Durability Design of Post-Tensioned Bridge Substructures

by

Jeffrey Steven West, B.S.C.E., M.S.

Dissertation

Presented to the Faculty of the Graduate School of

The University of Texas at Austin

in Partial Fulfillment

of the Requirements

for the Degree of

Doctor of Philosophy

The University of Texas at Austin

May 1999

Durability Design of
Post-Tensioned Bridge Substructures

Approved by
Dissertation Committee:

John E. Breen, Co-Supervisor

Michael E. Kreger, Co-Supervisor

Ned H. Burns

Ramon L. Carrasquillo

Harovel G. Wheat

to Pamela,
for your unending love,
support and patience

and to Jack and Bennett,
my wonderful sons who continue
to amaze me and remind me what
life is really about

Acknowledgements

I would like to begin by thanking my advisor, Dr. John Breen. I am extremely grateful for the many opportunities that you have given me to expand my horizons as an engineer far beyond the classroom and the research laboratory. I am very appreciative of the freedom I have had during my research, and the knowledge and experience I have gained as a result. I have learned a great deal from your enthusiasm for engineering, tact and ability to see the "big picture." Special thanks also goes to my second advisor, Dr. Michael Kreger. Our discussions on research, engineering, life after graduate school, golf and life in general have been invaluable to me. I have been very fortunate to round out my dissertation committee with three other great people: Dr. Ned Burns, Dr. Ramon Carrasquillo and Dr. Harovel Wheat. You have all been terrific, and I am very appreciative of the time each of you has taken to meet with me and discuss research over the years.

The research reported in this dissertation was performed under the Texas Department of Transportation Project 0-1405. I would like to thank our TxDOT Project Director Bryan Hodges for his support and advice throughout our research. I would also like to thank Dean Van Landuyt and Lloyd Wolf at TxDOT for their enthusiastic advice and assistance. Thanks also to Alan Kowalik in the Construction Division for loaning us the PR Monitor equipment for corrosion rate measurements.

Now on to the 1405 team of graduate students: Andrea Schokker, Brad Koester and Chuck Larosche. It has been a great pleasure to work with you all. Your friendship made the dirty, back-breaking, dehydrating days of never-ending work in the lab seem a whole lot better. I have been very fortunate to work with a team of people that I admire in many ways. Project 1405 has benefited from some great helpers, and in particular Diana Hun and John Riordan, who both survived "the summer of the reaction beams."

Several of my graduate student colleagues have been a big help to me. I would like to thank Trey Hamilton for his help and suggestions early on in the project, John Myers for his "concrete advice," Enrique Vaca for his guidance on epoxy coatings, chloride testing and numerous other corrosion-related subjects, and Stewart Verhulst for his help with the corrosion rate measurements on the beam specimens. Many other students helped out on the numerous concrete pours. There are too many of you to name, but I am

very grateful for your assistance. I have made many good friends at FSEL, and as we all eventually go our own way I will look forward to our mini-reunions at ACI conventions.

The extensive lab work would not have been possible without the help of the lab technical staff: Blake Stasney, Mike Bell, Wayne Fontenot and Ray Madonna. I am grateful for all of your assistance. On the administration side, my deepest gratitude goes to Laurie Golding, April Jenkins, Ruth Goodson and Regina Forward, whose help navigating the treacherous waters of purchasing and the university bureaucracy was priceless. Thanks also go to Carol Reese in the Construction Materials Research Group (18B) for her "scheduling help."

I would also like to thank several people from industry for their help and advice: George Somerville and Mike Webster at the British Cement Association, Giovanni Silvestri at VSL and Kerry Allen at DSI. I would like to thank Dr. Yoshito Tanaka at Shinko Wire for donating the prestressing strand used in the beam specimens. Special thanks go to Randy Poston and Jeff Wouters at WDP and Associates for the information on evaluating strand pitting, and for Jeff's help with the 3LP corrosion rate measurements.

I would like to thank my good friend Khaled Soudki at the University of Waterloo for his advice and encouragement throughout my pursuit of a Ph.D. I would also like express my gratitude to Dr. Sami Rizkalla at the University of Manitoba, for it was his talent, drive and most of all his infectious enthusiasm for structural engineering that made me decide I should be a structural engineer.

I would like to thank my parents, my mother-in-law, and my siblings for their love and encouragement, and for not continually asking me when I will be finished!

Finally, I must reserve my deepest gratitude for my wife Pamela. Your love, encouragement and support helped me through the lows, and made the highs that much better. Your patience and endurance is amazing as you handle a job and raise our two children, all with a graduate student for a husband. We now have the rest of our lifetimes for me to make it up to you.

Austin, Texas
May 1999

Jeff West

Durability Design of Post-Tensioned Bridge Substructures

Publication No._____

Jeffrey Steven West, Ph.D.
The University of Texas at Austin, 1999

Supervisors: John E. Breen and Michael E. Kreger

Bridge decks and superstructures have received considerable research and design effort to improve durability. While this effort has been successful in increasing the service life of the superstructure, bridge substructure condition may now limit service life.

Post-tensioning has been widely used in bridge superstructures, but has seen only limited application in bridge substructures. Post-tensioning can provide structural and economical benefits in substructure designs, and can possibly be used to improve durability.

The overall objective of this dissertation is to develop durability design guidelines for post-tensioned bridge substructures. The design guidelines are based on an extensive literature review and three experimental programs.

The literature review revealed a wealth of information on identifying durability concerns, concrete durability and corrosion protection measures for post-tensioned concrete structures.

A long term corrosion testing using large scale beams was developed to examine the effects of post-tensioning on corrosion protection through crack control. The beams are subjected to aggressive exposure and structural loading. Preliminary results indicate corrosion activity is decreased as the level of prestress increases, and that corrosion activity is largely confined to crack locations. This testing program is ongoing.

A long term exposure testing program using large scale column elements was developed to examine corrosion protection in vertical elements. Post-tensioned designs were compared to standard reinforced concrete designs. Corrosion activity during the reporting period was limited. Chloride samples showed substantially reduced chloride penetration for fly ash concrete. This testing program is ongoing.

A testing program with standard macrocell specimens was used to investigate corrosion protection for internal tendons in precast segmental construction. Findings indicated that match-cast epoxy joints are a necessity for corrosion protection of internal tendons. Severe corrosion damage was found on galvanized steel ducts, suggesting plastic ducts should be used in aggressive exposures. Gaskets used on the joint face around duct openings allowed moisture and chlorides to penetrate the joint. This testing program is ongoing.

Preliminary durability design guidelines were developed to identify durability concerns, to improve substructure durability using post-tensioning and to protect the post-tensioning system from corrosion. Because the experimental programs are on-going, the design guidelines are subject to change.

Table of Contents

List of Tables

List of Figures

Chapter 1:

Introduction

1.1 Bridge Substructure Durability

Durability is the ability of a structure to withstand various forms of attack from the environment. For bridge substructures, the most common concerns are corrosion of steel reinforcement, sulfate attack, freeze-thaw damage and alkali-aggregate reactions. The last three are forms of attack on the concrete itself. Much research has been devoted to these subjects, and for the most part these problems have been solved for new structures. The aspect of most concern for post-tensioned substructures is reinforcement corrosion. The potential for corrosion of steel reinforcement in bridges is high in some areas of Texas. In the northern regions, bridges may be subjected to deicing chemicals leading to the severe corrosion damage shown in Figure 1.1(a). Along the Gulf Coast, the hot, humid saltwater environment can also produce severe corrosion damage, as shown in Figure 1.1(b).

(a) Deicing Chemical Exposure

(b) Coastal Saltwater Exposure

"Attack from Above" **"Attack from Below"**

Figure 1.1 - Typical Corrosion Damage in Texas Bridge Substructures

The American Society of Civil Engineers (ASCE) produced a "report card" for America's infrastructure, as shown in Figure 1.2. Bridges faired better than most other areas of the infrastructure, receiving a grade of C-minus. However, a grade of C-minus is on the verge of being poor, and the ASCE comments that accompanied the grade indicated that nearly one third of all bridges are structurally deficient or functionally obsolete. What these statistics mean is that there are many bridges that need to be either repaired or replaced. This also means that more attention should be given to durability in the design process, since a lack of durability is one of the biggest contributors to the poor condition of the infrastructure.

Subject	Grade
Roads	D-
Bridges	C-
Mass Transit	C
Aviation	C-
Schools	F
Drinking Water	D
Wastewater	D+
Solid Waste	C-

"Nearly 1 of every 3 (31.4%) bridges is rated structurally deficient or functionally obsolete.

It will require $80 billion to eliminate the current backlog of deficiencies and maintain repair levels."

Figure 1.2 - ASCE Evaluation of Infrastruture Condition

Larosche[1.1] performed an analysis of bridge substructure condition in Texas using the TxDOT Bridge Inventory, Inspection and Appraisal System (BRINSAP). The BRINSAP system contains bridge condition rating information in a computer database of more than 30,000 bridges. Larosche determined the number of on-system concrete bridge substructures that had a condition rating indicating extensive minor deterioration or worse (condition rating of 5 or lower). Substructures with these condition ratings were deemed deficient for analysis purposes. The results of the analysis are plotted in Figure 1.3. In some districts, more than ten percent of the on-system bridges have deficient substructures. In general, bridges in the northern regions of the state appear to have a higher incidence of deficient substructures. Another interesting statistic is the superstructure condition rating for bridges with deficient substructures. The analysis of BRINSAP data indicated that the superstructure was in satisfactory condition in many instances of deficient substructures. This data, plotted in Figure 1.4, suggests that the substructure condition is controlling the service life of the bridge in many cases.

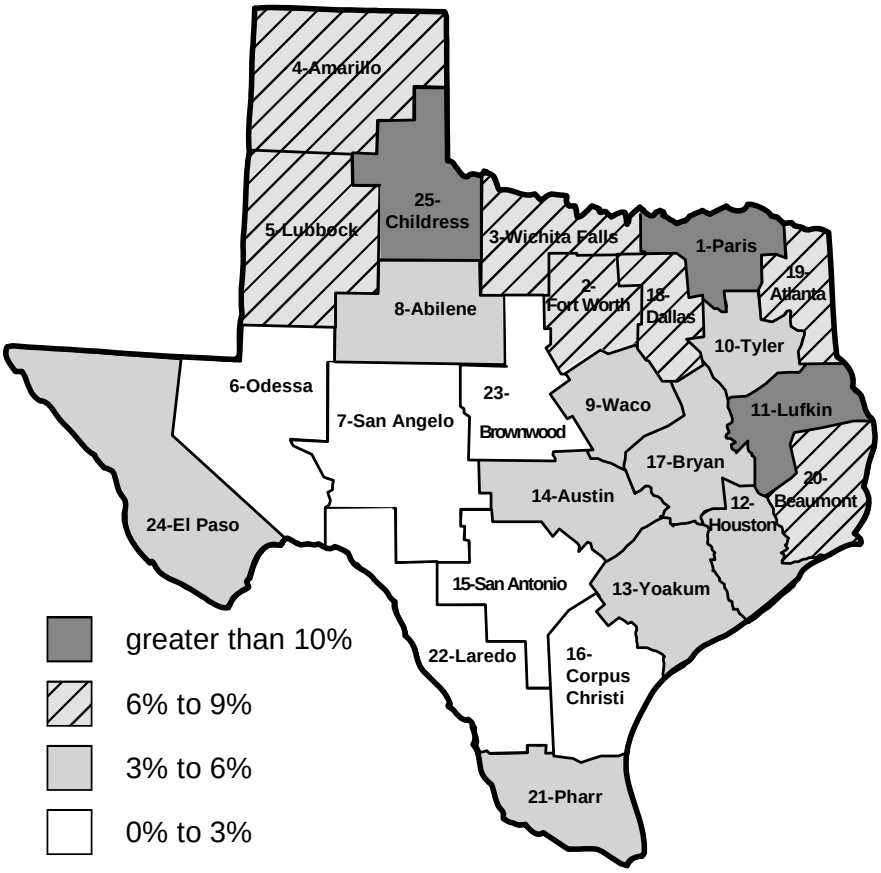

Figure 1.3 - Incidence of Deficient On-System Bridge Substructures in Texas[1.1]

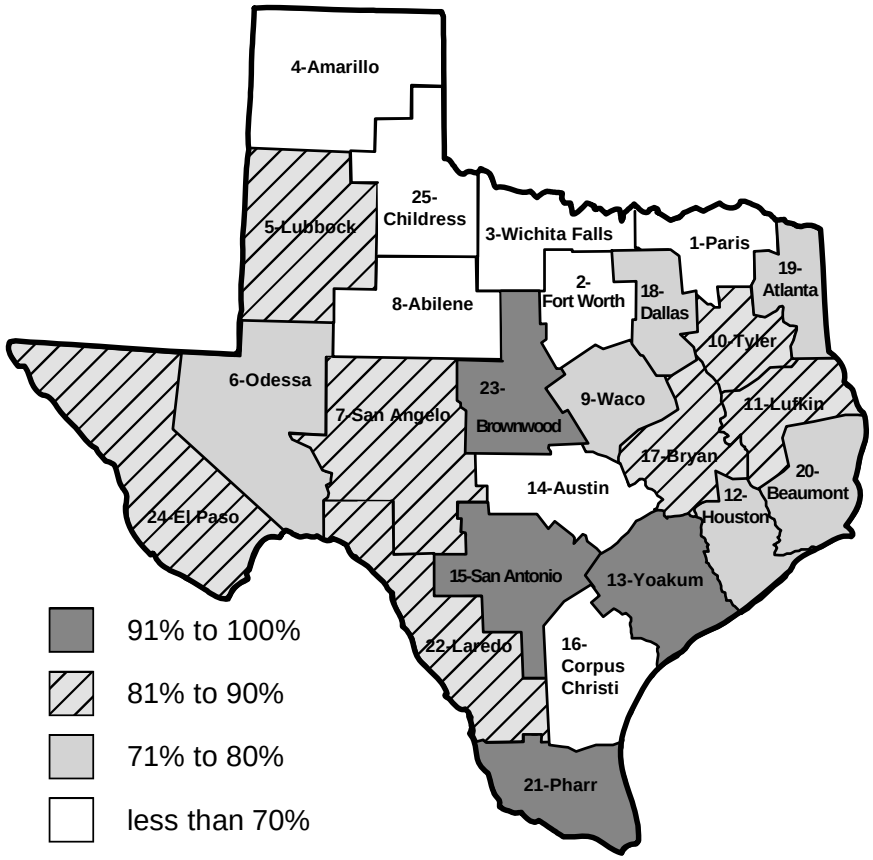

Figure 1.4 - Incidence of Bridges Where Substructure is Deficient but Superstructure Condtion is Satisfactory or Better[1.1]

The analysis of BRINSAP data suggests that more attention should be given to the durability of bridge substructures. However, two comments must be made at this point. The BRINSAP data does not indicate the source of deficiency. Therefore, a poor condition rating may reflect problems such as scour or vehicle impact, and not necessarily a lack of durability (see Larosche[1.1] for more discussion). The second issue is that the statistics presented in Figure 1.3 and Figure 1.4 are primarily for bridges that have been in existence for some time. The poor condition of many bridges may result from the lack of attention to durability at the time of construction. Advances have been made in recent years to improve substructure durability, including increased concrete cover, enhanced concrete quality and the use of epoxy-coated reinforcement. However, the effectiveness of these

changes is uncertain due to the short length of service, and a potential for further improvement exists.

1.2 Post-Tensioning in Bridge Substructures

1.2.1 Benefits of Post-Tensioning

Post-tensioning has been widely used in bridge superstructures, but has seen only limited applications in bridge substructures. There are many possible situations where post-tensioning can be used in bridge substructures to provide structural and economical benefits. Some possible benefits of post-tensioning are listed in Table 1.1.

Table 1.1 - Possible Benefits of Post-Tensioning

Benefit	Structural Behavior	Construction	Durability
Control of Deflections	✓		
Increased Stiffness	✓		
Improved Crack Control (higher cracking moment, fewer cracks, smaller crack widths)	✓		✓
Reduced Reinforcement Congestion	✓	✓	✓
Continuity of Reinforcement	✓		✓
Efficient utilization of high strength steel and concrete	✓		✓
Quick, efficient joining of precast elements	✓	✓	✓
Continuity between existing components and additions	✓	✓	✓

Although prestressing or post-tensioning is normally chosen for structural or construction reasons, many of the same factors can improve durability. For example, reduced cracking and crack widths offers the potential for improving the corrosion

protection provided by the concrete. Reduced reinforcement congestion and continuity of reinforcement means that it is easier to place and compact the concrete with less opportunity for voids in the concrete. Post-tensioning is often used in conjunction with precasting. Precast concrete offers improved quality control, concrete quality and curing conditions, all leading to improved corrosion protection. Bonded post-tensioning also provides the opportunity for multiple levels of corrosion protection for the prestressing tendon, as shown in Figure 1.5. Protection measures include surface treatments on the concrete, the concrete itself, the duct, the grout and strand or bar coatings such as epoxy or galvanizing. Post-tensioning also provides the opportunity to electrically isolate the prestressing system from the rest of the structure.

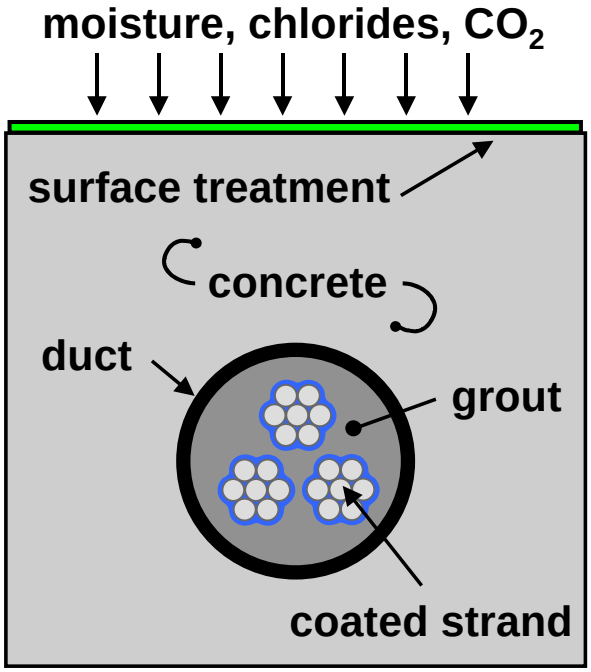

Figure 1.5 - Multi-Level Corrosion Protection for Bonded Post-Tensioning Tendons

1.2.2 Bridge Substructure Post-Tensioning Applications

Post-tensioning has been used successfully in many bridge substructures. The possible applications for post-tensioning are only limited by the imagination of the

designer. Several substructure post-tensioning applications are shown in Figure 1.6(a) through (h).

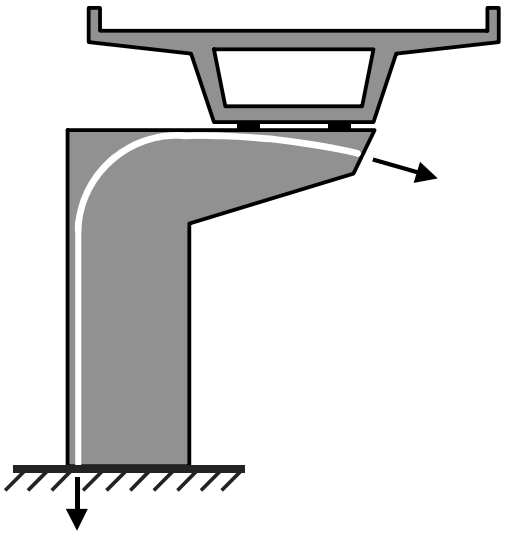

(a) Cantilever Substructure

Post-tensioning provides continuous reinforcement from the cantilever to the foundation. Deflection control and crack control are improved. Heavy reinforcement congestion in the joint region of the column is reduced.

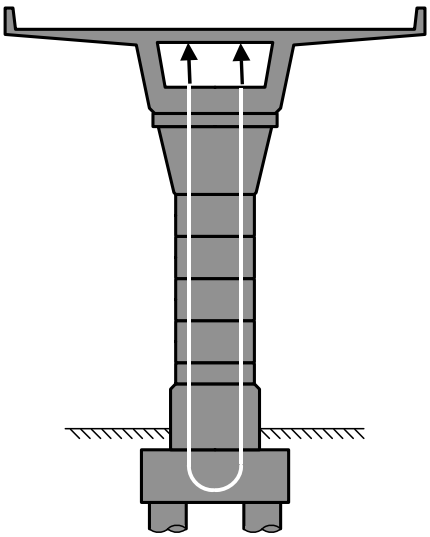

(b) Precast Segmental Hollow Pier

Post-tensioning provides continuous reinforcement in the substructure. Temporary post-tensioning is used during construction for structural integrity.

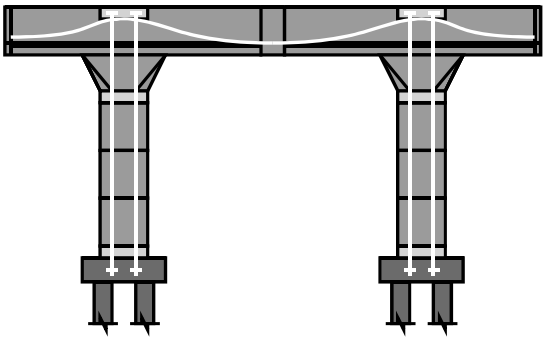

(c) Precast Frame Bent

Post-tensioning provides continuity of reinforcement and structural integrity for this entirely precast substructure. Construction proceeds rapidly, minimizing traffic interruption.

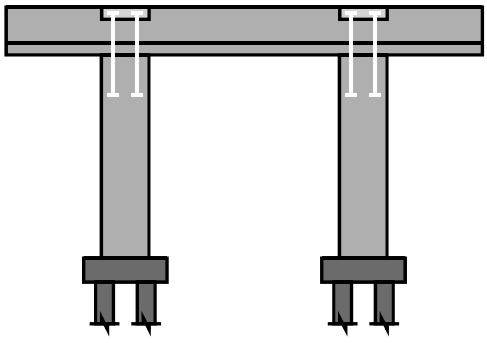

(d) Precast Bent Cap Post-Tensioned to Cast-in-Place Columns

Post-tensioning provides continuity between precast and cast-in-place components. Erection is rapid, minimizing traffic interruption.

Figure 1.6 - Applications of Post-Tensioning in Bridge Substructures

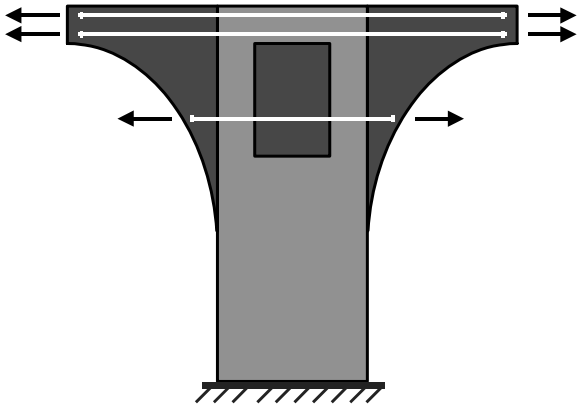

(e) Widening of Existing Substructure

Cantilever overhangs are added to allow widening of the bridge. Post-tensioning is used to provide continuous reinforcement and to improve shear transfer between the overhangs and existing substructure.

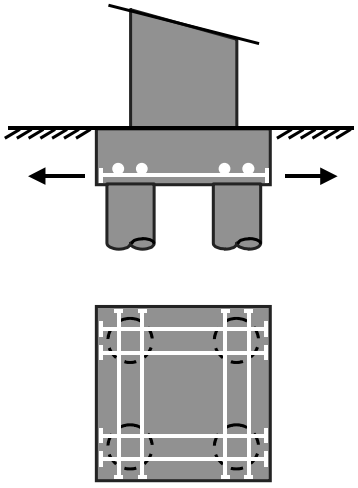

(f) Pile Cap

Post-tensioning is used to reduce the necessary size of the pile cap and the required steel area. The concentrated application of the post-tensioning anchorage forces is well suited to strut and tie methods of design for this element.

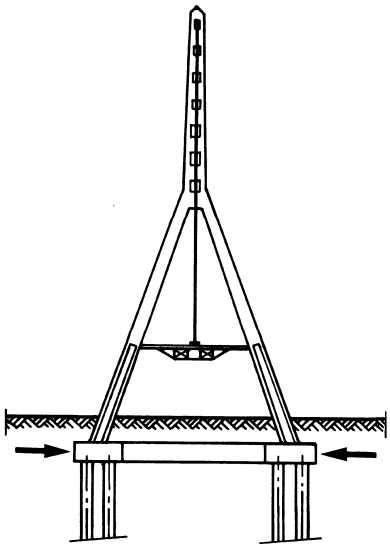

(g) Tie Beam[1,2]

High strength prestressing steel used for post-tensioning provides the necessary reinforcement for the large tension forces in the tie beam.

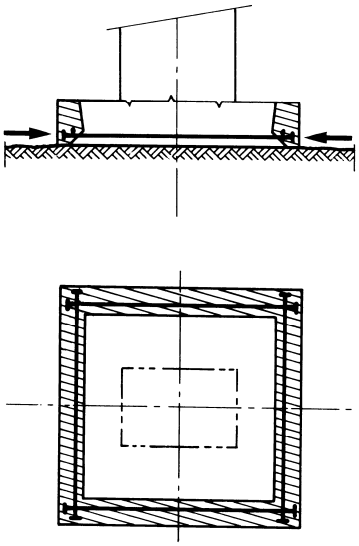

(h) Strengthening of Existing Footing[1,2]

Post-tensioning improves force transfer between existing and added concrete.

Figure 1.6 - Applications of Post-Tensioning in Bridge Substructures – Continued

1.3 Mixed Reinforcement in Structural Concrete

The recent development of the AASHTO LRFD (Load and Resistance Factor Design) Bridge Design Specifications[1.3] explicitly recognized the use of mixed reinforcement for the first time in American bridge and building codes. Mixed reinforcement, sometimes referred to as partial prestressing, describes structural concrete members with a combination of high strength prestressing steel and non-prestressed mild steel reinforcement. The relative amounts of prestressing steel and reinforcing bars may vary, and the level of prestress in the prestressing steel may be altered to suit specific design requirements. In most cases, members with mixed reinforcement are expected to crack under service load conditions (flexural cracks due to applied loading).

In the past, prestressed concrete elements have always been required to meet the classic definition of full prestressing where concrete stresses are kept within allowable limits and members are generally assumed to be uncracked at service load levels (no flexural cracks due to applied loading). The design requirements for prestressed concrete were distinctly separate from those for reinforced concrete (non-prestressed) members, and are located in different chapters or sections of the codes. The fully prestressed condition may not always lead to an optimum design. The limitation of concrete tensile stresses to below cracking can lead to large prestress requirements, resulting in very conservative designs, excessive creep deflections (camber) and the requirement for staged prestressing as construction progresses.

The use of varied amounts of prestressing in mixed reinforcement designs can offer several advantages over the traditional definitions of reinforced concrete and fully prestressed concrete:[1.4,1.5]

- Mixed reinforcement designs can be based on the strength limit state or nominal capacity of the member, leading to more efficient designs than allowable stress methods.
- The amount of prestressed reinforcement can be tailored for each design situation. Examples include determining the necessary amount of prestress to:
  - balance any desired load combination to zero deflections
  - increase the cracking moment to a desired value

  - control the number and width of cracks
- The reduced level of prestress (in comparison to full prestressing) leads to fewer creep and excessive camber problems.
- Reduced volume of steel in comparison to reinforced concrete designs.
- Reduced reinforcement congestion, better detailing, fewer reinforcement splices in comparison to reinforced concrete designs.
- Increased ductility in comparison to fully prestressed designs.

Mixed reinforcement can provide a desirable design alternative to reinforced concrete and fully prestressed designs in many types of structures, including bridge substructures. Recent research[1.6] at The University of Texas at Austin has illustrated the structural benefits of mixed reinforcement in large cantilever bridge substructures.

The opposition to mixed reinforcement designs and the reluctance to recognize mixed reinforcement in design codes has primarily been related to concerns for increased cracking and its effect on corrosion. Mixed reinforcement design will generally have more cracks than comparable fully prestressed designs. It has been proposed that the increased presence of cracking will lead to more severe corrosion related deterioration in a shorter period of time. Due to the widely accepted notion that prestressing steel is more susceptible to corrosion, and that the consequences of corrosion in prestressed elements are more severe than in reinforced concrete (see Section 2.3.2), many engineers have felt that the benefits of mixed reinforcement are outweighed by the increased corrosion risk. Little or no research has been performed to assess the effect of mixed reinforcement designs on corrosion in comparison to conventional reinforced concrete and fully prestressed designs.

1.4 Problem Statement

This dissertation represents a portion of the Texas Department of Transportation Research Project 0-1405: "Durability Design of Post-Tensioned Bridge Substructure Elements." The project title implies two main components to the research:

1. Durability of Bridge Substructures, and
2. Post-Tensioned Bridge Substructures.

The durability aspect is in response to the deteriorating condition of bridge substructures in some areas of Texas. Considerable research and design effort has been given to bridge deck design to prevent corrosion damage, while substructures have been largely overlooked. In some districts of the state, more than ten percent of the substructures are deficient, and the substructure condition is limiting the service life of the bridges.

The second aspect of the research is post-tensioned substructures. As described above, there are many possible applications in bridge substructures where post-tensioning can provide structural and economical benefits, and can possibly improve durability. Post-tensioning is now being used in Texas bridge substructures, and it is reasonable to expect the use of post-tensioning to increase in the future as precasting of substructure components becomes more prevalent and as foundation sizes increase.

Problem:

The problem that bridge engineers are faced with is that there are no durability design guidelines for post-tensioned concrete structures. Durability design guidelines should provide information on how to identify possible durability problems, how to improve durability using post-tensioning, and how to ensure that the post-tensioning system does not introduce new durability problems.

1.5 Research Objectives and Project Scope

1.5.1 Project Objectives

The research objectives for TxDOT Project 0-1405 are as follows:

1. To examine the use of post-tensioning in bridge substructures,
2. To identify durability concerns for bridge substructures in Texas,
3. To identify existing technology to ensure durability or improve durability,
4. To develop experimental testing programs to evaluate protection measures for improving the durability of post-tensioned bridge substructures, and
5. To develop durability design guidelines and recommendations for post-tensioned bridge substructures.

A review of literature early in the project indicated that post-tensioning was being successfully used in past and present bridge substructure designs, and that suitable post-

tensioning hardware was readily available. It was decided not to develop possible post-tensioned bridge substructure designs as part of the first objective for two reasons. First, other research[1.6,1.7,1.8] on post-tensioned substructures was already underway, and second, the durability issues warranted the full attention of Project 0-1405. The third objective was added after the project had begun. The initial literature review identified a substantial amount of relevant information that could be applied to the durability of post-tensioned bridge substructures. This allowed the scope of the experimental portion of the project to be narrowed. The final objective represents the culmination of the project. All of the research findings are to be compiled into the practical format of durability design guidelines.

1.5.2 Project Scope

The subject of durability is extremely broad, and as a result, so is the scope of Project 0-1405. Based on the project proposal and an initial review of relevant literature, the project scope and necessary work plan were defined. The scope of the research flows from the overall objective of developing durability design guidelines. The design guidelines must address two questions:

1. When is durability a concern?
2. How can durability be improved?

The project tasks related to these questions are illustrated in Figure 1.7 and Figure 1.8. The experimental work in the project involves the tasks listed in Figure 1.8.

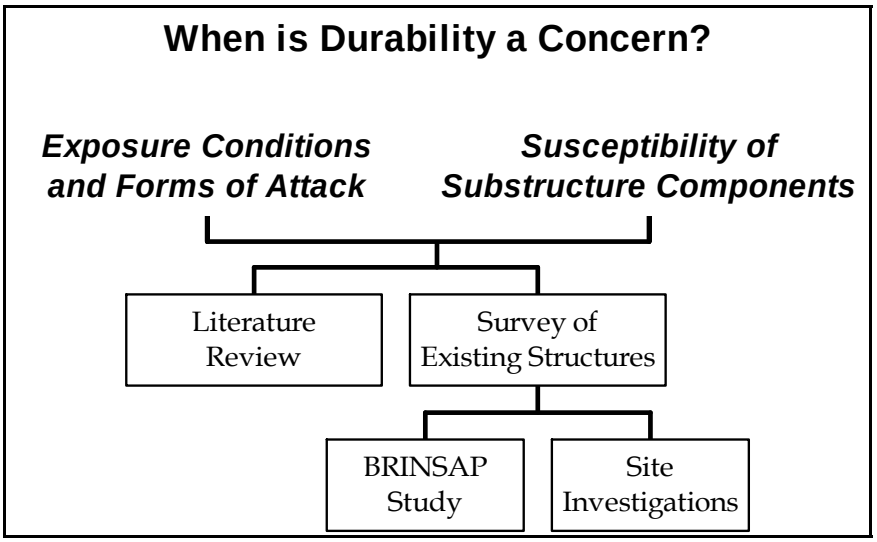

Figure 1.7 - Project Work Plan: Identifying Durability Concerns

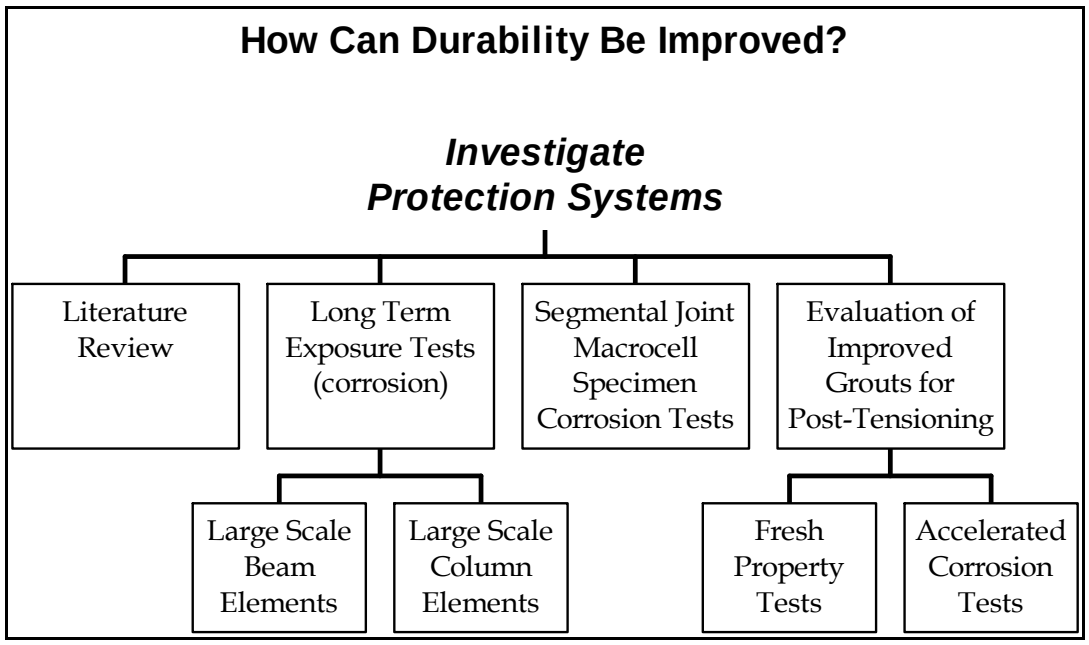

Figure 1.8 - Project Work Plan: Identifying Durability Protection Measures

A large amount of literature was found on the subject of concrete durability early in the project. Detailed information was available for sulfate attack, freeze-thaw damage and alkali-aggregate reaction. For this reason, it was decided to focus the experimental portion of the project on corrosion of reinforcement in post-tensioned concrete, as evident

in Figure 1.8. The detailed literature on concrete durability would be used to develop durability design guidelines on those aspects.

Four graduate students have worked on Project 0-1405 to date: the author, Brad Koester,[1.9] Chuck Larosche[1.1] and Andrea Schokker.[1.10] The work to date has been a cooperative effort, with students working together on various tasks. The involvement of graduate students in the various project tasks is shown in Table 1.2. The segmental joint macrocell specimens were developed and constructed by Rene Vignos[1.11] under Project 0-1264. These specimens were transferred to Project 0-1405 in 1995 for long term testing.

Project 0-1405 is not complete, as the long term beam and column exposure tests and the macrocell corrosion tests are ongoing. Additional graduate students will complete the project. The major tasks to be completed by future students include continued exposure testing and data collection, final autopsy of all beam, column and macrocell specimens and preparation of the final durability design guidelines.

Table 1.2 - Major Project Work Tasks and Contributions of Graduate Students

Project Task	Participants
Literature Review	West, Koester, Larosche, Schokker
Identification of Substructure Post-Tensioning Applications and Systems	West, Koester
Identification of Protection System Variables	West, Koester
Survey of Existing Structures	Larosche
Testing Program Design:	
Long Term Beam Exposure Tests	West
Long Term Column Exposure Tests	Larosche, West
Segmental Macrocell Corrosion Tests	Vignos
Evaluation of Improved Grouts for Post-Tensioning	Koester, Schokker, West
Fabrication of Test Specimens:	
Long Term Beam Exposure Tests	West, Schokker
Long Term Column Exposure Tests	Larosche, West
Segmental Macrocell Corrosion Tests	Vignos

Evaluation of Improved Grouts for Post-Tensioning	Koester, Schokker
Initial Exposure Testing:	
Long Term Beam Exposure Tests	West, Schokker
Long Term Column Exposure Tests	West, Schokker
Segmental Macrocell Corrosion Tests	Vignos, West
Evaluation of Improved Grouts for Post-Tensioning	Koester, Schokker
Limited Specimen Autopsies:	
Long Term Beam Exposure Tests	Schokker
Long Term Column Exposure Tests	Schokker
Segmental Macrocell Corrosion Tests	West
Preliminary Design Guidelines	West, Schokker

1.6 Dissertation Objectives and Scope

The scope of this dissertation represents the contribution of the author to TxDOT Project 0-1405. The specific objectives for this dissertation are:

1. To develop experimental testing programs to investigate the effect of post-tensioning for crack control on corrosion.
2. To develop experimental testing programs to investigate corrosion protection measures for post-tensioned concrete members.
3. To evaluate the effect of precast segmental joints on corrosion protection for internal post-tensioning tendons using macrocell corrosion test specimens.
4. To develop preliminary durability design guidelines for post-tensioned bridge substructures based on an in-depth review of related literature and preliminary experimental results.

Two exposure testing programs were developed to address the first and second objectives listed above. A third testing program was taken over from another research project to address Objective 3. Where possible, the testing programs were developed to address more than one objective as shown in Figure 1.9.

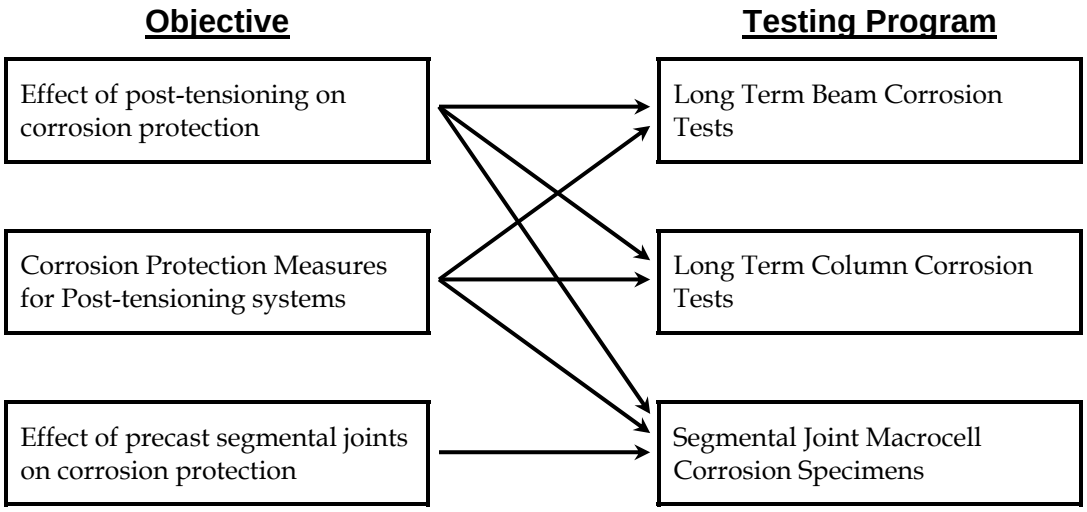

Figure 1.9 – Dissertation Research Objectives and Testing Programs

The core of the dissertation is organized into four chapters. Chapter 2 is an extensive literature review on various aspects of the durability of post-tensioned bridge substructures. The literature review begins with a discussion of exposure conditions and the forms of attack on durability for bridge substructures in Texas. Basic theory for corrosion of steel in concrete is presented, and an in-depth review on the effect of concrete cracking on corrosion is included. The effect of cracking is of great interest to this project since post-tensioning may be used to control cracking, and the effect on corrosion could influence mixed reinforcement designs. A large summary of corrosion protection measures for post-tensioned concrete structures is presented. Relevant literature on the subjects of sulfate attack, freeze-thaw damage and alkali-aggregate reaction was reviewed and presented in terms of exposure conditions, mechanism of attack, influencing factors and protection methods. Literature on the field performance of prestressed concrete bridges was reviewed to provide insight on the types of past and current problems experienced by post-tensioned bridges in service. A selected review of relevant experimental studies of corrosion in prestressed concrete is included. Lastly, crack prediction methods for structural concrete members are presented. The crack prediction methods were used in the design of the beam exposure test program and analysis of experimental results. The development of the experimental programs relied heavily on the reviewed literature. In particular, the effects of cracking on corrosion, field

performance of prestressed bridges and past prestressed concrete corrosion research were used to shape the beam exposure testing program.

Chapter 3 describes the long term beam exposure tests. A detailed discussion of the design of the test specimens and selection of variables is presented. Experimental data for the Phase I beam specimens is presented and analyzed, including cracking behavior, chloride penetration and ten months of half-cell potential measurements. Corrosion rate measurements at seven, twelve and fifteen months exposure are presented and analyzed. Preliminary conclusions for post-tensioning to improve corrosion protection, crack width prediction and corrosion rate measurements are presented.

Chapter 4 describes the long term column exposure tests. A detailed discussion of the design of the test specimens and selection of variables is presented. More than two years of experimental data in terms of half-cell potential measurements and chloride penetration is presented and analyzed. Preliminary conclusions are presented.

Chapter 5 describes the segmental joint macrocell corrosion specimens. The testing program was developed and implemented by Vignos.[1.11] Chapter 5 briefly describes the test specimens and variables, and presents and discusses four and a half years of exposure test data. One-half (nineteen of thirty-eight) of the macrocell specimens were subjected to a forensic examination after four and a half years of testing. A detailed description of the autopsy process and findings is included. Conclusions based on the exposure testing and forensic examination are presented.

Chapter 6 presents preliminary durability design guidelines for post-tensioned bridge substructures. These guidelines are primarily based on the literature reviewed in Chapter 2, but also include the preliminary findings from the experimental portion of the project described in Chapters 3, 4 and 5. The durability design process is described, and guidance is provided for assessing the durability risk and for ensuring protection against freeze-thaw damage, sulfate attack and corrosion of steel reinforcement. These guidelines will be refined and expanded by others on the project as more experimental data becomes available.

Chapter 7 presents a brief summary of the dissertation and overall conclusions. Recommendations for areas requiring further research are made.

Chapter 1 References:

1.1) **Larosche, C.J.,** "Test Method for Evaluating Corrosion Mechanisms in Standard Bridge Columns," Master of Science Thesis, The University of Texas at Austin, August 1999.

1.2) **Aeberhard, H.U., Ganz, H.R., Marti, P., and Schuler, W.,** Post-Tensioned Foundations, VSL International Ltd., Berne, Switzerland, 1988, 24 pp.

1.3) **AASHTO**, LRFD Bridge Design Specifications, 2nd Edition, American Association of State Highway and Transportation Officials, Washington, D.C., 1998.

1.4) **Billington, S.L.,** "Behavior of Two-Span Continuous Pier Caps With Varying Levels of Prestress," Master of Science Thesis, The University of Texas at Austin, December 1994.

1.5) **Thürlimann, Bruno,** "Considerations to the Design of Prestressed Concrete Bridges," *IABSE Proceedings,* No. 70, 1983, pp. 237-?.

1.6) **Armstrong, S.D., Salas, R.M., Wood, B.A., Breen, J.E. and Kreger, M.E.,** "Behavior and Design of Large Structural Bridge Pier Overhangs," Research Report 1364-1, Center for Transportation Research, The University of Texas at Austin, 1997, 272 pp.

1.7) **Billington, S.L.,** "Improving Standard Bridges Through Aesthetic Guidelines and Attractive, Efficient Concrete Substructures," Doctor of Philosophy Dissertation, The University of Texas at Austin, December 1997.

1.8) **Barnes, R.W.,** "Development of a High Performance Substructure System for Prestressed Concrete Girder Highway Bridges," Master of Science Thesis, The University of Texas at Austin, 1996.

1.9) **Koester, B.D.,** "Evaluation of Cement Grouts for Strand Protection Using Accelerated Corrosion Tests," Master of Science Thesis, The University of Texas at Austin, December 1995.

1.10) **Schokker, A.J.,** "Improving Corrosion Resistance of Post-Tensioned Substructures Emphasizing High Performance Grouts," Doctor of Philosophy Dissertation, The University of Texas at Austin, August 1999.

1.11) **Vignos, R.P.**, "Test Method for Evaluating the Corrosion Protection of Internal Tendons Across Segmental Bridge Joints." Master of Science Thesis, The University of Texas at Austin, May 1994.

gileswl.sa□□□□□□□□□□□□□□□□□□□□□□□□□□□□□□□□□□□□□□
□g□i□l□e□s□w□l□.□s□a□□□
□C□o□u□r□i□e□r□ □N□e□w□
□C□o□u□r□i□e□r□ □N□e□w□
□C□o□u□r□i□e□r□ □N□e□w□□□□□□□□□¸¸□□

Chapter 3:

Long Term Beam Corrosion Tests

3.1 Test Concept and Objectives

Post-tensioning may have two general effects on the durability or corrosion protection in flexural members. First, post-tensioning may improve the corrosion protection provided by the concrete by controlling the number and width of cracks in the concrete. In post-tensioned members where the concrete remains precompressed under service loading, it has been suggested that moisture and chloride penetration will be reduced as precompression limits microcracking within the structure of the concrete. The second effect is that additional components, the post-tensioning system, are introduced in the structure. Most of these components are steel, and thus introduce potential sources of corrosion damage if not given proper attention in the durability design process. Thus, the durability design process for post-tensioned elements must address how to best use post-tensioning to improve corrosion protection, while ensuring that the post-tensioning hardware is protected from corrosion damage.

The term prestressed concrete has traditionally been used to describe structural concrete that is prestressed such that elastic stresses in the gross concrete section do not exceed specified limits at service load levels. The extreme fiber stress in the precompressed tensile zone is normally limited to below the modulus of rupture of the concrete. This is the classic definition of full prestressing, and is equally applicable to pre-tensioned and post-tensioned concrete. As described in Chapter 2, many situations exist where it is desirable to reduce the amount of prestressing below that required by code elastic stress limits. In this situation, mild steel reinforcement may or may not be required to satisfy strength requirements, and the concrete will likely crack under service load levels. Because this is often desirable from structural and economical perspectives, it is important to evaluate its effect on the durability of the structure.

This portion of the research project consists of long term exposure testing of large structural concrete flexural members or beams. The specific objectives are to investigate:

1) The effect of post-tensioning on durability (corrosion protection) through crack control, and
2) The relative performance of a broad scope of corrosion protection variables for multistrand post-tensioning systems.

The experimental program uses large scale linear elements, designed as a beams. The beams are subjected to combined structural loading and aggressive exposure. The specimens are tested outside the Ferguson Structural Engineering Laboratory, and are exposed to cyclic wetting and drying with a 3% NaCl solution to promote accelerated corrosion. The majority of the specimens are continually subjected to service load conditions. The effect of post-tensioning is investigated for a range of prestressing from non-prestressed (reinforced concrete) to partially prestressed to fully prestressed. Variables investigated are the influence of crack width, high performance concrete, prestressing strand coatings, duct splices, high performance grout, and encapsulated post-tensioning systems.

The experimental program was implemented in two phases. The first phase, addressed in this chapter, was developed to investigate the influence of prestress level, cracking, high performance grout and post-tensioning duct splices. The second phase, detailed in Reference 3.1, investigates high performance concrete, high performance grout, prestressing strand coatings and an encapsulated post-tensioning system. The beam specimen design and loading is identical for the two phases of testing. The variables investigated in both phases are discussed briefly in this chapter. However, only the results from the first phase are presented and discussed.

3.2 Test Specimen

The test specimens in this experimental program are linear elements, designed as beams with a rectangular cross-section. The test specimens were developed for research purposes and are not necessarily representative of any particular bridge substructure element. Linear rectangular elements were chosen for the following reasons:

- results can be applied to bent cap and column elements directly and some results may be qualitatively applied to other elements such as pile caps
- all desired variables can be readily incorporated into design
- ease of construction, handling and placement
- simplicity of controlling and maintaining loading

The element dimensions and details were selected such that covers, reinforcement sizes, post-tensioning hardware and crack widths were on a similar order of magnitude as in practical applications, with consideration for handling and loading of the specimens. A minimum of two (2) tendons (multistrand) were used in all prestressed specimens to represent practical applications of post-tensioning in bridge substructures. Using commercially available multistrand post-tensioning hardware, the maximum number of strands as governed by several possible section dimensions are shown below.

Section:	**Max. No. of Strands:**	**Hardware:**
300 mm x 450 mm (12″ x 18″)	2	VSL Type E5-1
400 mm x 600 mm (16″ x 24″)	6	VSL Type E5-3
450 mm x 600 mm (18″ x 24″)	8	VSL Type E5-4

The Type E multistrand anchorage hardware manufactured by VSL Corporation[3.2] was selected because it is available in tendon configurations with as few as three strands. Most multistrand post-tensioning systems are not available in sizes smaller than five to seven strands per tendon. The 450 mm x 600 mm (18″ x 24″) section, accommodating up to eight strands in two tendons, was chosen to provide the most flexibility in the design of mixed reinforcement sections. For practical handling and loading, a nominal beam length of 15 feet was chosen.

3.2.1 Levels of Prestress

The effect of prestressing on corrosion protection is one of the main investigation areas for this testing program. In order to examine a broad range of prestressing, section reinforcement was proportioned for the following levels of prestress:

- non-prestressed
- 100% prestress based on service load/allowable stress design (100%S PS)
- 100% prestress based on ultimate (nominal) strength (100%U PS)
- intermediate level of mixed reinforcement with a nominal prestress amount between 50% and 75%

The amount of prestress, in percent, is defined as the tensile force component provided by prestressing steel at the nominal flexural capacity of the section. Prestress amounts of 100%U prestressed and the intermediate range of 50% to 75% would be traditionally classified as partial prestressing, and would be expected to crack at service load levels. These sections, and the non-prestressed section were designed using a strength design approach. The selected section dimensions and requirement for two tendons dictated the use of 8 strands for the 100%S PS section, 6 strands for the 100%U PS section, and 4 strands for the intermediate level of prestress (50% to 75%).

3.2.2 Section Design

The specimens used in this experimental program are not patterned after a prototype bridge element, and thus no specified design loading is available. Reinforcement was proportioned based on the total allowable service load moment (dead plus live) computed for the 100%S PS section (fully prestressed, service load design). Assuming a ratio of dead load to live load of 1.5, the calculated permissible total service load moment was used to compute the dead and live load moments. The factored moment was then computed and used to proportion the reinforcement for the remaining sections.

3.2.2.1 Calculation of Design Loading Based on 100%S PS Section

Determination of the design loading is shown schematically in Figure 3.1. The 100%S PS section is fully prestressed to meet the stress limits specified by Clause 5.9.4 of

AASHTO LRFD[3.3] (Clause 18.4 of ACI 318[3.4]). The section has eight prestressing strands in two tendons, and was analyzed assuming the following:

- Gross section properties, elastic stresses
- f'_c = 35 MPa (5 ksi)
- A_{ps} = eight 12.7 mm (0.5 in.) 7-wire prestressing strands, f_{pu} = 1860 MPa (270 ksi)
- $f_{pi} = 0.65f_{pu}$
- Long term losses = 15% ($f_{pe} = 0.55f_{pu}$)
- Maximum tendon eccentricity, e = 200 mm (8 in.) based on clear cover to duct of 65 mm (2.5 in.)
- Compute the total allowable moment assuming that the governing stress in the concrete (tensile or compressive) is at least 75% of the corresponding allowable value. (i.e., either $0.75f_{callow} \le f_{cmax} \le f_{callow}$ or $0.75f_{tallow} \le f_{tmax} \le f_{tallow}$)
- Neglect self weight of the beam (self weight is very small in comparison to applied forces)

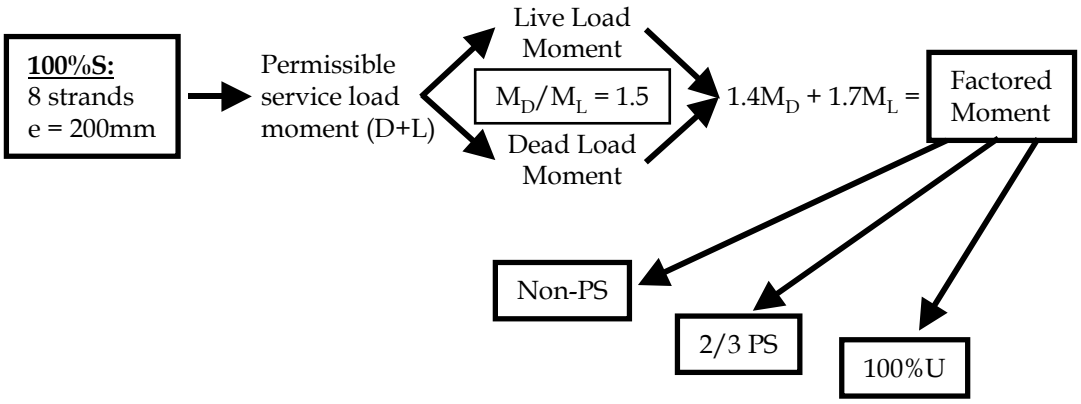

Figure 3.1 - Calculation of Design Moments

The 100%S PS section was analyzed for stresses in the concrete immediately after prestress transfer and under maximum applied loading. Calculated stresses and moments are shown in Appendix C. Based on these assumptions, a service load moment of 310 kN-m (2750 k-in.) was obtained with $f_t = 0.75f_{t_{allow}}$ governing. The tendon profile was draped to meet stress limits at the member ends. The tendon profile and allowable limits for the steel center of gravity (cgs) are shown in Figure 3.2.

The design moment for the remaining section types was calculated based on the maximum permissible service load moment as follows:

$M_{service}$ = 310 kN-m (2750 k-in.) (based on 100%S PS section)

M_D/M_L = 1.5 (assumed)

Therefore,

M_D = 186 kN-m (1650 k-in.)

M_L = 125 kN-m (1100 k-in.)

$M_{factored}$ = 472 kN-m (4180 k-in.)

$M_{nominal}$ = 525 kN-m (4650 k-in.) (for $\phi = 0.9$)

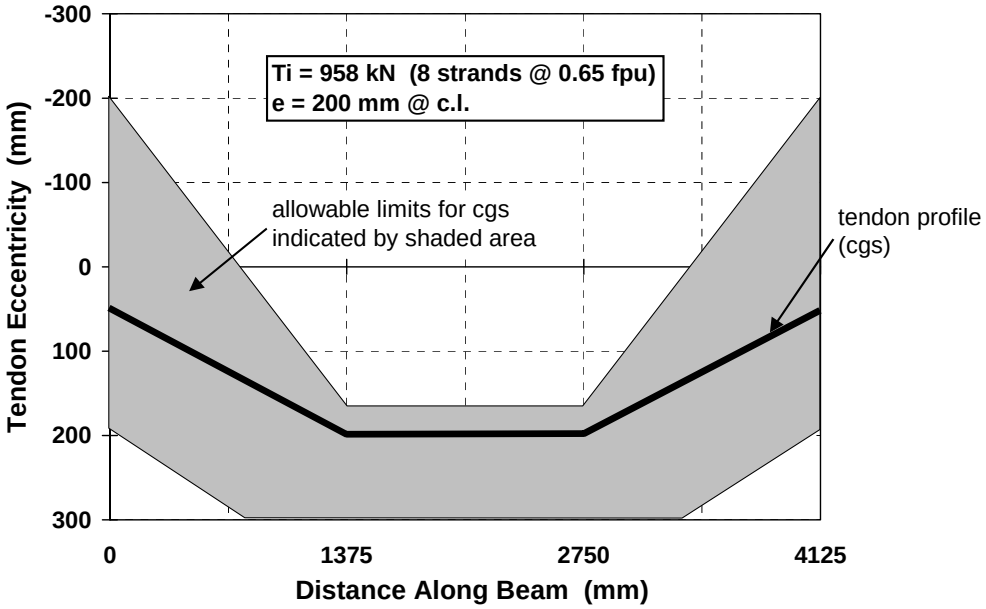

Figure 3.2 - 100%S PS Section Tendon Profile and Allowable Limits

3.2.2.2 Section Reinforcement

The required nominal flexural capacity, M_n, was used for the strength design of the remaining sections: Non-PS, 100%U prestressed and intermediate prestress (50% to 75%). The cross section size and desire for two tendons in each specimen dictated 6 strands in the 100%U PS section and 4 strands in the intermediate section (50% to 75% prestress). All sections were provided with two #5 bars (15.9 mm dia.) as compression steel.

Tension Reinforcement

The 100%S PS section was provided with two #3 bars (9.5 mm dia.) in the tension zone to aid construction of the reinforcement cages. This steel was not required as tension reinforcement to meet the reinforcement limits of AASHTO LRFD Clause 5.7.3.3[3.3] (Clause 18.8, ACI 318-95[3.4]), but was included in all calculations. The nominal flexural capacity of the 100%S PS section was computed to be 670 kN-m (5935 k-in.), well in excess of the required strength of 525 kN-m (4650 k-in.).

The 100%U PS section satisfied the strength requirements with six 12.7 mm (0.5″) dia. prestressing strands. The 100%U PS section was also provided with two #3 bars (9.5 mm dia.) in the tension zone to aid construction of the reinforcement cages. This steel was included in all calculations. The calculated flexural capacity was 529 kN-m (4685 k-in.) for this section.

The level of prestress for the intermediate section was determined by computing the necessary mild steel reinforcement to meet strength requirements in conjunction with the selected number of strands (in this case 4 strands). A mild steel area of 800 mm^2 (1.24 in^2) was required to provide the necessary flexural capacity. For this combination of strands and mild steel reinforcement, the level of prestress was calculated as 66.7% (2/3 PS). It was decided to use a constant number of mild steel bars for the 2/3 PS section and the Non-PS section in an attempt to emphasize the amount of prestress as the significant factor for crack widths. Four #4 bars (12.7 mm dia.) and four #3 bars (9.5 mm dia.) were selected to provide the necessary steel area.

The nominal strength requirements for the Non-PS section were met with a mild steel area of 1960 mm^2 (3.04 $in.^2$). Keeping the total number of bars at eight, six #6 bars (19 mm dia.) and two #4 bars (12.7 mm dia.) were selected.

The reinforcement details are shown in Figure 3.3 for the four section types and are summarized in Table 3.1. Bar sizes are shown in customary U.S. sizes, with metric equivalents listed below the table. Complete construction details of the four sections are shown in the detailed drawing set in Appendix C. A drawing list is provided in Figure C.1.

Table 3.1 – Summary of Section Details

Section	Prestressing Strands	Effective Prestress (after all losses)	Mild Steel Bars (tension)	Nominal Capacity
Non-PS	None	n/a	6-#6 and 2-#4	529 kN-m
2/3 PS	4 – 12.7 mm	$0.60f_{pu}$ = 1116 MPa	4-#4 and 4-#3	536 kN-m
100%U PS	6 – 12.7 mm	$0.60f_{pu}$ = 1116 MPa	2-#3	529 kN-m
100%S PS	8 – 12.7 mm	$0.56f_{pu}$ = 1042 MPa	2-#3	670 kN-m

Bar Sizes: #6 – 19 mm dia.
#4 – 12.7 mm dia.
#3 – 9.5 mm dia.

Conversion Factors: 1 in. = 25.4 mm
1 ksi = 6.895 MPa
1 k-in. = 0.11298 kN-m

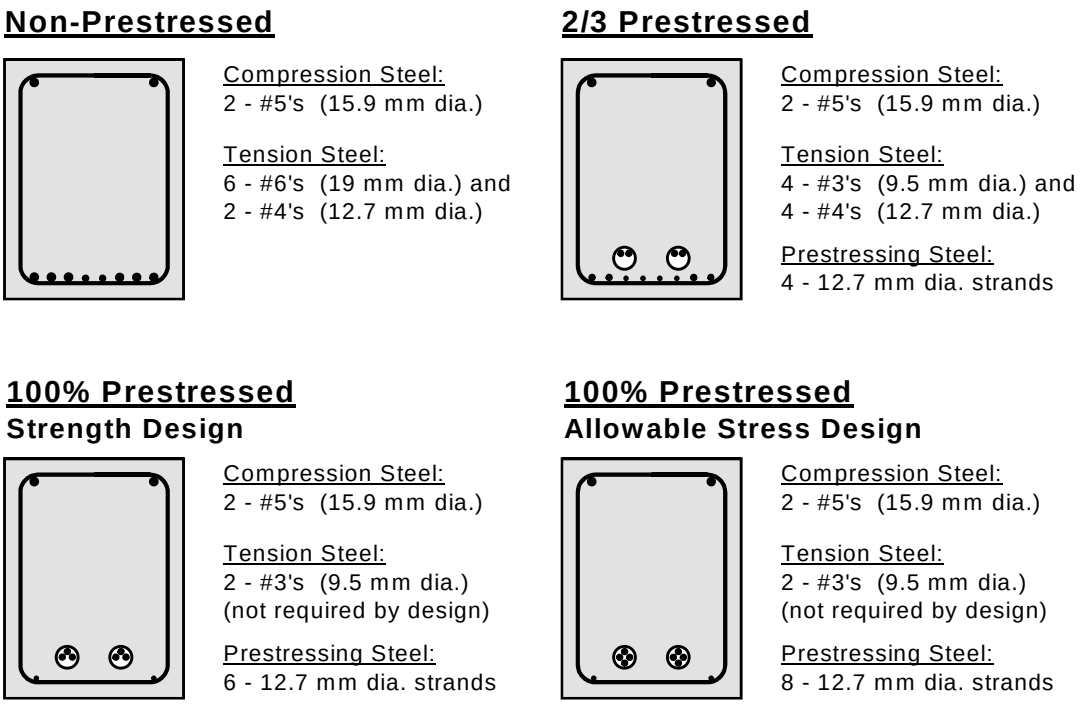

Figure 3.3 – Section Reinforcement Details

Shear Reinforcement

Shear reinforcement was proportioned for the shear force corresponding to development of the nominal flexural capacity of the sections. Stirrup layouts for all members are shown in Appendix C.

Anchorage Zone Reinforcement

General zone reinforcement for the post-tensioning anchorage forces was designed according to the recommendations of Breen et al.[3.5] General zone reinforcement was provided with closed stirrups according to the spacing shown in Appendix C. Local zone anchorage reinforcement in the form of spirals was based on the guidelines of the post-tensioning hardware supplier. Anchorage zone details and anchorage hardware are shown in Appendix C.

Post-Tensioning System

All prestressed sections utilized the same draped tendon profile (depression points at third points) shown in Figure 3.2 and Figure 3.4. As described in the previous section, this profile was chosen to satisfy allowable stresses at the ends of the 100%S PS members. The draped profile also ensures that all strands within the tendon are in contact (electrically), as this may influence corrosion behavior.

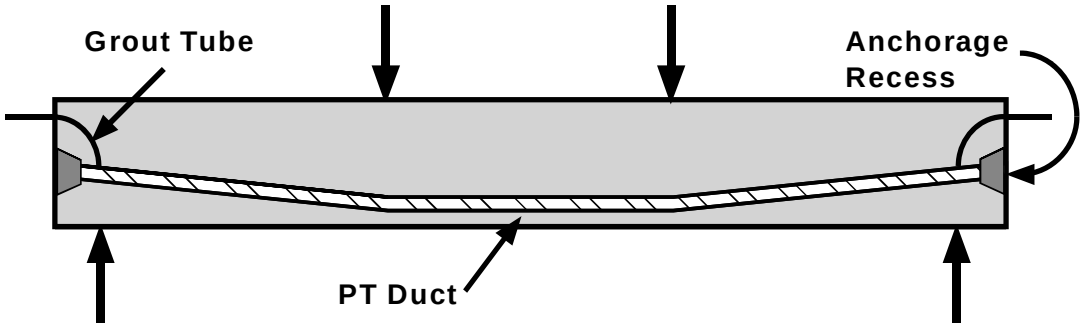

Figure 3.4 - Tendon Layout for Post-Tensioned Beams

The VSL Corporation Type E anchorage system[3.2] was used for all post-tensioned beams. The smallest available configuration in the Type E system is for a three strand tendon. This configuration (Type E5-3) was used for the 100%U PS and 2/3 PS sections. For the 2/3 PS section with only two strands per tendon, the E5-3 was used with the third strand opening unused. The 100%S PS section used the Type E5-4 configuration. The basic hardware for the E5-4 anchorage is shown in Figure 3.5. The anchorages were located inside a recessed pocket at both ends of the beams, as shown in Figure 3.4. Grouting was performed using grout tubes at both ends of the duct. Grout sleeves and

tubes were used for the 100%U PS and 100%S PS beams. The grout tube location is shown in Figure 3.4 for these section types. Grout tubes were placed through the third opening in the E5-3 anchor head for grouting the 2/3 PS beams. The duct profiles, grout tube locations and end pocket details are shown in Appendix C for each of the post-tensioned beam types.

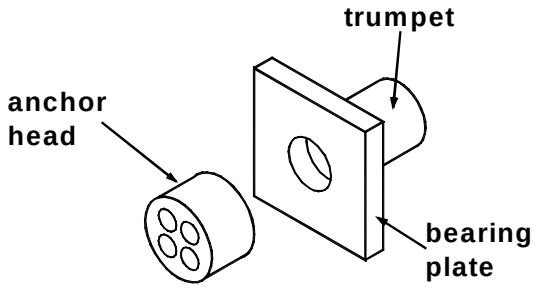

Figure 3.5 - VSL Type E5-4 Anchorage

3.2.3 Analysis of Section Behavior

Once the section details were defined, each section was thoroughly analyzed to determine its moment curvature behavior and applied moment - crack width behavior. Guidelines proposed by Armstrong et al[3.6] for crack width prediction in cracked prestressed members were used with the Gergely-Lutz[3.7] crack width expression to estimate the surface crack widths. The recommendations of Armstrong et al and the Gergely-Lutz expression are described in Section 2.8. The cracking moment for each section was computed based on the uncracked transformed section. The section was then analyzed as a cracked section at that moment to estimate the crack width immediately after cracking. Several additional points were calculated to define the applied moment - crack width relationship up to a maximum crack width of 0.46 mm (0.018 in.).

The sections were analyzed using the layer-by-layer strain compatibility section analysis technique.[3.8] A spreadsheet was developed by the author to automate the task of performing repeated analyses on the different section types. Moment-curvature and crack width analysis were performed neglecting long term material behavior. The basic assumptions for the analysis are listed below.

Concrete: f'_c = 35 MPa (5 ksi)

$f_r = 0.623\sqrt{f'_c}$ MPa $(7.5\sqrt{f'_c}$ psi)

ε_{cmax} = 0.0038

Hognestad parabolic stress-strain relationship[3.9]

no tension stiffening

Prestressing Steel:

bonded prestressing steel, low-relaxation seven-wire strand

stress-strain relationship modeled using a Ramberg-Osgood function[3.8]

Mild Steel: stress-strain relationship linear elastic to f_y, perfectly plastic to ε_{sh} = 0.010, strain hardening given by cubic polynomial[3.10]

The material stress-strain curves and expressions are shown in Figure 3.6, Figure 3.7 and Figure 3.8. The computed moment-curvature and moment-crack width curves are shown in Figure 3.9 and Figure 3.10.

$$f_c = f'_c\left[\left(\frac{2\varepsilon_c}{\varepsilon_o}\right)-\left(\frac{\varepsilon_c}{\varepsilon_o}\right)^2\right];\ \varepsilon_c \le \varepsilon_o$$

$$f_c = f'_c\left[1-0.15\left(\frac{\varepsilon_c-\varepsilon_o}{\varepsilon_{max}-\varepsilon_o}\right)\right];\ \varepsilon_o \le \varepsilon_c \le \varepsilon_{max}$$

$$\varepsilon_o = \frac{2f'_c}{E_c} \qquad \varepsilon_{max} = 0.0038$$

$$E_c = 12{,}411 + 3.17f'_c \quad \text{(MPa)}$$

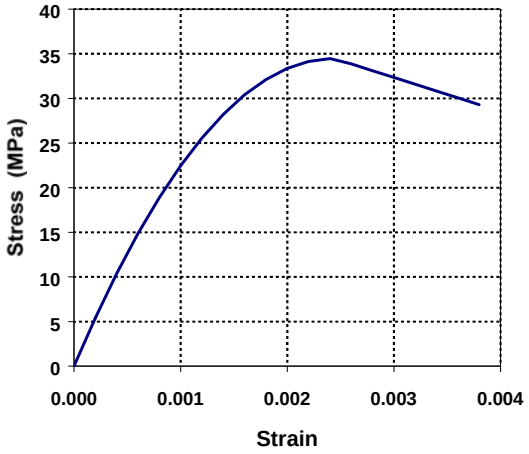

Figure 3.6 - Concrete Stress-Strain Curve

$$f_s = 200{,}000\varepsilon_s \;;\; \varepsilon_s \le \varepsilon_y$$
$$f_s = 400\ \text{MPa} \;;\; \varepsilon_y < \varepsilon_s \le 0.010$$
$$f_s = 297 + 13052\varepsilon_s - 143292(\varepsilon_s)^2 + 520200(\varepsilon_s)^3 \;;\; \varepsilon_s > 0.01$$

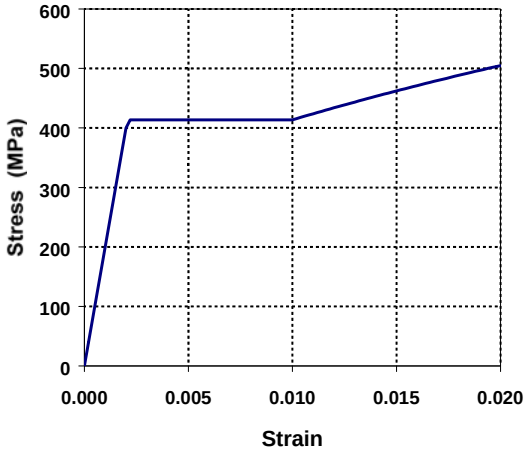

Figure 3.7 – Mild Steel Reinforcement Stress-Strain Curve

$$f_{ps} = 200{,}000\varepsilon_{ps}\left(0.025 + \frac{0.975}{\left[1 + (118\varepsilon_{ps})^{10}\right]^{0.10}}\right) \le 1860\ \text{MPa}$$

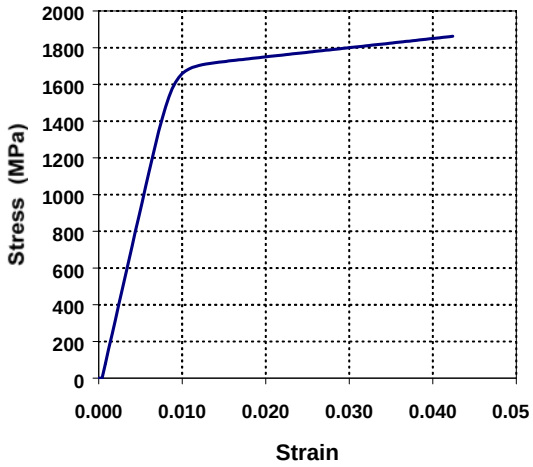

Figure 3.8 – Prestressing Strand Stress-Strain Curve

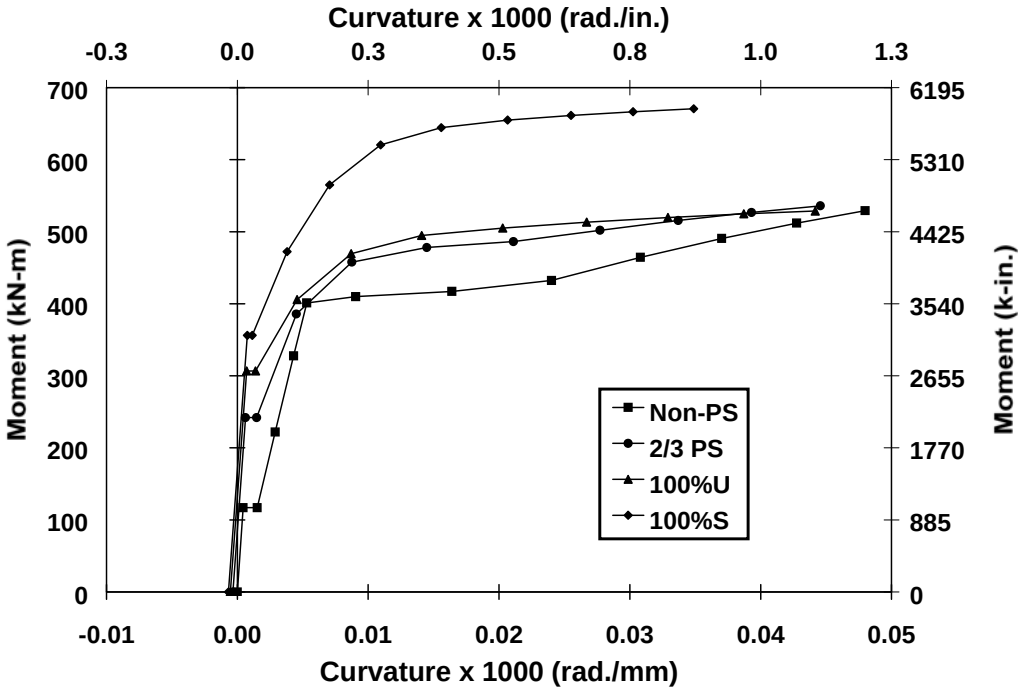

Figure 3.9 - Moment Curvature Behavior for All Sections

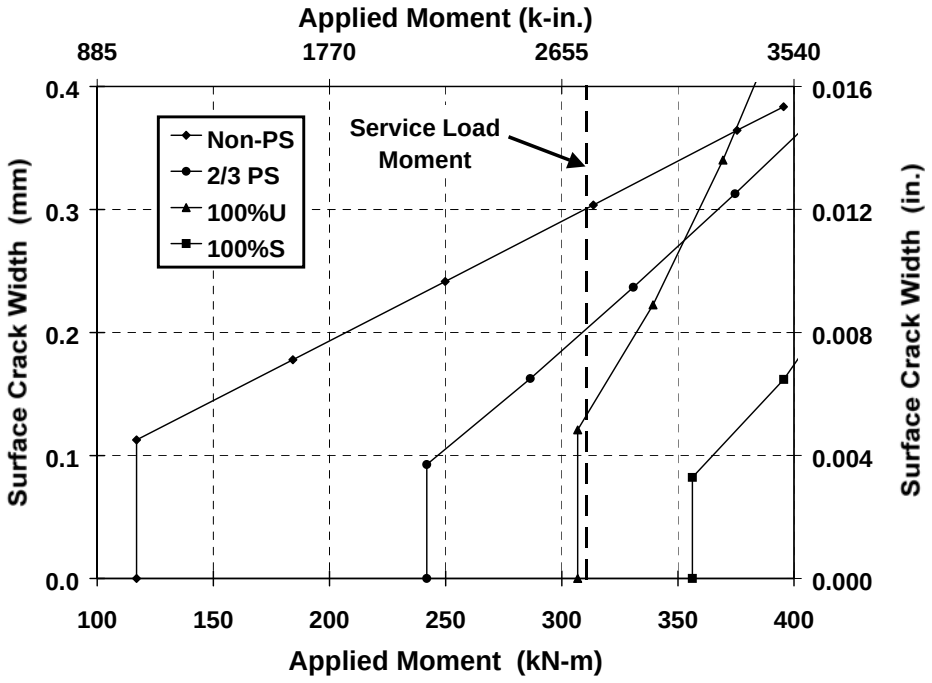

Figure 3.10 - Applied Moment - Estimated Crack Width Behavior for All Sections

Long term behavior of all sections was calculated according to the procedure proposed by Ghali and Favre.[3.11] This procedure uses basic equilibrium and strain compatibility without the use of empirical relationships. The procedure is general and can be applied to fully prestressed members (uncracked), cracked prestressed sections, sections with a combination of mild steel reinforcement and prestressed reinforcement and non-prestressed sections. This method was chosen to calculate long term prestress losses because the effect of non-prestressed reinforcement and/or the effect of cracking is directly included in the calculations of prestress losses. The procedure is analogous to the displacement method of structural analysis and has four main steps:[3.11]

1. Compute the initial stresses and strain profile for the section under the action of initial prestress forces and sustained loading.
2. Determine the hypothetical change in strain distribution due to creep and shrinkage of the concrete if they were free to occur during the time interval being considered. Determine the amount of relaxation of the prestressed reinforcement during the time interval.
3. Determine the total axial force (ΣN) and moment (ΣM) that would be required to restrain the deformations due to creep, shrinkage and relaxation (Step 2) using the age-adjusted modulus of elasticity of the concrete.
4. Eliminate the artificial restraint (Step 3) by applying $-\Sigma N$ and $-\Sigma M$ on the section using the age-adjusted section properties. The strain distribution at the end of the time increment is the sum of the strains computed in Steps 1 and 4. The corresponding stresses are determined by summing the stresses calculated in Steps 1, 3 and 4.

The procedure presented by Ghali and Favre is simple in concept but can be complicated to implement, particularly for cracked sections. The procedure was adapted by the author to use the layer-by-layer compatibility section analysis technique to determine stresses and resultant forces at the various steps. The adapted approach was programmed into a spreadsheet to allow rapid analysis of long term behavior for sections with any cross-section and combination of prestressed and mild steel reinforcement. The

recommendations of ACI Committee 209[3.12] were used to predict creep and shrinkage. An aging coefficient[3.11] is used in the analysis when computing ΣN and ΣM to reflect that these forces would be introduced gradually as the time dependent deformation occurs. Relaxation of the prestressing steel was predicted using the reduced relaxation approach[3.11] to account for the gradual reduction in prestress due to concrete creep and shrinkage.

The results of the long term analysis for each section are shown in Figure 3.11 through Figure 3.14. These figures show the initial strain profile and the strain profile after a duration of four years. The locations of the prestressing steel and mild steel reinforcement are indicated on the figures. A long term prestress loss (creep, shrinkage, relaxation) of 4.7% was calculated for the 100%S PS section. Prestress force increases of 5% and 4.3% were calculated for the 100%U PS and 2/3 PS sections, respectively, after four years of sustained loading. Prestress force increases rather than losses are obtained since these sections are cracked prior to and during sustained loading. This behavior is similar to that of reinforced concrete members under sustained loading (see Figure 3.14).

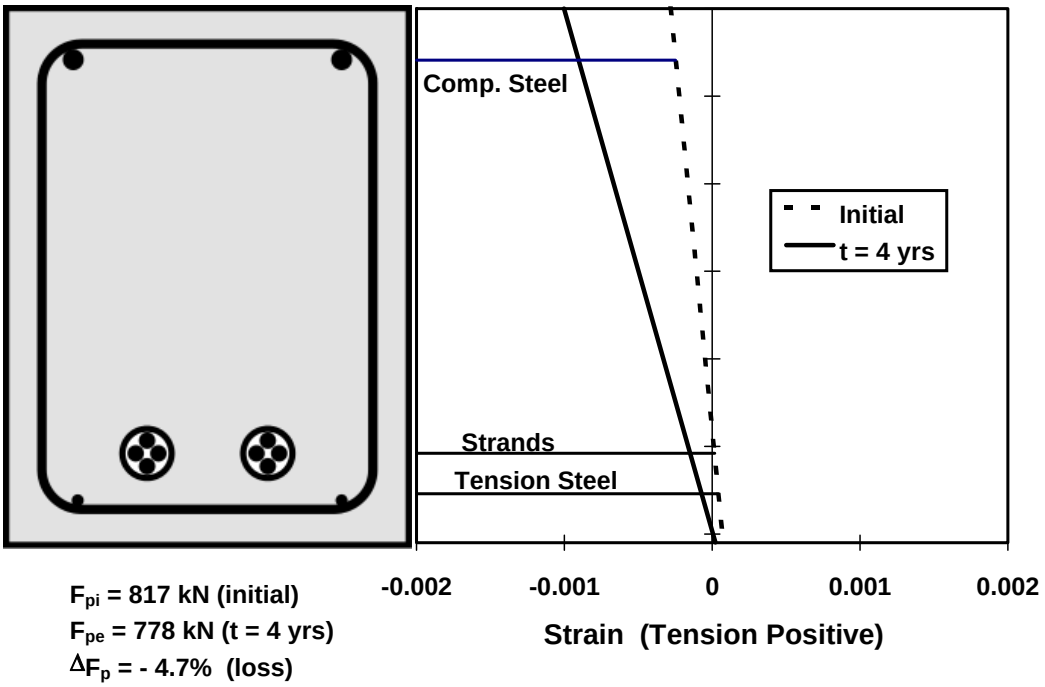

Figure 3.11 - Initial and Long Term Strain Profiles for 100%S PS Section

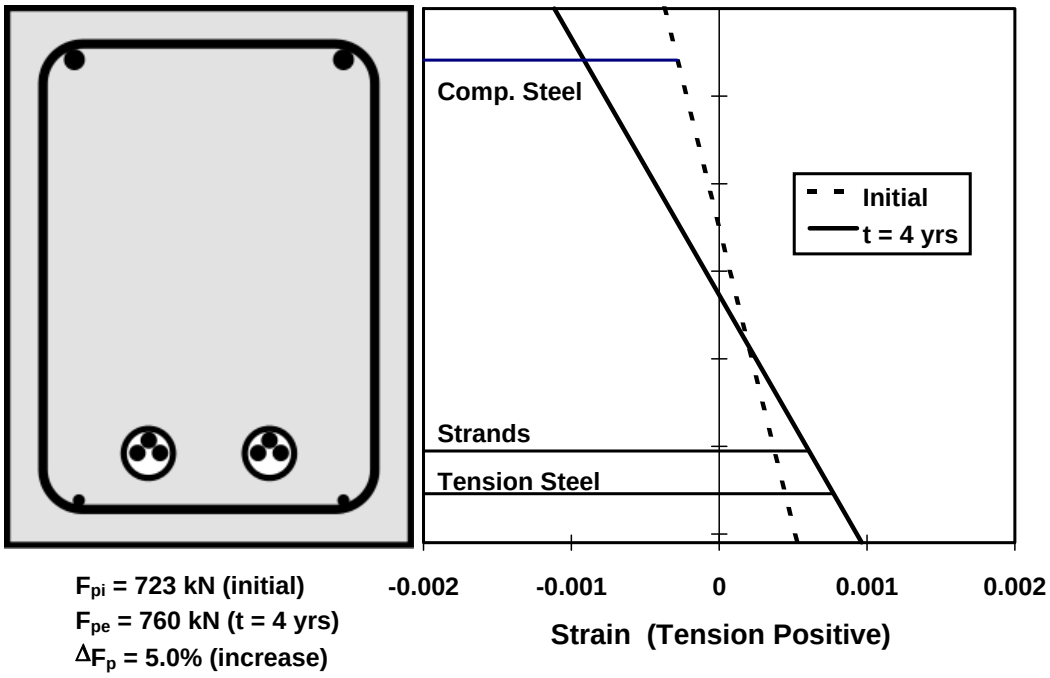

Figure 3.12 - Initial and Long Term Strain Profiles for 100%U PS Section

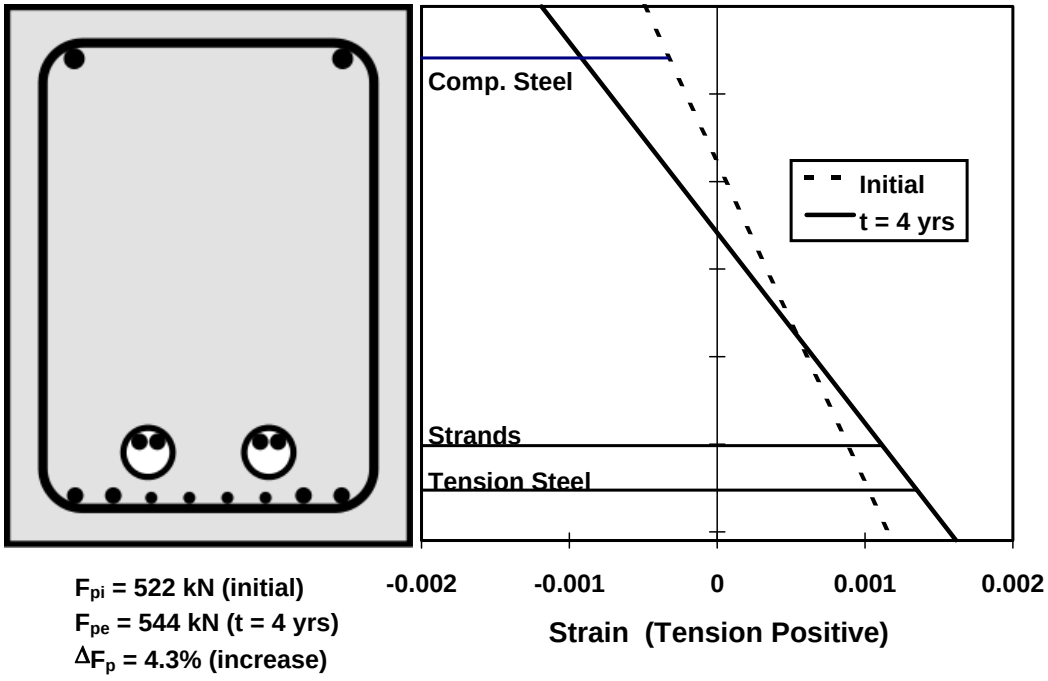

Figure 3.13 Initial and Long Term Strain Profiles for 2/3 PS Section

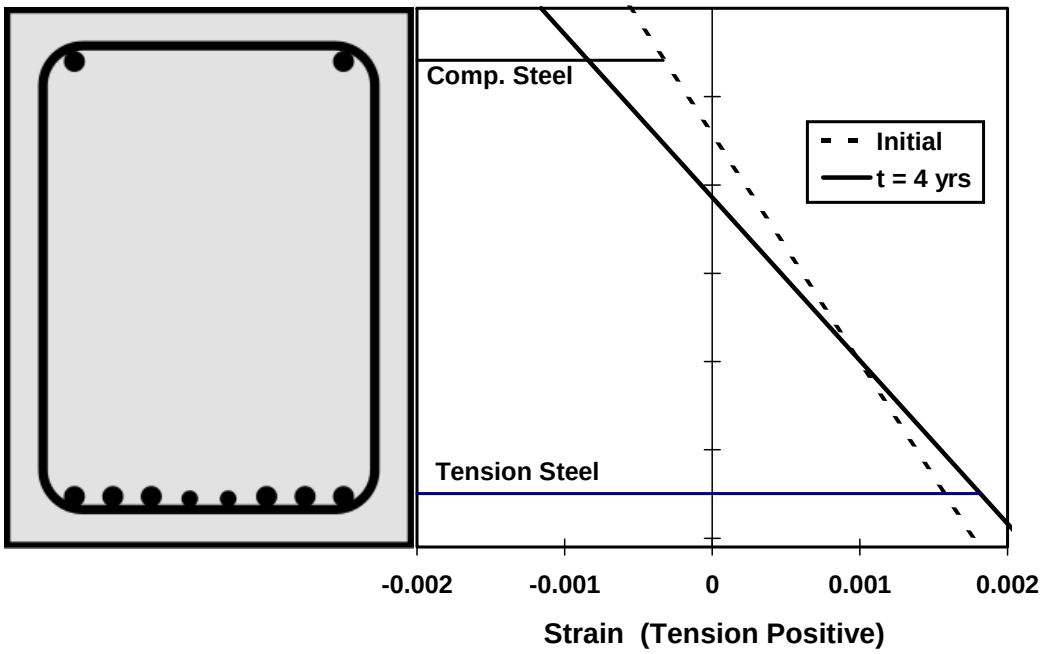

Figure 3.14 - Initial and Long Term Strain Profiles for Non-PS Section

3.3 Variables

A very broad scope of variables was selected for evaluation in the beam testing program. The variables fall into four main categories: level of prestress and crack width, concrete type, prestressing strand coatings and post-tensioning hardware protection. In addition to these variables, different post-tensioning duct splices are evaluated within the other variable categories.

The testing program was implemented in two phases. The first phase includes all of the specimens in the first category of variables (level of prestress and crack width), one specimen with high performance grout, and the evaluation of duct splices. The second phase includes the remaining three categories of variables.

3.3.1 Control Variables

Standard variables based on typical current practice were defined to represent control cases. These include concrete mix design, concrete clear cover, cement grout, duct and anchorage protection. Details of each are given below.

Concrete: based on TxDOT Specification[3.13] Item 421
TxDOT Class C concrete for bridge substructures
maximum w/c ratio = 0.533 (actual w/c will be closer to 0.45 based on slump requirements)
Type I cement
slump = 100 mm (4 in.)
maximum coarse aggregate size = 19 mm (3/4 in.)
retarder, Rheocrete 300-R
entrained air admixture
50 mm (2 in.) clear cover to main steel

Cement Grout: based on TxDOT Specification[3.13] Item 426.3.4a
w/c ratio = 0.44
Type I cement
expanding admixture, Intraplast-N

PT Duct: rigid galvanized steel duct

Anchor. Protection: based on TxDOT guidelines[3.14]

Type V State epoxy bonding compound
non-shrink grout patch (Euclid NS grout)

3.3.2 Phase I Variables

3.3.2.1 Level of Prestressing, Loading and Cracking

The inter-related effects of cracking and amount of prestressing on corrosion are given considerable emphasis in this experimental program. The effect of cracking is primarily investigated using standard variables and the three sections that would be expected to crack under service loads (Non-PS, 2/3 PS and 100% U). The range of crack widths investigated in this program is based on a survey of relevant literature regarding critical crack widths for corrosion and recommended allowable crack widths. Consideration was also given to the applied moment - crack width behavior computed for the sections (Figure 3.10). A broad range of crack widths was selected to provide a suitable evaluation of the effect of cracking on corrosion. The selected crack widths are 0.05 mm (0.002 in.), 0.1 mm (0.004 in.), 0.2 mm (0.008 in.), 0.3 mm (0.012 in.) and uncracked. To obtain this crack width range, the four cases shown in Table 3.2 were developed. This information is also presented in Figure 3.15. A total of eleven specimens are required to address the four loading cases. The four specimens under constant service load (loading case 1) are duplicated, giving a total of fifteen specimens in this category of variables.

Table 3.2 – Planned Crack Widths, Prestress Amounts and Loading

Loading Case	Crack Widths	Applicable Sections	Loading
1.) Constant Service Load	uncracked	100%S PS	service load
	0.1 mm	100%U PS	service load
	0.2 mm	2/3 PS	service load
	0.3 mm	Non-PS	service load
2.) Very Small Crack	0.05 mm	2/3 PS & 100%U PS	as needed and hold
3.) Unloaded	uncracked	Non-PS & 100%U PS	none

4.) Overload & Return to Service	as measured	Non-PS, 2/3 PS & 100%U PS	up to 1.33 x service load, then return to service load

Due to the large number of variables and uncertain nature of cracking, it was expected that some deviation from the planned crack width and loading combinations would occur. This is discussed in Section 3.8.

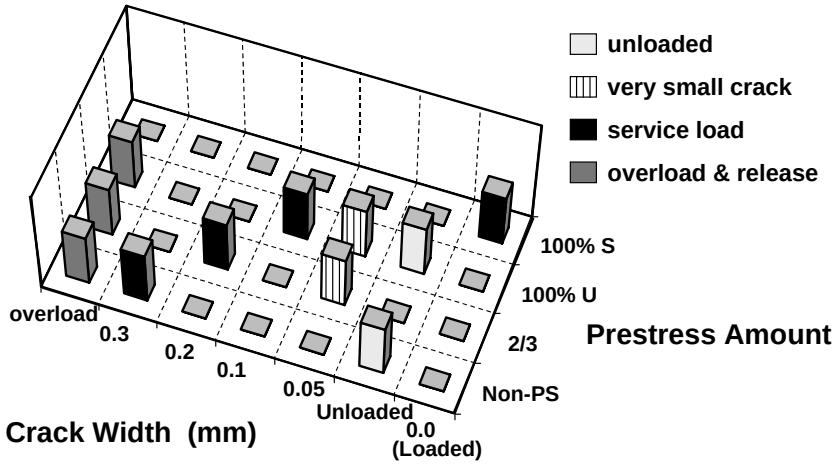

Figure 3.15 - Variables: Level of Prestress and Crack Widths

3.3.2.2 High Performance Grout: Fly Ash Grout

The use of high performance grouts for corrosion protection of the prestressing strands is investigated in this experimental program. The grout used in Phase I of the testing program was selected based on fresh property tests and accelerated corrosion tests performed by Schokker.[3.1] The fly ash grout selected contains 35% fly ash by weight, and has a low water-cementitious material ratio of 0.35. This grout had the best corrosion protection of all grouts investigated, and possessed excellent fresh properties with good resistance to bleed.

3.3.2.3 Duct Splices for Galvanized Steel Duct

In most practical applications, the post-tensioning ducts must be spliced at some location. It was decided to compare industry standard splices to heat shrink splices and unspliced duct. The effect of damaged splices was also examined. The two splices are shown in Figure 3.16. The industry standard splice consists of a 300 mm (1 ft) length of

oversized duct. Concrete is prevented from entering the splice by wrapping the ends with duct tape. The heat shrink splice consists of an 200 mm (8 in.) length of heat shrink tubing. The original diameter of the heat shrink tubing is 100 mm (4 in.). No mechanical connection was made between the two ducts being connected. For the damaged condition, poor or incomplete duct taping was used on the industry standard splice. For the damaged heat shrink splice, a 25 mm (1 in.) cut was made in the heat shrink tubing at the location where the ducts meet.

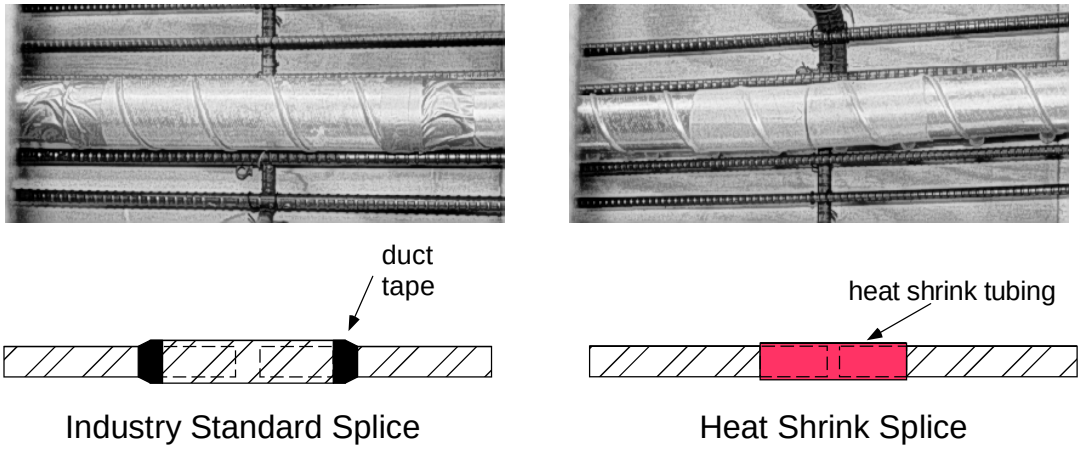

Figure 3.16 - Duct Splices

Three different comparisons were made for the duct splices:

1) Industry standard versus heat shrink
2) Industry standard versus unspliced
3) Effect of damage for industry standard and heat shrink splices

The configurations of the three splice comparisons are shown in Figure 3.17. Details of the splices and their locations for the various configurations are shown in Appendix C.

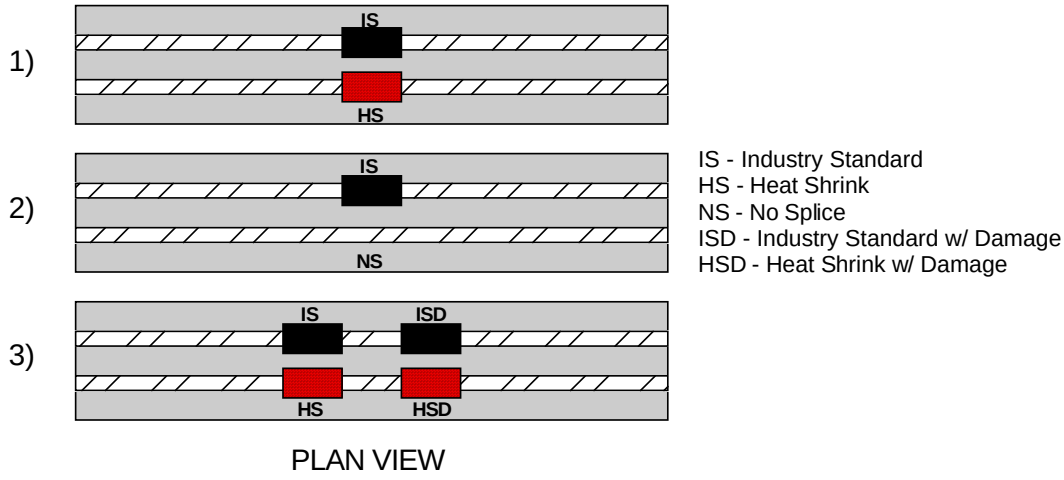

Figure 3.17 - Duct Splice Configurations

3.3.3 Phase II Variables

3.3.3.1 Concrete Type

Concrete plays an important role in corrosion protection of steel reinforcement. A tremendous amount of research has investigated the use of high performance concrete to improve corrosion protection. One of the objectives of this research program is to evaluate the effectiveness of high performance concrete as a function of cracking. The effect of cracking is important since the majority of past research on the effects of cracking on corrosion used poor or average concrete by modern standards. It is possible that cracking may have a more significant effect on the corrosion protection provided by high quality, low permeability concrete. The concrete selected for investigation in this research was based on practical considerations and a review of current literature. It was important to consider current and future trends in concrete technology in Texas to ensure that possible recommendations would be adopted by TxDOT and could be supplied by ready-mix concrete producers within the state. For this reason, it was decided to use fly ash based high performance concrete rather than silica fume or blast furnace slag. Although concrete using these pozzolanic admixtures have been shown to improve corrosion protection and durability, they are very uncommon in Texas, where fly ash is widely used and readily

available. Two different concrete mixes were selected for comparison to the standard substructure concrete. Each is described below.

TxDOT Class C Concrete with 25% Fly Ash

Partial cement replacement with fly ash has been shown to improve most aspects of concrete durability, as discussed in Section 2.4 and 2.5. Replacement amounts of 20% to 35% (by volume) are permissible under TxDOT Standard Specifications.[3.13] Cement replacement with fly ash is common practice in Texas bridges, normally at the contractor's request due to the low cost of fly ash in comparison to cement.

Traditionally, ASTM[3.15] Class C fly ash has been readily available in Texas as a by-product of burning lignite and/or sub-bituminous coals for electricity production within the state. However, due to recent increased construction and demand for fly ash, some ready-mix concrete producers have begun to use ASTM Class F fly ash from North Eastern states where bituminous coals are predominant. From a durability standpoint, ASTM Class F fly ash normally provides better durability performance through slightly lower permeability and better resistance to sulfate attack.

Due to the increasing use of fly ash in concrete, it was decided to investigate its effect on corrosion protection when fly ash is simply used as partial cement replacement and no other changes are made to the mix design. It was decided to use the standard TxDOT concrete for bridge substructures, and replace 25% of the cement (by weight) with fly ash. No other significant changes were made to the concrete mix, and the ratio of water to total cementitious materials was 0.44. At the time of construction, only Class F fly ash was available from local ready-mix suppliers, so Class F fly ash was used.

High Performance Concrete with Fly Ash

The second concrete type to be compared with the standard substructure concrete also contained 25% cement replacement with fly ash. However, the concrete mix design was modified to significantly lower the concrete permeability and increase concrete strength. This was primarily achieved by lowering the ratio of water to cementitious materials to 0.29. The low water content required large dosages of superplasticizer at the concrete plant and again immediately prior to placement to provide sufficient workability. ASTM Class F fly ash was also used in this concrete.

Effect of Cracking

In order to evaluate the effect of cracking , the two concrete types were each used with the Non-PS, 2/3 PS and 100%U PS sections at a constant service load level to produce a range of crack widths. This information is shown in Figure 3.18. A total of six specimens were required for this category of variables (3 sections x 2 variables).

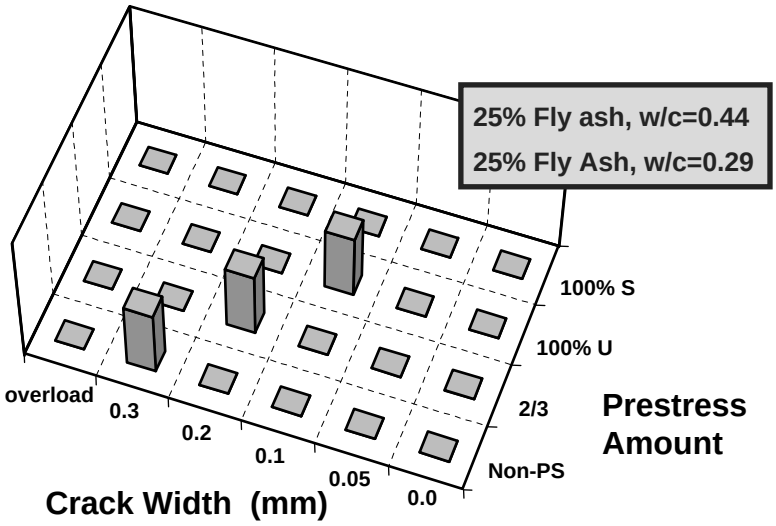

Figure 3.18 - Variables: Durable Concrete

3.3.3.2 Prestressing Strand Coatings

Two strand coatings were selected for investigation: epoxy coated and galvanized. The effect of coating damage is investigated for the epoxy coated strands. Damage was introduced on the strands of one tendon in the specimen, while the second tendon contains undamaged tendons. The different strand coatings are evaluated using the 2/3 PS section under constant service loading, as this section has the largest crack widths of the three post-tensioned sections at service loads. Two specimens were required for this category of variables (2 variables x 1 section).

Epoxy Coated Strands

The epoxy coated strand known as Flow-Gard-Bond, manufactured by Florida Wire and Cable, was investigated in this series of specimens. In this type of epoxy coating, the epoxy is applied while the strand is in its normal stranded condition. As a result, the

epoxy forms a perimeter barrier around the strand section, but does not fill the interstices of the strand.

Galvanized Strands

Florida Wire and Cable manufactures galvanized strand suitable for use in prestressed concrete. At present, structural applications of galvanized strand have been limited in North America. However, Germany and Japan have successfully used galvanized prestressing strand, and thus it was decided to investigate its performance in comparison to epoxy coated strands.

3.3.3.3 Post-tensioning System Protection

The post-tensioning system includes the prestressing strands, ducts and anchorages. Variables investigated in this category are related to grouting and encapsulated post-tensioning systems. The 2/3 PS section under constant service loads was also used to evaluate the variables in this category. Three specimens were used for this category of variables, one with high performance grout, one with poor grouting procedures and one with a proprietary encapsulated post-tensioning system.

High Performance Grout – Anti-Bleed Grout

The high performance grout used in Phase II of the testing program was also selected on the basis of fresh property tests and accelerated corrosion tests performed by Schokker.[3.1] The anti-bleed grout contains an anti-bleed chemical admixture with superplasticizer, and has a low water-cementitious material ratio of 0.33. This grout had very high resistance to bleed and good corrosion protection properties compared to most grouts investigated.

Poor Grouting Procedures

The effectiveness of grout for corrosion protection is dependent on the properties of the grout and on the placement of the grout. Incomplete or poor grouting will reduce the effectiveness of the grout as corrosion protection. All post-tensioned beams in this testing program were grouted according to the recommendations of the Post-Tensioning Institute.[3.16] In order to obtain a comparison between execution of the recommended procedures and poor grouting procedures, it was decided to intentionally grout one specimen using poor practices. The grouting procedure included delays of up to ten

minutes during grouting, allowing air to enter the pump and stopping the grouting process at the first sign of grout at the exit vent.

Encapsulated Systems

Encapsulated systems for post-tensioning were described in Section 2.4. VSL Corporation manufactures an encapsulated/electrically isolated multistrand post-tensioning system for severe environments. The smallest available configuration of the VSL Composite System is for a 5-12 tendon (twelve 0.5 in. (12.7 mm) strands). However, a two strand slab system known as the VSLAB+ System possesses many of the same properties as the Composite System, and can be accommodated into the test specimens. The VSLAB+ system uses an impermeable plastic duct system with special connections to the anchorage hardware to prevent moisture entry. A sealed end cap is provided to protect the strand ends. Although the strands are encapsulated, the anchorage is uncoated and therefore the system is not electrically isolated. The VSLAB+ system allows the effect of impermeable plastic ducts and protection of the anchorage to be investigated.

3.4 Experimental Program

A total of twenty-seven specimen types were developed to address the selected variables. The complete testing program is summarized in Table 3.3. A simple numbering scheme to identify each specimen is used in the table. The testing program was implemented in two phases, with sixteen specimens in Phase I and eleven specimens in Phase II. The first phase was constructed and implemented by the author. The second phase was constructed and implemented by Schokker.[3.1] The remainder of this chapter is devoted to the Phase I beam specimens only. All further information on the Phase II specimens is provided in Reference 3.1. Schematics of the beams in each phase are shown in Figure 3.19 and Figure 3.20 . The duct splice locations and types for each beam are shown in the figures.

Table 3.3 – Beam Experimental Program

	Main Variable	Section Type Non-PS	2/3 PS	100%U	100%S
Phase I	Unloaded	**1.1**		**3.1**	
	Very Small Crack		**2.1**	**3.2**	
	Constant Service Load	**1.2**	**2.2**	**3.3**	**4.1**
	Constant Service Load (duplicate)	**1.3**	**2.3**	**3.4**	**4.2**
	Overload and Return to Service	**1.4**	**2.4**	**3.5**	
	High Performance Fly Ash Grout		**2.11**		
Phase II	Standard Concrete with 25% Fly Ash	**1.5**	**2.5**	**3.6**	
	High Performance Fly Ash Concrete	**1.6**	**2.6**	**3.7**	
	Epoxy Coated Strands		**2.7**		
	Galvanized Strands		**2.8**		
	Poor Grouting Procedures		**2.9**		
	High Performance Anti-Bleed Grout		**2.10**		
	Encapsulated System w/ Plastic Duct		**2.12**		

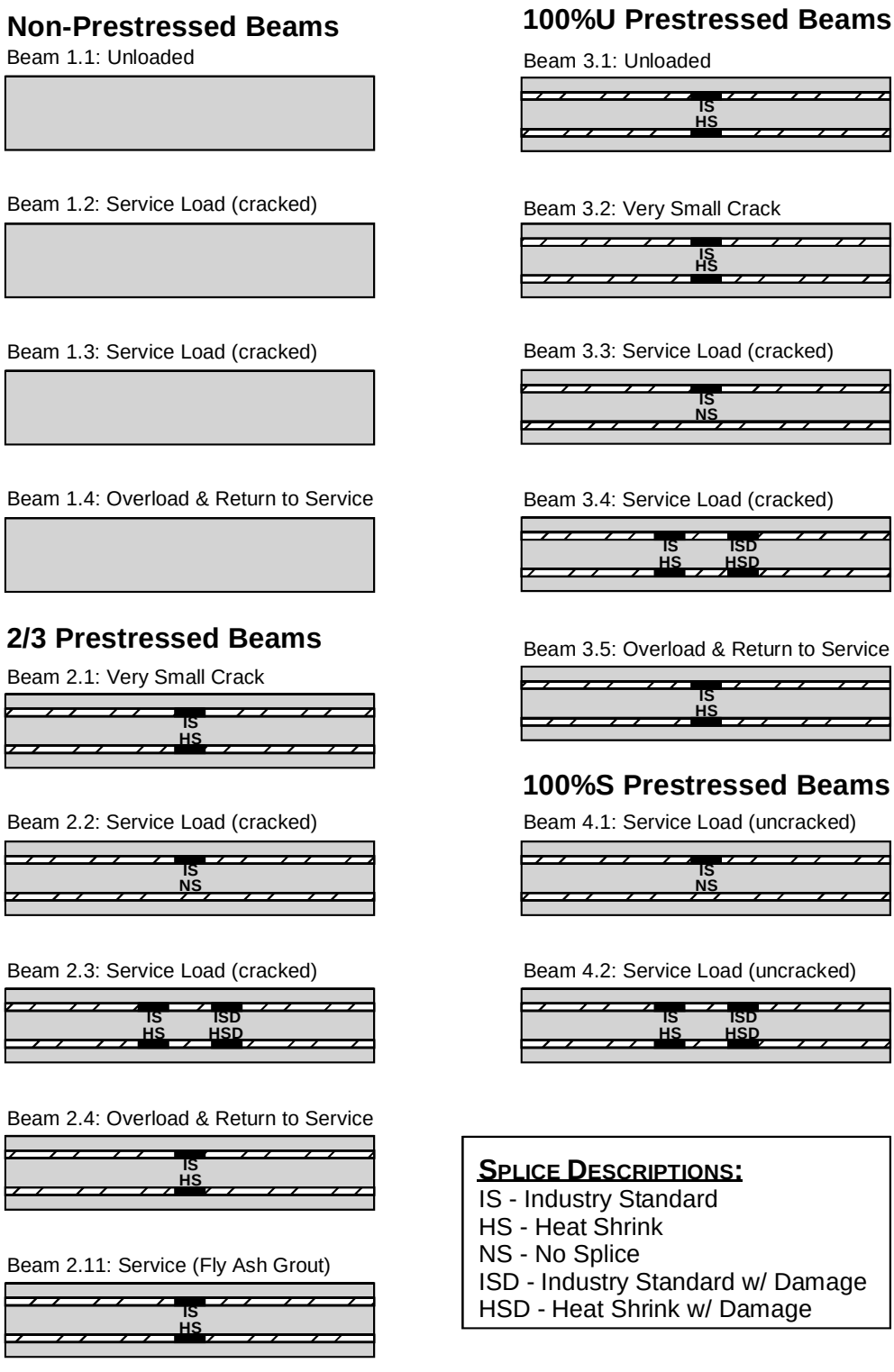

Figure 3.19 - Phase I Beams

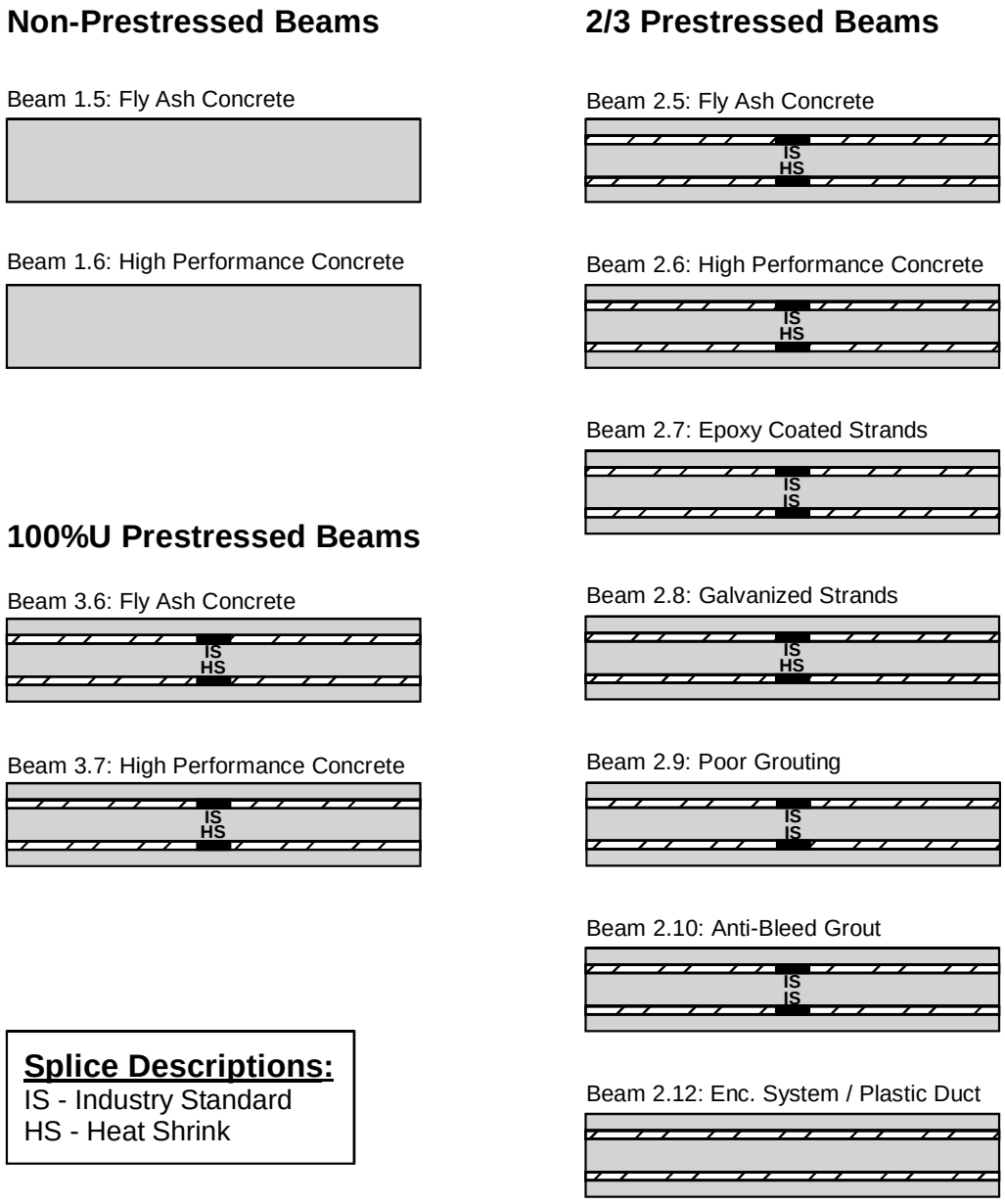

Figure 3.20 - Phase II Beams[3.1]

3.5 Experimental Setup

The experimental setup required the ability to subject the test specimens to sustained structural loading and corrosive environment. The sustained loading involved forces in excess of 225 kN (50 kips) applied on the beams. The exposure conditions were

selected as wet-dry cycling with a 3.5% salt (NaCl) solution. The salt concentration is based on the recommendations of ASTM G109.[3.17] The salt solution is applied on the cracked region of the elements for a period of two weeks, followed by a dry period of two weeks to complete one wet-dry cycle. Wet-dry cycling is expected to be continued for several years at this site. The large specimen size, number of specimens and long testing duration required a large outdoor area for exposure testing. The selection of an experimental setup was based on consideration of the following criteria:

Space: Total area required for placement of test specimens.

Volume of Concrete: Total volume of concrete for test specimens (and reaction beams if required).

Number of Specimens: Total number of specimens required to consider desired variables. Consideration given to the use of multiple variables in some specimens (strand and anchorage protection), where possible, depending on specimen orientation.

Construction Time: Time required for construction of test specimens (and reaction beams if required).

Salt Water Application: Ease of application, collection and removal of NaCl solution. Consideration given to sophistication of application/collection system (cost, construction time and reliability).

Exposure Surface: Coverage of cracked region with NaCl solution and protection from environment (wind, rain, limit evaporation).

Support System: Complexity (cost, construction time and reliability) of support system for test specimens.

Crack Measurement: Ease of taking measurements on cracked surfaces.

Control of Cracking During Loading: Ability to attain desired crack widths in a given specimen during application of loading.

The selection of an experimental setup and test procedure was based primarily on the concern for the application, collection and removal of the salt water solution. Due to the frequency of cycling and the considerable duration of the testing, a simple and reliable

system and procedure was desired. In addition, environmental regulations require all of the NaCl solution to be collected and disposed of in a sanitary sewer. Thus, the method for application and removal of the NaCl solution must minimize potential for leakage and spillage to the ground. For these reasons, a ponding system was selected over a system where the solution was pumped over the cracked region and collected in drip pans below the specimen. To accommodate this, it was decided to test the specimens in a typical negative moment tendon orientation, as shown in Figure 3.21. Other benefits of testing in this orientation include better control during loading, ease of crack measurements and the opportunity to evaluate multiple tendons in one specimen. In the latter case, the two tendons/ducts allows variables such as duct splices, strand coatings and coating damage to be compared to the control cases in a single specimen. This is not possible when the specimens are tested on their sides.

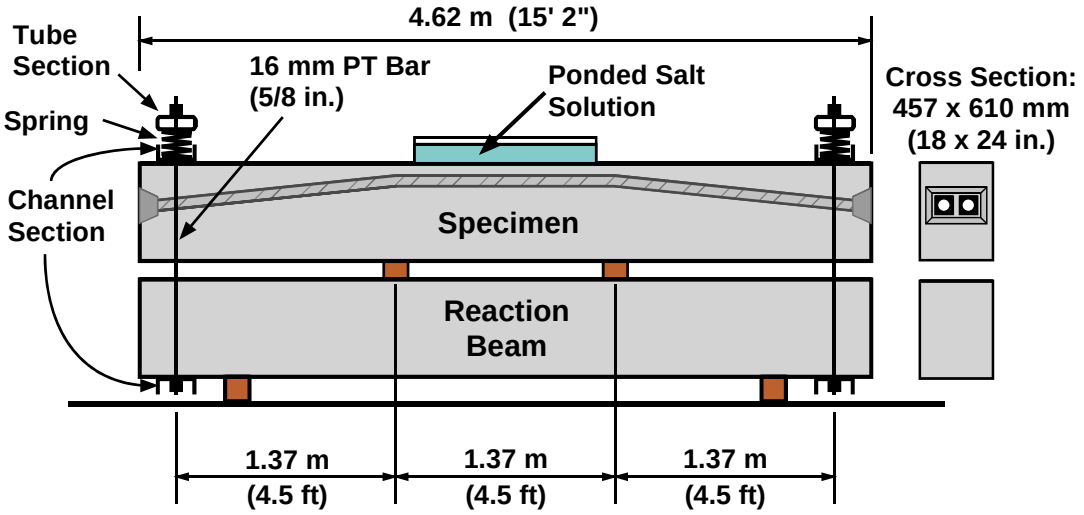

Figure 3.21 - Test Setup

The specimen is oriented tension side up and is paired with a reinforced concrete reaction beam. Salt water is ponded directly on the tension side over the middle third of the member using a plastic dike adhered to the concrete surface with marine sealant/adhesive. A wet-dry shop vacuum is used to remove the salt solution at the end

of the wet period. The ponded region is covered during the wet cycle to prevent contamination of the NaCl solution and to limit evaporation.

Loading is applied through a system of post-tensioning bars and railroad springs at the ends of the member and reactions at the third points along the member length. The railroad springs were used to minimize force losses due to time dependent deflections of the members. The spring stiffness was selected to limit force loss to 5% during the first year of sustained loading, with calculations based on the Non-PS beam section. It was decided not to use traditional methods to monitor the force in the loading system due to the cost of using load cells and due to the questionable long term reliability of strain gauges in an exterior exposure. Periodic re-loading of the beams will be necessary to ensure load levels remain within expected limits.

The reaction beam was designed as reinforced concrete. Other options investigated included prestressed concrete beams and steel beams. The decision to use non-prestressed, reinforced concrete beams was based on cost and construction time. The dimensions of the reaction beam were identical to the beam specimens. Reinforcement for the reaction beams was proportioned to provide excess strength in comparison to the specimens and to limit crack widths at service load levels. The nominal strength of the reaction beam was 700 kN-m (6180 k-in.). Maximum surface crack widths at the specimen service load level were computed as 0.2 mm (0.008 in.). Detailed drawings of the reaction beam are included in Appendix C.

The paved area at the north end of the Ferguson Structural Engineering Laboratory was selected for storage and testing of the beams, as shown in Figure 3.22. Figure 3.23 shows a top view of the beams with plywood covers on the ponded region of the beams.

Figure 3.22 - Beam Test Setup at North End of Ferguson Laboratory

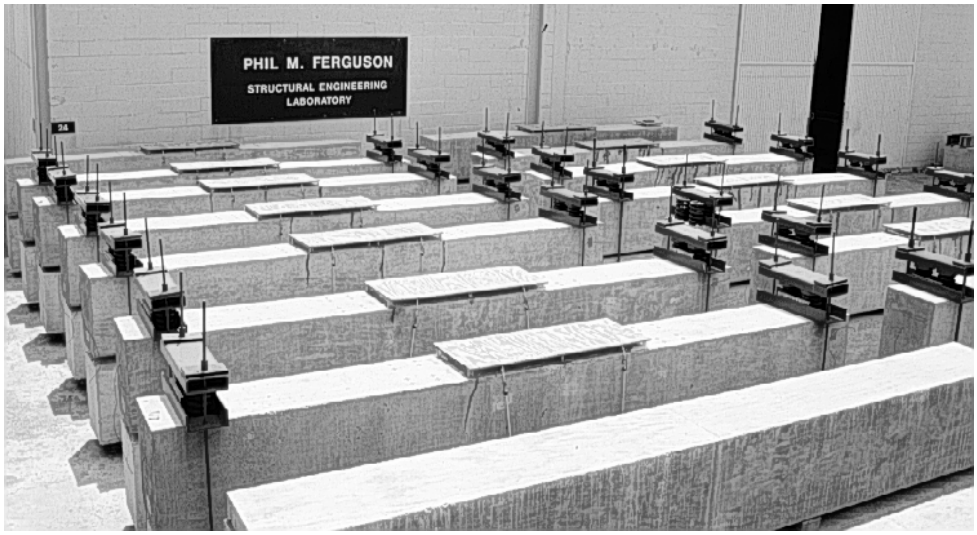

Figure 3.23 - Top View of Beams Showing Ponded Area (Covered)

3.6 Materials

Details of the materials used in Phase I of the testing program are summarized in Table 3.4. Where applicable, materials and proportions were selected to match Texas Department of Transportation Standard Specifications.[3.13,3.14] Concrete was supplied by a local ready-mix concrete producer. Grouts for post-tensioning were batched in using a medium sized mortar mixer (0.085 m^3 (3 ft^3)). Non-shrink grout for capping post-

tensioning anchorages was mixed in 18.9 liter (5 gal.) buckets using a paddle mixer mounted to a large hand-held drill. Mild steel reinforcement was supplied and fabricated according to design drawings by a local steel fabricator. Post-tensioning hardware was fabricated by the supplier. Complete details of specimen construction are provided Section 3.7.

Beam specimen concrete and reaction beam concrete was sampled for strength testing using typical practices. Average strengths for the two concrete types are listed in Table 3.4. Concrete cylinder strength data for the Phase I Beam Specimens is listed in Table 3.5. All cylinder strengths exceeded the minimum requirements for TxDOT Class C Concrete for Bridge Substructures.[3.13]

Table 3.4 - Construction Material Details: Phase I Beam Specimens

Item	Description			
Texas DOT Class C Concrete for Bridge Substructures	• w/c = 0.53 maximum allowable • w/c = 0.45 actual based on required slump • f'c = 25 MPa (3600 psi) minimum allowable • batch proportions: (per 0.764 m^3 (1 yd^3)) Coarse Aggregate (19 mm) 851 kg 1877 lbs Fine Aggregate 538 kg 1186 lbs Type I/II Cement 256 kg 564 lbs Water 115 kg 254 lbs Set retarder 710 ml 24 oz Entrained Air Admixture 118 ml 4 oz • cylinder strengths: 7-day 30.0 MPa 4345 psi (average) 28-day 36.7 MPa 5320 psi 56-day 37.9 MPa 5490 psi			
Reaction Beam Concrete	• w/c = 0.40 • f'c = 42 MPa (6000 psi) design strength • batch proportions: (per 0.764 m^3 (1 yd^3)) Coarse Aggregate (19 mm) 848 kg 1869 lbs Fine Aggregate 615 kg 1355 lbs Type I/II Cement 234 kg 517 lbs Water 95 kg 210 lbs Set retarder 603 ml 20.4 oz • cylinder strengths: 3-day 28.7 MPa 4160 psi (average) 28-day 36.7 MPa 5320 psi			
Texas DOT Grout for Post-Tensioning	• w/c = 0.44 • batch proportions: (per 0.028 m^3 (1 ft^3)) Type I Cement 37.4 kg 82.4 lbs Water 16.4 kg 36.2 lbs Expanding Admixture (Intraplast-N) 0.37 kg 0.82 lbs • cube strengths: 7-day 22.2 MPa 3215 psi (average) 28-day 28.8 MPa 4170 psi			
High Performance Fly Ash Grout for Post-Tensioning	• w/c = 0.35 • batch proportions: (per 0.028 m^3 (1 ft^3)) Type I Cement 28.9 kg 63.8 lbs Class C Fly Ash 12.4 kg 27.4 lbs Water 14.5 kg 31.9 lbs Superplasticizer 165 ml 5.6 oz • cube strengths: 7-day 38.4 MPa 5560 psi (average) 28-day 43.5 MPa 6310 psi			
Prestressing Strand	• 12.7 mm (0.5 in.) diameter seven wire strand • Grade 270 (1860 MPa, 270 ksi), low relaxation • Supplier: Shinko Wire, Inc.			
Mild Steel Reinforcement	• ASTM A615, Grade 60 (400 MPa, 60 ksi)			

Table 3.4 (Continued) – Construction Material Details: Phase I Beam Specimens

Item	Description
Steel Duct	• Corrugated, semi-rigid, galvanized steel duct • 54 mm (2-1/8 in.) outside diameter • Supplier: VSL Corporation, Inc.
PT Anchorage Hardware	• VSL Type E anchorage system • Supplier: VSL Corporation
Epoxy Bonding Agent	• Epoxy Adhesive Type V – General Epoxy Adhesive • Supplier: Industrial Coating Specialties Corp.
Non-Shrink Grout for Anchorage Protection	• Pre-bagged non-shrink grout mix • Trade Name: Euclid NS-Grout

Table 3.5 – Concrete Cylinder Strengths: Phase I Beam Specimens

Specimen Numbers	Average Cylinder Strength		
	7 Day	28 Day	56 Day
1.1, 1.2, 1.3	31.6 MPa (4590 psi)	35.9 MPa (5200 psi)	37.0 MPa (5360 psi)
1.4, 2.1, 2.2	28.3 MPa (4110 psi)	33.2 MPa (4810 psi)	36.1 MPa (5230 psi)
2.3, 2.4, 2.11	34.3 MPa (4970 psi)	41.4 MPa (6000 psi)	43.3 MPa (6280 psi)
3.1, 3.2, 3.3	n/a	37.0 MPa (5360 psi)	37.6 MPa (5450 psi)
3.4, 3.5	31.1 MPa (4510 psi)	39.7 MPa (5760 psi)	39.9 MPa (5780 psi)
4.1, 4.2	24.5 MPa (3550 psi)	33.0 MPa (4790 psi)	33.4 MPa (4840 psi)
Averages	30.0 MPa (4345 psi)	36.7 MPa (5320 psi)	37.9 MPa (5490 psi)

Grouts for post-tensioning were sampled according to PTI Specifications.[3.16] A minimum of three 50 mm (2 in.) restrained cubes were made from each batch of grout. Grout cubes were tested for compressive strength after seven days and twenty-eight days of curing. Grout cube strengths for the Phase I post-tensioned specimens are listed in Table 3.6. The PTI Specifications list minimum grout cube compressive strengths of 21 MPa (3000 psi) at seven days and 35 MPa (5000 psi) at twenty-eight days. On average, the TxDOT grout met the seven day strength requirement, but did not reach 35 MPa at twenty-eight days. The TxDOT Specifications[3.13] do not contain any minimum compressive strength provisions for grouts. The high performance grout with low water

content and 35% fly ash exceeded both the seven day and twenty-eight day strength by a considerable margin.

Table 3.6 - Post-Tensioning Grout Cube Strengths: Phase I Beam Specimens

Specimen Numbers	Grout Type	Average Cube Strength	
		7 Day	28 Day
2.1, 2.2, 2.3, 2.4	TxDOT Standard	24.3 MPa (3520 psi)	28.0 MPa (4070 psi)
3.1, 3.2, 3.3	TxDOT Standard	22.9 MPa (3325 psi)	24.9 MPa (3610 psi)
3.4, 3.5	TxDOT Standard	n/a	30.4 MPa (4400 psi)
4.1, 4.2	TxDOT Standard	19.3 MPa (2800 psi)	31.8 MPa (4620 psi)
Average:	TxDOT Standard	22.2 MPa (3215 psi)	28.8 MPa (4170 psi)
2.11	High Performance	38.4 MPa (5560 psi)	43.5 MPa (6310 psi)

3.7 Construction

All specimens and reaction beams were constructed at the Ferguson Laboratory. Specimens were constructed indoors and moved outside into position with a reaction beam prior to post-tensioning and loading. All construction, post-tensioning and loading was performed by the graduate and undergraduate research assistants working on the project.

3.7.1 Specimen Fabrication

Reinforcement cages were prepared following typical construction practices. All flexural reinforcement was cleaned prior to construction using a wire brush wheel on an angle grinder. Post-tensioning anchorage hardware and confinement reinforcement was sandblasted to remove visible rust. This was done so that any corrosion occurring from exposure testing would be clearly identifiable. Reusable wooden forms were constructed for casting the beams. Concrete was supplied by a local ready-mix producer, and poured using a concrete bucket on an overhead crane. Concrete was placed and vibrated with hand held concrete vibrators following typical practice. The concrete was wet cured for a minimum of three days. Forms were normally stripped after three days, and beams were moved if the concrete strength was sufficient. Beam specimens were constructed with the tension reinforcement on the bottom side of the beam so that cracking under load would

occur on a formed face. Specimens were turned over prior to moving into their final position. Several photos of the construction process are shown in Figure 3.24.

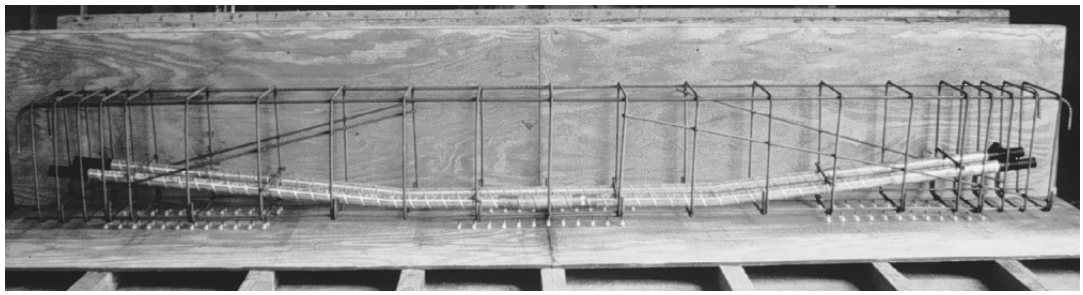

Reinforcement Cage with Ducts for Post-Tensioning

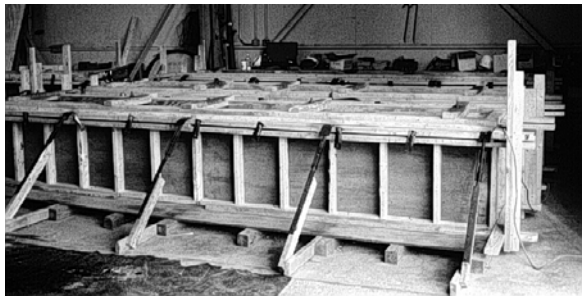

Formwork

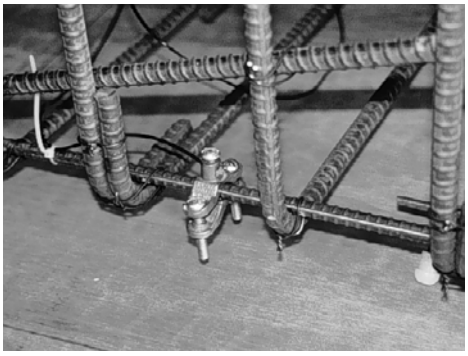

Ground Clamp to Attach Ground Wire

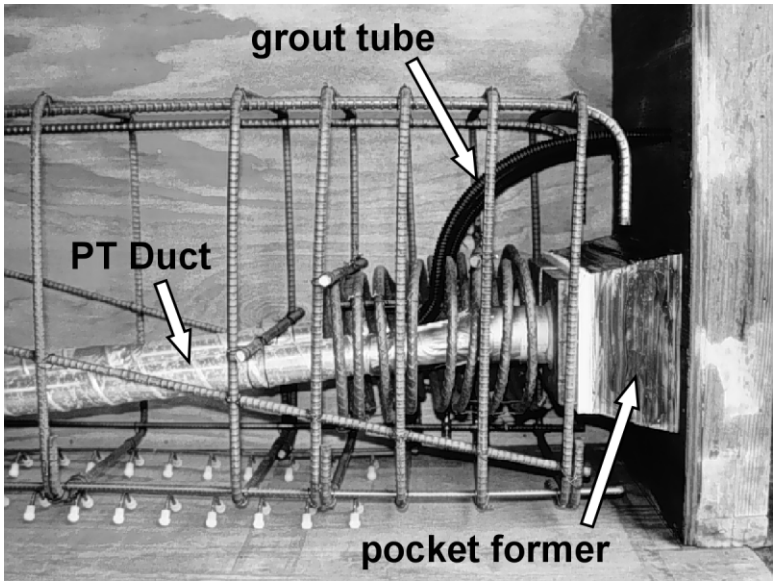

Anchorage Zone Details

Figure 3.24 - Beam Specimen Construction

3.7.2 Post-Tensioning

3.7.2.1 Prestress Losses

Elastic shortening, friction losses and anchorage seating were considered in the calculation of the post-tensioning jacking forces for each section type.

Elastic Shortening

Staged post-tensioning was used to minimize prestress losses due to elastic shortening. The post-tensioning sequence is shown in Figure 3.25. The final elastic shortening loss occurs in Tendon 1 as Tendon 2 is stressed from two thirds of the jacking force up to the total jacking force, T_j.

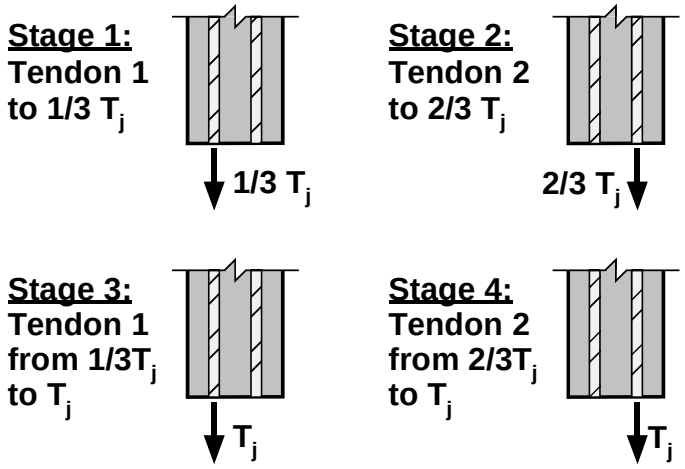

Figure 3.25 - Staged Post-Tensioning Sequence

Friction

Friction losses were small due to the short length of the beams and small variation in tendon path. The prestress loss due to friction at the midspan of the beams was computed to be 2.5% of the jacking force.

Anchorage Seating

Prestress losses due to anchorage seating were very critical due to the short beam length. Common practice is to use shims to compensate for anchorage seating losses in short tendons. The use of shims in the beam specimens was not practical due to the details of the anchorages and beam end pockets. Therefore, it was necessary to power seat the wedges to minimize seating losses. Most commercially available post-tensioning equipment has power seating capabilities incorporated into the stressing rams. However, for tendon sizes smaller than four strands and ram capacities less than 450 kN (100 kips), power seating is not available.[3.18] It was decided to use the available hydraulic rams at the Ferguson Laboratory in a configuration that would allow stressing and power seating of the wedges. Post-tensioning equipment is described in more detail in Section 3.7.2.2.

It was necessary to accurately determine the amount of anchorage seating loss for the anchorage hardware, tendon length and post-tensioning equipment to be used. A large, heavily reinforced concrete stressing block with the same length as the beams was available from a previous project at Ferguson Laboratory. Several pull off tests were used with the anchorage hardware and stressing equipment to determine necessary power seating forces to limit seating losses to tolerable levels. The setup for the pull off tests is shown in Figure 3.26. The procedure is as follows:

1. Stress the tendon to a trial jacking force based on the desired initial prestress and an assumed seating loss.
2. Power seat the wedges to a trial seating force.
3. Release the stressing ram.
4. Perform a pull off test to determine the actual force in the tendon. This is done by plotting the jacking force and stroke of the stressing ram as the tendon is re-stressed. A distinct slope change on a plot of T_j versus Δ will occur when the force in the stressing ram overcomes the force in the tendon.
5. Based on the trial jacking force and measured tendon force, determine the prestress loss and anchorage seating value. If unsatisfactory, de-tension the tendon, remove the wedges, and repeat the process using new values of assumed seating loss and power seating force.

The pull off tests determined a wedge seating force of approximately 80 kN (18 kips) would limit anchorage seating to 3.2 mm (1/8 in.). This seating loss could be easily accommodated by adjusting the jacking force.

The prestress losses, jacking forces and initial prestress for each of the post-tensioned beam types are summarized in Table 3.7. The total prestress loss due to elastic shortening, friction and seating was rounded up to 172 MPa (25 ksi) for each section type. Due to the small magnitude of the elastic shortening loss, it was decided to use the same jacking force for both tendons in a beam.

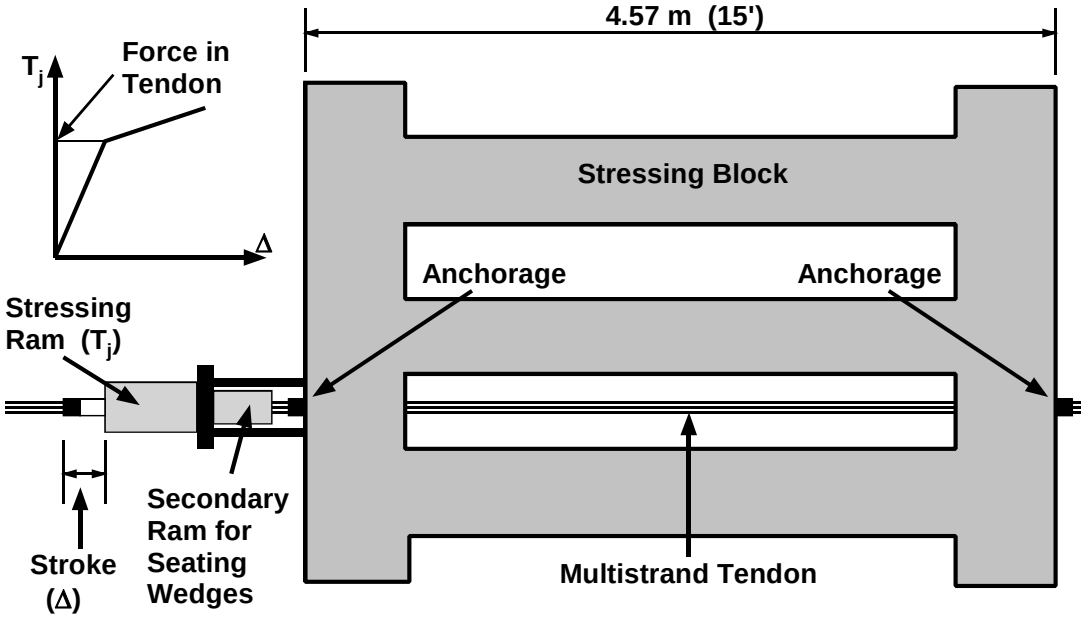

Figure 3.26 - Pull Off Test for Determining Anchorage Seating Loss

Table 3.7 - Initial Prestress, Prestress Losses and Jacking Forces

Item	2/3 PS Section: 2 strand tendon	100%U Section: 3 strand tendon	100%S Section: 4 strand tendon
Initial Prestress, f_{pi}	1117 MPa (162 ksi)	1117 MPa (162 ksi)	1041 MPa (151 ksi)
Elastic Shortening Loss	4.7 MPa (0.68 ksi)	7.2 MPa (1.04 ksi)	8.8 MPa (1.28 ksi)

Friction Loss	27.9 MPa (4.05 ksi)	27.9 MPa (4.05 ksi)	26.0 MPa (3.77 ksi)
Anchorage Seating Loss	130.3 MPa (18.9 ksi)	130.3 MPa (18.9 ksi)	130.3 MPa (18.9 ksi)
Jacking Stress, f_{pj}	1289 MPa (187 ksi)	1289 MPa (187 ksi)	1213 MPa (176 ksi)
Jacking Force	255 kN (57.2 kips)	383 kN (87.2 kips)	480 kN (108 kips)

3.7.2.2 Post-Tensioning Equipment

All equipment for post-tensioning was adapted from Ferguson Laboratory hydraulic equipment. The setup used for the 100%S PS beams is shown in Figure 3.27. Additional details are shown in Appendix C. The chair for post-tensioning was fabricated from a 50 mm (2 in.) thick steel plate and four 35 mm (#11) reinforcing bars. The stressing ram for the 100%S PS section had a capacity of 1335 kN (300 kips). This large ram was selected based on its internal diameter that could accommodate the four strand tendon. A smaller ram with 535 kN (120 kips) capacity was used for the 2/3 PS and 100%U PS beams. A system of two smaller rams and transfer bracket were used to power seat the anchorage wedges. The post-tensioning equipment was mounted on an electric forklift for ease of movement and height adjustment.

3.7.2.3 Post-Tensioning Procedure

Post-tensioning procedures were based on TxDOT Specifications[3.13] Item 426.9 and AASHTO LRFD Construction Specifications.[3.19] The main steps in the process are as follows:

1. Each individual strand was given an initial tension of approximately ten percent of the jacking force (per strand) to remove slack. Initial tensioning was performed using a small 107 kN (24 kip) ram.
2. After initial tensioning, all strands of the tendon were given a reference mark to measure elongation.
3. The tendons were stressed using a staged post-tensioning procedure, as described in Section 3.7.2.1. Prestress force was monitored using a pressure gauge on the hydraulic pump. At each stage, stressing ram stroke and tendon

elongation were measured to confirm force levels. Wedges were power seated at each stage.

4. At the completion of the four stressing stages, final tendon elongation was checked. If acceptable, equipment was removed and the strand ends were trimmed to 25 mm (1 in.) (none of the tendons required re-tensioning).

The 100%S PS sections required a small amount of preload before post-tensioning to keep concrete stresses within tolerable ranges. The preload was applied using the post-tensioning bar and spring loading system described in Section 3.5 and shown in Figure 3.21. The necessary applied moment was 56.5 kN-m (500 k-in.). This was below the cracking moment for the section (before post-tensioning).

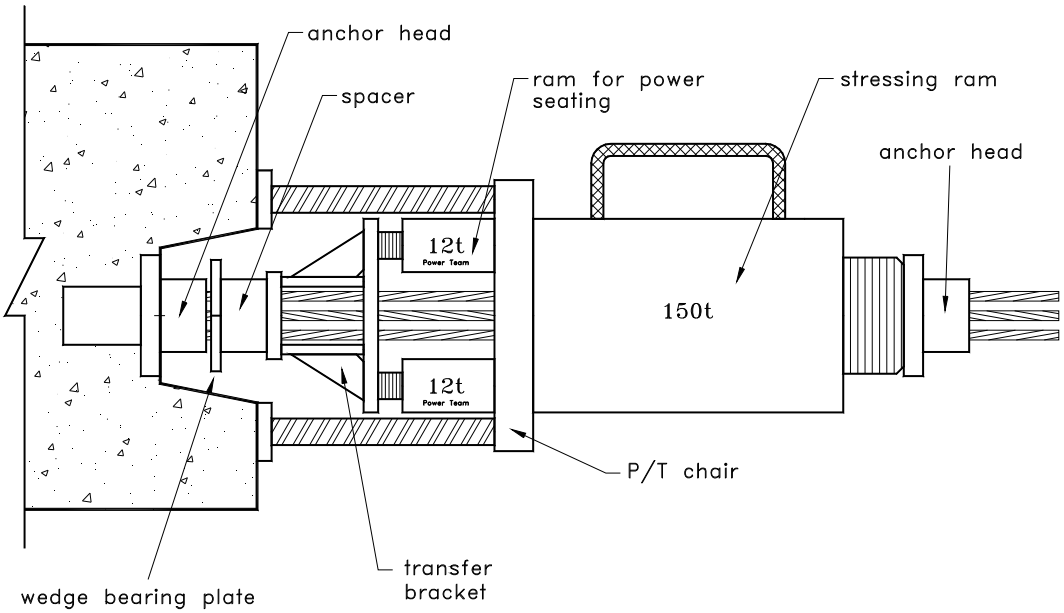

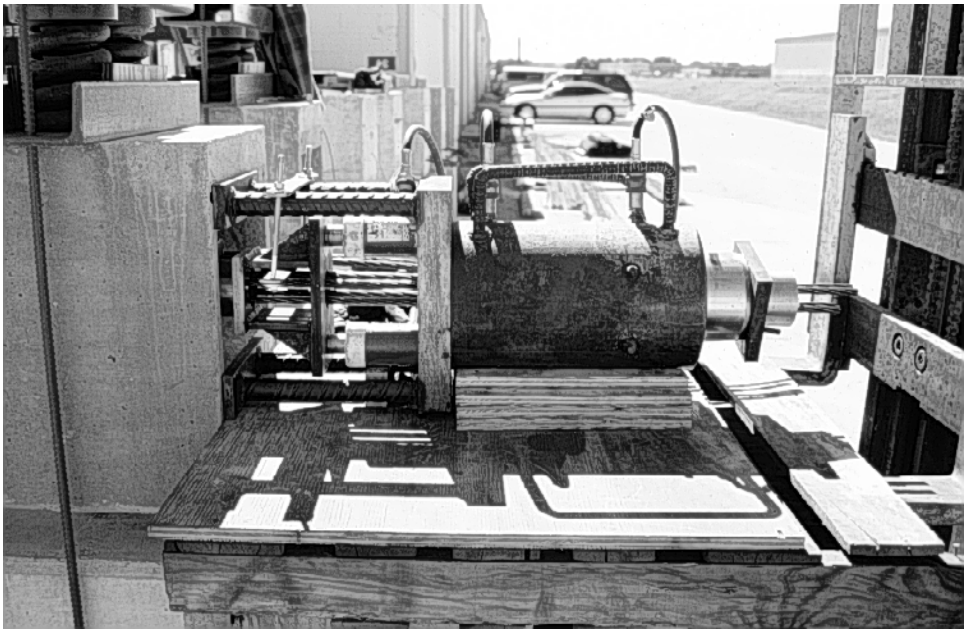

Figure 3.27 - Post-Tensioning Equipment for 100%S PS Beams

3.7.3 Grouting

Tendons were normally grouted within three days after post-tensioning. For Beam 2.1 the duration between stressing and grouting was more than two weeks. During this period the anchorage pockets were sealed using a plywood cover and silicone to prevent moisture entry. This duration is within PTI limits,[3.16] and temporary corrosion protections were not required.

All grouting procedures were performed according to the recommendations of the Post-Tensioning Institute[3.16] and TxDOT Specifications.[3.13] Grouts were mixed in a mortar mixer and pumped immediately using an electric grout pump. The grouting setup is shown in Figure 3.28. The inlet and vent 2 were provided using 19 mm (0.75 in.) grout tube with shut off valves. Vent 1 was provided by drilling from the tension face of the beam to the duct with a 12.7 mm (0.5 in.) diameter rotary hammer. Drilling was performed before the strands were placed and tensioned, and the duct was blown clean using compressed air. Vent 1 was closed using a dowel plug. Vent 1 was not required by the PTI Specifications,[3.16] but was included to ensure that the crest of the duct profile was completely filled during grouting.

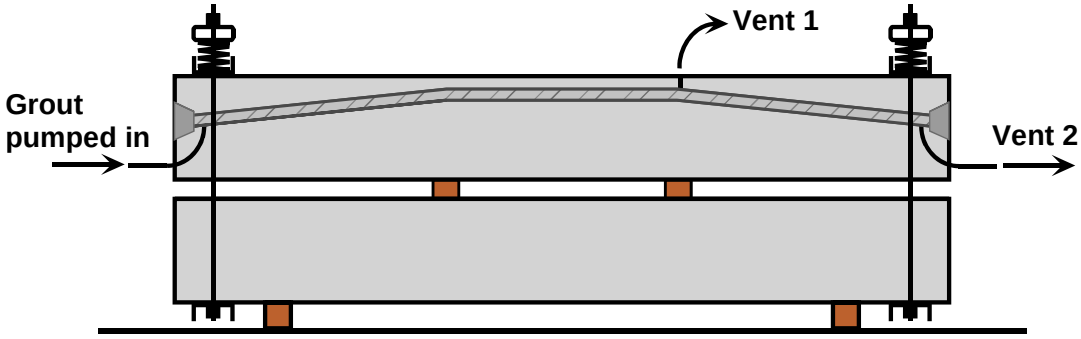

Figure 3.28 - Inlet and Vents for Grouting

Grouting began as soon as the grout was sufficiently mixed. Grout was transferred from the mixer using buckets, and poured into the pump reservoir through a screen to remove lumps, if any. The grout was continuously stirred in the reservoir to prevent segregation. Grout was pumped into each duct without stoppage. In all cases, the flow of grout filled the duct completely as it progressed along the duct length, and grout exited Vent 1 before reaching Vent 2. Once a continuous flow of grout was exiting Vent 1 with no slugs of air or water, Vent 1 was closed using a dowel. Pumping continued until a steady flow of grout was exiting Vent 2. At this time, Vent 2 was closed and the pump stopped. The pump was then restarted for a period of 2 to 3 seconds before closing the valve on the inlet tube. Grout bleed water was normally observed exiting from around the anchorage wedges immediately after the grouting operation had concluded.

3.7.4 Anchorage Protection

Corrosion protection for the anchorages and strand ends was provided by filling the anchorage pockets with a non-shrink grout. Procedures and materials were based on TxDOT Specifications.[3.14]

After grouting was completed, all exposed surfaces including the anchorage heads, bearing plates and sides of the pockets were cleaned with a wire brush to remove grout and rust. Each end pocket was photographed to provide a record of its condition before capping. This will provide a basis for comparison during forensic examination of the specimens at a later date. A sample photo is shown in Figure 3.29. Ground clamps were used to attach a lead wire to one strand in each tendon. This lead wire is used for

half-cell potential and corrosion rate measurements during testing. Ground clamps were attached on both tendons, one at each end of the beam.

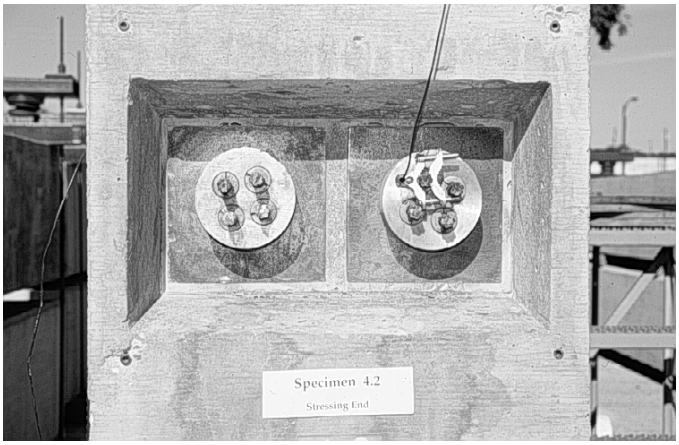

Figure 3.29 - Anchorage Pocket Immediately Before Capping

All exposed surfaces were coated with an epoxy bonding compound immediately prior to capping. After epoxy application, the end pockets were closed in with plywood. Silicone sealant was used to prevent leakage around the plywood. The pockets were with filled with a non-shrink grout mixture by pouring it through a tube as shown in Figure 3.30. The premixed grout contained silica sand and a non-shrink admixture. After the grout had hardened, the plywood was removed. In some cases, a small void remained at the top of the pocket. The entire beam end was rubbed with a mixture of cement, sand and latex bonding agent to provide a uniform finish and fill any voids in the end pocket.

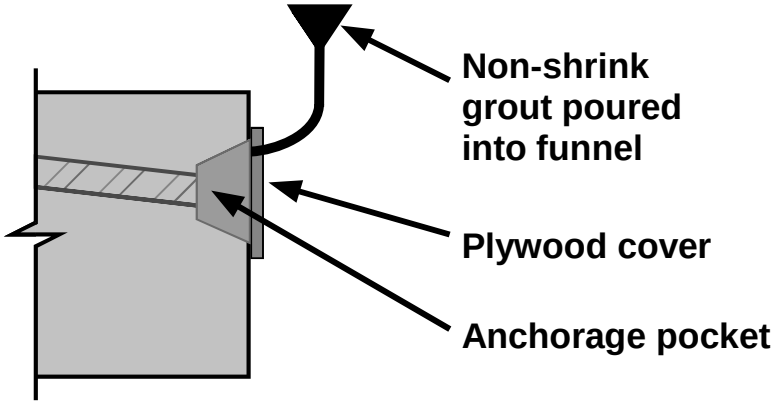

Figure 3.30 - Capping End Anchorages

3.8 Specimen Loading and Initial Crack Width Measurements

3.8.1 Specimen Load History

Loading was applied according to the planned loading cases (see Section 3.3.2.1 and Table 3.2). Due to variations in the concrete modulus of rupture and the inherent variability in crack prediction, some deviation from the planned loading cases occurred during loading. The actual loading histories for the Phase I beams are listed in Table 3.8. Beams 1.1 and 3.1 were not loaded, and are not listed in the table. Loading Step 1 corresponded to the actual (measured) cracking moment for the beam, with the exception of beams 3.2, 4.1 and 4.2 which were uncracked at service load levels.

Deviation from the planned loading cases occurred for Beams 3.2, 3.3 and 3.4. In all cases, the changes were required because the cracking moment was higher than predicted and exceeded the service load moment. The computed cracking moment for the 100%U PS beams was 305 kN-m based on the commonly assumed modulus of rupture of $0.623\sqrt{f'_c}$ MPa $(7.5\sqrt{f'_c}$ psi$)$. The actual cracking moments for Beams 3.3, 3.4 and 3.5 were 310 kN-m, 356 kN-m and 338 kN-m, respectively. Because the effect of cracking is one of the main objectives for the Phase I beam specimens, it was decided to temporarily increase loading on some of the 3 Series beams to produce the desired cracking patterns and levels. The planned and actual loading cases for the 3 Series beams (100%U PS) are shown in Table 3.9.

Table 3.8 - Beam Specimen Loading Histories

Beam No.	Loading Step 1 (M_{cr})	2	3	4	5	6	Note
1.2	0.48xM_S	0.55xM_S	0.77xM_S	1.0xM_S			
1.3	0.46xM_S	0.55xM_S	0.77xM_S	1.0xM_S			
1.4	0.48xM_S	0.55xM_S	0.77xM_S	1.0xM_S	1.25xM_S	1.0xM_S	
2.1	0.84xM_S						
2.2	0.79xM_S	0.90xM_S	1.0xM_S				

2.3	0.82xM_S	0.91xM_S	1.0xM_S				
2.4	0.85xM_S	0.92xM_S	1.0xM_S	1.25xM_S	1.0xM_S		
2.11	0.82xM_S	0.91xM_S	1.0xM_S				
3.2	1.0xM_S						2
3.3	1.0xM_S	1.1xM_S	1.15xM_S	1.25xM_S	1.0xM_S		3
3.4	1.15xM_S	1.25xM_S	1.0xM_S	1.25xM_S	1.33xM_S	1.0xM_S	3
3.5	1.09xM_S	1.16xM_S	1.25xM_S	1.0xM_S			
4.1	1.0xM_S						1
4.2	1.0xM_S						1

Notes:
1. Beam is uncracked at service load (as designed).
2. Loading case changed from very small crack to Constant Service Load (Uncracked).
3. Loading case changed from Constant Service Load to Overload and Return to Service.

Table 3.9 - Planned and Actual Load Cases for 100%U PS Beams

Beam	Planned Load Case	Actual Load Case	Comment
3.1	Unloaded	Unloaded	No change.
3.2	Very Small Crack	Constant Service Load (Uncracked)	Since the cracking moment for other 3 Series beams had exceeded the service moment, it was decided to leave this beam uncracked at service load. Comparisons can be made with Beams 3.1, 4.1 and 4.2.
3.3	Constant Service Load (Cracked)	Overload and Return to Service	A 25% temporary overload was required to produce three cracks in this beam. ($M_{cr} = 1.0M_{serv}$)
3.4	Constant Service Load (Cracked)	Overload and Return to Service	A 33% temporary overload was required to produce three cracks in this beam. ($M_{cr} = 1.15M_{serv}$)
3.5	Overload and Return to Service	Overload and Return to Service	No change. ($M_{cr} = 1.09M_{serv}$)

3.8.2 Loading Procedure and Measurement of Crack Widths

The beam specimens were loaded using two 535 kN (120 kip) hydraulic rams, one at each end of the beam. The loading hardware is shown in Figure 3.31. The ram reacts against a steel spreader beam, compressing the springs. Once the desired level of loading is attained, the force is locked in by tightening the nuts on the post-tensioning bars. An air driven pump was used to apply loading. Load levels were monitored using a pressure gauge on the pump.

Loading was applied according to the load histories listed in Table 3.8. At each loading stage, surface crack widths were measured on the tension face using a crack microscope. Five reference lines were drawn on the tension face of the beams as shown in Figure 3.32. Crack widths were measured where each crack crossed the five reference lines. The crack location was measured relative to the center of load application at one end of the beam.

Figure 3.31 - Beam Loading Apparatus

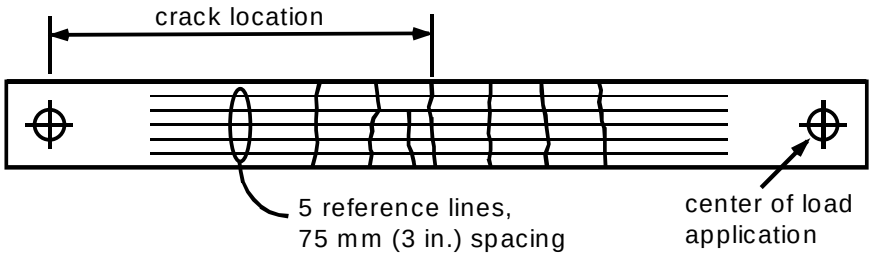

Figure 3.32 - Crack Width Measurement Locations

3.8.3 Measured Crack Data

Typical crack width data for each of the beam types is shown in Figure 3.33 through Figure 3.35. Data is shown for the 25% overload and return to service load case (Beams 1.4, 2.4 and 3.3). Maximum and minimum measured crack widths at each crack location are plotted. Schematics showing the beam reinforcement, post-tensioning ducts and duct splices are located at the top of each figure. Similar crack width plots for all Phase I beam specimens are included in Appendix C, Figures C.23 to C.33.

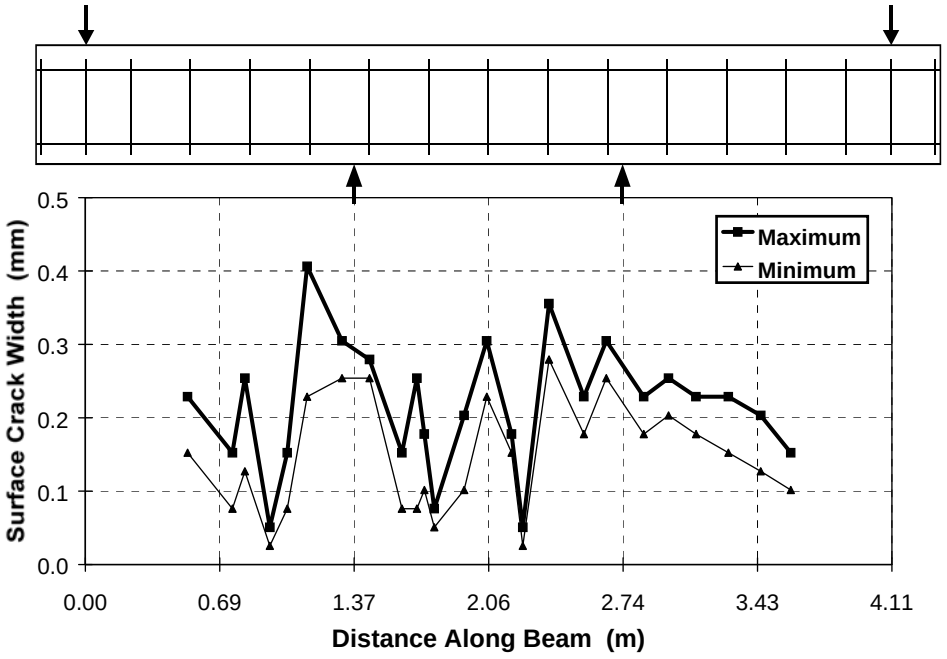

Figure 3.33 - Measured Crack Widths: Non-PS Beam at Service Load After 25% Overload

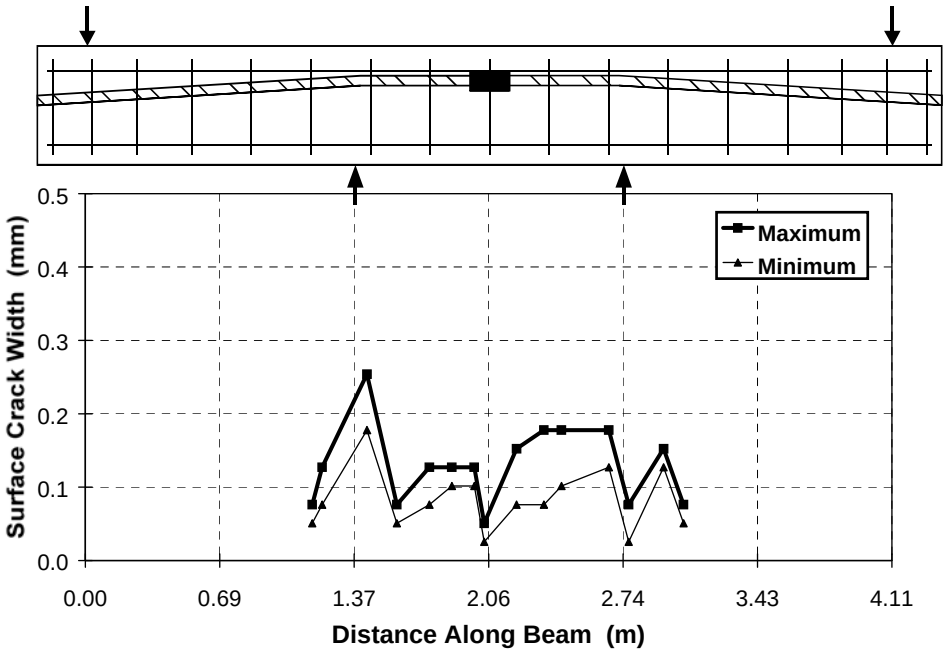

Figure 3.34 - Measured Crack Widths: 2/3 PS Beam at Service Load After 25% Overload

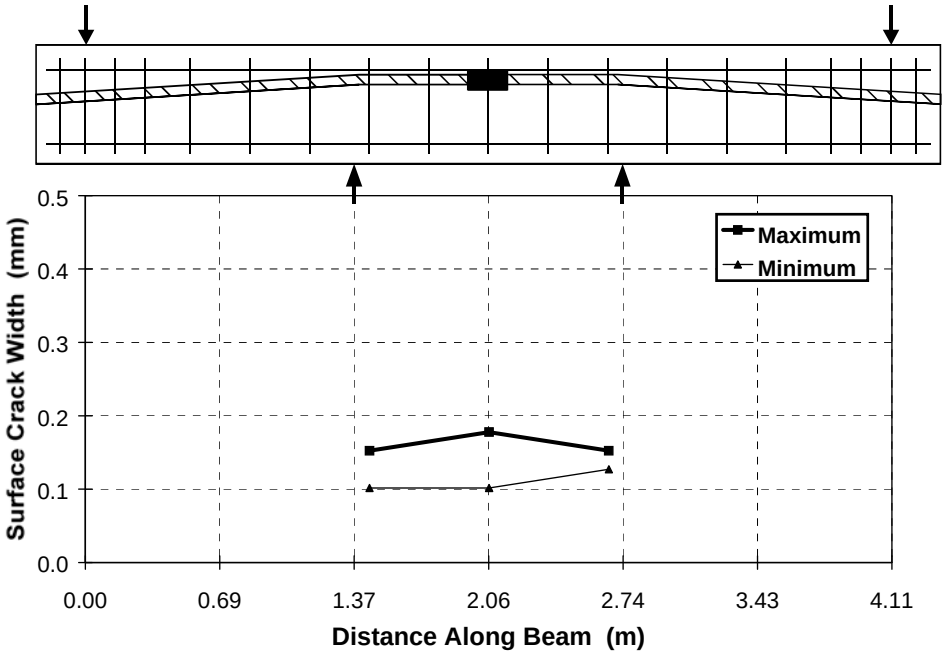

Figure 3.35 - Measured Crack Widths: 100%U PS Beam at Service Load After 25% Overload

Crack patterns on the tension face and side face of all Phase I beams are shown in Figure 3.36. The load and reaction points are indicated in the figure. Beams 1.1 and 3.1 are not shown since they are not loaded, and Beams 3.2, 4.1 and 4.2 are not shown since they are uncracked at service load levels.

The crack data in Figure 3.33 through Figure 3.36 and Appendix C clearly illustrates the effect of post-tensioning on cracking. The measured crack data shows the following trends:

- The number of cracks and extent of cracking is drastically reduced as the level of prestress increases. The Non-PS beams show a large number of cracks well distributed over a large area extending well outside the third points of the beam. The 2/3 PS beams show reduced cracking, confined primarily to the maximum moment region in the middle one-third of the beam. The 100%U PS beams have only three cracks, one near midspan and one near each support location.

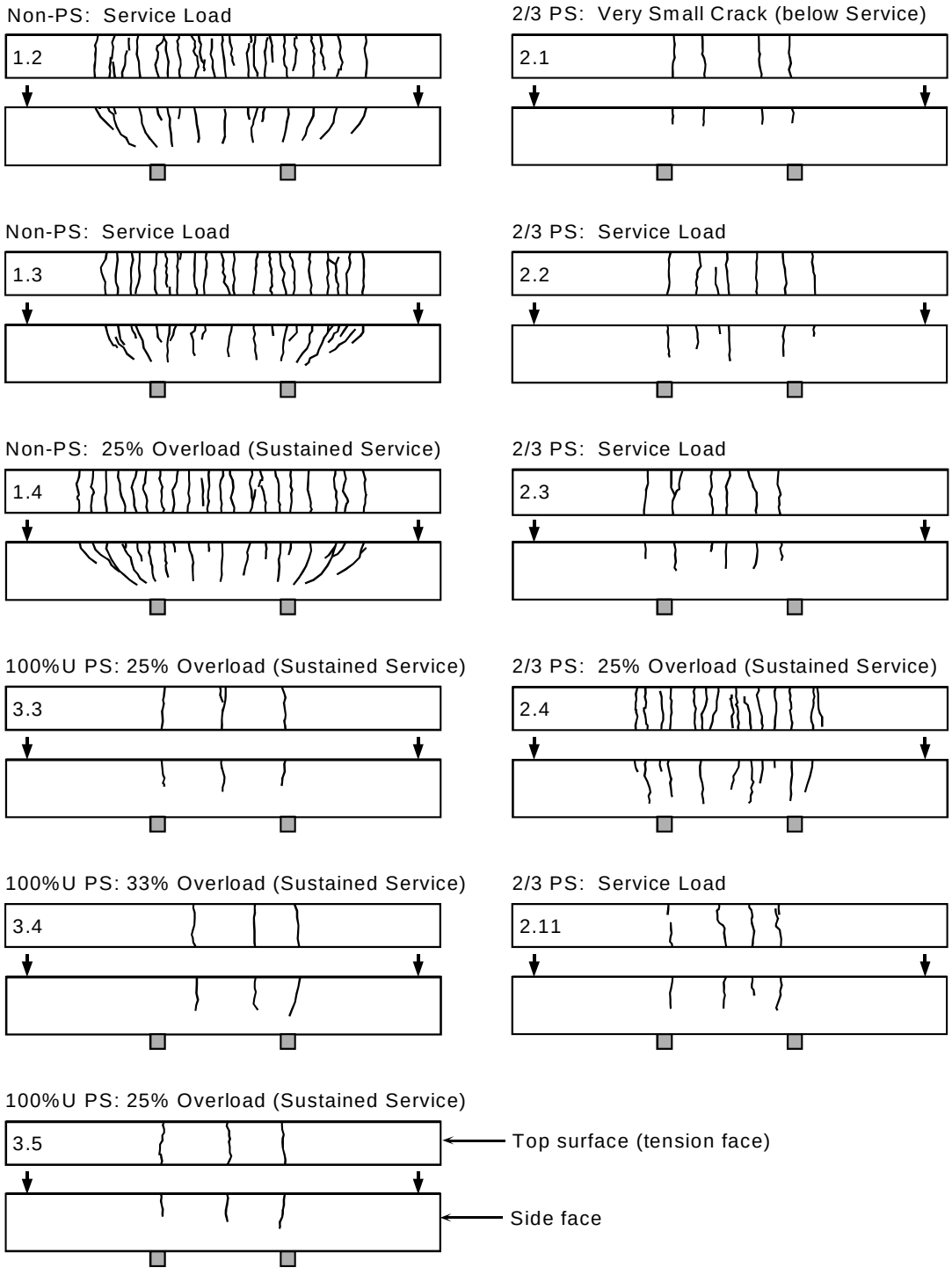

Figure 3.36 - Beam Specimen Crack Patterns

- The extent of cracking along the beam is well predicted by the cracking moments for the three beam types. Figure 3.37 shows the service load bending moment diagram with the computed cracking moments for the three section types that are cracked under service load.

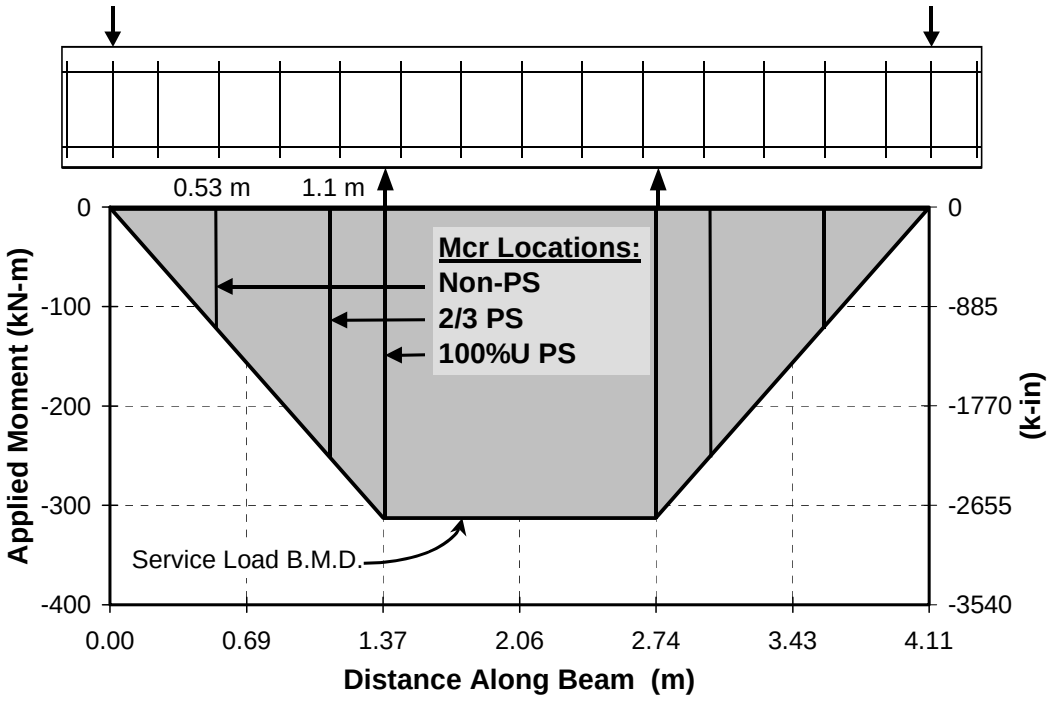

Figure 3.37 - Cracking Moment Locations Along Beam Length

- Cracks commonly occurred at stirrup locations. In many cases, the first cracks to form were located at stirrups, and in general cracks located at stirrups had larger crack widths than adjacent cracks.
- The maximum surface crack widths are reduced as the level of prestress increases. Referring to the data plotted in Figure 3.33, Figure 3.34 and Figure 3.35, most cracks in the Non-PS beam have a maximum width greater than 0.2 mm (0.008 in.), with the largest at 0.41 mm (0.016 in.). In the 2/3 PS beam, most cracks have a maximum width between 0.1 mm (0.004 in.) and 0.2 mm (0.008 in.) with the largest at 0.25 mm (0.010 in.). The cracks in the 100%U PS beam are consistent with maximum widths between 0.15 mm (0.006 in.) and 0.18 mm (0.007 in.). The maximum crack width reduction

from the 2/3 PS beam to the 100%U PS beam is not particularly significant. The most important difference between these levels of prestress is the reduction in the number of cracks.

3.9 Measurements During Exposure Testing

Specimen condition and corrosion activity are regularly monitored by collecting four forms of data: visual examination, half-cell potential readings, chloride penetration and corrosion rate measurements. Each is described below.

3.9.1 Visual Examination

The appearance of the specimens can indicate corrosion activity or distress. The beam specimens are regularly examined for signs of spalling, rust staining, changes in cracking and any other indication of distress.

3.9.2 Half-Cell Potential Readings

Half-cell potential readings can provide two forms of information regarding the condition of the beam specimens:

- The magnitude of half-cell potential readings indicate the probability of corrosion at a given location.
- The time at which corrosion initiation occurred can be determined from regular potential readings taken during testing.

Half-cell potential readings require a reference electrode, voltmeter and electrical connection to the reinforcement. Common reference electrode types include copper-copper sulfate and saturated calomel. Saturated calomel electrodes (SCE) are used in this testing program. As mentioned in Section 3.7.4, ground clamps were used to attach a wire to the prestressing tendons before capping the anchorages. In addition, two ground wires were attached to the reinforcement for each beam before placing concrete. The entire system of the reinforcement cage, ducts and prestressing tendons was found to be electrically continuous, and half-cell potential measurements using any of the lead wires should produce the same results.

Half-cell potential readings are taken at one month intervals, at the conclusion of the wet portion of the wet-dry exposure cycle. All measurements are performed according

to ASTM C876.[3.20] Half-cell potential measurements are taken on a grid over the tension surface of beams. The grid spacing is 150 mm (6 in.) along the length of the beam. The grid spacing across the width of the beam is dependent on the section reinforcement. Three evenly spaced rows are used for the Non-PS sections. Two additional rows along the line of the ducts are added in the 2/3 PS section. Four rows are used in the 100%U PS and 100%S PS sections: two along the line of the ducts, and two along the two mild steel reinforcing bars. The grid for the Non-PS beams is shown in Figure 3.38. Measurements are performed before the saltwater solution is removed from the ponded area at the conclusion of the wet portion of the exposure cycle. For readings outside of the ponded area, a wetting solution is used according to the requirements of ASTM C876.[3.20]

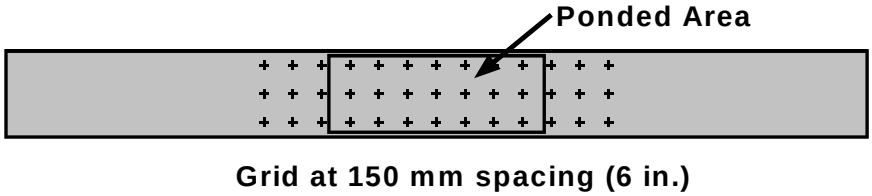

Figure 3.38 - Grid for Half-Cell Potential Readings: Non-PS Beams

The numerical significance of the half-cell potential readings (saturated calomel electrode) is shown in Table 3.10. The values reported in Table 3.10 were developed for uncoated reinforcing steel in concrete are not necessarily appropriate for post-tensioned concrete. In general, half-cell potential readings are not an effective method for monitoring corrosion activity in bonded post-tensioned structures. In structures with galvanized steel ducts, the prestressing tendon will be in contact with the duct in most cases and half cell potentials taken on the prestressing tendon may reflect the potential of the zinc on the galvanized steel duct. Because the potential of the zinc will be more negative than that of the tendon, this could lead to erroneous results and conclusions. However, due to the lack of other non-destructive methods for monitoring corrosion activity in post-tensioned concrete, it was decided to use regular half-cell potentials to monitor specimen condition. By considering both the magnitude and variation of the readings during testing it still may be possible to detect the onset of corrosion activity.

Table 3.10 - Interpretation of Half-Cell Potentials for Uncoated Reinforcing Steel[3.20]

Measured Potential (vs SCE)	Probability of Corrosion
more positive than –130 mV	less than 10% probability of corrosion
Between -130 mV and –280 mV	corrosion activity uncertain
more negative than –280 mV	greater than 90% probability of corrosion

3.9.3 Chloride Penetration

The role of chlorides in the corrosion process was discussed in Section 2.3. By regularly monitoring the penetration of chlorides into the concrete, it is possible to determine when chloride concentrations at the level of the steel reinforcement exceed the threshold for corrosion activity. Although this is not an absolute measurement of corrosion activity, it can be used in conjunction with other data to estimate whether corrosion initiation has occurred.

Chloride penetration is normally measured by collecting and testing samples from the concrete at varied depths. The most common method for obtaining samples is to use a rotary hammer (hammer drill). Holes are drilled to the desired depth and the powder is collected for analysis.

Concrete ponding blocks are used in this testing program to monitor chloride penetration in the beam specimens. The use of ponding blocks avoids drilling into the test area of the beam specimens which could possibly affect later results. The ponding blocks have dimensions of 300 x 300 x 150 mm (12 x 12 x 6 in.), and were based on the AASHTO test method for evaluating chloride ion permeability of concrete.[3.21] The specified block thickness was increased to 150 mm (6 in.) to allow sample collection at larger depths. Two blocks were cast during each specimen pour. One block was fitted with a plastic dike and is subjected to the same exposure regimen as the beams. The dike was placed on the bottom formed surface of the block since the beam ponded area is also a formed surface. The second block is used as a control specimen and is not subjected to saltwater exposure.

The control specimens are used to indicate the base level of chlorides in the concrete. Ponding blocks, shown in Figure 3.39, are stored outdoors with the beams.

Concrete powder samples are collected from the ponding block and control specimens at multiple depths to determine the extent of chloride penetration. Samples are analyzed for acid soluble chloride content using a specific ion probe (CL Test System by James Instruments). All sample collection and analysis procedures are based on AASHTO T260-94.[3.22] Samples are collected at regular time intervals to monitor the penetration of chlorides during exposure testing.

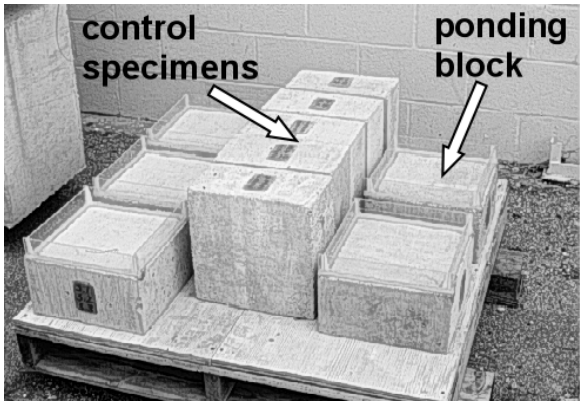

Figure 3.39 - Ponding Blocks for Beam Specimens

3.9.4 Corrosion Rate Measurement

Polarization resistance is a useful technique for measuring instantaneous corrosion rates under laboratory and field conditions. Polarization measurements are rapid, highly sensitive, non-destructive and can be performed repeatedly. The theory behind this technique is detailed in many references.[3.23,3.24,3.25,3.26] The theory states that within a small range of overvoltage (+/- 10 to 15 mV from the free corrosion potential), there is a linear relationship between applied current and electrode potential. The slope of the curve of ΔE versus $\Delta I_{applied}$ at the origin is defined as the polarization resistance, R_p (see Figure 3.40). The polarization resistance is inversely proportional to corrosion current, which in turn is directly proportional to corrosion rate. The computed corrosion rate can be compared to established guidelines to relate corrosion rate to corrosion damage. This method for

corrosion rate measurements is often referred to as linear polarization or the polarization resistance method.

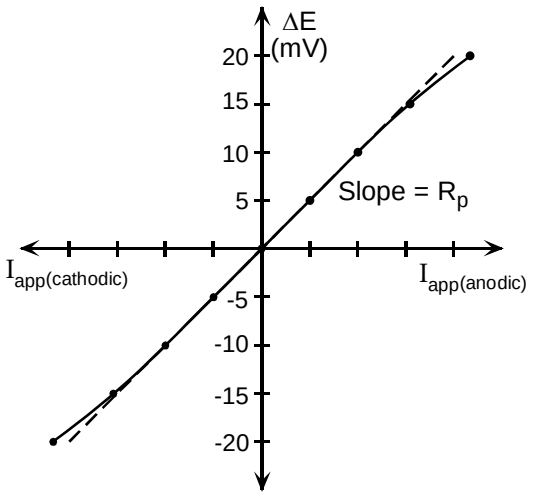

Figure 3.40 – Applied Current Linear Polarization Curve

The instantaneous corrosion current is related to the polarization resistance by the Stern-Geary equation shown below.[3.23,3.24]

$$i_{corr} = \frac{\beta_a \beta_c}{2.3(\beta_a + \beta_c)} \times \frac{1}{R_p} \qquad \textbf{Eq. 3.1}$$

where

i_{corr} = corrosion current, mA

β_a = anodic Tafel constant, mV

β_c = cathodic Tafel constant, mV

R_p = polarization resistance, Ohms

The rate of corrosion in terms of corrosion current density, i, can be calculated by dividing the corrosion current, i_{corr}, by the area of polarized steel, A_p.

$$i = \frac{i_{corr}}{A_p} \qquad \textbf{Eq. 3.2}$$

The term containing the Tafel constants in Eq. 3.1 is often replaced by a proportionality constant, B, as follows:

$$i_{corr} = \frac{B}{R_p} \qquad \textbf{Eq. 3.3}$$

where,

$$B = \frac{\beta_a \beta_c}{2.3(\beta_a + \beta_c)}$$

In order to accurately calculate the corrosion current, the anodic and cathodic Tafel constants must be known. The polarization resistance is primarily influenced by the corrosion current, I_{corr}, and is relatively insensitive to changes in the Tafel constants.[3.23] The value of the proportionality constant, B, ranges from 26 for actively corroding mild steel reinforcement in concrete to 52 for passive mild steel reinforcement in concrete.[3.27] There is no reported research on values of the constant B for prestressing steel in concrete.

3.9.4.1 Measurement of Polarization Resistance

The polarization resistance, R_p, can be measured using several different techniques.[3.24,3.25] The two most common methods used for reinforced concrete are the three electrode procedure, and electrochemical impedance spectroscopy (sometimes referred to as AC impedance). Each method has advantages and disadvantages.[3.25] The three electrode method is most common due to its simplicity and low equipment cost.

The basic components of the equipment for the three electrode method are shown in Figure 3.41. The working electrode is the steel reinforcement for which the corrosion rate is to be measured. The counter electrode is used to apply the polarizing current to the steel. The reference electrode measures the free corrosion potential of the working electrode and the change in potential of the working electrode due to the applied current from the counter electrode. The process of measuring the polarization resistance begins with measuring the free corrosion potential or open-circuit potential of the tested area of steel reinforcement (working electrode). The working electrode is then polarized in uniform increments from the free corrosion potential and the associated current is measured. The polarization resistance is taken as the slope of the curve when ΔE versus $\Delta I_{applied}$ is plotted (see Figure 3.40). This relationship is normally linear for a range of up to

+/- 10 mV from the free corrosion potential.[3.23] When corrosion activity is low, small changes in applied current will produce a large change in potential and the polarization resistance will be large. When corrosion activity is high, large changes in applied current are needed to produce the desired potential increment, resulting in a low polarization resistance.

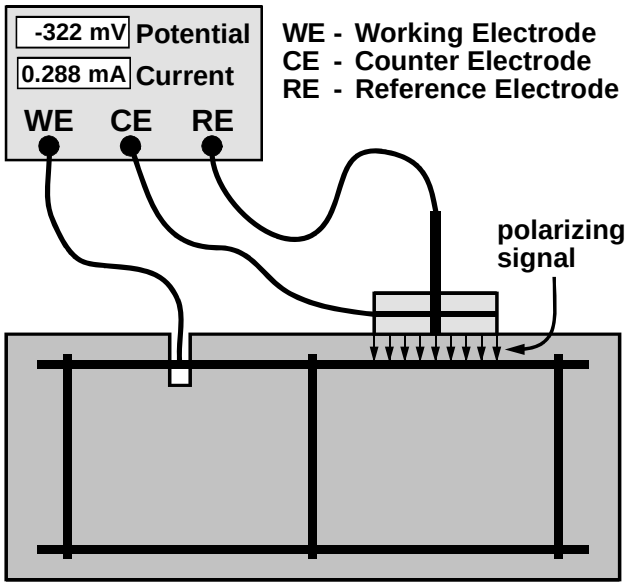

Figure 3.41 - Polarization resistance Apparatus (Schematic)

3.9.4.2 Errors in Corrosion Rates based on Polarization Resistance Measurements

The polarization resistance technique and apparatus were developed to measure corrosion rates of mild steel reinforcement in "regular" concrete. For this application in the laboratory setting, the polarization resistance technique provides excellent results when compared to direct corrosion rate measurements in macrocell corrosion specimens. In field applications, the results are felt to be somewhat less accurate, but still reliable. The inaccuracies arise from several sources:

- **Ohmic Electrolyte Resistance:** The configuration of the three electrode procedure for polarization resistance measurements in concrete results in a separation between the reference electrode and working electrode (see Figure 3.41). The separation provided

by the concrete cover introduces an error in the measurements due to ohmic electrolyte resistance, that is the resistance of the concrete. This resistance is also referred to as the solution resistance. The total resistance measured by the three electrode procedure is the sum of the polarization resistance, R_p and the solution resistance, R_s:

$$R_{tot} = R_p + R_s \qquad \textbf{Eq. 3.4}$$

In situations where the concrete resistance or solution resistance is high and the reference electrode can not be located close to the working electrode, the error introduced by solution resistance can be significant. The error introduced by solution resistance is unconservative since it increases the apparent polarization resistance, resulting in lower corrosion rates.

- **Uncertain polarized area:** Calculation of the corrosion rate or current density requires an accurate estimation of the polarized area of the working electrode (see Eq. 3.2). Normally, the polarized area is assumed to be that directly below the counter electrode, but it may unknowingly be smaller or larger. The use of a guard electrode has been shown to confine the current path between the counter electrode and the reinforcement, improving the accuracy of the corrosion rate measurement.[3.25] Other bars in the vicinity of the counter electrode may also affect the accuracy of the measurements. Diffusion of the current path also will result in larger polarized steel areas as the concrete cover increases.[3.25] Research has also shown that only the top half of the rebar (closest to the counter electrode) is effectively polarized.[3.25] This finding suggests that the polarized area is normally overestimated by a factor of two.
- **Uncertain Tafel constants:** Accurate calculation of corrosion current requires accurate values for the anodic and cathodic Tafel constants (see Eq. 3.1). However, because the Tafel constants β_a and β_c appear in both the numerator and denominator of the Stern-Geary equation (Eq. 3.1), the corrosion current is primarily a function of the polarization resistance and is relatively insensitive to changes in the Tafel constants.[3.23,3.24] For this reason, the values of the proportionality constant, B, proposed earlier are normally deemed sufficient. Inaccuracies resulting from uncertain Tafel constants may be avoided by using the results of polarization

resistance measurements for relative comparisons of corrosion activity measured under similar conditions.

- **Prestressed concrete:** Prestressed concrete introduces several factors that may produce errors in corrosion rates determined using the polarization resistance technique.
  - **prestressing strand** - affects Tafel constants, and area of polarized steel is uncertain because of seven wires in close proximity.
  - **prestressing strand inside duct** - may make potential measurements very small (possibly too small or erratic to be useful). Also affects Tafel constants. If duct is plastic, measurements can not be taken.
- **Erratic or very small polarization resistance:** Some situations and conditions may lead to unusable values of polarization resistance due to limitations in the technique and equipment. These include:
  - **epoxy coated reinforcement** - may make potential measurements very small (possibly too small or erratic to be useful). Also affects Tafel constants.
  - **large cover to reinforcement** - may make potential measurements very small (possibly too small or erratic to be useful).
  - **concrete with high resistivity or low permeability** - may make potential measurements very small (possibly too small or erratic to be useful). Concrete containing silica fume is an example of this.
  - **cracked concrete –** affects signal distribution in concrete.

3.9.4.3 Corrosion Measurements on Phase I Beam Specimens

There is no published work to date on using polarization resistance to monitor corrosion rates in pre-tensioned or post-tensioned concrete. Some of the factors listed above may have a significant influence on the usefulness of the technique in prestressed concrete. In spite of these potential limitations, it was decided to use polarization resistance as an evaluation method in this testing program since qualitative information and comparisons may still be possible. Relative corrosion rate measurements can provide an indication of relative corrosion rates between specimens with different variables. For example, the relative effectiveness of different corrosion protection measures may be

evaluated by comparing corrosion rates with those from "control" specimens. Also, regular measurements may indicate the onset of corrosion through increases in corrosion rate.

Corrosion rate measurements were taken three times during the first fifteen months of exposure testing. Measurements after seven months were performed using the PR-Monitor equipment. Measurements after one year of testing were performed using the 3LP equipment. Both the 3LP and PR Monitor were used to measure corrosion rate after fifteen months exposure. Both types of equipment use the three electrode technique. Two corrosion rate measurements were taken on each beam, one at midspan and one at 305 mm (12 in.) from midspan, as shown in Figure 3.42. The electrodes were centered over a stirrup at these locations. In the Non-PS and 2/3 PS beams, the electrode also covered several bars of the tension reinforcement.

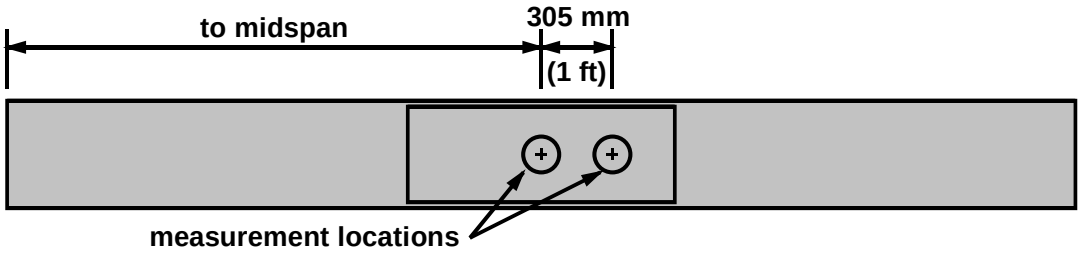

Figure 3.42 - Corrosion Rate Measurement Locations

The polarization resistance technique requires a direct electrical connection (ground connection) to the steel for which the corrosion rate is being measured. As mentioned in Section 3.9.2, ground wires were attached to the mild steel reinforcement and prestressing tendons during construction. Corrosion rate measurements require the concrete to be initially dry. A wetting solution is used to moisten the concrete surface immediately prior to testing.

3.9.4.4 PR-Monitor for Corrosion Rate Measurement

Corrosion rate measurements taken after seven and fifteen months of exposure testing were performed using the CORRTEST PR-Monitor Model IN-4500. The PR-Monitor device uses a portable computer to control the corrosion rate measurement process. The PR-Monitor compensates for the concrete resistance (IR drop) and has a guard electrode to confine the polarization signal. The default polarization scan uses six

steps of 5 mV, starting at -15 mV from the free corrosion potential and ending at +15 mV. The starting and ending potentials and voltage increment may be adjusted by the user in situations where the solution resistance is large in comparison to the polarization resistance. The increased potential range for the polarization scan can improve the accuracy of the measured polarization resistance when the solution resistance is high. At the end of the polarization scan, the concrete resistance or solution resistance is measured using AC impedance. A high frequency, low voltage AC signal is used to isolate the solution resistance. The computer performs a linear regression analysis on the polarization scan data and computes the total resistance, R_{tot}, as the slope of ΔE versus $\Delta I_{applied}$. The solution resistance, R_s, is subtracted from the total resistance to obtain the polarization resistance, R_p (see Eq. 3.4). The corrosion current is calculated assuming a proportionality constant, B, of 26 mV. When all measurements and calculations are complete, the computer displays the free corrosion potential, polarization resistance, concrete resistance and corrosion rate in mils per year. This information and the polarization scan data is also written to an output file. The corrosion rate can be converted to current density by dividing the corrosion rate in mils per year by 0.4568.[3.28] The corrosion current density can also be calculated using the measured polarization resistance and assumed polarized area. The corrosion severity is assigned based on the ranges listed in Table 3.11.

Table 3.11 - PR-Monitor Corrosion Severity Based on Current Density[3.28]

Corrosion Current Density	Corrosion Severity
Less than 0.1 μA/cm²	Passive
Between 0.1 and 0.5 μA/cm²	Low
Between 0.5 and 1.0 μA/cm²	Moderate
Greater than 1.0 μA/cm²	High

The guard ring is assumed to confine the polarized area of reinforcement to that of a circle with 152 mm (6 in.) diameter directly under the electrodes. The polarized steel surface area necessary to compute corrosion rate was calculated by multiplying the bar circumference by the lengths of the bars directly under the 152 mm (6 in.) diameter circle,

as shown in Figure 3.43. In the post-tensioned beams, twice the horizontal projection of the duct area under the circle was included when determining the polarized area. Calculated surface areas for each beam type are indicated in the figure. The wider duct spacing in the 100%S PS beams decreases the polarized area in comparison to the 100%U PS beams.

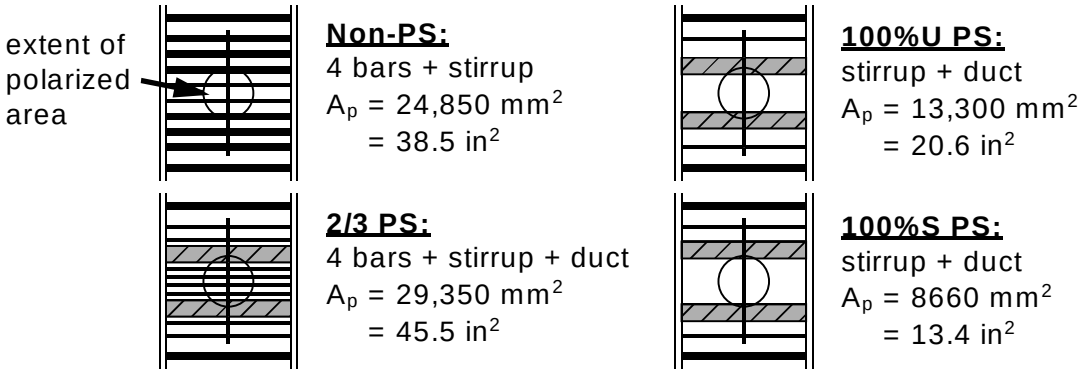

Figure 3.43 - Polarized Steel Surface Areas for PR-Monitor

3.9.4.5 3LP Equipment for Corrosion Rate Measurement

Corrosion rate measurements after twelve and fifteen months of exposure testing were performed using the 3LP Equipment developed by Kenneth C. Clear, Inc., USA. The 3LP device is manually operated, and polarization scan data is recorded by hand. The counter electrode is rectangular and current confinement is not provided. The equipment measures the half-cell potential of the reinforcement (working electrode) and the applied polarization current. The polarization scan uses three steps of 4 mV, starting at the free corrosion potential and ending at +12 mV. The concrete resistance is not measured by the 3LP device. The linear regression analysis on the polarization scan data must be performed using a hand calculator or computer to determine the total resistance, R_{tot}, as the slope of ΔE versus $\Delta I_{applied}$. No correction is made for the concrete resistance, and the polarization resistance, R_p, is simply taken as equal to the total resistance. The manufacturer recommends a proportionality constant, B, of 40.76 mV for calculating corrosion current. The manufacturer also provides guidance for relating corrosion current densities to expected corrosion damage. The SHRP Procedure Manual for Condition Evaluation of Bridges[3.29] indicates a proportionality constant, B, of 26 mV can be used with

the 3LP device. The interpretation guidelines listed in Table 3.11 are appropriate for the 3LP device if B = 26 mV is used.[3.29]

The counter electrode for the 3LP device is rectangular with dimensions of 178 mm by 76 mm (7 x 3 in.). The polarized steel surface area was calculated by multiplying the bar circumference by the bar length directly under counter electrode, as shown in Figure 3.44. Calculated surface areas for each beam type are indicated in the figure. The counter electrode was positioned such that it was not located over the ducts in the post-tensioned beams.

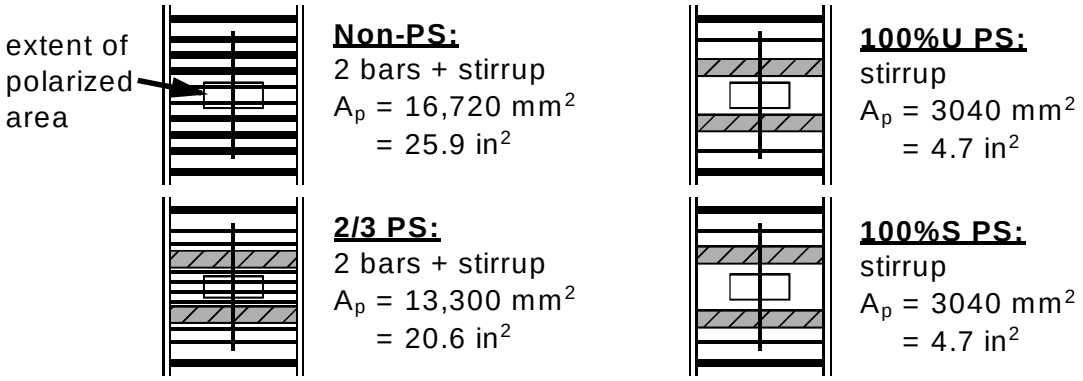

Figure 3.44 - Polarized Steel Surface Areas for 3LP

3.10 Exposure Testing Results

Exposure testing was initiated in December 1997. Exposure test data recorded up to September 25, 1998 is presented in this section. The data gathered during this period does not provide a strong indication of corrosion initiation in any of the Phase I beam specimens.

3.10.1 Visual Examination

Within the first two months of testing, rust stains were visible within the ponded area of several specimens. Rust staining was most prominent along cracks, but was also visible in uncracked concrete. In most cases, the rust staining may be attributed to corrosion of the bolster strips used to support the reinforcement during construction. This was also evidenced by spalling around the "feet" of many of the strips. The bolster strips were plastic tipped, but still corroded very early during testing. Typical rust staining is shown in Figure 3.45. The spots of rust appear aligned and at regular intervals, suggesting

bolster strip corrosion. The AASHTO LRFD Construction Specifications[3.19] require the use of plastic tipped or stainless steel tipped bar chairs and bolster strips on member faces that will be exposed to aggressive environments. The test results indicate that the plastic tips do not appear to be adequate for this purpose.

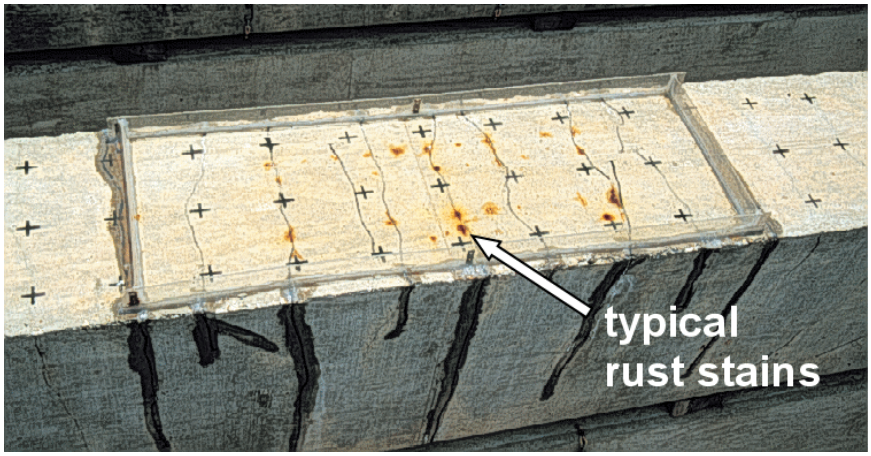

Figure 3.45 - Typical Rust Stains Due to Bolster Strip Corrosion

3.10.2 Half-Cell Potential Readings

Half-cell potential readings over the duration of testing are plotted in Figure 3.46 through Figure 3.49 for the four levels of prestress. The highest (most negative) half-cell reading for each beam is plotted in the figures. The ASTM guidelines for interpreting half-cell potentials (see Table 3.10) are indicated on the figures. Maximum potentials and the average potential within the ponded area are plotted for each beam in Appendix C, Figures C.34 to C.39. In most cases the maximum and average potentials are similar in magnitude.

Half-cell potential maps for all specimens are shown in Figure 3.50. The potential maps show fairly uniform variations in half-cell readings within the measurement area. In general, the potentials are lower outside of the ponded area, as would be expected.

It is important to emphasize that half-cell potentials are only an indicator of corrosion incidence, and a correlation with corrosion rate can not be made. The ASTM C876 guidelines (Table 3.10) only indicate the probability of corrosion. Very negative potentials can be used to suggest a higher probability of corrosion activity, but not necessarily a higher corrosion rate. Many factors can influence measured half-cell

potentials, including concrete cover thickness, concrete resistivity, concrete moisture content, different metals and availability of oxygen. In some cases, these factors can lead to very negative half-cell potentials with little or no corrosion activity. For this reason, it is important to consider the variation of half-cell potential measurements over an extended period of time in addition to the magnitude of the readings. A common trend observed in corrosion research is that a transition from fluctuating or steady more positive potentials to a stable condition of more negative potentials is normally associated with the onset of corrosion.[3.30,3.31]

The half-cell potential data for the Non-PS beams indicates a high probability of corrosion for all beams with the exception of the unloaded specimen (1.1). Readings for all 2/3 PS specimens suggest a high probability of corrosion. With the exception of specimen 3.4, data for the 100%U PS and 100%S PS specimens indicates a low or uncertain probability of corrosion. Potentials for specimen 3.4 (100%U PS) are slightly above the ASTM guideline for 90% probability of corrosion. Specimen 3.4 had a temporary 33% overload, the highest of all 3 Series beams.

The half-cell potentials for most beams show a gradual trend more negative over time. This trend is not indicative of a distinct initiation of corrosion, but does not preclude the presence of corrosion activity. Although no other outward signs of corrosion damage have been present during the reporting period, additional data in the form of a visual examination of the reinforcement condition should be considered to gain a more thorough assessment of corrosion activity.

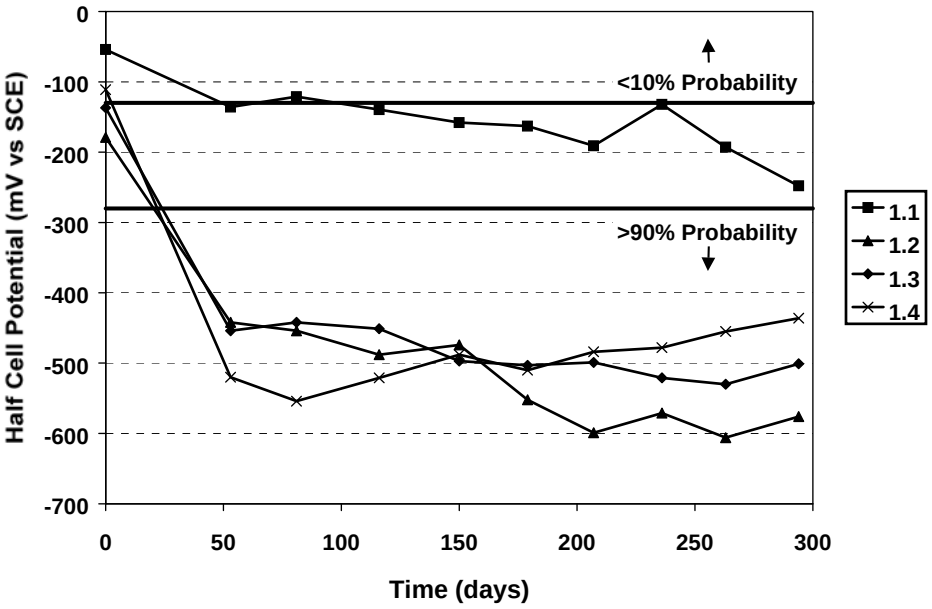

Figure 3.46 - Highest Half-Cell Potential Readings: Non-PS Beams

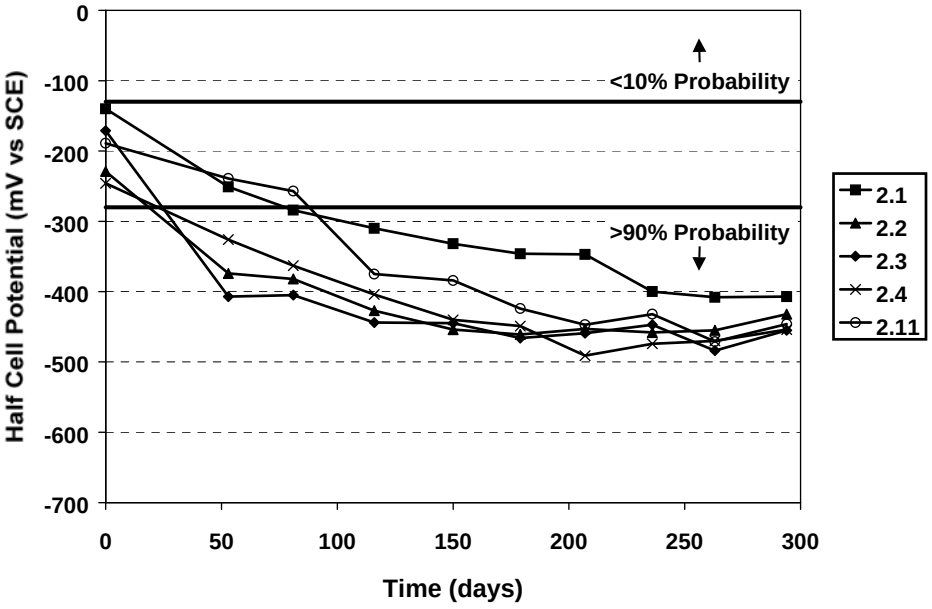

Figure 3.47 - Highest Half-Cell Potential Readings: 2/3 PS Beams

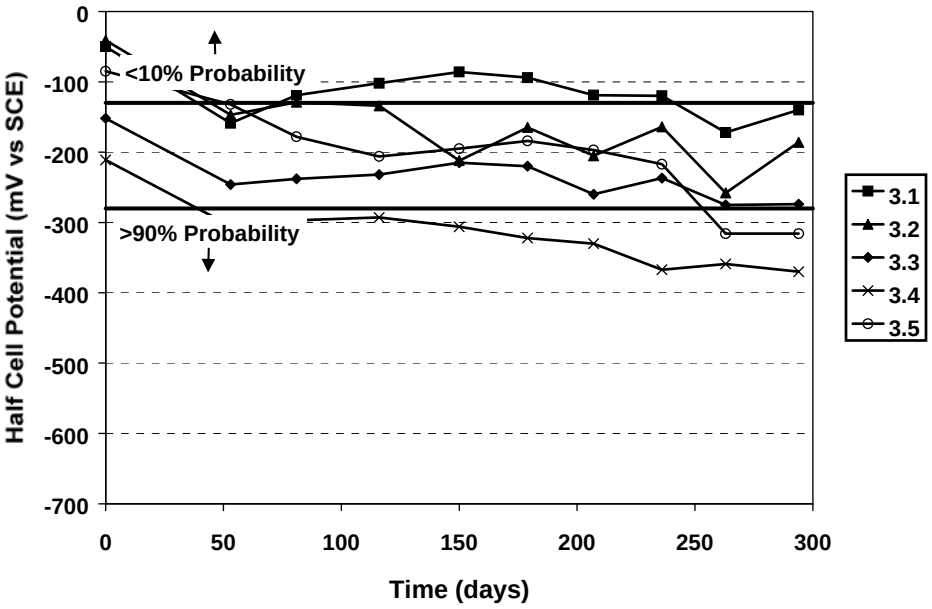

Figure 3.48 - Highest Half-Cell Potential Readings: 100%U PS Beams

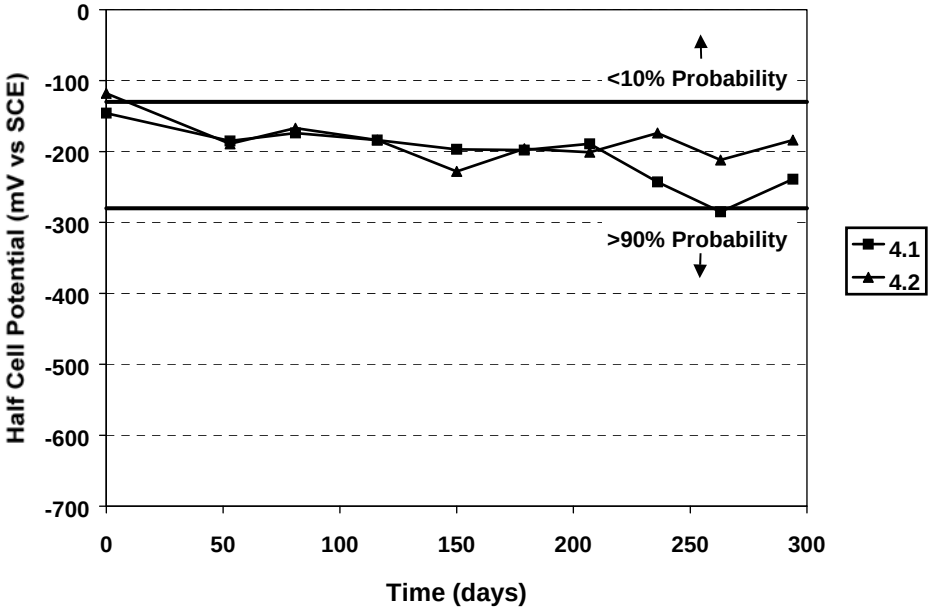

Figure 3.49 - Highest Half-Cell Potential Readings: 100%S PS Beams

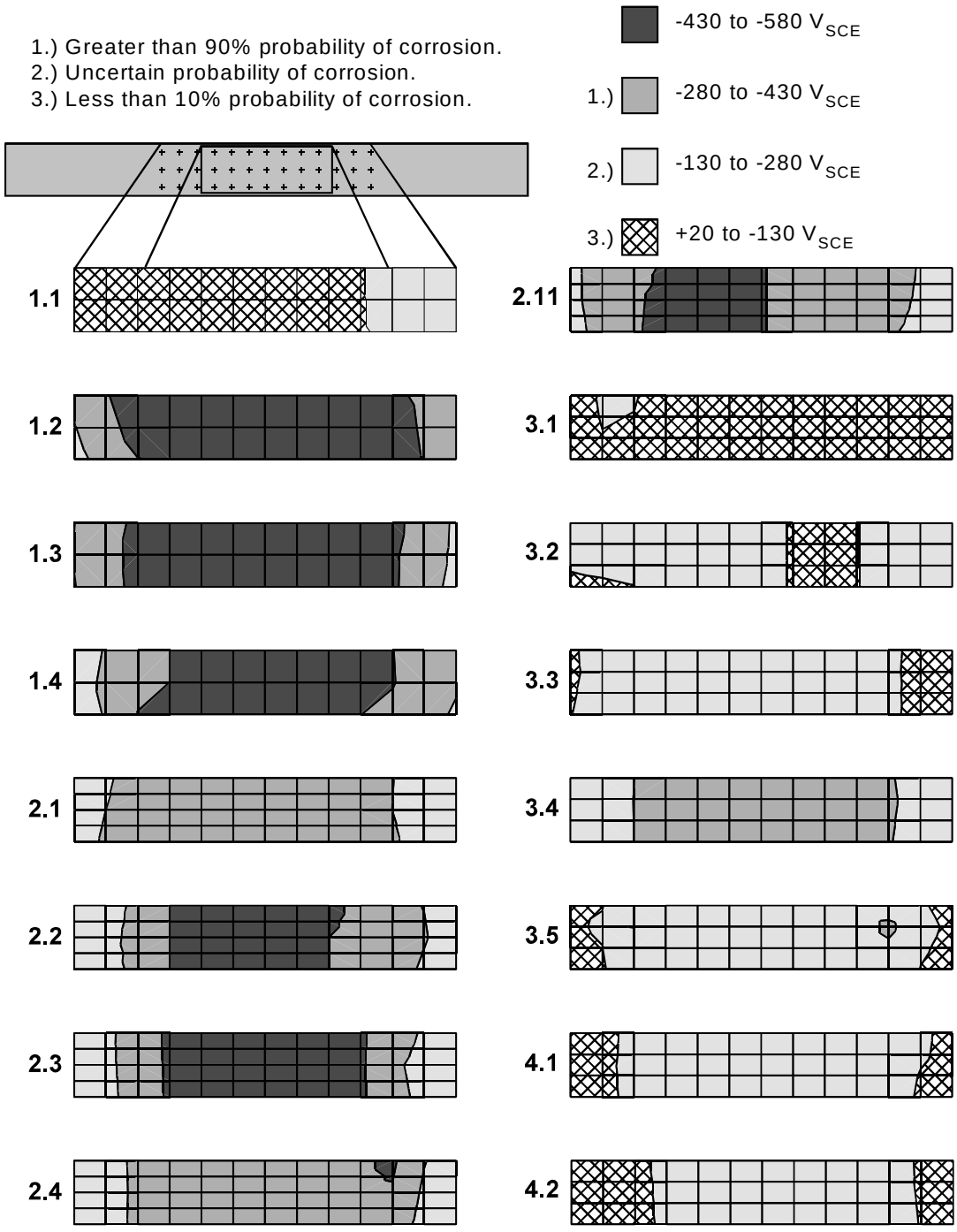

Figure 3.50 - Half-Cell Potential Maps for All Beam Specimens (Data as of September 25, 1998)

3.10.3 Chloride Ion Penetration

Concrete powder samples were collected from the saltwater exposed ponding blocks and from the non-exposed control blocks after seven months of exposure testing. Three sample depths were used, as shown in Figure 3.51. Two 1.5 gram samples were collected at each depth and analyzed for acid soluble chlorides using a specific ion probe.

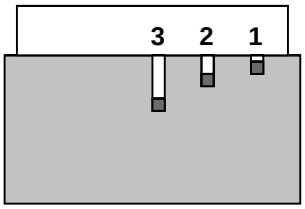

1.) Sample depth 6 to 19 mm (0.25 to 0.75 in.)
2.) Sample depth 19 to 21 mm (0.75 to 1.25 in.)
3.) Sample depth 44 to 57 mm (1.75 to 2.25 in.)

Figure 3.51 - Concrete Powder Sample Depths for Chloride Analysis

The results of the chloride analysis are plotted in Figure 3.52. All control samples had chloride contents below measurable levels (i.e., essentially zero). The chloride threshold for corrosion is indicated in the figure at 0.030% by weight of concrete. This value is intended as a guideline only, and is based on a chloride threshold value of 0.2% of the weight of cement.[3.32] Most chloride levels at a depth of 13 mm (0.5 in) are over the corrosion threshold, but decrease to zero at a depth of 25 mm (1 in.). This indicates that chlorides have penetrated to a depth between 13 mm and 25 mm.

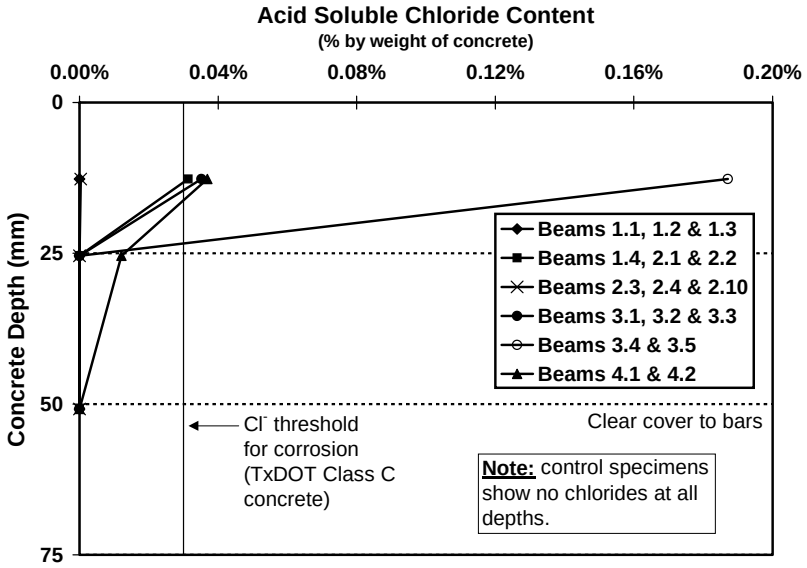

Figure 3.52 - Acid Soluble Chloride Profiles in Uncracked Concrete After Seven Months

3.10.4 Corrosion Rate Measurements

3.10.4.1 Seven Month Exposure Duration

Corrosion rate measurements were performed after seven months of exposure testing using the PR-Monitor equipment (see Section 3.9.4.4). Readings were taken midway (one week) through the dry portion of the exposure cycle. Corrosion rate readings in terms of corrosion current density are plotted in Figure 3.53 and listed in Table 3.12 for all specimens. Two readings were performed on each beam, one at midspan and one 305 mm (12 in.) from midspan. Corrosion currents for most beams are in the range of moderate and high corrosion activity. The corrosion rate for uncracked Beam 1.1 (non-prestressed, unloaded) is in the range of low corrosion activity. In general, the measured corrosion rates for the 100%U PS and 100%S PS beams are higher than those for the 2/3 PS and Non-PS beams. This trend in corrosion activity is contradictory to the half-cell potential readings.

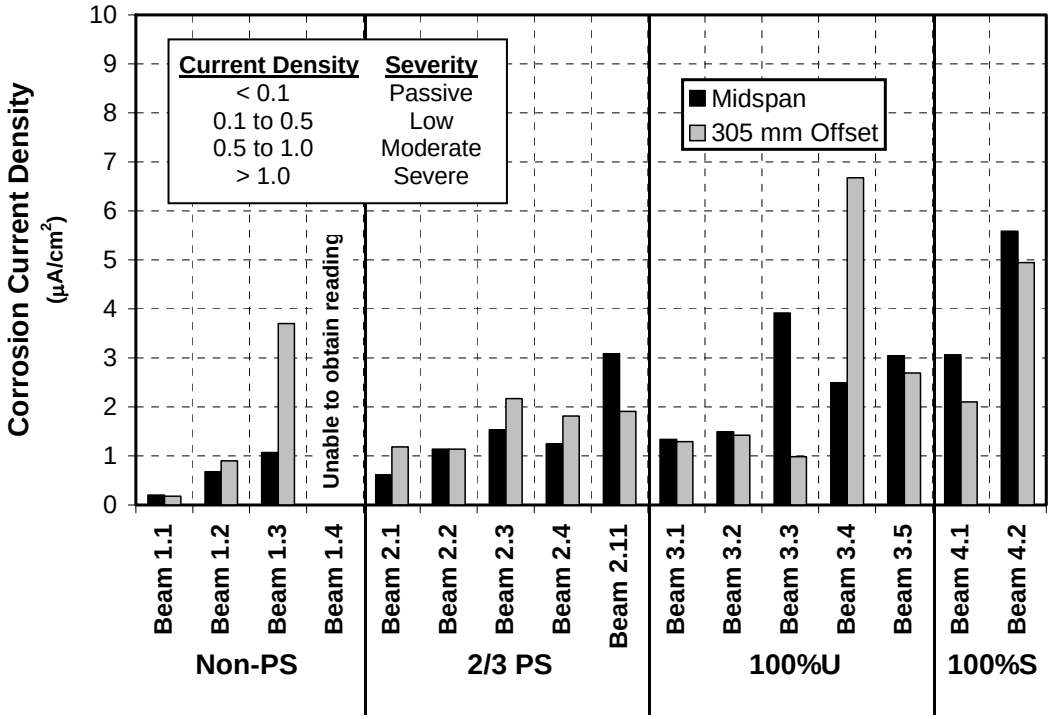

Figure 3.53 - Measured Corrosion Rates – Seven Month Exposure Duration (PR Monitor Equipment)

3.10.4.2 Twelve Month Exposure Duration

Corrosion rate measurements were performed after twelve months of exposure testing using the 3LP equipment (see Section 3.9.4.5). Readings were taken on day five of the two week dry portion of the exposure cycle. Corrosion rate readings in terms of corrosion current density are plotted in Figure 3.54 (note the greatly expanded scale in comparison to Figure 3.53) and listed in Table 3.12 for all specimens. Readings were taken at the same locations used with the PR-Monitor after seven months exposure. Corrosion rates for all beams except Beam 1.1 are very high. Although considerably lower than the other beams, the 3LP corrosion rate for Beam 1.1 has exceeded the threshold for severe corrosion activity. The relative corrosion rates between specimens show trends comparable to the data measured after seven months using the PR-Monitor. The measured corrosion rates for the 100%U PS and 100%S PS beams are again higher than those for the 2/3 PS and Non-PS beams, contrary to the relative corrosion activity indicated by the half-cell potential readings.

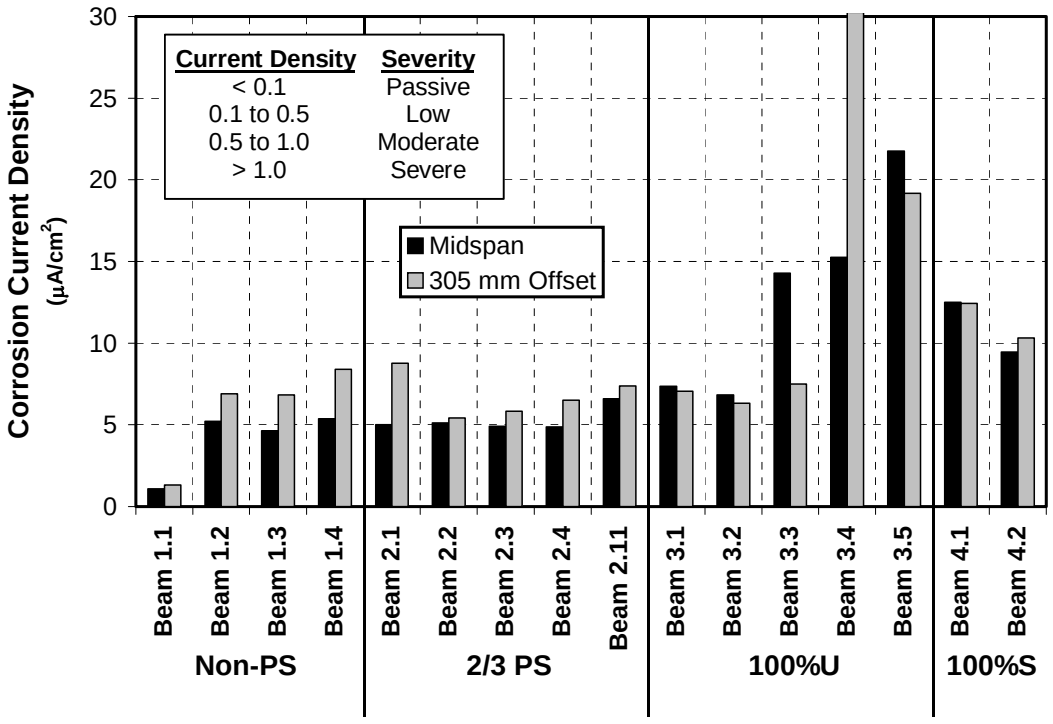

Figure 3.54 - Measured Corrosion Rates - Twelve Month Exposure Duration (3LP Equipment)

3.10.4.3 Fifteen Month Exposure Duration

Corrosion rate measurements were repeated after fifteen months of exposure testing using both the 3LP equipment and PR Monitor. Readings were taken sixteen days after the start of the dry portion of the exposure cycle (the dry period was extended beyond the normal two weeks because work was being performed on the beams). Corrosion current densities are plotted in Figure 3.55 and Figure 3.56 for the PR Monitor and 3LP, respectively (again, note the expanded scale in Figure 3.56 in comparison to Figure 3.55). All measured corrosion rates are summarized in Table 3.12.

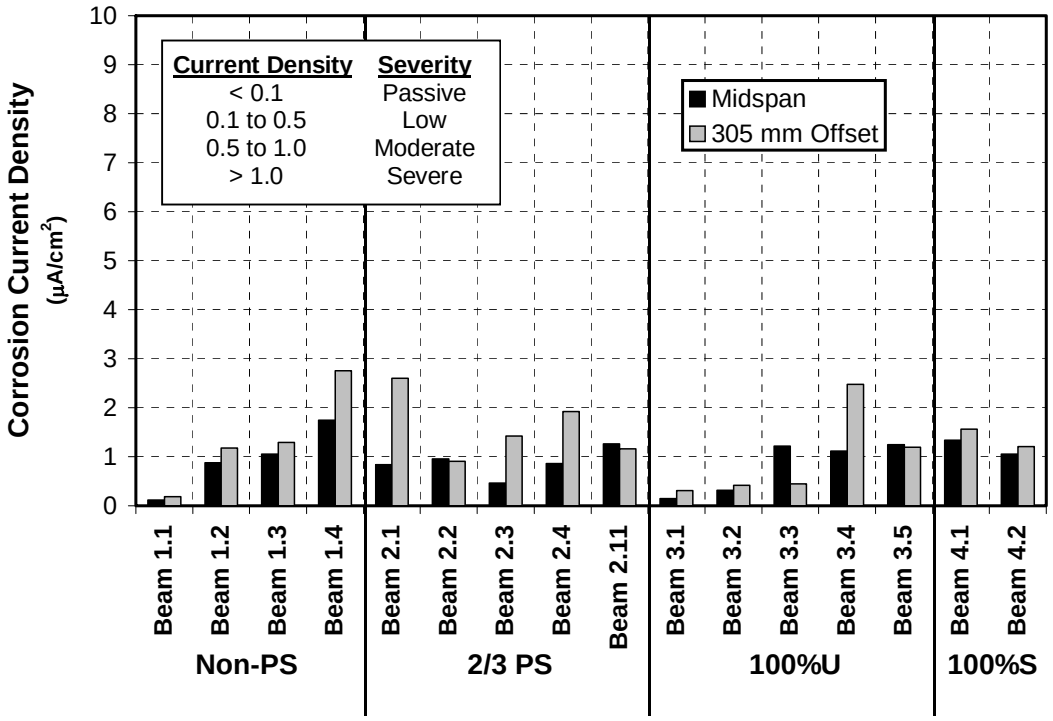

Figure 3.55 - Measured Corrosion Rates - Fifteen Month Exposure Duration (PR Monitor Equipment)

PR Monitor corrosion rates are high for many of the beams. Low corrosion activity is indicated in Beams 1.1, 3.1 and 3.2 and for some readings in other beams. The

fifteen month data can be compared to the seven month PR Monitor data shown previously in Figure 3.53. While many relative trends are similar (Beam 1.1 is very low and corrosion rates for the 100%U PS and 100%S PS beams are comparable to or higher than those for the 2/3 PS and Non-PS beams), the differences between the groups are much smaller. The corrosion rates for the 100%U PS and 100%S PS beams are greatly reduced from the seven month values.

The fifteen month 3LP data shows very high corrosion rates for all beams with the exception of Beam 1.1. Measured corrosion rates at fifteen months have decreased for several beams in comparison to the twelve month data shown previously in Figure 3.54. In general, the 3LP data is much more consistent between the twelve and fifteen month data. The overall trends in relative corrosion rates between beams at fifteen months are comparable to the data measured after twelve months.

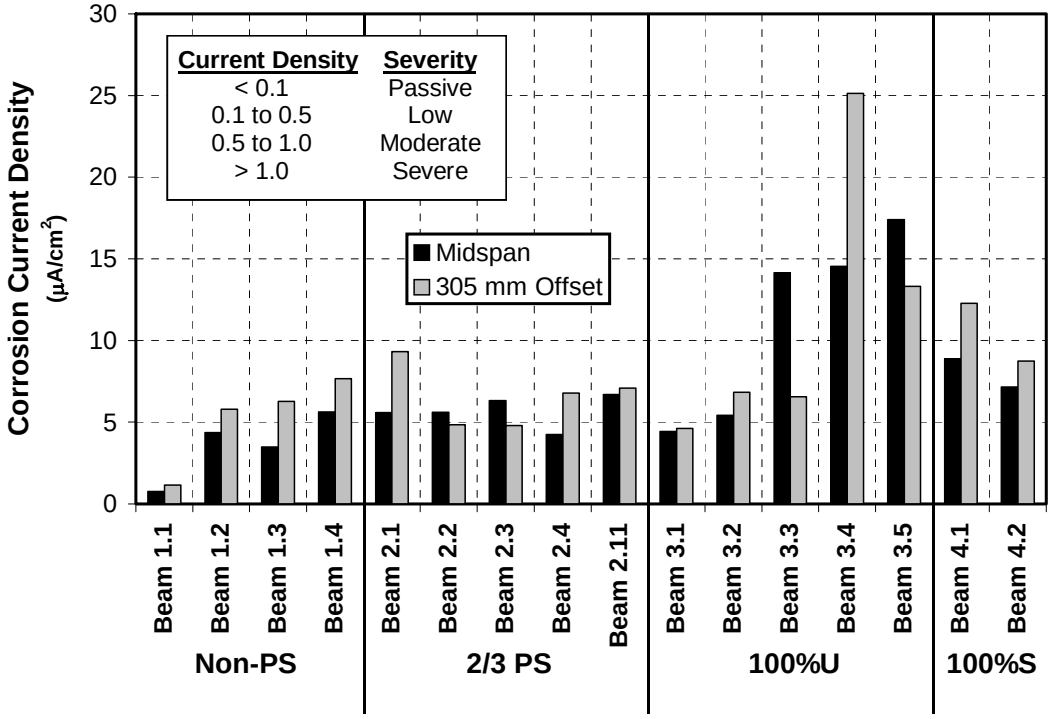

Figure 3.56 - Measured Corrosion Rates - Fifteen Month Exposure Duration (3LP Equipment)

Table 3.12 – Summary of Beam Corrosion Current Density Measurements

Specimen	Location	7 months PR Monitor μA/cm²	12 months 3LP μA/cm²	15 months PR Monitor μA/cm²	15 months 3LP μA/cm²
Beam 1.1	Midspan	0.18	1.09	0.12	0.76
	Offset	0.17	1.31	0.19	1.15
Beam 1.2	Midspan	0.65	5.22	0.88	4.37
	Offset	0.85	6.89	1.18	5.79
Beam 1.3	Midspan	1.01	4.64	1.06	3.50
	Offset	3.70	6.83	1.29	6.29
Beam 1.4	Midspan	no reading	5.37	1.74	5.64
	Offset	no reading	8.39	2.75	7.66
Beam 2.1	Midspan	0.47	5.00	0.84	5.58
	Offset	0.89	8.76	2.60	9.32
Beam 2.2	Midspan	0.85	5.12	0.95	5.61
	Offset	0.86	5.43	0.91	4.86
Beam 2.3	Midspan	1.15	4.93	0.47	6.32
	Offset	1.64	5.85	1.43	4.79
Beam 2.4	Midspan	0.94	4.88	0.86	4.25
	Offset	1.36	6.50	1.92	6.78
Beam 2.11	Midspan	2.33	6.61	1.26	6.70
	Offset	1.43	7.39	1.16	7.08
Beam 3.1	Midspan	0.61	7.37	0.14	4.44
	Offset	0.59	7.06	0.31	4.62
Beam 3.2	Midspan	0.68	6.84	0.31	5.43
	Offset	0.65	6.33	0.42	6.83
Beam 3.3	Midspan	1.78	14.27	1.21	14.14
	Offset	0.45	7.50	0.45	6.56
Beam 3.4	Midspan	1.14	15.25	1.12	14.53
	Offset	3.05	30.26	2.47	25.14
Beam 3.5	Midspan	1.40	21.77	1.24	17.41
	Offset	1.23	19.18	1.19	13.31
Beam 4.1	Midspan	2.14	12.51	1.34	8.88
	Offset	1.46	12.44	1.56	12.28
Beam 4.2	Midspan	3.90	9.47	1.06	7.16
	Offset	3.45	10.31	1.21	8.75

3.11 Analysis and Discussion of Results

3.11.1 Cracking Due to Applied Loading

The cracking behavior of the various beam types was described in Section 3.8.3. The prediction of the cracking moment and surface crack widths is discussed in more detail in the following sections.

3.11.1.1 Cracking Moment Prediction

The modulus of rupture for concrete is normally calculated based on the concrete cylinder strength as follows:

$$f_r = 0.62\sqrt{f'_c} \quad \text{(MPa)}$$
$$= 7.5\sqrt{f'_c} \quad \text{(ksi)} \qquad \textbf{Eq. 3.5}$$

The cracking moment for each beam specimen was computed using the calculated using the average concrete cylinder strength for each beam and the calculated modulus of rupture (Eq. 3.5). Concrete strength and cracking moment data is shown in Table 3.13 for all beams. Eq. 3.5 is a conservative estimate of modulus of rupture, and as a result, the calculated cracking moments were consistently lower than the cracking moments obtained during testing. Measured cracking moments ranged from very close to the estimated value to 31% higher than the estimated values. On average, the measured values were 1.11 times the estimated cracking moments.

The measured cracking moments were used to back-calculate the apparent modulus of rupture for each beam. This data is also listed in Table 3.13. The ratio of the modulus of rupture to the square root of the cylinder strength is normally taken as 7.5 in U.S. Customary Units (see Eq. 3.5). The corresponding value in metric is 0.62. Calculated values of this ratio are shown in Table 3.13. For metric units, the calculated ratio ranges from 0.62 to 0.86. In U.S. units, the range is 7.5 to 10.4. Given this range, it appears that the accepted values used in Eq. 3.5 are conservative and appropriate.

Table 3.13 - Cracking Moments and Concrete Strengths for All Beams

Beam	Cylinder Strength, f'_c (MPa)	f_r (Eq. 3.5) (MPa)	Cracking Moment Calculated (kN-m)	Measured (kN-m)	Meas/Calc	Apparent f_r (MPa)	$f_r/\sqrt{f'_c}$
1.2	35.9	3.7	118.9	150.3	1.26	4.7	0.79
1.3	35.9	3.7	118.9	142.9	1.20	4.5	0.75
1.4	33.2	3.6	115.0	150.3	1.31	4.7	0.81
2.1	33.2	3.6	239.9	262.7	1.10	4.3	0.75
2.2	33.2	3.6	239.9	244.0	1.02	3.7	0.65
2.3	41.4	4.0	251.2	255.3	1.02	4.1	0.64
2.4	41.4	4.0	251.2	262.7	1.05	4.4	0.68
2.11	41.4	4.0	251.2	255.3	1.02	4.1	0.64
3.3	37.0	3.8	310.5	310.7	1.00	3.8	0.62
3.4	39.7	3.9	314.3	356.7	1.13	5.4	0.86
3.5	39.7	3.9	314.3	337.8	1.07	4.7	0.75
				Avg.	1.11	Avg.	0.723
				Std. Dev.	0.10	Std. Dev.	0.076

3.11.1.2 Surface Crack Width Prediction

The measured applied moment – crack width relationship is plotted in Figure 3.57, Figure 3.58 and Figure 3.59 for the Non-PS, 2/3 PS and 100%U PS beams, respectively. Also shown in the plots are estimated crack widths using several different methods, including Gergely-Lutz,[3.6,3.7] CEB-FIP 1978 and 1990 Model Codes,[3.33,3.34] Batchelor and El Shahawi,[3.35] and Suri and Dilger[3.36] (each method was presented in Chapter 2). The Batchelor and El Shahawi and Suri and Dilger expressions were developed for partially prestressed concrete members only, and thus were not compared to the data for the Non-PS beams (Series 1).

The Gergely-Lutz expression provides a very good estimate of maximum surface crack width in the Non-PS beams (Series 1), as shown in Figure 3.57. The CEB-FIP 1978 Model Code (MC 78) underestimates crack widths at low load levels, and overestimates crack widths at service load levels. The CEB-FIP 1990 Model Code (MC 90) consistently underestimates the crack widths and is unconservative.

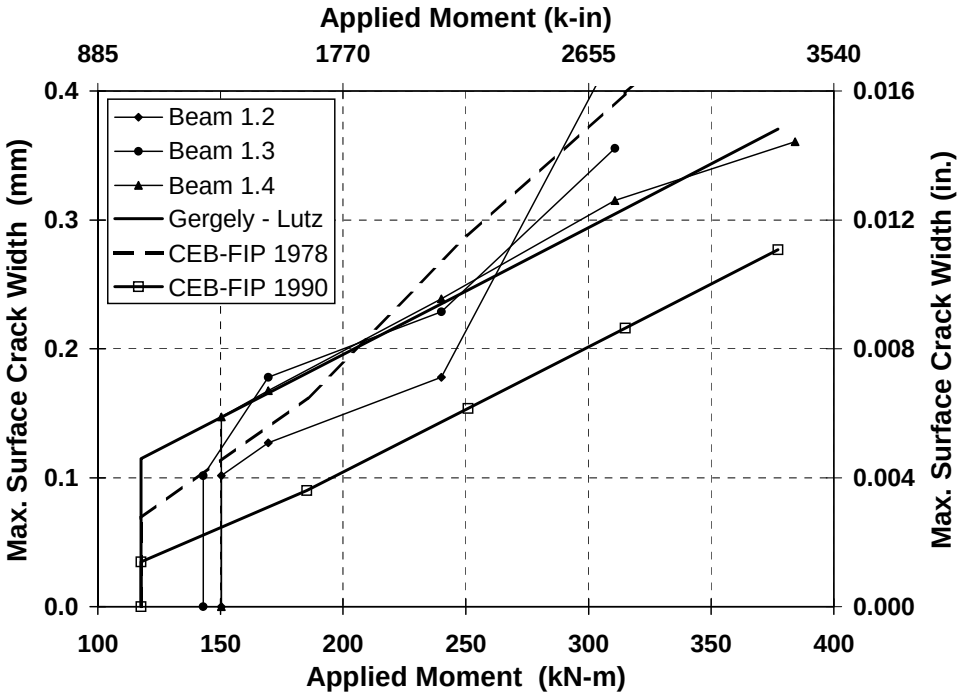

Figure 3.57 -Moment - Crack Width Relationship for Non-PS Beams

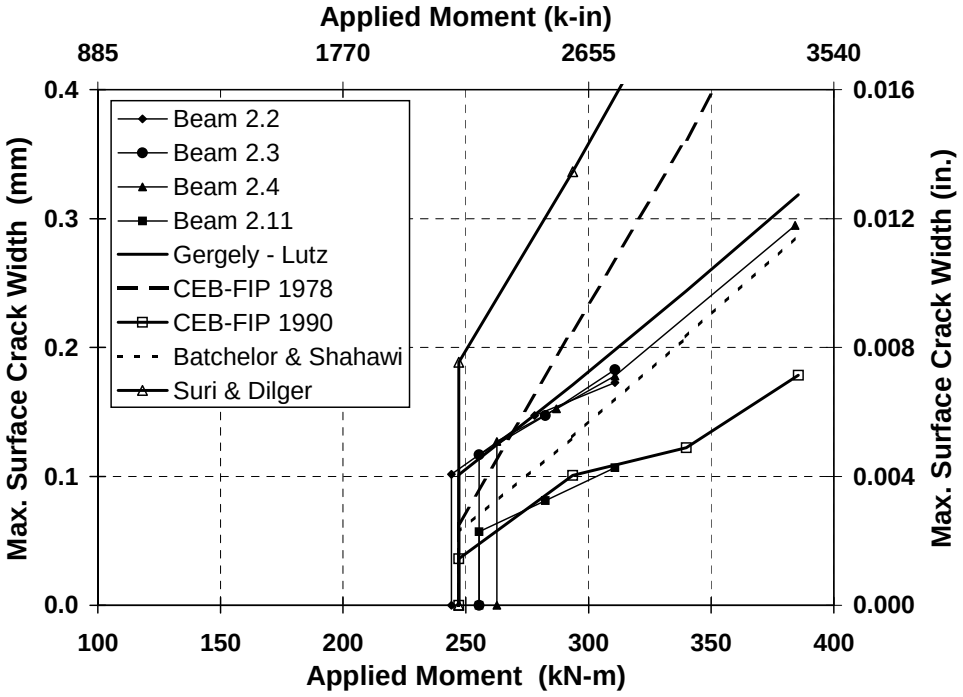

Figure 3.58 - Moment - Crack Width Relationship for 2/3 PS Beams

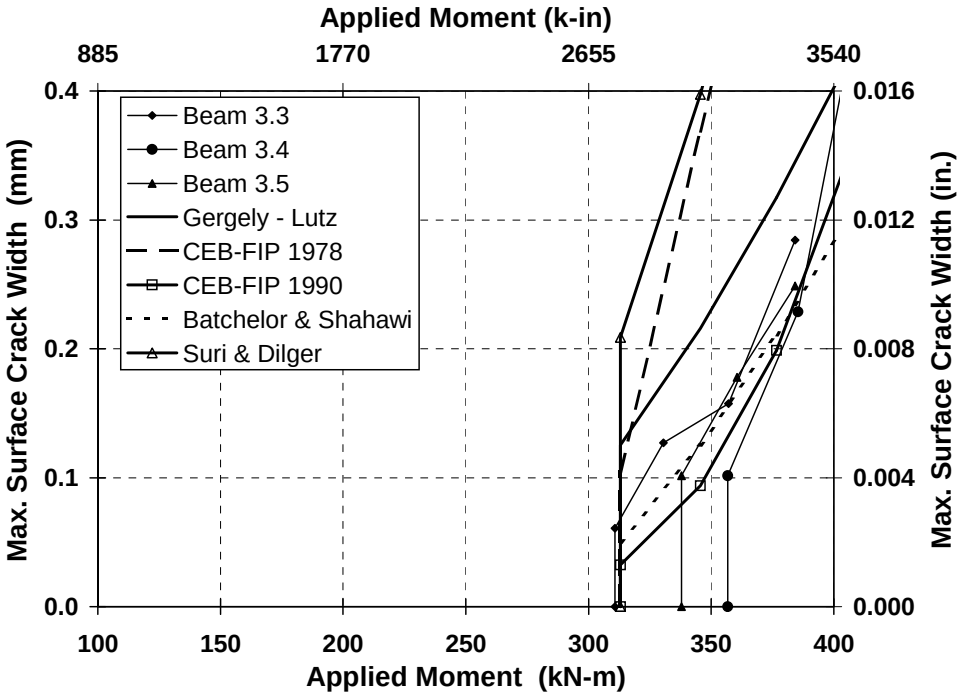

Figure 3.59 -Moment - Crack Width Relationship for 100%U PS Beams

The Gergely-Lutz expression provides an excellent estimation of surface crack width for the 2/3 PS beams. The MC 78 method and Suri and Dilger expression significantly overestimate the surface crack widths, and do not appear to be appropriate. The MC 90 method again underestimates crack widths by a sizeable margin. The Batchelor and El Shahawi expression provides a reasonably good prediction for crack widths, particularly at higher load levels.

The Batchelor and El Shahawi expression and MC 90 method provide the most accurate prediction of surface crack widths for the 100%U PS beams. The Gergely-Lutz expression overestimates the crack widths by a moderate margin. The MC 78 method and Suri and Dilger expression significantly overestimate the surface crack widths, and do not appear to be appropriate for the 100%U PS beams.

3.11.1.3 Evaluation of Prediction Methods

The basis for each of the crack width prediction methods is listed Table 3.14. Many crack width prediction methods are based on a statistical analysis of test data, including three of the five methods evaluated.

Table 3.14 - Crack Prediction Methods

Method	Basis	Variables Used
Gergely-Lutz	regression analysis	stress in non-prestressed reinforcement, concrete cover, area of concrete in tension around each reinforcing bar
CEB-FIP 1978 Model Code	basic principles (refined using test data)	avg. tension steel strain (accounting for tension stiffening), crack spacing, concrete cover, bar spacing, bar diameter, tension steel area, area of concrete in tension, strain profile in tension zone, tensile strength of concrete
CEB-FIP 1990 Model Code	basic principles (refined using test data)	length over which slip between steel and concrete occurs, difference between average steel and concrete strains (within length of slip), tension steel area, area of concrete in tension, tensile strength of concrete, bar diameter, bond stress
Batchelor and El Shahawi	regression analysis	stress in non-prestressed reinforcement
Suri and Dilger	regression analysis	stress in non-prestressed reinforcement, concrete cover, total tension steel area, area of concrete in tension

The accuracy of models based on regression analysis is highly dependent on the data considered and statistical methods used. It is apparent from Table 3.14 that the

variables used in the regression models differ considerably in some cases. The CEB-FIP 1978 Model Code estimates crack width as a function of the average crack spacing and the average strain in the tension steel, accounting for tension stiffening of the concrete. The CEB-FIP 1990 Model Code takes a slightly different approach, using the length of steel near a crack over which slip between the concrete and steel occurs instead of average crack spacing, and using the difference between the average steel and concrete strains within the length of slip.

The differences between the crack prediction methods can lead to large differences in results, as apparent in Figure 3.57, Figure 3.58 and Figure 3.59. In some cases it is possible to identify probable sources of error between the predicted and measured crack widths. Each crack prediction method is examined below.

Gergely-Lutz Expression[3.6,3.7]

The Gergely-Lutz crack width expression is based on a statistical analysis of a large set of test data from six different experimental investigations. All of the test data was for reinforced (non-prestressed) concrete members. The Gergely-Lutz expression provided an excellent estimation of maximum surface crack width for the Non-PS and 2/3 PS beam types in this testing program. Maximum crack widths for the 100%U PS beam type were overestimated by a moderate margin. The most likely source of error in prediction of crack widths for the 100%U PS beam type is the effective area of concrete in tension surrounding the tension reinforcement (see Section 2.8). Some of the calculation data is shown in Table 3.15 for the three section types. The Gergely-Lutz expression is shown in Eq. 3.6 (notation is given in Section 2.8). The effective area of concrete in tension, A_e, is considerably larger for the 100%U PS section due to the smaller effective depth of tensile reinforcement (non-prestressed and prestressed steel). It is possible that the effective area of concrete in tension is overestimated, leading to an overestimation of crack width. The height of the effective area of concrete in tension is almost one-third of the section depth for the 100%U PS section. Other crack width prediction methods, including MC 90, limit the height of the effective area of concrete in tension to $(h - c)/3$. This suggests that the Gergely-Lutz method could be overestimating the effective area of concrete in tension for the 100%U PS beam type.

$$w = 0.076\frac{h_2}{h_1} f_s (d_c A)^{1/3} = 0.076\left(\frac{h-c}{d-c}\right) f_s \left(d_c \frac{A_e}{m}\right)^{1/3} \quad \text{(units of 0.001 in.)} \qquad \textbf{Eq. 3.6}$$

Table 3.15 – Calculation Data for Gergely-Lutz Crack Width Expression

Variable	Non-PS	2/3 PS	100%U PS
effective area, A_e	55,742 mm²	69,677 mm²	83,613 mm²
effective depth, d	549 mm	536 mm	515 mm
height of effective area: 2(h – d)	121 mm (0.20h)	148 mm (0.24h)	190 mm (0.31h)
# bars and strands, m	8 bars	8 bars + 4 strands	2 bars + 6 strands
A_e/m	274 mm	229 mm	411 mm

CEB-FIP Model Code 1978[3.33]

The CEB-FIP Model Code 1978 (MC 78) method overestimated crack widths at most load levels for the three section types investigated. The MC 78 crack width model is based on the average crack spacing and average steel strain (accounting for tension stiffening), as shown in Eq. 3.7 (notation is given in Section 2.8). Selected measured and calculated crack width data is shown in Table 3.16.

$$w_k = S_m \varepsilon_{sm} \qquad \textbf{Eq. 3.7}$$

Table 3.16 – Selected Data for MC 78 Crack Width Expression

Variable	Non-PS	2/3 PS	100%U PS
applied moment	310 kN-m	310 kN-m	360 kN-m**
calculated crack spacing, S_m	167 mm	183 mm	295 mm
measured crack spacing, S_{meas}	135 mm	312 mm	574 mm
average steel strain, ε_{sm}	0.00137	0.00087	0.00092
maximum steel strain, ε_{s2}	0.00160	0.00107	0.00105
calculated crack width, w_c	0.39 mm	0.27 mm	0.46 mm
measured crack width, w_{meas}	0.36 mm	0.18 mm	0.19 mm
w_{meas}/S_{meas}	0.00267	0.00058	0.00033

**** Note:** The higher load level for the 100%U PS section corresponds to the moment required for multiple crack formation.

The relationship between measured crack width, measured crack spacing and calculated average steel strain is not a direct relationship for the three section types (levels of prestress) investigated in this testing program. As the level of prestress increases, the error in calculated crack width increases. If the measured crack spacing is substituted for the calculated crack spacing, the error in calculated crack widths will be even larger.

MC 78 appears to have two major deficiencies that make it unsuitable for estimating crack widths for a combination of mild steel and prestressed reinforcement. First, the average crack spacing is increasingly underestimated as the level of prestress increases. The error was almost 100% for the 100%U PS section. Second, the approach seems to be fundamentally flawed in that a direct relationship between crack width, crack spacing and average steel strain does not exist over a range of prestress.

CEB-FIP Model Code 1990[3.34]

The CEB-FIP Model Code 1990 (MC 90) method provided a very good estimate of crack widths for the 100%U PS section. Calculated crack widths for the Non-PS and 2/3 PS sections were consistently underestimated. The MC 90 crack width model is based on the length over which slip occurs between the steel and concrete near a crack and the difference between the average steel and concrete strains within this length, as shown in Eq. 3.8 (notation is given in Section 2.8). The term ($\varepsilon_{s2} - \beta\varepsilon_{sr2}$) represents the difference between steel and concrete strains within the length of slip, accounting for tension stiffening. Selected calculated and measured crack width data is shown in Table 3.17.

$$w_k = L_{max}(\varepsilon_{sm} - \varepsilon_{cm}) = L_{max}(\varepsilon_{s2} - \beta\varepsilon_{sr2}) \qquad \textbf{Eq. 3.8}$$

The basic concept for the MC 90 model appears more appropriate for mixed reinforcement elements than the MC 78 model. The length of slip (L_{max}) approach appears to better represent the actual cracking behavior for the levels of prestress investigated, particularly at higher prestress levels. The MC 90 model recognizes two different cracking conditions: single crack formation and stabilized cracking. Looking at the data in Table

3.17, the Non-PS beam type reaches the stabilized cracking condition soon after exceeding the cracking moment. In contrast, the 100%U PS section remained in the single crack formation condition over the range of loading investigated. This predicted behavior correlates well with observed crack formation where the Non-PS beams rapidly developed a large number of closely spaced cracks and the 100%U PS beams developed only three widely spaced cracks. The MC 90 expressions for determining L_{max} also account for the different bond properties of mild steel bars and prestressing steel.

Table 3.17 – Selected Data for MC 90 Crack Width Expression

$M_{applied}$ (kN-m)		L_{max} (mm)	Crack Type	ε_{s2}	ε_{sr2}	w_{calc} (mm)	w_{meas} (mm)
Non-PS							
M_{cr}	117.6	144	Single	0.00060	0.00079	0.035	0.070
	185.1	188	Stabilized	0.00095	0.00079	0.090	0.186
	250.9	188	Stabilized	0.00129	0.00079	0.154	0.264
M_{serv}	310.7	188	Stabilized	0.00160	0.00079	0.212	0.318
	377.1	188	Stabilized	0.00194	0.00079	0.277	0.367
2/3 PS							
M_{cr}	247.1	169	Single	0.00054	0.00147	0.036	0.107
	293.5	274	Single	0.00092	0.00164	0.101	0.160
M_{serv}	310.7	231	Stabilized	0.00107	0.00164	0.099	0.178
	339.8	231	Stabilized	0.00132	0.00164	0.122	0.206
	385.5	257	Stabilized	0.00174	0.00181	0.178	0.245
100%U PS							
$M_{cr,serv}$	313.0	163	Single	0.00050	0.00775	0.032	0.067
	345.5	262	Single	0.00089	0.00870	0.094	0.123
	376.6	372	Single	0.00134	0.00870	0.199	0.222
	406.7	484	Single	0.00182	0.00965	0.353	0.392

In spite of providing a better representation of the actual cracking behavior in terms of crack formation, the MC 90 model underestimates crack widths for the Non-PS and 2/3 PS beam types. As a concept, the MC 90 approach appears very good. However, many simplifications have been made in the model to facilitate hand calculation. Most notable are ε_{sr2} (cracked section steel strain at M_{cr}) and the steel stresses (σ_{s2} and $\Delta\sigma_p$)

under the desired loading. In addition, some of the calculations were derived for tension members and have been simply applied to flexural members. It is not clear whether the model has been calibrated for the simplified hand calculations. This could possibly lead to errors if more precise methods are used to determine the necessary stresses and strains.

Another possible source of difference between the estimated and measured crack widths is the strains used in Eq. 3.8. Many assumptions and approximations were necessary for the development of the tension stiffening model used to determine the strains influencing cracking. The term ($\varepsilon_{s2} - \beta\varepsilon_{sr2}$) in Eq. 3.8 represents the difference between the average steel and concrete strains within the length of slip. The variable β is an integration factor for the steel strain along the slip length, and is taken as 0.6 in most situations. Based on the calculated values of L_{max}, it appears that the value of β could range from zero to 0.6. Test data for each beam type is plotted in Figure 3.60, Figure 3.61 and Figure 3.62 along with calculated crack widths using $\beta = 0$ and $\beta = 0.6$. The range of β provides an upper and lower bound for the measured data for each of the three beam types.

Conceptually, the CEB-FIP 1990 Model Code method for crack width prediction is appealing, as it addresses many factors often overlooked. However, in its present form the estimated crack widths were unconservative for most of the beams testing in this research program.

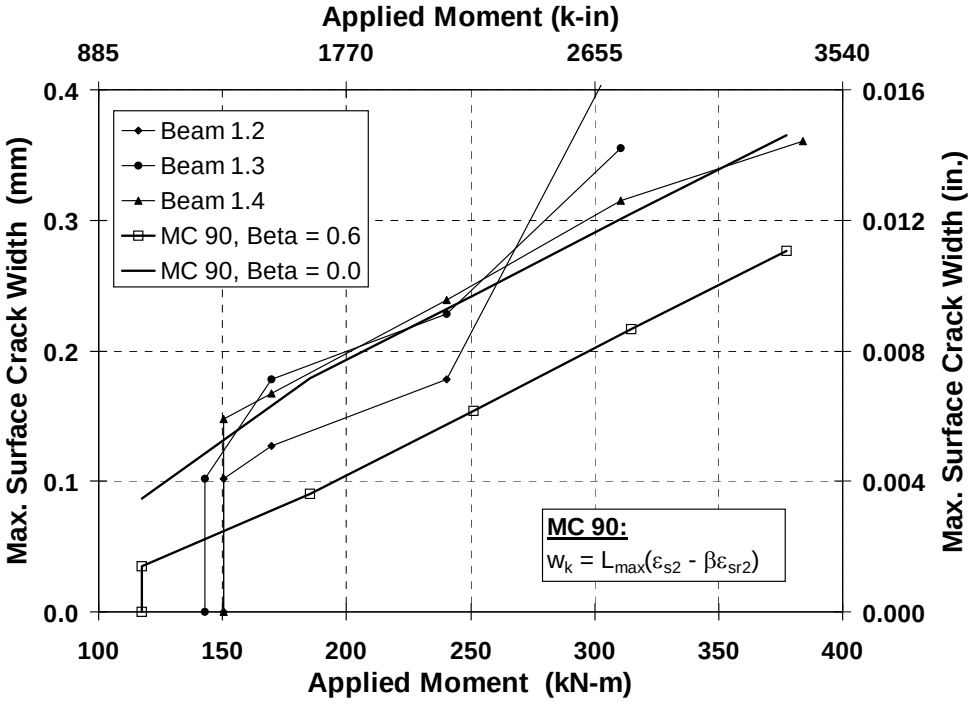

Figure 3.60 - MC 90: Upper and Lower Bound Crack Prediction for Non-PS Beams

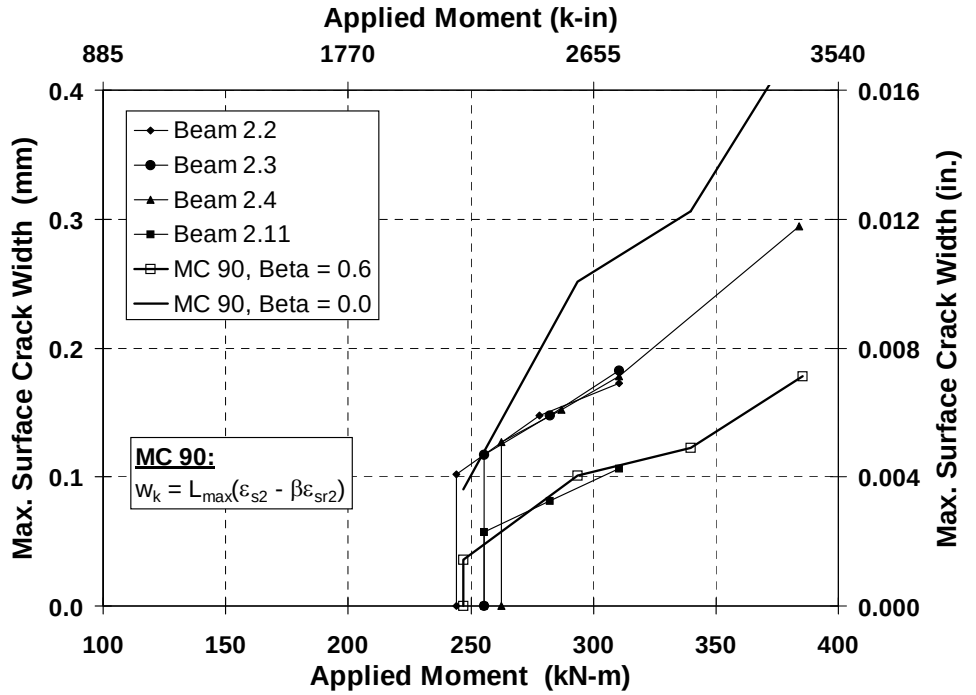

Figure 3.61 - MC 90: Upper and Lower Bound Crack Prediction for 2/3 PS Beams

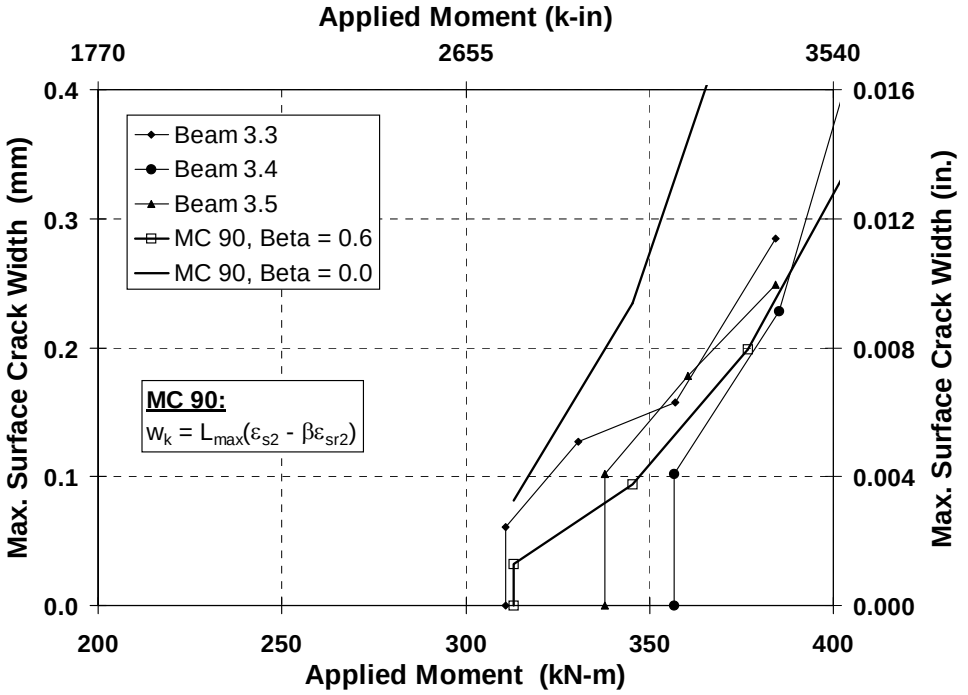

Figure 3.62 - MC 90: Upper and Lower Bound Crack Prediction for 100%U PS Beams

Batchelor and El Shahawi Expression[3.35]

The Batchelor and El Shahawi crack width expression is based on a statistical analysis of test data from five different experimental investigations of cracking in partially prestressed members. The Batchelor and El Shahawi expression, shown in Eq. 3.9, provided an excellent estimation of maximum surface crack width for the 2/3 PS and 100%U PS beam types. Notation for Eq. 3.9 is explained in Section 2.8. Batchelor and El Shahawi selected the simple form of Eq. 3.9 after concluding that the very large scatter of the test data did not justify a more complicated model. This simple model appears to be more than adequate for crack width prediction for the 2/3 PS and 100%U PS beam types.

$$w_{max} = \frac{0.96 f_s - 46}{1000} \quad \text{(mm)} \qquad \textbf{Eq. 3.9}$$

Suri and Dilger Expression[3.36]

The Suri and Dilger crack width expression is based on a statistical analysis of test data from 245 beams in eighteen different experimental investigations of cracking in partially prestressed members. The Suri and Dilger expression, shown in Eq. 3.10, significantly overestimated crack widths for the 2/3 PS and 100%U PS beam types. Notation for Eq. 3.10 is explained in Section 2.8.

$$w_{max} = k f_s c \left(\frac{A_t}{A_s + A_p} \right)^{0.5} \quad \text{(mm)} \qquad \textbf{Eq. 3.10}$$

It is difficult to determine any reasons for the poor performance of the Suri and Dilger expression. One possible explanation could be the variable A_t: the area of concrete in tension below the neutral axis. Most crack width prediction methods define the area of concrete in tension as only a portion of the concrete area below the neutral axis. MC 90 limits the effective area of concrete in tension to one-third of the concrete below the neutral axis. Overestimation of the concrete area in tension could account for overestimation of crack widths in the Suri and Dilger expression. In its present form, the Suri and Dilger does not appear to be suitable for the beam types investigated in this testing program.

3.11.2 Corrosion Rate Measurements

Several observations based on the corrosion rate measurements performed after seven, twelve and fifteen months of exposure testing are listed below. Discussion of the observations is provided in the following sections.

1. Moderate to high corrosion rates are indicated in the majority of test specimens by both the 3LP and PR Monitor equipment.
2. PR Monitor measurements at seven and fifteen months are similar in magnitude, as shown in Figure 3.63. The percent change from seven to fifteen months is plotted in Figure 3.64. Fifteen month data shows lower corrosion rates for several beams, particularly Beams 2.11, 3.1, 3.2 and 4.2.
3. 3LP measurements at twelve and fifteen months are also similar in magnitude, as shown in Figure 3.63, and indicate very high corrosion rates. Similar to the PR

Monitor data, fifteen month corrosion rates are lower for several beams in the 3 and 4 series (100%U PS and 100%S PS). The percent change from twelve to fifteen months is plotted in Figure 3.64. In general, the 3LP data is more consistent over time than the PR Monitor data.

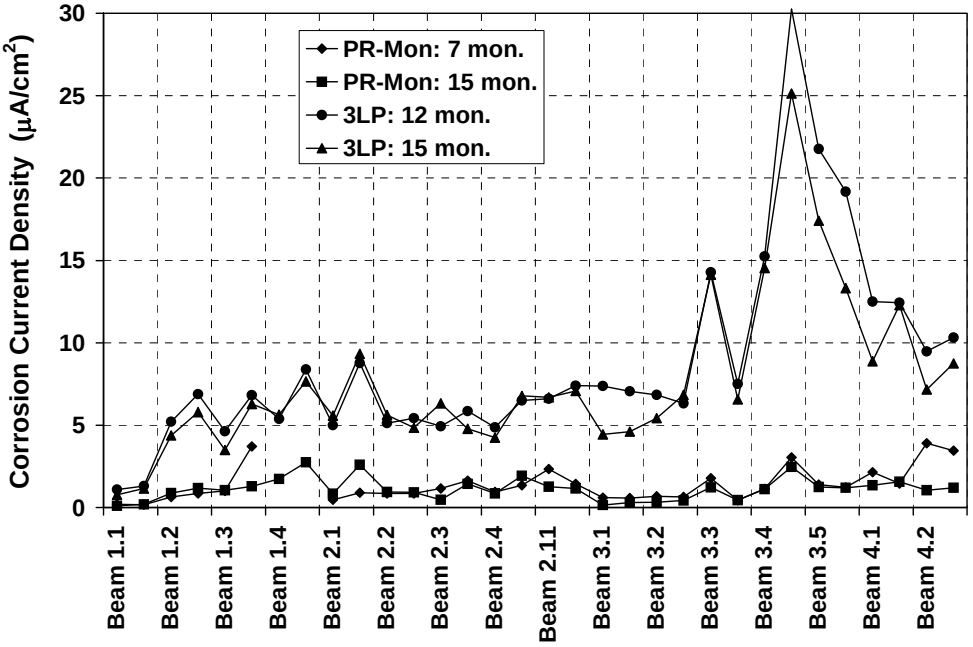

Figure 3.63 - Comparison of 3LP and PR Monitor Data

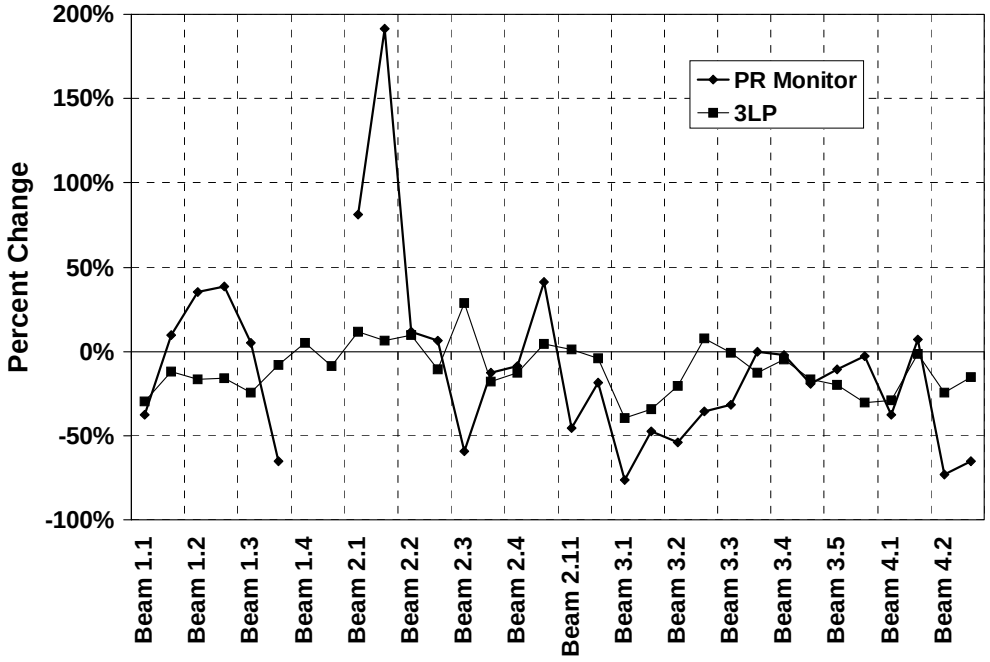

Figure 3.64 - Change in Measured Corrosion Rates Over Time (PR Monitor 7 to 15months, 3LP 12 to 15 months)

4. 3LP corrosion rates are consistently higher than PR Monitor corrosion rates, as shown in Figure 3.63. This observation, and observations 2 and 3 above, suggest that the 3LP data should not be directly compared to the PR Monitor data.
5. The measured corrosion rates indicate that corrosion activity is related to cracking. However, the data presents contradictory relationships:
    - Comparing the four series (levels of prestress), the measured corrosion rates tend to be highest in the specimens with more prestress and less cracking (Series 3 and 4, 100%U PS and 100%S PS respectively). These results are not intuitive and contradict the corrosion activity indicated by the half-cell potential readings.
    - Examining each series (level of prestress) individually, the results indicate that higher corrosion rates are associated with cracked concrete. These results are most pronounced in Series 1 and 3. Within the Non-PS beams (Series 1), the corrosion rate for Beam 1.1 (unloaded and uncracked) is much lower than the corrosion rates for the remaining Series 1 beams which are loaded and cracked. In 100%U PS beams (Series 3), Beam 3.1 and 3.2 are uncracked, while Beams 3.3, 3.4 and 3.5 are

cracked. Measured corrosion rates for Beams 3.1 and 3.2 are considerably lower than measured rates for the other Series 3 beams.

- Corrosion rate measurements on individual beams show higher corrosion rates at crack locations in comparison to uncracked locations. In Beams 2.1, 3.3, 3.4 and 3.5, crack patterns resulted in one reading at a crack location and one reading on uncracked concrete. In each case, the corrosion rate was higher for the measurement at the crack location. Seven and twelve month data is shown in Figure 3.65. These trends were also shown for fifteen month data.

Corrosion Rates (μA/cm²)		
Beam 2.1	**Midspan**	**Offset**
7 month	0.465	**0.893**
12 month	5.00	**8.76**
Beam 3.3	**Midspan**	**Offset**
7 month	**1.78**	0.447
12 month	**14.3**	7.50
Beam 3.4	**Midspan**	**Offset**
7 month	1.14	**3.05**
12 month	15.2	**30.3**
Beam 3.5	**Midspan**	**Offset**
7 month	**1.40**	1.23
12 month	**21.8**	19.2

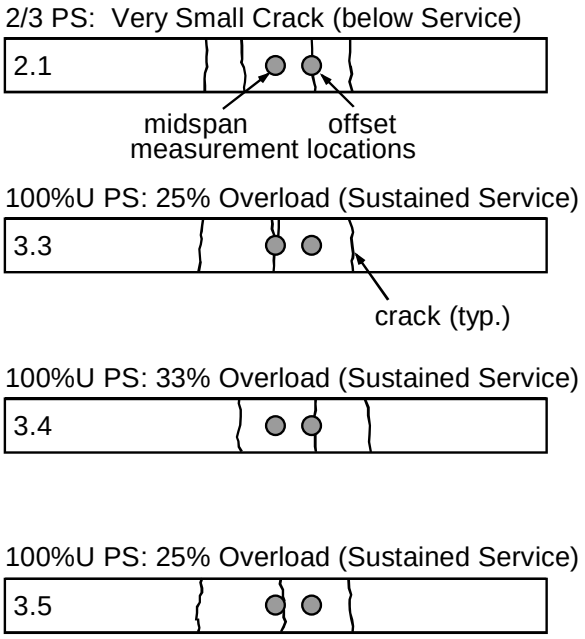

Figure 3.65 - Effect of Crack Location on Measured Corrosion Rate

3.11.2.1 High Corrosion Rates

Measured corrosion rates were very high, particularly those obtained using the 3LP device. The corrosion rate data illustrates the severe exposure conditions used in the test method. However, it is possible that the short dry period could contribute to overestimate corrosion rates if the moisture content of the concrete remained high during this short period. Elevated moisture content will decrease the resistivity of the concrete,

leading to higher corrosion rate measurements. Corrosion rates will decrease as the concrete dries out.

3.11.2.2 Changes in Corrosion Rates Over Time

The changes in corrosion rate over time can be examined by comparing the seven and fifteen month PR Monitor data (see Figure 3.63) and by comparing the twelve and fifteen month 3LP data (see Figure 3.63). The percent change for the PR Monitor and 3LP were shown previously in Figure 3.64.

The changes in measured corrosion rates over time are generally within +/- 50%, with corrosion rates decreasing more frequently than increasing. The largest measured increase occurred in Beam 2.1, where increases were almost 200% at the offset location. The 3LP data appears to be more consistent over time. This may be influenced by the shorter time period between readings for the 3LP readings. As mentioned previously, both the 3LP and PR Monitor data indicated a notable decrease in corrosion rate for several specimens, particularly Beams 3.1, 3.2 and 4.2. The changing moisture contents during the dry portion of the exposure cycle could possibly explain these lower corrosion rates at fifteen months. The fifteen month data was collected at the end of the two week dry portion of the exposure cycle, whereas the seven and twelve month data was collected midway through the dry period. It is possible that the longer dry period before the fifteen month measurements resulted in higher measured resistances and decreased corrosion activity in some specimens. This effect could be more pronounced for the uncracked specimens, including 3.1, 3.2 and 4.2.

The changes in measured corrosion rates for different specimens highlights the importance of regular measurements. In spite of the controlled environment (in comparison to structures in service), some corrosion rates increased and others decreased. Conclusions based on a single set of corrosion rate data should not be relied on to assess the condition of a specimen or structure.

3.11.2.3 Differences Between 3LP and PR Monitor Measured Corrosion Rates

The 3LP corrosion rates are significantly higher than the PR Monitor corrosion rates. The average difference for the fifteen month data was more than 700%, with maximum and minimum increases of 2968% and 178%, respectively (measured corrosion

rates for all specimens are listed in Table 3.12). The trends in corrosion activity indicated by the two devices are similar. This suggests that the large discrepancy in magnitude is likely due to inherent differences between the two devices.

The PR Monitor and 3LP equipment both use the three electrode technique for measuring polarization resistance. However, several differences exist between the two pieces of equipment. The 3LP equipment represents the first generation of polarization resistance equipment for measuring corrosion rates of steel in concrete. The PR Monitor reflects several advancements, including the use of a guard ring electrode to confine the polarizing signal of the counter electrode, and measurement of the concrete resistance to compensate for solution resistance. The possible effects of these differences are discussed below.

Polarized Area

The polarized area and the effect of the guard ring electrode could produce a significant difference between the 3LP and PR Monitor measurements. The unconfined counter electrode of the 3LP could lead to diffusion of the polarizing signal and a larger than expected polarized steel area. A larger polarized area would require more current to obtain the desired overvoltages, resulting in a lower polarization resistance and larger corrosion current, i_{corr}. If diffusion of the polarizing signal occurs but the polarized area is assumed to be that of the counter electrode, the corrosion rate or current density will be overestimated as shown in Figure 3.66.

The relationship between the polarized area and the measured polarization resistance is inversely proportional for a bar that is corroding uniformly. Thus, the error in the measured current density corresponds directly to the difference between the assumed polarized area and the actual polarized area. That is, if the actual polarized area is 50% larger than the assumed polarized area, the current density will be overestimated by 50%.

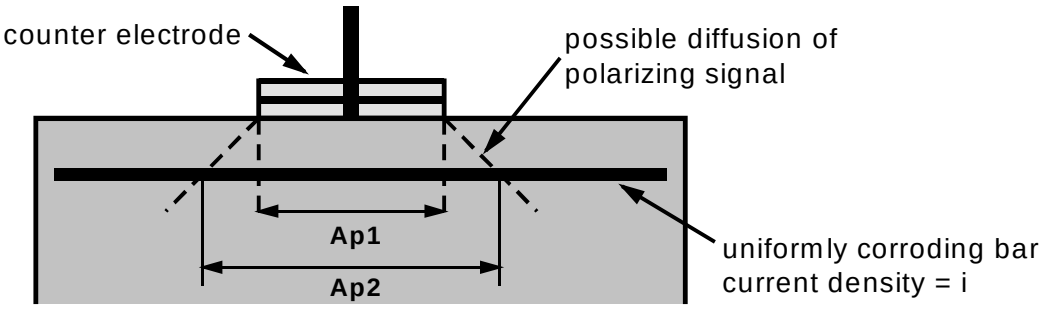

Case 1: Polarized area is A_{p1}

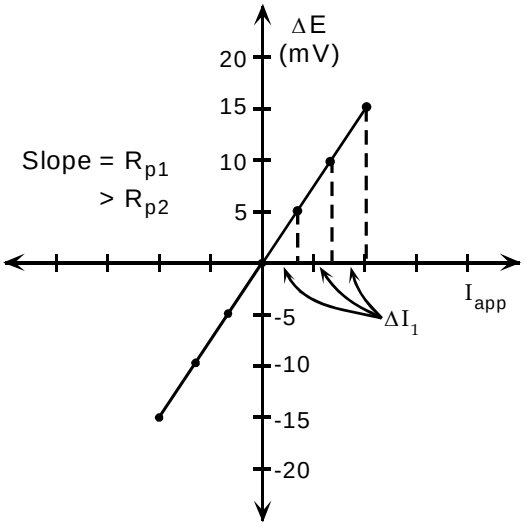

corrosion current, $i_{corr1} = \frac{B}{R_{p1}}$

current density, $i_1 = \frac{i_{corr1}}{A_{p1}} = \frac{B}{R_{p1}\,A_{p1}}$

Case 2: Assumed polarized area is A_{p1}, but actual polarized area is A_{p2}

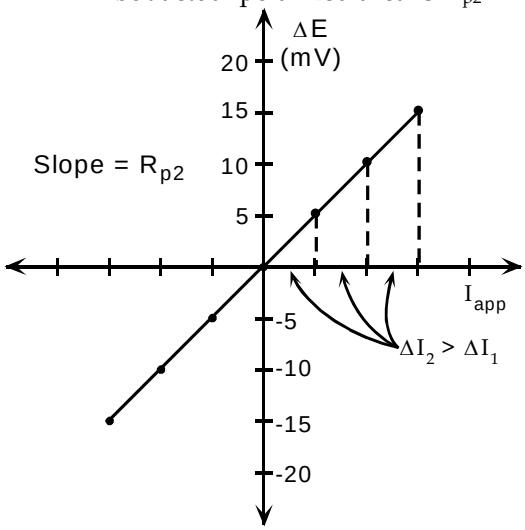

Since the polarized area is larger, more current is needed to polarize the steel. This results in a lower polarization resistance. As an example, assume $R_{p1} = 1.5\,R_{p2}$.

$$i_{corr2} = \frac{B}{R_{p2}} = \frac{1.5B}{R_{p1}}$$

$$i_2 = \frac{1.5B}{R_{p1}\,A_{p1}} \quad (A_{p1} \text{ assumed})$$

$\Rightarrow$ **$i_2 = 1.5 \times i_1$** **50% error**

Figure 3.66 - Overestimation of Corrosion Rate due to Unconfined Polarization

The unconfined signal in the 3LP equipment will almost certainly lead to an overestimation of the corrosion rate. The effect of diffusion of the polarizing current can be explored by assuming different diffusion profiles. Figure 3.67 shows the 100%U PS section with the 3LP counter electrode located directly over a stirrup. Projection lines are used to illustrate the assumed polarized area if diffusion of the polarizing signal occurred at 30 and 45 degrees. Figure 3.67 is not intended to suggest that the polarizing signal would diffuse linearly, but rather to indicate the effect of diffusion for polarized areas defined in this manner. The projected areas listed in Figure 3.67 are taken at a depth of 64 mm (2.5 in.) (clear cover to duct). The resulting polarized steel areas are listed in Table 3.18 for all four section types. The polarized areas for the 100%U PS and 100%S PS sections increase significantly since some portion of the ducts are now included. The last column of Table 3.18 lists the average difference between the 3LP and PR Monitor corrosion rates at fifteen months.

Table 3.18 – Polarized Steel Areas Assuming Diffusion of the Polarizing Signal

Section	Polarized Steel Area (mm^2)					Avg. Corr. Rate Increase**
	No Diffusion	30 deg. Projection	% increase	45 deg. Projection	% increase	
Non-PS	16,720	55,738	233%	67,392	303%	361%
2/3 PS	13,300	78,540	490%	146,438	1001%	483%
100%U PS	3,040	48,137	1483%	109,956	3517%	1440%
100%S PS	3,040	30,873	915%	109,956	3517%	612%

** Percent increase, 3LP over PR Monitor at 15 months exposure.

The data in Table 3.18 indicates that diffusion of the polarizing signal over an area equivalent to a 30 degree projection of the counter electrode could approximately account for the large difference between the 3LP and PR Monitor measurements. Although it is difficult to make any firm conclusions from the limited data, it does appear that diffusion of the polarizing signal in the 3LP equipment could have a significant effect on overestimation of the corrosion rates and could possibly account for the very large difference between 3LP and PR Monitor measurements.

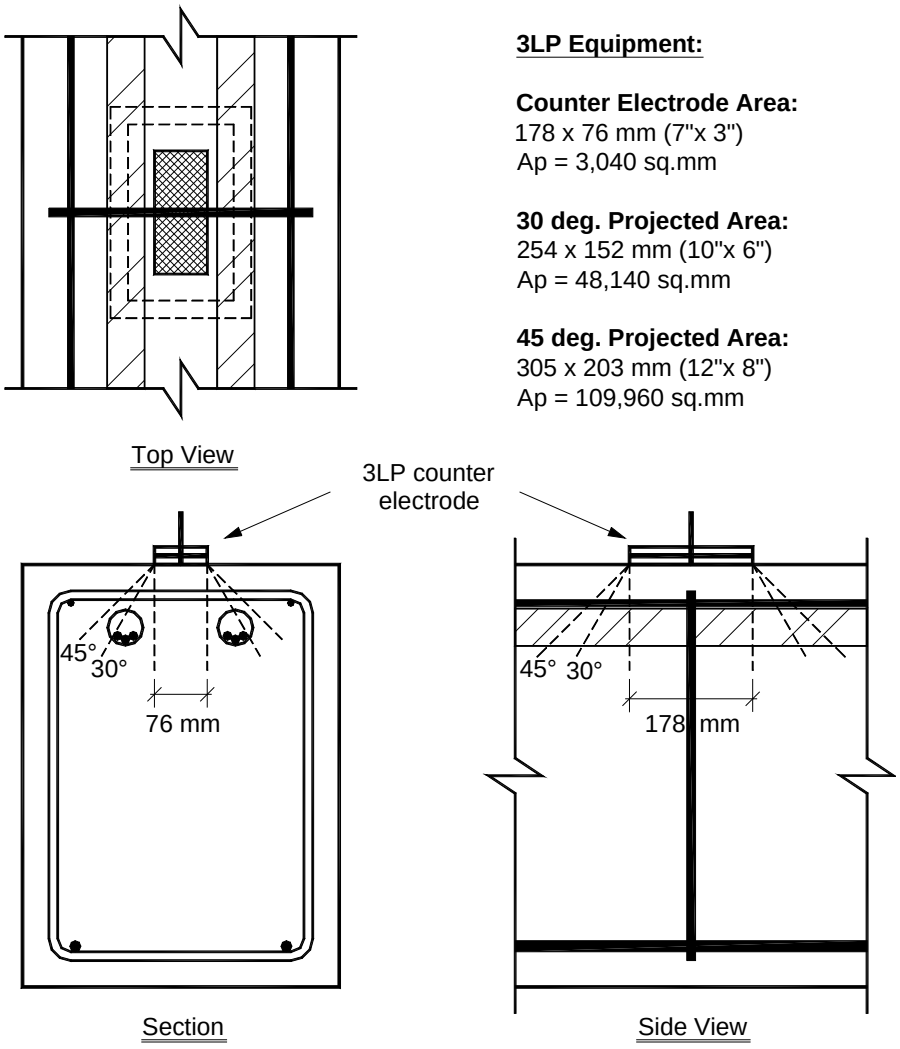

Figure 3.67 - 100%U PS Beam Type: Projected Areas for 3LP Counter Electrode

The importance of signal confinement can be further illustrated using the PR Monitor. A limited data set was collected to assess the effect of the guard ring electrode in the PR Monitor. Two corrosion rate measurements, one with the guard ring enabled and one with it disabled, were taken on two beams from each series. The measured corrosion rates are listed in Table 3.19. Measurements were taken at the beam midspan of the selected specimens. Additional measurements were taken at a 1.2 m (4 ft.) offset from midspan in two of the beams. For Beams 1.2 and 2.4, the effect of the guard ring was

negligible. However, for the remainder of the beams listed in Table 3.19, the effect of the guard ring is appreciable and the corrosion rates are considerably overestimated when the guard ring electrode is off. The effect is most pronounced in the 3 Series (100%U PS), where the error ranges from 67% to 124%. This supports the previous conclusion that the unconfined polarizing signal of the 3LP is possibly leading to overestimated corrosion rates.

Table 3.19 - PR Monitor: Effect of Guard Ring Electrode

Beam	Location	Corrosion Rate (μA/cm²)		% Difference
		Guard Ring On	Guard Ring Off	
Beam 1.2	Midspan	0.83	0.84	1.6%
Beam 1.4	Midspan	1.22	1.63	34.4%
Beam 1.4	1.2 m Offset	0.35	0.50	41.0%
Beam 2.2	Midspan	0.53	1.03	94.2%
Beam 2.4	Midspan	0.78	0.81	3.7%
Beam 3.2	Midspan	0.39	0.65	66.6%
Beam 3.5	Midspan	1.10	2.47	124.1%
Beam 3.5	1.2 m Offset	0.22	0.45	100.9%
Beam 4.1	Midspan	1.69	2.19	29.9%
Beam 4.2	Midspan	1.66	1.95	17.5%

Concrete Resistance Compensation

The PR Monitor uses AC impedance to assess the concrete or solution resistance, and adjusts the measured polarization resistance to account for this error (see Section 3.9.4.2). The 3LP equipment does not account for concrete resistance, and thus solution resistance could be a possible source of difference between the measured corrosion rates.

PR Monitor: $R_p = R_{tot} - R_s$ (R_s = solution resistance)

3LP: $R_p = R_{tot}$

Measured corrosion current and current density are inversely proportional to polarization resistance (see Eq. 3.1). If the solution resistance is not accounted for (as in the case of the 3LP), the assumed polarization resistance will be higher than the actual

polarization resistance. This will result in a measured corrosion rate lower than the actual rate. This would suggest that corrosion rate measurements obtained using the 3LP equipment could be too low or unconservative. However, the polarization resistances measured using the 3LP were consistently lower than those obtained with the PR Monitor, as shown in Figure 3.68 (data shown at fifteen months exposure). Since the corrosion rates obtained using the 3LP where significantly larger than those obtained using the PR Monitor (with compensation for solution resistance), it is difficult to make any conclusions regarding the effect of solution resistance on the measured corrosion rates. It is possible that the relatively moist condition of the concrete at the time of testing minimized the effect of solution resistance.

Relationship Between 3LP and PR Monitor Data

Other research and field experience with various devices for corrosion rate measurement has consistently shown that the 3LP equipment indicates corrosion rates higher than other devices. A number of corrosion rate measurements were performed on several bridges in Texas using the 3LP and PR Monitor.[3.37] The 3LP corrosion rates were consistently higher than the PR Monitor corrosion rates. A regression analysis indicated a linear relationship between the two data sets. However, due to the extremely limited data, it is not prudent to use this data further.

Another research study compared measured corrosion rates from several devices, including the 3LP, to known corrosion rates for laboratory test specimens.[3.25] A device known as GECOR (three electrode linear polarization device with solution resistance compensation) had corrosion rates very close to the actual rates. The 3LP device gave the highest corrosion rates. The researchers found a linear relationship between the logarithms of corrosion current measured by the two devices:[3.25,3.29]

$$\log(i_{GECOR}) = 0.92\log(i_{3LP}) - 0.90 \qquad \textbf{Eq. 3.11}$$

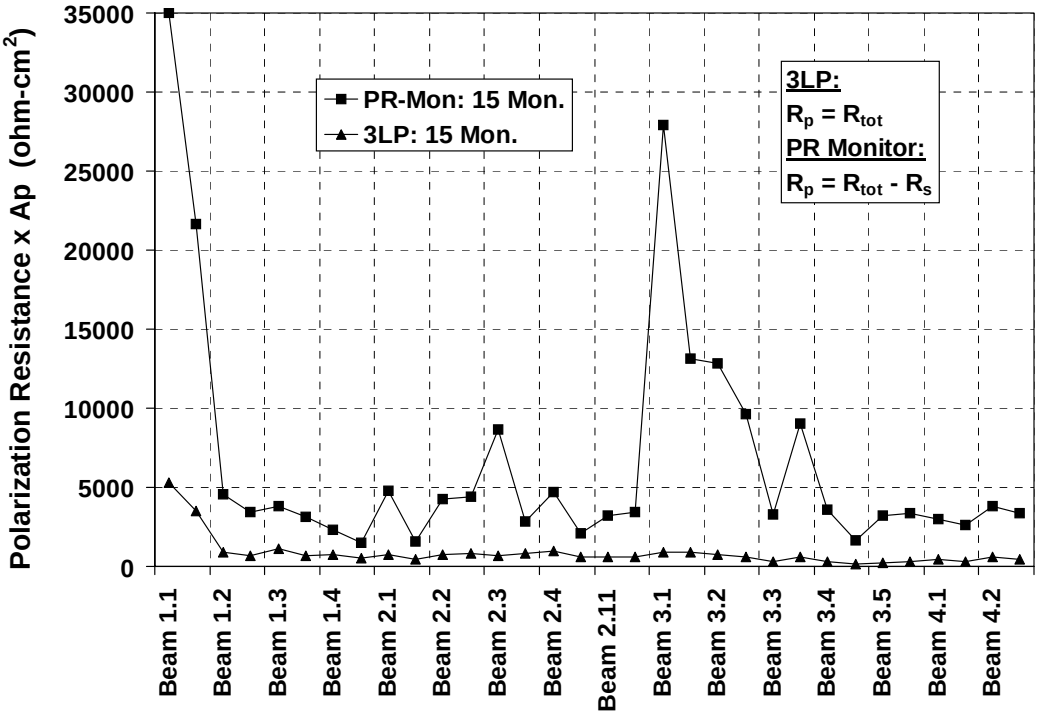

Figure 3.68 - Normalized Polarization Resistance Measured Using 3LP and PR Monitor

The corrosion rate data collected at fifteen months provides the opportunity for a direct comparison between the 3LP and PR Monitor data. When the entire data set is examined for a relationship between the two devices, the correlation is very poor. However, if each Beam Series is examined individually an approximate relationship can be determined. A linear regression analysis provided the best results. Correlation for the Non-PS and 2/3 PS beams is satisfactory, while correlation for the 100%U PS and 100%S PS beams is good. The calculated expressions are listed below.

Series 1, Non-PS: $i_{PR} = 0.3136(i_{3LP}) - 0.2277$ $(\mu A/cm^2)$ **Eq. 3.12**

Series 2, 2/3 PS: $i_{PR} = 0.3099(i_{3LP}) - 0.5560$ $(\mu A/cm^2)$ **Eq. 3.13**

Series 3, 100%U PS: $i_{PR} = 0.1022(i_{3LP}) - 0.2618$ $(\mu A/cm^2)$ **Eq. 3.14**

Series 4, 100%S PS: $i_{PR} = 0.09612(i_{3LP}) + 0.4014$ $(\mu A/cm^2)$ **Eq. 3.15**

Using Eq 3.11 and 3.12 through 3.15, calculated corrosion rates i_{GECOR} and i_{PR} were obtained using the 3LP data measured after fifteen months. The calculated corrosion rates are plotted together with the PR Monitor measured corrosion rates after fifteen months in Figure 3.69. The calculated PR Monitor values (i_{PR}) are similar to the measured data, indicating the reasonable accuracy of Eq. 3.12 to 3.15. The calculated GECOR values (i_{GECOR}) are lower than the measured PR Monitor data for Series 1 and 2, but similar for Series 3 and 4. The good correlation between the calculated GECOR and measured PR Monitor data lends credibility to the PR Monitor results, since the GECOR device had previously been found to give the best estimation of corrosion rates.[3.25]

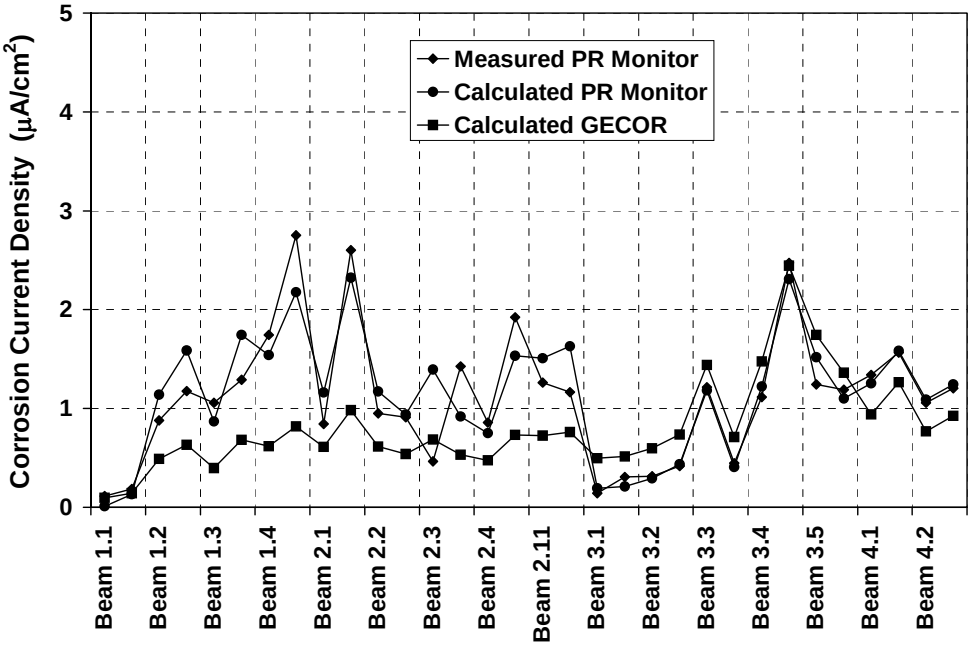

Figure 3.69 - Comparison of Measured and Calculated Corrosion Rates at 15 Months

The comparison of measured and calculated results makes it tempting to "correct" past and future 3LP data using Eq. 3.12 to 3.15. Figure 3.70 shows measured PR Monitor data at seven and fifteen months with calculated PR Monitor data at twelve months. The calculated twelve month data is based on the twelve month 3LP data and Eq. 3.12 to 3.15. The twelve month data significantly overestimates the corrosion currents for the Series 3 and 4 beams, illustrating the shortcomings of this approach. The conclusion to be drawn

from this comparison of data is that it is best to use a corrosion rate device with signal confinement, and it is important to account for solution resistance. That is, the PR Monitor should be used for future measurements. If this is not possible, the 3LP device could be used and the results "corrected" using the equations listed above. Correction of the 3LP data will improve the estimated corrosion rates, but it would be preferable to use the PR Monitor.

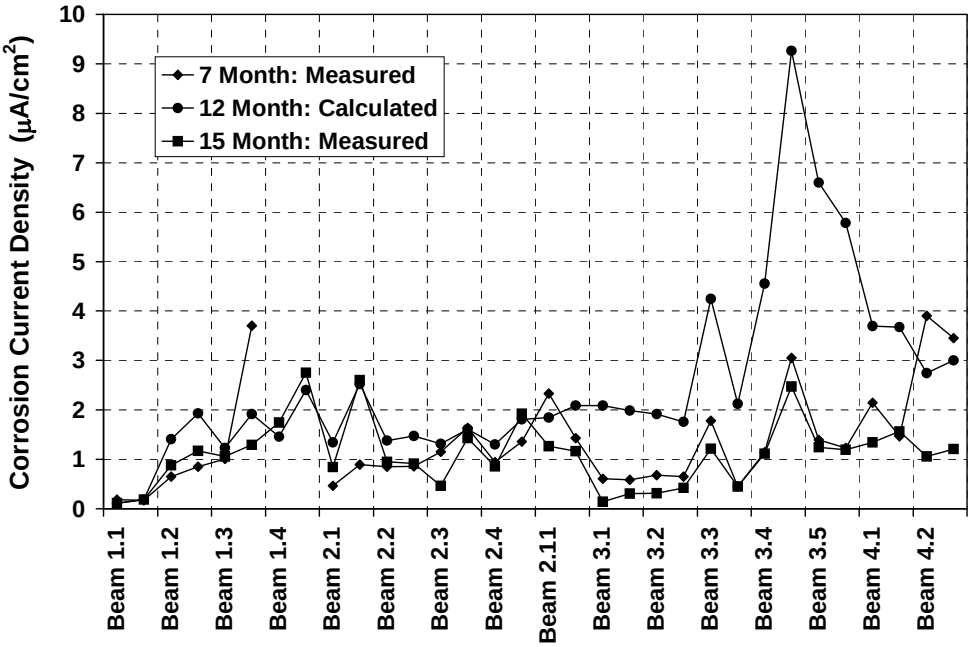

Figure 3.70 - Measured and Calculated PR Monitor Corrosion Rates

3.11.2.4 Effect of Cracks on Solution Resistance Measurement

The presence of cracks could affect the accuracy of the polarization resistance (total resistance) and the solution resistance measurements. Most guidelines for corrosion rate measurement suggest performing the tests on uncracked concrete.[3.25,3.29] The solution resistance measurements obtained from the PR Monitor appear to be influenced by the presence of cracks. Table 3.20 shows values of measured solution resistance for all specimens. Measured resistances at crack locations are consistently lower than readings at

uncracked locations. This trend is apparent by comparing cracked and uncracked beams, and also by comparing midspan and offset measurements on Beams 2.1, 3.3, 3.4 and 3.5.

In several cases, high corrosion rates measured by the PR Monitor occurred when the solution resistance was very close to the total measured resistance. Since the polarization resistance is computed as the difference between the measured total resistance and solution resistance, the polarization resistance was very low in these cases, leading to high corrosion rates. Errors in either the total resistance or solution resistance could lead to inaccurate corrosion rates and conclusions. The presence of cracks clearly has an effect on measurement of the polarization resistance and solution resistance. However, it is difficult to assess the effect of cracks on the accuracy of the estimated corrosion rates in the test data.

Table 3.20 - Effect of Cracking on Measured Solution Resistance (PR Monitor)

Beam	Location	Condition	Solution Resistance (Ohms)	
			7 Month	15 Month
Beam 1.1	**Midspan**	***Uncracked***	**1560**	**2904**
	Offset	***Uncracked***	**1339**	**1886**
Beam 1.2	Midspan	Cracked	605	644
	Offset	Cracked	424	598
Beam 1.3	Midspan	Cracked	397	580
	Offset	Cracked	No data	459
Beam 1.4	Midspan	Cracked	No data	249
	Offset	Cracked	No data	194
Beam 2.1	**Midspan**	***Uncracked***	**747**	**553**
	Offset	Cracked	508	291
Beam 2.2	Midspan	Cracked	573	460
	Offset	Cracked	471	514
Beam 2.3	Midspan	Cracked	459	602
	Offset	Cracked	427	536
Beam 2.4	Midspan	Cracked	618	654
	Offset	Cracked	330	336
Beam 2.11	Midspan	Cracked	350	401
	Offset	Cracked	322	326

Table 3.20 - Effect of Cracking on Measured Solution Resistance (PR Monitor) – Con't.

Beam	Location	Condition	Solution Resistance (Ohms)	
			7 Month	15 Month
Beam 3.1	**Midspan**	***Uncracked***	**1547**	**4216**
	Offset	***Uncracked***	**1118**	**3066**
Beam 3.2	**Midspan**	***Uncracked***	**923**	**1738**
	Offset	***Uncracked***	**942**	**1553**
Beam 3.3	Midspan	Cracked	652	796
	Offset	***Uncracked***	**1137**	**1682**
Beam 3.4	**Midspan**	***Uncracked***	**757**	**910**
	Offset	Cracked	367	480
Beam 3.5	Midspan	Cracked	524	685
	Offset	***Uncracked***	**641**	**894**
Beam 4.1	**Midspan**	***Uncracked***	**1166**	**1365**
	Offset	***Uncracked***	**877**	**1197**
Beam 4.2	**Midspan**	***Uncracked***	**753**	**833**
	Offset	***Uncracked***	**1062**	**1353**

3.11.3 Effect of Cracking and Level of Prestress

3.11.3.1 Half-Cell Potential Readings

The reported half-cell readings indicate that the level of corrosion activity is related to the amount of cracking. The measured potentials have been averaged for each series (prestress level) and are plotted in Figure 3.71. The highest (most negative) half cell potentials were measured for the Non-PS beams under service loading. Potentials become less negative as the level of prestress is increased. These measurements suggest that control of cracking can reduce corrosion activity and improve corrosion protection. This finding is based on short term data, and it will be important to see if this trend continues over long term exposure.

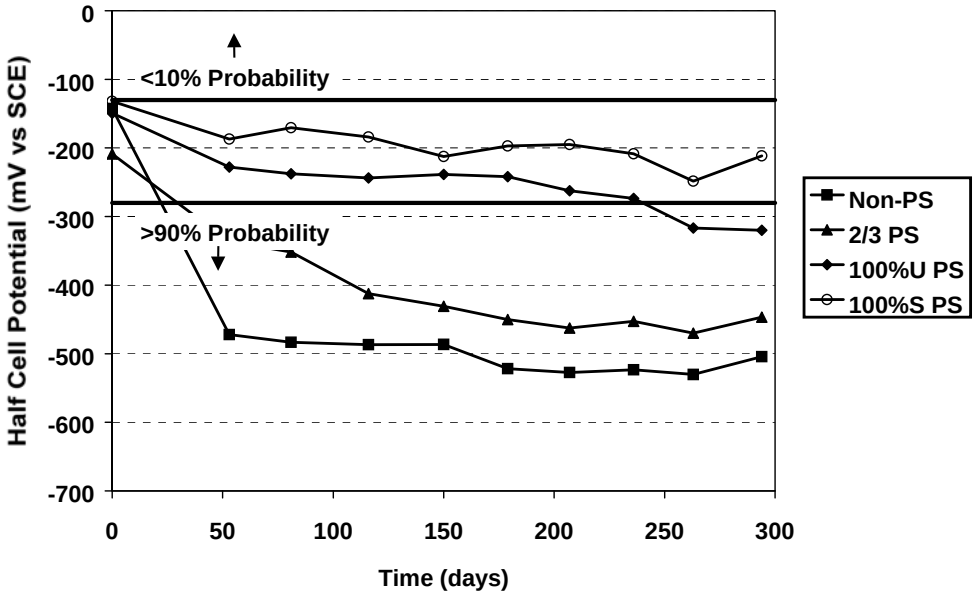

Figure 3.71 - Average Half-Cell Potentials for Each Series (Prestress Level)

The effect of post-tensioning in members that are not cracked is illustrated in Figure 3.72. Average half-cell potentials from the ponded region are plotted for the five beams that are uncracked. Several comparisons can be made:

- Beams 1.1 and 3.1 are unloaded. Measured potentials are similar in magnitude, with Beam 1.1 slightly more negative. These results suggest no significant effect of prestress on corrosion activity in unloaded beams.
- Beams 3.1 and 3.2 are 100%U PS, with 3.1 unloaded and 3.2 subjected to service loading (uncracked). Measured potentials for Beam 3.2 are more negative, suggesting a possible increase in corrosion activity due to loading. Although no visible cracks are present in Beam 3.2, concrete tensile stresses are present (by calculation) at the ponded surface. It is possible that this results in a higher concrete permeability in comparison to the precompressed ponded surface of Beam 3.1.
- Beams 4.1 and 4.2 are uncracked at service loading. Measured potentials for 4.1 and 4.2 are slightly more negative than Beam 3.2. This data suggests no improvement in corrosion protection is gained by increasing the prestress level from 100%U PS (nominal strength design) to 100%S PS (allowable stress design).

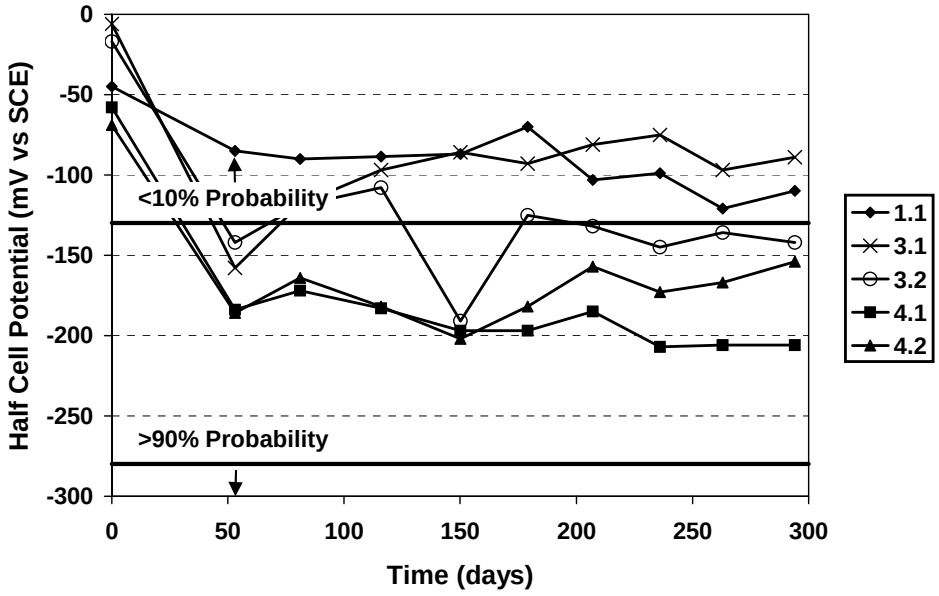

Figure 3.72 – Average Half-Cell Potentials for Uncracked Beams

3.11.3.2 Corrosion Rate Measurements

On the global scale, comparisons of corrosion rates between the different levels of prestress indicate that the 100%U PS and 100%S PS beams (Series 3 and 4) had corrosion rates comparable to or higher than Non-PS and 2/3 PS beams (Series 1 and 2). On the local scale, measured corrosion rates within Series 1, 2 and 3 indicate that higher corrosion rates are associated with cracking. Also, corrosion rates on beams where one measurement occurred at a crack location and the other on sound concrete showed higher corrosion rates at the crack locations.

Global Scale: Corrosion Rate and Level of Prestress

The observation that measured corrosion rates (from polarization resistance equipment) for prestressed members with limited or no cracking are similar to or higher than corrosion rates for heavily cracked, non-prestressed members does not match intuition. Normally, the use of prestress would be expected to improve corrosion protection by limiting the number and width of cracks. This trend was indicated by the measured half-cell potential data. Since the corrosion rate data measured after seven,

twelve and fifteen months of exposure indicates high corrosion rates for the 100%U PS and 100%S PS beams, the data warrants in-depth consideration.

It is possible that limitations or errors in the measurement of corrosion rate could explain the unexpected corrosion rates. As described in Section 3.9.4.2, many factors may introduce errors in measured corrosion rates. In this situation, the most likely errors are uncertain polarized area and unknown Tafel constants.

The effect of errors in the assumed polarized steel area was discussed in detail in Section 3.11.2.3. Underestimation of the polarized area was shown to lead to overestimation of corrosion rate. This effect was most pronounced for the 100%U PS and 100%S PS section types where diffusion of the polarizing signal could significantly increase the actual polarized area, resulting in overestimation of corrosion rates.

Calculation of the corrosion current based on measured polarization resistance requires knowledge of the Tafel constants for the conditions under investigation. The Tafel constants used in the calculations were developed for uncoated mild steel reinforcement in normal concrete. The presence of the prestressing strand and the galvanized steel duct could change the Tafel constants, affecting the accuracy of the results. Little or no research has been performed in this area, and no guidance is available at present.

Another possibility is that the intuitive assumption that prestressing will improve corrosion protection is not necessarily true, and thus the corrosion rate data is correct. Research by Schiessl and Raupach, reviewed in Appendix A, Section A.2.1.10, indicated that increased crack spacing would lead to higher corrosion rates at crack locations. Their explanation was that the ratio of cathode area to anode area increased as the crack spacing increased, resulting in high anodic current densities at the crack. The crack spacing in the 100%U PS (Series 3) beams is very large compared to the Non PS and 2/3 PS beams (Series 1 and 2). Thus, the conclusions of Schiessl and Raupach could offer an explanation for the high corrosion rates in Beams 3.3, 3.4 and 3.5, particularly at crack locations. However, the work of Schiessl and Raupach does not explain the high corrosion rates in the uncracked 100%S PS (Series 4) beams. It should also be mentioned that Schiessl and Raupach's conclusions on crack spacing were based on theoretical calculations that require simplifying assumptions, and were not confirmed experimentally. Continued exposure

testing and invasive or forensic examinations of the beams are required to fully assess the effect of cracking and level of prestress on corrosion.

Local Scale: Corrosion Rate At Crack Locations

On the local scale, the effect of cracks is to cause increased corrosion activity in the vicinity of the crack. As mentioned previously, this is particularly evident for beams where one measurement was taken at a crack location and the other measurement was taken on uncracked concrete. The effect of cracking was most pronounced in Beams 2.1, 3.3 and 3.4 (see Figure 3.65), where corrosion rates at crack locations were significantly higher than rates at uncracked locations. Since all other variables are essentially equal when comparing two readings from one beam, the higher corrosion rates at crack locations can be attributed to increased penetration of chlorides at the crack.

In many cases, flexural cracks coincided with stirrup locations, as discussed in Section 3.8.3. Therefore, it is assumed that corrosion of the stirrups is occurring at crack locations. This leads to an important observation; the corrosion rate measurement is an assessment of corrosion activity at a very local scale, in this case, the corrosion of a stirrup at a crack. This local condition could be similar whether the crack has occurred in a non-prestressed beam with many cracks, or in a prestressed beam with a very limited number of cracks. Therefore, corrosion rate measurements at cracks could be very similar for different levels of prestress and crack patterns.

The measured corrosion rate data collected in this testing program indicates that corrosion rates at cracks tend to be significantly higher than corrosion rates in uncracked concrete. This leads to the conclusion that the overall corrosion damage in a specimen is a function of the number of cracks in the beam. The question to debate is what criteria should be used to assess the severity of corrosion damage? Should it be the localized corrosion rate at a crack, or should it be the total amount of corrosion damage in the beam. In the latter case, post-tensioning would appear to improve corrosion protection by limiting the number of cracks and thus limiting the total amount of corrosion damage. This would be an appropriate conclusion if the corrosion at the cracks was not threatening to structural integrity. Continued long term exposure testing and invasive inspections are required to fully assess the effect of cracking.

The high corrosion rates at cracks located over stirrups warrant an additional observation. Since the crack is aligned with the stirrup, the potential for severe corrosion of the stirrup is very high. Corrosion damage to the stirrup could lead to deterioration of the shear strength of the beam. This aspect of corrosion in structural concrete is rarely considered, as most attention is given to deterioration of flexural capacity.

3.11.4 Effect of High Performance Fly Ash Grout and Duct Splice Types

The half-cell potential and corrosion rate data collected during the first ten months of exposure testing does not indicate any effect of the different grouts and duct splices investigated. These variables only influence corrosion protection for the post-tensioning tendons. It is not likely that significant corrosion activity has developed on the tendons during the relatively short exposure duration and additional test data will be necessary to evaluate these variables. It is possible that the effectiveness of the grout and duct splices may not be apparent until a forensic examination is performed on the beam specimens.

3.12 Summary and Conclusions

The ten month exposure duration reported in this chapter will ultimately represent only a short portion of the total exposure duration the for beam corrosion tests. The test data gathered during the first ten months of exposure indicates varied levels of corrosion activity, but does not suggest significant corrosion damage or corrosion related structural deterioration has occurred. Continued exposure testing and monitoring, combined with forensic examinations of the beams, will provide considerably more information and insight into corrosion in post-tensioned structural elements. The preliminary test data reported in this chapter does present some interesting conclusions. Because the conclusions are based on preliminary data, they could be subject to change.

3.12.1 Overall Performance

- Some minor signs of visible corrosion damage in terms of rust staining and spalling were present during the first ten months of exposure. The source of this damage appears to be corrosion of the plastic tipped bolster strips used to support the reinforcement cage during construction. These results suggest that plastic bolster strips and bar chairs should be used in aggressive exposures.

- No signs of corrosion of the reinforcement were present. This is not unexpected due to the short exposure duration and realistic specimen details and materials.
- Chloride measurements indicate chlorides have not penetrated to the level of the reinforcement in uncracked concrete.
- Half-cell potentials and corrosion rate measurements suggest a high probability of corrosion activity in more than half of the beam specimens.
- Actual assessment of the corrosion severity occurring during this exposure duration requires invasive techniques to provide a visual examination of the steel condition. This work will be performed and reported by Schokker.[3.1]

3.12.2 Assessing Corrosion Activity Using Half-Cell Potential Measurements

- Very negative half-cell potentials (more negative than the guidelines for high probability of corrosion) do not necessarily indicate that corrosion is occurring. Very negative half-cell potentials can result from sources other than significant corrosion activity, and therefore it is more important to consider the variation of half-cell potentials over time to assess corrosion activity.
- Although comparisons of half-cell potential data may be used with other forms of data to indicate the relative performance of the different beam types, the most important and appropriate use of the half-cell potential data is to indicate corrosion initiation by observing long term trends in the measured data. Therefore, continued regular measurements are very important.

3.12.3 Post-Tensioning to Improve Corrosion Protection

- Half-cell potential measurements suggest that corrosion activity is related to cracking. Increased cracking, in terms of number of cracks and crack widths, was associated with more negative half-cell potentials, indicating a higher probability of corrosion.
- A significant reduction in half-cell potentials was observed for the 100%U PS and 100%S PS beam types in comparison to the 2/3 PS and Non-PS beams. The difference between measurements for the 100%U PS and 100%S PS beams was not significant. This data suggests that the additional prestressing provided by the 100%S PS section may not be necessary from a durability standpoint.
- Corrosion rate measurements indicated corrosion activity is related to cracking.

  - Corrosion rate measurements on uncracked Beams 1.1, 3.1 and 3.2 were significantly lower than measured rates on companion cracked specimens.
  - Higher corrosion rates were measured at crack locations. This suggests that on a local scale cracks lead to increased corrosion activity in comparison to uncracked concrete.
- Corrosion rate measurements at crack locations in post-tensioned beams were as high or higher than corrosion rates at cracks in non-prestressed beams. This illustrates the significance of cracking on corrosion, at least in the short term.
- Assessing the effect of post-tensioning on corrosion protection depends on the criteria used to quantify the severity of corrosion. If corrosion rates at crack locations are used as criteria, there appears to be little or no positive effect of post-tensioning. If overall corrosion damage in the structural element is considered, post-tensioning improves corrosion protection by limiting the number of cracks and thus limiting the total deterioration due to corrosion.
- Overall, the preliminary test data indicates that corrosion protection can be improved through crack control with post-tensioning.

3.12.4 Crack Width Prediction for Structural Concrete with Mixed Reinforcement

- Comparison of measured crack data with several crack prediction models produced widely varying results. This finding suggests that not all crack prediction methods are appropriate for structural concrete members with a combination of mild steel and prestressed reinforcement.
- The Gergely-Lutz crack width model[3.7] provided an excellent prediction of maximum crack widths for the Non-PS and 2/3 PS beams, and a conservative estimate for the 100%U PS beams. The Gergely-Lutz model was applied using the recommendations of Armstrong et al.[3.6] This model is relatively easy to apply, and is recommended for sections with mixed reinforcement.
- The Batchelor and El Shahawi crack width expression[3.35] provided a very good prediction of maximum crack widths for the 2/3 PS and 100%U PS beams. This very simple model is also recommended for sections with mixed reinforcement.

3.12.5 Corrosion Rate Measurements Using Polarization Resistance

- Corrosion rate measurements were obtained using the three electrode procedure to measure polarization resistance. Two different devices were used: 3LP and PR Monitor. The PR Monitor uses a guard electrode for signal confinement and compensates for concrete resistance.
- Corrosion rates obtained using the 3LP device were extremely high and did not correlate with specimen condition and half-cell potentials. The PR Monitor indicated lower corrosion activity than the 3LP, although moderate to high corrosion rates were indicated for most beams.
- The corrosion activity indicated by both devices, and in particular the 3LP, contradicted the half-cell potential measurements for some specimens. In general, the highest corrosion rates were obtained for the 100%U PS beams, while the most negative half-cell potentials were measured for the Non-PS beams. Numerous possible factors were investigated, but no firm conclusions could be made other than several limitations exist for the 3LP device and the polarization resistance technique in general.
- The PR Monitor appears to provide a better assessment of corrosion rate than the 3LP device. Because of differences between the devices, it is not recommended to directly compare corrosion rates obtained using the 3LP and PR Monitor.
- The 3LP device suffers from an unconfined polarizing signal. As a result, the polarized area of steel will unknowingly be larger than expected in most cases, resulting in an overestimation of corrosion rate.
- The three electrode technique for measuring polarization resistance appears to be most useful for relative comparisons of corrosion activity rather than a quantitative assessment of corrosion rate. Relative comparisons should only be made for similar beams and similar conditions, and therefore the comparison of corrosion rates for the different levels of prestress investigated is questionable.
- In view of the preceding conclusions, corrosion rate measurements in post-tensioned concrete structures should be approached with caution and should not be relied on as a sole method to evaluate corrosion activity.

- Regular corrosion rate measurements over time are needed to assess the amount of corrosion related distress in structural concrete. Discrete measurements may occur at instances where corrosion rates are higher or lower than normal, and give a false indication of the specimen or structural element condition.
- The PR Monitor is recommended for future corrosion rate measurements in this testing program. The 3LP device could be used as a second choice. 3LP corrosion rates could be "corrected" using the expressions developed in Section 3.11.2.3 for an improved estimate of corrosion rates.

3.12.6 Conclusion

The research program described in this chapter has the potential to provide some very useful and important findings on the durability of post-tensioned bridge elements. The preliminary findings are encouraging, but long term exposure testing and a thorough forensic examination at the conclusion of testing are necessary for complete results.

The long term beam corrosion tests will continue exposure testing for an undetermined time of at least several years. Specimen condition monitoring with half-cell potentials, chloride measurements and corrosion rate measurements is essential as it provides a continual evaluation of specimen condition and may detect changes in corrosion activity. The data also provides additional information to support final forensic examination findings. Finally, comparison of long term monitoring data and forensic examination results provides an assessment of the monitoring techniques in post-tensioned concrete. This is important information needed for the condition evaluation of post-tensioned bridge structures.

Chapter 3 References

3.1) **Schokker, Andrea J.,** "Improving Corrosion Resistance of Post-Tensioned Substructures Emphasizing High Performance Grouts," Doctor of Philosophy Dissertation, The University of Texas at Austin, May 1999.

3.2) "VSL Post-Tensioning Systems," Product Information Pamphlet, VSL Corporation, (undated).

3.3) **AASHTO**, LRFD Bridge Design Specifications, 2nd Edition, American Association of State Highway and Transportation Officials, Washington, D.C., 1998.

3.4) **ACI Committee 318,** "Building Code Requirements for Structural Concrete" (ACI 318-95), American Concrete Institute, Detroit, MI, 1995, 369 pp.

3.5) **Breen, J.E., Burdet, O., Roberts, C., Sanders, D. and Wollman, G.,** "Anchorage Zone Reinforcement for Post-Tensioned Concrete Girders," NCHRP Report 356, Transportation Research Board, Washington, D.C., 1994, 204pp.

3.6) **Armstrong, S.D., Salas, R.M., Wood, B.A., Breen, J.E. and Kreger, M.E.,** "Behavior and Design of Large Structural Bridge Pier Overhangs," Research Report 1364-1, Center for Transportation Research, The University of Texas at Austin, 1997, 272 pp.

3.7) **Gergely, P., and Lutz. L.A.,** "Maximum Crack Width in Reinforced Concrete Flexural Members," ACI SP-20, American Concrete Institute, Detroit, MI, 1968, pp. 87-117.

3.8) **Collins M.P., and Mitchell, D.,** Prestressed Concrete Structures, Prentice Hall, NJ, 1991.

3.9) **Park R., and Paulay, T.,** Reinforced Concrete Structures, John Wiley and Sons, Inc., New York, 1975.

3.10) **Klingner, R.,** "Advanced Reinforced Concrete Structures," Course Notes CE383N, The University of Texas at Austin, 1994.

3.11) **Ghali, A., and Favre, R.**, Concrete Structures: Stresses and Deformations, 2nd. Edition, E & FN Spon, London, 1994. (see also Ghali, A., "Stress and Strain Analysis in Prestressed Concrete: A Critical Review," *PCI Journal*, Vol. 34, No. 6, November-December 1989, pp. 80-97.)

3.12) **ACI Committee 209,** "Prediction of Creep, Shrinkage and Temperature Effects in Concrete Structures" (ACI 209R-92), American Concrete Institute, Detroit, Michigan, 1992.

3.13) Standard Specifications for Construction of Highways, Streets and Bridges, Texas Department of Transportation, March 1995.

3.14) Standard Specifications for Construction of Highways, Streets and Bridges, Special Provision to Item 426 (Prestressing), Sub-Section: Construction Methods, Texas

Department of Transportation, 1995. (also, personal communication with Dean Van Landuyt, Texas Department of Transportation, April 1997.)

3.15) **ASTM,** "Standard Specification for Coal Fly Ash and Raw or Calcined Natural Pozzolan for Use as a Mineral Admixture in Concrete," ASTM C618-98, American Society for Testing and Materials, Philadelphia, PA, 1998.

3.16) **PTI Committee on Grouting Specifications,** "Guide Specification for Grouting of Post-Tensioned Structures," 5th Draft, Post-Tensioning Institute, Phoenix, AZ, November 1997, 37 pp.

3.17) **ASTM**, "Standard Test Method for Determining the Effects of Chemical Admixtures on the Corrosion of Embedded Steel Reinforcement in Concrete Exposed to Chloride Environments," ASTM G109-92, American Society for Testing and Materials, Philadelphia, PA, 1992.

3.18) **Silvestri, Giovanni**, Personal Communication, VSL Corporation, Grand Prairie, TX, March 1997.

3.19) **AASHTO**, LRFD Bridge Construction Specifications, 1st Edition, American Association of State Highway and Transportation Officials, Washington, D.C., 1998.

3.20) **ASTM**, "Standard Test Method for Half-Cell Potentials of Uncoated Reinforcing Steel in Concrete," ASTM C876-91, American Society for Testing and Materials, Philadelphia, Pa., 1991.

3.21) **AASHTO**, Standard Method of Test for Resistance of Concrete to Chloride Ion Penetration," AASHTO Designation T 259-80, American Association of State Highway and Transportation Officials, Washington, D.C., 1980.

3.22) **AASHTO**, Standard Method of Test for Sampling and Testing for Chloride Ion in Concrete and Concrete Raw Materials," AASHTO Designation T 260-94, American Association of State Highway and Transportation Officials, Washington, D.C., 1994.

3.23) **Fontana, M.G.,** Corrosion Engineering, 3rd Edition, McGraw-Hill, Inc., New York, New York, 1986.

3.24) **Jones, D.A.,** Principles and Prevention of Corrosion, 2nd Edition, Prentice Hall, Inc., Upper Saddle River, NJ, 1996.

3.25) **Flis, J., Sehgal, A., Li, D., Kho, Y, Sabol, S., Pickering, H., Osseo-Asare, K, and Cady, P.D.,** "Condition Evaluation of Concrete Bridges Relative to Reinforcement Corrosion, Volume 2: Method for Measuring the Corrosion Rate of Reinforcing Steel," SHRP-S/FR-92-104, Strategic Highway Research Program, Washington, D.C., 1992, 105 pp.

3.26) **Clear, K.,** "Measuring the Rate of Corrosion of Steel in Field Concrete Structures," Transportation Research Record 1211, pp. 28-37, 1989.

3.27) **Andrade, C., Castelo, V., Alonso, C. and Gonzalez, J.A.,** "The Determination of Corrosion Rate of Steel Embedded in Concrete by the Polarization Resistance and AC Impedance Methods," Corrosion Effect of Stray Currents and the Techniques for Evaluating Corrosion of Rebars in Concrete, ASTM STP 906, V. Chaker, Editor, American Society for Testing and Materials, Philadelphia, PA, 1986, pp. 43-63.

3.28) **CONCORR, Inc.,** "FHWA – SHRP Showcase: Assessment of Physical Condition of Concrete Bridge Components," Federal Highway Administration, Washington, D.C., July 1996.

3.29) **Cady, P., and Gannon, E.,** "Condition Evaluation of Concrete Bridges Relative to Reinforcement Corrosion, Volume 8: Procedure Manual," SHRP-S/FR-92-330, Strategic Highway Research Program, Washington, D.C., 1992, 124 pp.

3.30) **Kahhaleh, K.Z.,** "Corrosion Performance of Epoxy-Coated Reinforcement," Doctor of Philosophy Dissertation, The University of Texas at Austin, May 1994.

3.31) **Wheat, H.G., and Eliezer, Z.,** "Some Electrochemical Aspects of Corrosion of Steel in Concrete," *Corrosion*, Vol. 41, No. 11, November 1985, pp. 640-645.

3.32) **ACI Committee 222,** "Corrosion of Metals in Concrete," ACI 222R-96, American Concrete Institute, Detroit, Michigan, 1996.

3.33) **CEB-FIP,** Model Code for Concrete Structures: CEB-FIP International Recommendations, 3rd Edition, Comité Euro-International du Béton, Paris, 1978, 348 pp.

3.34) **CEB-FIP,** CEB-FIP Model Code for Concrete Structures 1990, Bulletin D'Information No. 213/214, Comité Euro-International du Béton, Lausanne, May 1993, 437 pp.

3.35) **Batchelor, B.DEV., and El Shahawi, M.,** "A Review of Cracking of Partially Prestressed Concrete Members," *Canadian Journal of Civil Engineering*, Vol. 12, 1985, pp. 645-652.

3.36) **Suri, K.M., and Dilger, W.H.,** "Crack Width of Partially Prestressed Concrete Members," *ACI Journal,* Vol. 83, No. 5, September-October 1986, pp. 784-797.

3.37) **Verhulst, S.M.,** "Evaluation and Performance Monitoring of Corrosion Protection Provided by Fiber-Reinforced Composite Wrapping," Master of Science Thesis, The University of Texas at Austin, May 1999.

Chapter 4:

Long Term Column Corrosion Tests

4.1 Test Concept and Objective

The applications of post-tensioning in bridge columns or piers have been limited in comparison to flexural members. However, some situations do exist where post-tensioning can provide an efficient structural solution. Some examples include columns or piers where large bending moments are encountered during construction or in service, or in precast segmental construction. In the latter case, post-tensioning provides continuity in the structure. Similar to flexural members, post-tensioning may have two general effects on corrosion protection in columns or piers. First, post-tensioning may improve the corrosion protection provided by the concrete by controlling cracking in the concrete. Post-tensioning may also be used to control or prevent tensile stresses across segmental joints or construction joints in columns. The second effect is that the post-tensioning system introduces additional components that may be susceptible to corrosion damage. Thus, durability design for post-tensioned columns must address how to use post-tensioning to improve corrosion protection and how to protect the post-tensioning hardware from corrosion damage.

This portion of the research project consists of long term exposure testing of large structural concrete columns or vertical members. The specific objectives are to investigate:

1) The effect of post-tensioning on durability (corrosion protection) through precompression of the concrete and precompression of construction joints, and
2) The relative performance of various aspects of corrosion protection for post-tensioning.

The experimental program uses large scale circular column specimens subjected to combined structural loading and aggressive exposure. The columns are cast-in-place on a large concrete foundation. The specimens are tested outside the Ferguson Structural Engineering Laboratory, and are continuously exposed to saltwater to promote corrosion

activity. The majority of the columns are subjected to simulated service load conditions. The effect of post-tensioning is compared to the standard non-prestressed (reinforced concrete) column. Variables investigated are the joint between the column and foundation, loading, concrete type, prestressing bar coatings, and type of post-tensioning duct. Exposure testing began in July of 1996. This chapter describes the specimen design and variables, and presents exposure testing results through September of 1998.

4.2 Test Specimen

The test specimens in this experimental program are circular cast-in-place columns. The columns were patterned after standard Texas Department of Transportation (TxDOT) multi-column substructures. Although post-tensioning would not normally be used in this type of column, it was selected for research purposes for several reasons, including constructability, size limitations and familiarity. The column dimensions and details were selected such that covers, reinforcement sizes and post-tensioning hardware were on a similar order of magnitude as in practical applications, with consideration for construction and loading of the specimens. A nominal column diameter of 460 mm (18 in.) and height of 1.83 m (6 ft) were selected.

4.2.1 Column Design Loading

The test specimen design process began with determining the applied loading for the columns. It was decided to deviate from the design process used for the beam corrosion tests to determine the loading for the columns. In many cases, typical bridge column reinforcement is based on minimum reinforcement requirements, and the nominal capacity of the column is well in excess of the design loading dictated by analysis of the bridge. Thus, it was decided to obtain design loading for a typical TxDOT multi-column bridge substructure. The test specimen reinforcement would be proportioned to meet minimum requirements and column capacity would be compared against the design loading. The design loading would be applied on the columns during testing. This approach would provide a more realistic representation of the typical relationship between bridge column capacity and design loading.

4.2.1.1 Prototype Substructure

The prototype bridge substructure selected for analysis was a three column frame bent from an overpass structure, as shown in Figure 4.1. The bridge carried two lanes of traffic and one shoulder. The substructure was cast-in-place reinforced concrete (non-prestressed). The circular columns had a 762 mm (30 in.) diameter, and a clear height of 4.88 m (16 ft). The bent cap was rectangular in section with dimensions of 838 mm (33 in.) by 914 mm (36 in.). The bent was skewed to the roadway alignment at 45 degrees. The superstructure consisted of five Type C precast, pretensioned bridge girders with a 22.86 m (75 ft) span, and a 200 mm (8 in.) thick cast-in-place concrete deck.

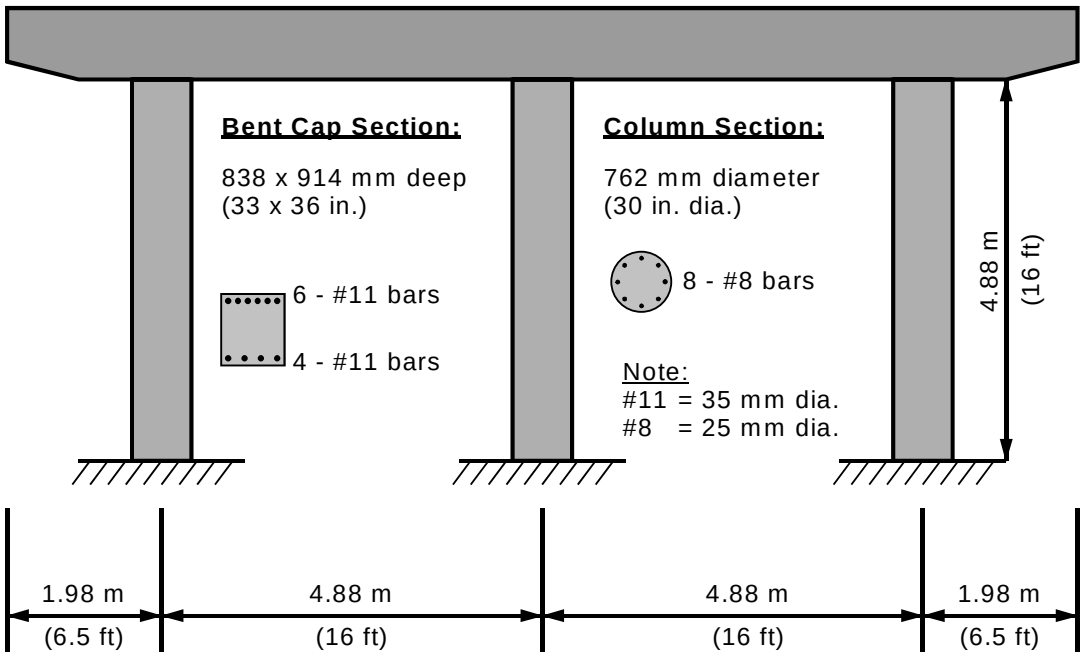

Figure 4.1 - Prototype Multi-Column Substructure

4.2.1.2 Substructure Analysis

The three column frame bent was analyzed using a plane frame analysis program. AASHTO LRFD[4.1] was used for design loading on the bridge. Elastic uncracked transformed section properties were used for the columns. The bent cap was divided into several segments and the analysis was performed assuming an initial moment of inertia of 40% of the gross moment of inertia. The initial analysis results were then used to refine

the moment of inertia for each segment based on the calculated end moments for each segment. Depending on the magnitude and direction of the end moment, the gross transformed moment of inertia or elastic cracked section moment of inertia (positive or negative bending) was assigned to each end, and the average was computed for each segment The frame was then re-analyzed and the various combinations of axial load and moment for the columns were determined. The calculated column forces are shown in Table 4.1. Columns 1 and 3 are the outside columns. Loading on the substructure was not symmetric due to the shoulder, producing different force combinations for the two columns. The critical combination was taken at the top of column 3, since this combination produced the largest eccentricity (ratio of moment to axial load).

Table 4.1 - Calculated Column Forces for Prototype Substructure (unfactored)

Location	Data	Column 1		Column 3	
Column Base	$\mathbf{N_{max}}$	1781 kN	(400.4 kips)	994 kN	(223.4 kips)
	$\mathbf{M_{max}}$	55.8 kN-m	(494.4 k-in.)	74.6 kN-m	(660.0 k-in.)
	e = M/N	30.5 mm	(1.2 in.)	76.2 mm	(3.0 in.)
Column Top	$\mathbf{N_{max}}$	1716 kN	(385.7 kips)	**928 kN**	**(208.7 kips)**
	$\mathbf{M_{max}}$	144.8 kN-m	(1281.6 k-in.)	**118.0 kN-m**	**(1044.0 k-in.)**
	e = M/N	83.8 mm	(3.3 in.)	**127 mm**	**(5.0 in.)**

The design loading from the prototype analysis was scaled for use with the column specimens. Axial forces are scaled by the square of the ratio of column diameters. Bending moments are scaled by the cube of the ratio of column diameters. Calculation of the column specimen design forces is as follows:

$$N_{specimen} = \left(\frac{D_{specimen}}{D_{prototype}}\right)^2 \times N_{prototype}$$

$$= \left(\frac{457\ mm}{762\ mm}\right)^2 \times (928\ kN)$$

$$= 334\ kN \quad (75.2\ kips)$$

$$M_{specimen} = \left(\frac{D_{specimen}}{D_{prototype}}\right)^3 \times M_{prototype}$$

$$= \left(\frac{457\ mm}{762\ mm}\right)^3 \times (118\ kN-m)$$

$$= 25.5\ kN-m \quad (225\ k-in.)$$

Assuming an average load factor of 1.5, the factored design forces are:

N_f	=	501 kN	(112.6 kips)
M_f	=	38.2 kN-m	(338.6 k-in.)

4.2.2 Reinforced Concrete Column Design

The smallest circular column used by TxDOT[4.2] is 460 mm (18 in.) diameter. This column was selected as the non-prestressed or reinforced concrete design in the research program. The 460 mm column is provided with six #6 (19 mm) bars for longitudinal reinforcement. Spiral reinforcement is #3 (9.5 mm) at a 152 mm (6 in) pitch. Clear cover to the spiral is 50 mm (2 in.). The concrete used in the columns was TxDOT Class C concrete, with a minimum compressive strength of 25 MPa (3600 psi). The reinforced concrete section is shown in Figure 4.2.

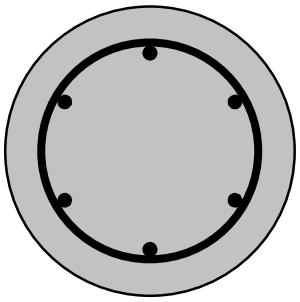

Main Reinforcement:
6 - #6 (19 mm) bars

Spiral:
#3 (9.5 mm) at
152 mm (6 in.) pitch

Column Diameter: 460 mm (18 in.)
Clear Cover to Spiral: 50 mm (2 in.)

Figure 4.2 - Reinforced Concrete Column Section Details

The reinforced concrete section was analyzed using a layer-by-layer strain compatibility section analysis technique[4.3] to produce an axial force-moment interaction diagram. A spreadsheet was developed by the author to automate the analysis process. The basic assumptions for the analysis were listed previously in Section 3.2.3. The

concrete compressive strength used in the calculations was 25 MPa (3600 psi) (minimum allowable for TxDOT Class C concrete). The calculated interaction diagrams are shown in Figure 4.3. Curves are plotted for the nominal capacity (N_n, M_n) and the factored resistance (ϕN_n, ϕM_n). The factored resistance is well in excess of the factored loading.

The elastic decompression moment for the column was calculated for the design service loading as follows:

$$f_{tensile} = 0 = \frac{P_{service}}{A_{tr}} - \frac{M_{decomp.}}{S_{tr}}$$

$$M_{decomp.} = \left(\frac{S_{tr}}{A_{tr}}\right) P_{serv} = \left(\frac{10.147 x 10^6\ mm^3}{176{,}903\ mm^2}\right)\left(\frac{334\ kN}{1000}\right)$$

$$= 19.2\ kN - m \quad (169.4\ k - in.)$$

The service load moment of 25.5 kN-m (225 k-in.) exceeds the decompression moment for the reinforced concrete column design.

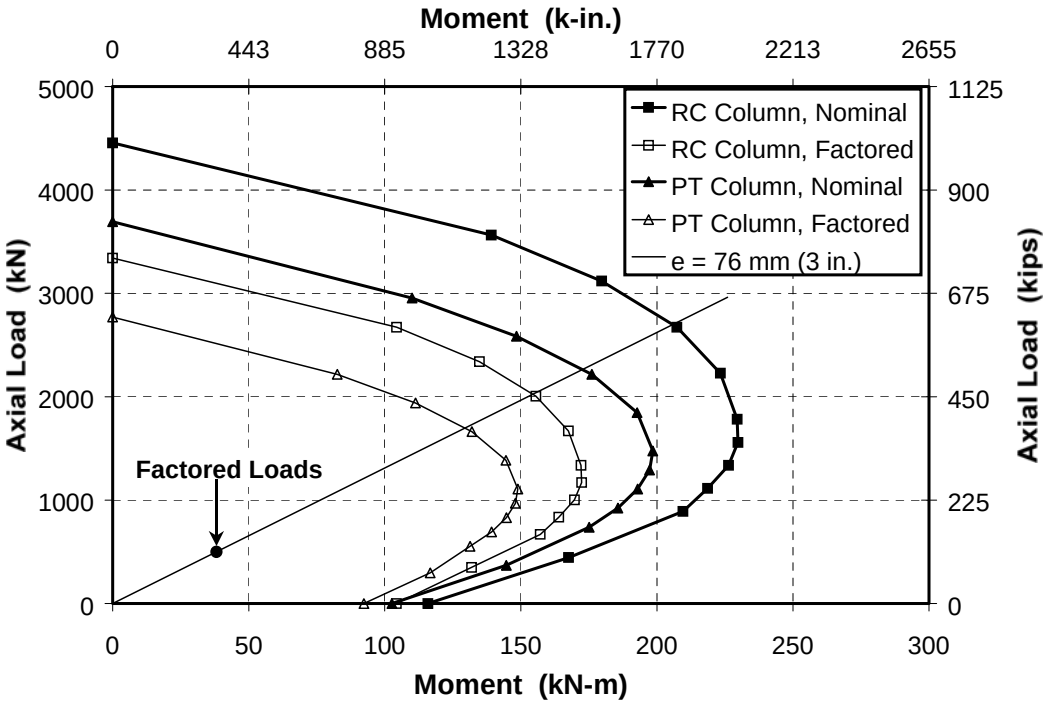

Figure 4.3 - Column Interaction Diagrams, Nominal Resistance and Factored Resistance

4.2.3 Post-Tensioned Column Design

The post-tensioned column design was based on practical considerations. The design concept for the post-tensioned column was to keep the same mild steel reinforcement from the reinforced concrete column design, and to add prestressed steel to provide continuity between the column and foundation and increase the decompression moment, which could improve durability at construction joints. The mild steel column reinforcement would not extend into the foundation or the bent cap. The longitudinal mild steel was left in the column for several reasons, including the need for confinement and concerns for creep. Due to the relatively small size of the test specimens, it was decided to use threaded prestressing bars rather than seven-wire strand for post-tensioning. The use of threadbar minimized anchorage seating losses and provided simple details for anchoring the bars in the foundation while accommodating a construction joint at the column-foundation interface. The column-foundation joint is discussed in Section 4.3.2.

Since only the post-tensioning bars would provide continuity between the column and other elements, a minimum of four prestressing bars would be required to effectively develop flexural capacity about more than one axis. Four 16 mm (5/8 in.) prestressing bars were selected. A minimum effective prestress of 60% of ultimate ($f_{pe} = 0.6f_{pu}$) was used for design and analysis purposes. The post-tensioned column section details are shown in Figure 4.4.

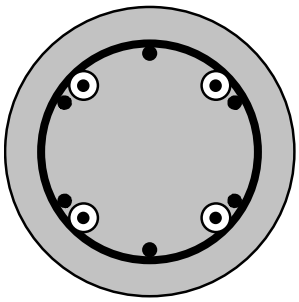

Main Reinforcement:
6 - #6 (19 mm) bars**
4 - 16 mm (5/8 in.) PT bars
$f_{pe} = 0.6f_{pu}$

Spiral:
#3 (9.5 mm) at
152 mm (6 in.) pitch

Column Diameter: 460 mm (18 in.)
Clear Cover to Spiral: 50 mm (2 in.)

** Only PT bars provide continuity to foundation

Figure 4.4 - Post-Tensioned Column Section Details

The elastic decompression moment was calculated for the post-tensioned column at the critical section (neglecting the mild steel reinforcement) as follows:

$$f_{tensile} = 0 = \frac{P_{service} + F_p}{A_{tr}} - \frac{M_{decomp.}}{S_{tr}}$$

$$M_{decomp.} = \left(\frac{S_{tr}}{A_{tr}}\right)\left(P_{serv} + F_p\right) = \left(\frac{9.382 \times 10^6\ mm^3}{164{,}173\ mm^2}\right)\left(\frac{334\,kN + 4(117.3\,kN)}{1000}\right)$$

$$= 45.9\ kN - m \quad (406\ k - in.)$$

The decompression moment for the post-tensioned column exceeds the applied service load moment of 25.5 kN-m (225 k-in.) by a considerable margin.

The post-tensioned column section was analyzed using the layer-by-layer strain compatibility section analysis technique described previously. The stress-strain curve for the high strength prestressing bars was modeled using a Ramberg-Osgood function,[4.3] as shown in Figure 4.5. The concrete strength assumed for the calculations was 25 MPa (3600 psi). An axial force-moment interaction diagram was produced for the post-tensioned column at the critical section (neglecting the mild steel reinforcement). The calculated interaction diagrams are shown in Figure 4.3. Curves are plotted for the nominal capacity (N_n, M_n) and the factored resistance (ϕN_n, ϕM_n). The interaction diagram for the post-tensioned section shows a lower nominal capacity than the reinforced concrete column,

particularly for axial loads higher than 500 kN. This illustrates the effect of post-tensioning on the axial load carrying capacity of columns. Although the post-tensioned column had a lower strength than the reinforced concrete column, the factored resistance of the post-tensioned columns far exceeded the factored loads (Figure 4.3).

$$f_{ps} = E_{ps}\varepsilon_{ps}\left(0.01293 + \frac{0.987}{\left[1+\left(238.5\varepsilon_{ps}\right)^{8}\right]^{0.125}}\right)$$

$$\leq 1035 \text{ MPa}$$

$$E_{ps} = 200{,}000 \text{ MPa}$$

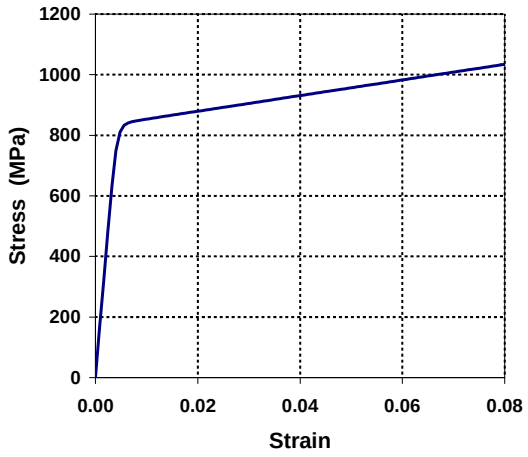

Figure 4.5 - Prestressing Bar Stress-Strain Curve

Long term prestress losses were calculated using the approach proposed by Ghali and Favre (see Section 3.2.3). The assumed concrete strength was increased from 25 MPa (3600 psi) to 35 MPa (5000 psi) to better reflect tested cylinder strengths obtained for the columns. The column mild steel reinforcement was included the long term analysis. Initial calculations were performed using an initial prestress value of $0.6f_{pu}$. Calculated average prestress losses under sustained service loading were approximately 10% after 1000 days. Since the desired effective prestress was $0.6f_{pu}$, it was decided to increase the initial level of prestress to $0.68f_{pu}$. Calculations were performed for periods of 500, 1000 and 1500 days, for both loaded and unloaded post-tensioned columns. The results are listed in Table 4.2. Losses are not uniform in the loaded case due to the eccentric loading. The calculated losses indicate that with an initial prestress of $0.68f_{pu}$ the effective prestress in the columns will meet or exceed the design value for an experiment duration longer than 1500 days.

The effect of the mild steel reinforcement on the prestress losses was investigated by excluding the mild steel from the prestress loss calculations. This resulted in an

average prestress loss of 12.75% after 1500 days of loading compared to an average loss of 11% when the mild steel is included.

Table 4.2 - Long Term Prestress Losses

Time Period (days)	Prestress Loss ΔF_{p1}	Prestress Loss ΔF_{p2}
Case 1: Loaded, $f_{pi} = 0.68f_{pu}$		
500	10.7%	8.8%
1000	11.5%	9.6%
1500	11.9%	9.9%
Case 2: Unloaded, $f_{pi} = 0.68f_{pu}$		
500	7.8%	7.8%
1000	8.4%	8.4%
1500	8.8%	8.8%

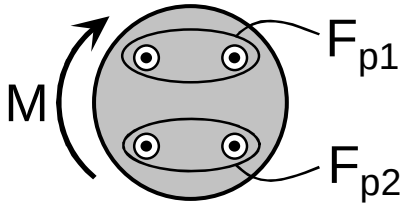

4.3 Variables

A number of variables were selected for consideration column corrosion tests. The variables fall into five main categories: column to foundation joint, concrete type, loading, prestressing bar coatings and post-tensioning duct types.

4.3.1 Control Variables

Standard variables based on typical current practice were defined to represent control cases. These include concrete mix design, concrete clear cover, cement grout and post-tensioning duct. Details of each are given below.

Concrete:

based on TxDOT Specification[4.4] Item 421
TxDOT Class C concrete for bridge substructures
maximum w/c ratio = 0.533 (actual w/c will be closer to 0.45 based on slump requirements)
Type I cement
slump = 100 mm (4 in.)
maximum coarse aggregate size = 19 mm (3/4 in.)
retarder, Rheocrete 300-R
entrained air admixture
50 mm (2 in.) clear cover to main steel

Cement Grout:	based on TxDOT Specification[4.4] Item 426.3.4a
	w/c ratio = 0.44
	Type I cement
PT Duct:	rigid galvanized steel duct

4.3.2 Column to Foundation Connection

The construction joint between the column and foundation presents a possible weak link in corrosion protection since it represents a pre-formed crack that could open under loading. This problem is aggravated by the potential exposure conditions at the column-foundation interface, since the joint could be directly exposed to moisture and chlorides in coastal and de-icing chemical exposures. One of the objectives for this research program is to investigate the influence of the column-foundation cold joint on chloride ion movement and corrosion activity. Three configurations were selected, as shown in Figure 4.6.

The standard doweled joint has six mild steel dowels (#6 (19 mm dia.) bars) cast into the foundation to provide continuity with the column. The column reinforcement is lapped with the dowels, and the column is cast-in-place on the foundation. In the second configuration, continuity between the column and foundation is provided with four post-tensioned bars (16 mm (5/8 in.) dia.). A short length of threadbar with bearing plate and nut is cast into the foundation for each post-tensioned bar. The bars protrude from the foundation to permit coupling with the column post-tensioning bars during column construction. After the column is cast-in-place, it is post-tensioned to the foundation. The no joint configuration represents the condition of a column or trestle pile in deep water. The column is cast-in-place on the foundation for this configuration, but no dowel steel is used and an end cover of 50 mm (2 in.) is provided for all column longitudinal reinforcement. An epoxy bonding agent was used to prepare the foundation surface immediately prior to casting the no joint type columns.

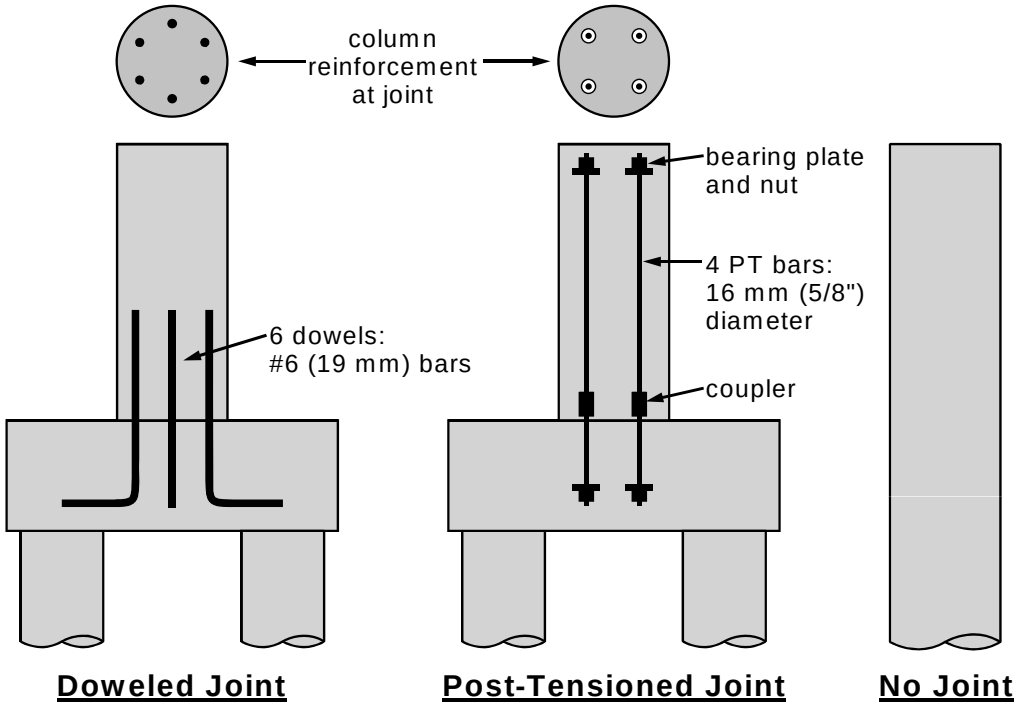

Figure 4.6 - Column-Foundation Joint Configurations

4.3.3 Loading

Two loading conditions were considered: unloaded and service load. The columns were subjected to the combined axial load and moment conditions obtained from the prototype substructure analysis for the service load condition:

$N_{service}$ = 334 kN (75.2 kips)

$M_{service}$ = 25.5 kN-m (225 k-in.)

The unloaded case was included since it could represent a worse case condition for allowing moisture and chloride penetration at the column-foundation construction joint.

4.3.4 Concrete Type

Partial cement replacement with fly ash has been shown to improve most aspects of concrete durability, as discussed in Section 2.4.3. Replacement amounts of 20% to 35% (by volume) are permissible under TxDOT Standard Specifications.[4.4] Cement replacement with fly ash is common practice in Texas bridges, normally at the contractor's request due to the low cost of fly ash in comparison to cement.

Due to the increasing use of fly ash in concrete, it was decided to investigate its effect on corrosion protection when fly ash is simply used as partial cement replacement and no other changes are made to the mix design. It was decided to use the standard TxDOT concrete for bridge substructures in most specimens, and replace 35% of the cement by volume (31% replacement by weight) with fly ash in two columns. No other significant changes were made to the concrete mix. ASTM[4.5] Class C fly ash was supplied by the ready-mix concrete supplier.

4.3.5 Prestressing Bar Coatings

Two prestressing bar coatings are investigated in the long term column exposure tests. Epoxy-coated and zinc galvanized prestressing bars are compared to uncoated prestressing bars. The coated bars were compared directly to uncoated bars within individual specimens, as shown in Figure 4.7.

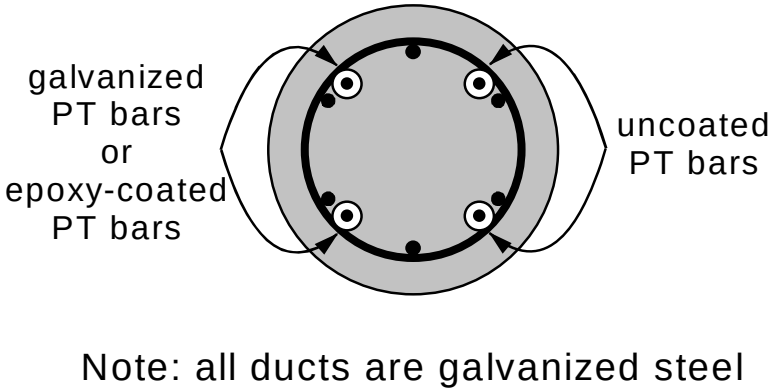

Figure 4.7 - Comparison of Coated and Uncoated Prestressing Bars

4.3.5.1 Epoxy-coated Bars

High strength threaded bars commonly used for post-tensioning may be specified with epoxy coating. Epoxy-coated threadbars are coated according to ASTM A775-97,[4.6] the same standard used for epoxy coating mild steel reinforcement. Anchorage hardware, including bearing plates, nuts and couplers are also epoxy-coated. Nuts and couplers are proportioned to allow free movement over the threads without damaging the epoxy coating.

4.3.5.2 Galvanized Bars

Threaded galvanized prestressing bars are commercially available in standard sizes and strengths of threadbar for prestressing. The high strength prestressing bars are galvanized according to strict specifications to minimize the potential for hydrogen embrittlement. Similar to the epoxy-coated prestressing bars, bearing plates, nuts and couplers are also galvanized. Nuts and couplers are proportioned to limit damage to the zinc coating.

4.3.6 Post-Tensioning Ducts

Impermeable plastic ducts are compared to standard galvanized steel ducts. Due to the short column height, duct splices were not necessary in the column specimens, and thus were not introduced as a test variable. The performance of plastic ducts was compared directly to galvanized steel ducts within individual specimens as shown in Figure 4.8. Uncoated post-tensioning bars were used in columns where duct type was evaluated.

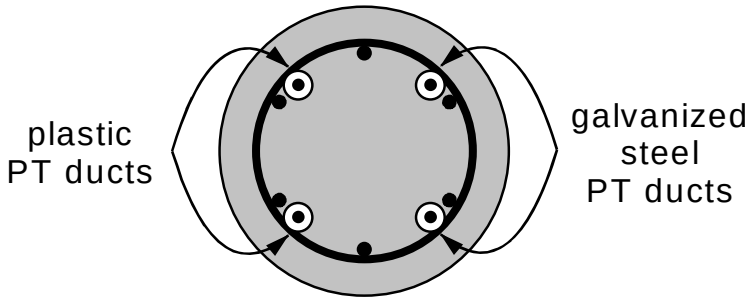

Figure 4.8 - Comparison of Galvanized Steel and Plastic Ducts for Post-Tensioning

4.4 Experimental Program (Specimen Types)

A total of ten specimen types were needed to address the selected variables. The complete experimental program is listed in Table 4.3. A specimen notation scheme used throughout the testing program is shown after the table.

Table 4.3 – Column Specimen Types and Variables

Specimen	Foundation Connection	Concrete Type	Loading	PT Protection
1 DJ-TC-N	Doweled	Class C	Unloaded	n/a
2 PT-TC-N-PD	Post-tensioned	Class C	Unloaded	Plastic Duct
3 NJ-TC-N	No Joint	Class C	Unloaded	n/a
4 DJ-TC-S	Doweled	Class C	Service	n/a
5 PT-TC-S-PD	Post-tensioned	Class C	Service	Plastic Duct
6 NJ-TC-S	No Joint	Class C	Service	n/a
7 PT-TC-S-EB	Post-tensioned	Class C	Service	Epoxy-coated PT Bar
8 PT-TC-S-GB	Post-tensioned	Class C	Service	Galvanized PT Bar
9 DJ-FA-S	Doweled	35% Fly Ash	Service	n/a
10 PT-FA-S-PD	Post-tensioned	35% Fly Ash	Service	Plastic Duct

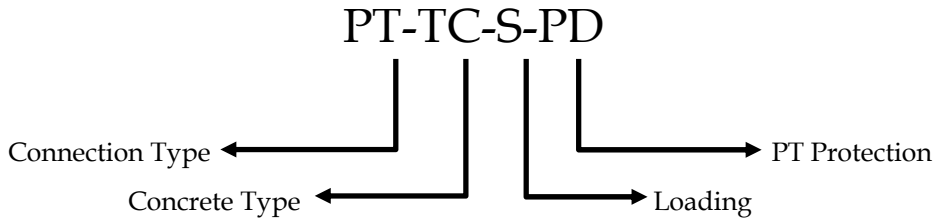

Connection Type:
- DJ = Doweled Joint
- PT = Post-tensioned Joint
- NJ = No Joint

Concrete Type:
- TC = TxDOT Class C
- FA = 35% Fly Ash

PT Protection:
- PD = Plastic Duct*
- EB = Epoxy-coated PT Bar**
- GB = Galvanized PT Bar**
- Blank = Not applicable (i.e., no PT)

Loading:
- N = No Load
- S = Service Load

Notes:

* plastic ducts used for bars 1 and 2, galvanized steel ducts used for bars 3 and 4

** epoxy-coated or galvanized bars used for bars 1 and 2, uncoated bars used for bars 3 and 4

4.5 Experimental Setup

Due to the specimen size and expected long duration of the exposure testing, it was decided to place the column testing program outside of the Ferguson Laboratory. A suitable location was found adjacent to the Construction Materials Research Group building. The ground was leveled and a layer of gravel was placed over heavy plastic sheeting. The design requirements for the experimental setup included:

- provide simulated foundation for the column specimens,
- permit loading of the columns without requiring the lab strong floor, and
- accommodate exposure conditions consisting of saltwater continuously ponded around column base and regular application of saltwater to one face of columns.

The experimental setup is shown schematically in Figure 4.9. It was decided to use a large reinforced concrete foundation to support the columns, provide load reactions and hold ponded saltwater. The dimensions of the foundation are 4.67 m (15.33 ft) long, 915 mm (36 in.) wide and 460 mm (18 in.) high. A 152 x 152 mm (6 x 6 in.) curb was provided around the top surface of the foundation to contain ponded saltwater. The foundation size was dictated by the necessity of moving the foundation with a forklift from inside the laboratory to its final outdoor position. Each foundation accommodates five column specimens, although only two columns are shown in place in Figure 4.9. Loading is applied on the columns using a stiffened loading plate on top of the column and four 25 mm (1 in.) threaded prestressing bars. These bars have been referred to as "tie-down bars" in the figure to avoid confusion with the internal post-tensioning bars used in selected specimens. The loading system is self-reacting, as the foundation provides the reaction for both the column and prestressing bars. Eccentric loading is achieved by adjusting the level of loading in the bars to apply the desired moment and axial force. A photo of the complete experimental setup is shown in Figure 4.10. Two foundations were used to accommodate the ten specimens.

The reinforced concrete foundation was designed using a strut and tie model to resist the complex pattern of reaction forces and post-tensioning forces. All foundation reinforcement was epoxy-coated to prolong the life of the foundation. The top surface and curbs of the foundation were painted with swimming pool paint to improve water-

tightness of the ponded area and to limit penetration of chlorides into the foundation. High performance concrete containing fly ash was used to further improve the durability of the foundation. Concrete for the foundations was selected from a list of design mixes supplied by a local ready-mix concrete producer. Concrete for the non-prestressed column foundation had a design strength of 55 MPa (8000 psi) and contained 30% fly ash by weight. Concrete for the post-tensioned column foundation had a design strength of 96 MPa (14,000 psi) and contained 26% fly ash by weight. Details of the foundation concrete are listed in Table 4.4. Details of the foundation reinforcement and loading plates are included in Appendix D.

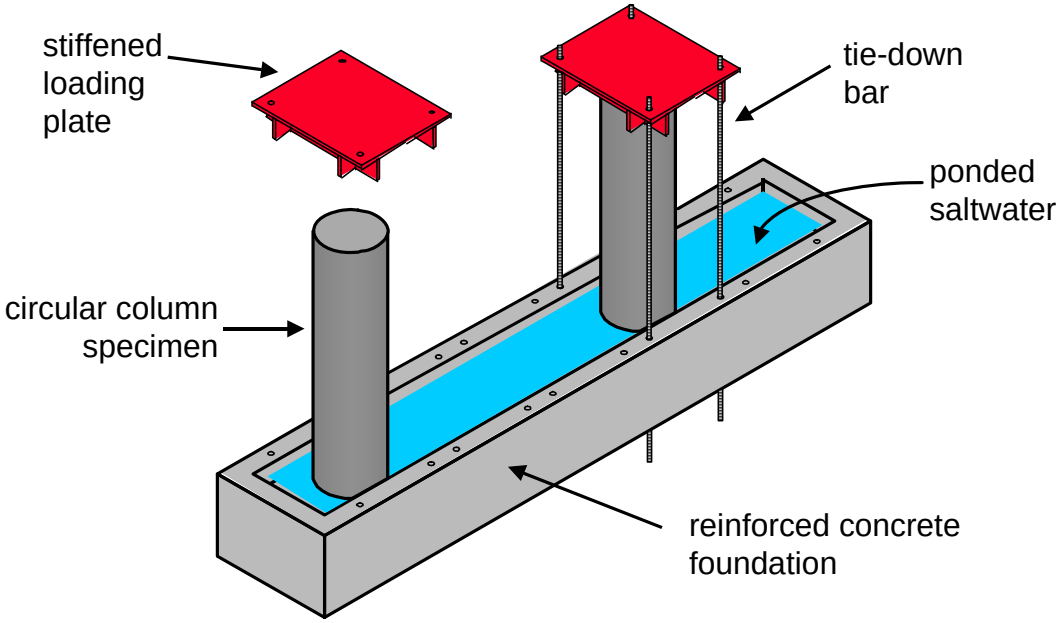

Figure 4.9 - Long Term Column Corrosion Test Setup – Schematic

Figure 4.10 - Long Term Column Corrosion Test Setup

The applied loading is to be sustained on the columns for the duration of exposure testing. The effect of concrete creep and shrinkage on the loading system was investigated using the procedure proposed by Ghali and Favre, (see Section 3.2.3). The loading system was treated as external prestressing in the calculations, and loading force losses were estimated for various time periods. Due to the relatively low axial force on the column, average loading force losses (i.e., in the tie down bars) for the post-tensioned columns were only 6.6% for the period of 500 days from first loading. Losses were even lower for the reinforced concrete column, reaching 3.6% over the first 500 days of loading. Due to their small magnitude, it was decided not to complicate the loading system by introducing springs in an attempt to reduce the losses. Rather, it was decided to simply re-apply the loading forces on the columns every twelve to sixteen months. Column specimens were re-loaded in December 1997. The re-loading procedure was completed in less than one day.

4.5.1 Exposure Conditions

Exposure conditions for the column specimens consist of saltwater continuously ponded around the base of the columns to simulate a coastal exposure. The effect of de-

icing salts dripping from the superstructure or saltwater spray is simulated by trickling saltwater on one face of each column for a period of six to eight hours every two weeks. A small electric pump and system of hoses is used to provide the trickled water, as shown in Figure 4.11. Valves are used at each column to control the flow rate to provide equal flow of trickled water to each column. Flow rates are determined manually by measuring the length of time to fill a known volume. The saltwater used in this testing program is a 3.5% solution of NaCl in tap water. The salt concentration is based on the recommendations of ASTM G109.[4.7]

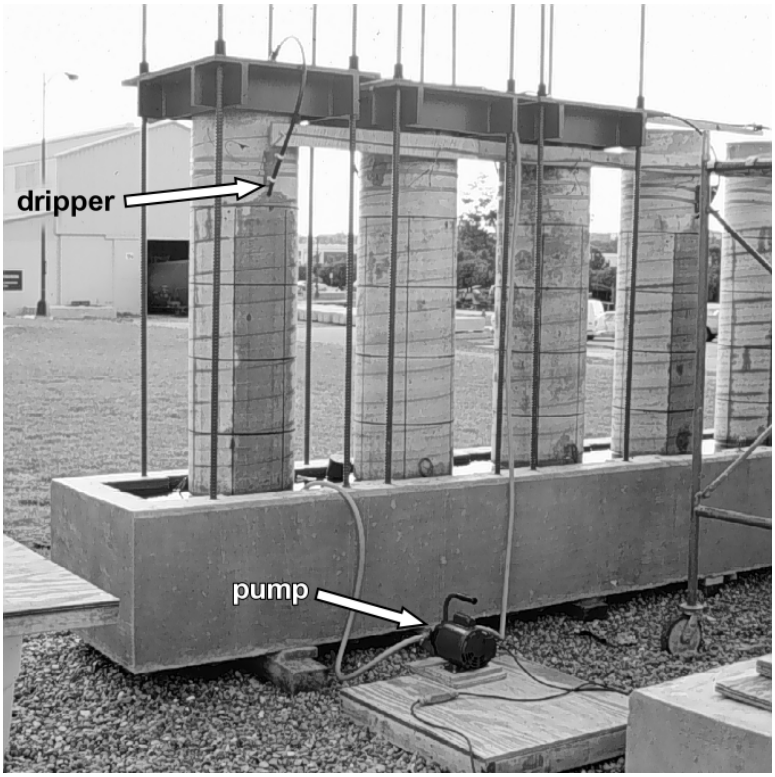

Figure 4.11 - Trickled Saltwater Exposure for Columns

4.5.2 Specimen Locations

The locations of the column specimens on the two foundations are shown in Figure 4.12. All references are made with respect to the North direction. The mild steel reinforcement and post-tensioning bars were numbered according to the scheme shown in Figure 4.12. The curved arrows in the figure indicate the direction of applied moment on

each column. Columns without arrows were not loaded. A capital "D" is used to indicate the location of the dripper for trickled water on each column. The dripper was located on the tension side of the column for loaded columns. Plastic ducts, epoxy-coated post-tensioning bars and galvanized post-tensioning bars were placed in PT Bar Locations 1 and 2 in the appropriate specimens. Locations 3 and 4 have uncoated post-tensioning bars and galvanized steel ducts in these specimens.

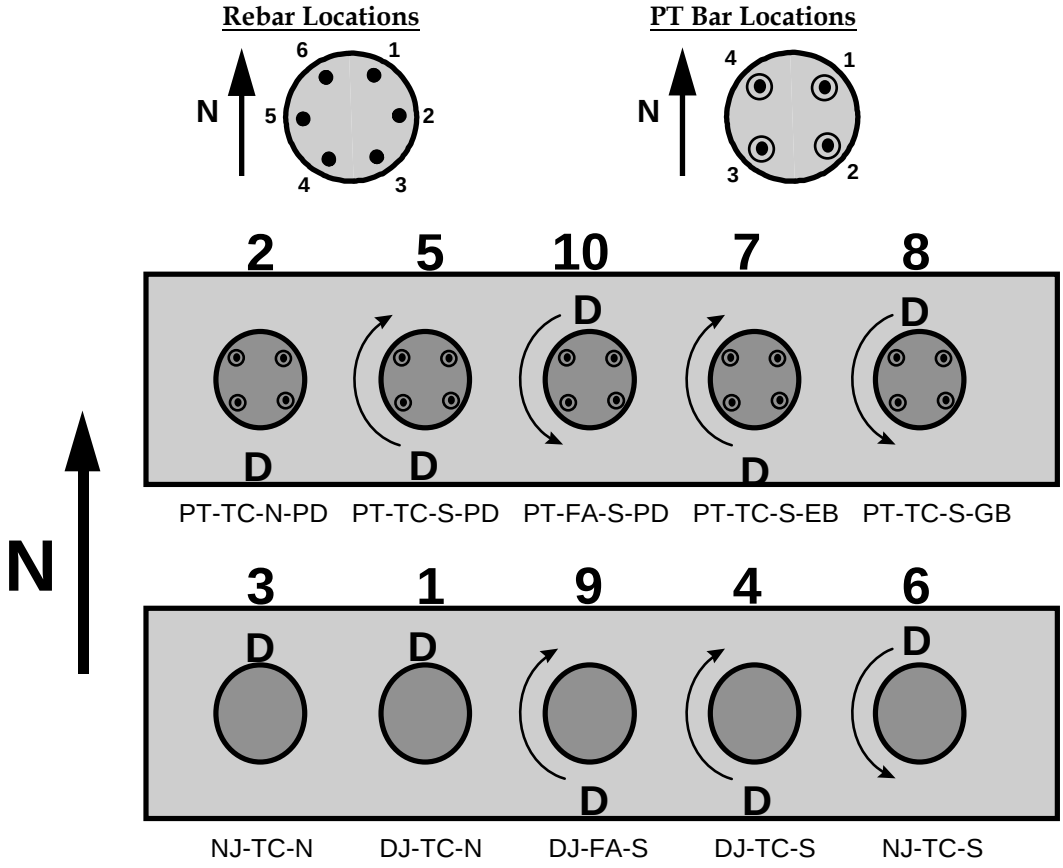

Figure 4.12 - Column Specimen Locations and Related Test Details

4.6 Materials

Similar to the beam corrosion tests, materials and proportions were selected to match Texas Department of Transportation Standard Specifications[4.4] where possible. Concrete was supplied by a local ready-mix concrete producer. Grouts for post-tensioning

were batched in 18.9 liter (5 gal.) buckets using a paddle mixer mounted to a large hand-held drill. Mild steel reinforcement was supplied and fabricated by a local steel fabricator. Post-tensioning hardware was fabricated by the supplier. The materials used in the column corrosion tests are summarized in Table 4.4. Complete details of specimen construction are provided in Section 4.7.

Table 4.4 - Construction Material Details: Column Specimens

Item	Description			
Column Concrete: Texas DOT Class C Concrete for Bridge Substructures	• w/c = 0.45 (based on slump, max. allowable w/c = 0.53) • f'c = 25 MPa (3600 psi) minimum allowable • batch proportions: (per 0.764 m^3 (1 yd^3)) Coarse Aggregate (19 mm) — 851 kg — 1877 lbs Fine Aggregate — 538 kg — 1186 lbs Type I/II Cement — 256 kg — 564 lbs Water — 115 kg — 254 lbs Set retarder — 710 ml — 24 oz Entrained Air Admixture — 118 ml — 4 oz • cylinder strengths: (average) 7-day — 30.0 MPa — 4358 psi 14-day — 36.2 MPa — 5250 psi 28-day — 36.4 MPa — 5284 psi			
Column Concrete: Texas DOT Class C Concrete with 31% Fly Ash by Weight	• w/(c +p) = 0.42 • f'c = 25 MPa (3600 psi) minimum allowable • batch proportions: (per 0.764 m^3 (1 yd^3)) Coarse Aggregate (19 mm) — 834 kg — 1855 lbs Fine Aggregate — 586 kg — 1245 lbs Type I/II Cement — 164 kg — 362 lbs Class C Fly Ash — 73 kg — 162 lbs Water — 100 kg — 220 lbs Set retarder — 591 ml — 20.0 oz Entrained Air Admixture — 104 ml — 3.5 oz • cylinder strengths: (average) 7-day — 30.7 MPa — 4447 psi 28-day — 44.6 MPa — 6473 psi			
Foundation Concrete Mix 1 (for RC Columns, Capitol Aggregates Mix 241)	• w/(c + p) = 0.39 • f'c = 55 MPa (8000 psi) design strength • batch proportions: (per 0.764 m^3 (1 yd^3)) Coarse Aggregate (19 mm) — 812 kg — 1790 lbs Fine Aggregate — 513 kg — 1131 lbs Type I/II Cement — 238 kg — 525 lbs Class C Fly Ash — 102 kg — 225 lbs Water — 134 kg — 295 lbs Set Retarder — 665 ml — 22.5 oz • avg. cylinder strengths: 28-day — 42.9 MPa — 6220 psi			

Table 4.4 (Continued) – Construction Material Details: Column Specimens

Item	Description			
Foundation Concrete Mix 2 (for PT Columns, Capitol Aggregates Mix 246)	• w/(c + p) = 0.25 • f'c = 96 MPa (14,000 psi) design strength • batch proportions: (per 0.764 m^3 (1 yd^3)) Coarse Aggregate (12.7 mm) — 812 kg — 1665 lbs Fine Aggregate — 513 kg — 1371 lbs Type I/II Cement — 238 kg — 714 lbs Class C Fly Ash — 102 kg — 254 lbs Water — 134 kg — 240 lbs Superplasticizer — 4730 ml — 160 oz • cylinder strengths: (average) 7-day — 35.2 MPa — 5102 psi 14-day — 52.0 MPa — 7536 psi 28-day — 58.5 MPa — 8478 psi			
TxDOT Grout for Post-Tensioning (see note at end of Section 4.7.4)	• w/c = 0.44 • batch proportions: (per 0.028 m^3 (1 ft^3)) Type I Cement — 37.4 kg — 82.4 lbs Water — 16.4 kg — 36.2 lbs			
Threaded Prestressing Bars	• 16 mm (5/8 in.) diameter high strength threaded prestressing bar • Grade 157 (1080 MPa, 157 ksi) • Supplier: Dywidag Systems, Inc.			
Mild Steel Reinforcement	• ASTM A615, Grade 60 (400 MPa, 60 ksi)			
Steel Duct	• Corrugated, semi-rigid, galvanized steel duct • 40 mm (1.575 in.) outside diameter • Supplier: Dywidag Systems, Inc.			
Plastic Duct	• Corrugated, flexible plastic duct • 51 mm (2 in.) outside diameter • Supplier: Dywidag Systems, Inc.			
Epoxy Bonding Agent	• Sikadur 32 High-Mod - Epoxy Bonding Adhesive • Supplier: Sika			

Column specimen concrete and foundation concrete were sampled for strength testing using typical practices. Concrete cylinder strength data for the column specimens is listed in Table 4.5 and Table 4.6. All cylinder strengths exceeded the minimum requirements for TxDOT Class C Concrete for Bridge Substructures.[4.4] Foundation concrete strengths did not reach their design values, but were deemed sufficient. The foundation concrete mix designs were selected from a catalog of concrete mixes available from the ready-mix concrete supplier. Grout for post-tensioning was not sampled for strength testing, as this is not required by TxDOT specifications.[4.4]

Table 4.5 – TxDOT Class C Concrete Cylinder Strengths

Column Numbers	Average Cylinder Strength 7 Day	14 Day	28 Day
1, 3, 4, 6	33.0 MPa (4791 psi)	42.6 MPa (6177 psi)	42.0 MPa (6091 psi)
2, 5, 9, 10	27.0 MPa (3924 psi)	29.8 MPa (4324 psi)	30.9 MPa (4478 psi)
Averages	30.0 MPa (4358 psi)	36.2 MPa (5250 psi)	36.4 MPa (5284 psi)

Table 4.6 - 35% Fly Ash Concrete Cylinder Strengths

Column Numbers	Average Cylinder Strength 7 Day	14 Day	28 Day
7	35.2 MPa (5107 psi)	41.6 MPa (6028 psi)	46.2 MPa (6706 psi)
8	26.1 MPa (3788 psi)	n/a	43.0 MPa (6240 psi)
Averages	30.7 MPa (4447 psi)	n/a	44.6 MPa (6473 psi)

4.7 Construction

The column foundations were constructed inside the Ferguson Laboratory. Column reinforcement was prepared and placed on the foundations inside the lab. The foundations were then moved outside and into their final position prior to casting of the columns. Post-tensioning and loading of the columns took place in their final position. All construction, post-tensioning and loading was performed by the graduate and undergraduate research assistants working on the project.

4.7.1 Foundations

All foundation reinforcement was epoxy-coated. Reinforcement assemblies were prepared following typical construction practices for epoxy-coated reinforcement. Epoxy-coated tie wire was used, and all cut ends and damaged areas were repaired using appropriate patching materials. Reusable wooden forms were constructed for casting the foundations. Concrete was supplied by a local ready-mix producer, and poured using a concrete bucket on an overhead crane. Concrete was placed and vibrated with hand held

concrete vibrators following typical practice. The concrete was wet cured for a minimum of three days. Several photos of the foundation reinforcement are shown in Figure 4.13.

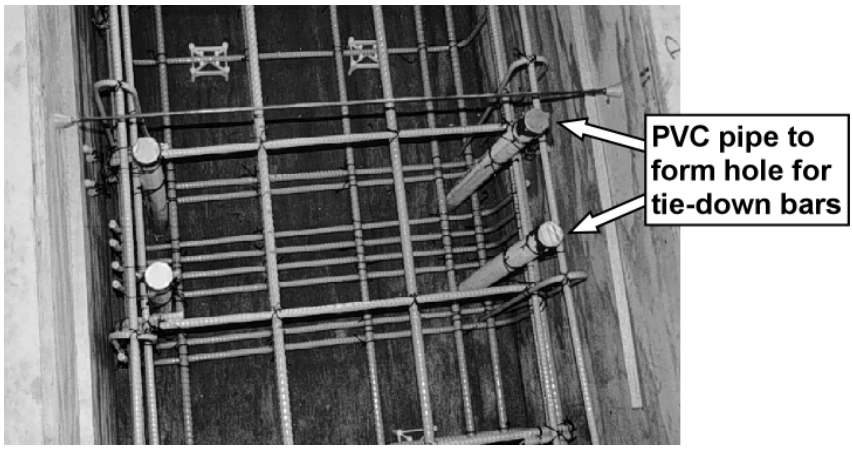

Top View

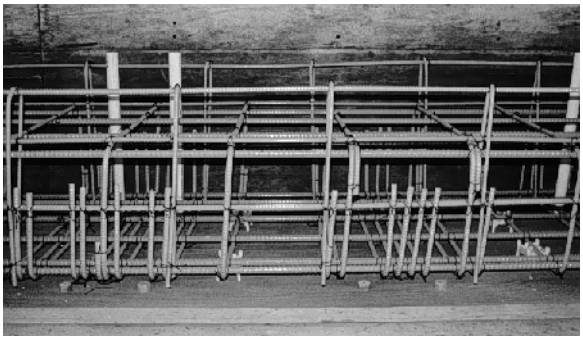

Side View

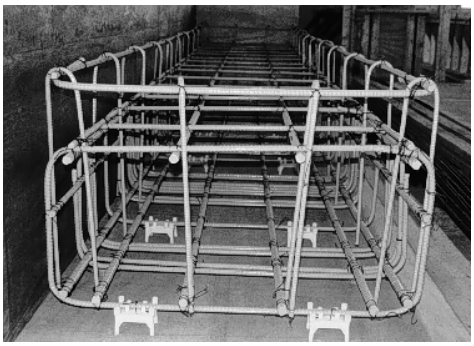

End View

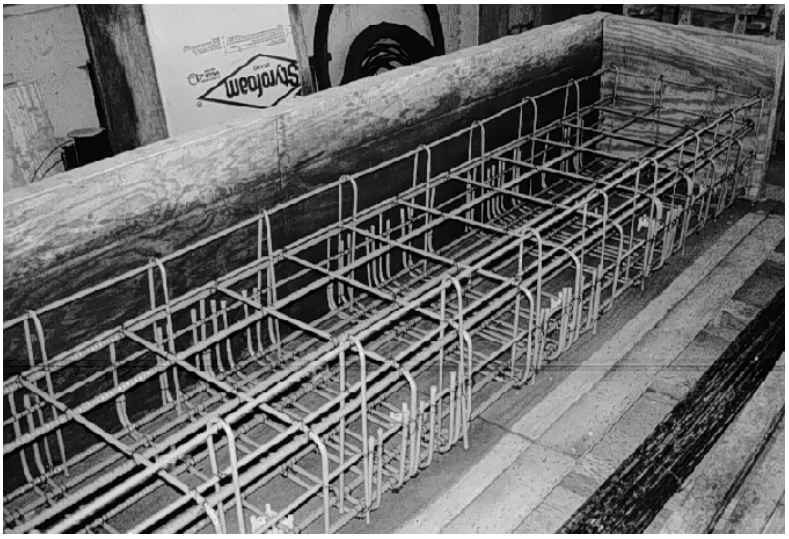

Overall View

Figure 4.13 - Foundation Reinforcement

4.7.2 Columns

Column reinforcement and post-tensioning hardware were assembled and placed on the foundation inside the lab. Ground clamps were used to attached a ground wire to the mild steel reinforcement for half-cell potential measurements during testing. Cardboard tube forms were used to form the columns. Tubes were fixed in position using a wooden frame to prevent movement during concrete casting. Concrete was tremied into the columns using a concrete bucket mounted on a forklift. Column construction is shown in Figure 4.14.

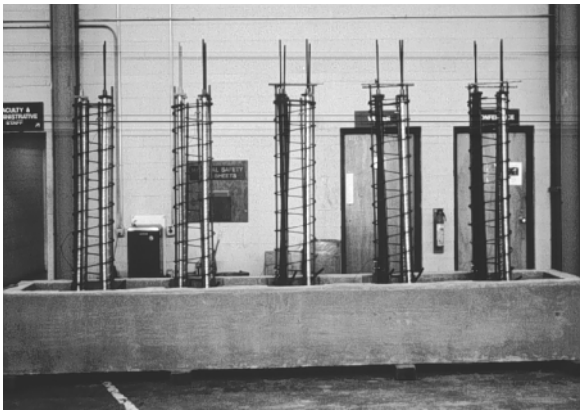

Column Reinforcement on Foundation

Ground Clamp to Attach Ground Wire

Pouring Column Concrete with Tremie Tube Attached to Concrete Bucket

Figure 4.14 - Column Construction

The post-tensioned columns required several additional details. As described in Section 4.3.2, short lengths of post-tensioning bar were cast into the foundation to provide anchorage for the column post-tensioning bars. Figure 4.15 shows the four post-tensioning bars protruding from the foundation. Shallow, square pockets were formed around each bar to accommodate rubber gaskets to seal the "dead end" of the post-tensioning ducts. The column post-tensioning bars were coupled to the protruding bars prior to placement of the ducts. The assembled reinforcement and post-tensioning hardware are shown in Figure 4.15. Plastic grout tubes were attached to the ducts near the base of the column, as visible in Figure 4.15. The post-tensioned columns were cast to a reduced height of 1.68 m (5.5 ft) to permit later capping of the columns to protect the post-tensioning anchorages. Four of the six reinforcing bars and the spiral reinforcement were reduced in length to accommodate the reduced column height. The remaining two vertical bars were extended full height with the post-tensioning bars to provide continuity with the concrete cap. After post-tensioning and grouting was completed, one full turn of the spiral reinforcement was placed around the protruding bars, and the column was capped with concrete to its full height. The configuration of the column immediately prior to capping is shown in Figure

4.15. Ground clamps were used to attach ground wires to the post-tensioning bar ends prior to capping.

4.7.3 Column Post-Tensioning

The column post-tensioning process was simpler than that for the beam specimens. Due to the specimen size, straight tendon path and use of post-tensioning bars rather than strands, prestress losses during stressing were negligible. The post-tensioning jacking force, F_{pj}, was taken equal to the initial prestress force, F_{pi} ($0.68f_{pu}A_{pbar}$ = 133 kN (30 kips)).

Each bar was post-tensioned individually. The post-tensioning hardware consisted of a steel post-tensioning chair and 534 kN (120 kips) hollow stressing ram, as shown in Figure 4.16. A short extension bar was temporarily coupled to the bar to be stressed to provide the necessary length to pass through the stressing ram. The post-tensioning force during stressing was monitored using a load cell and by a pressure gauge on the hydraulic pump. Once the desire force was achieved, the nut on the post-tensioning bar was tightened to refusal using a large wrench to minimize seating losses.

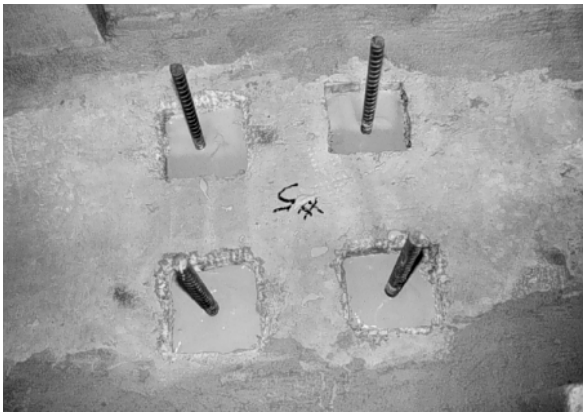

PT Bars Protruding from Foundation

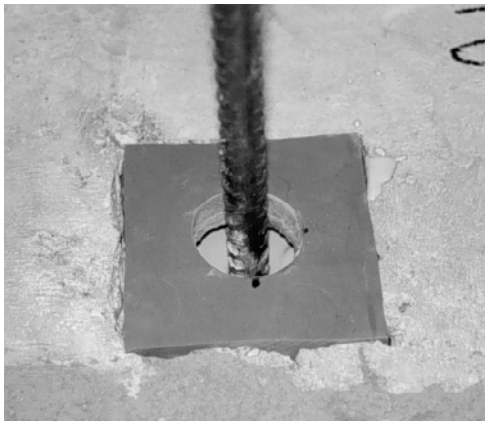

Gasket Around Post-Tensioning Bar

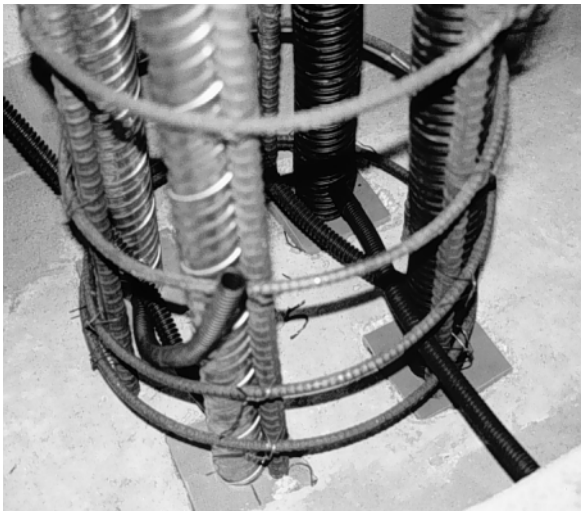

Reinforcement, Ducts and Grout Tubes

Top of Column Prior to Capping

Figure 4.15 - Post-Tensioned Column Construction Details

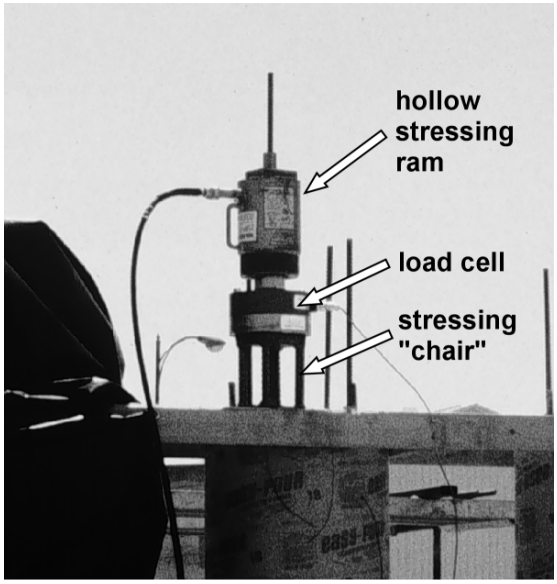

Figure 4.16 - Column Post-Tensioning

4.7.4 Grouting

The post-tensioned columns were grouted immediately following post-tensioning. All grouting procedures were performed according to

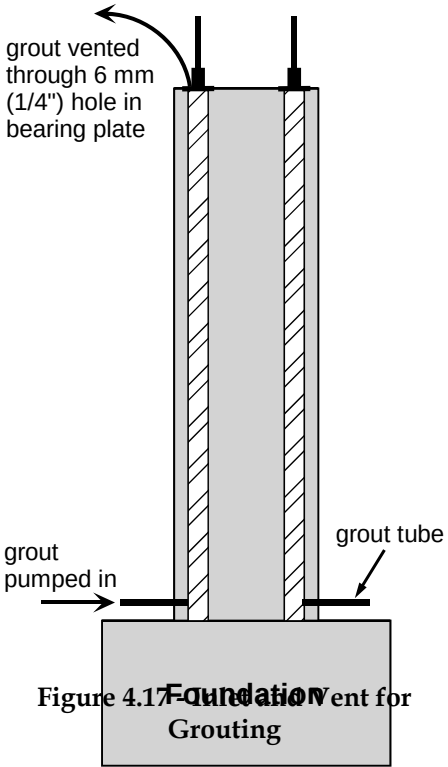

Figure 4.17 - Duct and Vent for Grouting

TxDOT Specifications.[4.4] The grouting setup is shown in Figure 4.17. A 19 mm (0.75 in.) grout tube with shut off valve was used for the inlet. The vent at the top of the column was provided by drilling a 6 mm (0.25 in.) hole through the bearing plate adjacent to the nut. Grouts were mixed in large buckets using a paddle mixer on a large hand held drill, and pumped immediately using an electric grout pump. Grout was poured into the pump reservoir through a screen to remove lumps, if any. The grout was continuously stirred in the reservoir to prevent segregation. Grout was pumped into each duct without stoppage. Once a continuous flow of grout was exiting the vent with no slugs of air or water, the vent was closed by hammering a wooden dowel into the hole. The pump was then restarted for a period of 2 to 3 seconds before closing the valve on the inlet tube.

Important Note

After the column grouting had been completed, the possibility of an error in the post-tensioning grout came to light. It is possible that incorrectly labeled cement barrels may have resulted in partial or complete cement replacement with Class F fly ash. The amount of fly ash, if any, is not certain. If the fly ash content is high, very little hydration will have occurred, and the effect of this on the experimental results is not certain. Persons performing invasive inspections or autopsies on the columns should be aware of the possibility of fly ash in the grout. The most likely columns to contain fly ash grout are PT-TC-S-EB and PT-TC-S-GB.

4.7.5 Column Loading

The column specimens were loaded (where applicable) after all construction was completed. The top surface of the columns was prepared using Plaster-of-Paris to level the surface and provide even bearing for the stiffened loading plates (details of the loading plates are shown in Appendix D). Column loading was performed using the apparatus shown in Figure 4.18. The necessary applied forces are shown in Figure 4.19. A separate hydraulic pump was used for each ram, and the forces T_1 and T_2 were applied simultaneously in four increments of 22% and a final increment of 11%. The applied forces were monitored during each increment using load cells and pressure gauges on each pump. Tie-down bar nuts were tightened to refusal using a large wrench once the desired forces had been attained. The identical apparatus and procedure is used for

regular re-loading of the columns to restore any losses resulting from creep and shrinkage of the concrete.

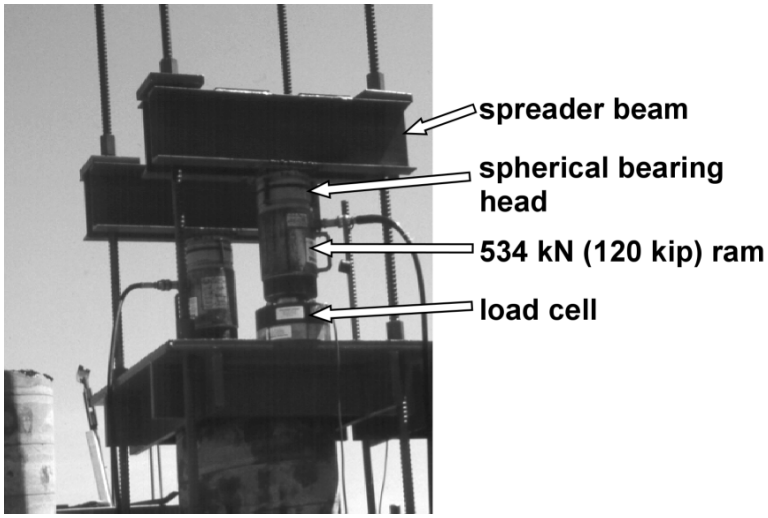

Figure 4.18 - Column Loading Apparatus

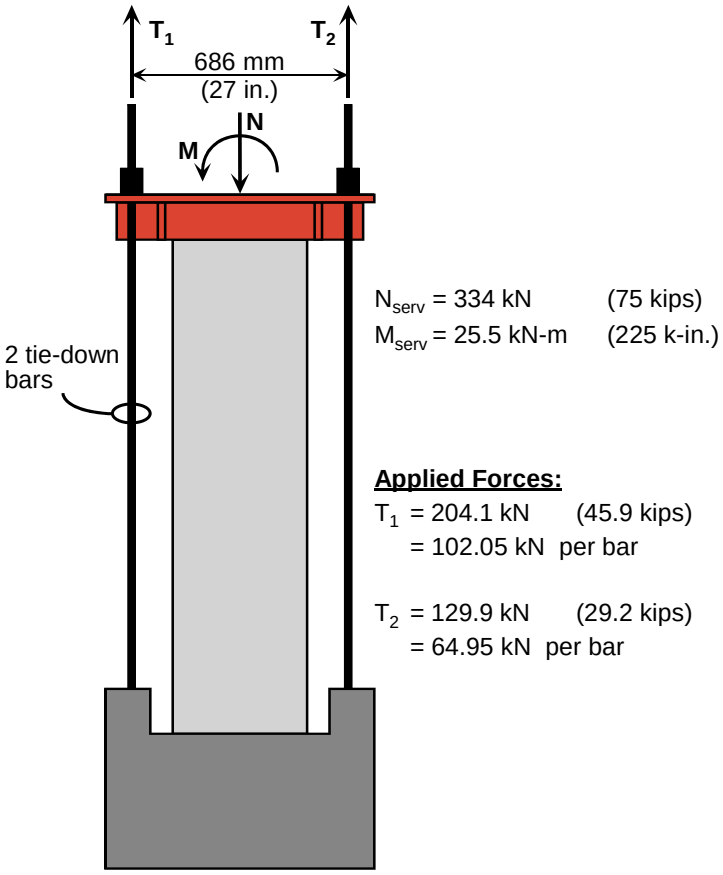

Figure 4.19 - Column Loading Forces

4.8 Measurements During Exposure Testing

Column specimen condition and corrosion activity are regularly evaluated using visual observations and half-cell potential readings, and by measuring chloride ion penetration. Each is described below.

4.8.1 Visual Examination

The appearance of the specimens can indicate corrosion activity or distress. The beam specimens are regularly examined for signs of spalling, rust staining, cracking and any other indication of distress.

4.8.2 Half-Cell Potential Readings

Half-cell potential readings can indicate the probability of corrosion at a given location, and can be used to detect corrosion initiation if regular measurements are taken during testing. Half-cell potential readings require a reference electrode, voltmeter and electrical connection to the reinforcement. As mentioned in Section 4.7, ground clamps were used to attach ground wires to the mild steel reinforcement and post-tensioning bars during construction.

Half-cell potential readings are taken at one month intervals on a grid over the surface of the columns. The grid consists of six vertical lines, one located over each of the six vertical reinforcing bars, and three horizontal lines. The horizontal lines are spaced at 610 mm (24 in.), starting at 75 mm (3 in.) from the column base. The lowest horizontal reference line is below the level of continuously ponded saltwater. In order to limit the volume of data, readings are taken on every second reinforcing bar. This accounts for nine half-cell potential measurements on each column: bars 1, 3, and 5 (see Figure 4.12) at the bottom, mid-height and top reference lines as shown in Figure 4.20. Twelve additional measurements are performed on the post-tensioned columns: each post-tensioned bar at the bottom, mid-height and top reference lines.

The ground wires from each column were connected to a central switching box. The box contains a small voltmeter and a switching system to select the desired column or post-tensioning bar within a given column. The reference electrode is plugged into the measurement system at each column location. The switching box is shown in Figure 4.21.

Half-cell readings are performed according to ASTM C876.[4.8] For measurements at the mid-height and top reference lines, the concrete is dampened using the wetting solution specified in ASTM C876. The numerical significance of the half-cell potential readings was shown previously in Table 3.10. As mentioned in Chapter 3, half-cell potential readings are generally not an effective method for evaluating corrosion activity in bonded post-tensioned structures. However, by considering both the magnitude and variation of the readings during testing it may be possible to detect the onset of corrosion activity.

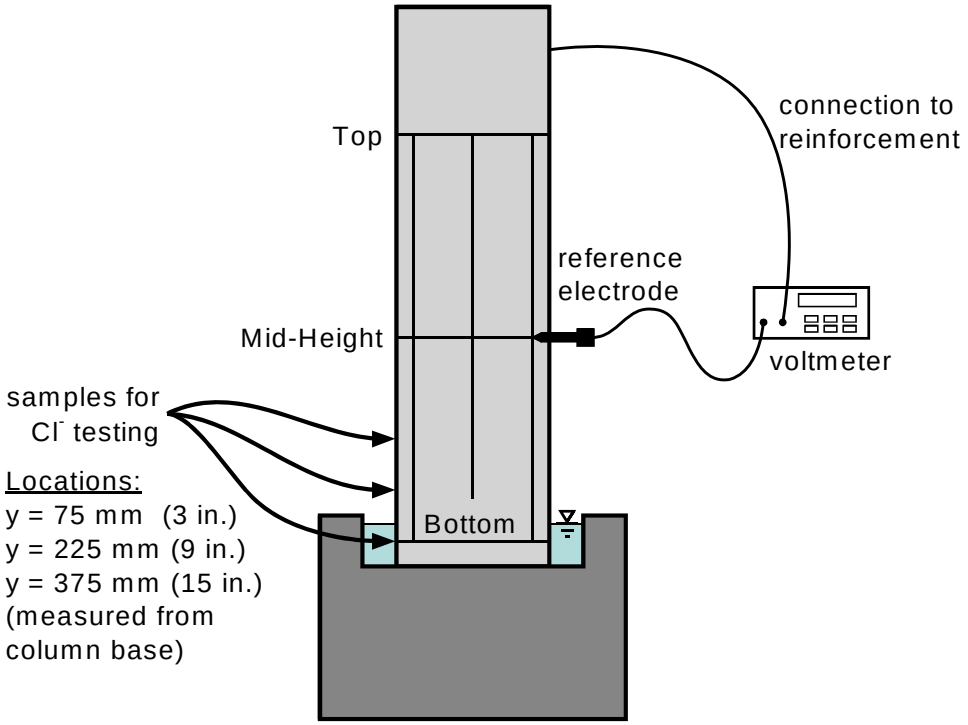

Figure 4.20 - Half-Cell Potential Measurement and Chloride Sample Locations

Figure 4.21 - Switching Box and Voltmeter for Column Half-Cell Potential Readings

4.8.3 Chloride Penetration

Measurement of chloride levels in several of the columns were used to monitor two phenomena:

1. **The penetration of chlorides into the concrete.** By regularly measuring chloride levels it is possible to determine when chloride concentrations at the

level of the steel reinforcement exceed the threshold for corrosion activity. Although this is not an absolute measurement of corrosion activity, it can be used in conjunction with other data to estimate whether corrosion initiation has occurred.

2. **The vertical migration of chlorides due to capillary action.** Reinforcement corrosion is frequently observed above the high tide line in marine structures. Chloride measurements in this testing program may determine the significance of capillary rise or wicking action to this form of corrosion damage.

Concrete powder samples were taken from selected columns at three locations and depths. Samples were taken at 75 mm (3 in.), 225 mm (9 in.) and 375 mm (15 in.) from the column base to evaluate vertical migration of chlorides, as shown in Figure 4.20. Three sample depths (12.7 mm, 25.4 mm, 50.8 mm (0.5 in., 1 in., 2 in.)) were collected at each location to evaluate the depth of chloride penetration.

Concrete powder samples were obtained using a rotary hammer (hammer drill) with a 12.7 mm (0.5 in.) bit. A special collection system was needed for the concrete powder since the samples were being taken from a vertical surface. A modified Shop-Vac was used for this purpose. A coffee filter was folded into a cone shape and placed part way into the vacuum nozzle. A small vacuum upholstery attachment was fitted over the filter to prevent it from being sucked into the vacuum. The wide mouth of the upholstery attachment was held directly under the drill bit while drilling to collect the powder while the suction drew the powder into the filter. After collecting a desired sample, the filter was removed and the concrete powder transferred to a plastic bag for later weighing and analysis. The filter was discarded and the upholstery brush was cleaned with distilled water to prevent contamination of later samples. Samples were analyzed for acid soluble chloride content using a specific ion probe (CL Test System by James Instruments). All sample collection and analysis procedures were based on AASHTO T260-94.[4.9]

Samples were collected for chloride analysis after one and a half years of exposure. Additional samples will be taken after two and a half years of exposure. Future samples will be collected with increasing regularity as dictated by specimen condition.

4.9 Experimental Results

Exposure testing was initiated in July 1996. Exposure test data recorded up to September 17, 1998 is presented in this section. The data gathered during this period does not provide a strong indication of corrosion initiation in any of the column specimens.

4.9.1 Visual Examination

No cracking or spalling has been observed in the column specimens during the reported exposure duration. After approximately one year of exposure, several very localized small areas of rust staining were observed in two columns. The rust stains were located at or below the level of continuously ponded saltwater. Half-cell readings in the vicinity do not suggest increased corrosion activity. The highly localized nature and early appearance suggests these stains have resulted from corrosion of bar chairs or tie wire.

4.9.2 Half-Cell Potential Readings

The volume of half-cell potential data collected during the reporting period is very large. Measurements were collected on twenty-five occasions from July 1996 to October 1998, producing 225 data points for each non-prestressed column and 525 data points for each post-tensioned column. Typical half-cell potential data is shown for three columns, NJ-TC-N, DJ-TC-N and PT-TC-N-PD, in Figure 4.22 through Figure 4.25. Data for column PT-TC-N-PD is split into two figures, one for mild steel reinforcement, and one for post-tensioning bars. The ASTM guidelines indicating high, low or uncertain corrosion probability are shown at the right of the figures. It is clear from these figures that presentation of all the half-cell potential data for a given column serves little purpose other than to illustrate the type and volume of data. Average half-cell potentials were calculated for measurements at the column base, mid-height and top. This data is more useful for showing trends in corrosion activity for the columns and the effect of variables. Average potential readings for all columns are included in Appendix D, Figures D.7 to D.16. The general trend in half-cell data is that the potentials become more negative moving from the top of the column to the base.

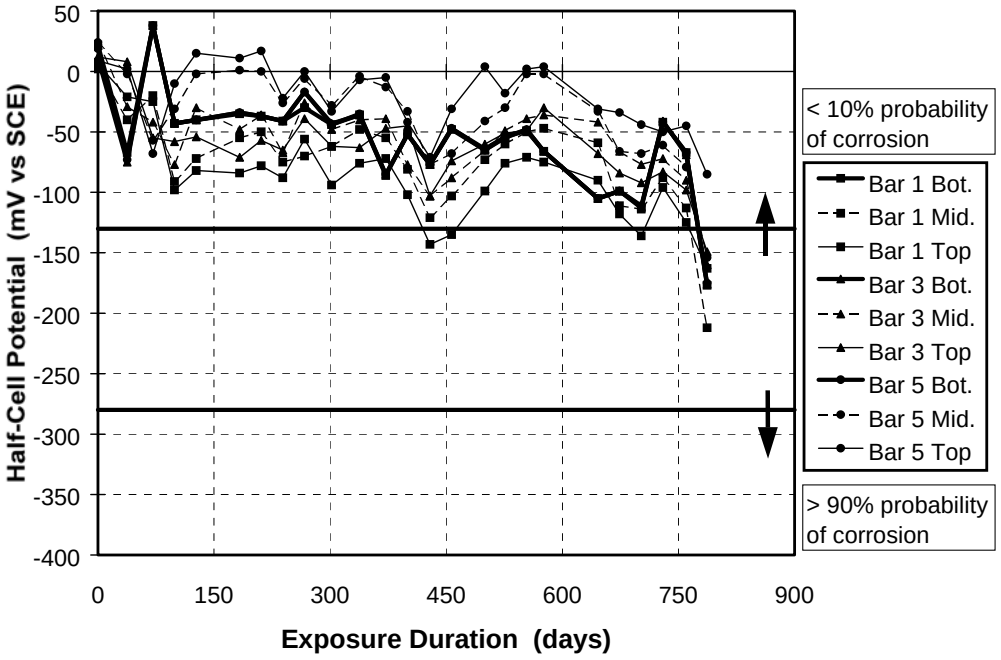

Figure 4.22 - All Half-Cell Potential Readings: Column NJ-TC-N

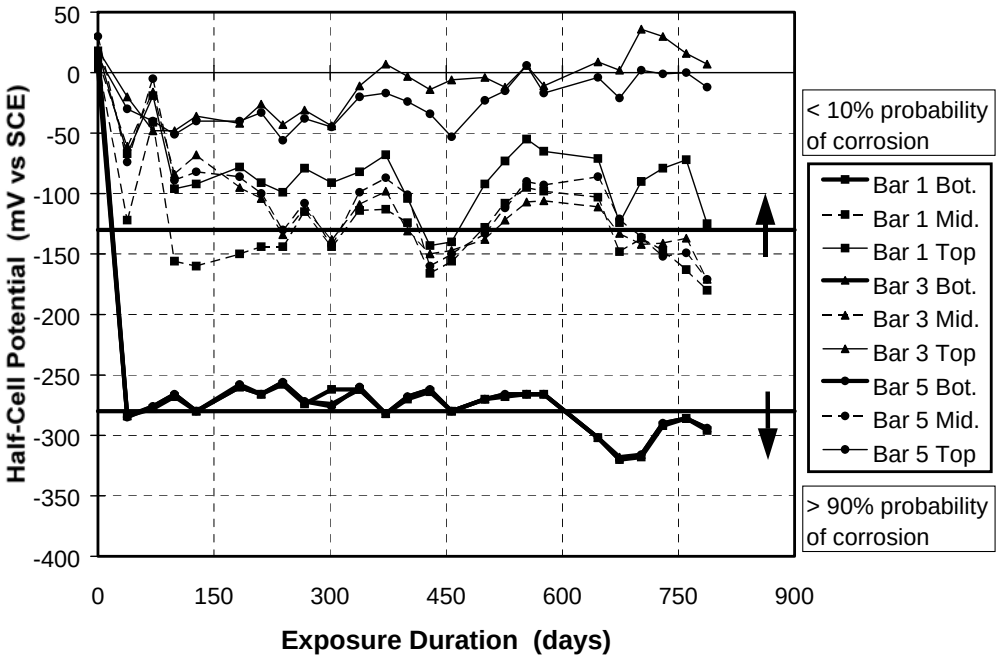

Figure 4.23 - All Half-Cell Potential Readings: Column DJ-TC-N

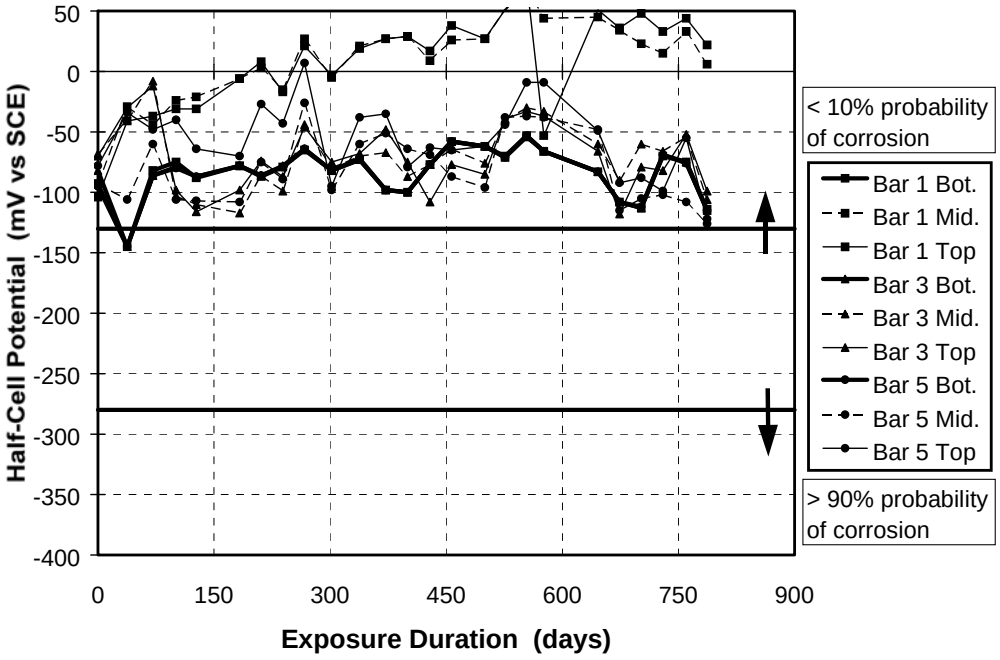

Figure 4.24 - All Half-Cell Potential Readings: Column PT-TC-N-PD - Rebar

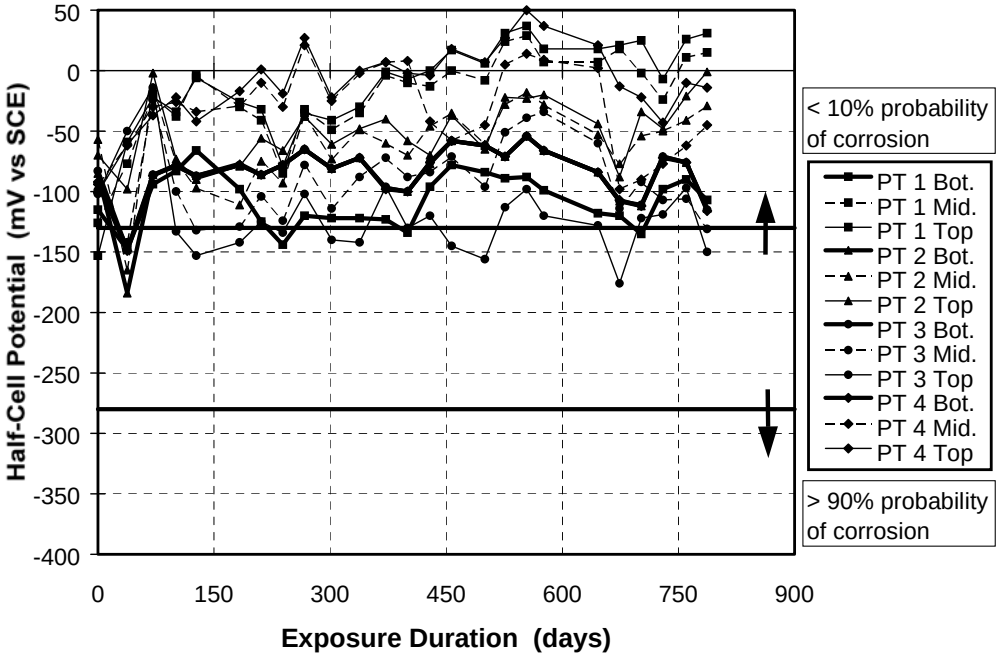

Figure 4.25 - All Half-Cell Potential Readings: Column PT-TC-N-PD - PT Bars

The relative performance of the columns is illustrated by plotting the average half-cell potentials at the column base. Average rebar potentials for the non-prestressed columns are shown in Figure 4.26. Figure 4.27 and Figure 4.28 show average rebar and post-tensioning bar measurements, respectively, for the post-tensioned columns. The data plotted in these three figures is very similar. The lowest (least negative) potentials generally coincide with specimens that are not loaded. The highest (most negative) potentials were measured for the no joint column under service loading (NJ-TC-S).

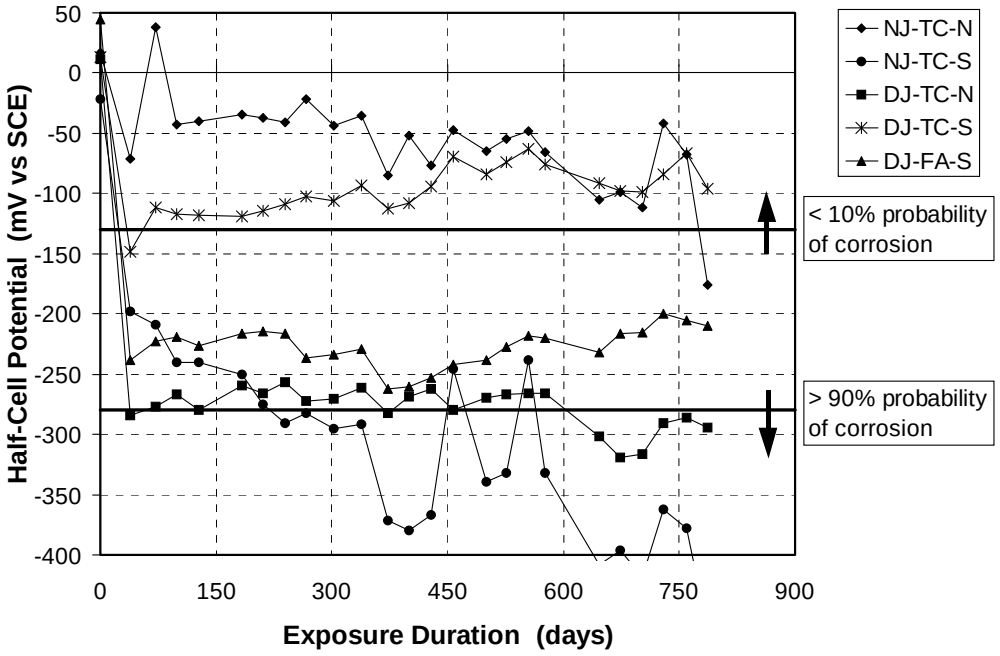

Figure 4.26 - Average Half-Cell Potentials at Column Base: Non-Prestressed Columns

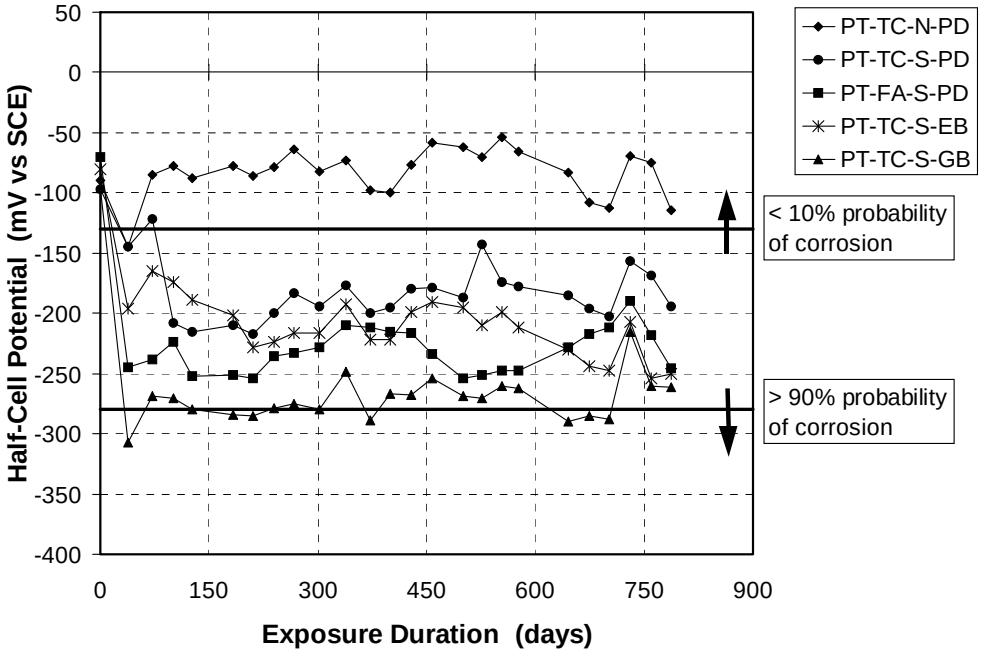

Figure 4.27 - Average Half-Cell Potentials at Column Base: PT Columns - Rebar

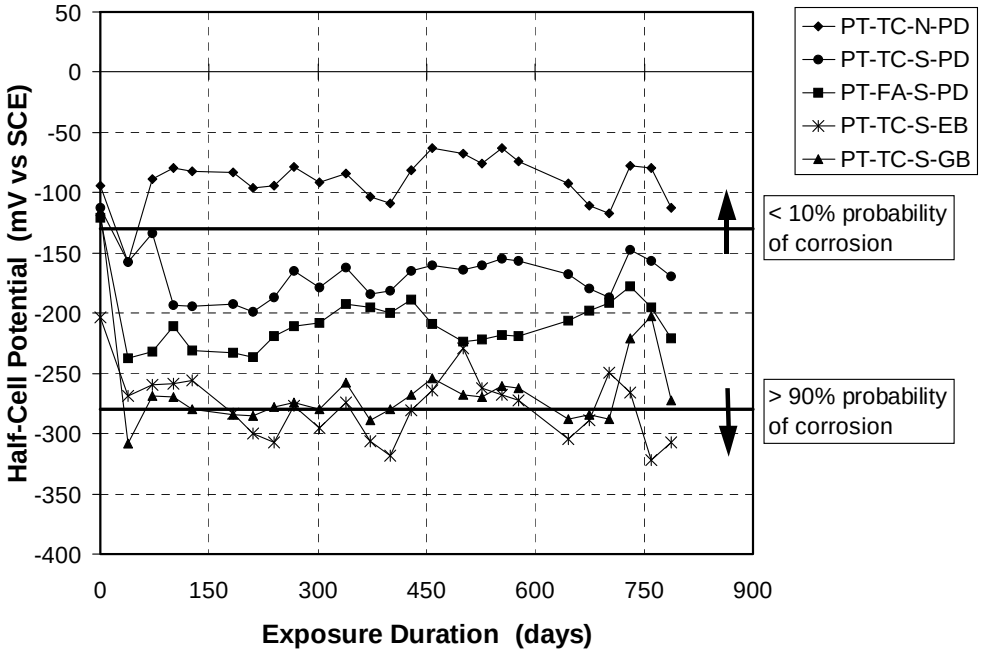

Figure 4.28 - Average Half-Cell Potentials at Column Base: PT Columns - PT Bars

4.9.3 Chloride Ion Measurements

Concrete powder samples for chloride analysis were collected after eighteen months of exposure testing. Four columns were selected for sampling to provide a representative indication of the major variables affecting chloride ion penetration: joint type and concrete type. The columns selected were NJ-TC-S, DJ-TC-S, PT-TC-S-PD and DJ-FA-S.

As described in Section 4.8.3, samples were collected at three vertical distances from the column base. Samples were collected at three concrete depths at each location. The concrete powder samples were taken from the side of the column opposite from the dripper locations. Two 12.7 mm (0.5 in.) diameter holes were drilled at each height, and the powder was collected into a single bag. The powder was mixed thoroughly and portioned into three 1.5 gram samples to be analyzed for acid soluble chlorides using a specific ion probe.

The results of the chloride analysis are plotted in Figure 4.29 through Figure 4.32. Three chloride profiles are plotted in each figure, one for each sample depth. The clear cover to the spiral reinforcement is 50 mm (2 in.) in these columns. Samples at that depth would be indicative of chloride levels near the reinforcement. The chloride threshold for corrosion is indicated in the figures as 0.030% by weight of concrete. This value is intended as a guideline only, and is based on the widely accepted chloride threshold value of 0.2% of the weight of cement.[4.10] This threshold value is for concrete with Portland cement, and could be different for concrete containing fly ash or other mineral admixtures.

In general, the chloride profiles decrease rapidly with height, and chloride levels at a height of 375 mm (15 in.) are very close to zero in all columns. Chloride levels at a depth of 13 mm (0.5 in) have exceeded the corrosion threshold near the base of the column in all specimens sampled. The no joint and doweled joint columns with TxDOT Class C concrete show chloride levels in excess of the corrosion threshold at a depth of 25 mm (1 in.) at the column base. The doweled joint specimen is the only column where chloride levels exceed the corrosion threshold at the level of reinforcement, as shown in Figure 4.30.

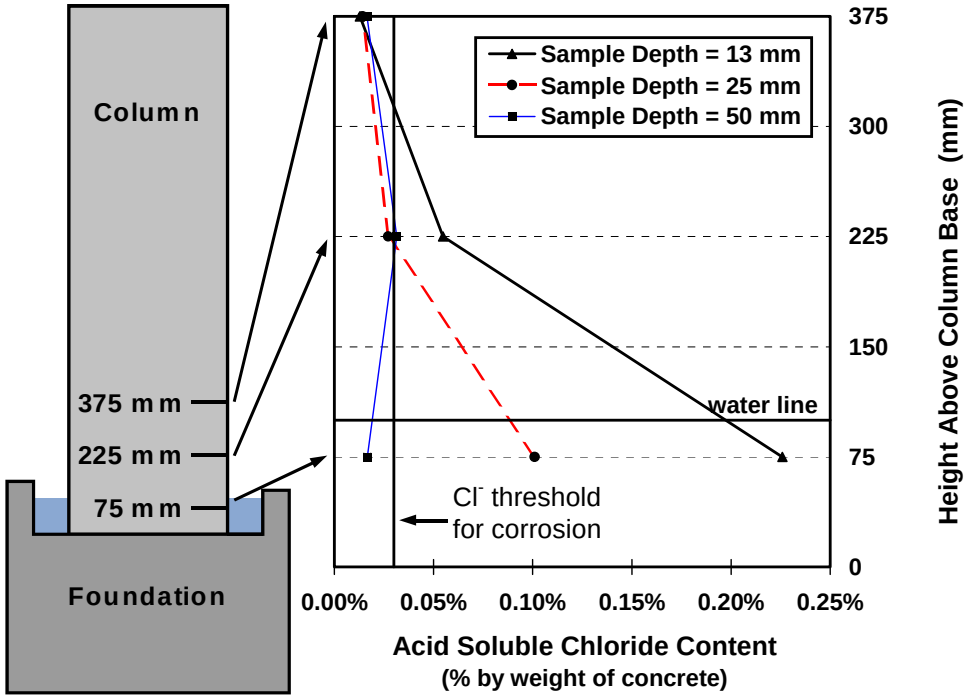

Figure 4.29 - Column NJ-TC-S Chloride Profiles

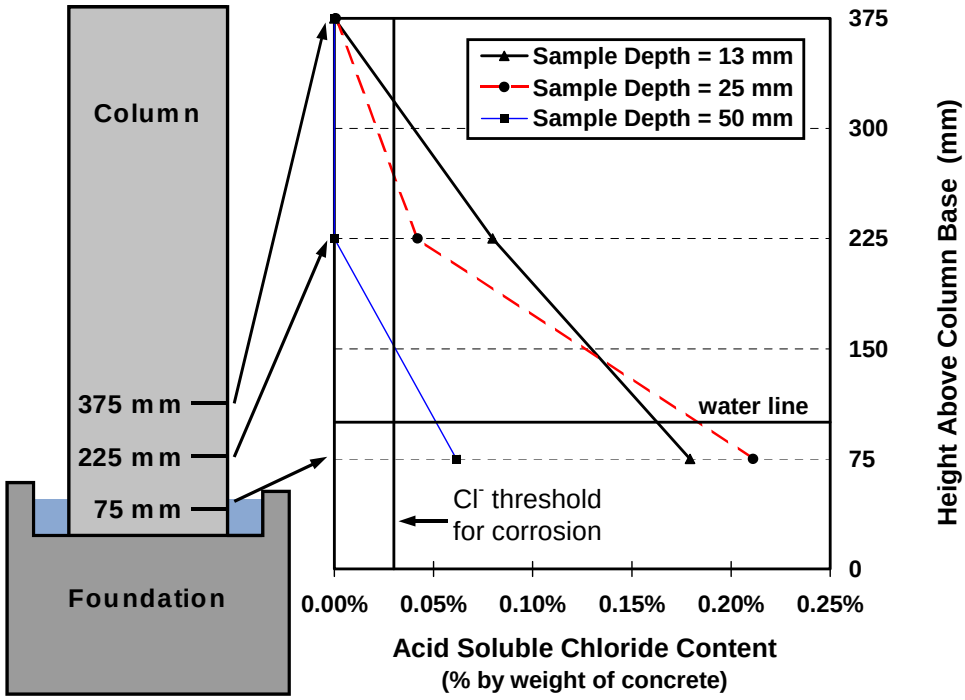

Figure 4.30 - Column DJ-TC-S Chloride Profiles

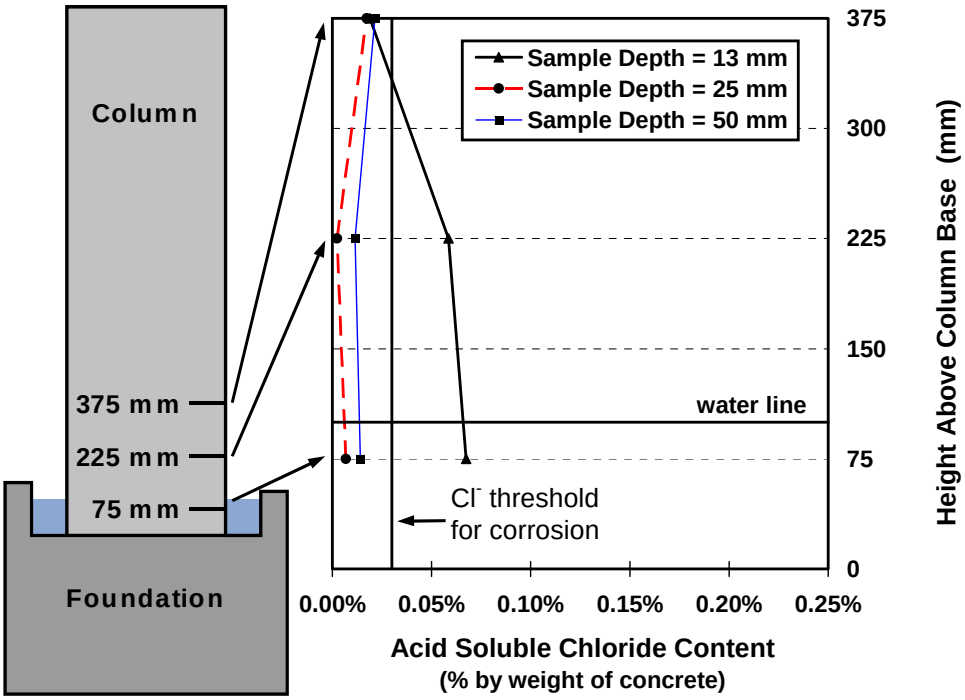

Figure 4.31 - Column DJ-FA-S Chloride Profiles

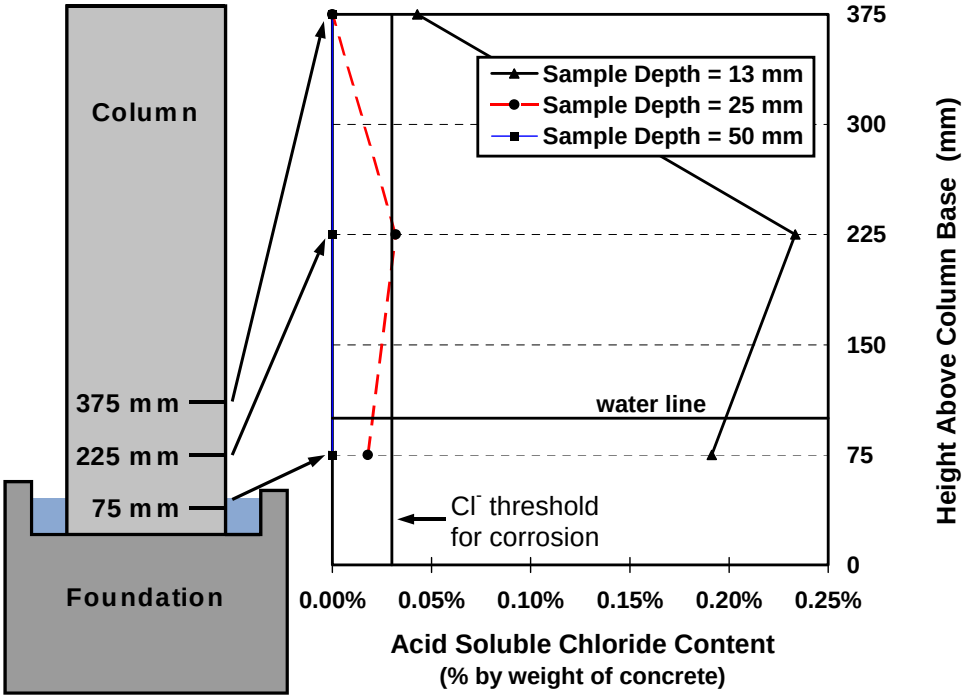

Figure 4.32 - Column PT-TC-S-PD Chloride Profiles

4.10 Analysis and Discussion of Results

4.10.1 Half-Cell Potential Measurements

4.10.1.1 Using Half-Cell Potential Data to Compare Specimen Performance

The half-cell potential measurements represent the largest volume of collected data to monitor specimen condition during testing. Evaluation of many of the variables at this stage of testing must rely largely on the half-cell potential data. Before entering into an in depth analysis of the half-cell potential data, it is important to emphasize that half-cell potentials are only an indicator of corrosion incidence, and a correlation with corrosion rate can not be made. The ASTM C876[4.8] guidelines for interpreting potentials indicate the probability of corrosion. Very negative potentials can be used to suggest a higher probability of corrosion activity, but not necessarily a higher corrosion rate.

Many factors can influence measured half-cell potentials, including concrete cover thickness, concrete resistivity, concrete moisture content, different metals and availability of oxygen. Therefore, comparisons of half-cell potentials for different test specimens should only be made for measurements taken under similar conditions.

Finally, the most useful application of half-cell potential measurements is possible when regular measurements are made over an extended period, as in this testing program. A common trend observed in corrosion research is that a transition from fluctuating or steady more positive potentials to a stable condition of more negative potentials is normally associated with the onset of corrosion.[4.11,4.12] Transition to stable potentials within the range of –400 mV to –650 mV is frequently associated with a loss of passivity and corrosion initiation.[4.11,4.12]

4.10.1.2 Very Negative Half-Cell Potentials

The average potentials at the column base are at or near the ASTM guideline for high corrosion probability for several column specimens, as shown in Figure 4.33. However, this does not necessarily mean that corrosion is occurring for two reasons.

First, the readings at the column base are taken below the water level where the concrete is continually submerged. When the oxygen supply is restricted, as in the case of submerged concrete, the rate of the cathodic reaction is reduced and the corroding system

is said to be under diffusion control. A system under diffusion control is illustrated by mixed potential theory in Figure 4.34.[4.13] Because the slope of the cathodic reaction becomes very steep, the corrosion potential at equilibrium is very negative and the corrosion rate is small. Thus, very negative half-cell potentials in submerged concrete should not necessarily be interpreted as an indication of significant corrosion activity.[4.8,4.14]

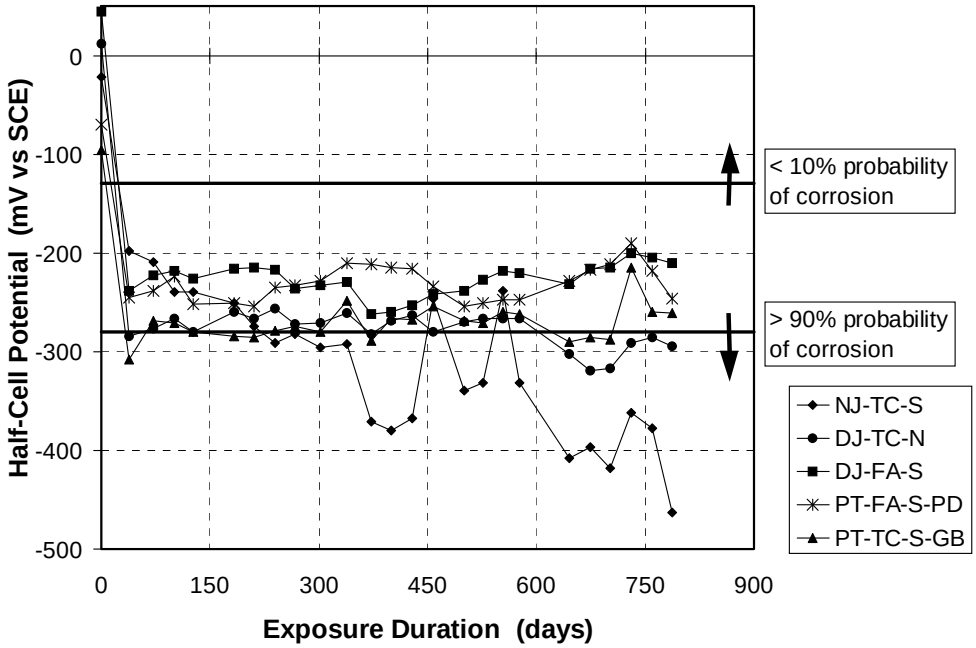

Figure 4.33 - Very Negative Half-Cell Potentials at Column Base in Selected Specimens

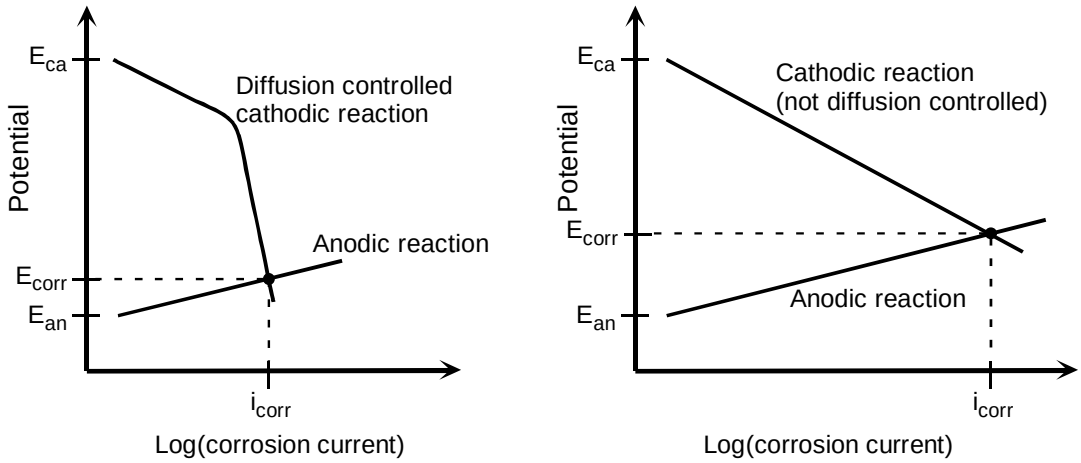

Figure 4.34 - Effect of Diffusion Controlled Cathodic Polarization (Lack of Oxygen) on Corrosion Potential and Current

The second factor to consider is the changes in potential measurements over time. When the readings over the duration of testing are considered, most specimens show consistent half-cell potentials since the start of exposure with no significant deviations, with the exception of NJ-TC-S. Normally, the onset of corrosion would be indicated by a well defined transition to stable, more negative potentials. Since this has not occurred in most columns, it is likely that the steel is not corroding. For column NJ-TC-S, a continuing trend of more negative potentials could suggest an initiation of corrosion activity.

4.10.1.3 Effect of Trickled Saltwater on Half-Cell Potentials

The proximity of the reinforcement to the trickled saltwater on one face of the columns has a clear effect on the measured half-cell potentials. Typical half-cell potential data at the mid height of a reinforced concrete column with fly ash concrete is shown in Figure 4.35. Data is plotted for three of the six mild steel bars. The relative positions of the bars are shown in the diagram on the lower right, and the location of the dripper is indicated by the letter "D." The half-cell potentials for the bar closest to the location of the dripper were consistently more negative than those for the other bars. In Figure 4.35, bar 3 is closest to the source of trickled water. This data suggests higher moisture and chloride contents in the vicinity of bar 3, and a higher probability of corrosion activity. This trend was seen in all ten of the columns, for both the mild steel bars and post-tensioned bars.

4.10.2 Effect of Joint Type

The experimental data reported in this chapter gives some indications of the effect of joint type on corrosion activity. However, some of the indications are contradictory, and overall it is difficult to draw firm conclusions.

Figure 4.36 shows average half-cell potentials at the column base for each of the three joint types, both loaded and unloaded. Looking at the data for unloaded columns, the doweled joint column has the most negative potentials, followed by the post-tensioned joint and no joint. The trend is reversed for the loaded columns, with the no joint configuration most negative and doweled joint least negative. The same trends are indicated by half-cell data at the column mid-height and top (data not shown).

Conceptually, the doweled joint would be expected to provide the least corrosion protection. This is indicated by the unloaded column data, but not when the columns are loaded.

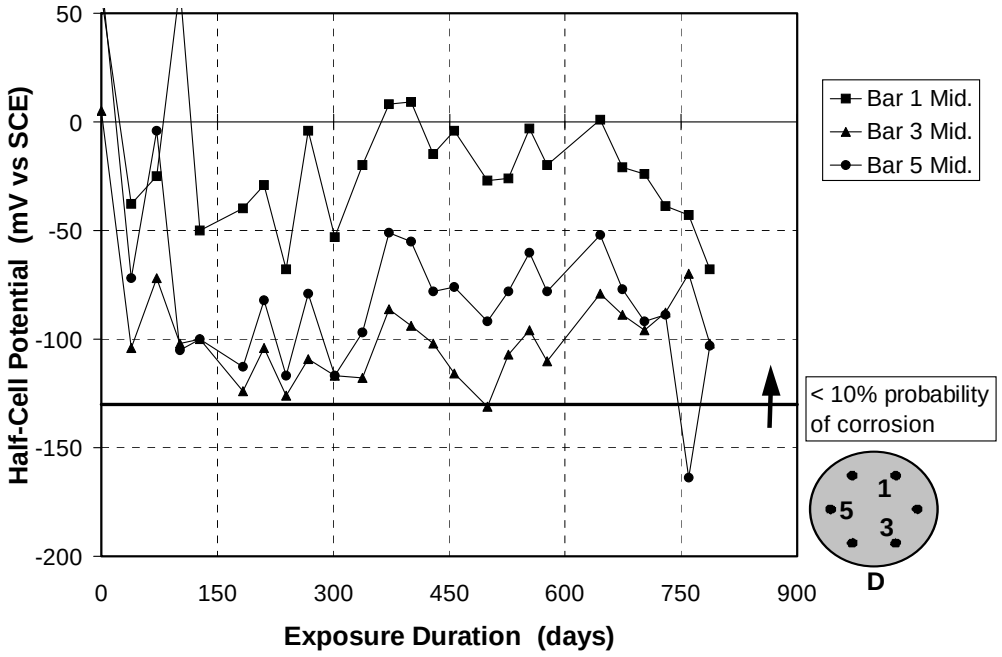

Figure 4.35 - Effect of Dripper Proximity on Half-Cell Potentials (Specimen DJ-FA-S)

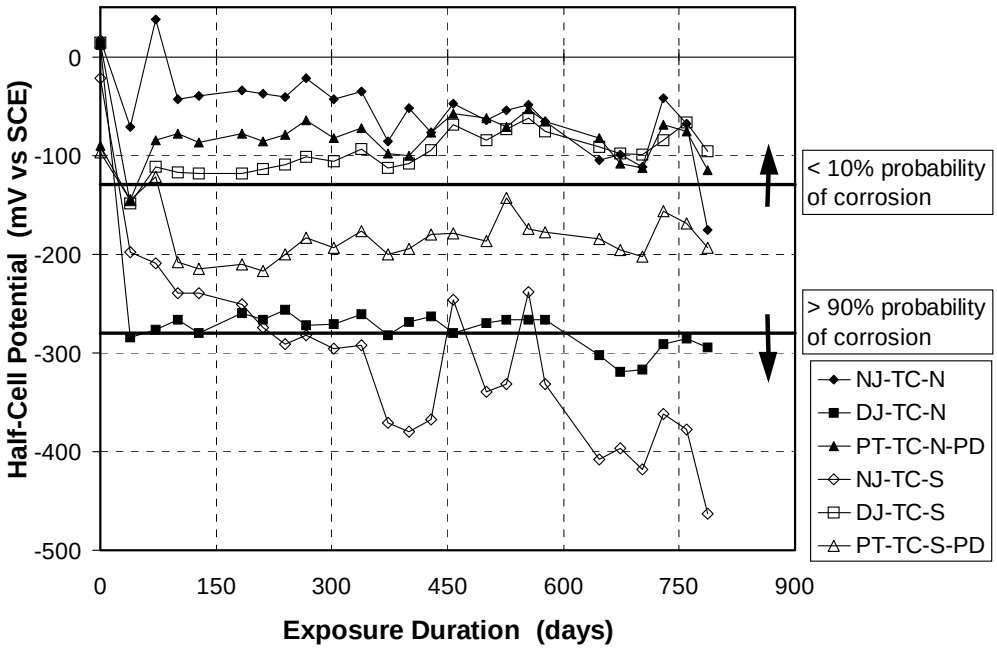

Figure 4.36 - Effect of Joint Type: Average Rebar Half-Cell Potentials at Column Base

The measured chloride profiles shown in Figure 4.29, Figure 4.30 and Figure 4.32 for columns NJ-TC-S, DJ-TC-S and PT-TC-S-PD, respectively, indicate a clear effect of joint type on chloride penetration. Chloride penetration into the concrete and vertical movement of chlorides is similar for the no joint and doweled joint columns. The post-tensioned column shows high chloride levels at a depth of 13 mm (0.5 in.). However, at greater depths the measured chlorides are significantly lower in comparison to the no joint and doweled joint. These preliminary results indicate that post-tensioning at the construction joint may reduce chloride penetration at the column base and improve corrosion protection.

4.10.3 Effect of Loading

The effect of loading on corrosion activity is illustrated in Figure 4.36. Each joint type is shown for the loaded and unloaded condition. The no joint and the post-tensioned joint show an increased probability of corrosion activity for the loaded condition. The doweled joint shows the opposite trend, with a higher probability of corrosion activity for the unloaded case.

The applied service loading exceeds the decompression moment for the reinforced concrete columns. Therefore, the service load case would be expected to produce more severe conditions for moisture and chloride penetration at the joint. This presumption is borne out by the no joint configuration, but not by the doweled joint.

The columns selected for chloride analysis did not include the unloaded condition, and therefore the effect of loading on chloride penetration can not be directly evaluated at this time. The half-cell potential data presents conflicting results for the effect of loading, and further data is needed to make firm conclusions.

4.10.4 Effect of Concrete Type

Half-cell potentials for the two columns with fly ash concrete (DJ-FA-S and PT-FA-S-PD) are plotted together with their companion specimens (DJ-TC-S and PT-TC-S-PD) in Figure 4.37. In both cases, the half-cell potentials for the fly ash concrete are more negative than for the control concrete. This data could suggest that the probability of corrosion is higher in the columns with fly ash.

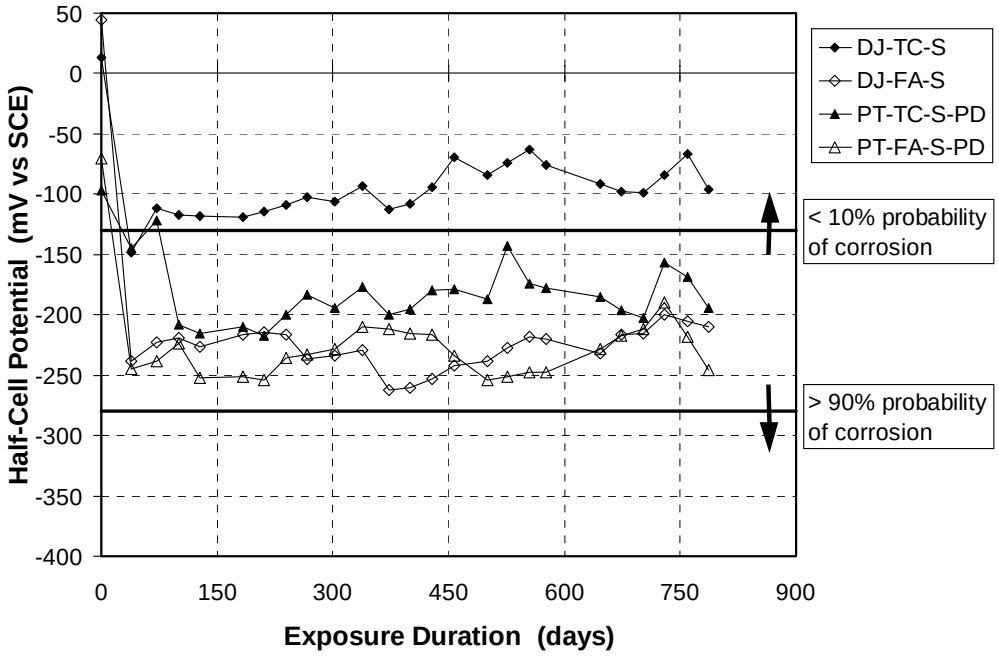

Figure 4.37 - Effect of Concrete Type: Average Rebar Half-Cell Potentials at Column Base

The measured chloride profiles for columns DJ-TC-S and DJ-FA-S (Figure 4.30 and Figure 4.31) show significantly lower chloride levels at all locations and depths for the fly ash concrete. The use of fly ash as partial cement replacement has been shown to reduce concrete permeability, as discussed in Section 2.4.3, and this is clearly demonstrated by the test data.

The chloride profile data suggests that comparison of the half-cell potential data for columns with fly ash concrete and plain Portland cement concrete may not be valid. The measured half-cell potentials will be affected by the ionic properties of the concrete, which may be vastly different for concrete with and without fly ash. Therefore, the conclusion that one may be tempted to draw from Figure 4.37 could be incorrect. In view of the chloride data and possible shortcomings of the half-cell potentials, it may be concluded that the use of fly ash as partial cement replacement improves corrosion protection by limiting penetration of chlorides.

4.10.5 Effect of Post-Tensioning Bar Coatings

The effectiveness of post-tensioning bar coatings and duct types is difficult to assess from half-cell potential readings. Several possible complications exist:

- ASTM C876[4.8] guidelines for interpreting half-cell potentials are for uncoated reinforcing steel in concrete and may not be appropriate for bonded post-tensioned reinforcement.
- Galvanized ducts may result in very negative half-cell potentials if the tendon is in contact with the duct.
- Impervious plastic ducts will prevent measurements on tendons since the duct will act as a barrier to the ion flow necessary for half-cell potential readings.

Half-cell potential measurements were collected for the bonded post-tensioning bars in all of the post-tensioned columns. This data can be examined, but the possible errors listed above must be considered before making any conclusions.

Average post-tensioned bar (PT bar) half-cell potential data at the column base is shown in Figure 4.38 and Figure 4.39 for the five post-tensioned columns. Average potentials from PT Bars 1 and 2 are plotted in Figure 4.38, and averages from PT Bars 3 and 4 are shown in Figure 4.39. Duct and bar configurations at the various locations are listed in Table 4.7.

Table 4.7 – Duct and Post-Tensioned Bar Configurations

Specimen	PT Bars 1 and 2	PT Bars 3 and 4
PT-TC-N-PD	uncoated bars, plastic ducts	uncoated bars, galv. ducts
PT-TC-S-PD	uncoated bars, plastic ducts	uncoated bars, galv. ducts
PT-FA-S-PD	uncoated bars, plastic ducts	uncoated bars, galv. ducts
PT-TC-S-EB	epoxy-coated bars, galv. ducts	uncoated bars, galv. ducts
PT-TC-S-GB	galvanized bars, galv. ducts	uncoated bars, galv. ducts

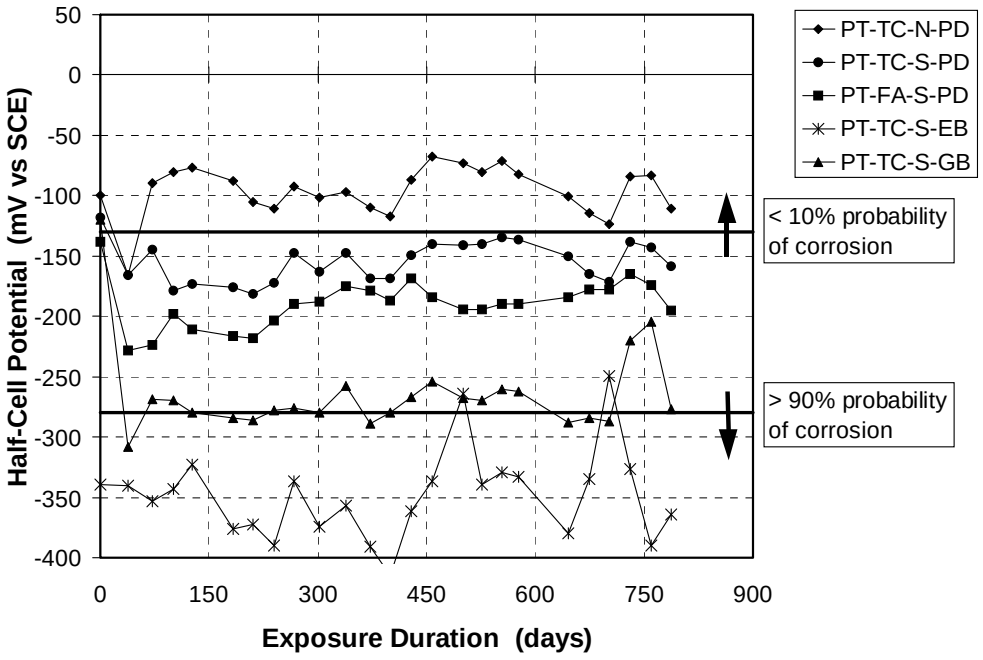

Figure 4.38 - Average PT Bar Half-Cell Potentials at Column Base: PT Bars 1 and 2

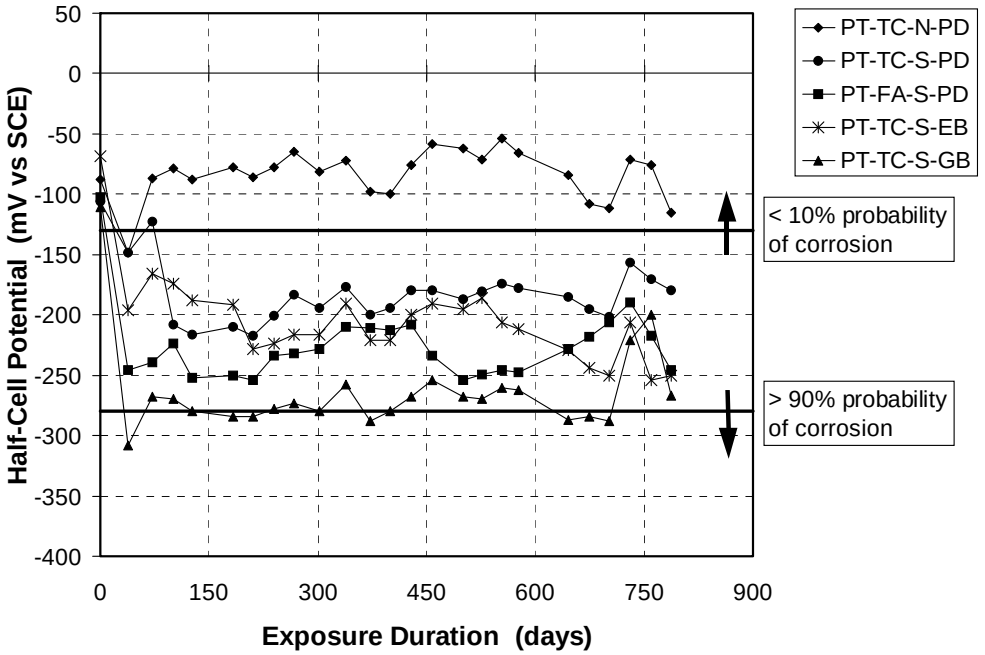

Figure 4.39 – Average PT Bar Half-Cell Potentials at Column Base: PT Bars 3 and 4

The half-cell potentials for the epoxy-coated post-tensioning bars (PT-TC-S-EB, PT Bars 1 and 2) are very negative in comparison to all other PT bar potentials. This trend was also evident for potentials at the mid-height and top of the columns (data not shown). Other research[4.15] has reported half-cell potentials for epoxy-coated rebar more negative than uncoated bars in some instances, and less negative in others. Several other researchers cited in Reference 4.11 consistently found epoxy-coated bars to have more negative half-cell potentials than uncoated bars. These studies all found the epoxy-coated bars to be in good condition when removed from the concrete, indicating that the very negative half-cell potentials should not be misinterpreted as more severe corrosion activity. The very negative half cell potentials and low corrosion rates can be explained by mixed potential theory for a diffusion controlled system, as described in Section 4.10.1 and Figure 4.34. The epoxy coating protects the steel reinforcement from corrosion by acting as a barrier to moisture, chlorides and oxygen. If corrosion develops at a defect or holiday in the coating, the corrosion rate is normally limited by the cathodic reaction since the epoxy coating restricts oxygen reduction away from the holiday (the anodic reaction will be

occurring on the depassivated steel at the holiday). The resulting polarization produces low corrosion rates in spite of negative corrosion potentials.

There is essentially no difference between the potentials for the galvanized post-tensioning bars (1 and 2) and the uncoated bars (3 and 4) in column PT-TC-S-GB. Zinc is more active than iron in the Electromotive Force (EMF) Series,[4.13] and therefore will produce more negative half-cell potentials under similar conditions. This is not indicated by the test data.

4.10.6 Effect of Duct Type

Half-cell potentials for post-tensioning bars in galvanized steel ducts are consistently more negative than potentials in plastic ducts. This is illustrated in Figure 4.40 for two columns (PT Bars 1 and 2 have plastic ducts, PT Bars 3 and 4 have galvanized steel ducts). Half-cell potential measurements should not be possible for tendons in plastic ducts since the duct will prevent the necessary ion flow between the working electrode (bar) and reference electrode. Thus, two possible conclusions can be proposed:

1. The duct is not impervious, and the measurements can be assumed accurate.
2. The post-tensioning bar is in electrical contact with the mild steel reinforcement, and the half-cell potential measurements are actually for the mild steel and not the tendon.

The more plausible conclusion is the second. The post-tensioning bars extend out of the duct at the top of the column. The spiral reinforcement in the column cap could provide electrical continuity between the post-tensioning bars and the mild steel reinforcement in the columns (see Figure 4.15). Therefore, the ground wire connected to the post-tensioning bar would not be isolated from the other reinforcement. The overall conclusion is that the effect of duct type can not be determined using half-cell potential data.

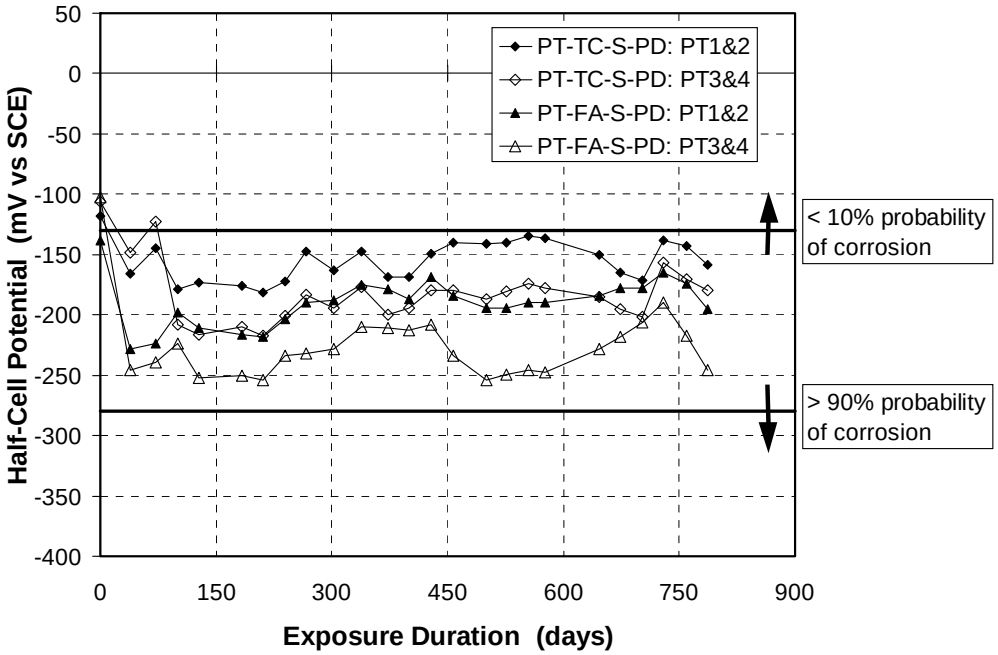

Figure 4.40 - Effect of Duct Type: Average PT Bar Half-Cell Potentials at Column Base

4.11 Summary and Conclusions

The twenty-six month exposure duration reported in this chapter represents only a portion of the expected exposure duration for the column corrosion tests. The test data gathered during this period indicates relatively stable conditions for most of the column specimens. Half-cell potential and chloride penetration data suggests some specimens may be experiencing corrosion activity, but no significant corrosion damage or corrosion related structural deterioration has occurred. Continued exposure testing and monitoring, combined with partial and complete forensic examinations of the columns will provide considerably more information and insight into corrosion in post-tensioned structural elements. Some preliminary conclusions may be drawn from the test data. However, these conclusions could be subject to change as more data is accumulated.

4.11.1 Overall Performance

- No significant corrosion damage was apparent during twenty-six months of severe, accelerated exposure conditions. This is not unexpected due to the relatively short exposure duration and realistic specimen details and materials.
- Chloride analysis of samples taken from four columns indicated chloride levels in one column were in excess of the threshold for corrosion at the level of reinforcement. This suggests that conditions may be appropriate for corrosion initiation during the exposure duration reported in this chapter.
- Half-cell potential data does not strongly suggest corrosion initiation in any of the column specimens. Data for column NJ-TC-S (no joint, TxDOT Class C concrete, service load) is beginning a transition to more negative potentials, possibly indicating an onset of corrosion activity.
- An actual assessment of corrosion severity can not be made from the half-cell potential and chloride penetration data. An invasive inspection including a visual examination of the steel condition is necessary to determine corrosion severity. This work will be performed and reported by Schokker.[4.16]

4.11.2 Post-Tensioning to Improve Corrosion Protection

- Measured chloride profiles near the column to foundation construction joint indicate a reduction in chloride penetration for post-tensioned columns in comparison to non-prestressed doweled connections and the no joint condition. This preliminary data suggests post-tensioning could improve corrosion protection by reducing the penetration of moisture and chlorides.
- Half-cell potential data indicates an uncertain probability of corrosion activity in post-tensioned columns. Data for non-prestressed columns suggests both higher and lower probabilities of corrosion in some instances. The half-cell potential data for the reporting period does not indicate a clear effect of joint type on corrosion activity.

4.11.3 Fly Ash as Partial Cement Replacement in Concrete

- The use of fly ash as partial cement replacement significantly reduced chloride penetration and vertical migration of chlorides in the column specimens. The fly ash concrete used in the testing program was standard TxDOT concrete for bridge

substructures with 35% of the cement replaced with fly ash (35% by volume, 31% by weight). No special measures such as increased cement content or reduced water-cement ratio were taken to reduce the permeability and increase the strength of the concrete. These findings suggest that simply replacing a portion of the cement with fly ash can improve corrosion protection for bridge columns. This practice has already been adopted by many contractors to reduce concrete costs.

4.11.4 Effectiveness of Coated Post-Tensioning Bars and Plastic Ducts

- The use of galvanized and epoxy-coated post-tensioning bars and plastic ducts is expected to improve corrosion protection in comparison to uncoated bars and galvanized steel ducts. The inherent limitations of half-cell potential measurements and low probability of corrosion activity during the reporting period do not permit an assessment of these corrosion protection measures. The best indication of the relative performance of coated and uncoated post-tensioning bars and the different ducts will be provided by a forensic examination at a later stage of exposure.

4.11.5 Assessing Corrosion Activity Using Half-Cell Potential Measurements

- Very negative half-cell potentials (more negative than the guidelines for high probability of corrosion) do not necessarily indicate that corrosion is occurring. Very negative half-cell potentials can result from sources other than significant corrosion activity, and therefore it is more important to consider the variation of half-cell potentials over time to assess corrosion activity.
- Half-cell potential measurements proved to have limited usefulness in determining the relative performance of the variables in this testing program. The different materials investigated, the nature of half-cell potentials and the general complexity of the corrosion process resulted in data that did not indicate clear differences in corrosion activity and specimen performance.
- The best use of the half-cell potential data will be to indicate the initiation of corrosion by observing long term trends in the measured data. Therefore, continued regular measurements are very important.

4.11.6 Conclusion

Similar to the long term beam corrosion tests, the research program described in this chapter has the capacity to provide useful and important findings on the durability of post-tensioned bridge elements. The preliminary findings are limited, but suggest the use of post-tensioning and fly ash can improve the durability of bridge substructures.

The long term column corrosion tests will continue exposure testing for an undetermined time. Regular half-cell potential and chloride ion measurements are essential to monitor specimen condition and detect changes in corrosion activity. Long term exposure testing and a thorough forensic examination at the conclusion of testing are necessary for complete results and the development of durability design guidelines.

Chapter 4 References

4.1) **AASHTO**, LRFD Bridge Design Specifications, 2nd Edition, American Association of State Highway and Transportation Officials, Washington, D.C., 1998.

4.2) **Texas State Department of Highways and Public Transportation,** Bridge Design Guide, First Edition, Austin, Texas, 1990.

4.3) **Collins M.P., and Mitchell, D.,** Prestressed Concrete Structures, Prentice Hall, NJ, 1991.

4.4) Standard Specifications for Construction of Highways, Streets and Bridges, Texas Department of Transportation, March 1995.

4.5) **ASTM,** "Standard Specification for Coal Fly Ash and Raw or Calcined Natural Pozzolan for Use as a Mineral Admixture in Concrete," ASTM C618-98, American Society for Testing and Materials, Philadelphia, PA, 1998.

4.6) **ASTM**, "Standard Specification for Epoxy-Coated Reinforcing Steel Bars," ASTM A775-97, Philadelphia, PA, 1997.

4.7) **ASTM**, "Standard Test Method for Determining the Effects of Chemical Admixtures on the Corrosion of Embedded Steel Reinforcement in Concrete Exposed to Chloride Environments," ASTM G109-92, American Society for Testing and Materials, Philadelphia, PA, 1992.

4.8) **ASTM**, "Standard Test Method for Half-Cell Potentials of Uncoated Reinforcing Steel in Concrete," ASTM C876-91, American Society for Testing and Materials, Philadelphia, Pa., 1991.

4.9) **AASHTO**, Standard Method of Test for Sampling and Testing for Chloride Ion in Concrete and Concrete Raw Materials," AASHTO Designation T 260-94, American Association of State Highway and Transportation Officials, Washington, D.C., 1994.

4.10) **ACI Committee 222,** "Corrosion of Metals in Concrete," ACI 222R-96, American Concrete Institute, Detroit, Michigan, 1996.

4.11) **Kahhaleh, K.Z.,** "Corrosion Performance of Epoxy-Coated Reinforcement," Doctor of Philosophy Dissertation, The University of Texas at Austin, May 1994.

4.12) **Wheat, H.G., and Eliezer, Z.,** "Some Electrochemical Aspects of Corrosion of Steel in Concrete," *Corrosion*, Vol. 41, No. 11, November 1985, pp. 640-645.

4.13) **Fontana, M.G.,** Corrosion Engineering, 3rd Edition, McGraw-Hill, Inc., New York, New York, 1986.

4.14) **Elsener, B., and Böhni, H.,** "Potential Mapping and Corrosion of Steel in Concrete," Corrosion Rates of Steel in Concrete, ASTM STP 1065, Berke, N.S., Chaker, V., and Whiting, D., Editors, American Society for Testing and Materials, Philadelphia, PA, 1990, pp. 143-156.

4.15) **Vaca-Cortes, Enrique**, "Corrosion Performance of Epoxy-Coated Reinforcement in Aggressive Environments," Doctor of Philosophy Dissertation, The University of Texas at Austin, May 1998.

4.16) **Schokker, Andrea J.,** "Improving Corrosion Resistance of Post-Tensioned Substructures Emphasizing High Performance Grouts," Doctor of Philosophy Dissertation, The University of Texas at Austin, May 1999.

Chapter 5:

Macrocell Corrosion Tests: Corrosion Protection for Internal Prestressing Tendons in Precast Segmental Bridges

5.1 Test Concept and Objective

Post-tensioning in precast concrete segmental bridge construction may be in the form of internal bonded tendons, external tendons, or a combination of both. Current specifications[5.1] require the use of match-cast epoxy joints with internal tendons. Epoxy joints were introduced to enhance force transfer across the segmental joint and to seal the joint against moisture ingress. More recently, epoxy joints have been recognized as an absolute requirement for durability when internal tendons are used.

Corrosion protection for bonded internal tendons in precast segmental construction can be very good. Within the segment, internal tendons are well protected by the high quality concrete, duct and cement grout. The potential weak link in corrosion protection is at the joint between segments. The ducts for internal tendons are not continuous across the joints, and no special coupling of tendon ducts is made with match-cast joints. Thus, the joint represents a pre-formed crack at the same location where there is a discontinuity in the duct. In saltwater exposures or in areas where de-icing salts are used, the joint could possibly allow moisture and chlorides to reach the tendon and cause corrosion. Since the tendons provide structural continuity, tendon rupture due to corrosion might lead to collapse of the bridge. This potential corrosion problem was confirmed in the U.K. with the collapse of the Ynys-y-Gwas Bridge in Wales.[5.2] The design and details of that bridge were considerably different from North American practice. These details, including thick, highly permeable mortar joints between segments, played a large role in the collapse. The collapse of this bridge contributed to moratorium on precast segmental bridges in the U.K.

The overall performance of precast segmental bridges in North America has been very favorable,[5.3] and there have been no reported cases of corrosion of internal tendons in North American precast segmental construction with epoxy joints. However, given the concerns raised by the U.K. experience, and the relative youth of precast segmental construction in North America (the first precast segmental bridge with internal tendons and epoxied joints in the U.S.A. was constructed in 1972), it is prudent to examine the potential for corrosion problems and get a better understanding of the protective mechanisms with the design details used in North America.

The objectives of this research program are:

1. To evaluate the potential for corrosion of internal tendons at joints in typical precast segmental construction,
2. To examine the effect of typical North American design and construction details on corrosion protection for internal tendons,
3. To examine methods for improving corrosion protection for internal tendons.

Based on these objectives, it was necessary to select or develop a test method with the following requirements:

- The test method should provide meaningful comparisons in a reasonable amount of time (less than 5 years).
- The test method should accommodate the desired variables in a realistic manner.
- The test method should allow measurement of both macrocell and microcell corrosion.
- The test method should be as standardized as possible to allow comparisons with past and future testing, and provide reproducible results.

The test method and experimental program described in this section were developed and implemented by Rene Vignos.[5.4] Vignos patterned the test method after ASTM G109 - "*Standard Test Method for Determining the Effects of Chemical Admixtures on the Corrosion of Embedded Steel Reinforcement in Concrete Exposed to Chloride Environments.*"[5.5]

The standard macrocell corrosion specimens were modified to examine prestressing tendons in grouted ducts and simulate segmental joints. A full description of the development of the testing program and details of the experiment setup are provided in Reference 5.4. A summary of the test specimens, variables and measurements is provided in the following sections. Exposure testing was initiated by Vignos in August 1993.

5.2 Test Specimen

The specimens used in this program are patterned after the standard ASTM G109[5.5] macrocell specimen developed to evaluate the effect of concrete admixtures on the corrosion of mild steel reinforcement. The standard specimens consisted of a single concrete block with two layers of mild steel reinforcement. During macrocell corrosion, the top layer of steel acts as the anode and the bottom layer acts as the cathode. Several modifications were made to the ASTM G109 specimens to evaluate corrosion protection for internal tendons in segmental bridge construction. These included the introduction of a transverse joint in the concrete block to allow the effect of the segmental joint type to be evaluated, the use of a grouted prestressing strand in the top layer (anode) and the addition of longitudinal compressive stress on the specimen to simulate prestress in the structure. The specimen configuration is shown in Figure 5.1.

Each specimen consists of two match-cast segments. Continuity between the segments is provided by a 12.7 mm (0.5 inch) diameter, seven-wire prestressing strand inside a grouted duct, representing a typical bonded internal tendon in segmental bridge construction. The duct is cast into each of the match-cast segments and is not continuous across the joint. Due to the small specimen size, the strand can not be post-tensioned effectively. To simulate precompression across the joint due to post-tensioning, the pairs of match-cast segments were stressed together using external loading frames.

Similar to ASTM G109, two 12.7 mm (#4) mild steel bars were used as the cathode. These bars would represent non-prestressed reinforcement within the segment. The use of two bars increases the ratio of cathode area to anode area, accelerating macrocell corrosion. The cathode bars were discontinuous across the transverse joint, consistent with precast segmental construction. The end cover for the cathode bars at the segmental joint was 6 mm (0.25 in.). Following ASTM G109, the exposed length of the anode and

cathode were limited to 125 mm (5 in.) by painting the steel with epoxy paint as shown in Figure 5.2.

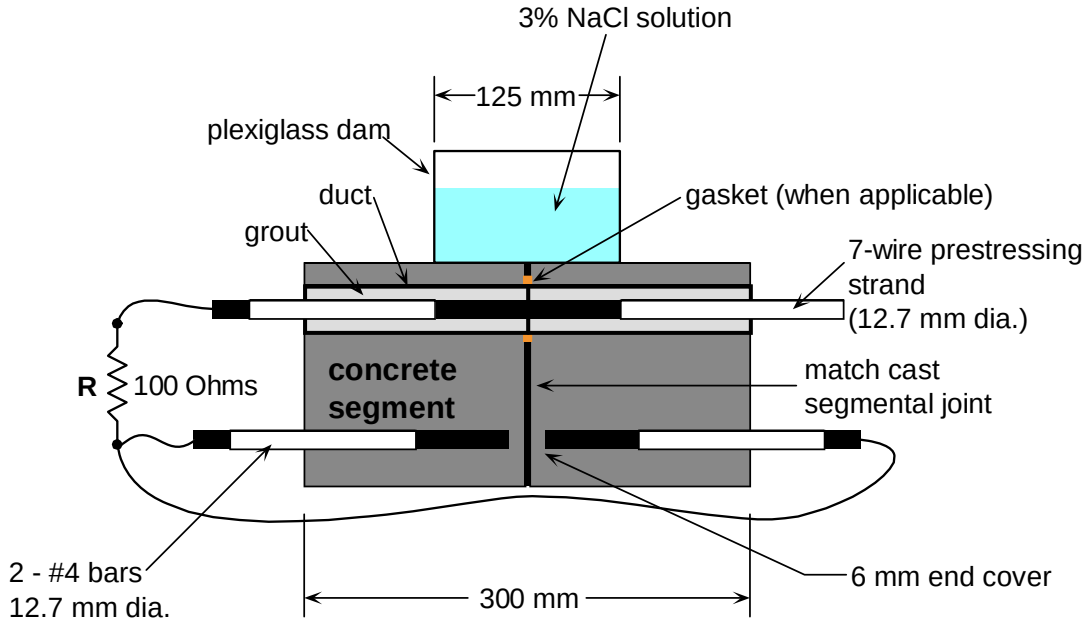

Figure 5.1 - Macrocell Specimen Details

Electrical contact must exist between the anode and cathode for macrocell corrosion to develop. This is achieved in the test specimen by wiring the protruding ends of the anode and cathode steel together, as shown in Figure 5.1. Zinc ground clamps are used to connect the wire to the steel. A 100 Ohm resistor is placed in the wire connection between the anode and cathode, as shown in Figure 5.1, to allow assessment of the corrosion current by measuring the voltage drop across the resistor ($I_{corr} = V_{meas}/R$).

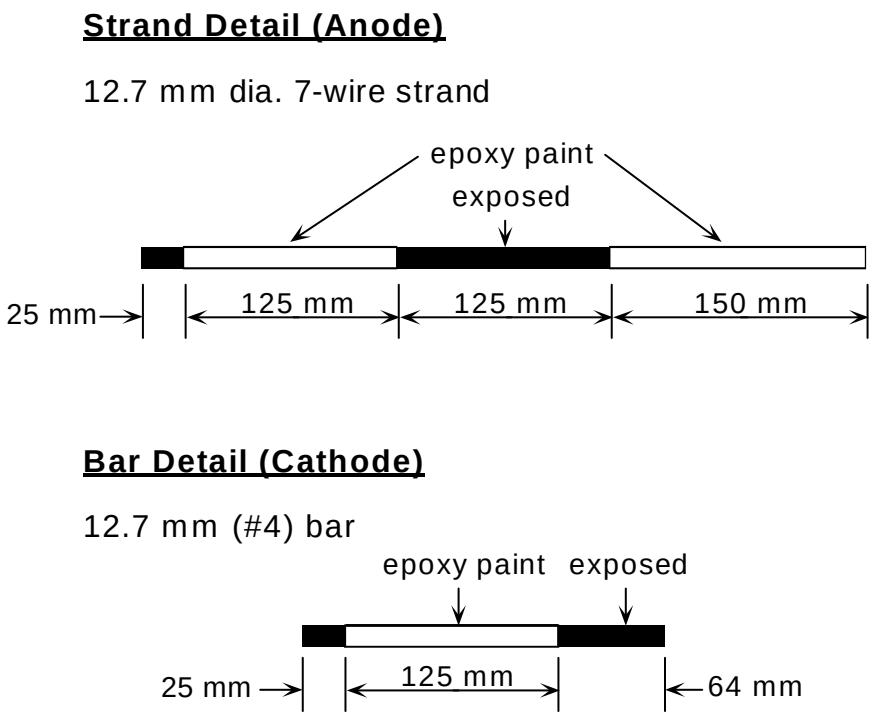

Figure 5.2 - Anode and Cathode Bar Details

Exposure conditions for the specimens consist of a 4 week cycle of 2 weeks dry and 2 weeks wet. During the wet period of the cycle, a portion of the top surface of the specimen is ponded with 3.5% NaCl solution, as shown in Figure 5.1. At the end of the wet period, the NaCl solution is removed from the Plexiglas dam using a wet/dry vacuum.

5.3 Variables

A broad scope of protection variables were selected for investigation in this program. These variables cover four components of the precast concrete segmental bridge related to corrosion of internal tendons. Included are; joint type, duct type, joint precompression and grout type.

5.3.1 Joint Type

Precast segmental joints are either dry or wet. Wet joints include mortar joints, concrete joints and epoxy joints. Dry joints and epoxy joints require match casting, and are the most common segmental joints used in North America. When match-cast epoxy joints are used, the entire face of the segment is coated with a thin layer of epoxy immediately before each segment is placed in the bridge. The segments are held firm contact with temporary post-tensioning while the epoxy cures and the prestressing tendons are placed and stressed. In some situations, a small gasket is used around each duct opening to prevent epoxy from entering the duct when the segment is placed and initially stressed. If a gasket is not used, the duct is swabbed out immediately after initial stressing to prevent epoxy from blocking the duct.

To address typical North American practice, dry joints and epoxy joints, with and without gaskets, were selected for investigation in this testing program. All joint types were match-cast. The AASHTO Guide Specification for Segmental Bridges[5.1] does not permit the use of dry joints with internal tendons. However, dry joints were included as a worst case scenario for comparison purposes. The epoxy jointed specimens were assembled according to standard practice. Both match cast faces were coated with epoxy and the segments were pushed together. The joint was precompressed at 345 kPa (50 psi) for 48 hours after which the specimens were unloaded and re-loaded to the desired level of precompression (Section 5.3.3). In the epoxy/gasket joint, a foam gasket was glued to the face of one segment around the duct opening prior to application of the epoxy. Details of the foam gasket are shown in Figure 5.3. In the epoxy joint without a gasket, the duct was

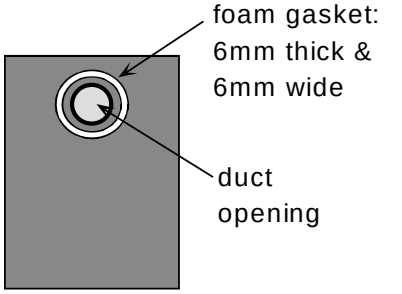

Figure 5.3 - Gasket Details

swabbed out immediately after stressing to 345 kPa to prevent the epoxy from blocking the duct.

5.3.2 Duct Type

Two duct types were investigated; standard galvanized steel duct and plastic duct. Due to size limitations, PVC pipe was used for the plastic duct.

5.3.3 Joint Precompression

The joint precompression refers to the level of prestress provided by the internal and/or external tendons in the bridge. Three levels of precompression were selected; 35 kPa, 345 kPa and $7.88\sqrt{f'_c}$ kPa (5 psi, 50 psi and $3\sqrt{f'_c}$ psi). The lowest level of 35 kPa could represent the level of precompression encountered in a precast segmental column under self weight. The precompression of 345 kPa is based on the AASHTO Guide Specifications.[5.1] The highest precompression value of $7.88\sqrt{f'_c}$ kPa corresponds to 1310 kPa (190 psi) for this testing program.

5.3.4 Grout Type

Three cement grout types were selected for evaluation; normal grout (plain cement grout, no admixtures, w/c = 0.40), grout with silica fume (13% cement replacement by weight, w/c = 0.32, superplasticizer added) and grout with a commercial calcium nitrite corrosion inhibitor (w/c = 0.40). Grout mix proportions are provided in Section 5.4.

5.3.5 Specimen Types

A total of nineteen specimen types were selected to address all of the variables. Each specimen type was duplicated for a total of thirty-eight specimens. Details of the specimen types and corresponding designations are listed in Table 5.1. The notation used in the specimen designations is as follows:

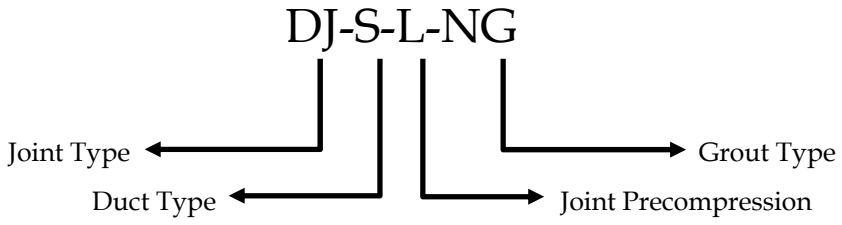

Joint Type:

DJ = Dry Joint
SE = Standard Epoxy
EG = Epoxy with Gasket

Duct Type:

S = Steel
P = Plastic

Joint Precompression:

L = Low: 35 kPa
M = Medium: 345 kPa
H = High: $7.88\sqrt{f'_c}$ kPa (1310 kPa)

Grout Type:

NG = Normal Grout
SF = Silica Fume Added
CI = Corrosion Inhibitor

Table 5.1 - Specimen Types and Variables

Specimen No.	Specimen Name	Duct Type	Joint Precompression	Grout Type
Dry Joints:				
1,2	DJ-S-L-NG	Steel	35 kPa	Normal
7,8	DJ-S-M-NG	Steel	345 kPa	Normal
11,12	DJ-S-H-NG	Steel	1310 kPa	Normal
31,32	DJ-P-L-NG	Plastic	35 kPa	Normal
33,34	DJ-P-M-NG	Plastic	345 kPa	Normal
3,4	DJ-S-L-CI	Steel	35 kPa	Corrosion Inhibitor
9,10	DJ-S-M-CI	Steel	345 kPa	Corrosion Inhibitor
Standard Epoxy Joints:				
15,16	SE-S-L-NG	Steel	35 kPa	Normal
21,22	SE-S-M-NG	Steel	345 kPa	Normal
27,28	SE-S-H-NG	Steel	1310 kPa	Normal
35,36	SE-P-L-NG	Plastic	35 kPa	Normal
37,38	SE-P-M-NG	Plastic	345 kPa	Normal
17,18	SE-S-L-CI	Steel	35 kPa	Corrosion Inhibitor
23,24	SE-S-M-CI	Steel	345 kPa	Corrosion Inhibitor
29,30	SE-S-H-CI	Steel	1310 kPa	Corrosion Inhibitor
19,20	SE-S-L-SF	Steel	35 kPa	Silica Fume
Epoxy/Gasket Joints:				
5,6	EG-S-L-NG	Steel	35 kPa	Normal
25,26	EG-S-M-NG	Steel	345 kPa	Normal
13,14	EG-S-H-NG	Steel	1310 kPa	Normal

5.4 Materials

Details of the materials used in this testing program are summarized in Table 5.2. All materials and proportions were selected to match segmental bridge usage as closely as possible. Concrete was batched using a six cubic foot mixer in the laboratory. Grouts were batched in five gallon buckets using a paddle mixer mounted to a drill press. Complete details of specimen construction are provided in Reference 5.4.

Table 5.2 - Material Details

Item	Description		
Segment Concrete	• w/c = 0.44, f'c = 34.5 MPa (5000 psi)		
	• batch proportions:	Coarse Aggregate	174 kg (19 mm max.)
		Fine Aggregate	136 kg
		Type I/II Cement	68 kg
		Water	30 kg
	• cylinder strengths:	7-day	31 MPa
		28-day	35.5 MPa
Normal Grout	• w/c = 0.40		
	• batch proportions:	Type I/II Cement	13.08 kg
		Water	5.28 kg
Corrosion Inhibitor Grout	• w/c = 0.40		
	• corrosion inhibitor:	calcium nitrite	
	• batch proportions:	Type I/II Cement	13.08 kg
		Water	5.28 kg
		Corrosion Inhibitor	187 ml
Silica Fume Grout	• w/c = 0.32		
	• silica fume:	Sikacrete 950DP	
	• superplasticizer:	WRDA-19	
	• batch proportions:	Type I/II Cement	9.86 kg
		Water	3.62 kg
		Silica Fume	1.48 kg
		Superplasticizer	88.5 ml
Prestressing Strand	• 12.7 mm (0.5 in.) diameter seven wire strand • Grade 270 (1860 MPa, 270 ksi), low relaxation		
Mild Steel Reinforcement	• 12.7 mm diameter bars (#4) • ASTM A615, Grade 60 (400 MPa, 60 ksi)		
Steel Duct	• Corrugated, semi-rigid, galvanized steel duct for post-tensioning • 30 mm (1-3/16 in.) outside diameter		
Plastic Duct	• ASTM D1785 PVC pipe • 33 mm (1-5/16 in.) outside diameter, 25.4 mm (1 in.) inside diameter		
Segment Epoxy	• B-73 Mid-Range two-part span epoxy		

5.5 Measurements During Exposure Testing

Two forms of regular measurements are taken to evaluate macrocell and microcell corrosion in the test specimens. Macrocell corrosion current can be measured directly as described in Section 5.2. In addition, the probability of macrocell corrosion can be estimated using half-cell potential measurements. Microcell corrosion cannot be measured directly, however, significant half-cell potential readings in the absence of measured macrocell corrosion current would indicate a high probability for microcell corrosion.

5.5.1 Macrocell Corrosion Current Measurements

The nature of the macrocell specimen allows direct measurement of the macrocell corrosion current. Macrocell corrosion currents provide three forms of information:

- The time at which corrosion began can be determined from regular measurements during testing.
- Corrosion rate or severity can be calculated from corrosion current measurements.
- The polarity of the corrosion current indicates which steel is corroding (prestressing strand or mild steel reinforcing bars).

The corrosion current is determined by measuring the voltage drop across a resistor placed between the anode and cathode steel, as shown in Figure 5.4. The corrosion current, I_{corr}, is calculated dividing the measured voltage drop by the known resistance (Ohm's Law). Each specimen is connected to a data acquisition system, allowing voltages (currents) for all specimens to be measured simultaneously. Corrosion currents are measured at one week intervals.

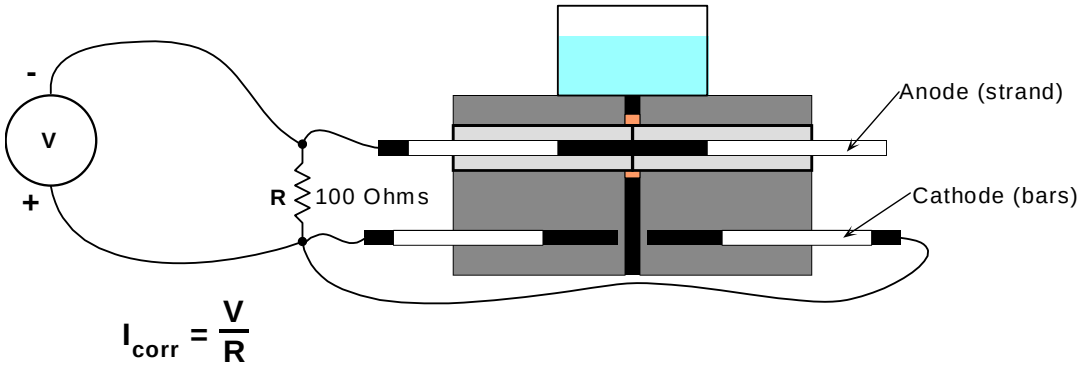

Figure 5.4 - Macrocell Corrosion Current Measurement

During corrosion, the electrons liberated at the anode travel through the electrical connection provided by the wire and resistor to the cathode. Since current moves in the direction opposite to electron flow, the current in the macrocell flows from the cathode to the anode. With the leads of the voltage measuring device attached as indicated in Figure 5.4, the measured voltage across the resistor will have a positive polarity if the anodic reaction is occurring on the prestressing strand. Thus, the polarity of the measured voltage allows the direction of the electron flow to be determined, indicating whether or not the expected corrosion cell has developed.

5.5.2 Half-Cell Potential Readings

Half-cell potential readings also provide three forms of information regarding the condition of the specimen:

- The magnitude of half-cell potential readings indicate the probability of corrosion at a given location.
- The time at which corrosion initiation occurred can be determined from regular potential readings taken during testing.
- Significant half-cell potentials in the absence of macrocell corrosion currents suggest the occurrence of microcell corrosion.

Half-cell potential readings are taken every two weeks at the start of the wet period and the start of the dry period. All measurements are performed according to ASTM C876[5.6] using a saturated calomel electrode (SCE). Three half-cell potential measurements are made manually on each specimen, as shown in Figure 5.5. One measurement is taken

with the Plexiglas dam filled with NaCl solution and the electrode immersed in the solution. Two measurements are taken directly on the surface of each segment with the dam empty. The surface of the concrete is damp for these readings. In all cases, electrical contact between the anode and cathode is interrupted to ensure that the half-cell potential reading is for the strand only.

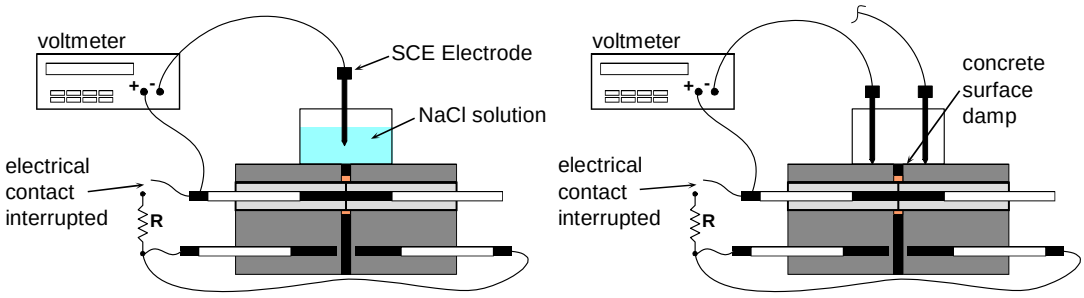

Figure 5.5 - Half-Cell Potential Readings

The numerical significance of the half-cell potential readings is shown in Table 5.3, as defined by ASTM C876. This standard was developed for half-cell potential readings of uncoated reinforcing steel in concrete, and therefore the values reported in Table 5.3 may not necessarily be appropriate for grouted prestressing strand in concrete. In general, half-cell potential readings are not an effective method for monitoring corrosion activity in bonded post-tensioned structures. In structures with galvanized steel ducts, the prestressing tendon will be in contact with the duct in most cases and half cell potentials taken on the prestressing tendon may in fact reflect the potential of the zinc on the galvanized steel duct. Because the potential of the zinc will be more negative than that of the tendon, this could lead to erroneous results and conclusions. In situations where the tendon is completely encapsulated in an impervious plastic duct system, half-cell potentials are not possible since the duct will act as a barrier to the ion flow necessary for half-cell potential readings.

In spite of these issues, half-cell potential readings are used effectively in the macrocell corrosion specimens in this testing program for two reasons. Firstly, in all cases the prestressing tendon is not in contact with the galvanized duct. Secondly, for both galvanized ducts and plastic ducts the discontinuity in the duct at the segmental joint

should allow ion movement and measurement of half-cell potentials. However, it is still possible that the presence of the duct, whether galvanized steel duct or plastic, may affect the magnitude of the half-cell potentials. Thus, it is important to consider both the magnitude and variation of the measured potentials over time.

Table 5.3 – Interpretation of Half-Cell Potentials for Uncoated Reinforcing Steel[5.6]

Measured Potential (vs SCE)	Probability of Corrosion
more positive than –130 mV	less than 10% probability of corrosion
Between -130 mV and –280 mV	corrosion activity uncertain
more negative than –280 mV	greater than 90% probability of corrosion

5.6 Exposure Test Results

Exposure testing was initiated on August 23, 1993. Exposure testing continued without interruption until January 13, 1998, a period of four years and five months. At that time, one specimen from each pair of duplicates was removed for forensic examination. Exposure testing for the remaining nineteen specimens was restarted in April 1998, and continues at present. Exposure testing results from the initiation of testing up to January 13, 1998 are reported in the following sections. The recorded data for this period indicates that twelve of the thirty-eight specimens have experienced an initiation of corrosion. Of these twelve, only seven had measurable corrosion activity as of January 13, 1998.

5.6.1 Macrocell Corrosion Current Results

The variation of macrocell corrosion current over time was plotted for all specimens and included in Appendix E. The macrocell corrosion current plots for most specimens show stable corrosion currents close to zero, and thus can be considered as not corroding. Twelve specimens displayed a clear initiation of corrosion. Macrocell corrosion current data for these specimens are plotted in Figure 5.6 through Figure 5.9.

From these figures, it is evident that only specimens DJ-S-H-NG-1, DJ-S-H-NG-2, DJ-S-L-CI-1, DJ-S-M-CI-1, DJ-P-L-NG-1, DJ-P-M-NG-2 and SE-S-M-NG-2 show continued corrosion activity.

When examining the plots of corrosion current, the "polarity" of the current is important. As described in Section 5.5.1, the measured voltages and thus the corrosion currents should be positive if the assumed macrocell corrosion mechanism has developed. Negative corrosion currents indicate that a reversed corrosion cell has developed. That is, the prestressing strand is acting as the cathode, while the mild steel reinforcing bars are actively corroding.

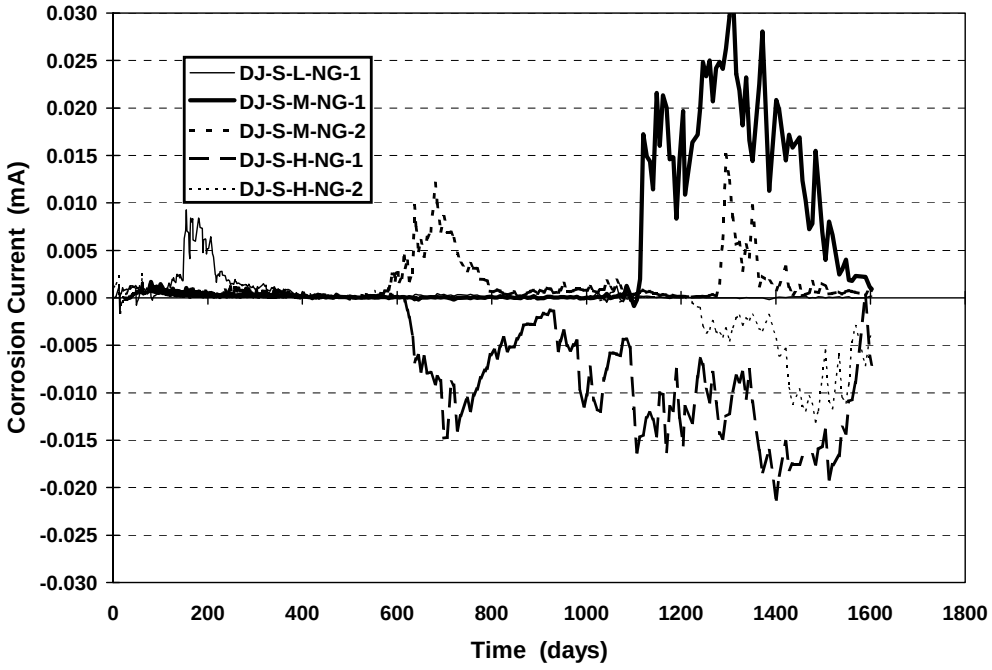

Figure 5.6 - Macrocell Corrosion Current: Dry Joint, Steel Duct and Normal Grout

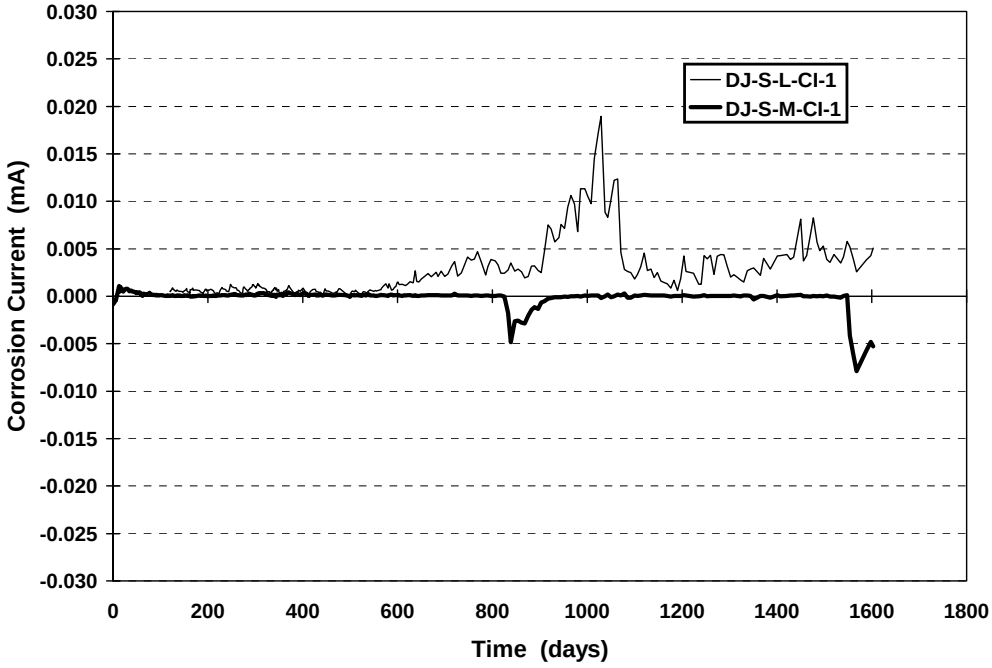

Figure 5.7 - Macrocell Corrosion Current: Dry Joint, Steel Duct and Corrosion Inhibitor in Grout

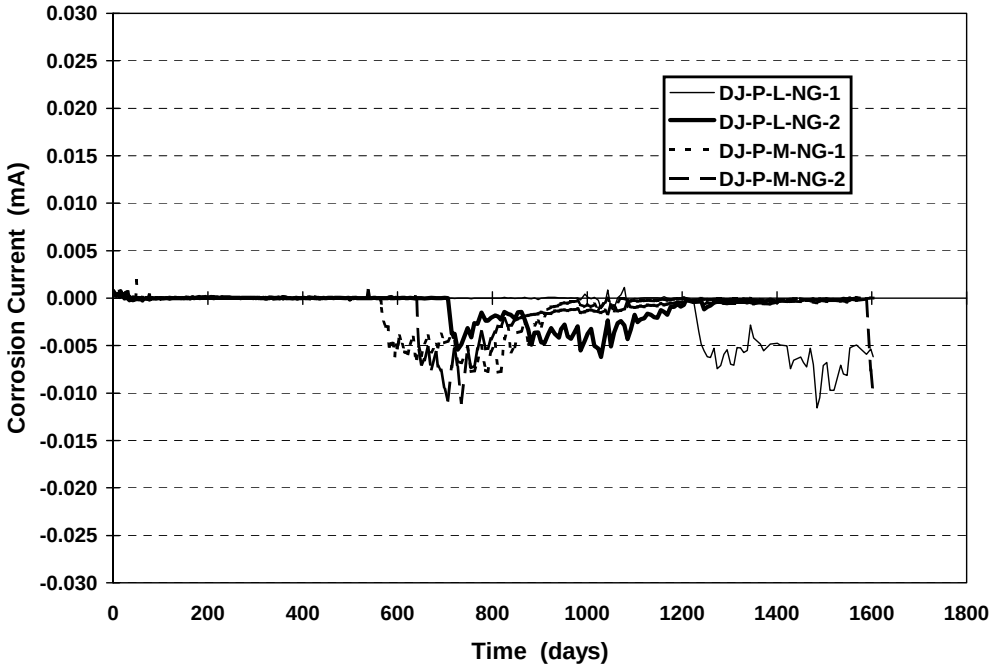

Figure 5.8 - Macrocell Corrosion Current: Dry Joint, PVC Duct and Normal Grout

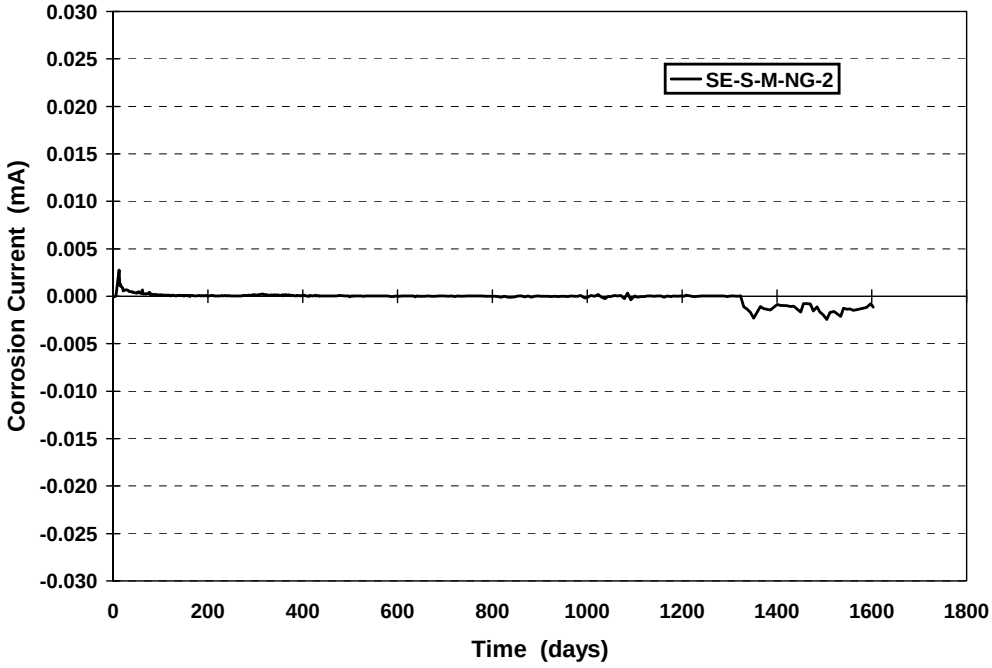

Figure 5.9 - Macrocell Corrosion Current: Standard Epoxy Joint, Steel Duct and Normal Grout

5.6.2 Half-Cell Potential Readings

Three half-cell potential readings were made on each specimen at the start of both the dry and wet period of the cycles. When this data was examined for each specimen, little or no difference was observed between the three readings and thus only the half-cell potential readings immersed in the salt solution (see Figure 5.5) were plotted. These charts are included in Appendix E. The ASTM C876[5.6] guidelines of -130 mV and -280 mV (Table 5.3) are shown on each figure.

The half-cell potential measurements for most specimens suggest a low probability of corrosion or uncertain corrosion activity. Eight specimens, DJ-S-L-NG-1, DJ-S-M-NG-1, DJ-S-M-NG-2, DJ-S-H-NG-1, DJ-S-H-NG-2, DJ-S-L-CI-1, DJ-S-M-CI-1 and SE-S-M-NG-2, show half-cell potentials indicating a high probability of corrosion for some duration. These specimens also showed increased macrocell corrosion current, as described in the previous section. Half-cell potential readings for these specimens, along with the other four specimens with macrocell corrosion current activity, are plotted in Figure 5.10

through Figure 5.13. The specimens plotted in each figure correspond to the same specimens in Figure 5.6 through Figure 5.9.

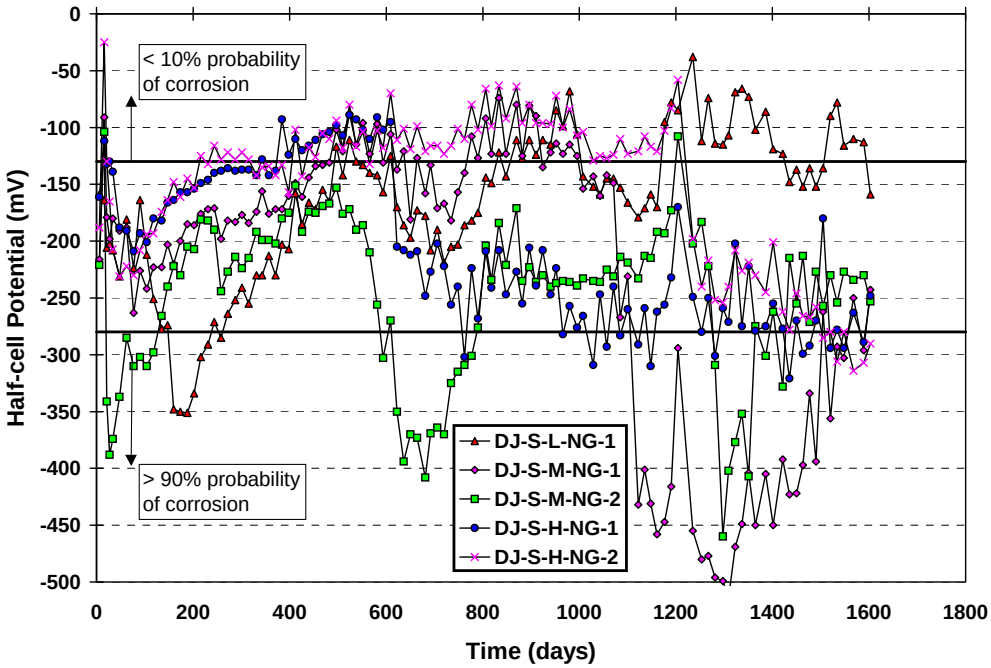

Figure 5.10 - Half-Cell Potentials: Dry Joint, Steel Duct and Normal Grout

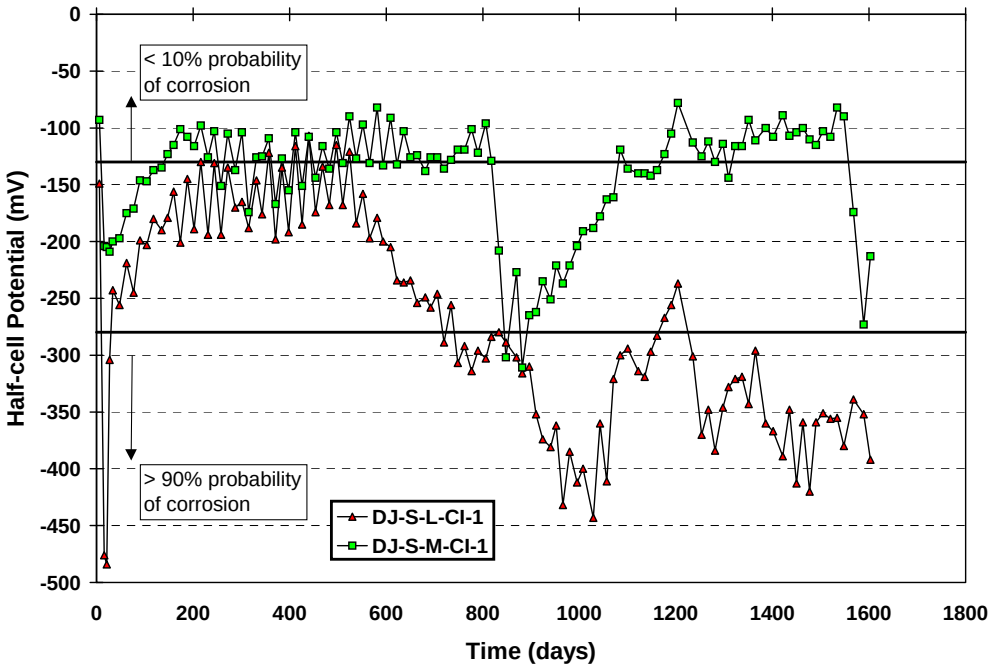

Figure 5.11 - Half-Cell Potentials: Dry Joint, Steel Duct and Corrosion Inhibitor

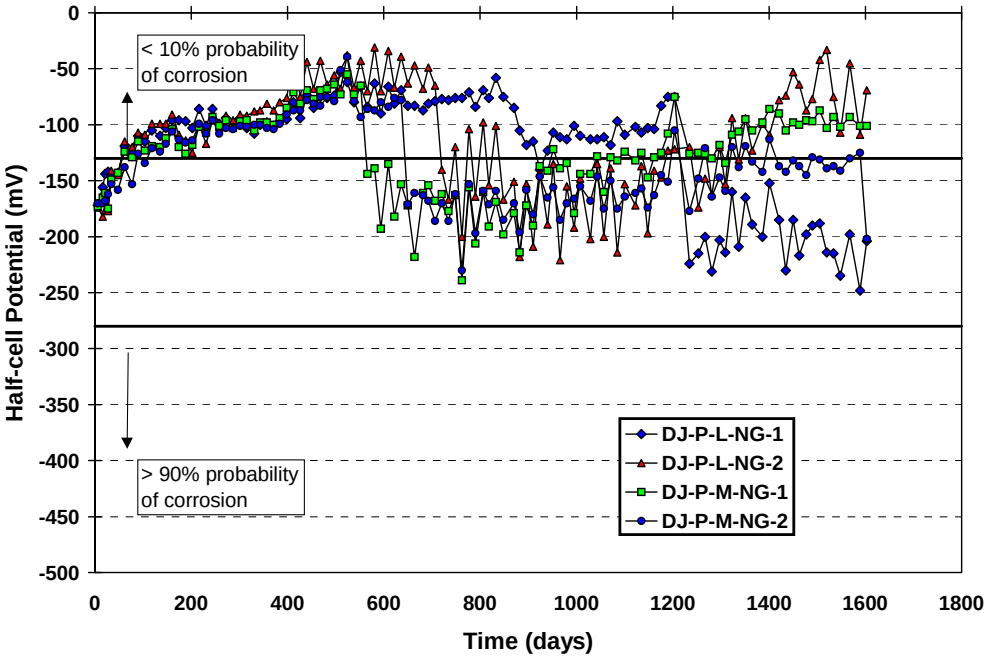

Figure 5.12 - Half-Cell Potentials: Dry Joint, PVC Duct and Normal Grout

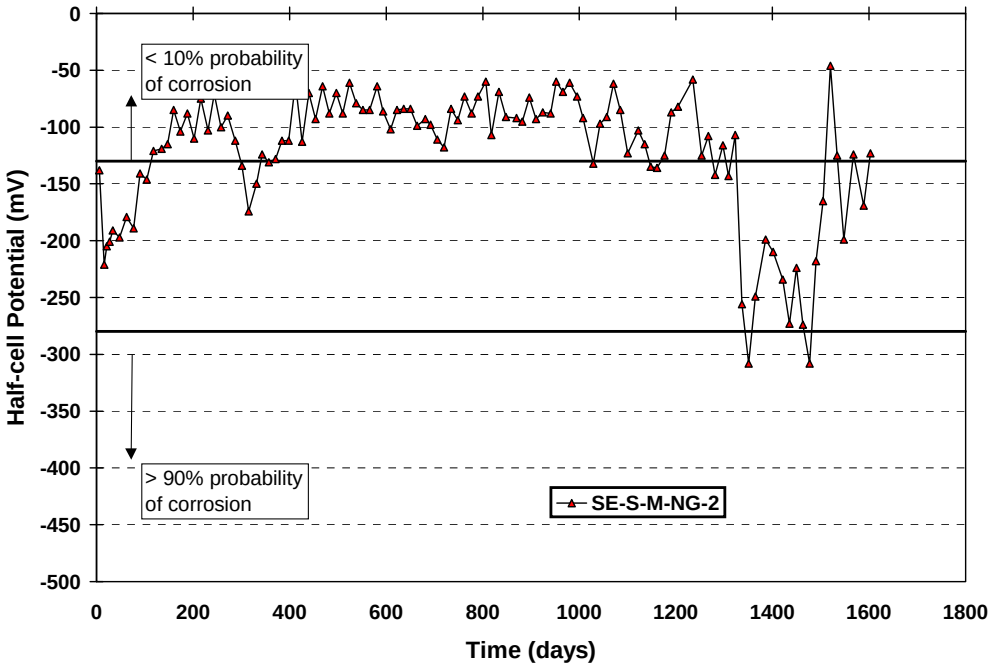

Figure 5.13 - Half-Cell Potentials: Standard Epoxy Joint, Steel Duct and Normal Grout

5.6.3 Analysis and Discussion of Exposure Test Results

5.6.3.1 Time to Initiation of Corrosion

The length of exposure before corrosion initiation is detected may be used to evaluate the effectiveness of corrosion protection variables. For the purposes of this research program, the initiation of corrosion is defined as:

a) a sudden and significant increase in measured corrosion current

and/or b) half-cell potential measurements more negative than -280 mV

and/or c) a sudden and significant change (more negative) in half-cell potential

Criterion (a) is evaluated by examining the plots of macrocell corrosion current over time for a significant increase in corrosion current. Criteria (b) is based on the guidelines of ASTM C876,[5.6] as described in Section 5.5.2. However, the non-typical details of the macrocell specimens in this program may affect the reliability of the ASTM C876 guidelines, and corrosion may occur at potentials less negative than -280 mV. For this

reason, Criterion (c) is included, where plots of half-cell potential over time are examined for a significant change more negative.

Twelve specimens displayed some amount of increased corrosion activity or an initiation of corrosion, as described in Sections 5.6.1 and 5.6.2 and plotted in Figure 5.6 through Figure 5.13. Using these plots and the above definitions for corrosion initiation, the approximate times to the initiation of corrosion for these specimens are listed in Table 5.4. The seven specimens that were exhibiting corrosion activity as of January 1998 are shown in bold in the table.

Table 5.4 - Time to Initiation of Corrosion

Specimen Name	Time to Corrosion		Comments
	Macrocell Current	Half-Cell Potentials	
DJ-S-L-NG-1	128 days	129 days	- strand is corroding - corrosion current reduced to zero after 400 days
DJ-S-M-NG-1	1110 days	1110 days	- strand is corroding - corrosion current reduced to zero near 1600 days
DJ-S-M-NG-2	580 days	588 days	- strand is corroding - two distinct periods of corrosion activity - corrosion current reduced to zero near 1400 days
DJ-S-H-NG-1	**615 days**	**616 days**	**- mild steel bars are corroding**
DJ-S-H-NG-2	**1250 days**	**1225 days**	**- mild steel bars are corroding**
DJ-S-L-CI-1	**580 days**	**714 days**	**- strand is corroding**
DJ-S-M-CI-1	**833 days**	**842 days**	**- mild steel bars are corroding - two distinct periods of corrosion activity**
DJ-P-L-NG-1	**1250 days**	**1225 days**	**- mild steel bars are corroding**
DJ-P-L-NG-2	710 days	714 days	- mild steel bars are corroding - corrosion current decreased to zero at 1200 days
DJ-P-M-NG-1	565 days	560 days	- mild steel bars are corroding - corrosion current decreased to zero after 950 days
DJ-P-M-NG-2	**640 days**	**644 days**	**- mild steel bars are corroding - corrosion current decreased to zero after 1100 days then suddenly increased near 1600 days**
SE-S-M-NG-2	**1330 days**	**1337 days**	**- mild steel bars are corroding - corrosion current is very small**

Discussion: Time to Corrosion

In general, the correlation between times to corrosion initiation based on macrocell current and half-cell potential is very good. The initiation of corrosion based on macrocell corrosion current was very clear for all specimens. The time to corrosion based on half-cell potentials was estimated using Criterion (b) for most specimens. In some cases, it was apparent that Criterion (c) better indicated the onset of corrosion. Examples include specimen DJ-S-H-NG-1 and all of the specimens with plastic ducts.

The largest difference between times given by the two types of data occurs for Specimen DJ-S-L-CI-1. This data suggests that corrosion initiation occurred when the half-cell potentials first indicated a trend towards –280 mV, rather than the point at which the guideline of -280 mV was reached. When the data for DJ-S-L-CI-1 is re-evaluated based on this observation, the time to initiation of corrosion based on half-cell potentials is determined to be approximately 590 days which corresponds well with the estimate based on corrosion current.

The length of time to corrosion for each of the twelve specimens showing activity is plotted in Figure 5.14. The times to corrosion for the twelve specimens do not indicate any trends in the effect of the variables. The three levels of joint precompression investigated do not appear to affect the time to corrosion. Conceptually, higher precompression may be expected to limit moisture and chloride ion penetration at the joint. The results presented in Figure 5.14 do not indicate this trend. The data does not indicate any effect of duct type or grout type.

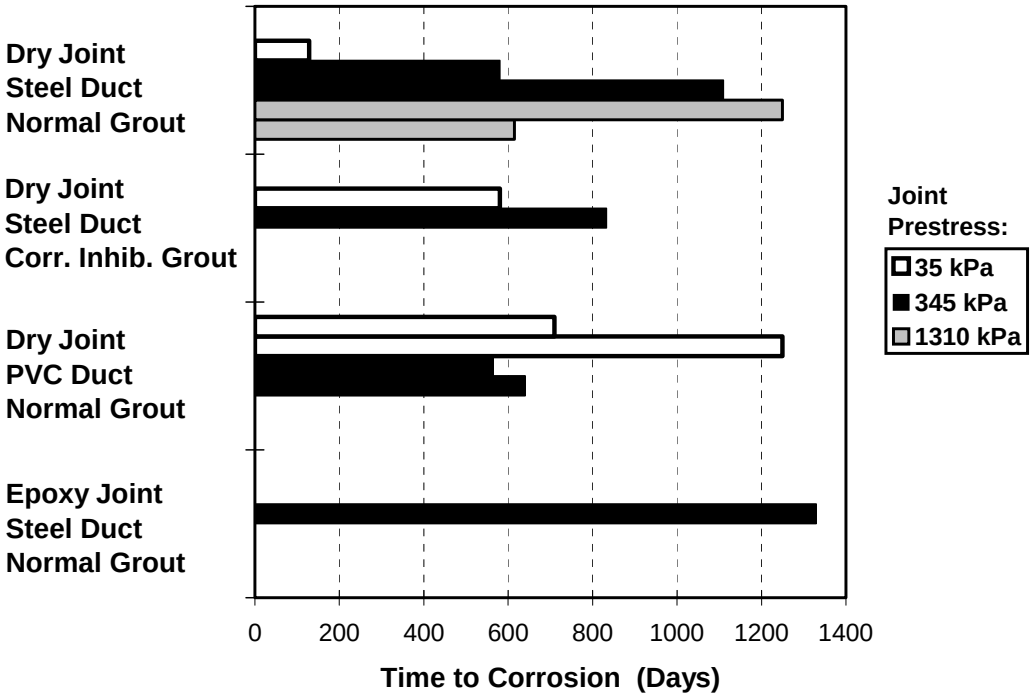

Figure 5.14 - Time to Corrosion Initiation for Active Specimens

5.6.3.2 Corrosion Rate or Severity

Corrosion severity is commonly evaluated in three ways using measured macrocell corrosion currents; weighted average corrosion current, corrosion current density and metal loss.

Weighted Average Corrosion Current

The weighted average corrosion current over the duration of testing, I_{wa}, is computed using the following expression:

$$I_{wa} = \frac{\Sigma I_{ai} T_i}{\Sigma T_i} \quad i=1,n \qquad \textbf{Eq. 5.1}$$

where, I_{ai} = average current in time interval i

T_i = duration of time interval i

n = number of measurements

The effect of different time intervals between readings requires a weighted average. Table 5.6 gives weighted averages for the active specimens. ASTM G109[5.5] defines failure as an average corrosion current of 10 μA (0.010 mA). All specimens are considerably below this value.

Corrosion Current Density

The corrosion current density is the amount of corrosion current per unit surface area of the anode, calculated as the weighted average corrosion current divided by the total anode surface area.

$$\text{Corrosion Current Density} = \frac{I_{wa}}{A_{surf}} \ (\mu A / cm^2) \qquad \textbf{Eq. 5.2}$$

The anode surface area (A_{surf}) is taken as the total (nominal) surface area of the anode bar, assuming that corrosion is occurring over the entire exposed length of the anode. For this testing program, the non-typical macrocell specimens make estimation of the anode surface area very difficult. If the strand is the anodic site, the total surface area is computed as the sum of the surface areas of each of the 7 wires of the strand. The presence of the duct and segmental joint raise further questions as to whether corrosion will occur over the exposed length of strand. For specimens in which the corrosion macrocell is reversed the anode cross-sectional area is the area of the two reinforcing bars. However, chlorides may not have reached the entire bar length.

The uncertainty surrounding the computation of A_{surf} significantly affects the usefulness of calculated values of corrosion current density. For analysis purposes, the following values of A_{surf} were used:

For normal macrocell corrosion: (positive I_{wa})	use A_{surf} based on total surface area of 7 wires (125 mm (5 in.) exposed length)
For reversed macrocell corrosion: (negative I_{wa})	use A_{surf} based on surface area of two 12.7 mm (#4) bars (125 mm (5 in.) exposed length)

Guidelines have been proposed[5.7,5.8,5.9] to assess the rate of corrosion based on corrosion current densities, as shown in Table 5.5. Calculated values of corrosion current density are shown in Table 5.6. The computed corrosion current densities for all specimens are all well within the range of negligible corrosion. However, because the corroded surface area is uncertain, overestimation of A_{surf} could produce unconservative results.

Table 5.5 - Corrosion Severity Based on Current Density[5.7,5.8,5.9]

Corrosion Current Density	Corrosion Severity
Less than 0.1 μA/cm²	Negligible
Between 0.1 and 0.2 μA/cm²	Low (threshold for active deterioration mechanism)
Between 0.2 and 0.5 μA/cm²	Moderate

Metal Loss

The amount of steel "consumed" by macrocell corrosion is directly related to the total amount of electrical charge, or number of electrons, exchanged between the anode and cathode. One amp of corrosion current consumes 1.04 grams of steel (iron) per hour.[5.10] The total amount of current passed, or charge flux, is computed by numerically integrating the macrocell corrosion current data over the duration of exposure. Although an absolute measurement of corrosion severity is difficult to obtain using metal loss (charge flux), a relative comparison of corrosion severity between specimens is possible. Calculated values of metal loss are listed in Table 5.6.

As mentioned in Section 5.6.1, ASTM G109[5.5] defines failure as an average macrocell corrosion current over the duration of testing of more than 10 μA. For an average corrosion current of 10 μA and the exposure duration of four years and five months, a metal loss of 400 milligrams (0.014 oz) would be expected (calculations are included in Appendix E). The most severe corrosion has occurred in specimens with dry joints, galvanized steel ducts and normal grout. Calculated metal loss for these specimens is less than 250 mg ((0.0088 oz). Calculated metal loss for the single epoxy joint specimen

showing corrosion activity is very low (10 mg (0.00035 oz)), reflecting the long time to corrosion initiation and low corrosion current. In general, the calculated values of metal loss suggest corrosion activity is minor in most specimens.

Table 5.6 – Calculated Weighted Average Current, Current Density and Metal Loss for Active Specimens

No.	Specimen Name	Weighted Average Corrosion Current (μAmps)	Corrosion Current Density (μA/cm²)	Metal Loss (mg)
1	DJ-S-L-NG-1	0.499	0.004	20
7	DJ-S-M-NG-1	4.517	0.039	181
8	DJ-S-M-NG-2	1.307	0.011	52
11	DJ-S-H-NG-1	-5.960	0.060	238
12	DJ-S-H-NG-2	-1.346	0.013	54
31	DJ-P-L-NG-1	-1.394	0.014	56
32	DJ-P-L-NG-2	-1.216	0.012	49
33	DJ-P-M-NG-1	-1.187	0.012	48
34	DJ-P-M-NG-2	-1.162	0.012	46
3	DJ-S-L-CI-1	2.659	0.023	106
9	DJ-S-M-CI-1	-0.294	0.003	12
22	SE-S-M-NG-2	-0.236	0.002	9

Note: Negative Average Corrosion Current indicates mild steel bars are corroding.

Discussion: Corrosion Rate Calculations

The corrosion rate calculations for weighted average corrosion current, corrosion current density and metal loss indicate that the corrosion activity for all specimens is considerably lower than what would be defined as failure.

The calculated corrosion rates using the three different methods are plotted in Figure 5.15 where the relative performance of the twelve specimens is the same for all three cases. All three corrosion rate calculations are related to the charge flux or the number of electrons exchanged between the anode and cathode. The charge flux is calculated by integrating the corrosion current over time:

$$\text{Charge Flux} = \int I_{corr} dt \equiv \sum I_{ai} T_i \quad (i = 1, n) \quad \text{(Coulombs)}$$

where, I_{corr} = instantaneous corrosion current
I_{ai} = average current in time interval i
T_i = duration of time interval i
n = number of measurements

The calculation of charge flux appears in the computation of weighted average corrosion current, current density and metal loss:

$$\text{Weighted Avg. Current, } I_{wa} = \frac{\int I_{corr}\,dt}{t_d} \equiv \frac{\sum I_{ai} T_i}{\sum T_i} \quad \text{(amps)}$$

$$\text{Current Density} = \frac{I_{wa}}{A_{surf}} \equiv \frac{\int I_{corr}\,dt}{t_d} \times \frac{1}{A_{surf}} \quad (\text{amps}/\text{cm}^2)$$

$$\text{Metal Loss} = \int I_{corr}\,dt \times \left(\frac{1\ \text{hr}}{3600\ \text{sec}} \times \frac{1.04\text{g}}{\text{amp} - \text{hr}} \times \frac{1000\text{mg}}{\text{g}} \right) (\text{mg})$$

where, t_d = duration of testing
A_{surf} = corroded surface area

In general, any one of the three forms of corrosion rate calculations would be appropriate for comparing the performance of the protection variables. Calculated metal loss will be used for discussion purposes in the remainder of this document.

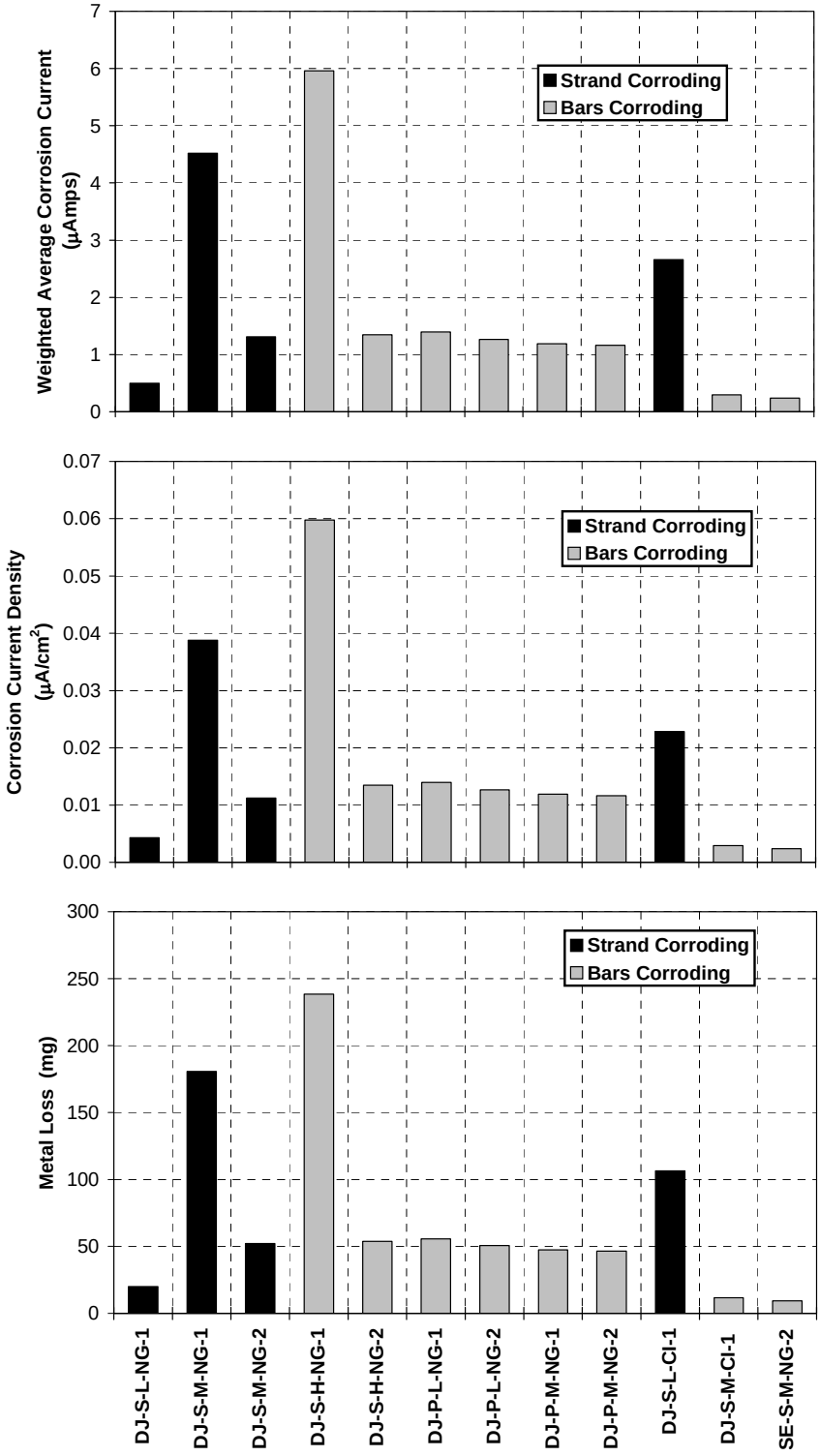

Figure 5.15 - Calculated Corrosion Rates for Active Specimens

The corrosion rate calculations provide a means for relative comparison of corrosion activity in the different specimens. However, it is difficult to use the calculated corrosion rates to obtain an absolute measure of corrosion severity. Corrosion current density can be used for this purpose if the area over which corrosion is occurring is known. The non-typical details of the segmental macrocells make estimation of the corroded surface area uncertain at best, and thus the use of corrosion current density to assign a corrosion severity using Table 5.5 is questionable for this testing program.

The effect of the different variables (other than joint type) is not clear based on the calculated corrosion rates (Figure 5.15). Similar to the time to corrosion data, computed values of metal loss do not indicate improved corrosion protection for the three levels of joint precompression. Also, the effect of duct type and grout type is unclear.

5.7 Forensic Examination

After 1603 days of exposure testing (four years and five months), one specimen from each identical pair was removed from testing for forensic examination or autopsy. The objectives of the forensic examination are as follows:

1. Obtain visual evaluation of corrosion damage on duct, strand and mild steel reinforcement.
2. Obtain visual evaluation of joint condition.
3. Determine chloride ion penetration at locations adjacent to and away from the segmental joint.
4. Examine mechanisms of corrosion in segmental macrocell corrosion specimens.

The notation scheme shown in Figure 5.16 was assigned for record keeping purposes. "Clamp end" refers to the end of the specimen where ground clamps were attached to complete the macrocell circuit. Segment B was cast first. Segment A was match-cast against Segment B. All specimens were numbered on Side C at the clamp end. This ensured that the orientation of all specimens was known throughout the forensic examination process. The notation scheme will be referred to throughout this chapter.

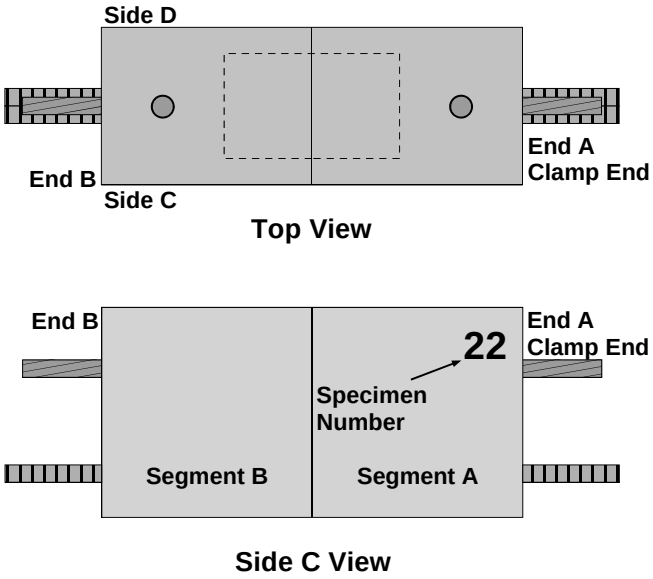

Figure 5.16 - Specimen Labeling Scheme

5.7.1 Procedure

5.7.1.1 Specimen Condition at End of Testing

The exterior surfaces of each specimen were examined for cracking and rust staining upon removal from testing. Duct ends were examined for grout voids and rust stains. The joint perimeter was examined for visible salt stains, joint epoxy and grout.

5.7.1.2 Concrete Powder Samples for Chloride Analysis

One of the objectives of the forensic examination is to determine the influence of the three joint types on the penetration of moisture and chlorides. It was expected that chloride contents could be higher in the vicinity of the joint, particularly for dry joint specimens. To examine the influence of joint type on chloride penetration, concrete powder samples were collected at multiple depths and locations to determine chloride ion profiles adjacent to the joint and away from the joint. Sample locations are shown in Figure 5.17. Concrete powder samples were collected using a rotary hammer and following a procedure based on AASHTO T 260-94.[5.11] Two 1.5 g samples were collected

at each depth. Samples were analyzed for acid soluble chlorides using a specific ion probe (CL Test System by James Instruments).

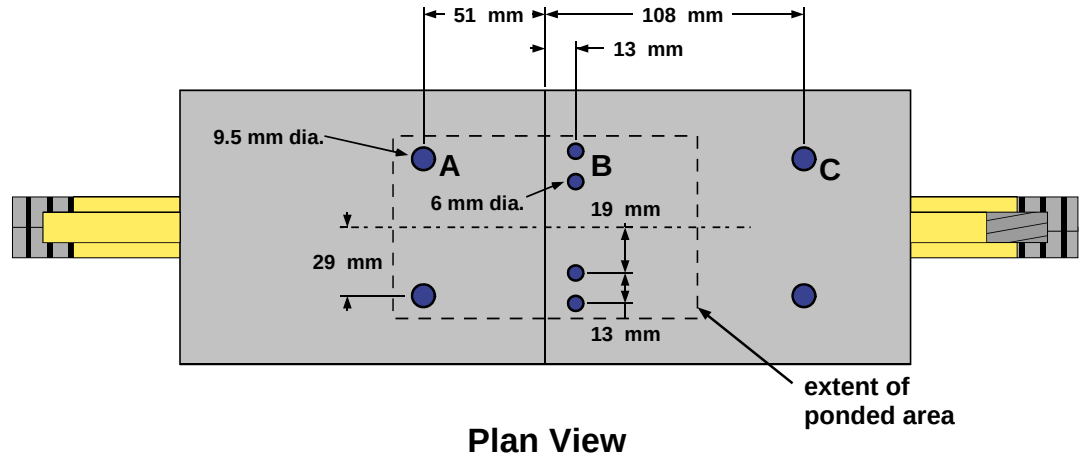

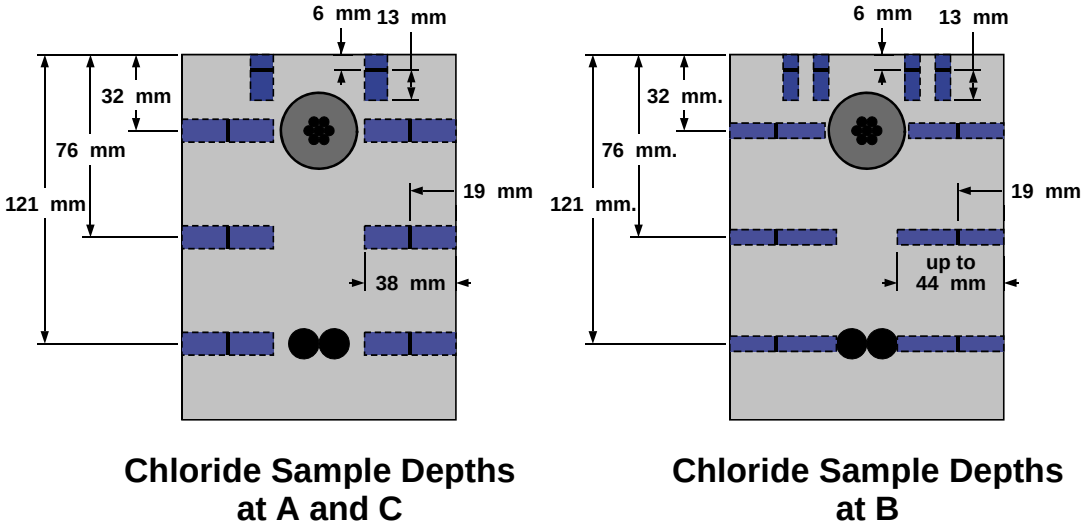

Figure 5.17 - Chloride Sample Locations

Location A

Samples at A were taken at a distance of 51 mm (2 in.) from the segmental joint using a 9.5 mm (3/8 in.) dia. drill bit. Two holes were drilled at each depth to obtain a sufficient amount of powder for testing. The first sample was taken on the top surface of

the specimen. Initially, the holes were drilled to a depth of 6 mm (0.25 in.). The holes and bit were then cleaned, and the holes were drilled an additional depth of 13 mm (0.5 in.). An average depth of 13 mm (0.5 in.) was assumed for this sample. The remaining three samples at location A were obtained by drilling into the sides of the specimen. One hole was drilled into each side of the specimen at the desired depths. The holes were drilled to an initial depth of 19 mm (0.75 in.) so that the collected sample will be from concrete directly below the ponded area. Following cleaning, the holes were drilled an additional 13 to 19 mm (0.5 to 0.75 in.) to obtain the sample amount (total depth up to 38 mm).

Location B

Samples at B were collected at a distance of 13 mm (0.5 in.) from the segmental joint. Due to the close proximity of the joint, a smaller bit size of 6 mm (0.25 in.) was used for these samples. The procedure for obtaining the powder samples at location B is similar to that a location A with some minor modifications due to the smaller drill bit size. Four holes were required for the sample on the top surface of the specimen, and the holes for the other samples were drilled slightly deeper (up to 44 mm (1.75 in.)) to obtain the necessary sample amount.

Location C

Samples at C were taken at a distance of 108 mm (4.25 in.) from the segmental joint. The procedure for collecting samples at C is identical to that for samples at A.

5.7.1.3 Longitudinal Saw Cuts

Four longitudinal saw cuts were made on each specimen to facilitate removal of the duct/strand unit and mild steel bars. Saw cuts were made to a depth of 38 mm (1.5 in.) at the level of the tendon and bars, as shown in Figure 5.18. These cuts are referred to as the strand cut line and bar cut line respectively. The specimen remained intact after cutting, but was easily opened using a hammer and chisel. Saw cuts were performed using a high torque circular saw fitted with a diamond dry-cut concrete blade.

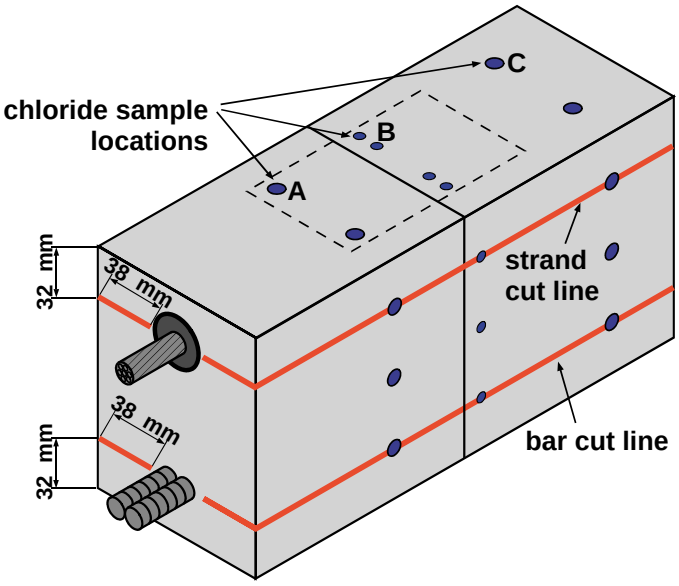

Figure 5.18 - Longitudinal Saw Cuts

5.7.1.4 Expose and Remove Duct and Strand

The duct was exposed by opening the specimen at the strand cut line, as shown in Figure 5.19. The duct and strand were then removed from the concrete as one unit. The concrete surrounding the duct was examined for voids, cracks, rust staining, salt collection and damage. After thorough examination, the duct was cut open by making two longitudinal cuts along the sides of the duct/strand unit using a small air-driven grinder. The grout was examined for voids and cracks and indications of moisture and chloride ingress. If desired, grout samples were taken from the grout for chloride analysis at this time (see Section 5.7.1.5). The grout was then carefully removed, exposing the strand for examination. The extent and severity of corrosion on both the strand and duct was rated according to the corrosion rating scheme described in Section 5.7.3.

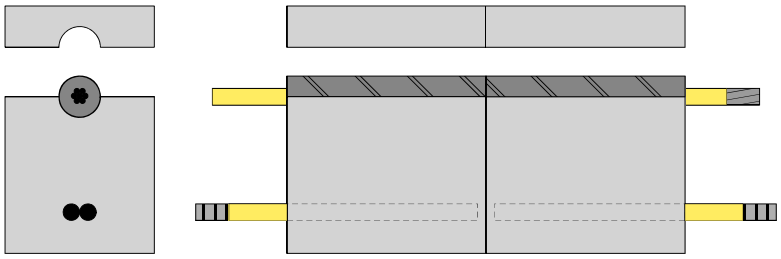

Figure 5.19 - Specimen Opened to Expose Duct/Strand

5.7.1.5 Grout Samples for Chloride Analysis

Grout samples were collected from selected specimens for chloride analysis. Samples were carefully removed from the strand at the location of the joint and at a distance of 50 mm (2 in.) from the joint. The grout pieces were crushed between two steel plates and ground into powder using a mortar and pestle. Grout powder samples were analyzed for acid soluble chlorides using a specific ion probe (CL Test System by James Instruments).

5.7.1.6 Expose and Remove Mild Steel

The mild steel bars were exposed by opening the specimen at the bar cut line, as shown in Figure 5.20. The bars were then removed from the concrete for examination. The extent and severity of corrosion on the bars was rated according to the corrosion rating scheme described in Section 0. The concrete surrounding the bars was examined for voids, rust staining, salt collection and any damage.

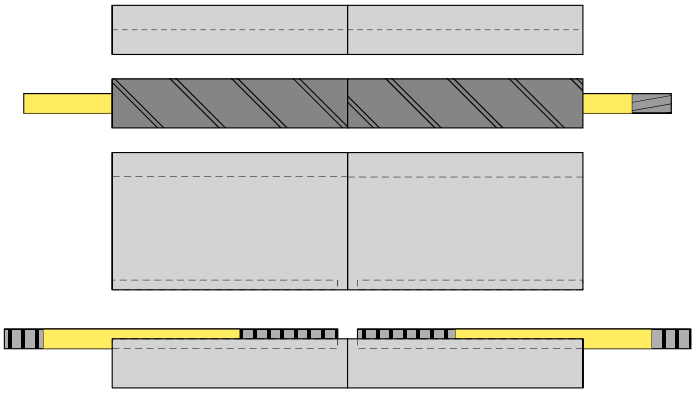

Figure 5.20 - Specimen Opened to Expose Mild Steel Bars

5.7.1.7 Examine Joint Condition

In the dry joint specimens, the specimen readily separated into its two segments after the duct/strand unit was removed (Section 5.7.1.4). This allowed the condition of the joint face to be examined directly for cracking, rust staining, evidence of moisture and chloride penetration and general soundness of the joint.

The intention of the epoxy joint is to bond the two segments together. As a result, it was not possible to examine the joint in the same manner as the dry joint specimens. An

indication of the epoxy joint condition was obtained by examining several sections through the joint, as shown in Figure 5.21. The saw cuts at the strand line and bar line (Section 5.7.1.3) revealed the epoxy joint condition at sections 1 and 3 in Figure 5.21. An addition longitudinal saw cut was made at the mid-height of the specimen to obtain a third section through the joint (Joint Section 2 in the figure). The joint was also examined around the perimeter of the specimen. The joint sections were examined for indications of voids in the epoxy or the presence of moisture, salt or corrosion products.

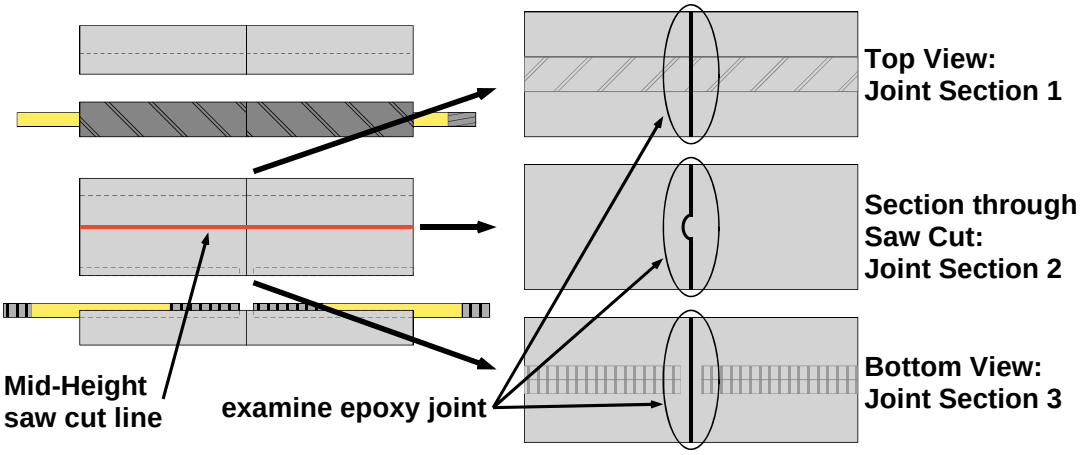

Figure 5.21 - Examining Epoxy Joint Condition

5.7.2 Autopsy Program

One specimen from each duplicate pair of specimen types was selected for forensic examination. For dry joint specimens, it was arbitrarily decided to autopsy specimen number 1 of each pair. For epoxy jointed specimens, it was decided to autopsy specimen number 2 of each pair so that the one epoxy joint specimen showing corrosion activity (SE-S-M-NG-2) would be included.

Chloride samples were collected from ten of the nineteen specimens autopsied. The ten specimens were selected to provide a representative sample and address the major variables expected to influence chloride penetration. The mid-height cut for epoxy jointed specimens was performed on six of the twelve specimens with epoxy joints. Specimens selected were standard epoxy joints and epoxy/gasket joints at each of the three levels of

joint precompression. Details of the nineteen specimens selected for autopsy are listed in Table 5.7.

Table 5.7 - Specimens Selected for Forensic Examination

Specimen	Time to Corrosion	Corrosion Location	Corrosion Activity	Chloride Samples	Mid-Height Cut
DJ-S-L-NG-1	128 days	Strand	Inactive	A, B, C	n/a
DJ-S-M-NG-1	1110 days	Strand	Inactive	A, B	n/a
DJ-S-H-NG-1	615 days	Bars	Active	A, B	n/a
DJ-P-L-NG-1	1250 days	Bars	Active	A, B	n/a
DJ-P-M-NG-1	565 days	Bars	Inactive	None	n/a
DJ-S-L-CI-1	580 days	Strand	Active	A, B	n/a
DJ-S-M-CI-1	835 days	Bars	Inactive	A, B	n/a
SE-S-L-NG-2	n/a	n/a	n/a	A, B, C	Yes
SE-S-M-NG-2	1330 days	Bars	Active	A, B	Yes
SE-S-H-NG-2	n/a	n/a	n/a	A, B	Yes
SE-P-L-NG-2	n/a	n/a	n/a	None	No
SE-P-M-NG-2	n/a	n/a	n/a	None	No
SE-S-L-CI-2	n/a	n/a	n/a	None	No
SE-S-M-CI-2	n/a	n/a	n/a	None	No
SE-S-H-CI-2	n/a	n/a	n/a	None	No
SE-S-L-SF-2	n/a	n/a	n/a	None	No
EG-S-L-NG-2	n/a	n/a	n/a	A, B	Yes
EG-S-M-NG-2	n/a	n/a	n/a	None	Yes
EG-S-H-NG-2	n/a	n/a	n/a	none	Yes

5.7.3 Evaluation and Rating of Corrosion Found During Forensic Examination

A generalized evaluation and rating system was developed to quantify the severity and extent of corrosion damage in the test specimens. The procedure is presented in a universal form with the intention of applying the same rating system to other situations. The length of strand, mild steel reinforcement or galvanized steel duct was subdivided into eight increments. At each increment, the steel was examined and a rating was assigned to describe the corrosion severity within that increment. The ratings for the eight increments were summed to give a total corrosion rating for the element that could

be compared for different specimens. By assigning a corrosion severity at eight locations, both the extent and severity of corrosion is considered using this approach.

The corrosion severity ratings are described below. The rating system is essentially the same for prestressing strand, mild steel reinforcement and galvanized duct, with some modifications to reflect unique corrosion aspects of each type of steel. In general, the evaluation system doubles the severity rating for each category of increasing corrosion damage.

5.7.3.1 Prestressing Strand

The strand was examined at eight intervals, as indicated in Figure 5.22. The interval sizes have been adjusted to provide four intervals in the unpainted region of the strand, and two intervals in each of the painted regions at both ends. Corrosion ratings were assigned to indicate the severity of corrosion on the outer six wires of the strand and on the center wire (after de-stranding) at each interval to address the possibility of different corrosion activity on the strand exterior and interstices between wires. The corrosion rating system for prestressing strand is described in Table 5.8. The total strand corrosion rating was calculated as follows:

$$\text{Strand Corrosion Rating} = \sum_{i=1}^{8} R_{outer,i} \times n_i + R_{center,i} \qquad \textbf{Eq. 5.3}$$

where,

$R_{outer,i}$ = outer wires corrosion rating, interval i
n_i = number of corroded outer wires, interval i
$R_{center,i}$ = center wire corrosion rating, interval i
i = interval, 1 to 8

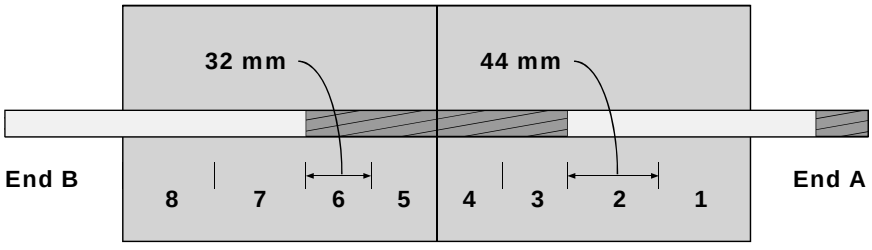

Figure 5.22 - Intervals for Corrosion Ratings on Prestressing Strand

Table 5.8 - Evaluation and Rating System for Corrosion Found on Prestressing Strand

Code	Meaning	Description	Rating
NC	No Corrosion	No evidence of corrosion.	0
D	Discoloration	No evidence of corrosion, but some discoloration from original color.	1
L	Light	Surface corrosion on less than one half of the interval, no pitting. Surface corrosion can be removed using cleaning pad.	2
M	Moderate	Surface corrosion on more than one half of the interval, no pitting. **and/or** Corrosion can not be completely removed using cleaning pad.	4
P1	Mild Pitting	Broad shallow pits with a maximum pit depth not greater than 0.5 mm (.02 in).	8
P2	Moderate Pitting	Pitting where the maximum pit depth ranged between 0.5 and 1.0 mm (.02 and .04 in.).	16
P3	Severe Pitting	Pitting where the maximum pit depth is greater than 1.0 mm (.04 in.).	32

The corrosion rating system for prestressing strand was adapted from Poston[5.12] and Hamilton.[5.13] The use of a cleaning pad to assess corrosion severity was proposed by Sason[5.14] for classifying the degree of rusting on prestressing strand for new construction. The recommended cleaning pad is a 3M Scotch Brite Cleaning Pad. The pad is held by hand and rubbed longitudinally along the strand axis with a pressure similar to that used when cleaning pots and pans. The classification of pitting severity was based on tensile tests performed on corroded prestressing strand.[5.15] The tests were used to assign a reduced tensile capacity of 97% GUTS to pitting damage at the level of P1. Moderate pitting (P2) was assigned a capacity of 90% GUTS, and severe pitting (P3) 77% GUTS. In general, the presence of any pitting visible to the unaided eye is deemed cause for rejection in new construction.[5.14]

5.7.3.2 Mild Steel Reinforcement

The mild steel reinforcing bars were examined at eight intervals, as indicated in Figure 5.23. The interval sizes have been adjusted to provide four intervals in the unpainted region of the bars, and two intervals in the painted regions at both ends. Corrosion ratings were assigned to indicate the severity of corrosion on the top and bottom surfaces of each bar to reflect the possibility of different corrosion severity and extent. The corrosion rating system is described in Table 5.9. The total bar corrosion rating was calculated as follows:

$$\text{Bar Corrosion Rating} = \sum_{i=1}^{8} R_{Bar1Top,i} + R_{Bar1Bot,i} + R_{Bar2Top,i} + R_{Bar2Bot,i} \qquad \textbf{Eq. 5.4}$$

where,
$R_{Bar1Top,i}$ = Bar 1, top surface corrosion rating, interval i
$R_{Bar1Bot,i}$ = Bar 1, bottom surface corrosion rating, interval i
$R_{Bar2Top,i}$ = Bar 2, top surface corrosion rating, interval i
$R_{Bar2Bot,i}$ = Bar 2, bottom surface corrosion rating, interval i
i = interval, 1 to 8

Table 5.9 - Evaluation and Rating System for Corrosion Found on Mild Steel Bars

Code	Meaning	Description	Rating
NC	No Corrosion	No evidence of corrosion	0
D	Discoloration	No evidence of corrosion, but some discoloration from original color	1
L	Light	Surface corrosion on less than one half of the interval, no pitting. Surface corrosion can be removed using cleaning pad.	2
M	Moderate	Surface corrosion on more than one half of the interval, no pitting. **and/or** Corrosion can not be completely removed using cleaning pad.	4
P	Pitting	Pits visible to unaided eye.	8
AR	Area Reduction	Measurable reduction in bar cross-sectional area due to corrosion	R^2

R = Estimated cross-sectional area reduction in percent

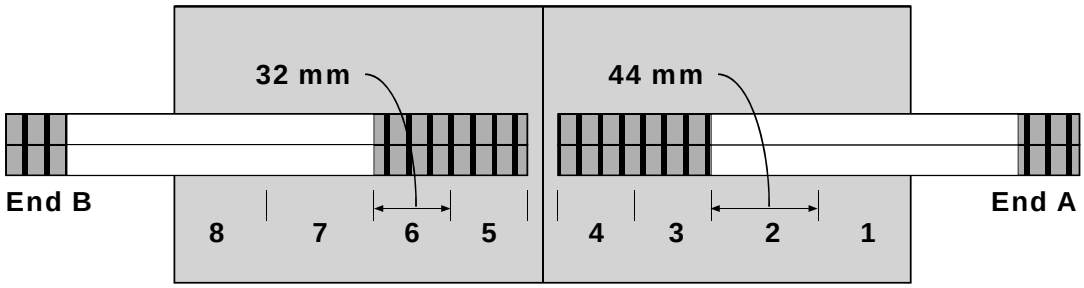

Figure 5.23 – Intervals for Corrosion Ratings On Mild Steel Bars

5.7.3.3 Galvanized Steel Duct

The galvanized steel duct was examined eight equal intervals of 38 mm (1.5 in.), as indicated in Figure 5.24. At each location, corrosion ratings are assigned to indicate the severity of corrosion on the top and bottom surfaces of the inside and outside of each duct to reflect the possibility of different corrosion severity and extent. The corrosion rating system is described in Table 5.10. The total duct corrosion rating was calculated as follows:

$$\text{Duct Corrosion Rating} = \sum_{i=1}^{8} R_{\text{TopOuter},i} + R_{\text{BotOuter},i} + R_{\text{TopInner},i} + R_{\text{BotInner},i} \qquad \textbf{Eq. 5.5}$$

where,

$R_{\text{TopOuter},i}$ = top outer surface corrosion rating, interval i
$R_{\text{BotOuter},i}$ = bottom outer surface corrosion rating, interval i
$R_{\text{TopInner},i}$ = top inner surface corrosion rating, interval i
$R_{\text{BotInner},i}$ = bottom inner surface corrosion rating, interval i
i = interval, 1 to 8

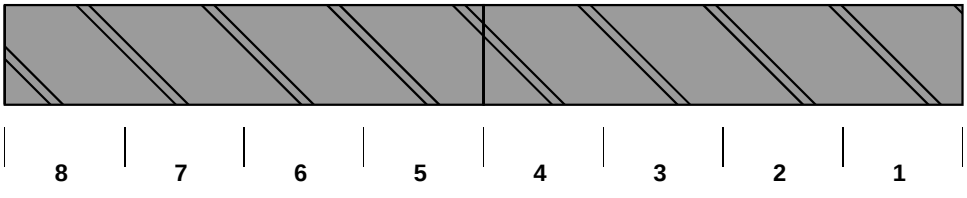

Figure 5.24 - Intervals for Corrosion Ratings on Galvanized Duct

Table 5.10 – Evaluation and Rating System for Corrosion Found on Post-tensioning Duct

Code	Meaning	Description	Rating
NC	No Corrosion	No evidence of corrosion	0
D	Discoloration	No evidence of corrosion, but some discoloration from original color	1
L	Light	Surface corrosion on less than one half of the interval, no pitting.	2
M	Moderate	Surface corrosion on more than one half of the interval, no pitting.	4
S	Severe	Corrosion completely covers the interval. **and/or** Presence of pitting.	8
H	Hole Through Duct	Hole corroded through duct. Used in conjunction with ratings D, L, M and S.	$32 + A_h$

A_h = Area of hole(s) in mm^2

5.7.4 Forensic Examination Results

A brief summary of the forensic examination results is provided for each specimen in the following sections. In the interest of space, photos of specimen condition are not provided for each specimen. Instead, typical photos of the different findings are shown where appropriate. Several addition photos are used in the discussion of results (Section 5.8).

5.7.4.1 Specimen DJ-S-L-NG-1

Severe corrosion was found on the galvanized steel duct in both segments, as shown in Figure 5.25. The corroded area was

Corrosion Ratings:	Strand	26
	Bars	12
	Duct	528

centered on the segmental joint. Two large holes, and several small holes were produced by corrosion action on the top surface of the duct. A smaller area of severe corrosion was also found on the bottom surface of the duct in the vicinity of the joint. Duct corrosion produced a 160 mm (6.25 in.) long crack on the top surface of the specimen. The crack had a maximum width of 0.18 mm (0.007 in.). The crack extended the full depth of cover to the duct, and was clearly visible when the specimen was opened at the strand cut line.

(a) Outside Surface of Duct (joint location at left end)

(b) Inside Surface of Duct (joint location at left end)

Figure 5.25 - Severe Duct Corrosion Damage

One interval each of light and moderate corrosion was found on both the outer wires and the center wire of the prestressing strand. Corrosion was located near end A where the epoxy paint had peeled off of the strand, as shown in Figure 5.26. No corrosion was found in the unpainted length of the strand.

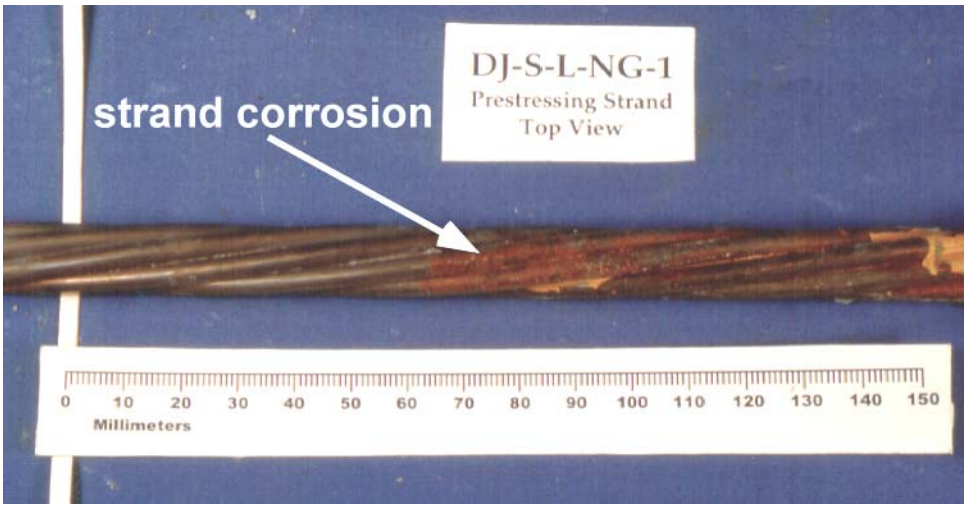

Figure 5.26 - Moderate Prestressing Strand Corrosion Where Epoxy Paint Peeled Away (Segmental Joint Location Indicated by Vertical White Line)

Several small patches of light corrosion were found on the top and bottom surfaces of the mild steel bars.

Heavy rust and salt stains were found on the surface of the grout, as shown in Figure 5.27. The heaviest concentrations were in the vicinity of the holes in the duct. Three large voids were found in the grout. The voids appear to have resulted from insufficient grout fluidity rather than due to trapped air or bleed water collection. Several of the small holes in the duct were located over a grout void near the joint.

The match-cast dry joint was intact with no voids or cracks. Some grout infiltrated the joint during grouting. The extent of infiltration was approximately 15 mm, uniform around the duct opening. Some rust stains were visible around the duct opening. The entire face of the joint was covered with a white residue that may be salt or leaching.

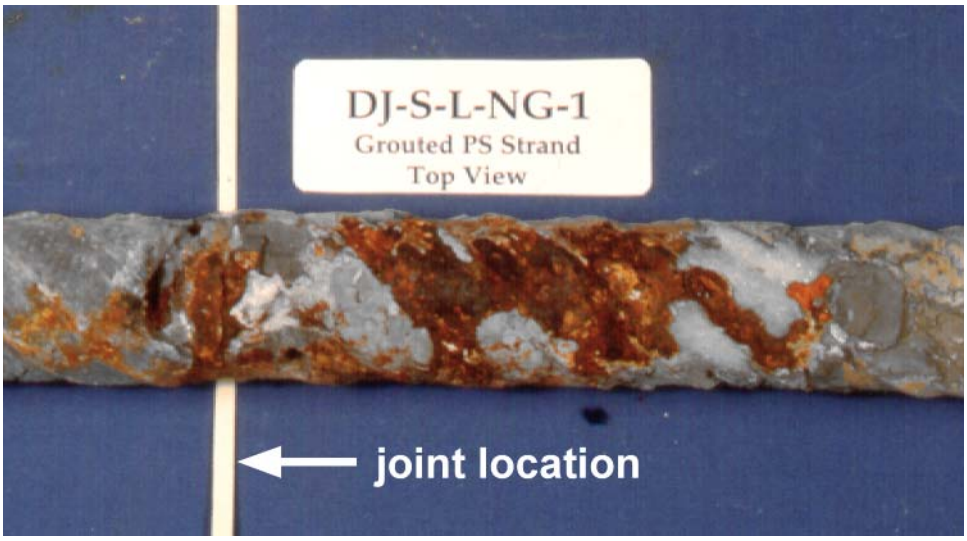

Figure 5.27 - Heavy Rust Staining on Grout Surface

5.7.4.2 Specimen DJ-S-M-NG-1

Corrosion Ratings:	Strand	43
	Bars	12
	Duct	325

Significant corrosion was found on the galvanized steel duct, with the heaviest areas located in the vicinity of the dry segmental joint. On the top surface, a large hole more than 25 mm (1 in.) long and 6 mm (0.25 in.) wide resulted from corrosion action. Some corrosion damage was also observed on the bottom surface of the duct, including a small hole. Duct corrosion produced a 150 mm (5.75 in.) long crack on the top surface of the specimen. The maximum crack width was 0.08 mm (0.003 in.).

A small area of moderate surface corrosion was found on the unpainted region of the prestressing strand. This area was limited to one wire of the strand, and was approximately 38 mm (1.5 in.) long. Large areas of epoxy paint had peeled off of the strand. Several intervals of moderate and light corrosion were found on both the outer wires and center wire throughout the areas where the paint had peeled.

Several small patches of light corrosion were found on the top and bottom surfaces of the mild steel reinforcement.

A large void, 95 mm (3.75 in.) long was observed in the top surface of the grout at the joint. The hole in the duct directly corresponded to the grout void in segment B. Salt crystals were visible in the void. The void appears to have resulted from insufficient grout fluidity rather than from bleed water collection or trapped air.

The match-cast dry joint was intact with no voids or cracks. The entire joint surface was covered with a white residue. A large area of rust staining was present on the face of the joint around the duct opening, as shown in Figure 5.28.

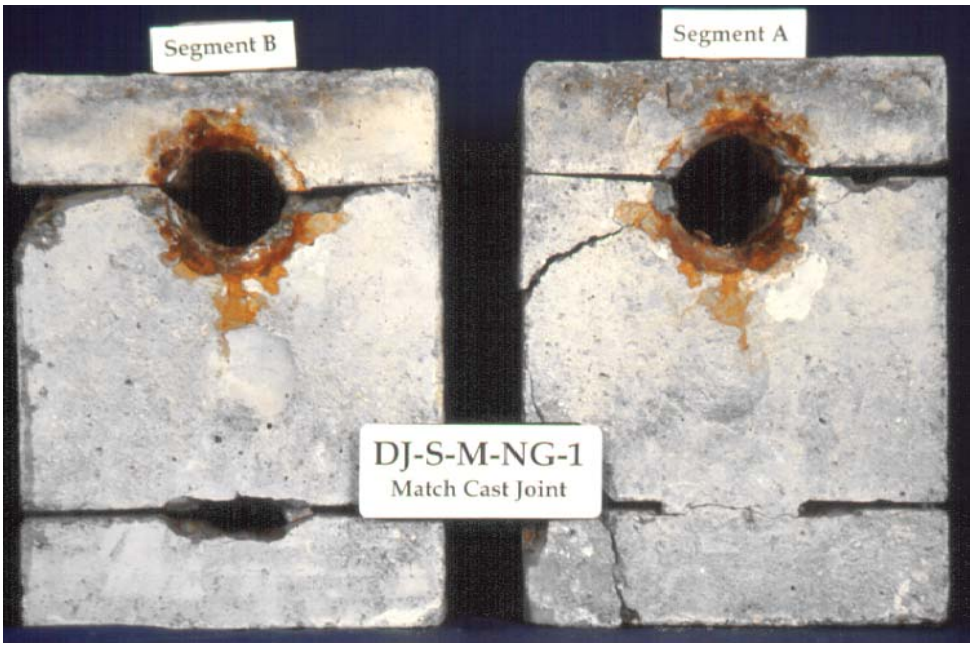

Figure 5.28 - Rust Staining Around Duct Opening in Dry Joint Face

5.7.4.3 Specimen DJ-S-H-NG-1

Corrosion Ratings:	Strand	38
	Bars	60
	Duct	64

Moderate to heavy corrosion was found on the top and bottom surfaces of the galvanized steel duct in the immediate vicinity of the joint. One small hole resulted from corrosion action. Duct corrosion produced a 70 mm (2.75 in.) long crack on the top surface of the specimen. The maximum crack width was 0.025 mm (0.001 in.).

No corrosion was found on the outer wires of the strand in the unpainted length. Large areas of the epoxy paint peeled away at both ends of the strand. Very small patches of discoloration and light corrosion were found where the paint had peeled. The center wire of the strand had light corrosion along its entire length.

Several large areas of moderate corrosion were found on the mild steel bars. The most severe corrosion was found on the underside of the bars in segment B, within the unpainted length of the bars. Several pits were found in this area. Corrosion of the bars in segment B resulted in cracking of the concrete at end B and on the bottom surface of segment B, as shown in Figure 5.29. The cracks have been highlighted in the photo for illustration purposes

A large void, 65 mm (2.56 in.) long was observed in the top surface of the grout in segment A, near the joint. The maximum depth of the void was 6 mm (0.25 in.). The hole in the duct was located over the grout void. Salt crystals were visible in the void. The void appears to have resulted from insufficient grout fluidity rather than from bleed water collection or trapped air.

Bottom Surface End B of Specimen

Figure 5.29 - Cracking Due to Rebar Corrosion

The match-cast dry joint was intact with no cracks or voids. No infiltration of grout was observed at the joint. Some rust stains were visible around the bottom of the duct opening. The entire joint face was covered with a white residue, either salt or leaching.

5.7.4.4 Specimen DJ-P-L-NG-1

Corrosion Ratings:	Strand	6
	Bars	17
	Duct	0

The plastic ducts were intact, with no signs of damage. Some salt deposits were visible on the exterior of the duct in the vicinity of the joint. The top surface of the specimen was uncracked.

No corrosion was found on the unpainted region of the prestressing strand. One very small patch of light corrosion was found in an area where the epoxy paint had peeled away. Some discoloration was found on the center wire of the strand.

Several patches of light and moderate corrosion were found on the mild steel reinforcement. One large area, approximately 38 mm (1.5 in.) long, of moderate corrosion was found on the bottom surface of one bar. This corrosion was located within the unpainted length of the bar.

Large areas of salt deposits were found on the surface of the grout at the segmental joint when the duct was removed. It is assumed that the salt reached the grout through the joint in the duct. Long, thin voids were found on the top surface of the grout. Total length of void was 142 mm (5.6 in.). The voids appear to have resulted from insufficient grout fluidity.

The concrete surface of the match-cast dry joint was intact with no voids or cracks. It is apparent that some grout leaked from the duct at the segmental joint during grouting. Approximately 30% of the joint area was covered with grout. The entire joint surface not filled with grout was covered with a white residue. No rust stains are present on the face of the joint.

5.7.4.5 Specimen DJ-P-M-NG-1

Corrosion Ratings:	Strand	9
	Bars	24
	Duct	0

The plastic ducts were intact, with no signs of damage. The top surface of the specimen was uncracked.

No corrosion was found on the unpainted region of the prestressing strand. Several small areas of discoloration were visible where the epoxy paint had peeled away.

One interval of light corrosion and two intervals of discoloration were found on the center wire of the strand.

Several patches of light and moderate corrosion were found on the top and bottom surfaces of the unpainted length of the mild steel reinforcement. One pit was found on the top of one bar bear the joint. A large area of light corrosion was found where the epoxy paint had peeled away.

Several long, thin voids were found on the top surface of the grout. Two smaller, wider voids were also found, including one were the strand was visible. The voids appear to have resulted from insufficient grout fluidity.

The concrete surface of the match-cast dry joint was intact with no cracks, but one small void at the top corner of segment A. Some grout leakage was apparent around the bottom of the duct opening. The entire joint surface was covered with a white residue. No rust stains were found on the face of the joint.

5.7.4.6 Specimen DJ-S-L-CI-1

Corrosion Ratings:	Strand	114
	Bars	4
	Duct	42

Extensive corrosion was found on the surface of the galvanized steel duct, centered on the joint. On the top surface of the duct, entire length of duct under the ponded region of the specimen was heavily corroded. On the bottom surface of the duct, severe corrosion damage was confined to the immediate vicinity of the duct. No holes were found in the duct. Duct corrosion produced a 240 mm (9.5 in.) long crack on the top surface of the specimen. The maximum crack width was 0.20 mm (0.008 in.).

A small area of light corrosion was found on the unpainted region of the prestressing strand. This area was limited to the crevice between two wires of the strand, and was approximately 13 mm (0.5 in.) long. Very large areas of epoxy paint had peeled off of the strand. Patches of light to moderate corrosion were found throughout the areas where the paint had peeled, including one interval with broad, shallow pitting. The entire length of the center wire was covered with moderate corrosion.

Two small patches of light corrosion were found on the mild steel reinforcement.

Heavy rust stains were found on the surface of the grout in the vicinity of the joint. The entire top surface of the grout in segment A was covered with salt crystals. Three

voids were visible in the grout, all located away from the joint. The voids appear to have resulted from insufficient grout fluidity.

The concrete surface of the match-cast dry joint was intact with no voids or cracks. Significant grout leakage occurred during grouting, and approximately 80% of the joint surface was covered with grout, as shown in Figure 5.30. Rust and salt stains are present on the face of the joint around the duct opening.

Figure 5.30 – Grout Infiltration Into Joint: Specimen DJ-S-L-CI-1

5.7.4.7 Specimen DJ-S-M-CI-1

Corrosion Ratings:	Strand	24
	Bars	20
	Duct	151

A large area of moderate to severe corrosion was found on the galvanized steel duct in the vicinity of the dry segmental joint. Two small holes were found on the top surface of the duct, and one small hole was found on the bottom surface. Duct corrosion produced a 57 mm (2.25 in.) long crack on the top surface of the specimen. The maximum crack width was 0.05 mm (0.002 in.).

No corrosion was found on the outer wires within the unpainted length of the strand. Large areas of epoxy paint had peeled off of the strand, and one interval of light corrosion and several areas of discoloration were found where the paint had peeled. The center wire of the strand was discolored near the ends and had five intervals of light surface corrosion.

Several small patches of light corrosion were found on the top and bottom surfaces of the mild steel reinforcement. Two areas of moderate corrosion were found on

the underside of the mild steel reinforcement. All corrosion was found in the unpainted length of the bars.

Several voids were observed in the top surface of the grout away from the joint. The void appears to have resulted from insufficient grout fluidity. Rust and salt stains were visible on the surface of the grout in the vicinity of the joint.

The match-cast dry joint was intact with no voids or cracks. A sizeable area of the joint face was covered with grout due to leakage at the joint. The remainder of the joint surface was covered with a white residue. Minor rust stains were present on the face of the joint around the duct opening.

5.7.4.8 Specimen SE-S-L-NG-2

Corrosion Ratings:	Strand	13
	Bars	6
	Duct	22

Severe corrosion was found on the galvanized steel duct in segment B. Corrosion damage was located under the ponded area of the segment and was centered approximately 25 mm (1 in.) from the joint. Light corrosion was found on the top surface of the duct in segment A. No holes were evident in the duct. Duct corrosion produced a 64 mm (2.5 in.) long crack in the top surface of segment B. The maximum crack width was 0.08 mm (0.003 in.). Some epoxy was visible on the inside of the duct at the joint. It appears that this epoxy was smeared into the duct when the duct was swabbed out after initial stressing, as is shown in Figure 5.31 for SE-S-H-NG-2. This specimen was chosen as it had the largest area of smeared epoxy inside the duct.

Several intervals of discoloration were found on the outer wires and the center wire of the strand. No corrosion was found on the prestressing strand.

One area of light and moderate corrosion was found on the underside of the mild steel bars in Segment B.

Some light rust stains and salt crystals were found on the surface of the grout at the joint. Several voids were found in the grout, apparently resulting from lack of grout fluidity.

The epoxy segmental joint was intact with no signs of moisture, salt or rust penetration. Examination of three sections through the joint showed it to be completely filled with epoxy and free from voids or cracks.

5.7.4.9 Specimen SE-S-M-NG-2

Corrosion Ratings:	Strand	2
	Bars	16
	Duct	61

Severe corrosion was found on the galvanized steel duct in segment B. Corrosion damage was located under the ponded area of the segment and was centered approximately 25 mm (1 in.) from the joint. Corrosion was severe enough to perforate the duct in segment B, allowing penetration of moisture and chlorides into the grout. Light corrosion and discoloration was found on the top surface of the duct in segment A. Duct corrosion produced a 70 mm (2.75 in.) long crack in the top surface of the specimen. The crack was primarily in segment B, and only extended 13 mm (0.5 in.) into segment A. The maximum crack width was 0.05 mm (0.002 in.).

No corrosion was found on the outer wires of the prestressing strand. Two intervals of discoloration were found on the center wire.

A large area of moderate surface corrosion was found on the underside of the mild steel bars in segment A. Corrosion was confined to the unpainted length of the bars. The bars in segment B were free of corrosion.

Rust staining was found on the surface of the grout at the location of the hole in the duct. A large void at the grout tube location at end B exposed the strand. It appears this void resulted from incomplete filling of the duct.

The epoxy segmental joint was intact with no signs of moisture, salt or rust penetration. Examination of three sections through the joint showed it to be completely filled with epoxy and free from voids or cracks.

5.7.4.10 Specimen SE-S-H-NG-2

Corrosion Ratings:	Strand	3
	Bars	0
	Duct	8

Discrete areas of light corrosion were found on the duct in both segments. Corrosion damage was located under the ponded area of the segment and was centered approximately 25 mm (1 in.) from the joint in both segments. No cracks were found on the top surface of the specimen. Some epoxy was

smeared into the galvanized duct when the duct was swabbed out after initial stressing, as shown in Figure 5.31. The area of epoxy has been cross-hatched for illustrative purposes.

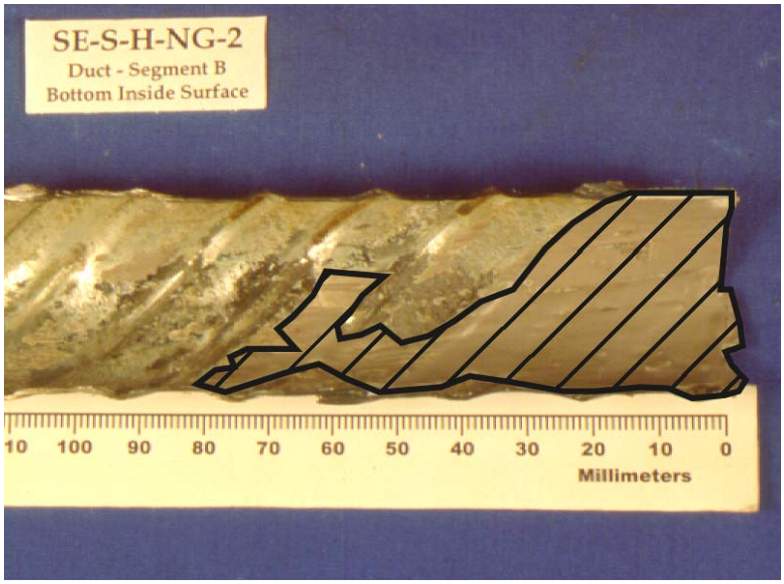

Figure 5.31 - Joint Epoxy Smeared Inside Galvanized Duct During Swabbing

No corrosion was found on the outer wires of the prestressing strand. Three intervals of discoloration were found on the center wire.

No corrosion was found on the mild steel bars.

Several long, thin voids were observed in the grout, primarily in segment A. The voids were up to 6 mm (0.25 in.) deep, and appear to have resulted from insufficient grout fluidity.

The epoxy segmental joint was intact with no signs of moisture, salt or rust penetration. Examination of three sections through the joint showed it to be completely filled with epoxy and free from voids or cracks.

5.7.4.11 Specimen SE-P-L-NG-2

The plastic ducts were intact, with no signs of damage. The top surface of the specimen was uncracked. Some epoxy was

Corrosion Ratings:	Strand	5
	Bars	0
	Duct	0

smeared into the duct when the duct was swabbed out after initial stressing, as shown in Figure 5.32. Ducts from both segments are shown in the photo.

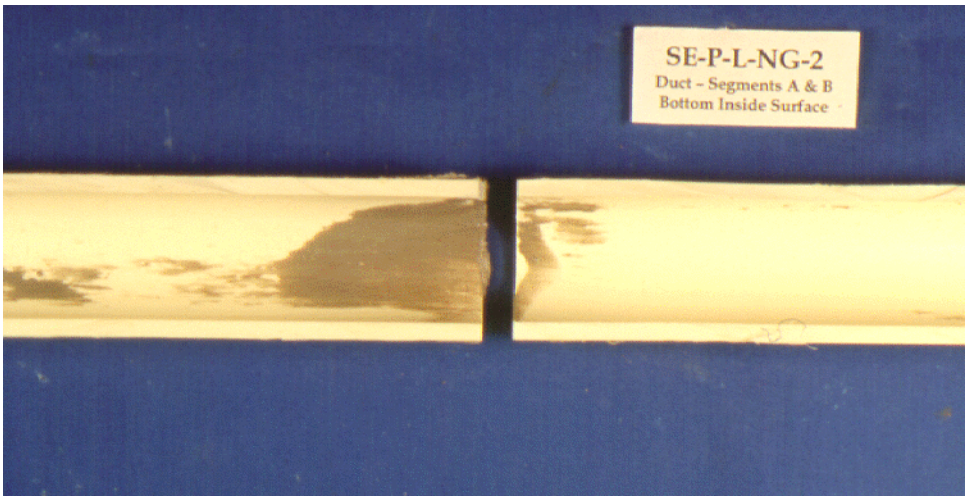

Figure 5.32 - Joint Epoxy Smeared Inside Plastic Duct During Swabbing

No corrosion was found on the outer wires of the prestressing strand. Three intervals of discoloration and one location of light corrosion were found on the center wire.

No corrosion was found on the mild steel bars.

A large void was found along the top surface of the grout. The void was 150 mm (6 in.) long and up to 15 mm (0.6 in.) wide. The maximum depth of the void was 6 mm (0.25 in.). This void appears to be an air pocket or possibly may have resulted from incomplete filling of the duct. No signs of salt were evident.

The epoxy segmental joint was intact around its perimeter, with no signs of moisture, salt or rust penetration at the strand and bar cut lines.

5.7.4.12 Specimen SE-P-M-NG-2

The plastic ducts were intact, with no signs of damage. The top surface of the specimen was uncracked.

Corrosion Ratings:	Strand	6
	Bars	0
	Duct	0

No corrosion was found on the outer wires of the prestressing strand. Six intervals of discoloration were found on the center wire.

No corrosion was found on the mild steel bars.

Several large voids were present in the grout. Voids were both longitudinal and transverse. The strand was exposed at one location. The voids appear to be caused by lack of grout fluidity. No signs of salt were evident.

The epoxy segmental joint was intact around its perimeter, with no signs of moisture, salt or rust penetration at the strand and bar cut lines.

5.7.4.13 Specimen SE-S-L-CI-2

Corrosion Ratings:	Strand	24
	Bars	0
	Duct	85

Discrete areas of corrosion were found on the duct in both segments. In segment A, light corrosion was centered approximately 35 mm (1.375 in.) from the joint. In segment B, severe corrosion was centered 42 mm (1.65 in.) from the joint. Corrosion damage produced several small holes through the duct in segment B. No cracks were found on the top surface of the specimen. Some epoxy was smeared into the duct when the duct was swabbed out after initial stressing.

Several areas of discoloration were found on the outer wires and center wire of the prestressing strand.

No corrosion was found on the mild steel bars.

Rust and salt stains were found on the surface of the grout in segment B. It appears that moisture and chlorides penetrated through the hole in the duct in this area. Several voids were observed in the grout. The voids appear to have resulted from trapped air or bleed water collection.

The epoxy segmental joint was intact around its perimeter, with no signs of moisture, salt or rust penetration at the strand and bar cut lines.

5.7.4.14 Specimen SE-S-M-CI-2

Corrosion Ratings:	Strand	2
	Bars	0
	Duct	114

Discrete areas of corrosion were found on the duct in both segments. In segment A, light corrosion and discoloration was centered approximately 38 mm (1.5 in.) from the joint. A large area of severe corrosion was centered 42 mm (1.65 in.) from the joint in segment B. Corrosion damage produced a large hole through the duct in segment B. No cracks were found on the top surface of the

specimen. Some epoxy was smeared into the duct when the duct was swabbed out after initial stressing.

Two intervals of discoloration were found on the center wire of the strand.

No corrosion was found on the mild steel bars.

Rust and salt stains were found on the surface of the grout in segment B in the vicinity of the hole in the duct in this area. One void was present in the grout of segment A, apparently resulting from insufficient grout fluidity. The prestressing strand was exposed at this location.

The epoxy segmental joint was intact around its perimeter, with no signs of moisture, salt or rust penetration at the strand and bar cut lines.

5.7.4.15 Specimen SE-S-H-CI-2

Corrosion Ratings:	Strand	3
	Bars	1
	Duct	10

Discrete areas of light corrosion were found on the duct in both segments. In both segments, corrosion was centered approximately 38 mm (1.5 in.) from the joint. No cracks were found on the top surface of the specimen. Some epoxy was smeared into the duct when the duct was swabbed out after initial stressing.

Three intervals of discoloration were found on the center wire of the strand.

No corrosion was found on the mild steel bars.

Two voids were found in the grout, one located at the joint and one at end A. Both voids appear to have resulted from insufficient grout fluidity.

The epoxy segmental joint was intact around its perimeter, with no signs of moisture, salt or rust penetration at the strand and bar cut lines.

5.7.4.16 Specimen SE-S-L-SF-2

Corrosion Ratings:	Strand	12
	Bars	0
	Duct	12

Discrete areas of corrosion were found on the duct in both segments. An area of light corrosion was centered approximately 40 mm (1.57 in.) from the joint in segment A. In segment B, moderate corrosion was centered 38 mm (1.5 in.) from the joint No cracks were found on the top surface of the specimen.

Some epoxy was smeared into the duct when the duct was swabbed out after initial stressing.

Two areas of light surface corrosion were found on the outer wires of the prestressing strand where some of the epoxy paint had peeled away. Two intervals of discoloration were found on the center wire of the strand.

No corrosion was found on the mild steel bars.

A long, thin, shallow void was found in the grout of segment B. Several small voids and many tiny air bubbles were visible in segment A grout. These voids appear to have resulted from trapped air or possibly bleed water collection.

The epoxy segmental joint was intact around its perimeter, with no signs of moisture, salt or rust penetration at the strand and bar cut lines.

5.7.4.17 Specimen EG-S-L-NG-2

Corrosion Ratings:	Strand	2
	Bars	0
	Duct	54

Discrete areas of light corrosion were found on the duct in both segments. Light corrosion damage was centered approximately 45 mm (1.75 in.) from the joint in segment A. A small hole was found in the corroded area of segment A. Light and severe corrosion was found in segment B, with the heaviest corrosion centered 45 mm (1.75 in.) from the joint. No cracks were found on the top surface of the specimen. No epoxy was visible on the interior of the duct.

No corrosion was found on the outer wires of the prestressing strand. Two intervals of discoloration were found on the center wire.

No corrosion was found on the mild steel bars.

A large, deep void in the grout was located at the segmental joint. The void appears to have resulted from insufficient grout fluidity. Rust and salt stains were present on the surface of the grout under the hole in the duct.

The epoxy segmental joint was intact with no signs of moisture, salt or rust penetration. Examination of three sections through the joint showed it to be completely filled with epoxy and free from voids or cracks. The gasket was visible at the strand cut line.

5.7.4.18 Specimen EG-S-M-NG-2

Corrosion Ratings:	Strand	23
	Bars	0
	Duct	237

A large area of severe duct corrosion was found centered on the segmental joint. Corrosion damage resulted in three holes in the duct, including one large hole in segment B at the joint. Duct corrosion produced a 100 mm (4 in.) long crack in the top surface of specimen. The maximum crack width was 0.13 mm (0.005 in.). No epoxy was visible on the interior of the duct.

Several areas of discoloration were found on the outer wires of the prestressing strand where the epoxy paint had peeled away. One location of discoloration was found on the center wire.

No corrosion was found on the mild steel bars.

Several large voids were found on the top surface of the grout. In most cases, the voids were less than 6 mm (0.25 in.) deep. One void was deep enough to expose the strand. The voids appear to have resulted from insufficient grout fluidity. Heavy rust and salt stains were present in the vicinity of the joint and the holes in the duct. The large hole in the segment B duct corresponded directly with a void in the grout.

The side and bottom perimeter of the joint were intact and appeared filled with epoxy. A thin void was visible at the joint on the top surface. Sections through the joint at the mid-height, bar cut line and strand cut line showed it to be completely filled with epoxy and free from voids or cracks. However, the gasket appears to have prevented complete bonding of the segments immediately above the duct opening. As a result, the top portion of the specimen above the strand cut line separated at the joint during autopsy. When the face of the joint was examined, incomplete epoxy coverage was revealed as shown in Figure 5.33. Salt and rust stains were visible on the joint.

Figure 5.33 - Incomplete Epoxy Coverage In Epoxy/Gasket Joint (EG-S-M-NG-2)

5.7.4.19 Specimen EG-S-H-NG-2

Corrosion Ratings:	Strand	16
	Bars	1
	Duct	78

A small area of light corrosion was centered 32 mm (1.25 in.) from the joint in segment A. The corroded area did not extend to the joint. In segment B, severe corrosion extended from the joint for a distance of 75 mm (3 in.). Corrosion damage resulted in two holes in this area. No cracks were visible on the concrete surface. No epoxy was visible on the interior of the duct.

No corrosion was found on the outer wires of the prestressing strand. The entire length of the center wire was covered with light surface corrosion.

One small area of discoloration was found on the mild steel bars.

Two large voids were found on the top surface of the grout, one located at the joint and one located under the grout tube in segment A. The voids appear to be caused by trapped air or collection of bleed water. One of the holes in the duct corresponded with the grout void at the joint. Rust and salt stains were present in the vicinity of the joint and the holes in the duct.

Similar to specimen EG-S-M-NG-2, the side and bottom perimeter of the joint were intact and appeared filled with epoxy, but a thin void was visible at the joint on the top surface of the specimen. Sections through the joint at the mid-height and bar and strand cut lines showed it to be completely filled with epoxy and free from voids or cracks. However, the gasket again appears to have prevented complete bonding of the segments immediately above the duct opening. As a result, the top portion of the specimen above

the strand cut line separated at the joint during autopsy. Salt penetration and rust stains were visible on the joint.

5.7.4.20 Corrosion Ratings

The strand, bar and duct corrosion ratings for all specimens are plotted in Figure 5.34 through Figure 5.36 and listed in Table 5.11. Average, standard deviation and median values are listed at the bottom of the table.

In order to put the corrosion ratings in perspective, a "Threshold of Concern" was assigned at a corrosion rating of 50 for the strands, bars and ducts. This threshold is used to indicate corrosion related deterioration deemed severe enough to warrant concern. The threshold of concern is useful to illustrate that in most cases the observed corrosion was negligible from a practical standpoint. In general, corrosion ratings greater than 50 corresponded to pitting corrosion for strands and bars, and holes in the galvanized steel duct caused by corrosion.

Table 5.11 - Corrosion Ratings for all Specimens

Specimen Name	Corrosion Rating		
	Strand	Bars	Duct
DJ-S-L-NG-1	26	12	528
DJ-S-M-NG-1	43	12	325
DJ-S-H-NG-1	38	60	64
DJ-P-L-NG-1	6	17	0
DJ-P-M-NG-1	9	24	0
DJ-S-L-CI-1	114	4	42
DJ-S-M-CI-1	24	20	151
SE-S-L-NG-2	13	6	22
SE-S-M-NG-2	2	16	61
SE-S-H-NG-2	3	0	8
SE-P-L-NG-2	5	0	0
SE-P-M-NG-2	6	0	0
SE-S-L-CI-2	24	0	85
SE-S-M-CI-2	2	0	114
SE-S-H-CI-2	3	1	10
SE-S-L-SF-2	12	0	12
EG-S-L-NG-2	2	0	54
EG-S-M-NG-2	23	0	237
EG-S-H-NG-2	16	1	78
Average	19.5	9.1	94.3
Std. Dev.	25.3	14.3	132.6
Median	12	1	54

Specimen DJ-S-L-CI-1 had the most severe strand corrosion, with an corrosion rating of 114 compared to the average of 19.5 and median of 12. This was the only specimen with a strand corrosion rating greater than 50. Specimen DJ-S-H-NG-1 had the most severe mild steel reinforcement corrosion with a rating of 60 compared to the average of 9.1 and median of 1. This was the only specimen with a bar corrosion rating greater than 50. Specimen DJ-S-L-NG-1 had the worst duct corrosion with a rating of 528 compared to the average of 122.9 and median of 79. In each case, the specimen with the largest corrosion rating was several times higher than the average and median values. The average rating is larger than the median rating for all three ratings. The difference is largest for the mild steel bars, where the average is almost an order of magnitude larger than the median. This trend illustrates that the worst performance generally occurred in a limited number of specimens.

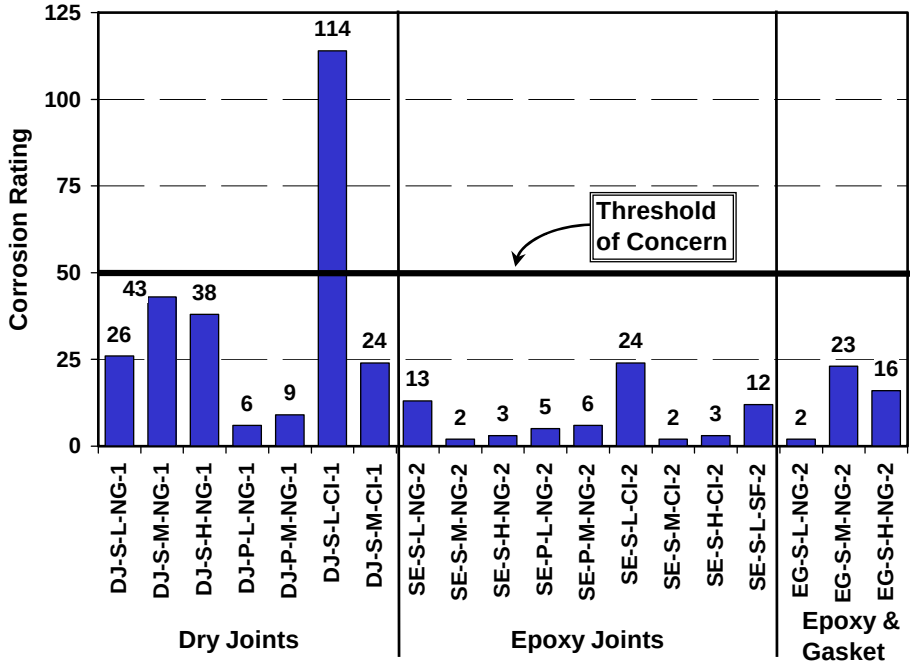

Figure 5.34 - Strand Corrosion Ratings for All Specimens

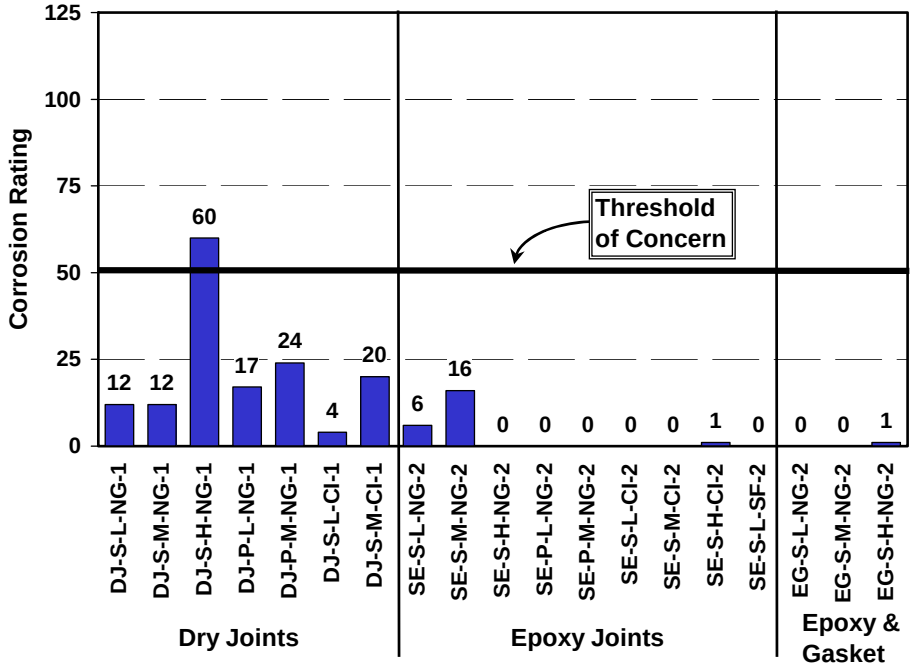

Figure 5.35 - Mild Steel Bar Corrosion Ratings for all Specimens

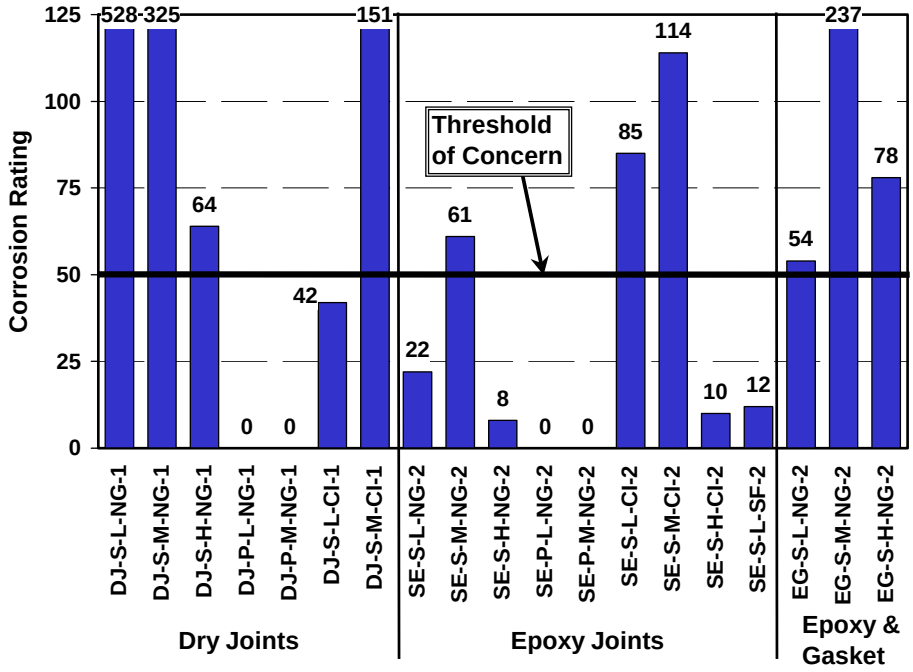

Figure 5.36 - Duct Corrosion Ratings for all Specimens

5.7.4.21 Chloride Analysis

Concrete powder samples were collected from six dry joint specimens and four epoxy joint specimens for chloride analysis (procedure described in Section 5.7.1.2). In addition, samples were collected from the grout in these specimens for chloride analysis. Concrete chloride ion profiles for these ten specimens are included in Appendix E.

The chloride ion profiles in the concrete revealed distinct trends in chloride ion penetration in dry joint and epoxy joint specimens. In general, the dry joint specimens showed significantly higher chloride contents adjacent to the joint in comparison to measurements away from the joint. In the epoxy joint specimens, the chloride profiles were essentially the same near and away from the joint. Typical profiles are show in Figure 5.37 and Figure 5.38 for specimens DJ-S-L-NG-1 and SE-S-L-NG-2. Values plotted in the figures are acid soluble chloride levels, expressed as a percentage of concrete weight. The chloride threshold for corrosion is indicated in the figures at 0.033%. This value is intended as a guideline only, and is based on the widely accepted chloride threshold value of 0.2% of the weight of cement.[5.16] In the dry joint specimens, the

chloride contents were well above the corrosion threshold over the depth of the specimen. In some cases, chloride contents at 51 mm from the joint were higher in the dry joint specimens in comparison to those with epoxy joints. Samples collected at location C, 108 mm from the joint, showed negligible chloride levels in both dry and epoxy joint specimens.

The chloride profile near the joint for specimen DJ-S-L-CI-1 was very low in comparison to the other dry joint specimens tested, as shown in Figure 5.39. During the autopsy process, it was discovered that a significant grout leak had occurred at the joint in this specimen. Approximately 80% of the dry joint face was covered with grout, and in essence this joint became a thin mortar joint. The presence of grout in the joint could explain the lower chloride penetration at the joint in comparison to the other dry joint specimens.

The chloride profile for specimen SE-S-M-NG-2 displays a discontinuity in the measurements adjacent to the joint, as shown in Figure 5.40. Chloride measurements near and away from the joint decrease to zero by mid-height of the specimen. However, chloride levels increase dramatically at the level of the mild steel bars near the joint. This discontinuity could be dismissed as an error in sampling or testing, however in this case corrosion was found on the mild steel at this location, suggesting the results are valid. Three possible explanations may account for this:

1. The chloride measurements at mid height and the level of the strand are in error. This is unlikely, since chloride profiles measured for other epoxy joint specimens do not indicate increased penetration of chlorides at the joint, and all show chloride levels decreasing rapidly to zero over the height of the specimen.
2. The concrete or mild steel bars were contaminated with chlorides prior to or during construction. This is unlikely since construction was performed under carefully controlled conditions.
3. Saltwater leakage from the ponded area ran down the exterior of the specimen to the bottom where it entered the concrete. The top surface and sides of the specimen are sealed with epoxy according to ASTM G109[5.5] requirements, while the bottom is not. This mechanism is common in bridges, and the epoxy sealant on the top and sides would amplify the effect leading to increased chloride levels

near the bottom surface. This is the most likely explanation for the increased chloride levels and mild steel corrosion.

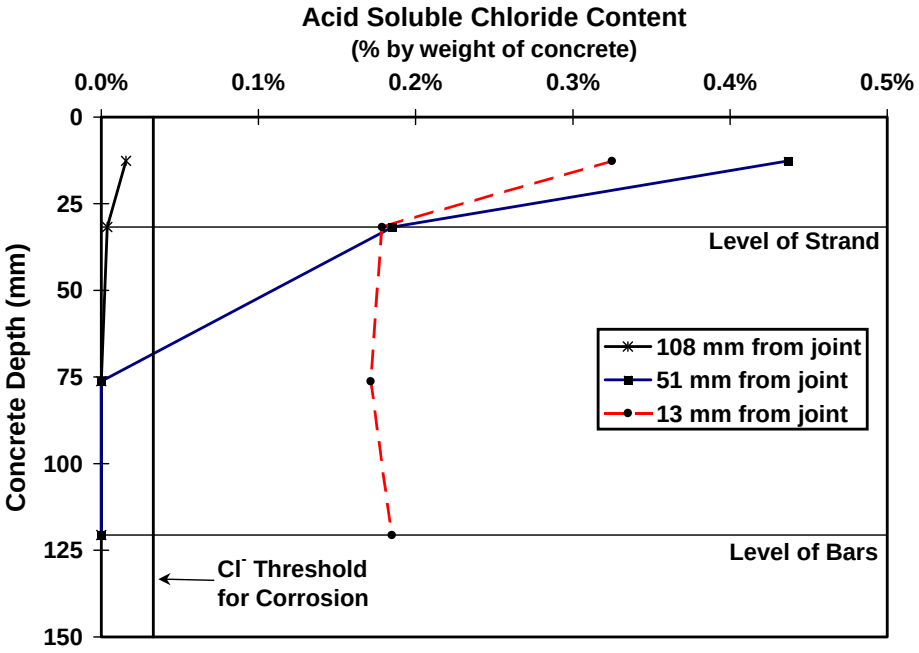

Figure 5.37 - Concrete Chloride Ion Profiles for Specimen DJ-S-L-NG-1

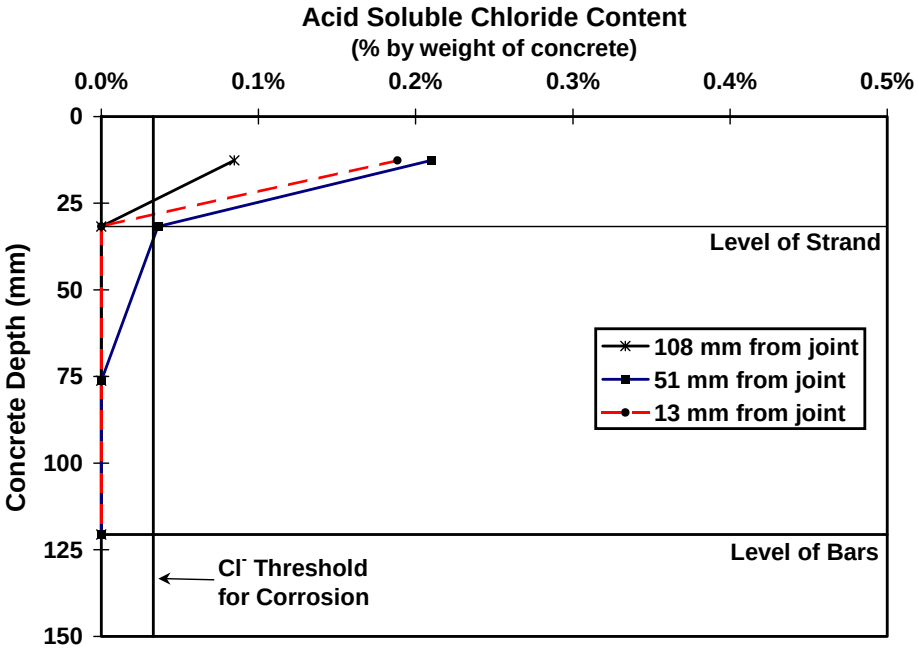

Figure 5.38 – Concrete Chloride Ion Profiles for Specimen SE-S-L-NG-2

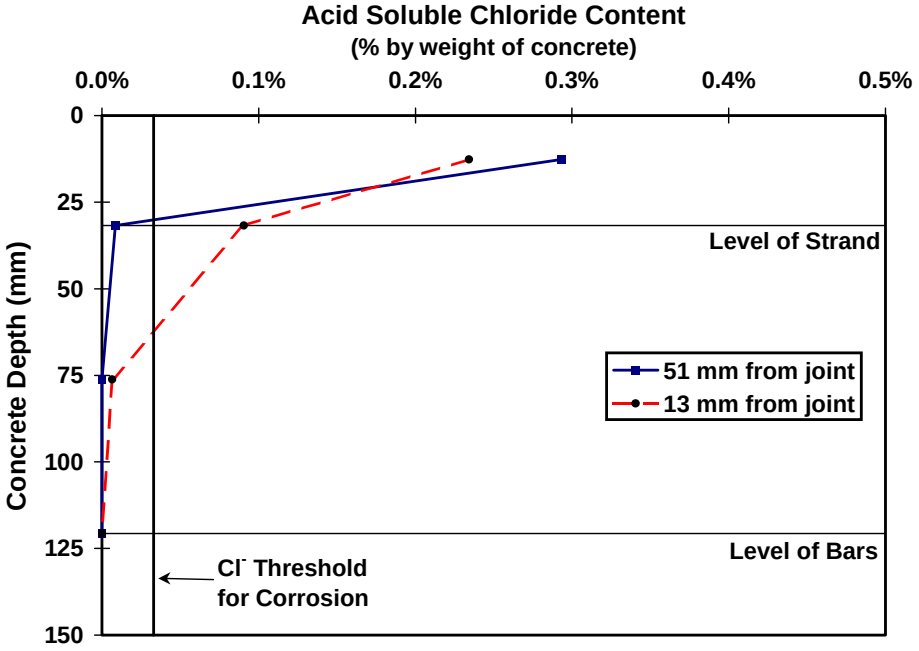

Figure 5.39 - Concrete Chloride Ion Profiles for Specimen DJ-S-L-CI-1

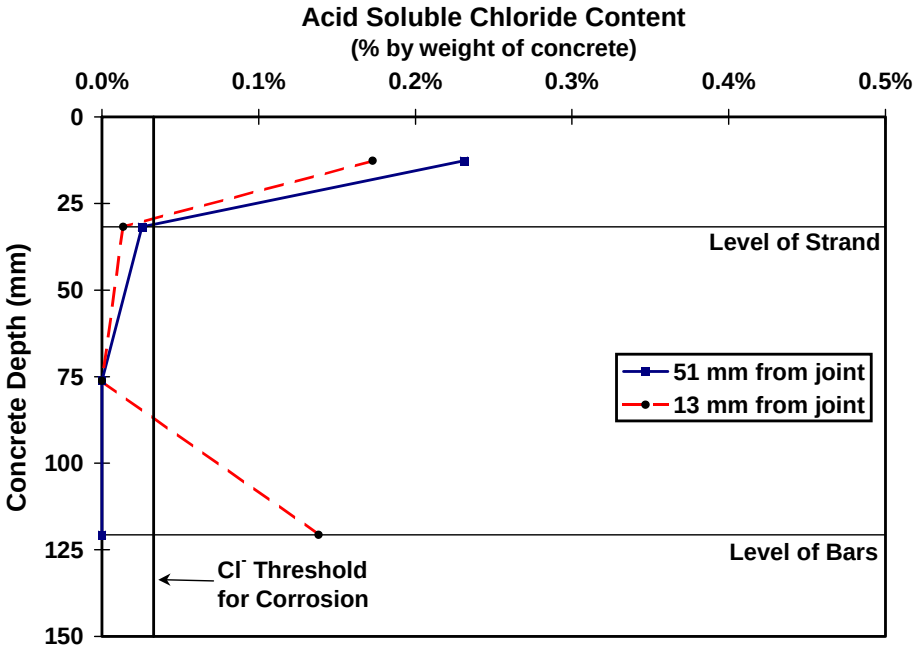

Figure 5.40 - Concrete Chloride Ion Profiles for Specimen SE-S-M-NG-2

The results of the chloride analysis on grout samples are shown in Figure 5.41. The values are plotted as acid soluble chlorides, as a percentage of the grout weight. The chloride threshold for corrosion in grout is taken as approximately 0.14%, assuming a chloride threshold 0.2% of by weight of cement and a water-cement ratio of 0.44. The dry joint specimens show very high chloride contents, particularly in the vicinity of the joint. The two dry joint specimens with steel ducts and low precompression (DJ-S-L-NG-1 and DJ-S-L-CI-1) also show large chloride contents inside the duct, 50 mm (2 in.) from the joint. The dry joint specimen with a plastic duct, DJ-P-L-NG-1, showed a high chloride content at the joint, but only negligible chlorides 50 mm inside the duct. The four epoxy joint specimens analyzed show very low or unmeasurable chlorides at the joint. At a distance of 50 mm inside the duct, all samples showed unmeasurable chloride levels for the epoxy joint specimens.

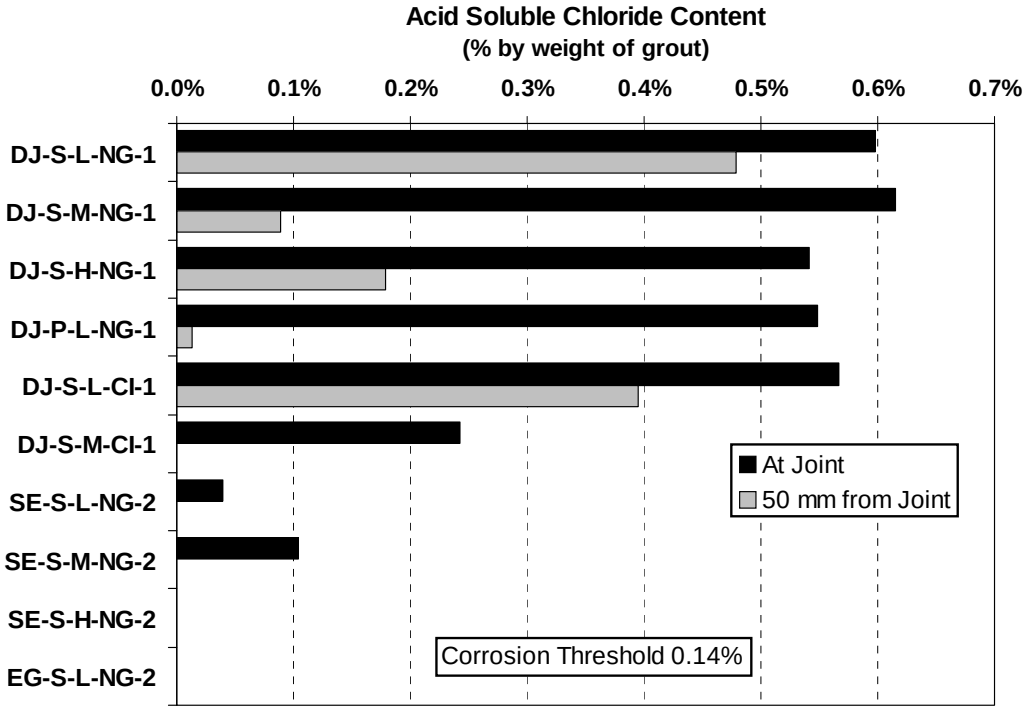

Figure 5.41 - Measured Chloride Contents in Post-tensioning Grout

5.8 Discussion of Results

The effect of many of the variables investigated in this testing program can be demonstrated based on nearly four and a half years of severe exposure test data and the thorough forensic examination of each specimen type. The discussion of results in the following sections describes the effect of the test variables.

5.8.1 Overall Performance

The performance of the macrocell corrosion specimens in this testing program is very good. After four years and five months of testing, only twelve of thirty-eight specimens displayed corrosion activity. Computed values of weighted average corrosion current are well below the failure value proposed by ASTM G109. Forensic examination of each specimen type revealed that corrosion damage to prestressing strand and mild steel reinforcement was not severe. Only one prestressing strand was found to have pitting corrosion, and no mild steel bars were found to have measurable area reduction. Similar

testing programs using macrocell corrosion specimens normally report severe corrosion damage and specimen failure in less than four and a half years. Part of a corrosion study on epoxy-coated reinforcement at The University of Texas at Austin[5.17] used modified macrocell corrosion specimens. Severe corrosion damage indicated by concrete cracking and rust staining was observed in less than three years of testing. Testing was concluded after four and a half years of exposure due to severe deterioration in some specimens.

The main objective for this testing program was to examine corrosion protection for internal prestressing tendons in precast segmental bridges. The relative performance of the specimens in this testing program can be seen by looking at the corrosion ratings for the prestressing strand, ordered from lowest to highest. This data is plotted in Figure 5.42. At the top half of the list are standard epoxy joints and dry joints with plastic ducts. At the bottom of the list are dry joints, two of the three epoxy/gasket joints and one of the epoxy joints with corrosion inhibitor in the grout.

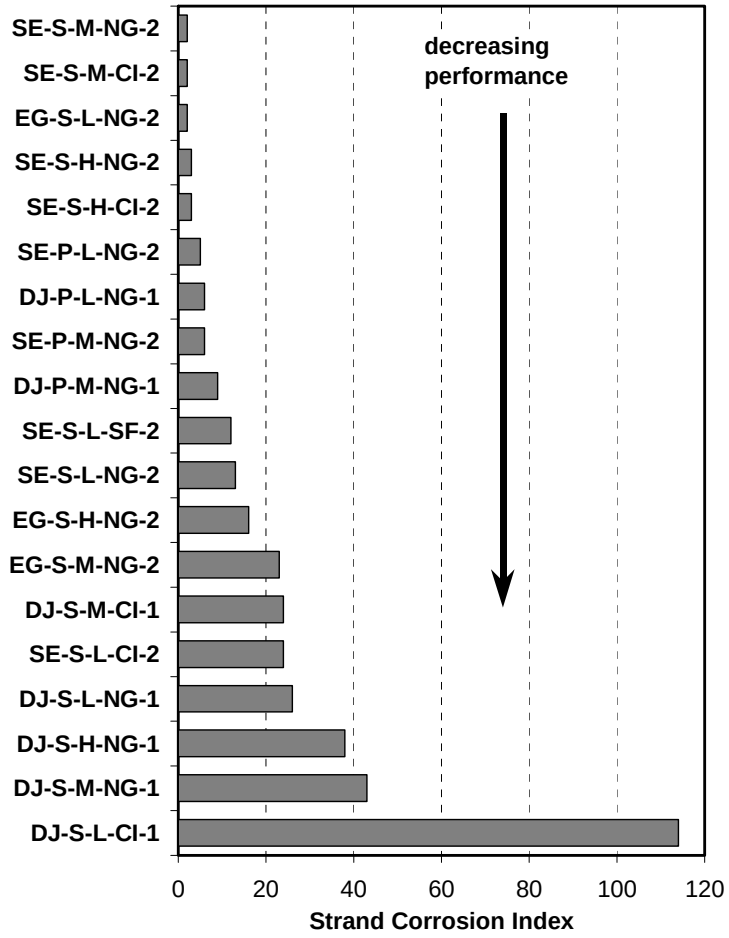

Figure 5.42 - Corrosion Ratings for Prestressing Strand Ordered According to Performance

The overall performance of the specimens in this testing program can also be compared by considering the total corrosion rating, obtained by summing the ratings for strand, bars and duct. This data is plotted in Figure 5.43. Similar to Figure 5.42, the best performance occurred with standard epoxy joints. Plastic ducts performed well with both dry and epoxy joints. The worst performance occurred for dry joints with steel ducts. The ordering in Figure 5.43 is strongly influenced by the duct corrosion rating.

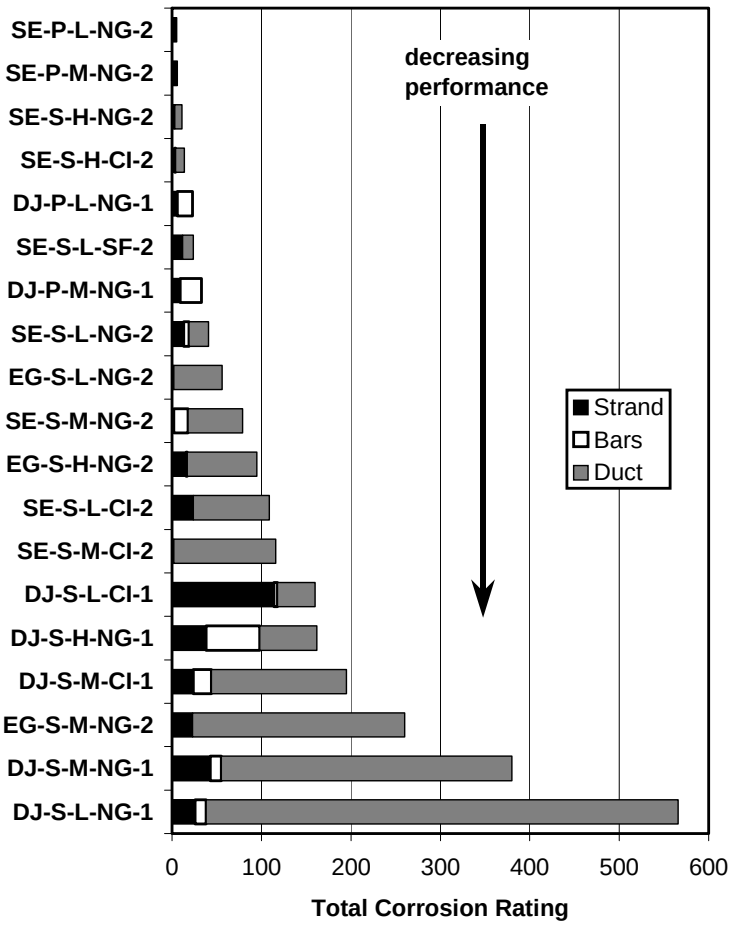

Figure 5.43 - Total Corrosion Rating Ordered According to Performance

5.8.2 Effect of Joint Type

Of the four variable groups investigated, joint type appears to have the most significant effect on the performance of the specimens. In general, dry joints performed very poorly, with corrosion currents for seventy-eight percent of the specimens indicating corrosion activity. One out of the eighteen specimens with a standard epoxy joint showed corrosion activity. This specimen was the most recent to display an onset of corrosion, and measured corrosion currents were very small and indicated a reversed macrocell. Autopsy of this specimen confirmed the mild steel reinforcement was corroding rather than the prestressing strand. None of the six epoxy/gasket joint specimens displayed corrosion currents indicating an onset of corrosion. However, autopsies revealed

increased corrosion of the galvanized steel duct in two epoxy/gasket specimens. The effect of joint type on the measured and observed results is described below.

Galvanized Steel Duct Corrosion

The extent and severity of duct corrosion was significantly affected by the joint type. The photos in Figure 5.44 show typical corrosion of the galvanized steel duct in each of the three joint types. Two epoxy/gasket joint specimens are shown to illustrate the two levels of performance observed for this joint type. The specimens have been cut open at the level of the duct, and the photo shows the top surface of the specimen and a top view of the duct still embedded in the concrete. In three of the four specimens shown, the top surface of the concrete had a longitudinal crack due to corrosion (the crack has been highlighted in the photo). The black arrow indicates the location of the segmental joint.

In general, the duct corroded area and corrosion severity were less for epoxy joints and corrosion induced cracking on the concrete surface was more severe for dry joints. Duct corrosion was centered on the segmental joint in all of the dry joint specimens. Corrosion was not centered on the joint in the standard epoxy joint, suggesting corrosion was caused by moisture and chloride migration through the concrete with no discernible influence from the joint. Two of the three epoxy/gasket joint specimens autopsied indicated that the gasket interfered with epoxy coverage in the vicinity of the duct. When the joint was sound, the duct corrosion in the epoxy/gasket joint was less severe than the dry joints and was not centered on the joint, similar to the standard epoxy joint. However, when epoxy coverage was not complete the corrosion was severe and led to concrete cracking. Duct corrosion was centered on the joint, suggesting that moisture and chlorides penetrated at the joint. These results indicate that the standard epoxy joint consistently provides the best corrosion protection and is less likely influenced by quality control in the construction process. The results also indicate that the complications introduced in the process by adding gaskets are counter productive since corrosion resistance was reduced when compared to the epoxy joint without a gasket.

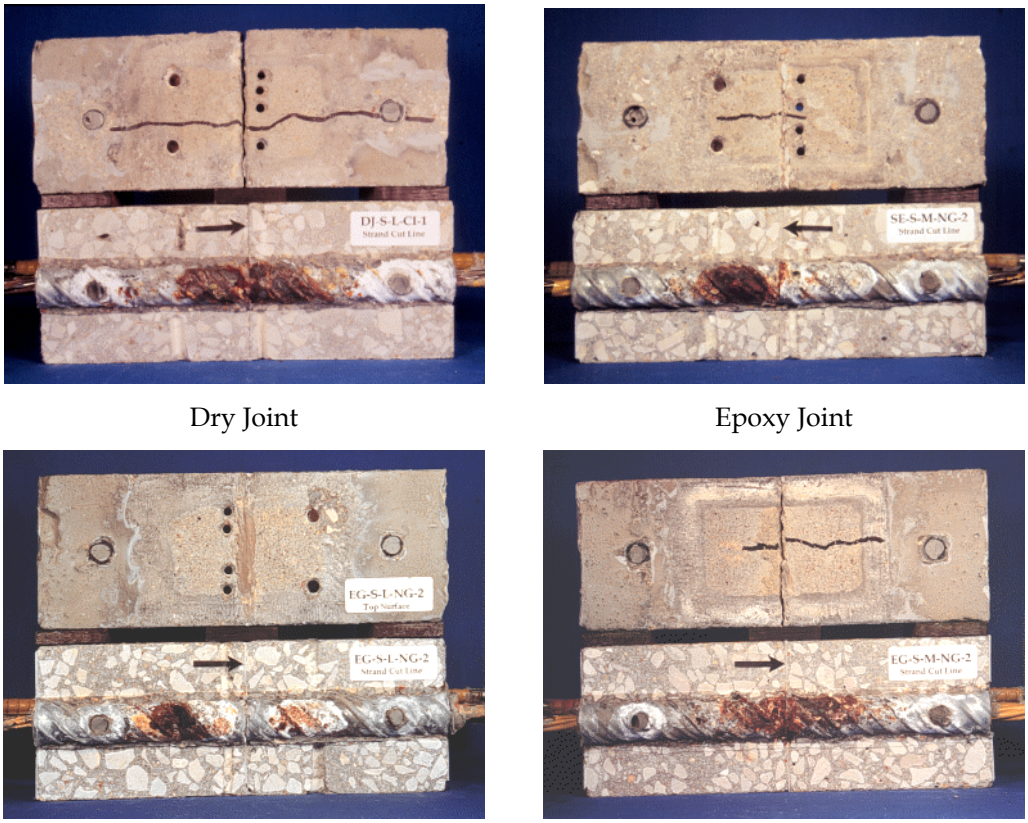

Dry Joint | Epoxy Joint

Sound Epoxy/Gasket Joint | Poor Epoxy/Gasket Joint

Figure 5.44 – Galvanized Steel Duct Corrosion: Effect of Joint Type

Prestressing Strand Corrosion

Macrocell corrosion current data measured during exposure testing indicated that corrosion of the prestressing strand was only occurring in four dry joint specimens. The prestressing strand corrosion found during the forensic examination would be considered very mild or negligible for all specimens with the exception of specimen DJ-S-L-CI-1 (dry joint, steel duct, low precompression, corrosion inhibitor grout). In general, the strand corrosion found in the dry joint specimens was worse than in the epoxy joint specimens (see Figure 5.42). Light to moderate surface corrosion was found on the strand in all of the dry joint specimens where galvanized steel ducts were used. In the standard epoxy and epoxy/gasket joints, corrosion ratings for most specimens were very low (less than 10). Corrosion ratings higher than ten resulted primarily from discoloration on the strand.

Patches of light strand corrosion were found in only three of the twelve epoxy joint specimens, and no moderate or pitting corrosion was found.

Mild Steel Reinforcement Corrosion

Corrosion current data indicated that corrosion of mild steel reinforcement was occurring in seven dry joint specimens and one standard epoxy joint specimen. Forensic examination revealed reinforcing bar corrosion in all of the dry joint specimens, one small area of discoloration in two epoxy joint specimens and light corrosion in two epoxy joint specimens. Two thirds of the epoxy joint specimens had no discoloration or corrosion of the mild steel bars. The highest mild steel corrosion rating for epoxy joint specimens occurred in Specimen SE-S-M-NG-2. This was the only epoxy joint specimen where corrosion currents indicated activity during exposure testing. The measured chloride profile for this specimen (see Section 5.7.4.21 and Figure 5.40) suggests that elevated chloride levels at the bottom of the specimen resulted from an external source of moisture and chlorides rather than from penetration at the epoxy joint or through the concrete.

Chloride Penetration

Chloride penetration was higher for dry joint specimens in all cases. Measured chloride ion profiles indicated chloride contents in excess of the corrosion threshold in the vicinity of the dry joints. Chloride profiles adjacent to the joint and away from the joint were similar in the epoxy joint specimens, suggesting no influence from the joint. Crystalline salt deposits were observed on the interior of the ducts in the dry joint specimens, clearly indicating moisture and chlorides had penetrated through the joint. Chloride analysis performed on samples from the grout showed very high chloride contents for dry joint specimens, even at distances of 50 mm (2 in.) from the joint. Grout chloride contents in epoxy joint specimens were very low or negligible. While dry joints are not permitted with internal tendons, this penetration of chlorides through the dry joint faces could result in accelerated corrosion of the mild steel reinforcement near the joint face when used with external tendons.

Grouting

Grout leaked into the joint region in five of the seven dry joint specimens. The extent of the leak ranged from very minor around the duct opening to almost 80% of the

joint face covered with grout. No grout leakage was found in the standard epoxy joint and epoxy/gasket joint specimens.

5.8.3 Effect of Duct Type

Duct Corrosion

Galvanized steel ducts were corroded in all cases. Duct corrosion led to concrete cracking on the top surface of the specimen in eight of the fifteen specimens with galvanized steel ducts. No cracks were found in specimens with plastic ducts. Galvanized steel ducts were perforated by corrosion action in nine of fifteen specimens, allowing direct ingress of moisture and chlorides. Plastic ducts were not affected by exposure testing, and remained intact as a barrier in the corrosion protection system.

The concrete cover in these specimens was lower than would be allowed by specification, and this contributed to the severe galvanized duct corrosion in a short period of time. However, the test results indicate the potential corrosion problems when using galvanized ducts in aggressive exposures. The relative performance of the galvanized and plastic ducts is not affected by the low cover, and plastic ducts performed extremely well in spite of the small cover.

Prestressing Strand Corrosion

Little or no strand corrosion was found dry joint and epoxy joint specimens with plastic ducts. Strand corrosion ratings for the four plastic duct specimens autopsied were all less than 10, with only discoloration found on the strand in most cases. Light to moderate surface corrosion and some pitting was found on the strands in galvanized steel duct specimens with dry joints.

Reversed Macrocell

Macrocell corrosion current data for the four dry joint specimens with plastic ducts indicated that the mild steel bars were corroding instead of the prestressing strand. Forensic examinations performed on two of the plastic duct specimens confirmed that the mild steel reinforcement was the primary corrosion site. This data suggests that the plastic ducts provided improved corrosion protection for the prestressing strand in the dry joint specimens. As a result, the mild steel reinforcement became the preferential site for corrosion.

5.8.4 Effect of Joint Precompression

Reinforcement Corrosion

The three levels of joint precompression show no clear, consistent trends in strand corrosion or mild steel reinforcement corrosion.

Duct Corrosion

Corrosion of the galvanized steel duct appears to be somewhat influenced by the level of joint precompression, particularly for dry joints. The extent and severity of duct corrosion was quantified previously using the duct corrosion ratings described in Section 0. The severity of duct corrosion can also be quantified by considering the length and width of cracking in the concrete (concrete and clear cover is comparable in all specimens). As described in Section 5.7.4, many specimens with galvanized steel ducts experienced cracking on the top surface of the specimen as a result of duct corrosion. A crack rating can be obtained for each specimen by multiplying the crack length by the maximum crack width.

The duct corrosion ratings and crack ratings for the autopsied specimens with steel ducts are plotted in Figure 5.45. The effect of joint precompression on duct corrosion can be seen by comparing similar specimens where the joint precompression is the only variable. For example, consider DJ-S-L-NG-1, DJ-S-M-NG-1 and DJ-S-H-NG-1. The corrosion and crack ratings for these specimens decrease as the joint prestress increases, suggesting improved corrosion protection. A similar trend is present for the pair of specimens with a dry joint and corrosion inhibitor grout (DJ-S-L-CI-1 and DJ-S-M-CI-1). Duct corrosion in the standard epoxy joint specimens was not influenced by the presence of the joint (see Section 5.8.2), and thus the joint precompression does not appear to affect duct corrosion. Two of the epoxy/gasket joint specimens, EG-S-M-NG-2 and EG-S-H-NG-2, had partially defective joints resulting in chloride ingress at the joint. The duct corrosion and crack ratings for these two specimens again shows reduced corrosion damage for the specimen with higher joint prestress. The most significant effect would be expected to occur for dry joint specimens, as demonstrated in Figure 5.45.

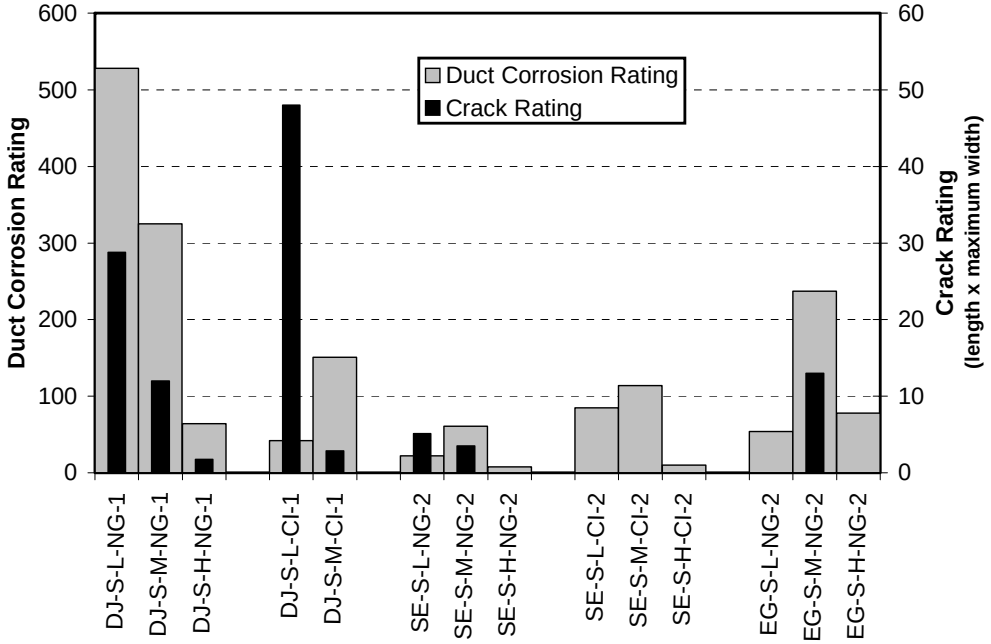

Figure 5.45 - Effect of Joint Precompression on Duct Corrosion

5.8.5 Effect of Grout Type

Measured macrocell corrosion currents indicated that the prestressing strand was corroding in four specimens; DJ-S-L-NG-1, DJ-S-M-NG-1, DJ-S-M-NG-2 and DJ-S-L-CI-1. Metal loss calculations (based on corrosion current measurements) indicated that specimens DJ-S-M-NG-1 and DJ-S-L-CI-1 had experienced the most significant corrosion damage. Three of these four specimens were autopsied (DJ-S-M-NG-2 continues exposure testing). Corrosion ratings for the three autopsied specimens are listed in Table 5.12. The most severe corrosion, including the only pitting corrosion, was found in the specimen with corrosion inhibitor grout.

Table 5.12 - Effect of Grout Type - Strand Corrosion Ratings

Specimen	Strand Corrosion Rating	Comments
DJ-S-L-NG-1	26	Light to moderate corrosion
DJ-S-M-NG-1	43	Light to moderate corrosion
DJ-S-L-CI-1	114	Light to moderate corrosion with pitting on three wires

Based on this limited data, there does not appear to be any improvement in corrosion protection when calcium nitrite corrosion inhibitor is used in cement grout, and its use may in fact be detrimental.

The dosage of corrosion inhibitor used in this testing program was the same dosage normally used for concrete (~20 liters/m^3 concrete). The effectiveness of calcium nitrite corrosion inhibitor relies on the ratio of calcium nitrite solids to cement solids. Due to the higher cement content of grout in comparison to concrete, the dosage used in this testing program may be too low for the corrosion inhibitor to be effective. In spite of this, it is very concerning that calcium nitrite appears to have worsened corrosion in comparison to plain grout.

Other research has found calcium nitrite corrosion inhibitor to be detrimental to corrosion protection when used in cement grouts. Koester[5.18] performed anodic polarization tests on grouted prestressing strand to investigate the corrosion protection provided by various cement grouts. These tests found that calcium nitrite significantly reduced the time to corrosion in comparison to plain grout, and had no effect on corrosion rate after the initiation of corrosion. The calcium nitrite dosage was adjusted to account for the higher cement content in grout for those tests. Calcium nitrite has shown good results when used in concrete.[5.10,5.19,5.20] However, further investigation is warranted before calcium nitrite corrosion inhibitor should be used in cement grout.

The grout containing 13% silica fume was used only in specimens with a standard epoxy joint. Macrocell corrosion currents did not indicate an initiation of corrosion in these specimens. Forensic examination of specimen SE-S-L-SF-2 found small areas of light corrosion on the prestressing strand and a total corrosion rating of 12. This data does not indicate a positive or negative effect of using silica fume in cement grout at this time.

5.8.6 Grout Voids

Voids were found in the grout of all nineteen specimens autopsied. In fourteen of the specimens, the shape and appearance of the voids suggests that they resulted from insufficient fluidity. In four specimens, voids appear to have resulted from air pockets or possibly bleed water collection. In the remaining specimen, the void may be attributed to incomplete filling of the duct during grouting. In some cases, voids were small and/or

shallow. However, in several cases, voids were extensive and deep and the prestressing strand was exposed. Typical voids are shown in Figure 5.46.

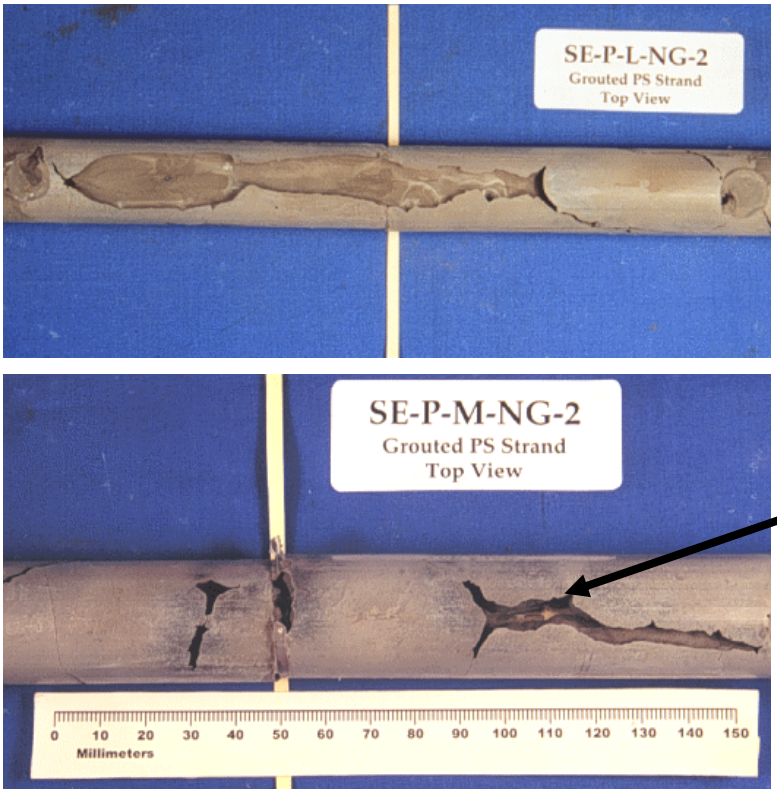

Figure 5.46 – Typical Grout Voids

Normally, if the void does not expose the prestressing tendon it is not deemed a concern. However, during the forensic examination it was discovered that five specimens had holes corroded through the galvanized steel duct at the location of a void. In two of these specimens, large holes in the duct corresponded directly to the voids in shape and size. An example of this is shown in Figure 5.47 for specimen DJ-S-M-NG-1. These findings suggest that the presence of a void in the grout may lead to more severe corrosion of the galvanized steel duct. The duct is intended to provide corrosion protection for the tendon, and any holes in the duct resulting from corrosion action effectively eliminate the duct as a protection barrier for the tendon.

Figure 5.47 - Hole in Duct Corresponding to Grout Void

5.8.7 Reversed Corrosion Macrocell

The macrocell corrosion current data indicates that eight of the twelve specimens displaying an initiation of corrosion have developed reversed corrosion macrocells where the mild steel reinforcing bars are corroding (anodic reaction) instead of the prestressing strand. The direction of corrosion current in the macrocell specimens is indicated by the polarity of the measured voltages (see Section 5.5.1).

The development of a reversed macrocell in typical macrocell specimens is unlikely and is not addressed by ASTM G109.[5.5] The development of the reversed corrosion macrocell in this testing program may be attributed to the transverse segmental joint. The use of a dry joint is particularly severe, as indicated by the experimental data. A

possible mechanism is shown in Figure 5.48. The dry joint allows easy penetration of chlorides to the bottom layer of steel. The small end cover for the bottom bars (6 mm (0.25 in.)) provides little protection from lateral migration of the chlorides and the steel becomes quickly depassivated while the prestressing steel benefits from the additional protection provided by the grout and duct. It is assumed that the added protection is primarily due to the extra thickness of the grout over the strand in comparison to the end cover for the bars. Although the duct is discontinuous at the joint, it may also contribute to corrosion protection. These conditions are conducive to the formation of a reversed corrosion macrocell.

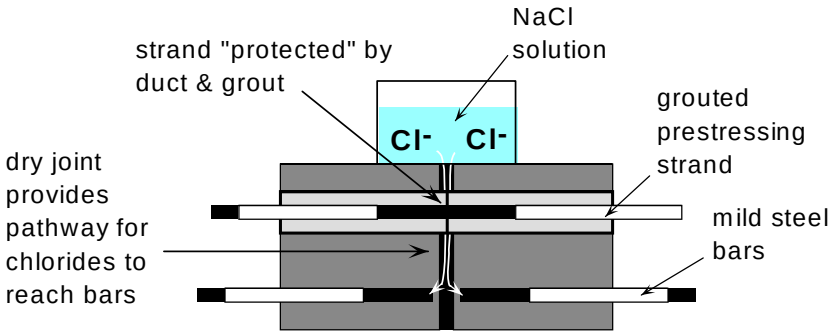

Figure 5.48 - Mechanism for Development of Reversed Macrocell in Dry Joint Specimens

The occurrence of a reversed macrocell was confirmed by forensic examination. Of the nineteen specimens autopsied, exposure test data indicated a reversed macrocell in five specimens (DJ-S-H-NG-1, DJ-P-L-NG-1, DJ-P-M-NG-1, DJ-S-M-CI-1 and SE-S-M-NG-2). Corrosion of the mild steel reinforcement was found in each of these five specimens. Chloride profiles (where available) indicated chloride levels in excess of the corrosion threshold in each case.

5.8.8 Test Measurements

Comparison Between Half-Cell Potentials and Macrocell Corrosion Current

In Section 5.6.3.1, the time to corrosion initiation was evaluated using both macrocell corrosion currents and half-cell potentials. Both forms of measurement were

equally appropriate for estimating the point at which corrosion began, provided that both the magnitude and variation of half-cell potentials were considered.

The overall trends in specimen behavior were also illustrated equally well by macrocell corrosion currents and half-cell potentials. As a typical example, the half-cell potentials and corrosion currents for specimen DJ-S-L-CI-1 (dry joint, steel duct, low precompression and corrosion inhibitor grout) are plotted together in Figure 5.49. The ASTM guidelines for half-cell potentials are included in the figure. The more negative half-cell potentials correspond directly with increasing corrosion current. The reduced corrosion current near 1100 days is also paralleled by a change (more positive) in half-cell potentials. At 1200 days, the corrosion current has reduced to near zero and the half-cell potentials dropped out of the 90% probability of corrosion range. Beyond 1200 days, corrosion current gradually increases, and half-cell potentials again move into the range for 90% probability of corrosion.

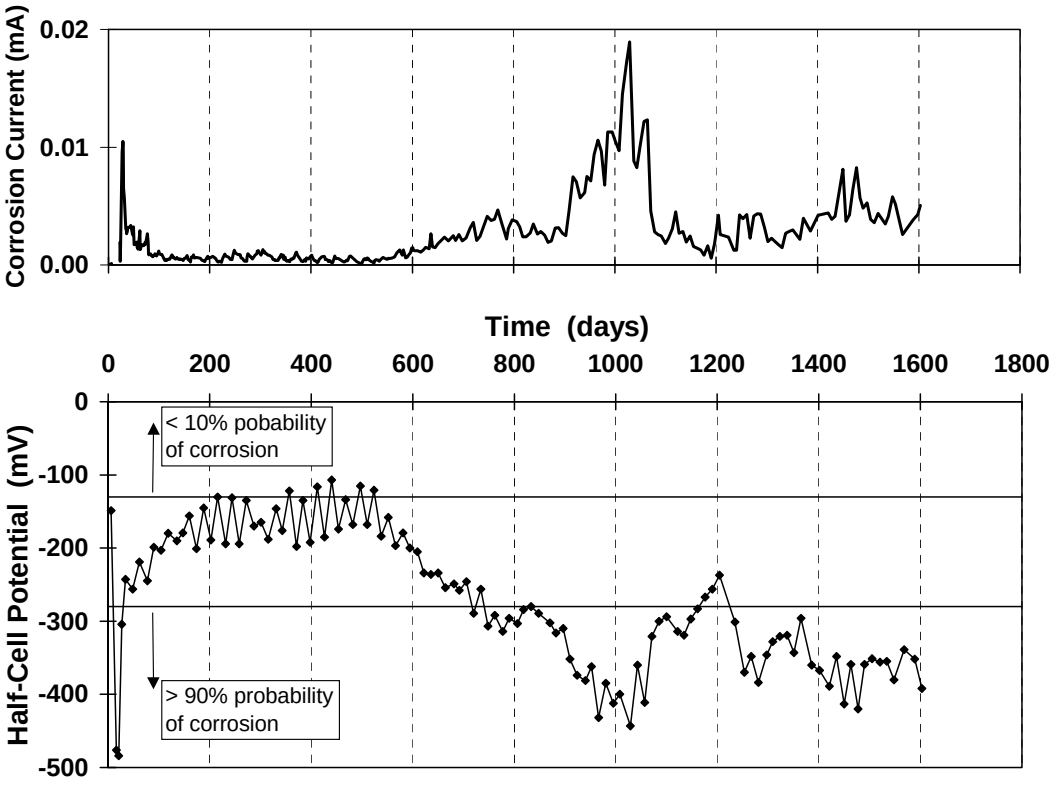

Figure 5.49 - Comparison Between Corrosion Current and Half-Cell Potential Readings

Half-cell potential readings can readily be taken in concrete structures, where corrosion current can not be measured directly. The good correlation between half-cell potentials and corrosion current obtained in this testing program suggests that regular half-cell potentials taken throughout the service life of a structure could be used to reliably detect the onset of corrosion. This would provide a very useful tool for owners with the desire and resources to monitor their structures regularly. However, the conditions in a structure may differ considerably from those in the experimental specimens, and this may affect the reliability of the half-cell potentials. One particular item of concern is that in the macrocell specimens the prestressing strand was not in contact with the galvanized steel duct. In a structure, this case would be uncommon. Thus, half cell potentials taken on the prestressing tendon may in fact reflect the very negative potential of the zinc on the galvanized steel duct, leading to erroneous results and conclusions. In situations where the tendon is completely encapsulated the duct will act as a barrier to the ion flow necessary for half-cell potential readings. In the experimental specimens, it is possible that the discontinuity in the duct at the segmental joint facilitated measurement of half-cell potentials.

Reversed Macrocell Corrosion

The occurrence of a "reversed" macrocell (i.e. bottom layer of steel corroding rather than the top layer) was confirmed by forensic examination. In each case, the polarity of the macrocell corrosion current correctly indicated which layer of steel was the anodic site.

Comparison Between Macrocell Corrosion Current and Forensic Examination

Macrocell corrosion specimens are particularly appealing for corrosion research since the corrosion current can be measured directly. As described in the Section 5.5.1, regular measurement of the corrosion current allows easy determination of the time to corrosion and calculation of the corrosion severity. Forensic examination of the macrocell specimens at the end of testing allows a comparison between the results measured during testing and the observed damage at the end of testing.

The calculated values of metal loss for the prestressing strand or bars are plotted with the corresponding corrosion ratings from specimen autopsies in Figure 5.50 and Figure 5.51. In general, the specimens with the highest calculated metal loss also had the

highest corrosion ratings, particularly for the mild steel bars. However, some discrepancies exist, particularly for the strand corrosion. All of the specimens that were autopsied had some light corrosion or discoloration on the prestressing strand, resulting in low but non-zero corrosion ratings. However, measured corrosion currents for only three of the specimens that were autopsied had indicated corrosion of the prestressing strand was occurring.

A number of factors may contribute to the observed differences between calculated corrosion severity (metal loss) and observed corrosion damage. Firstly, the extremely light corrosion and discoloration seen on many of the strands during autopsy may result from microcell corrosion activity or macrocell corrosion currents too low to be measured. The second factor is the age of the specimens. During the nearly four and a half years of exposure testing, it is possible that corrosion is occurring on both layers of steel. In the dry joint specimens, measured chloride contents were in excess of the corrosion threshold at the level of the mild steel reinforcement. If corrosion is occurring on both layers of steel, the macrocell corrosion current would correctly indicate which layer of steel was experiencing the more severe corrosion activity, but the other layer of steel would be overlooked and the charge flux calculated from macrocell corrosion current would underestimate the actual corrosion severity or metal loss. It is possible that this may be occurring for some of the dry joint specimens, and that the reduction in corrosion activity (decreasing corrosion current) displayed by several specimens is a reflection of corrosion activity on both layers of steel.

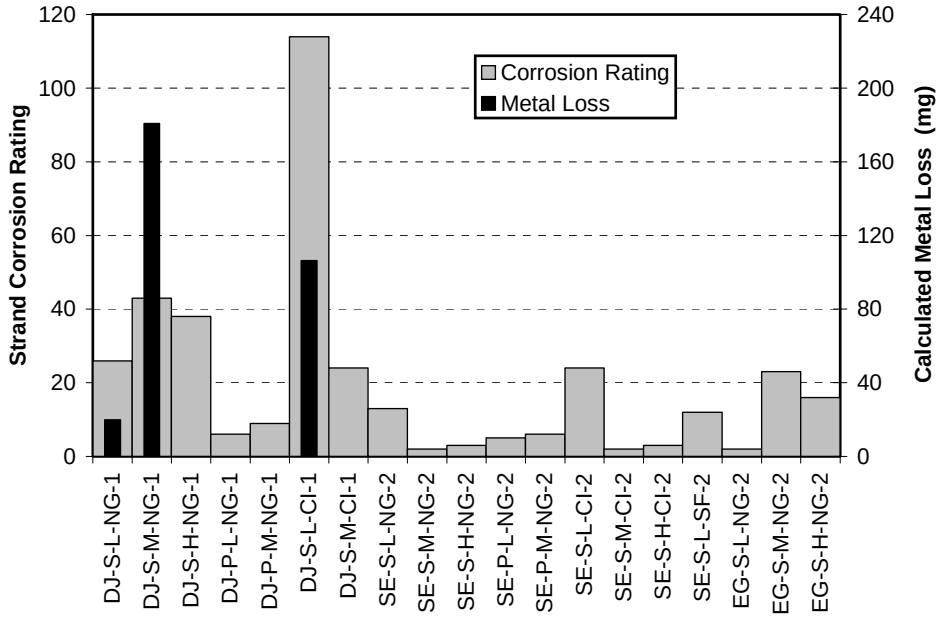

Figure 5.50 - Comparison of Corrosion Rating and Metal Loss for Prestressing Strand

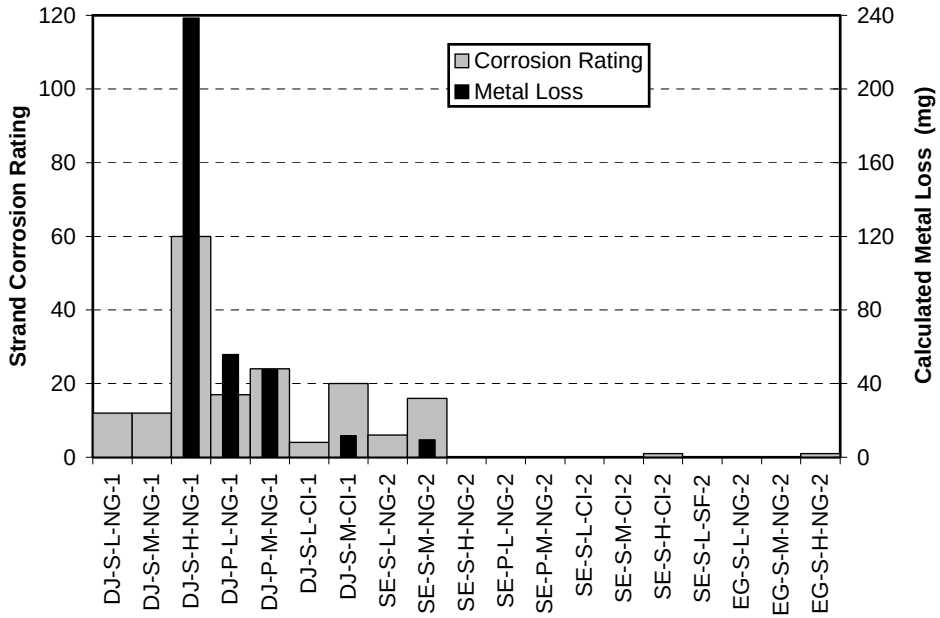

Figure 5.51 - Comparison of Corrosion Ratings and Metal Loss for Mild Steel Bars

The phenomenon described in the preceding paragraph illustrates a possible limitation of the macrocell corrosion specimen. Due to the small specimen size, long term

exposure testing may allow moisture and chloride penetration to both layers of steel. If the macrocell specimens are used to evaluate corrosion resistant steels (epoxy coated or galvanized bars, or well protected bonded post-tensioning tendons), it is possible that macrocell corrosion will not develop. The driving force for macrocell corrosion is the potential difference between the two levels of steel resulting from variations in chloride and moisture concentration. In a long term test, this potential difference may disappear due to advanced moisture and chloride penetration before corrosion can be initiated on the steel.

5.9 Summary and Conclusions

Several interesting observations can be drawn after nearly four and a half years of extreme, accelerated exposure testing. Since the majority of corrosion activity has occurred in specimens with dry joints (eleven of twelve specimens with corrosion), these conclusions are based on a limited data set and therefore could be subject to change.

At present, exposure testing is continuing for nineteen specimens (one of each specimen type). Continued exposure testing may provide additional results to assist comparison of variables.

5.9.1 Overall Performance

- Overall performance of the segmental macrocell corrosion specimens in this program is very good with only minor corrosion detected in a limited number of specimens.
- Metal loss calculations indicate that corrosion to date is minor or negligible.
- Possible strength degradation, in the form of pitting corrosion on prestressing strand, was found in only one specimen.

5.9.2 Assessing Corrosion Activity Using Half-Cell Potential Measurements

- The magnitude of half-cell potential measurements may not necessarily indicate the severity of corrosion activity. Very negative half-cell potentials may result from sources other than significant corrosion activity. Low half-cell potentials (more positive than guidelines for high probability of corrosion) may be measured for conditions of corrosion activity. Therefore it is important to consider the variation of half-cell potentials over time to assess corrosion activity and detect the initiation of corrosion.

5.9.3 Segmental Joints

- All long term and significant corrosion has occurred in specimens with dry joints. Seventy-eight percent (eleven of fourteen) of the dry joint specimens displayed corrosion activity. Specimens with dry joints showed increased chloride penetration and increased corrosion of galvanized steel duct, prestressing strand and mild steel reinforcement. Test results indicate that dry joints do not provide corrosion protection for internal tendons where aggressive exposure may occur.
- The mild steel reinforcement is corroding instead of the prestressing strand in seven of the eleven dry joint specimens with corrosion activity. This occurrence is attributed to penetration of chlorides at the dry segmental joint and indicates a possible increased corrosion threat for mild steel reinforcement within the segment when dry joints are used. This could occur in bridges with external tendons, and highlights the importance of clear cover over the ends of longitudinal bars in the segments.
- One out of twenty-four specimens with epoxy joints has shown corrosion activity. This specimen was the most recent to display an onset of corrosion, and measured corrosion current was very small. Autopsy of this specimen confirmed that the mild steel reinforcement was corroding rather than the prestressing strand. Measured chloride profiles for this specimen suggested that corrosion resulted from an external source of moisture and chlorides rather than from penetration at the epoxy joint or through the concrete.
- Only very minor prestressing strand corrosion was found in specimens with epoxy joints. Corrosion of the galvanized steel duct was reduced in extent and severity in specimens with epoxy joints. The experimental data to date indicates that thin epoxy joints provide substantially improved corrosion protection for internal tendons in segmental construction.
- The use of gaskets in epoxy joints may interfere with epoxy coverage on the joint. Autopsied epoxy/gasket joint specimens found incomplete epoxy coverage near the duct openings, leading to increased chloride penetration and duct corrosion. The observed deficiencies occurred in carefully controlled laboratory conditions, and could possibly be worse under field conditions.

5.9.4 Ducts for Internal Post-tensioning

- Strand corrosion was not detected during exposure testing in any epoxy joint specimens with plastic ducts. Reversed macrocell corrosion developed in the four dry joint specimens with plastic ducts. Formation of the reversed corrosion macrocells indicates that the plastic duct is providing improved corrosion protection for the prestressing strand (tendon), even when penetration of chlorides at the dry joints has caused rebar corrosion.
- Forensic examination revealed only very minor corrosion or discoloration on the prestressing strand from specimens with plastic ducts.
- Galvanized steel ducts were corroded in all cases. Duct corrosion led to concrete cracking along the line of the tendon in many specimens. Ducts were corroded through in nearly two-thirds of the specimens, eliminating the duct as corrosion protection for the prestressing tendon. The concrete cover in the test specimens was lower than specification, contributing to the poor performance of the galvanized duct in such a short period of time. However, test results indicate the potential for durability problems when using galvanized ducts in aggressive exposures.
- Specimens with plastic ducts and epoxy joints had the best overall performance in the testing program (in terms of strand, mild steel and duct corrosion).

5.9.5 Joint Precompression

- The range of joint precompression investigated did not affect the time to corrosion or corrosion severity for steel reinforcement.
- In dry joint specimens with steel ducts, corrosion of the steel duct decreased as joint prestress increased.

5.9.6 Grouts for Bonded Post-tensioning

- The most severe corrosion of the prestressing tendon was found where calcium nitrite corrosion inhibitor was used in the grout. Test results suggest calcium nitrite should not be used in cement grouts.
- Two specimens with silica fume in the grout (and epoxy joints) did not show corrosion activity.

5.9.7 Conclusions

The results of this testing program indicate that epoxy joints provide excellent corrosion protection for internal tendons in segmental construction. The very poor corrosion performance of dry joints confirms the necessity for match-cast epoxy joints when internal tendons are used. Test results also indicate a possible increased risk for corrosion of the segment reinforcement when dry joints are used with external post-tensioning.

The use of gaskets in epoxy joints does not appear to be beneficial from a durability standpoint. Test results illustrated the potential for incomplete epoxy coverage when gaskets were used around duct openings, leading to increased chloride penetration and corrosion damage.

The excellent performance exhibited by plastic ducts indicates that they should be used in all situations where aggressive exposure may occur.

The experimental results mirror the performance of precast segmental bridges in North America to date. This experience and these research findings suggest that current practice and specifications are working well for corrosion protection of internal tendons in segmental construction. The research findings indicate that corrosion protection can be improved through the use of epoxy joints without gaskets in all precast segmental construction, and the use of plastic ducts for internal tendons.

Chapter 5 References

5.1) **AASHTO**, Guide Specifications for Design and Construction of Segmental Concrete Bridges, American Association of State Highway and Transportation Officials, Washington, D.C., 1989.

5.2) **Woodward, R.J. and Williams, F.W.,** "Collapse of the Ynys-y-Gwas Bridge, West Glamorgan," *Proceeding of The Institution of Civil Engineers*, Part 1, Vol. 84, August 1988, pp. 635-669.

5.3) **Miller, Maurice D.**, "Durability Survey of Segmental Concrete Bridges," *PCI Journal*, Vol. 40, No. 3, May-June 1995, pp. 110-123.

5.4) **Vignos, R.P.**, "Test Method for Evaluating the Corrosion Protection of Internal Tendons Across Segmental Bridge Joints." Master of Science Thesis, The University of Texas at Austin, May 1994.

5.5) **ASTM**, "Standard Test Method for Determining the Effects of Chemical Admixtures on the Corrosion of Embedded Steel Reinforcement in Concrete Exposed to Chloride Environments," ASTM G109-92, American Society for Testing and Materials, Philadelphia, PA, 1992.

5.6) **ASTM**, "Standard Test Method for Half-Cell Potentials of Uncoated Reinforcing Steel in Concrete," ASTM C876-91, American Society for Testing and Materials, Philadelphia, Pa., 1991.

5.7) **Broomfield, J.P., Rodriguez, J., Ortega, L.M., and Garcia, A.M.**, "Corrosion Rate Measurement and Life Prediction for Reinforced Concrete Structures," Proceedings of the 5th International Conference on Structural Faults and Repair held on June 29, 1993, Vol. 2, Venue, University of Edinburgh, pp 155-163.

5.8) **Al-Qadi, I.L., Peterson, J.E., and Weyers, R.E.**, "A Time to Cracking Model for Critically Contaminated Reinforced Concrete Structures," Proceedings of the 5th International Conference on Structural Faults and Repair held on June 29, 1993, Vol. 3, Venue, University of Edinburgh, pp 91-99.

5.9) **Concrete Reinforcing Steel Institute**, "CRSI Performance Research: Epoxy-Coated Reinforcing Steel," Interim Report, CRSI, Schaumburg, Ill, January 1992.

5.10) **Virmani, Y.P., Clear, K.C., and Pasko, T.J.**, "Time-to-Corrosion of Reinforcing Steel in Concrete Slabs, Vol. 5,: Calcium Nitrite Admixture or Epoxy-Coated Reinforcing Bars as Corrosion Protection Systems," Report No. FHWA/RD-83/012, Federal Highway Administration, Washington, D.C., September 1983, 71p.

5.11) **AASHTO.** "Sampling and Testing for Chloride Ion in Concrete and Concrete Raw Materials," AASHTO T 260-94, American Association of State Highway and Transportation Officials, Washington, D.C., 1994.

5.12) **Poston, R.W.,** "Improving Durability of Bridge Decks by Transverse Prestressing," Doctor of Philosophy Dissertation, The University of Texas at Austin, 1984.

5.13) **Hamilton, H.R.,** "Investigation of Corrosion Protection Systems for Bridge Stay Cables," Doctor of Philosophy Dissertation, The University of Texas at Austin, 1995.

5.14) **Sason, A.S.,** "Evaluation of Degree of Rusting on Prestressed Concrete Strand," *PCI Journal*, Vol. 37, No. 3, May-June 1992, pp. 25-30.

5.15) **Wouters, J.P.,** Personal Communication, Whitlock Dalrymple Poston and Associates, Inc., Manassas, Virginia, July 1998.

5.16) **ACI Committee 222,** "Corrosion of Metals in Concrete," ACI 222R-96, American Concrete Institute, Detroit, Michigan, 1996.

5.17) **Vaca-Cortes, Enrique**, "Corrosion Performance of Epoxy-Coated Reinforcement in Aggressive Environments," Doctor of Philosophy Dissertation, The University of Texas at Austin, May 1998.

5.18) **Koester, B.D.,** "Evaluation of Cement Grouts for Strand Protection Using Accelerated Corrosion Tests," Master of Science Thesis, The University of Texas at Austin, December 1995.

5.19) **Berke, N.S., Dallaire, M.P., Hicks, M.C. and Hoopes, R.J.,** "Corrosion of Steel in Cracked Concrete," *Corrosion*, Vol. 49, No. 11, November 1993, pp. 934-943.

5.20) **Pfeifer, D.W., Landgren, J.R. and Zoob, A.,** "Protective Systems for New Prestressed and Substructure Concrete," FHWA/RD-86/193, Federal Highway Administration, Washington, D.C., April 1987.

Chapter 6:

Durability Design Guidelines

6.1 Introduction

Designing for durability requires the same thought process as design for any other limit state or form of structural loading. The engineer must first assess the type of loading to be considered, and determine its intensity. Then, the engineer must determine the effects of the loading on the structure and design the structure to resist the loading through careful proportioning and detailing. The various components of the structure may have different design requirements depending on their function, and these requirements must be identified and addressed. A simplified analogy between durability design and design for structural loading is illustrated in Figure 6.1. Although the two processes are similar, the "precision" of design for durability can be significantly different from design for structural loading. The types and intensities of design requirements or loading can be assessed with similar accuracy in both cases. However, the resistance of the structure to durability attack can not be determined with the same level of certainty as in the estimation of the resistance of the structure to structural loading. This lack of precision is reflected in the durability design process, as will be discussed in this chapter.

Durability design guidelines should provide the engineer with the following information:

- How to determine when different forms of attack on durability should be considered.

  The engineer should be able to establish when durability must be considered as a limit state in the design process, and identify which forms of attack will occur in a given situation. Due to the varied climate, geology and geography of Texas, durability may play a significant role in the design process for some situations, while in others it may not.

- How to evaluate the severity of attack on structural durability in a given situation.

Once it has been determined that certain forms of durability problems may occur, the possible severity of attack needs to be assessed.

- How to determine what level of protection is necessary for the various components of the structure.

  The required level of protection for the structural components is a function of the forms and severity of attack that may be encountered in a particular situation. It is also strongly affected by the susceptibility of the various components of the substructure to the expected forms of attack.

- What measures can be employed to provide the necessary level of protection.

  Once the required level of protection has been determined, the engineer should be presented with design options to provide the necessary level of protection for durability.

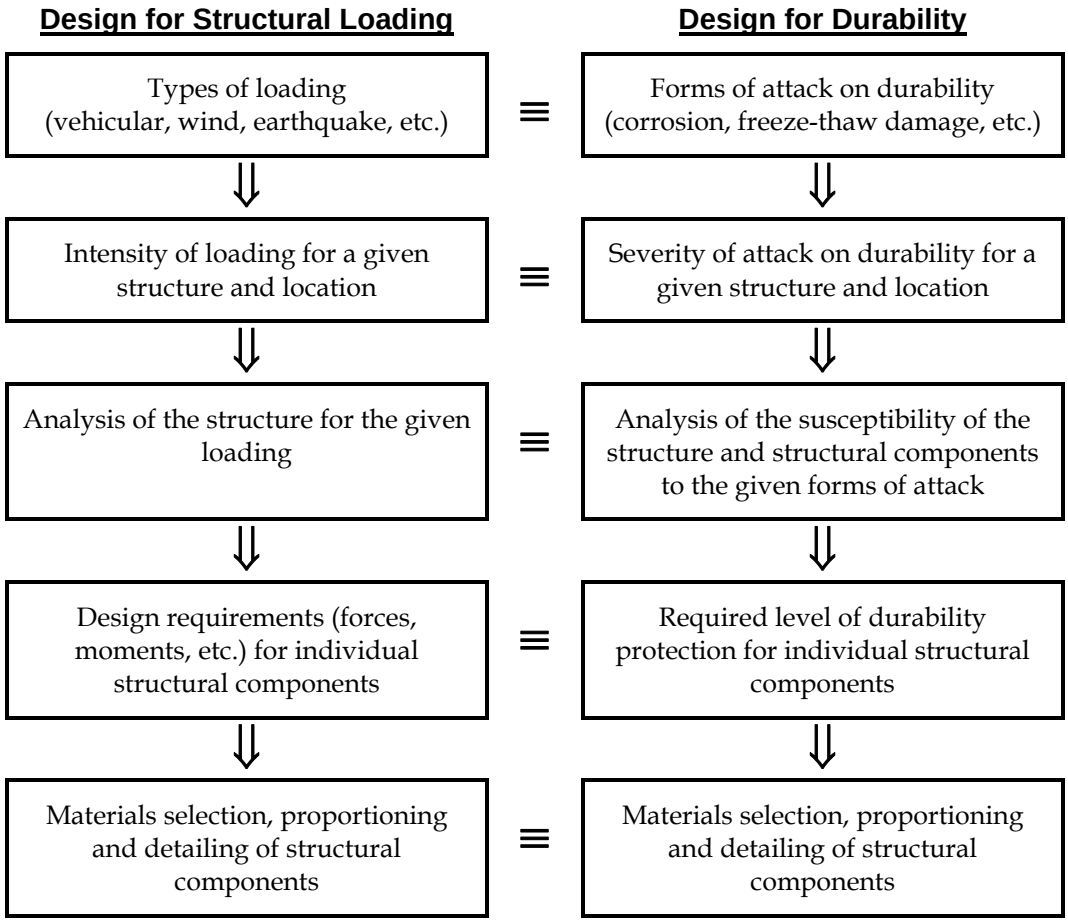

Figure 6.1 - Simplified Analogy Between Design for Structural Loading and Durability

The fundamental objective of durability research is to apply the research findings in the form of durability design guidelines. This is the goal of TxDOT Project 0-1405, where the final product will be durability design guidelines for post-tensioned bridge substructures. The portion of Project 0-1405 covered by this dissertation is insufficient by itself to develop comprehensive durability design guidelines for post-tensioned bridge substructures. However, the literature review and preliminary research findings from the different testing programs can be used to develop the groundwork for durability design guidelines. It is expected that the design guidelines will be refined and expanded as the project is completed and more information and detailed experimental results become available. Preliminary durability design guidelines are presented in the remainder of this chapter. The following subject areas are discussed:

- Assessing the environmental exposure (forms of attack) for bridges in Texas.
- Assessing the severity of attack on durability.
- Assessing the susceptibility of substructure components to attack on durability.
- Determining the required level of protection for durability.
- Protection measures for durable post-tensioned concrete structures.

6.2 Assessing the Environmental Exposure Condition

The environmental exposure conditions at a given location dictate what forms of durability attack may occur on the structure. The substructure exposure conditions in Texas were discussed previously in Section 2.2.4, and are shown in Figure 6.2. This figure indicates three different exposure conditions in Texas for bridge substructures: coastal exposure, freezing exposure and sulfate soils. Depending on the type of exposure, various forms of attack may be expected to occur, as indicated in Figure 6.2. For a given bridge location, Figure 6.2 can be used to determine the forms of environmental durability problems that may be encountered.

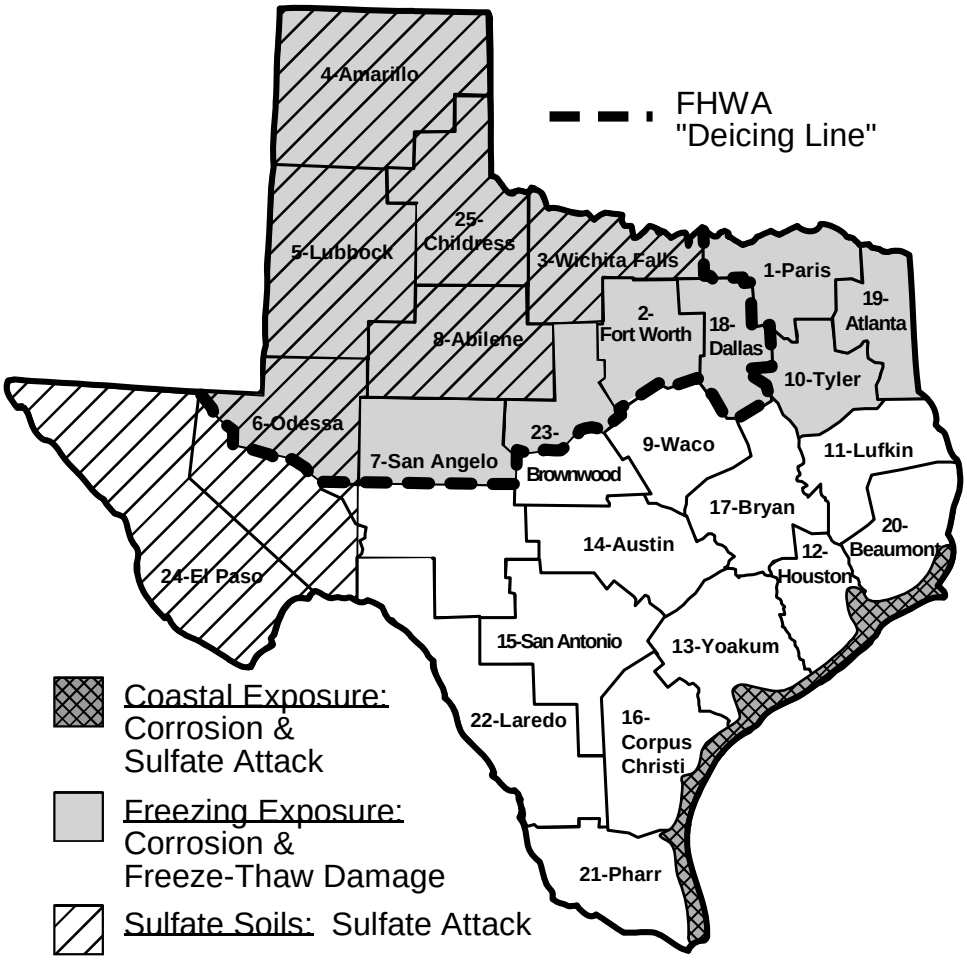

Figure 6.2 – Global Substructure Exposure Conditions for Bridges in Texas

6.3 Assessing the Severity of Durability Attack

Once it has been determined that a particular form of durability distress may occur in an environment, the severity of the attack must be established.

6.3.1 Severity of Environmental Conditions for Freeze-Thaw Damage

The severity of the Texas environment for freeze-thaw damage in bridge structures was reported by Watkins[6.1] and discussed in Section 2.5.2. Based on an analysis of climate data and deicing chemical usage in Texas, Watkins developed the chart shown in Figure 6.3 to assess the degree of severity of freeze-thaw damage in Texas.

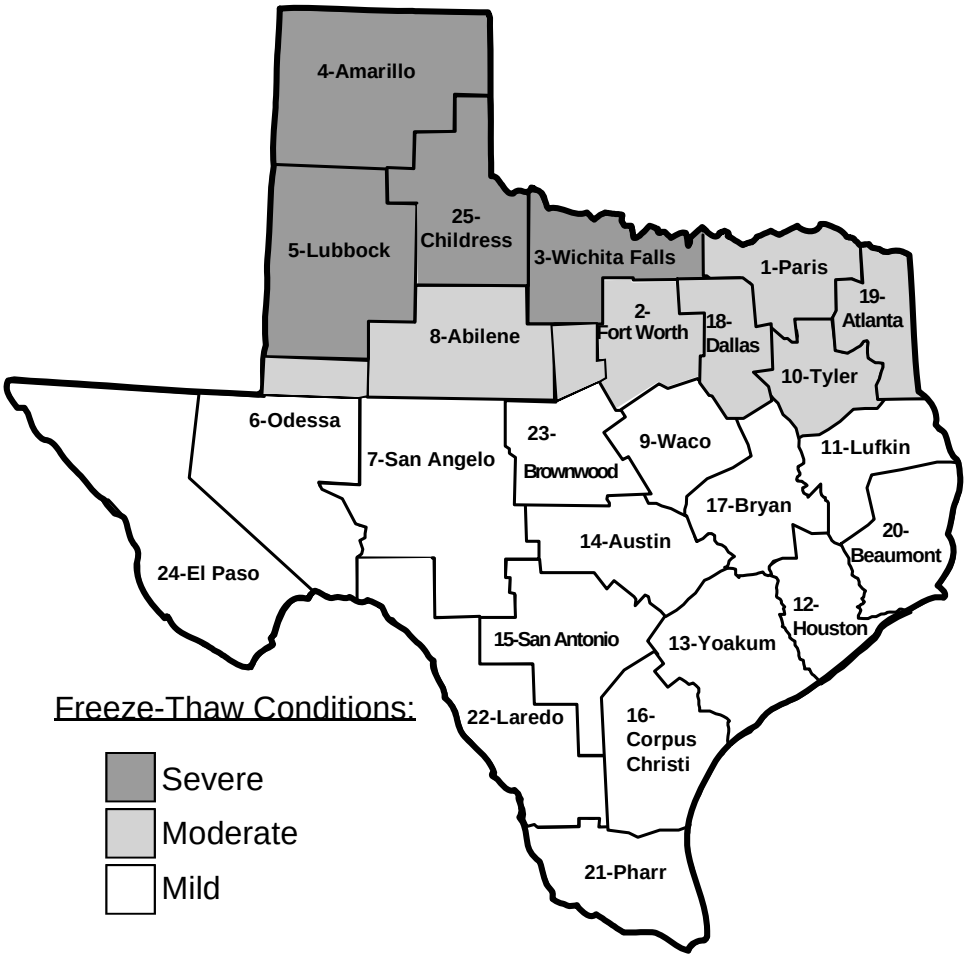

Figure 6.3 – Environmental Freeze-Thaw Damage Severity Ratings

6.3.2 Severity of Environmental Conditions for Sulfate Attack

Sulfate attack may occur due to sulfate soils or sulfates in seawater. The sulfate concentration in soils may vary considerably within the large region of Figure 6.2 where sulfate soils are indicated. ACI Committee 201[6.2] provides guidelines for assessing the degree of sulfate attack based on sulfate concentrations in soils and water. These guidelines are listed in Table 6.1. In coastal regions or in areas where sulfate soils are suspected, the seawater and/or soil should be analyzed for sulfate content to assess the severity of sulfate attack based on Table 6.1.

Table 6.1 – Environmental Sulfate Attack Severity Ratings[6.2]

Sulfate Content	Mild	Moderate	Severe	Very Severe
Water soluble SO_4 in soil, %	0.00-0.10	0.10-0.20	0.20-2.00	Over 2.00
SO_4 in water, ppm	0-150	150-1500	1500-10,000	Over 10,000

6.3.3 Severity of Environmental Conditions for Corrosion

Coastal Exposure

The saltwater environment and high average annual temperature of the coastal exposure along the Gulf of Mexico provides severe conditions for reinforcement corrosion. All structures located within the coastal region indicated in Figure 6.2 should be considered as having severe environmental exposure conditions for corrosion.

Freezing Exposure

The environmental exposure conditions for corrosion are potentially severe in the areas of Texas where freezing may occur. The severity of the exposure is dependent on the type and amount of deicing agents used during winter months. If chloride-based deicing chemicals are used, the potential for corrosion will be high. A survey of TxDOT deicing chemical usage for the winter of 1996-1997 indicated that in all districts where deicing chemicals were used, chloride-based deicing agents had been applied.[6.1] If non-chloride-based deicing chemicals are used, then the potential for corrosion will be very low.

The duration during which chloride-based deicing chemicals are used will also affect the corrosion severity. Logically, districts with the coldest temperatures during the winter months and highest number of freeze-thaw cycles will receive more deicing chemical applications, and thus experience more severe conditions for corrosion.

The severity of environmental conditions for corrosion in freezing exposures can be assessed using the climate data gathered by Watkins[6.1] and the FHWA Deicing Line. A corrosion severity rating of mild, moderate or severe is assigned depending on annual temperature data for the region, as shown in Figure 6.4. These severity ratings assume that chloride-based deicing chemicals are used. If deicing chemicals are not used, or if

non-chloride-based chemicals are used, the corrosion severity may be taken as mild. This decision should be made with caution, since ice removal procedures may change during the service life of the structure.

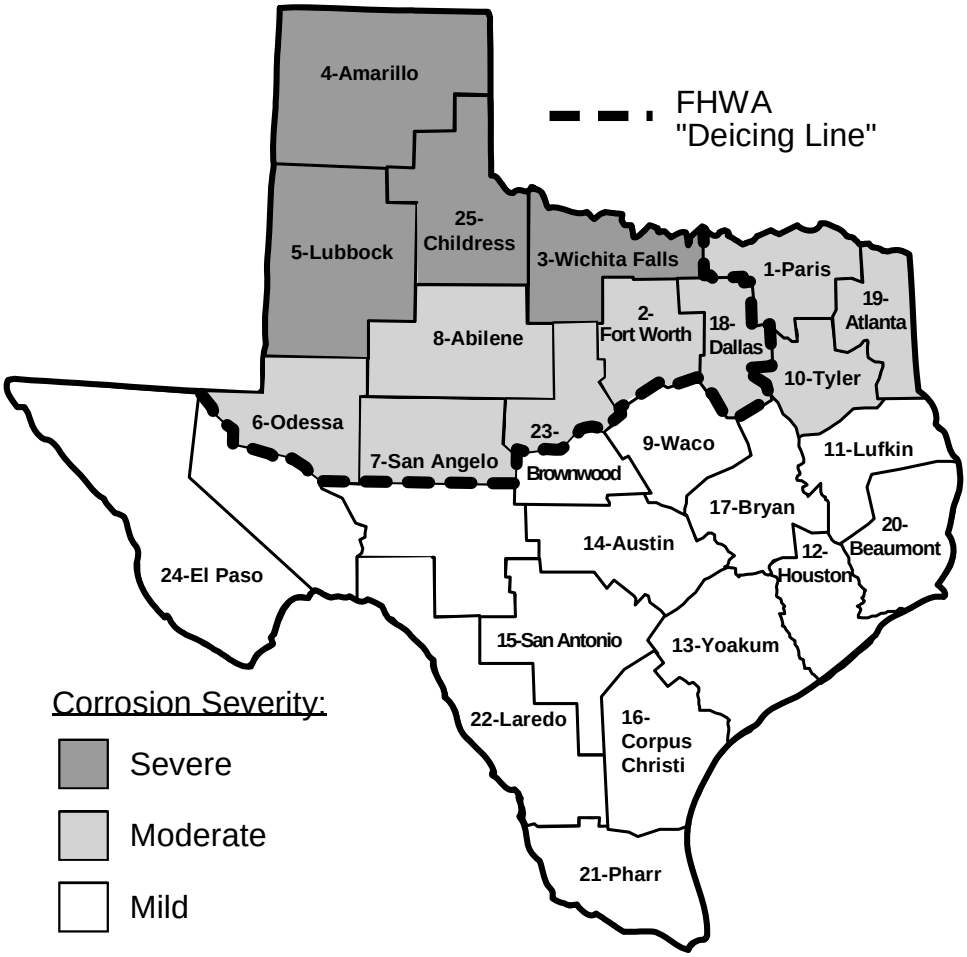

Figure 6.4 – Environmental Corrosion Severity Ratings for Freezing Exposures Where Chloride-Based Deicing Chemicals are Used

6.4 Assessing the Substructure Component Exposure Condition

The exposure conditions for a specific structural component can have a significant effect on the severity of attack on that element. Different components of the substructure may experience more or less severe deterioration than would be expected for a given environment. The severity of the local exposure conditions is a function of the

temperature, presence of moisture, availability of oxygen and exposure to aggressive agents for a particular substructure component.

The significance of member exposure condition can be illustrated using examples. The direct exposure to aggressive agents plays a role in whether deterioration will occur. In a region with sulfate soils, only components directly in contact with the soils are at risk for sulfate attack. Therefore, pile caps or other foundation elements may require sulfate resistant cements and the use of mineral admixtures, but the columns and bent caps of the substructure may not. Another example occurs in areas where deicing chemicals are used. If drainage of chloride-laden moisture from the superstructure onto the substructure is prevented, the corrosion risk for the substructure will be low. However, if drainage is poor or superstructure joints leak, moisture and chlorides may contact the substructure and cause corrosion damage. Thus, the design and details of the superstructure may influence the substructure durability requirements. The availability of oxygen is a significant factor for corrosion. Substructure components that are continually submerged will experience only limited corrosion damage due to lack of oxygen. The local temperature conditions for a structural element will affect the severity of freeze-thaw damage. Elements that are buried or have one or more surfaces in contact with the ground will benefit from the insulation provided by the soil, and may experience less severe freeze-thaw damage.

6.4.1 Susceptibility of Substructure Components to Freeze-Thaw Damage

Watkins[6.1] developed a comprehensive bridge member exposure rating system for freeze-thaw damage. The criteria for the rating system consists of the member exposure to freezing and thawing, moisture and deicing chemicals, as described in Table 6.2. The exposure ratings of low, medium and high were assigned values of one, two and three, respectively. The exposure categories were given importance factors of 20% for deicing chemical exposure, 40% for moisture exposure and 40% for freeze-thaw cycle exposure.[6.1] The member exposure severity considering these criteria is determined as follows:

$$\text{Member Exposure Severity, } S_{member} = 0.2R_{d1} + 0.4R_{m1} + 0.4R_{ft}$$

$$= \text{Severe Exposure} \quad \text{for } S_{member} = 3.0$$

$$= \text{Moderate Exposure} \quad \text{for } 2.0 \leq S_{member} < 3.0$$

$$= \text{Mild Exposure for} \quad S_{member} < 2.0$$

where,

R_{d1} = Deicing Chemical Exposure (1, 2 or 3 for low, medium or high rating)

R_{m1} = Moisture Exposure (1, 2 or 3 for low, medium or high rating)

R_{ft} = Freeze-Thaw Cycle Exposure (1, 2 or 3 for low, medium or high rating)

The member exposure rating system was used to assign an exposure severity for various bridge members, as listed previously in Table 2.14. Member Exposure Severity ratings for different substructure components are listed in Table 6.3. Sample calculations for bridge piers are shown below.

Sample Calculations for a Bridge Pier:

Deicing Chemical Exposure = Medium (may receive salt spray)

Moisture Exposure = Medium (not likely exposed to run-off)

Freeze-Thaw Cycle Exposure = High (exposed to air on all sides)

S_{member} = 0.2(2) + 0.4(2) + 0.4(3)

= 2.4 $\Rightarrow$ **Moderate** Member Exposure Severity

Table 6.2 - Member Exposure Criteria for Freeze-Thaw Damage[6.1]

Exposure Rating	Deicing Chemical Exposure, R_{d1}	Moisture Exposure, R_{m1}	Freeze-Thaw Cycle Exposure, R_{ft}
Low (1)	Deicing chemicals are not used on or around this member, or member is located underground or in water insulated from deicing chemical exposure.	Members that are not likely to become critically saturated such as vertical walls or members located inside a covered structure.	Members which are insulated from freeze-thaw cycles by soil or water so that it does not freeze. Member located inside temperature controlled buildings.
Medium (2)	Members that do not receive direct application of deicing chemicals, but may receive salt spray if deicing chemicals are used.	Water is not likely to pond on concrete surface or member will not be exposed to run-off.	Member exposed to circulating air on only one side or has thick member dimensions (> 200 mm (8 in.)).
High (3)	Horizontal concrete surfaces which receive direct application of deicing chemicals or are likely to be in contact with water that contains deicing chemicals, or members located directly below open bridge	Member on which water is likely to pond or member which receives frequent direct contact with drainage or run-off water.	Member exposed to air circulation on more than one side or members with thin dimensions (> 200 mm (8 in.)).

	expansion joints.		

Table 6.3 – Freeze Thaw Damage Member Exposure Severity Ratings for Selected Substructure Components

Member Exposure	Substructure Component
Mild Exposure	• Drilled Shafts • Prestressed Piling • Abutments • Buried Pile Caps
Moderate Exposure	• Bridge Piers • Columns • Drilled Shafts in Water • Exposed Pile Caps
Severe Exposure	• Bent Caps

6.4.2 Susceptibility of Substructure Components to Sulfate Attack

The approach used in the preceding section for freeze-thaw damage can be applied to determining the susceptibility of substructure components to sulfate attack. Proposed exposure rating criteria for sulfate attack is shown in Table 6.4. The rating system considers sulfate soil environments and coastal environments separately. For soil environments, the member exposure severity is a function of the sulfate soil exposure and moisture exposure. In the coastal environment, the exposure severity is dictated by the exposure zones described in Section 2.2.1 and shown in Figure 2.1. For sulfate soil environments, sulfate soil exposure and moisture exposure were given equal importance when determining exposure severity ratings. For coastal environments, the member exposure severity ratings are directly a function of the sulfate seawater exposure. The exposure rating system was used to assign exposure condition ratings for various bridge substructure components listed in Table 6.5 using the following procedure.

Sulfate Soil Environments:

Member Exposure Severity, $S_{member} = 0.5R_{soil} + 0.5R_{m2}$

Sulfate Seawater Environments:

Member Exposure Severity, $S_{member} = 1.0Rsea$

with,

S_{member} = Severe Exposure for $S_{member} = 3.0$

S_{member} = Moderate Exposure for $2.0 \le S_{member} < 3.0$

S_{member} = Mild Exposure for $S_{member} < 2.0$

where,

R_{soil} = Sulfate Soil Exposure (1, 2 or 3 for low, medium or high rating)

R_{m2} = Moisture Exposure (1, 2 or 3 for low, medium or high rating)

R_{sea} = Sulfate Seawater Exposure (1, 2 or 3 for low, medium or high rating)

Table 6.4 - Member Exposure Rating Criteria for Sulfate Attack

Exposure Rating	Sulfate Soil Environment		Coastal Environment
	Sulfate Soil Exposure, R_{soil}	**Moisture Exposure, R_{m2}**	**Sulfate Seawater Exposure, R_{sea}**
Low (1)	Members not in direct contact with sulfate soils.	Members that remain dry or members located inside a covered structure.	Members in the atmospheric zone of the structure.
Medium (2)	Members not in direct contact with sulfate soils, but may be splashed with sulfate-laden moisture.	Members where water is not likely to pond on concrete surface or where member will not be exposed to run-off.	Members in the splash zone of the structure.
High (3)	Members in direct contact with sulfate soils.	Members exposed to continuous moisture or members which receive frequent contact with drainage or run-off water.	Members in the tidal zone or submerged zone of the structure.

Table 6.5 – Sulfate Attack Member Exposure Severity Ratings for Selected Substructure Components

Member Exposure	Substructure Component	
	Sulfate Soil Environment	**Coastal Environment**
Mild Exposure	• Bent Caps • Bridge Piers (no soil at base) • Columns (no soil at base)	• Bent Caps (atmospheric zone) • Bridge Piers (atmospheric zone) • Columns (atmospheric zone)
Moderate Exposure	• Abutments • Bridge Piers (soil at base) • Columns (soil at base)	• Bent Caps (splash zone) • Bridge Piers (splash zone) • Columns (splash zone)
Severe Exposure	• Drilled Shafts • Prestressed Piling • Pile Caps	• Bridge Piers (tidal and submerged zone) • Columns (tidal and submerged

		zone) • Drilled Shafts • Prestressed Piling • Pile Caps

6.4.3 Susceptibility of Substructure Components to Reinforcement Corrosion

Proposed exposure rating criteria for the susceptibility of substructure components to corrosion is shown in Table 6.6. The rating system considers freezing environments and coastal environments separately. For freezing environments, the member exposure severity is a function of the chloride-based deicing chemical exposure. If non-chloride deicing chemicals are used, the exposure rating will be mild in most cases. In the coastal environment, the member exposure severity is dictated by the exposure zones described in Section 2.2.1 and shown in Figure 2.1. The exposure rating system was used to assign member exposure condition ratings for various bridge substructure components as listed in Table 6.7 using the following procedure.

Freezing Environments:

Member Exposure Severity, $S_{member} = 1.0R_{d2}$

Coastal Environments:

Member Exposure Severity, $S_{member} = 1.0R_{salt}$

with,

S_{member} = Severe Exposure for $S_{member} = 3.0$

S_{member} = Moderate Exposure for $2.0 \leq S_{member} < 3.0$

S_{member} = Mild Exposure for $S_{member} < 2.0$

where,

R_{d2} = Deicing Chemical Exposure (1, 2 or 3 for low, medium or high rating)

R_{salt} = Saltwater Exposure (1, 2 or 3 for low, medium or high rating)

Table 6.6 - Member Exposure Rating Criteria for Reinforcement Corrosion

Member Exposure	Freezing Environment Deicing Chemical Exposure, R_{d2}	Coastal Environment Saltwater Exposure, R_{salt}
Low (1)	Deicing chemicals are not used on or around this member, or member is located underground or in water insulated from deicing chemical exposure.	not applicable
Medium (2)	Members that do not receive direct application of deicing chemicals, but may receive salt spray if deicing chemicals are used.	Members in the submerged zone of the structure.
High (3)	Horizontal concrete surfaces which receive direct application of deicing chemicals or are likely to be in contact with water that contains deicing chemicals, or members located directly below open bridge expansion joints.	Members in the tidal zone, splash zone or atmospheric zone of the structure.

Table 6.7 – Reinforcement Corrosion Member Exposure Severity Ratings for Selected Substructure Components

Member Exposure	Substructure Component	
	Freezing Environment	**Coastal Environment**
Mild Exposure	• Drilled Shafts • Prestressed Piling • Pile Caps (buried)	• not applicable
Moderate Exposure	• Columns Adjacent to Roadways • Bridge Piers Adjacent to Roadways	• Drilled Shafts in Water • Prestressed Piling • Pile Caps (submerged)
Severe Exposure	• Bent Caps at Expansion Joints • Bridge Piers at Expansion Joints • Columns at Expansion Joints • Abutments at Expansion Joints	• Bent Caps • Abutments • Bridge Piers • Columns • Pile Caps (not submerged)

6.5 Establishing the Required Level of Protection for Durability

At this point, it is prudent to make a statement about the "precision" of durability design. The preceding sections have described criteria for assessing the types and severity

of attack on structural durability, and for assessing the susceptibility of substructure components to these attacks. It must be emphasized that these are general criteria, and are certainly open to interpretation by the designer for each structure and environment. Many factors may influence the severity and nature of the attack, and many factors are involved in determining the necessary protection measures to guard against premature deterioration. In almost all cases, the effect of various protection measures in terms of length of service life can not be determined with any level of accuracy. For this reason, it was decided to simplify environmental and member exposure severity ratings to mild, moderate and severe, and to assign three levels of protection: none, intermediate and maximum. The use of more precise definitions of exposure severity or protection levels is simply not justified.

The required level of protection against the different forms of durability attack is a function of the severity of the environment (environmental exposure) and the susceptibility of the individual substructure components to attack (member exposure). The required level of protection can be generalized for all forms of durability. Based on the environmental exposure severity and the member exposure severity, the required level of protection is determined using Table 6.8.

Table 6.8 – Required Level of Protection Based on Exposure Conditions

Member Exposure	Environmental Exposure		
	Mild	**Moderate**	**Severe**
Mild	None	None	None
Moderate	None	Intermediate	Maximum
Severe	None	Maximum	Maximum

6.6 Protection Measures for Durable Structures

Once the required level of protection has been determined, the appropriate protection measures should be selected. Due to the many uncertainties involved in determining service life and the effect of different protection measures on service life, it is

not appropriate to prescribe specific measures to achieve a decisive level of protection or service life. The purpose of this section is to present options for protection measures against the various forms of environmental attack. Increasing protection is provided primarily by adding measures to create a multilevel protection scheme. Protection measures for intermediate and maximum protection against freeze-thaw damage, sulfate attack and corrosion are presented in the following sections. These measures have been obtained from the literature review described in Chapter 2. Protection measures for corrosion in post-tensioned substructures have been supplemented with the preliminary results of the testing programs described in Chapters 3, 4 and 5.

6.6.1 Protection Measures for Freeze-Thaw Damage

6.6.1.1 General Requirements for Freeze-Thaw Environments

- **Structural Form:** Attention should be given to structural form and layout to minimize contact with deicing chemical run-off and splashing (see Section 2.4.1).
- **Water-Cement Ratio:** The maximum water-cement ratio shall be limited to 0.45 for thin members and members exposed to deicing chemicals, either directly or in the form of run-off. This requirement may be relaxed to 0.50 for all other situations.
- **Coarse Aggregate:** Coarse aggregate should be frost resistant. Standard test methods including ASTM C666,[6.3] C671[6.4] and C682[6.5] may be used to evaluate the suitability of aggregates.
- **Surface Treatment:** Concrete surface treatments may be employed to limit moisture penetration (see Section 2.4.3.4).

6.6.1.2 Specific Requirements for Intermediate and Maximum Protection Levels

The most significant factor for protection against freeze-thaw damage is the concrete pore structure. Recommendations for total average air content in the concrete are listed in Table 6.9 for intermediate and maximum protection. Required total concrete air contents are specified as a function of the maximum coarse aggregate size. The total concrete air contents should be attained using an appropriate air entraining admixture with consideration for the amount of entrapped air (total air content equals entrained air

plus entrapped air). The volume of entrapped air is a function of the concrete mix proportions and aggregate characteristics. The field tolerance for average total concrete air content is plus or minus 1.5%.

Table 6.9 - Required Total Concrete Air Content for Protection Against Freeze-Thaw Damage[6.1]

Protection Level	Maximum Aggregate Size					
	9.5 mm (3/8″)	12.7 mm (1/2″)	19 mm (3/4″)	25 mm (1″)	38 mm (1.5″)	50 mm (2″)
Intermediate	6%	5.5%	5%	5%	4.5%	4%
Maximum	8%	7%	6.5%	6%	5.5%	5%

6.6.2 Protection Measures for Sulfate Attack

Several options or approaches may be taken to provide a desired level of protection against sulfate attack in concrete structures. It is left to the discretion of the designer to select the preferred combination of protection measures listed in Table 6.10. Cement types are according to ASTM C150.[6.6] Fly ash classifications are according to ASTM C618.[6.7] Construction of concrete structures exposed to sulfate soils or water should adhere to the special construction procedures described in Section 8.6.7 of the AASHTO LRFD Construction Specifications.[6.8]

Table 6.10 - Protection Measures for Sulfate Attack

Protection Level Options		Cement Type	Maximum w/(c + p) Ratio	Mineral Admixture
Intermediate	1	Type II	0.50	not required
	2	Type I	0.50	see Table 6.11
Maximum	1	Type V	0.45	not required
	2	Type I or II	0.45	see Table 6.11
	3**	Type V	0.45	see Table 6.11

** highest level of protection

Table 6.11 - Mineral Admixture Quantities for Sulfate Attack

Mineral Admixture	Amount	Comment
Class F Fly Ash	15% to 40% cement replacement by weight	Class F fly ash is the preferred choice for sulfate attack conditions
Class C Fly Ash	15% to 40% cement replacement by weight	Class C fly ash must not be used without special considerations, as it may reduce sulfate resistance. Depending on the mineralogy of the Class C fly ash, intergrinding of the fly ash with cement clinker and gypsum may improve sulfate resistance. See Ref. 6.9 for detailed information.
Silica Fume	5% to 20% cement replacement by weight, **or** up to 10% addition by weight of cement	

6.6.3 Protection Measures for Reinforcement Corrosion

6.6.3.1 General Requirements for Environments Where Corrosion is a Concern

- **Structural Form:** Attention should be given to structural form and layout, as described in Section 2.4.1. Factors to consider include drainage, joint locations, splashing effects and geometry effects.
- **Reinforcement Congestion:** Reinforcement details should be carefully considered to avoid congestion that may interfere with concrete placement and compaction. Options such as headed reinforcement and prestressing may be required to avoid congestion.
- **Crack Control:** Cracking should be minimized. Unintended cracking due to plastic shrinkage and settlement, drying shrinkage, thermal effects and differential settlement should be controlled through detailing and proper curing conditions. Intended

cracking due to structural loading should be minimized through reinforcement detailing. The use of prestressing to control cracking may be an option.

> *Preliminary test results from the experimental programs described in this testing program suggest that limiting the number of cracks and increasing crack spacing using prestressing may improve corrosion protection. The required amount of prestressing will vary for different structural components and loading conditions.*

- **Location of Post-Tensioning Anchorages:** Post-tensioning anchorages should not be located where direct exposure to moisture and chlorides may occur. If anchorages must be located near expansion joints, member ends should be detailed to prevent exposure to chloride-laden moisture (see Section 2.4.4.5).
- **Segmental Joints:** All precast segmental construction must use match-cast epoxy joints. The use of gaskets around duct openings on joint faces is discouraged. The preferred option is to swab the ducts immediately after segment placement and initial stressing to prevent epoxy from blocking the duct.
- **Surface Treatment:** Concrete surface treatments may be employed to limit moisture penetration (see Section 2.4.3.4).
- **Concrete Cover:** AASHTO LRFD[6.10] concrete cover requirements of Clause 5.12.3 should be used.
- **Minimum Cement Content of Concrete:** Minimum cement contents should be dictated by TxDOT Specifications[6.11] or AASHTO LRFD Specification[6.10] Table C5.4.2.1-1 or AASHTO LRFD Construction Specification[6.8] Clause 8.2.
- **Reinforcing Bar Supports:** Non-metallic (plastic) bar chairs and bolster strips should be used at all locations where supports bear against forms for exposed concrete surfaces.

  > *Plastic tipped bar chairs and bolster strips corroded in beam and column test specimens, producing concrete spalling and extensive rust staining.*

- **Construction Procedures:** Construction of concrete structures exposed to saltwater should adhere to the special procedures described in Clause 8.6.6 of the AASHTO LRFD Construction Specifications.[6.8]

6.6.3.2 Specific Measures for Intermediate Corrosion Protection

Table 6.12 - Intermediate Corrosion Protection Measures

Design Component	Protection Requirements	Comments
Concrete:		
w/c ratio	0.45 maximum	
mineral admixtures	optional	Mineral admixtures such as fly ash and silica fume may be required to meet permeability requirements. Required mineral admixture quantities can be determined based on permeability, workability and strength requirements.
permeability	medium to low	Rapid chloride ion permeability according to AASHTO T277[6.12] or ASTM C1202.[6.13] Concrete permeability requirements are similar to those proposed for performance based specifications for concrete.[6.14] Reduced permeability may be achieved using low water-cement ratios and mineral admixtures.
Mild Steel Reinforcement	epoxy-coated reinforcement	Coating quality is extremely important to the effectiveness of epoxy-coated reinforcement, as indicated by recent research[6.15,6.16] and the poor durability performance of some structures with epoxy-coated bars.
Prestressing Strand	bare strands (uncoated)	Increased protection options may not be warranted at the intermediate protection level.
Post-Tensioning Duct	plastic ducts should be used vacuum testing or pressure testing for leaks should be performed prior to grouting	Plastic ducts should be used with watertight couplers for duct splices and connection to anchorage hardware. Plastic duct systems may be tested for air leaks prior to grouting. Leaks should be identified and sealed to ensure a waterproof protection barrier for the tendon.
Post-Tensioning Grout	$w/c \leq 0.44$	Standard grout[6.11] should be adequate for intermediate protection levels, provided that proper grouting procedures are used (see Section 2.4.4.4). The use of expanding admixtures and corrosion inhibitors should be discouraged based

		on experimental results.[6.17,6.18] If large vertical distances are encountered in the tendon profile, the use of Post-Tensioning Grout Option 2 in Table 6.13 should be considered.

Table 6.12 - Intermediate Corrosion Protection Measures - Continued

Design Component	Protection Requirements	Comments
Anchorage Protection	anchorages should be located in recessed pockets pockets should be filled with non-shrink concrete or mortar pocket surfaces and exposed anchorage components should be coated with an epoxy bonding agent prior to filling	Requirements are based on TxDOT Specifications[6.19] and practice, and past research (see Section 2.7).
Post-Tensioning System	standard post-tensioning systems	Increased protection options may not be warranted at the intermediate protection level.

6.6.3.3 Specific Measures for Maximum Corrosion Protection

Table 6.13 - Maximum Corrosion Protection Measures

Design Component	Protection Requirements	Comments
Concrete:		
w/c ratio	0.40 maximum	Water-cement ratios as low as 0.27 have been used successfully to produce high strength, low permeability concrete for bridges.
mineral admixtures	optional	Mineral admixtures such as fly ash and silica fume will be required to meet reduced permeability requirements in almost all cases. Required mineral admixture quantities can be determined based on permeability, workability and strength requirements. Quantities such as those recommended for protection against sulfate attack (Table 6.11) should be sufficient for corrosion protection.

permeability	low or very low	Rapid chloride ion permeability according to AASHTO T277[6.12] or ASTM C1202.[6.13] Concrete permeability requirements are similar to those proposed for performance based specifications for concrete.[6.14] Reduced permeability may be achieved using low water-cement ratios and mineral admixtures.

Table 6.13 - Maximum Corrosion Protection Measures - Continued

Design Component	Protection Requirements	Comments
Mild Steel Reinforcement: Option 1	epoxy-coated reinforcement – where possible, all fabrication including assembly of reinforcement cages should be performed prior to epoxy coating	Reinforcement coating after fabrication of the cages was done for the construction of the Great Belt Link in Denmark.[6.20] This is intended to minimize coating damage due to bending and assembly of the cages. Past research[6.15,6.16] and poor durability performance of some structures with epoxy-coated bars have emphasized the importance of coating quality.
Mild Steel Reinforcement: Option 2	stainless steel reinforcement	Research has shown excellent corrosion resistance of stainless steel reinforcement in concrete in comparison to galvanized and epoxy-coated reinforcement.[6.21,6.22,6.23] Evaluation of cost data has shown increases of 6% to 16% in overall project costs when stainless steel reinforcement is specified.[6.22] When life cycle costs are considered, stainless steel may be more cost effective than its alternatives.
Prestressing Strand	epoxy-coated and filled strands	Research[6.18,6.24] has demonstrated excellent performance of epoxy-coated strand in comparison to bare strand.
Post-Tensioning Duct	plastic ducts should be used vacuum testing or pressure testing for leaks should be performed prior to grouting	Plastic ducts should be used with watertight couplers for duct splices and connection to anchorage hardware. Plastic duct systems may be tested for air leaks prior to grouting. Leaks should be identified and sealed to ensure a waterproof protection barrier for the tendon.
Post-Tensioning Grout: Option 1	w/(c + p) = 0.35 30% Fly ash by weight superplasticizer as needed for fluidity	Grout based on research by Schokker.[6.25] This grout offers excellent corrosion protection. Superplasticizer dosage should be determined using a flow cone test for fluidity (ASTM C939[6.26]).

Post-Tensioning Grout: Option 2	w/c = 0.32 anti-bleed admixture superplasticizer as needed for fluidity	Grout based on research by Schokker.[6.25] This grout offers good corrosion protection and high resistance to bleed, and should be used in situations where large variations in height occur along the tendon profile. Superplasticizer dosage should be determined using a flow cone test for fluidity.[6.26] Anti-bleed admixture dosage should be based on the Gelman Pressure Test (see Ref. 6.18 and 6.25).

Table 6.13 - Maximum Corrosion Protection Measures – Continued

Design Component	Protection Requirements	Comments
Anchorage Protection	anchorages should be located in recessed pockets pockets should be filled with non-shrink concrete or mortar pocket surfaces and exposed anchorage components should be coated with an epoxy bonding agent prior to filling	Requirements are based on TxDOT Specifications[6.19] and practice, and past research (see Section 2.7).
Post-Tensioning System	specialized encapsulated post-tensioning systems for aggressive environments should be used. (e.g., VSL CS-Super Post-Tensioning System)	Encapsulated and electrically isolated post-tensioning systems meet many of the suggestions of the U.K. Concrete Society Report on Durable Bonded Post-tensioned Concrete Bridges.[6.27] The cost of the VSL CS-Super Post-tensioning System is approximately 10% to 12% higher than standard VSL multi-strand tendon anchorage systems.[6.28] The anchorages are less expensive due to the use of the composite bearing plate (less steel), but the PT-Plus plastic duct is more expensive than galvanized steel duct.[6.28] When overall project costs are considered, a project cost increase of much less than 10% would be expected.

6.7 Durability Design Procedure

The preceding sections have presented a generalized procedure for bridge substructure durability design. The steps of the durability design process are summarized below.

1. Determine the location and general configuration of the bridge under consideration.
2. Use Figure 6.2 to determine what forms of attack on durability may be expected for the given location and environment.
3. Assess the severity of the environmental exposure using Figure 6.3 for freeze-thaw damage, Table 6.1 for sulfate attack and Figure 6.4 for corrosion in deicing chemical exposures. For corrosion in coastal exposures, the environmental exposure may be taken as severe.
4. Assess the severity of the member exposure for each substructure component using Table 6.2 for freeze-thaw environments, Table 6.4 for sulfate attack environments, and Table 6.6 for reinforcement corrosion environments.
5. Determine the required level of protection for each substructure component and form of attack using Table 6.8.
6. Select the necessary protection measures from those presented in Section 6.6.

Chapter 6 References:

6.1) **Watkins, D.A.,** "Specification of Air Entrainment for Freezing and Thawing Environments," Master of Science Thesis, The University of Texas at Austin, August 1997.

6.2) **ACI Committee 201,** "Guide to Durable Concrete" (ACI 201.2R-92), American Concrete Institute, Detroit, MI, 1992, 41 pp.

6.3) **American Society for Testing and Materials,** "Standard Test Method for Resistance of Concrete to Rapid Freezing and Thawing," ASTM C666-97, Philadelphia, PA, 1997.

6.4) **American Society for Testing and Materials,** "Standard Test Method for Critical Dilation of Concrete Specimens Subjected to Freezing," ASTM C671-94, Philadelphia, PA, 1994.

6.5) **American Society for Testing and Materials,** "Standard Practice for Evaluation of Frost Resistance of Coarse Aggregates in Air-Entrained Concrete by Critical Dilation Procedures," ASTM C682-98, Philadelphia, PA, 1998.

6.6) **American Society for Testing and Materials,** "Standard Specification for Portland Cement," ASTM C150-97a, Philadelphia, PA, 1997.

6.7) **American Society for Testing and Materials,** "Standard Specification for Coal Fly Ash and Raw or Calcined Natural Pozzolan for Use as a Mineral Admixture in Concrete," ASTM C618-98, Philadelphia, PA, 1998.

6.8) **AASHTO**, LRFD Bridge Construction Specifications, 1st Edition, American Association of State Highway and Transportation Officials, Washington, D.C., 1998.

6.9) **Freeman, R.B.,** "Optimization of the Physical and Compositional Characteristics of Fly Ash Cement for the Production of Sulfate Resistant Concrete," Doctor of Philosophy Dissertation, The University of Texas at Austin, August 1992.

6.10) **AASHTO**, LRFD Bridge Design Specifications, 2nd Edition, American Association of State Highway and Transportation Officials, Washington, D.C., 1998.

6.11) Standard Specifications for Construction of Highways, Streets and Bridges, Texas Department of Transportation, March 1995.

6.12) **American Association of State Highway and Transportation Officials,** "Rapid Determination of the Chloride Permeability of Concrete," AASHTO T277, Washington, D.C., 1983.

6.13) **American Society for Testing and Materials,** "Standard Test Method for Electrical Indication of Concrete's Ability to Resist Chloride Ion Penetration," ASTM C1202-97, Philadelphia, PA, 1997.

6.14) **Goodspeed, C.H., Vanikar, S., and Cook, R.A.,** "High Performance Concrete Defined for Highway Structures," *Concrete International*, Vol. 18, No. 2, February, 1996, pp. 62-67.

6.15) **Vaca-Cortes, Enrique**, "Corrosion Performance of Epoxy-Coated Reinforcement in Aggressive Environments," Doctor of Philosophy Dissertation, The University of Texas at Austin, May 1998.

6.16) **Kahhaleh, K.Z.,** "Corrosion Performance of Epoxy Coated Reinforcement," Doctor of Philosophy Dissertation, Department of Civil Engineering, The University of Texas at Austin, May 1994.

6.17) **Koester, B.D.,** "Evaluation of Cement Grouts for Strand Protection Using Accelerated Corrosion Tests," Master of Science Thesis, The University of Texas at Austin, December 1995.

6.18) **Hamilton, H.R.,** "Investigation of Corrosion Protection Systems for Bridge Stay Cables," Doctor of Philosophy Dissertation, The University of Texas at Austin, September 1995.

6.19) Standard Specifications for Construction of Highways, Streets and Bridges, Special Provision to Item 426 (Prestressing), Sub-Section: Construction Methods, Texas Department of Transportation, 1995. (also, personal communication with Dean Van Landuyt, Texas Department of Transportation, April 1997.)

6.20) **Vincentsen, L.J. and Henriksen, K.R.**, "The Great Belt Link - Built to Last," *Concrete International*, Vol. 14, No. 7, July, 1992, pp. 30-33.

6.21) **Rasheeduzzafar, Dakhil, F.H., Bader, M.A., and Kahn, M.M.**, "Performance of Corrosion Resisting Steels in Chloride-Bearing Concrete," *ACI Materials Journal*, Vol. 89, No. 5, September-October 1992, pp. 439-448.

6.22) **McDonald, D.B., Sherman, M.R., Pfeifer, D.W., and Virmani, Y.P.**, "Stainless Steel Reinforcing as Corrosion Protection," *Concrete International*, Vol. 17, No. 5, May 1995.

6.23) **McDonald, D.B., Pfeifer, and Blake, G.T.,** "The Corrosion Performance of Inorganic, Ceramic and Metallic-Clad Reinforcing Bars and Solid Metallic Reinforcing Bars in Accelerated Screening Tests," FHWA-RD-96-085, Federal Highway Administration, Mclean, Va, October 1996, 112 pp.

6.24) **Perenchio, W.F., Fraczek, J., and Pfeifer, D.W.,** "Corrosion Protection of Prestressing Systems in Concrete Bridges," NCHRP 313, Transportation Research Board, Washington, D.C., 1989, 25 pp.

6.25) **Schokker, Andrea J.,** "Improving Corrosion Resistance of Post-Tensioned Substructures Emphasizing High Performance Grouts," Doctor of Philosophy Dissertation, The University of Texas at Austin, August 1999.

6.26) **American Society for Testing and Materials,** "Standard Test Method for Flow of Grout for Preplaced-Aggregate Concrete (Flow Cone Method)," ASTM C939-97, Philadelphia, PA, 1997.

6.27) "Durable Bonded Post-Tensioned Concrete Bridges," Technical Report No. 47, The Concrete Society, Slough, Berkshire, U.K., August 1996, 64 pp.

6.28) **Silvestri, Giovanni**, VSL Corporation, Grand Prairie, Texas, Personal Communication, June 1996.

Chapter 7:

Summary and Conclusions

7.1 Research Summary

The research described in this dissertation deals with the interrelationship between bridge substructure durability and the use of post-tensioning in bridge substructures. The durability of bridge substructures has not received the same level of attention in research and design that bridge decks have. In some situations the substructure durability is now controlling the service life of the bridge, signaling the need for increased attention to the durability of bridge substructures. Post-tensioning can provide an efficient substructure design option in many cases. Post-tensioning in substructures has not been widely used to date, but its use is expected to increase in the future. Post-tensioning can improve substructure durability, but it introduces additional factors that must be considered during the durability design process. These issues illustrated the need for durability design guidelines for post-tensioned bridge substructures, and TxDOT Project 0-1405 was developed with the following objectives:

1. To examine the use of post-tensioning in bridge substructures,
2. To identify durability concerns for bridge substructures in Texas,
3. To identify existing technology to ensure durability or improve durability,
4. To develop experimental testing programs to evaluate protection measures for improving the durability of post-tensioned bridge substructures, and
5. To develop durability design guidelines and recommendations for post-tensioned bridge substructures.

Project 0-1405 has a very broad scope. A large research program involving an in depth literature review and several experimental testing programs was developed to address the objectives. Four graduate students have worked on Project 0-1405 to date, and

additional graduate students will see the project to its completion through long term exposure testing and forensic examinations.

This dissertation represents the author's contribution to Project 0-1405. The project aspects covered in this document include an extensive literature review on the subject of bridge substructure durability and corrosion in prestressed concrete (Chapter 2), the development and implementation of long term exposure testing programs for beam and column elements (Chapter 3 and Chapter 4), and long term monitoring and specimen autopsy for a macrocell corrosion specimen study of corrosion in precast segmental bridges (Chapter 5). Preliminary durability design guidelines for post-tensioned bridge substructures were presented in Chapter 6 based on the reviewed literature and early experimental results. The three testing programs are ongoing and will be completed by others.

Chapter 2 presents a literature review of several key aspects related to durability of post-tensioned bridge substructures. The literature review was used to develop the long term beam and column testing programs. It was also used to present a summarize a wealth of information on concrete durability and on corrosion protection for post-tensioned concrete. This resource was used extensively in the development of the preliminary durability design guidelines presented in Chapter 6.

Chapter 3 presents preliminary exposure test data for the long term beam corrosion tests. The early test data indicates varied levels of corrosion activity, but no visible corrosion related structural deterioration is apparent. Continued exposure testing and monitoring, combined with forensic examinations of the beams, will provide considerably more information and insight into corrosion in post-tensioned structural elements. Some preliminary conclusions have been made based on the results for this reporting period. Because the conclusions are based on preliminary data, they could be subject to change.

Chapter 4 presents twenty-six months of exposure test data. The results gathered during this period indicate relatively stable corrosion activity for most of the column specimens. Half-cell potential and chloride penetration data suggests some specimens may be experiencing corrosion activity, but no significant visual indications of corrosion damage have been observed. Continued exposure testing and monitoring, combined with

partial and complete forensic examinations of the columns will provide considerably more information and insight into corrosion in post-tensioned structural elements. Some preliminary conclusions have been drawn from the test data, but could be subject to change as more data is accumulated.

Chapter 5 describes four and a half years of exposure testing for a macrocell corrosion testing program for internal tendons in precast segmental bridges. Almost all of the corrosion activity measured during this period occurred in specimens with match-cast dry joints (eleven of twelve specimens with corrosion). One half of the macrocell specimens were removed from testing for a complete forensic examination. The remaining specimens continue to undergo exposure testing. A number of conclusions are presented based on the exposure test data and autopsy results. Continued exposure testing may provide additional results to assist comparison of variables.

7.2 Conclusions

7.2.1 Long Term Beam Exposure Tests

7.2.1.1 Overall Performance

- No significant indications of corrosion damage were present during ten months of exposure. Some rust staining and spalling was evident due to corrosion of the steel bolster strips.
- Chloride measurements indicate chlorides have not penetrated to the level of the reinforcement in uncracked concrete.
- Half-cell potentials suggest a high probability of corrosion activity in more than half of the beam specimens.
- Actual assessment of the corrosion severity occurring during this exposure duration requires invasive techniques to provide a visual examination of the steel condition.

7.2.1.2 Post-Tensioning to Improve Corrosion Protection

- Half-cell potential measurements suggest that increased corrosion activity is related to increased numbers and widths of cracks.

- A significant reduction in half-cell potentials was observed for the 100%U PS and 100%S PS beam types in comparison to the 2/3 PS and Non-PS beams, suggesting that prestress may improve corrosion protection.
- Corrosion rate measurements indicated corrosion activity is related to cracking:
  - Corrosion rate measurements on uncracked Beams 1.1, 3.1 and 3.2 were significantly lower than measured rates on companion cracked specimens.
  - Higher corrosion rates were measured at crack locations, suggesting that on a local scale cracks lead to increased corrosion activity in comparison to uncracked concrete.
- Corrosion rate measurements at crack locations in post-tensioned beams were as high or higher than corrosion rates at cracks in non-prestressed beams. This illustrates the significance of cracking on corrosion, at least in the short term.
- Assessing the effect of post-tensioning on corrosion protection depends on the criteria used to quantify the severity of corrosion. If corrosion rates at crack locations are used as criteria, there appears to be little or no positive effect of post-tensioning. If overall corrosion damage in the structural element is considered, post-tensioning improves corrosion protection by limiting the number of cracks and thus limiting the total deterioration due to corrosion.
- Overall, the preliminary test data indicates that corrosion protection can be improved through crack control with post-tensioning.

7.2.1.3 Crack Width Prediction for Structural Concrete with Mixed Reinforcement

- Comparison of measured crack data with several crack prediction models produced widely varying results. This finding suggests that not all crack prediction methods are appropriate for structural concrete members with a combination of mild steel and prestressed reinforcement.
- The Gergely-Lutz crack width model provided an excellent prediction of maximum crack widths for the Non-PS and 2/3 PS beams, and a conservative estimate for the 100%U PS beams.
- The Batchelor and El Shahawi crack width expression provided a very good prediction of maximum crack widths for the 2/3 PS and 100%U PS beams.

7.2.1.4 Corrosion Rate Measurements Using Polarization Resistance

- Corrosion rate measurements were obtained using two different devices: 3LP and PR Monitor.
- Corrosion rates obtained using the 3LP device were extremely high and did not correlate with specimen condition and half-cell potentials. The PR Monitor indicated lower corrosion activity than the 3LP, although moderate to high corrosion rates were indicated for most beams.
- The corrosion activity indicated by both devices, and in particular the 3LP, contradicted the half-cell potential measurements for some specimens. Numerous possible factors were investigated, but no firm conclusions could be made other than several limitations exist for the 3LP device and the polarization resistance technique in general.
- The PR Monitor appears to provide a better assessment of corrosion rate than the 3LP device. Because of differences between the devices, it is not recommended to directly compare corrosion rates obtained using the 3LP and PR Monitor.
- The 3LP device suffers from an unconfined polarizing signal, and corrosion rates will be overestimated in most cases.
- The three electrode technique for measuring polarization resistance appears to be most useful for relative comparisons of corrosion activity under similar conditions rather than a quantitative assessment of corrosion rate.
- Regular corrosion rate measurements over time are needed to assess the amount of corrosion related distress in structural concrete. Discrete measurements may occur at instances where corrosion rates are higher or lower than normal, and give a false indication of the specimen or structural element condition.

7.2.2 Long Term Column Exposure Tests

7.2.2.1 Overall Performance

- No significant corrosion damage was apparent during twenty-six months of severe, accelerated exposure conditions.
- Chloride analysis of samples taken from four columns indicated chloride levels in one column were in excess of the threshold for corrosion at the level of reinforcement.

- Half-cell potential data does not strongly suggest corrosion initiation in any of the column specimens.
- An actual assessment of corrosion severity can not be made from the half-cell potential and chloride penetration data. An invasive inspection including a visual examination of the steel condition is necessary to determine corrosion severity.

7.2.2.2 Post-Tensioning to Improve Corrosion Protection

- Measured chloride profiles near the column to foundation construction joint indicate a reduction in chloride penetration for post-tensioned columns in comparison to non-prestressed doweled connections and the no joint condition. This preliminary data suggests post-tensioning could improve corrosion protection by reducing the penetration of moisture and chlorides.
- Half-cell potential data indicates an uncertain probability of corrosion activity in post-tensioned columns. The half-cell potential data for the reporting period does not indicate a clear effect of joint type on corrosion activity.

7.2.2.3 Fly Ash as Partial Cement Replacement in Concrete

- The use of fly ash as partial cement replacement significantly reduced chloride penetration and vertical migration of chlorides in the column specimens. The fly ash concrete used in the testing program was standard TxDOT concrete for bridge substructures with 35% of the cement replaced with fly ash (35% by volume, 31% by weight). These findings suggest that simply replacing a portion of the cement with fly ash can improve corrosion protection for bridge columns.

7.2.2.4 Effectiveness of Coated Post-Tensioning Bars and Plastic Ducts

- The use of galvanized and epoxy-coated post-tensioning bars and plastic ducts is expected to improve corrosion protection in comparison to uncoated bars and galvanized steel ducts. The inherent limitations of half-cell potential measurements and low probability of corrosion activity during the reporting period do not permit an assessment of these corrosion protection measures. The best indication of the relative performance of coated and uncoated post-tensioning bars and the different ducts will be provided by a forensic examination at a later stage of exposure.

7.2.2.5 Assessing Corrosion Activity Using Half-Cell Potential Measurements

- Half-cell potential measurements proved to have limited usefulness in determining the relative performance of the variables in this testing program. The different materials investigated, the nature of half-cell potentials and the general complexity of the corrosion process resulted in data that did not indicate clear differences in corrosion activity and specimen performance.
- The best use of the half-cell potential data will be to indicate the initiation of corrosion by observing long term trends in the measured data. Therefore continued regular measurements are very important.

7.2.3 Segmental Joint Macrocell Specimens

7.2.3.1 Overall Performance

- Overall performance of the segmental macrocell corrosion specimens in this program is very good with only minor corrosion detected in a limited number of specimens.
- Metal loss calculations indicate that corrosion to date is minor or negligible.
- Possible strength degradation, in the form of pitting corrosion on prestressing strand, was found in only one specimen.

7.2.3.2 Segmental Joints

- All long term and significant corrosion has occurred in specimens with dry joints where eleven of fourteen specimens displayed corrosion activity. Test results indicate that dry joints do not provide corrosion protection for internal tendons where aggressive exposure may occur.
- The mild steel reinforcement is corroding instead of the prestressing strand in seven of the eleven dry joint specimens with corrosion activity. This occurrence is attributed to penetration of chlorides at the dry segmental joint and indicates a possible increased corrosion threat for mild steel reinforcement within the segment when dry joints are used. This could occur in bridges with external tendons, and highlights the importance of clear cover over the ends of longitudinal bars in the segments.
- One out of twenty-four specimens with epoxy joints has shown corrosion activity. Autopsy of this specimen confirmed that the mild steel reinforcement was corroding

rather than the prestressing strand. Measured chloride profiles for this specimen suggested that corrosion resulted from an external source of moisture and chlorides rather than from penetration at the epoxy joint or through the concrete.

- Only very minor prestressing strand corrosion was found in specimens with epoxy joints. Corrosion of the galvanized steel duct was reduced in extent and severity in specimens with epoxy joints. The experimental data to date indicates that thin epoxy joints provide substantially improved corrosion protection for internal tendons in segmental construction.
- The use of gaskets in epoxy joints may interfere with epoxy coverage on the joint. Autopsied epoxy/gasket joint specimens found incomplete epoxy coverage near the duct openings, leading to increased chloride penetration and duct corrosion.

7.2.3.3 Ducts for Internal Post-tensioning

- Strand corrosion was not detected during exposure testing in any epoxy joint specimens with plastic ducts. Reversed macrocell corrosion developed in the four dry joint specimens with plastic ducts. Formation of the reversed corrosion macrocells indicates that the plastic duct is providing improved corrosion protection for the prestressing strand (tendon), even when penetration of chlorides at the dry joints has caused rebar corrosion.
- Forensic examination revealed only very minor corrosion or discoloration on the prestressing strand from specimens with plastic ducts.
- Galvanized steel ducts were corroded in all cases. Duct corrosion led to concrete cracking along the line of the tendon in many specimens. Ducts were corroded through in nearly two-thirds of the specimens, eliminating the duct as corrosion protection for the prestressing tendon. Test results indicate the potential for durability problems when using galvanized ducts in aggressive exposures.
- Specimens with plastic ducts and epoxy joints had the best overall performance in the testing program in terms of strand, mild steel and duct corrosion.

7.2.3.4 Joint Precompression

- The range of joint precompression investigated did not affect the time to corrosion or corrosion severity for steel reinforcement.

7.2.3.5 Grouts for Bonded Post-tensioning

- The most severe corrosion of the prestressing tendon was found where calcium nitrite corrosion inhibitor was used in the grout. Test results suggest calcium nitrite should not be used in cement grouts.
- Two specimens with silica fume in the grout (and epoxy joints) did not show corrosion activity.

7.2.4 Durability Design Guidelines

- Preliminary durability design guidelines for post-tensioned bridge substructures were developed.
- Durability design guidelines provide information on assessing the types and severity of attack on durability for a given location in Texas. Guidance is provided for determining the required level of protection for durability, and options for protection measures are included.
- The preliminary durability design guidelines are based primarily on reviewed literature, and should be refined and expanded as experimental results become available.

7.3 Recommendations for Future Research

There are many unanswered questions at the conclusion of this dissertation. However, the broad scope of the testing programs and continued exposure testing will provide many opportunities to answer most of these questions. Several possible areas of future research that may not be addressed by the testing programs in Project 0-1405 are listed below.

- **Calcium Nitrite Corrosion Inhibitor:** Calcium nitrite performed poorly in the grout of one segmental joint macrocell corrosion specimen. However, it is apparent that the calcium nitrite dosage may have been too low for use in grout in this case. A small testing program considering varied calcium nitrite dosages in grout tested under non-accelerated (no imposed current or potential) corrosion test conditions could provide a final conclusion on the effectiveness of this corrosion inhibitor in grout.

- **Construction Requirements for Precast Segmental Columns:** Standard practice is to subject all match-cast segmental joints with epoxy to a precompression of 345 kPa (50 psi) for a period of forty-eight hours from the time of segment placement. This precompression is to ensure uniform epoxy coverage on the face of the segment during the epoxy curing period. While this requirement may be necessary in precast segmental superstructures, it is possible that this level of superimposed precompression may not be necessary in segmental columns where the self weight of the segments could provide the precompression. This needs to be investigated.
- **Crack Prediction:** If the long term exposure test data indicates a clear influence of cracking on corrosion related deterioration, better crack control provisions need to be developed. Crack prediction models should determine both the crack spacing and width, and must address mixed reinforcement designs.
- **Corrosion Rate Measurements:** Existing field evaluation techniques for measuring corrosion rate in reinforced concrete, such as polarization resistance, need to be evaluated for use in mixed reinforcement and fully post-tensioned designs. Additional factors such as the presence of the post-tensioning duct and prestressing strand requires investigation.
- **Condition Evaluation of Post-Tensioned Structures:** Additional techniques for assessing the extent and severity of corrosion in post-tensioned concrete elements need to be developed. Many techniques have been proposed, but all have met with only limited success to date.

Appendix A:

Crack Widths and Corrosion: Literature Review

This appendix provides a review of literature on the relationship between cracking and corrosion in structural concrete. The literature review covers the following sections:

A.1 Technical Organizations

A.1.1 Design Codes and Specifications

A.1.2 Technical Committee Recommendations

A.2 Research - Crack Widths and Corrosion

A.2.1 Reinforced Concrete Research - Short Term Corrosion Tests

A.2.2 Reinforced Concrete Research - Long Term Corrosion Tests

A.2.3 Prestressed Concrete Research

A discussion of each of the two main sections is provided in Section 2.4.2.

This literature review was originally prepared in 1994. Brad Koester[A.1] contributed to Sections A.2.1 and A.2.2 of the original draft.

The literature review was expanded and revised in 1996 and 1999.

A.1 Technical Organizations

The following sections present the recommendations and guidelines, related to cracking and the prevention of corrosion, published by various technical organizations around the world. These publications include major building and bridge codes and specifications for structural concrete in North America, Europe and Japan, and the publications of several technical committees from the American Concrete Institute (ACI) and the Comite Euro-International Du Beton (CEB). Some of the publications do not address crack control as a method of corrosion protection, specifying other measures instead. These publications have been discussed briefly for the completeness of the literature summary.

A.1.1 Design Codes and Specifications

A.1.1.1 ACI 318-95

The American Concrete Institute (ACI) Publication ACI 318-95, "Building Code Requirements for Structural Concrete,"[A.2] is widely used for the design of structural concrete. Although ACI 318-95 has an entire chapter devoted to durability (Chapter 4), the effect of cracking on durability is not addressed. Rather, protection against corrosion of reinforcement is addressed through specification of a maximum water-cement ratio, minimum concrete strength and maximum chloride ion content for concrete mix constituents. The control of crack widths in ACI 318-95 is addressed implicitly in Clause 10.6 (Distribution of flexural reinforcement in beams and one-way slabs). For reinforcement with nominal yield strength less than 40 ksi (300 MPa), no specific requirements are necessary. For reinforcement with yield strengths exceeding 40 ksi, Clause 10.6.4 provides an empirical expression based on the Gergely-Lutz equation for crack widths,[A.3] written in a form that emphasizes reinforcement details (spacing and cover) and the level of stress in the bars at service load levels. The quantity "Z" is calculated using equation (10-4) of Clause 10.6.4 (shown below) and is compared to the limits of 175 kips/in (30.6 kN/mm) for interior exposure and 145 kips/in (25.4 kN/mm) for exterior exposure. A specific definition is not given for interior or exterior exposures. These limits for Z correspond to surface crack widths of 0.016 in. (0.4 mm) for interior exposures and 0.013 in. (0.34 mm) for exterior exposures. The basis of selection for the limiting values of Z (allowable crack widths) is not provided in either ACI 318-95 or its commentary.

$$Z = f_s \sqrt[3]{d_c A} \qquad \text{(kips/in. or kN/mm)} \qquad (10\text{-}4)^{A.2}$$

where:

f_s = calculated stress in reinforcement at service loads

d_c = thickness of concrete cover measured from extreme tension fiber to center of bar or wire closest thereto

A = effective tension area of concrete surrounding the flexural tension reinforcement and having the same centroid as that reinforcement, divided by the number of bars or wires

Equation (10-4) is a modification of the Gergely-Lutz[A.3] expression described in Section 2.8. By comparing Equation (10-4) with the Gergely-Lutz equation, the following definition is obtained for Z:

$$Z = \frac{w}{(7.6x10^{-5})\beta} \qquad \text{(units of kip/in. for Z and inches for w)}$$

For beams, β may be taken as 1.2, and the limiting values of Z corresponding to the desired maximum surface crack widths are obtained.

Although the approach of Section 10.6 is to address reinforcement details and to de-emphasize crack widths, from the preceding discussion, it is clear that the underlying principle remains to be allowable crack widths. The move by ACI away from crack widths to the quantity Z was primarily for legal reasons. Due to the nature of cracking and the wide variability involved in predicting crack widths, comparison of predicted crack widths to the measured crack widths in situ often revealed inconsistencies which were used either justly or unjustly in cases of dispute. Thus, by utilizing the parameter Z which has no physical meaning, measured crack widths could no longer be compared to Code provisions for crack control, avoiding unnecessary legal action on the basis of cracking.

As mentioned previously, the limiting values of Z are proposed for interior and exterior exposures. For severe exposures, no explicit recommendations are made. Instead, Clause 10.6.5 states:

> "**10.6.5** - Provisions of 10.6.4 are not sufficient for structures subjected to very aggressive exposure or designed to be watertight. For such structures, special investigations and precautions are required."

Unfortunately, no special investigations or precautions are suggested. The commentary for 10.6.5 provides the following comments:

> "**R10.6.5** - Although a number of studies have been conducted, clear experimental evidence is not available regarding the crack width beyond which a corrosion danger exists. Exposure tests indicate that concrete quality, adequate compaction and ample concrete cover may be of greater importance for corrosion protection than crack width at the concrete surface. The limiting values for Z were, therefore, chosen primarily to give reasonable reinforcing details in terms of practical experiences with existing structures."

The implicit provisions for crack control described above are intended for mild steel reinforcement. ACI 318-95 does not provide any form of similar requirements for the

use of prestressing steel in prestressed elements or mixed reinforcement (partial prestressing) schemes. Clause 18.1.3 states that Clause 10.6 shall not apply to prestressed concrete. However, it should be noted that ACI 318-95 does not recognize the partial prestressing or prestressed components that are designed to be cracked under service load levels.

A.1.1.2 AASHTO LRFD Bridge Design Specifications

The American Association of State Highway and Transportation Officials (AASHTO) LRFD Bridge Design Specifications[A.4] list cracking as an action to be considered at the Service Limit State (Clause 5.5.2). The AASHTO LRFD Specifications address crack control implicitly through detailing requirements in Clause 5.7.3.4. This clause uses a similar approach to ACI 318-95,[A.2] with slight modifications. A modified form of the Gergely-Lutz expression is used, but re-arranged such that a limiting stress at service loads is computed as a function of reinforcement detailing and the quantity Z. The procedure is as follows:

$$f_{sa} \le \frac{Z}{\sqrt[3]{d_c A}} \le 0.6 f_y \qquad (5.7.3.4\text{-}1)^{A.4}$$

where:

f_{sa} = calculated stress in reinforcement at service loads

d_c = thickness of concrete cover measured from extreme tension fiber to center of bar or wire closest thereto

A = effective tension area of concrete surrounding the flexural tension reinforcement and having the same centroid as that reinforcement, divided by the number of bars or wires

Another difference between the AASHTO LRFD Specifications and ACI 318-95 is that the AASHTO document specifies slightly stricter limits on the value of Z. The limits for Z are 170 kips/in. (29.8 kN/m) for moderate exposure conditions, 130 kips/in. (23 kN/m) for severe exposure conditions and 100 kips/in. (17.5 kN/mm) for buried structures. These values correspond to allowable surface crack widths of 0.0155 in. (0.39 mm), 0.0118 in. (0.33 mm) and 0.009 in. (0.24 mm), respectively.

The commentary states the following regarding Equation 5.7.3.4-1:

> "There appears to be little or no connection between surface crack width and corrosion. Thicker or additional cover for reinforcement will result in greater surface crack widths. These wider crack widths are not detrimental to the corrosion protection of the reinforcement."[A.4]

The commentary goes on to state that in view of the above statement, Equation 5.7.3.4-1 should only be used for concrete cover less than or equal to 2 in. (50 mm). If the cover

exceeds 2 in. (50 mm), a limiting value of 2 in. (50 mm) should be used in Equation 5.7.3.4-1.

For aggressive exposure or corrosive environments, the commentary states:

> "… additional protection beyond that provided by satisfying Equation 5.7.3.4-1 may be provided by decreasing the permeability of the concrete and/or waterproofing the exposed surface."[A.4]

The commentary also states

> "Structures subjected to very aggressive exposure are beyond the scope of these provisions. For such conditions, more restrictive limits on crack widths may be required. Narrower surface crack widths may be obtained by using the recommendations in ACI 350R."[A.4] (see Section A.1.2.4 for ACI 350R)

The AASHTO LRFD Specifications permit the use of partially prestressed members (i.e., prestressed members designed to crack under service load conditions (may or may not contain non-prestressed mild steel reinforcement)). Crack control for partial prestressed members is referred to Clause 5.7.3.4, described above. In this situation, bonded prestressing steel is included in the calculation of "A," and the increase in stress in the prestressing steel beyond decompression is used in place of f_{sa} in Equation 5.7.3.4-1. The values of Z are unchanged for partial prestressed members.

For fully prestressed members (uncracked at service load levels) Clause 5.9.4.2.2 limits the allowable concrete tensile stresses under service loads after losses to the following:

$6\sqrt{f'_c}$ psi ($0.5\sqrt{f'_c}$ MPa)	for components with bonded prestressing tendons or reinforcement subjected to moderate (or better) exposure conditions
$3\sqrt{f'_c}$ psi ($0.25\sqrt{f'_c}$ MPa)	for severe corrosive exposure conditions such as coastal areas
No tension	for members with unbonded prestressing tendons

In addition to crack control through detailing requirements, the AASHTO LRFD Specifications address corrosion protection in Section 5.12: Durability. Corrosion protection provisions consist of specification of minimum concrete cover for reinforcement. Requirements are given for various elements and exposure conditions. In general, these minimum cover requirements are the same as ACI 318-95 cover requirements. The minimum covers listed in Clause 5.12.3 may be reduced by 20% for water-cement ratios less than 0.40, and should be increased by 20% for water-cement ratios greater than 0.50. In addition to minimum cover requirements, Section 5.12 indicates that protection against chloride-induced corrosion can be provided by epoxy coating or galvanizing mild steel reinforcement, prestressing steel and post-tensioning ducts and hardware. Clause 5.12.4 allows the cover requirements for interior exposure to be used if

epoxy-coated reinforcement is used. No other information is given regarding corrosion protection or implementation of the positive corrosion protection described above.

A.1.1.3 CAN3-A23.3-M84

The Canadian Standards Association Publication CAN3-A23.3-M84, "Design of Concrete Structures for Buildings,"[A.5] uses the same approach for crack control as ACI 318-95. No explicit guidelines for crack widths are given, and crack control is implicitly considered by the distribution of mild steel flexural reinforcement in Clause 10.6.4. The approach used in Clause 10.6.4 is identical to Clause 10.6.4 of ACI 318-95. Similarly, the implied allowable surface crack widths are also 0.016 in. (0.4 mm) for interior exposures and 0.013 in. (0.33 mm) for exterior exposures.

An important difference between the crack control provisions of CAN3-A23.3-M84 and ACI 318-95 is that the Canadian Standard provides information for crack control for partially prestressed members. Clause 18.9.3 of CAN3-A23.3-M84 applies to prestressed members which are cracked under service loads (i.e. the allowable concrete tensile stress under service loads is exceeded). Clause 18.9.3.3 is based on the same form of the Gergely-Lutz crack width expression as Clause 10.6.4 for non-prestressed sections (Equation (10-4)), but with stricter limits for Z. The specified maximum limits for Z in partially prestressed members are 20 kN/mm (115 kips/in.) for interior exposure and 15 kN/mm (85 kips/in.) for exterior exposure. These values of Z correspond to surface crack widths of 0.26 mm (0.010 in.) and 0.20 mm (0.008 in.). The commentary for Clause 18.9.3.3 states that the stricter limits applied to partially prestressed members are necessary due to "uncertainties in computing crack widths for partially prestressed members and because prestressing steel is more susceptible to corrosion."[A.5]

A.1.1.4 Ontario Highway Bridge Design Code - 1991

Section 8-11 of the Ontario Highway Bridge Design Code (OHBDC)[A.6] contains the minimum requirements for durability of concrete structures. The emphasis of this section is the protection of reinforcement and other hardware from corrosion. The OHBDC addresses durability through concrete cover and protective coatings. Concrete covers are specified for various members types and exposure conditions. Protective coatings are required on reinforcement, anchorages, internal post-tensioning ducts and hardware specified for use within 100 mm (4 in.) of a surface subjected to moisture containing de-icing chemicals. Recommended protective coatings include, in general, epoxy, painting, galvanizing and metalizing. Corrosion resistant material (e.g. polyethylene) may be used for internal post-tensioning ducts in place of protective coating in this situation.

Crack control is addressed separately by the OHBDC in Section 8-12. Crack control is provided by emphasizing the distribution of reinforcement rather than by emphasizing crack widths. A parameter β_2 is computed based on the details of the section, the level of stress in the steel and the ratio of the moment at which the tensile concrete stress reaches $0.4f_{cr}$ to the moment under service loads.

$$\beta_2 = (0.9\,s_c + 2.0\,c_c)\,f_s\left[1 - (M_w / M_s)^2\right]$$

where

f_s = tensile stress in non-prestressed reinforcing bar nearest to the tensile face at the serviceability limit state, MPa (may be taken as 240 MPa (35 ksi) in non-prestressed members)

s_c = clear space between reinforcing bars nearest to the tension face, mm

c_c = clear cover to the reinforcing bar nearest to the tension face, mm

M_w = moment at a section when a tensile stress of $0.4f_{cr}$ is induced in the concrete, N-mm

f_{cr} = cracking strength of concrete

M_s = moment at a section at a serviceability limit state load, N-mm.

Limits for β_2 are given as 50 kN/mm (285 kips/in.) for non-prestressed members and 30 kN/mm (170 kips/in.) for prestressed members. These values correspond to average crack widths at the level of the reinforcement of 0.25 mm (0.010 in.) and 0.15 mm (0.006 in.) for non-prestressed and prestressed members, respectively.[A.7] It is important to emphasize that these crack width limits are specified for the crack width at the level of the steel rather than at the surface of the concrete, as in most cases. The crack widths specified above correspond to flexural crack widths at first loading of a member.

A.1.1.5 CEB-FIP Model Code 1990

The Comite Euro-International Du Beton (CEB) Bulletin No. 213/214 reports the CEB-FIP Model Code 1990.[A.8] The CEB-FIP Model Code addresses cracking as a specific limit state in Section 7.4 of the Model Code. The design criteria for cracking is that the functional requirements, durability and appearance of the structure should not be affected by cracking. This criteria may be satisfied by analytical procedures (calculated crack widths versus tolerable limits) or by practical detailing rules. This approach is applied to both non-prestressed and prestressed members, with slightly different requirements for each.

Analytical Procedures (Crack Widths)

A very complex crack prediction method is presented in the 1990 Model Code. The predicted characteristic crack widths are compared to allowable limits. The crack prediction method is described in detail in Section 2.8.

For non-prestressed reinforcement, the nominal limit of surface crack width is 0.30 mm (0.012 in.) for exposure conditions including humid environments, with or without de-icing agents and seawater environments. This limit is assumed to be satisfactory for both appearance and durability. For a dry environment, this limit may be relaxed.

For prestressed reinforcement, stricter requirements for crack widths are proposed. Surface crack width limitations are given for various exposure conditions for

both post-tensioned and pre-tensioned members, as shown in Table A.1. As the environmental conditions become more severe, cracking is not permitted by not allowing tension in the section. This requirement may be relaxed to a surface crack width of 0.20 mm (0.008 in.) if coated tendons or an impermeable duct are used.

Table A.1 - Surface Crack Width Limits for Prestressed Members (CEB-FIP Model Code 1990)

Exposure Condition	Post-tensioned	Pre-tensioned
Dry Environment	0.008in. (0.20mm)	0.008in. (0.20mm)
Humid Environment	0.008in. (0.20mm)	Decompression
Humid Envir. with Frost & De-icing Agents	No Tension Allowed Within Section OR Use coated tendons or impermeable ducts (w = 0.2mm)	
Seawater Environment		

An important note to accompany this information is given in the commentary for subsection 7.4.1.1:

> "... due to the actual state of the art and the highly probabilistic nature of the related phenomena, such nominal crack width values may only serve as a means to apply the design criterion..., and can in no case be compared to actual crack widths measured in situ."[A.8]

Practical Detailing Rules

As an alternative to calculating crack widths, crack control may also be provided by satisfying the provisions of Section 7.4.4 of the CEB-FIP Model Code. Provisions for reinforcement details are given as maximum bar diameter and maximum bar spacing as a function of steel stress, for both reinforced sections and prestressed sections. This information is shown in Table A.2. The steel stresses are to be calculated under quasi-permanent loads for reinforced concrete and under frequent loads and the characteristic value of prestress for prestressed sections. When these detailing provisions are used, surface crack widths will not generally exceed the value of 0.30 mm (0.012 in.) for reinforced elements and 0.20 mm (0.008 in.) for prestressed elements.

Table A.2 - Maximum Bar Diameter and Spacing for Which No Crack Width Calculation is Needed (CEB-FIP Model Code 1990)

Steel Stress (MPa)	Maximum Bar Diameter (mm)		Maximum Spacing (mm)	
	Reinforced Sections	Prestressed Sections	Reinforced Sections	Prestressed Sections
160	32	25	300	200
200	25	16	250	150
240	20	12	200	100
280	14	8	150	50
320	10	6	100	--
360	8	5	60	--
400	6	4	--	--
450	5	--	--	--

A.1.1.6 British Standard CP110

The British Standards Institution Publication CP 110, "Code of Practice for The Structural Use of Concrete"[A.9] addresses cracking as a separate limit state. The general requirement of Clause 2.2.3.2 is that "cracking of concrete should not adversely affect the appearance or durability of the structure."[A.9] To meet this requirement, some "reasonable limits" are provided. A formula for computing surface crack width is provided in Appendix A of CP 110.

For reinforced concrete members, CP 110 limits surface crack widths to 0.3 mm (0.012 in.). For severe environments, such as alternate wetting and drying or exposure to seawater, the surface crack width is limited to 0.004 times the nominal cover to the main reinforcement. For 50 mm (2 in.) cover, surface crack widths would be limited to 0.2 mm (0.008 in.).

For prestressed concrete elements in which cracking is allowed (i.e. the design flexural tensile stress of the concrete is exceeded), the surface crack width is limited to 0.2 mm (0.008 in.) by CP 110. In severe environments, such as alternate wetting and drying or exposure to seawater, this limit is reduced to 0.1 mm (0.004 in.).

A.1.1.7 SIA Standard 162

The Swiss Society of Engineers and Architects Standard 162, "Concrete Structures,"[A.10] addresses cracking as a limit state. The general approach of SIA Standard 162 is to limit crack width through detailing and arrangement of reinforcement. Crack widths are not explicitly calculated and checked. Provisions are provided for normal requirements and for severe requirements. Normal requirements are defined as conditions where:

- Physical and chemical actions are insignificant
- Cracking produces no damage

- No special requirements regarding watertightness apply
- Cracking does not detract from the appearance of the structure

Severe requirements are defined as conditions where:

- Physical and chemical actions are significant
- Cracking can produce damage
- Watertightness is required
- Limiting crack widths is desirable for aesthetic reasons

For normal requirements, minimum reinforcement is specified to limit crack width in Clause 3.33.4. These requirements are based upon developing the tensile force corresponding to the initial formation of cracks, without yielding. The minimum area of reinforcement is given by

$$A_{s,min} = \frac{\alpha\beta f_{ct} A_{ct}}{f_y}$$

where:

α = factor to account for the influence of bar spacing

for spacing:	$\leq$ 100 mm	$\alpha = 1.0$
	150 mm	$\alpha = 1.1$
	200 mm	$\alpha = 1.2$
	250 mm	$\alpha = 1.3$
	300 mm	$\alpha = 1.4$

β = factor used to calculate the tensile force corresponding to the initial formation of cracks, taking into account the stress distribution:

for rectangular sections in flexure:	$\beta = 0.5$
for T or I shapes in flexure:	$\beta = 0.3$
for box girders in flexure:	$\beta = 0.3$
for members in direct tension:	$\beta = 0.8$ for $h < 0.3$ m
	$\beta = 0.5$ for $h > 0.8$ m
	(interpolate for $0.3 < h < 0.8$ m)

f_{ct} = design value of concrete tensile strength

= 2 MPa for $f_{cube} < 25$ MPa ($f'_c < 21.25$ MPa)

= 2.5 MPa for $f_{cube} > 25$ MPa ($f'_c > 21.25$ MPa)

A_{ct} = critical tension zone of the uncracked concrete section

f_y = design value of yield stress of reinforcing steel (≤ 460 MPa (66.7 ksi))

For severe requirements, the minimum reinforcement required for normal conditions is to be increased by 30%. In addition, stresses in reinforcing steel and increases in stress in prestressing steel are limited according to Clause 3.33.5. Under the actions of all long term loads and one variable load, the stresses in the reinforcing steel and increases in stress in prestressing steel must not exceed the allowable stresses shown in Figure A.1.

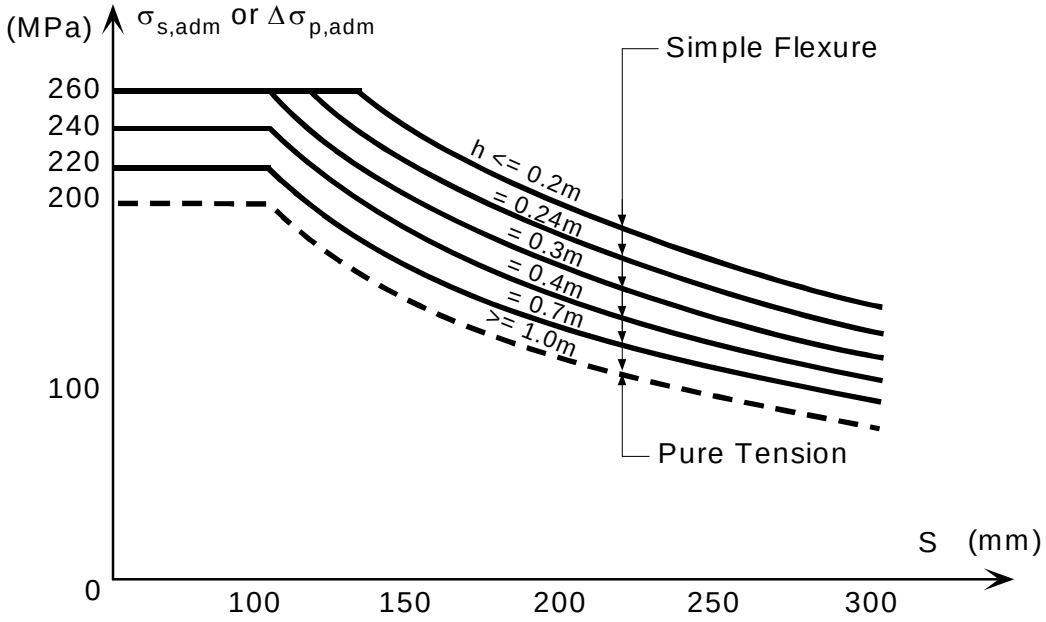

Figure A.1 -Limitation of Cracking Due to Loads (Severe Requirements): Stress in Reinforcing Steel and Increases in Stress in Prestressing Steel (SIA 162[A.10])

A.1.1.8 Standard Specification for Design and Construction of Concrete Structures-JSCE

The Japan Society of Civil Engineers (JSCE) publication SP-1, "Standard Specification for Design and Construction of Concrete Structures - 1986, Part 1 (Design),"[A.11] addresses cracking as a serviceability limit state. The provisions of Section 7.3 are intended to ensure that cracking does not impair the function, durability and appearance of concrete structures. The approach of the JSCE Standard is to ensure that computed surface crack widths satisfy permissible limits. For the purposes of defining permissible crack widths, three exposure conditions are considered: normal, corrosive and severely corrosive. Severely corrosive environments applies to marine structures exposed to tides and splashing. A corrosive environment is defined as severe alternate wetting and drying or marine structures submerged in seawater. Normal conditions constitute all other exposures.

Permissible surface crack widths specified by the JSCE Standard are defined in terms of the amount of concrete cover in Clause 7.3.3. Different crack widths are specified depending on the exposure condition and the type of steel, as shown in Table A.3. A procedure for computing surface crack widths in reinforced concrete and prestressed concrete members is given in Clause 7.3.4.

The JSCE standard specifies the concrete covers as a function of exposure condition, as shown in Table A.4. Thus, for a reinforced concrete beam, the range of permissible surface crack widths would be 0.15 mm (0.006 in.), 0.20 mm (0.008 in.) and 0.21 mm (0.0083 in.) for normal, corrosive and severely corrosive environments, respectively. For a prestressed concrete beam in a normal environment, the permissible surface crack width would be 0.12 mm (0.0047 in.). A permissible crack width for prestressing steel in a corrosive or severely corrosive environment is not given in Table 3. The commentary to Clause 7.3.3 advises that prestressed concrete members used in these environments should be designed to prohibit the formation of flexural cracks.

Table A.3 -Permissible Surface Crack Width (JSCE SP-1[A.11])

Type of Reinforcement	Environmental Conditions Reinforcement		
	Normal	Corrosive	Severe Corrosive
Deformed and Plain Bars	0.005 x cover	0.004 x cover	0.0035 x cover
Prestressing Steel	0.004 x cover	No cracking	No cracking

Table A.4 - Basic Concrete Cover (JSCE SP-1[A.11])

Environmental Conditions	Slabs	Beams	Columns
Normal	25 mm (1.0 in.)	30 mm (1.2 in.)	35 mm (1.4 in.)
Corrosive	40 mm (1.6 in.)	50 mm (2.0 in.)	60 mm (2.4 in.)
Severe Corrosive	50 mm (2.0 in.)	60 mm (2.4 in.)	70 mm (2.75 in.)

A.1.2 Technical Committee Recommendations

A.1.2.1 ACI 201.2R-92

The ACI Publication ACI 201.2R-92, "Guide to Durable Concrete"[A.12] does not address the subject of crack control for the prevention of reinforcement corrosion in concrete. Rather, recommendations are given for corrosion prevention through the use of

concrete with low permeability, mix proportioning (w/c ratio), workmanship, curing, concrete cover, drainage, chloride limitations for mix constituents and positive protection systems, including waterproof membranes and epoxy coated reinforcement.

A.1.2.2 ACI 222R-96

The ACI Publication ACI 222R-96, "Corrosion of Metals in Concrete"[A.13] provides a discussion of the role of cracking on corrosion. However, it does not provide crack width or detailing requirements for prevention of corrosion. ACI 222R-96 provides the following discussion on crack widths:

> "Studies have shown that cracks less than about 0.3 mm (0.012 in.) have little influence on the corrosion of reinforcing steel.[A.14] Other investigators have shown that there is no relationship between crack width and corrosion.[A.15,A.16,A.34] Furthermore, there is no direct relationship between surface crack width and the internal crack width. Consequently, it has been suggested that the control of surface crack widths in design codes is not the most rational approach[A.43]."

A.1.2.3 ACI 224R-90

ACI Publication ACI 224R-90, "Control of Cracking in Concrete Structures",[A.17] gives additional guidance for crack control in concrete members. Chapter 4 of ACI 224R-90 provides several methods for predicting crack widths in flexural members, including the Gergely-Lutz equation.[A.3] In Section 4.4, a table of tolerable surface crack widths as a function of exposure condition is provided. The predicted maximum widths for a given member must meet the tolerable crack widths to ensure satisfactory durability. Tolerable surface crack widths are given for various exposure conditions including dry air, humidity or soil, de-icing chemicals, seawater with wetting and drying and water retaining structures. The recommended values are shown in Table A.5 of this report.

Table A.5 - Tolerable Surface Crack Widths at the Tensile Face of Reinforced Concrete Members (ACI 224R-90)

Exposure Condition	Tolerable Crack Width
Dry Air	0.016 in. (0.40mm)
Humidity or Soil	0.012 in. (0.30mm)
De-icing Chemicals	0.007 in. (0.18mm)
Seawater: wetting and drying	0.006 in. (0.15mm)
Water Retaining Structures	0.004 in. (0.10mm)

With regard to the recommended tolerable surface crack widths, Section 4.4 emphasizes the following:

> "It is important to note that these values of crack width are not always a reliable indication of the corrosion and deterioration to be expected. In particular, a larger cover, even if it leads to a larger surface crack width, may sometimes be preferable for corrosion control in certain environments. Thus the designer must exercise engineering judgment on the extent of crack control to be used."

The allowable surface crack widths proposed by ACI 224R-90 are based on a paper by E.G. Nawy.[A.18] Nawy summarizes typical allowable crack widths reported by several researchers, the CEB and the U.S. Bureau of Public Roads. The tolerable crack widths presented in ACI 224R-90 appear to be strongly influenced by those recommended by the U.S. Bureau of Public Roads,[A.19] shown in Table A.6. The USBPR values are for maximum crack width at the level of the reinforcement. No source is given for these recommendations. It should be noted that all of the work reported in the paper by Nawy, the basis of Table 4.1 in ACI 224R-90 (Table A.5 in this report), is in excess of 30 years old.

ACI 224R-90 addresses flexural crack control in prestressed members in Section 4.5. This section is intended for "partially prestressed members" which may be cracked under service loading. ACI 224R-90 suggests that crack control for this type of element is mainly for aesthetic reasons and that in situations where live loading is transitory, the residual crack width is normally small (0.001 in. to 0.003 in. (0.025 mm to 0.076 mm)) and crack control is not necessary. Some discussion is provided for calculation of crack widths using equations developed for reinforced concrete members (non-prestressed). With regard to allowable crack widths, ACI 224R-90 reports that some researchers indicate that corrosion may be a greater concern in prestressed concrete due to the smaller area of steel, thus suggesting stricter crack width limitations. However, ACI 224R-90 also indicates that other researchers have reported that there is no relationship between cracking and corrosion and thus does not offer any recommendations. In closing, ACI 224R-90 suggests that crack width limits for prestressed members should consider the magnitude and fluctuation of the live load. Unfortunately, no further guidelines are given.

Table A.6 - Maximum Permissible Crack Width at Level of Reinforcement at Working Load Level (U.S. Bureau of Public Roads[A.19])

Exposure Conditions	D.L. causes comp., L.L. causes tension	D.L. causes tension, L.L. causes tension
Air, or when a protective membrane is applied to surface	0.012 in. (0.30 mm)	0.010 in. (0.25 mm)
Salt air, water and soil	0.010 in. (0.25 mm)	0.008 in. (0.20 mm)
De-icing chemicals, humid tropical climate	0.008 in. (0.20 mm)	0.006 in. (0.15 mm)
Seawater and seawater spray; alternate wetting and drying	0.008 in. (0.20 mm)	0.006 in. (0.15 mm)

A.1.2.4 ACI 350R-89

ACI Publication ACI 350R-89, "Environmental Engineering Concrete Structures",[A.20] provides recommendations for the structural design and construction of structures used in water and wastewater treatment facilities. For this type of structure, minimal cracking is a paramount requisite and emphasis is placed on structural design that minimizes the possibility of cracking and provides resistance to chemical attack. Thus, the guidelines provided by ACI 350R-89 are of some interest to the durability design of bridge substructures in severe environments.

The structural design process presented in ACI 350R-89 is based on the requirements of ACI 318-95[A.2] with special limitations for application to environmental structures to minimize leakage and improve durability in the extreme environment of environmental service. Both strength design procedures and working stress design procedures are addressed by ACI 350R-89 for this type of structure.

For strength design, the importance of the service limit state (i.e. minimized leakage and cracking) is considered indirectly by increasing the required strength of the members. The load factor for lateral liquid pressure (F) is increased from 1.4 to 1.7. The required strength to resist factored loads, U, is further increased by sanitary durability coefficients as follows:

a) In calculations for reinforcement in flexure, the required strength should be 1.3U

b) In calculations for reinforcement in direct tension, the required strength should be 1.65U

c) In calculations for the shear capacity provided by mild steel reinforcement, use $\phi V_s > 1.3(V_u - \phi V_c)$

d) In calculations for compressive regions of concrete in flexure or under axial load, the required strength should be 1.00U (unmodified)

The sanitary durability coefficients used to increase U were based on crack width requirements. No discussion as to the development of these coefficients is given in ACI 350R-89.

For working stress design, reduced allowable stresses are specified for both concrete and mild steel reinforcement. In addition, spacing requirements are specified for different bar sizes as a function of service load stress. Recommended allowable stresses for concrete are shown in Table A.7. These working stresses are specified in terms of f'c for all strengths of concrete. The minimum compressive strength for concrete recommended by ACI 350R-89 is 3500 psi. This value is increased to 4000 psi if the concrete is subjected to severe and frequent freezing and thawing. Maximum allowable working stresses for mild steel reinforcement are given in Table A.8 for a maximum bar spacing of 12 in (304.8 mm).

For both strength design and working stress design, crack control is addressed through the quantity Z, as defined in Section 2.1.1 of this report. For environmental structures, two levels of sanitary exposure are considered: normal and severe. Normal sanitary exposure is defined as "liquid retention (watertight), exposure to liquids with pH > 5 or exposure to sulfate solutions less than 1500 ppm. Severe sanitary exposures are conditions in which the limits defining normal sanitary exposures are exceeded."[A.20] For normal exposures, a maximum Z value of 115 kips/in. (20 kN/mm) is specified. This corresponds to a surface crack width of 0.010 in. (0.25 mm). For severe sanitary exposure conditions, a maximum Z value of 95 kips/in. (16.6 kN/mm) is specified, corresponding to a surface crack width of 0.0087 in. (0.22 mm).

Table A.7 - Recommended Allowable Concrete Stresses (psi) (ACI 350R-89)

Description	Stress
Flexure;	
Extreme fiber stress in compression	0.45 f'c
Extreme fiber stress in tension in plain concrete footings and walls	$1.6\sqrt{f'_c}$
Shear;	
Beams with no web reinforcement	$1.1\sqrt{f'_c}$
Joists with no web reinforcement	$1.2\sqrt{f'_c}$
Members with web reinforcement or properly combined bent bars and vertical stirrups	$5\sqrt{f'_c}$
Slabs and footings (peripheral shear)	$2\sqrt{f'_c}$
Bearing;	
On full area	0.25 f'c
On one-third area or less	0.375 f'c

Table A.8 - Recommended Stresses for Reinforcement at Service Loads for a Maximum Spacing of 12 in. (304.8 mm) (ACI 350R-89)

Bar Sizes	Exposure Condition	Maximum stress at service load	
		Grade 60	Grade 40
All sizes	Members in direct tension All Exposures	20 ksi (138 MPa)	14 ksi (96 MPa)
#3, #4, #5	Flexural Members Severe Exposure	22 ksi (152 MPa)	20 ksi (138 MPa)
	Flexural Members Normal Sanitary Exposure	27 ksi (186 MPa)	20 ksi (138 MPa)
#6, #7, #8	Flexural Members Severe Exposure	18 ksi (124 MPa)	18 ksi (124 MPa)
	Flexural Members Normal Sanitary Exposure	22 ksi (152 MPa)	20 ksi (138 MPa)
#9, #10, #11	Flexural Members Severe Exposure	17 ksi (117 MPa)	17 ksi (117 MPa)
	Flexural Members Normal Sanitary Exposure	21 ksi (145 MPa)	20 ksi (138 MPa)

A.1.2.5 CEB Information Report No. 183

The Comite Euro-International Du Beton (CEB) Publication No. 183, "Durable Concrete Structures,"[A.21] uses the same crack control provisions as the CEB-FIP Model Code 1990.[A.8] However, some additional comments are provided in CEB No. 183.

For ordinary reinforcement, CEB No. 183 reports that surface crack widths in the range of 0.30 mm to 0.40 mm (0.012 in. to 0.016 in.) are only of minor importance compared with the thickness and quality of the concrete cover. For severe exposure conditions, CEB No. 183 states:

> "... high corrosion rates may occur in the region of cracks. Again, limitation of crack width is not sufficient to avoid attack on the reinforcement. In such cases, special protective measures must be taken (e.g. sealing the concrete surface or the use of epoxy coated reinforcement)."[A.21]

For prestressing steel, CEB No. 183 reports that due to the possibility of brittle failure, cracks crossing the prestressing steel in outdoor conditions can only be allowed in post-tensioned members, provided that the surface crack width is less than 0.20 mm (0.008 in.) and there is no source of chloride attack. Cracking must not be allowed in pre-tensioned members due to the lack of extra protection provided by the post-tensioning duct and grout. For exposures in which a source of chloride attack is present (de-icing salts or seawater), no tension is allowed for both post-tensioned and pre-tensioned elements, unless the tendons are coated. In this case, surface crack widths are to be limited to less than 0.20 mm (0.008 in.).

A.1.2.6 Durability of Concrete Structures - State of the Art

In the 1982 CEB State of the Art Report, "Durability of Concrete Structures,"[A.22] the importance of crack widths is addressed. It is simply stated that in the region of cracks in structural concrete, carbonation can penetrate much faster than in uncracked concrete. This leads to quicker corrosion initiation in the region. It is also said that cracks cannot be limited in such a way as to eliminate corrosion of the reinforcing steel during the life of the structure. The document further states that,

> "... the width of cracks is no longer to be regarded as a major factor in corrosion protection of the reinforcement. Carbonation in the region of smaller cracks will reach the reinforcement only at a later time than in that of wider cracks. From this point, however, the rate of corrosion is almost independent of the crack width, as the diffusion of oxygen is in general not influenced by the width of cracks."[A.22]

A.1.2.7 CEB Manual on Cracking and Deformations

In the CEB Manual on Cracking and Deformations,[A.23] there are four reasons cited for the control of crack widths. The reasons are listed in the document in the following order:

1. Appearance
2. Water tightness and Gas tightness
3. Corrosion Protection
4. Other Functional Requirements

Appearance was listed as the first reason to control cracking in structural concrete. It was suggested to limit cracks to those which cannot be seen in areas where concrete is exposed. There was question as to what this limit should be, and how it should be quantified.

A series of surveys to assess public reaction to cracks were carried out. The results showed that surface cracks wider than about 0.25 mm to 0.30 mm (0.010 in. to 0.012 in.) can lead to public concern. It was understood that this could not be a conclusive range of crack width levels for the following reasons. Very small cracks can be seen if material leaches from these cracks, or if dirt is present in the areas surrounding the cracks. The viewing distance to the crack also has an influence on whether or not the crack will cause public concern. Engineers are then advised to make their own assessment in each particular situation.

Corrosion protection is listed as the third reason to control cracking, and is referred to as the "most commonly quoted reason for controlling cracking". Again references such as Houston, Atimtay, and Ferguson[A.25] and Schiessl[A.38,A.39] are cited to show that crack control will only delay the onset of almost certain corrosion. It is stated that crack width has a negligible effect on the long-term corrosive damage of a structure during its lifetime.

The crack control section concludes by saying that, "corrosion protection is probably the least convincing reason, since, at best, cracking is only of secondary importance in controlling corrosion."[A.23] Since aesthetic and functional requirements vary from situation to situation, the CEB model code leaves crack control as an issue for the engineer and client to come to agreement on.

A.2 Research - Crack Widths and Corrosion

A tremendous amount of research has been performed over the last several decades on the subject of corrosion of steel reinforcement in concrete. The broad scope of the research programs including specimen types, exposure conditions, loading conditions, test duration, test methods, measurement methods and protection variables is staggering. In spite of the large amount of work in this area, little or no general conclusions have been made, largely due to the wide variation in testing methods and variables. In the following sections, an attempt has been made to review available literature on the subject of the influence of crack widths on corrosion. In Section A.2.1, research for reinforced (non-prestressed) concrete is reported. Section A.2.3 summarizes research in which the influence of prestressing on cracking and corrosion was investigated. For organizational purposes, the reviewed literature on reinforced concrete has been split into short term and long term tests. Experimental programs with duration's of 10 or more years have been designated as long term tests. All others have been classified as short term.

A.2.1 Reinforced Concrete Research - Short Term Corrosion Tests

A.2.1.1 Kahhaleh, K.Z.

Kahhaleh[A.24] performed a series of beam exposure tests to evaluate the performance of epoxy coated reinforcement in structural members. The variables investigated in this program were reinforcement usage, loading condition (crack width), damage to epoxy coating and repair procedures. The reinforcement usage included longitudinal bars, stirrups and spliced bars with patched ends. The loading conditions considered were:

- no imposed load
- load applied to produce a specified crack width (0.013 in., 0.33 mm); load removed during exposure
- load applied to produce a specified crack width (0.013 in., 0.33 mm); load held during exposure

The concrete used in the test beams was designed to have a reduced strength and increased permeability to accelerate corrosion. The concrete had an average compressive strength f'c of 3700 psi (25.5 MPa) and used Type I cement with a water-cement ratio of 0.62. A concrete cover of 2 in. (50 mm) was used for all specimens. The midspan region of the beams was subjected to wet-dry cycles 14 days in length. The wet portion of the cycle consisted of 3 days of continuous wetting with 3.5% NaCl solution. The specimen was then allowed to dry for the remaining eleven days of the cycle.

After accelerated exposure testing for a period of 392 days, the following conclusions regarding cracking and corrosion were made:

1. **Cracking:** Corrosion of epoxy coated bars was initiated much earlier in cracked members than in uncracked members. However, specific crack widths, measured during testing, did not show an influence on corrosion initiation and progression.
2. **Effectiveness of Epoxy Coating:** Cracked specimens with damaged coating showed the worst corrosion damage. Patched areas also experienced significant corrosion in cracked members. Where damaged or patched areas coincided with cracks, significant localized pitting was observed on longitudinal bars.
3. **Corrosion Mechanism:** In cracked specimens, corrosion was initiated at crack locations and spread to adjacent areas, undercutting the epoxy coating. Differential chloride distributions and moisture gradients influenced by the presence of cracks generated large potential differences when coupled with damage to the epoxy coating. This provided the driving force for macrocell corrosion to initiate and proceed.

A.2.1.2 Houston, J.T., Atimtay, E. and Ferguson, P.M.

Houston, Atimtay and Ferguson[A.25] performed an experimental study of corrosion in representative elements from highway structures. A large number of variables was considered: type of reinforcing steel, cement type, water-cement ratio, aggregate type, concrete permeability, bar size and spacing, cover, casting position, concrete cracking, steel

working stress and prestressing. This broad approach was intended to isolate the most critical parameters. The experimental program involved exposure testing of 40 beam elements and 42 slab elements for periods of up to 34 months. Exposure conditions consisted of daily spraying with 3% salt solution.

On the basis of the experimental results, the following observations related to cracking and corrosion were made:

1. **Critical Crack Width:** In many cases, corrosion was initiated at flexural crack widths greater than 0.005 in. (0.13 mm). However, for specimens with a cover of 1 in. (25 mm), limitation of crack widths to less than 0.004 in. (0.10 mm) did not ensure prevention of corrosion.
2. **Influence of Concrete Cover:** For shallow covers (1 in. (25 mm)), uniform corrosion of reinforcement was observed. For covers larger than 2 in. (50 mm), corrosion initiation was associated primarily with crack locations. However, larger covers were effective in minimizing continued corrosion by inhibiting the development of longitudinal splitting. The range of covers considered was 1, 2 and 3 in. (25, 50 and 75 mm).
3. **Stress Corrosion:** For the investigated levels of working stress in the mild steel reinforcement (20, 30 and 35 ksi (138, 207 and 241 MPa)), stress corrosion was not an apparent factor in the corrosion process. (normally stress corrosion cracking in reinforcement is only a concern for prestressing steels - individual wire diameters less than 4 mm (0.16 in.), cold worked and subjected to a permanent tension exceeding 400 MPa (60 ksi))
4. **Level of Stress/Crack Widths:** For the reinforcement stress levels considered (20, 30 and 35 ksi (138, 207 and 241 MPa)), the increased crack width associated with the increasing stress was not a significant factor in the corrosion process. This suggests that corrosion was unaffected by the range of crack widths considered.
5. **Prestressing:** Corrosion of the 3/8 in. (9.5 mm) diameter prestressing strand was similar to that of the unstressed #6 (19 mm dia.) bars in the same specimens. The effect of improved durability (crack control) through prestressing was not investigated in this research.

A.2.1.3 Vennesland, O. and Gjorv, O.E.

Gjorv and Vennesland[A.26] reported the findings of an experimental study of the effects of cracks on corrosion in submerged concrete structures. An experimental technique was developed to simulate the conditions in a submerged concrete structure where a galvanic cell is developed between exposed steel at crack locations (acting as the anode) and the embedded system of rebar (acting as the cathode). In such a system, the corrosion rate is dependent on the rate of oxygen diffusion to the cathode and on the relative areas of the cathode and anode. In a large submerged concrete structure, the amount of embedded steel acting as the cathode may be considerably larger than the small exposed steel area at the crack locations, developing a considerable corrosion rate in spite of the low oxygen concentration and diffusion rate.

The experimental procedure utilized 10 x 10 x 50 cm (4 x 4 x 20") cracked concrete prisms as the anodic region and a stainless steel plate as the cathode. The diffusion rate of oxygen onto a stainless steel plate was determined experimentally to be approximately 100 times larger than the oxygen diffusion rate through the concrete cover of the concrete prism. This allowed the use of a comparatively small stainless steel plate to model a large embedded rebar system with a cathode to anode area ratio of approximately 10.[A.5] The entire system was submerged in synthetic seawater and was monitored to determine corrosion rates and instantaneous potentials. The concrete prisms were reinforced with a single 10 mm (0.4 in.) diameter deformed bar. The water cement ratio of the concrete was 0.5. Prior to initiating the corrosion test, each specimen was cracked under three point loading. The range of surface crack widths considered was 0.1 to 2.0 mm (0.004 to 0.079 in.). The specimens where then sealed with a neoprene based glue, leaving only the crack location exposed. The corrosion tests were run for a period of four months.

In general, the findings of this research indicated that for crack widths less than 0.4 mm to 0.5 mm (0.016 to 0.020 in.) corrosion was not significant (critical crack width). This was attributed to "clogging" of the cracks. The cracks did lead to an initiation of corrosion, but the products from the corrosion reaction were found to deposit in the cracks, thereby inhibiting further corrosion. Several specimens indicated that the critical crack width for corrosion could be as high as 0.6 mm (0.024 in.).

A.2.1.4 Lin, C.Y.

Lin[A.27] reported an experimental study of the effects of crack widths on corrosion of reinforcing steel in concrete beams exposed to seawater. The beams had dimensions of 76 x 152 x 914 mm long (3 x 6 x 36" long). The concrete used Type I cement and had a water cement ratio of 0.50. The beams were precracked to desired crack widths of 0.10 mm, 0.15 mm, & 0.18 mm (0.004, 0.006 and 0.007 inches). Some of the beams were subjected to sustained loading to keep the cracks open, while others were cracked and then unloaded. The corrosion testing was performed by completely immersing the beams in a tank of seawater and impressing a constant current between the reinforcing steel and an aluminum counter electrode. The direction of the impressed current was such that the reinforcement served as the anode. The corrosion testing was continued until initiation of a longitudinal crack along the line of the reinforcing steel, resulting from deposition of the corrosion products, was observed. Due to the impressed current, formation of the longitudinal cracks occurred quickly. Testing periods ranged from two to ten days.

Related to crack widths and the effects on corrosion, the research produced two significant findings:

1. For the specimens subjected to sustained loading, the crack width did not affect the amount of corrosion (for the range of crack widths considered).
2. For the specimens which were cracked and subsequently unloaded, the amount of corrosion was significantly less (up to five times) than the beams subjected to sustained loading. On the basis of this observation, Lin recommended that for corrosion control, cracks should not be permitted under sustained or frequent loads.

A.2.1.5 Makita, M., Mori, Y. and Katawaki, K.

Makita, Mori and Katawaki[A.28] reported the results of an experimental program studying the marine corrosion behavior of reinforced concrete. Concrete specimens were partially submerged in seawater and were examined for a relationship between crack width and extent of corrosion. The specimens were 75 cm long (30 in.) and were made with concretes having water cement ratios ranging from 0.40 to 0.70. Several of the specimens were precracked. The initial crack widths were not reported by the authors. The specimens were left at the exposure site for a period of 1000 days.

At the completion of exposure testing, crack widths were measured in all specimens. The measured surface crack widths ranged from 0.05 mm to 0.3 mm (0.002 to 0.012 in.). The specimens were subsequently autopsied to determine the locations and extent of corrosion. Makita et al reported that there did not appear to be a correlation between surface crack width and corrosion, for both the precracked specimens and the initially uncracked specimens.

A.2.1.6 Misra, S. and Uomoto, T.

Misra and Uomoto[A.29] conducted three series of tests to clarify the characteristics of corrosion occurring under a combination of different conditions. Two of the series were unloaded (uncracked) and tested under various exposure conditions in a laboratory. The third series consisted of four beams tested at a marine exposure site and two beams subjected to aggressive exposure conditions in a laboratory setting. Two of the specimens at the marine site were precracked to examine the effect of cracking on corrosion. The beams had dimensions of 100 x 200 x 2100 mm long (4 x 8 x 84 in. long) and were reinforced with two D6 (< #3) bars top and two D16 (~ #5) bars bottom. The clear cover over the stirrups was 10 mm (0.4 in.). The concrete had a water/cement ratio of 0.55. The two precracked beams were subjected to four-point loading to produce a tensile strain of 0.0011 in the bottom reinforcement. The beams were unloaded prior to transportation to the exposure site and were not loaded during exposure allowing the cracks to "close". One uncracked and one cracked beam were removed from the exposure site after one year. The remaining two beams were removed after a total of two years exposure.

After one year of the study, it was found that corroded areas in uncracked specimens were the same as corroded areas in uncracked portions of the cracked specimens. However, in the cracked central portion of the precracked beams, increased corrosion was observed. This led to the conclusion that the increased corrosion could be attributed to the flexural cracking in the central portions of these members.

Misra and Uomoto did not make any conclusions regarding critical crack width values. However, their data suggested that crack widths above 0.5 mm (0.020 in.) are sufficient to cause a harsh cycle of crack initiation and propagation. The test results show that corrosion in specimens with crack widths greater than or equal to about 0.5 mm (0.020 in.) was significant enough to cause additional longitudinal cracks along the reinforcing steel. This process initiated a rapid growth, or vicious cycle, of corrosion along the reinforcement. It was shown that the presence of shear reinforcement provided sufficient confinement to restrain the growth of corrosion induced longitudinal cracks along the main reinforcing bars.

A.2.1.7 Okada, K. and Miyagawa, T.

Two series of tests to examine the influence of cracks on the mechanism and rate of corrosion of reinforcing steel were carried out by Okada and Miyagawa.[A.30] In the first series of tests, the influence of cracks on the corrosion rate of reinforcing steel was investigated. In the second series, the influence of chosen variables on the mechanisms of crack corrosion was investigated. The two main variables chosen in this study were water-cement ratio, and crack width. This experiment was based on the theory that cracks in reinforced concrete structures make reinforced concrete so heterogeneous as to cause macrocells to develop in the cracked regions. It was suggested that the region near a crack may act as an anode.

Two sizes of specimens were used in the first series. Continuous immersion specimens had dimensions of 150 x 100 x 1000 mm long (6 x 4 x 40 in. long), and were reinforced with D10 (~ #3) bars. The clear cover to the reinforcement was 15 mm (0.6 in.) and specimens had pre-formed cracks of 0, 5, 10 or 25 mm (0, 0.2, 0.4 or 1.0 in.). The water/cement ratio was 0.65. The wetting and drying specimens were macrocell specimens and had 100 x 100 mm (4 x 4 in.) sections, with lengths up to 3 m. Clear cover was 20 mm (0.8 in.) for these specimens. The water/cement ratio was 0.70. The relative lengths of anode steel and cathode steel were varied to examine effects of cathode to anode area ratio.

Measures of macrocell current in the first test series showed that during immersion of specimens in sodium chloride solution, macrocell potential and current dropped with time. However, when specimens were allowed to dry, the current density increased. Close agreement between observed loss of steel area, and that calculated from the quantity of macrocell activity was found. This confirmed that macrocell current density is directly related to the rate of corrosion.

The specimens in the second series had cross-sections of 50 x 50 mm (2 x 2 in.). Specimen lengths were varied up to 1 m (40 in.). Water/cement ratios of 0.4, 0.5, 0.6 and 0.7 were used. Specimens were loaded to in tension to produce cracks (up to 0.3 mm (0.012 in.)) or were provided with pre-formed cracks (10 mm (0.4 in.)). Some specimens had 3.13% NaCl added to the mixing water.

In the second series, in which the mechanisms of crack corrosion were observed, conclusions regarding the effects of water-cement ratio and crack width on macrocell corrosion were drawn. It was concluded that as the water-cement ratio of concrete increases, corrosion of reinforcing steel accelerates. In addition, water-cement ratio influences both the macrocell corrosion rate at cracks, and the mechanism of corrosion. When the ratio was 0.40 or 0.50, potential difference increased with increasing crack width. According to the experimental results, the critical crack width is between 0.1 and 0.2 mm (0.004 and 0.008 in.). However, as water-cement ratio increased, there was less correlation between crack width and potential difference.

A.2.1.8 Swamy, R.N.

There exists evidence that there is an interaction between cover-to-steel and crack-width on the durability of reinforcing steel in concrete. Swamy[A.31] carried out a series of tests on concrete specimens reinforced with plain, epoxy coated, and galvanized steel. The

specimens were a series of square concrete prisms containing a central reinforcing bar with embedment length of 760 mm (30 in.). The reinforcing bars had varying epoxy coating thickness of 100 μm, 200 μm, and 300 μm (4, 8 and 12 mils). Tests were also conducted using galvanized reinforcement without epoxy coatings. The specimens were subject to two exposure conditions. The first was a natural marine exposure in a tidal zone, and the other was an accelerated cyclic sea water immersion test in the laboratory. The accelerated test was a wet and dry cycle of six hours each to simulate low tide. Prior to the tests, all of the test prisms were loaded in tension resulting in surface crack widths of 0.11 to 0.25 mm (0.0043 to 0.010 in.). During the tests, the specimens were subjected to their environments in the loaded condition, with steel stress adjusted to approximately 200 MPa (29 ksi).

According to the study, no corrosion protection measure could overcome the negative impact of insufficient cover, poor concrete quality, or excessive cracking. Although the study was primarily concerned with different protection measures (such as epoxy coatings and galvanized strand), conclusions were made regarding the role of critical crack widths and adequate concrete cover on corrosion of reinforcement. The results of the study suggest that a balance between both concrete cover and crack width is necessary. With large cover, there exists larger crack widths at the surface of the concrete, but also a lower number of 'critical' crack widths. This type of interaction lead to what was suggested as an optimum range of both covers and crack widths in concrete specimens. With optimum concrete cover ranging from 50 to 70 mm (2 to 2-3/4 in.), crack widths from 0.10 to 0.15 mm (0.004 to 0.006 in.) were considered critical. Although it was concluded that cover to steel is the most critical factor in preserving the electrochemical stability of steel, results obtained from this study suggest that concrete cover, quality, and crack width play all play an interactive role in the durability of reinforced concrete structures.

A.2.1.9 Berke, N.S., Dalliare, M.P., Hicks, M.C., and Hoopes, R.J.

Berke et al[A.32] performed a series of tests to address the corrosion of cracked reinforced concrete members and to evaluate the effectiveness of calcium nitrite corrosion inhibitor. The specimens used in this program were beams, based on the ASTM G109 macrocell specimens. Dimensions of the beams were 6 x 6 x 30 in. long (152 x152 x 762 mm long). Reinforcement was identical to standard macrocell specimens, with one #4 (0.5 in. dia.) bar as the anode and two #4 bars as the cathode. Clear cover was 1-1/2 in. (38 mm). As in typical macrocell specimens, electrical contact between the layers of steel was provided using wire and a 10 Ohm resistor. Electrical contact is necessary for macrocell corrosion to develop, and the use of the resistor allows direct measurement of the corrosion current. The beams were initially cracked with the single #4 bar in tension, using a loading machine. The average crack width was 0.008 in. (0.2 mm). Shims were placed in the cracks and specimens were unloaded during exposure testing. Exposure consisted of ponding the cracked surface with 3% NaCl solution on a 4 week cycle (2 weeks wet, 2 weeks dry). Exposure testing was continued for 16 months.

A total of 8 beams were tested using concrete meeting minimum ACI Specifications[A.2] (w/c = 0.40). 4 of the beams had calcium nitrite added.

Destructive examination of the specimens at the conclusion of testing found the majority of corrosion below the crack. The beams without corrosion inhibitor showed more severe corrosion and spreading of the corrosion several diameters from the crack.

Comparison of average macrocell corrosion current and total macrocell corrosion showed a dramatic improvement using calcium nitrite. Observed corrosion in these specimens was negligible in comparison to the specimens without calcium nitrite.

Overall, the results show that a crack width of 0.008 in. (0.2 mm) was insufficient to prevent corrosion with a 1-1/2 in. (38 mm) cover. The addition of calcium nitrite proved effective in limiting corrosion at a crack width of 0.008 in. (0.2 mm).

A.2.1.10 Schiessl, P., and Raupach, M.

Schiessl and Raupach[A.33] performed a laboratory and theoretical study investigating the dominant variables influencing corrosion in cracked reinforced concrete.

The laboratory study consisted of small reinforced concrete beams subjected to saltwater exposure. The beam dimensions were 97 x 150 x 700 mm long (3.8 x 5.9 x 27.6 in.). The beams were subjected to sustained loading to produce one crack at midspan. Investigated crack widths were 0.1 mm, 0.2 mm, 0.3 mm and 0.5 mm (0.004 in., 0.008 in., 0.012 in. and 0.020 in.). The effect of water-cement ratio (0.5 and 0.6) and concrete cover (15 mm (0.6 in.) and 35 mm (1.4 in.) was investigated. The maximum exposure duration was two years. The number of specimens in the study was not clear, but data for twelve specimens was plotted in several figures. The results of the laboratory study summarized as follows:

1. **Corrosion Mechanism:** The anodic reaction occurs at the crack location. The regions outside the crack behave cathodically up to a distance of 200 mm (7.9 in.) on either side of the crack. The cathodic current density decreases with distance from the crack due to increasing electrolyte resistance.
2. **Effect of Concrete Cover:** Increased concrete cover significantly reduced the calculated steel mass loss due to corrosion.
3. **Effect of Water-Cement Ratio:** Reducing the w/c ratio from 0.6 to 0.5 reduced calculated mass loss in the crack zone, particularly within the first six months of exposure. The influence of w/c ratio was less pronounced after 2 years of exposure.
4. **Effect of Crack Width:** Corrosion rates and mass loss increased with increasing crack widths. However, the influence of crack width was deemed much less than the influence of concrete cover and w/c ratio.

The laboratory study was followed by a series of calculations to further investigate the influence of cracking on corrosion. Based on the observed corrosion mechanism in the laboratory study, the corrosion process at a crack was modeled as “macrocorrosion” cells with an anode at the crack and large cathodes between the cracks. The reader is referred to the paper for more information on the model and assumptions. The results of the corrosion theory calculations are summarized as follows:

1. **Effect of Crack Spacing:** The corrosion rate (mass loss) increased as the crack spacing increased. These results can be explained by the area effect, or the ratio of cathode area to anode area. For a given corrosion current flowing in the corrosion cell, the corrosion current density increases as the electrode area decreases. The corrosion rate or metal loss is related to the current density at the anode. As the ratio of cathode area to anode area increases the anodic current density increases. If the crack spacing decreases, the available cathodic area is reduced and the anodic current density decreases.

2. **Effect of Reducing Bar Diameter to Limit Crack Widths:** Limiting crack widths by reducing the bar size (keeping total steel area constant) resulted in an increase in loss of reinforcement cross-section. This occurrence was attributed to an increase in total surface area of steel.

   Schiessl and Raupach conclude their paper with the following statement:

   "The calculations and the results of the laboratory tests clearly indicate that the problem of reinforcement corrosion in crack zones cannot solely be solved by crack width limitation in the range from roughly 0.3 to 0.5 mm; corrosion protection must be assured primarily through adequate concrete quality and cover."[A.33]

A.2.2 Reinforced Concrete Research - Long Term Corrosion Tests

A.2.2.1 Tremper, B.

Tremper[A.34] reported the findings of a long term exposure test on small scale reinforced concrete members. The members were concrete blocks with dimensions of 8 x 8 x 2.5 inches (200 x 200 x 63 mm), reinforced with steel wires or deformed bars. Different concrete mixes with either well graded aggregate or poorly graded aggregate were used to represent different placement qualities. The water cement ratios of the concrete ranged from 0.40 to 0.75. The minimum cover to the reinforcement was 1-1/8 in. (28.6 mm) The specimens were loaded as beams to produce surface crack widths of 0.005 in., 0.010 in., 0.020 in., and 0.050 in. (0.127 mm, 0.254 mm, 0.508 mm and 1.27 mm). The specimens were then unloaded and taken to a coastal exposure site. The specimens were placed on racks, cracked side upwards, but were not in direct contact with the seawater. Tremper indicated that the exposure conditions would not be considered as particularly severe.

After ten years of continuous exposure testing, the specimens were autopsied. All reinforcement was found to be free of corrosion, except in the regions of cracks. However, this corrosion was deemed minor. Tremper concluded that for the conditions considered in these tests, occasional "large cracks" (within the range of cracks considered) do not promote serious corrosion of reinforcing steel.

A.2.2.2 Ohta, T.

Long term exposure tests on reinforced concrete beams exposed to sea air were conducted by Ohta.[A.35] One hundred and forty nine pairs of reinforced concrete beams (1000 x 150 x 150 mm (39.4 x 6 x 6 in.)) with open cracks were exposed for two to twenty years. The main reinforcement was one or two deformed 13 mm (1/2 in.) bars with 6 mm

(1/4 in.) stirrups. The cements used were ordinary Portland cement, blast furnace slag cement, and Portland fly-ash cement. The specimens were exposed near the beach line in Ramoi, facing the Sea of Japan. The variables measured were carbonation of the concrete, chloride ion content in concrete, electrical potential and corrosion of the reinforcing steel. The cross sectional area of the reinforcing steel was measured to determine the extent of corrosion.

The loss of sectional area of reinforcing steel after ten years of exposure is plotted on Weibull probability paper in Figure A.2 and Figure A.3. The results are summarized as follows:

1. Crack widths did not correlate significant loss of the cross sectional area of steel for 20 mm (0.8 in.) cover after ten years (Figure A.2).
2. For 40 mm (1.6 in.) cover, there appeared to be a relationship between the amount of corrosion and crack widths (Figure A.3).
3. Corrosion was only slight for covers of 50 mm and 68 mm (2 in. and 2-2/3 in.).

It was then concluded that the rate of progress of depassivation depends on crack width when cover is thick, and when term of exposure is short.

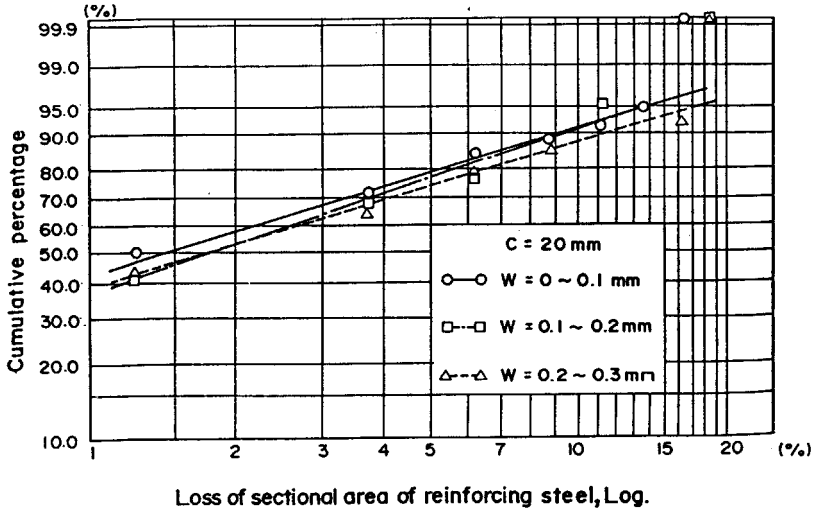

Figure A.2 - Loss of Cross-Sectional Area After 10 Years, 20 mm (0.79 in.) cover (Ohta[A.35])

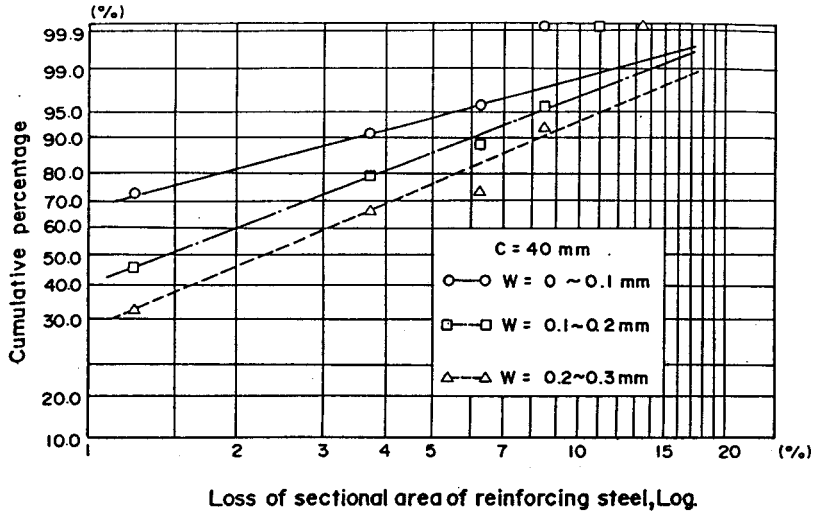

Figure A.3 - Loss of Cross-Sectional Area After 10 Years, 40 mm (1.57 in.) cover (Ohta[A.35])

Results after 20 year of the study:

1. The effect of crack widths on corrosion disappeared for even the 40 mm (1.6 in.) cover specimens (Figure A.4).
2. Specimens with 20 mm (0.8 in.) cover were very heavily corroded, and longitudinal cracks along the reinforcement were observed

It was concluded from these tests that cover, and not crack width played the most important role in the control of corrosion of reinforcing steel in concrete.

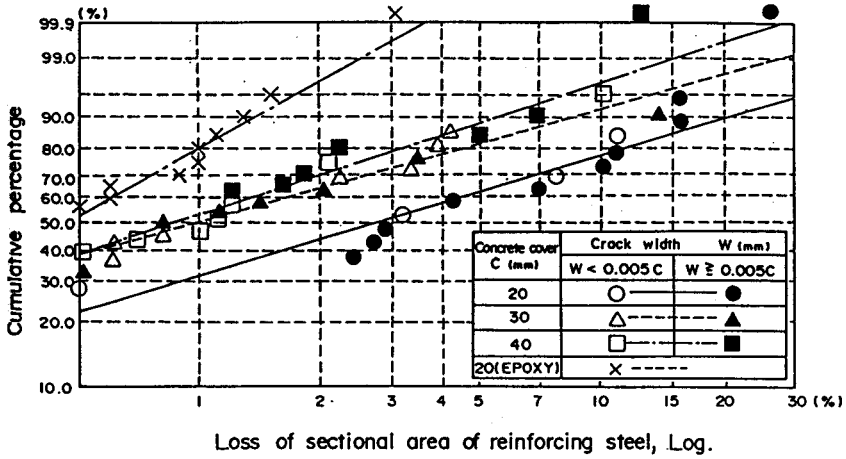

Figure A.4 - Loss of Cross-Sectional Area After 20 Years (Ohta[A.35])

A.2.2.3 Francois, R and Arliguie, G.

Francois and Arliguie[A.36] drew similar conclusions through a series of tests on cracked reinforced concrete specimens. The test program involved sixty-eight reinforced concrete beams, and covered a test period of ten years. The beams were 150 x 280 mm (6 x 11 in.) in cross section, and 3 m (118 in.) in length. Two exposure conditions were used. One was a salt fog produced by means of four vaporizers using compressed air at 0.1 MPa, and salt water at 3.5% NaCl by weight. The other environment was a mixture of 50% CO_2 and air, with relative humidity kept between 40% and 70%.

Results of their study suggest that the existence of cracks, and not their width, is the significant parameter in the corrosion of reinforcing steel. The study did not report how different values of crack width influenced corrosion, but only said that crack widths were less than 0.5 mm (0.02 in.). It was also observed that crack width influenced the speed at which corrosion began. Since this onset time was a relatively short, the influence of crack width was limited in general. Instead, the findings support the idea that concrete cover is directly related to the rate of corrosion. It was suggested that this is because the capacity of concrete to absorb aggressive agents increases with the thickness of cover.

A.2.2.4 O'Neil, E.F.

In a study by E.F. O'Neil,[A.37] several reinforced concrete beams were placed at the Weathering Exposure Station at Treat Island, Cobstock Bay, Eastport, and Lubec in Maine. The length of the study was 25 years (1950 to 1975). The purpose of the test was to obtain information on the long-term weathering of air-entrained, and non-air-entrained concrete beams containing steels of different composition, types of deformation, and different levels of stress. Though the study of crack widths on corrosion was not a primary objective, data obtained during these tests show some relationship between stress levels in the steel and corrosion rates. These stress levels correspond directly to the crack widths observed in the specimens.

The test consisted of a series of 82 reinforced concrete beams. 22 beams were made with air-entrained concrete, and the rest were done without air-entrainment to evaluate the durability of air entrained concrete specimens in severe environments. Thirty nine percent of the beams had cover depths of 50 mm (2 in.), while the rest had 19 mm (3/4 in.) cover. The reinforcing steel used conformed to ASTM A 16-50T for rail-steel rebar, or to A 15-50T for billet-steel rebar. All specimens were loaded to put tensile steel under stress, with the exception of the control specimens. The loaded stress levels in the steel were 0, 138, 207, 276, and 345 MPa (0, 20, 30, 40 and 50 ksi). Beams were exposed to twice daily tidal cycles. Since tides reached as high as 9.15, the beams were also subjected to considerable head during wetting. In addition, the beams were subjected to freeze-thaw during the winter months.

After 5 years of exposure, all of the beams with non-air entrained concrete had extensively deteriorated due to freezing and thawing. After 25 years, 18 of the beams with air entrained concrete remained, however only 13 were in testable condition. At this time, 11 of the beams were tested and autopsied.

Corrosion of the reinforcing steel in beams stressed to 138 MPa (20 ksi) could not be matched with the flexural cracks in the beams. Beams stressed to 345 MPa (50 ksi) did

show corrosion of steel matched with the flexural cracking in those regions. Since the 345 MPa (50 ksi) beams had crack widths of 0.4 mm (0.016 in.) or greater, it was concluded in the study that crack widths of 0.4 mm (0.016 in.) or higher were necessary to produce corrosion at flexural cracks.

The results could not show a definite relationship between the steel stress levels and corrosion that would indicate more or less corrosion for lower stress levels. The study generally did find that steel at higher stress levels produced larger flexural cracks, and therefore would allow for greater penetration of water and oxygen.

A.2.2.5 Schiessl, P.

Schiessl[A.38,A.39] found, through a series of long-term tests, that the decisive parameter for the control of corrosion was the carbonation of the concrete, and not the width of cracks in the concrete.

The test specimens used in the comprehensive study consisted of 1.95 m rectangular beams (150 x 250 mm (6 x 9.8 in.)). The reinforcing steel consisted of 2 deformed 8 mm (0.31 in.) bars, and one plain 4 mm (0.16 in.) bar. Concrete covers were 2.5 cm and 3.5 cm (1 in. and 1.38 in.), and stirrups (8 mm deformed bars) were provided on only one-half of each specimen. After 28 days the concrete strength was 250 kg/cm^2 (3600 psi (24.8 MPa)). The beams were subjected to normal city air, polluted industrial air, and salty sea air. The pairs of beams were braced against each other at the quarter points by use of an intermediate piece, and stressed together with screw bolts. The beam pairs were situated such that the top of one beam faced upward, while the other faced downward. Permanent crack widths produced by this type of loading ranged from 0.15 mm to 0.40 mm (0.006 to 0.016 in.).

Schiessl concluded from these tests that the limiting of crack widths only serves to limit the amount of cracks with high corrosion intensity. These areas of high local corrosion intensity often give rise to longitudinal cracking along the reinforcing steel. This in turn can cause spalling of the concrete cover. Schiessl acknowledged that there is a wide range of opinion regarding acceptable crack widths, typically ranging from 0.1 mm to 1.0 mm (0.004 to 0.04 in.). He reasons, however, that the corrosion rate of reinforcing steel in carbonated concrete is almost independent of crack width and cover. That is, the influence of the crack width on corrosion intensity decreases with increased exposure time.

Schiessl explains that there are two phases in the corrosion of reinforcing steel. The first phase involves the depassivation of the reinforcing steel. This depassivation is dependent on both the cover depth and crack width. The alkaline nature of the surrounding concrete provides a passive layer around the reinforcing steel, thus preventing corrosion. CO_2 from the atmosphere reacts with hydroxides in the concrete (carbonation). Experiments showed that large covers slowed the process sufficiently enough to protect the steel inside. However, tests also revealed that cracks speed up the process, and that the rate was dependent on width.

The second phase begins once corrosion has initiated. Results from his studies showed that the rate of corrosion, once initiated, was independent of crack width and cover. Since the first phase is relatively short in duration compared to the length of the

longer term exposure tests, and since it is only a matter of time before corrosion initiates regardless of crack widths, it is concluded that there is no long term relationship between crack widths and rates of corrosion.

Schiessl does not propose any specific limiting value of crack width because his research shows that there is no value of crack width below which protection against corrosion could be guaranteed. Test results show that, for even a specimen with 25 mm (1 in.) cover, and a crack width of 0.15 mm (0.006 in.), there still exists a 40% probability that corrosion will appear.

A.2.2.6 Tuutti, K.

Tuutti[A.40] studied the effects of cracks in the concrete cover on the corrosion of reinforcing steel through a review of available literature. Tuutti also agrees that permissible crack width reported in the literature range from 0.1 mm to 1.0 mm (0.004 to 0.04 in.). In addition, it was also noted that a few authors had shown that cracks widths as small as 0.01 mm (0.0004 in.) give rise to corrosion attacks. Shown in the report are the findings of Rehm and Moll (1964). In these findings, specimens with relatively low concrete quality (w/c ratio 0.8) showed signs of corrosion for crack widths above 0.1 mm (0.004 in.). When only the crack width varied, it was shown that the corrosion varied with the crack width. However, these results were then supplemented by the results of Schiessl's 10 year study.[A.38,A.39] These results showed that,

> "corrosion in the uncracked zones always occurred as soon as the carbonation front had penetrated to the steel, in which the thickness of the concrete cover determines the initiation time, given the same concrete."[A.38]

It was stated that for short term duration, corrosion was dependent on a limiting crack width value. The value of this limiting crack width was not explicitly defined, as it depends on the concrete quality and other factors.

Cited in this paper are the results of work by Tremper,[A.34] in which concrete quality, as well as crack widths were variables studied. Crack widths varied from 0.13 mm to 1.3 mm (0.005 to 0.05 in.), and w/c ratios varied from 0.40 to 0.75. Specimens were exposed for a period of 10 years. Results showed that corrosion attacks occurred in the cracks and in their immediate surroundings in all cases.

Tuutti concludes that cracks in the concrete cover do not change the basic mechanisms of corrosion, but instead only have local effects. It is theorized that corrosion initiates when a threshold concentration of an initiating substance is achieved at the surface of the steel. The rate of corrosion is then determined by the flows of these substances to the area. So basically it is only the local flows of these substances that are changed by the crack widths.

A.2.2.7 Beeby, A.W.

Beeby[A.41,A.42,A.43] examined the relationship of cracking to corrosion of reinforcing steel. Based on his own studies, the works of Schiessl,[A.38,A.39] and others, he concludes that crack widths have little influence on corrosion. He also says that current guidelines for controlling crack widths are unnecessary.

This argument is based on the idea that cracking influences the onset of corrosion locally, but has a negligible long-term effect. He acknowledged that some short term tests (2 years) revealed an influence of crack widths on corrosion. Also cited were the results of Houston, Atimtay, and Ferguson[A.25] (see earlier discussion of this work). These results showed that crack widths had only a minimal effect on the corrosion of 84 beam and slab units exposed for up to two years with daily spaying of salt solution. Several other tests were cited to support the claim that crack widths have an overall minimal effect on the corrosion of steel in concrete.

Also used to support his claim that crack control guidelines are unnecessary is the work by Husain and Ferguson[A.44] regarding crack widths at the level of steel in concrete. In this study, it was found that there does not exist a definite relationship between the widths of surface cracks, and the widths of cracks at varying steel depths. Therefore, it is argued, the use of a surface crack width value can be completely arbitrary with regard to the actual situation in the field.

A.2.3 Prestressed Concrete Research

In comparison to corrosion research for reinforced concrete, very little research has been performed for prestressed concrete. In particular, the effectiveness of prestressing as corrosion protection through crack control has rarely been addressed. Some researchers have studied the corrosion of prestressed concrete, but in many cases, the specimens were not cracked or subjected to structural loading. Others, such as Houston et al[A.25] (see Section A.2.1.2) did not consider the effect of crack widths nor special measures for protection of the prestressing system. The research summarized in this section is all considered as short term exposure.

A.2.3.1 Poston, R.W.

Poston[A.45] performed an experimental program to examine transverse post-tensioning as a method for improving the durability of bridge decks. The effectiveness of the prestressing as a corrosion protection scheme was evaluated using representative full thickness (8″) bridge deck specimens subjected to an aggressive chloride environment. The laboratory specimens modeled the negative moment region of the bridge deck over an interior support (girder). The durability of prestressed bridge decks (100% prestressing) and conventionally reinforced bridge decks (no prestressing) were investigated.

Since the postulated mechanism by which the durability of a prestressed bridge deck is improved involves the control or elimination of cracking, crack width was included as a variable. The non-prestressed specimens and some of the prestressed specimens were loaded to produce surface crack widths of 0.015 in. (0.38 mm). The remaining prestressed specimens were loaded to the same load used to open the cracks of 0.015 in. in the non-prestressed specimens. This produced surface cracks of 0.002 in. (0.051 mm) in the prestressed specimens. Other variables included the type of prestressing system (unbonded or bonded), black or epoxy coated non-prestressed reinforcement (in all specimens) and concrete cover of 2 or 3 in. (50 or 75 mm). The concrete used in all of the specimens had a compressive strength f'c of 5100 psi (35.2 MPa) and used Type I cement with a water cement ratio of 0.44. The exposure conditions consisted of one wet-dry cycle every 14 days, continued for 17 cycles or 8 months. The wet portion of the cycle consisted

of 3.5% saltwater solution ponded on the specimens for two days. The specimens were then allowed to dry for the remaining nine days of the cycle. On the second day (during the wet portion), the specimens were subjected to five repeated loading cycles to produce the desired crack width. The same loading pattern was also applied on the ninth day, during the drying portion of the cycle.

From the accelerated exposure tests, the following observations related to cracking and corrosion were made:

1. **Corrosion Occurrence:** Corrosion of non-prestressed reinforcement initiated and occurred only at the location of flexural cracks. In many cases, corrosion had spread over a distance of 6 to 10 bar diameters (uncoated bars). The incidence and extent of corrosion was much less for the epoxy coated bars.
2. **Crack Width:** For both non-prestressed and prestressed specimens loaded to produce crack widths of 0.015 in. (0.38 mm), the incidence and extent of corrosion was similar. Virtually no incidence of corrosion of non-prestressed reinforcement was observed in the prestressed specimens with a crack width of 0.002 in. (0.051 mm). This represents the most significant effect of prestressing/crack control on reinforcement corrosion.
3. **Penetration of Chloride Ion:** Prestressing had little effect on chloride ion penetration in regions of uncracked concrete. However, chloride ion concentrations at crack widths of 0.002 in. (0.051 mm) were approximately 60% less than at crack widths of 0.015 in. (0.38 mm).
4. **Concrete Cover:** For the conditions and time length of the exposure testing in this study, no difference was observed for the two levels of cover considered.

A.2.3.2 Moore, D.G., Klodt, D.T., and Hansen, J.

As part of a large experimental program, Moore et al[A.46] performed a series of corrosion tests on pre-tensioned beams. The purpose of the tests was to evaluate:

- effect of voids between steel and concrete
- effect of concrete cover
- effect of live loads
- effect of sizable tensile cracks in concrete
- effect of accidental overloading (cracking followed by load reduction and cracks closing)

A total of 16 beams were tested. The dimensions of the beams were 4 x 6 in (102 x 152 mm) and 6.5 ft (1.98 m) long. The beams were pre-tensioned using two 3/8 in. (9.5 mm) dia., Gr 270 (1860 MPa) prestressing strands. One strand was placed near the compression face and the other near the tension face such that concentric prestressing was achieved. The concrete used Type I cement with w/c = 0.40. The compressive strength was 6300 psi (43.4 MPa). Concrete cover ranged from 1/2 in. to 2 in. (12.7 mm to 50 mm). Exposure conditions consisted of ponding with 3.5% NaCl solution. Exposure testing was continued for a period of 10 months.

The beams were loaded (3-point) in pairs, back to back. Various levels of load were used to evaluate increasing levels of extreme fiber stress. These included 1300 psi (8.96 MPa) compression, zero stress, 250 psi (1.72 MPa) tension, 500 psi (3.44 MPa)tension and 1000 psi (6.88 MPa) tension. The necessary applied load levels were calculated based on the desired stresses in an elastic uncracked section. The beams loaded to 1000 psi tension had a maximum average surface crack width of 0.008 in. (0.2 mm). All other specimens were "uncracked" under load. Two additional specimens were loaded to produce a surface crack width of 0.004 to 0.006 in. (0.1 to 0.15 mm), and then unloaded to zero extreme fiber stress (load corresponding to decompression at extreme fiber, assuming and elastic, uncracked section). No cracks were detectable upon load reduction.

The results of the exposure tests related to cracking and corrosion are summarized as follows:

1. **Effect of Cracks:** The most serious corrosion was observed in the beams with open cracks. Pitting corrosion was observed at cracks as small as 0.004 in. (0.1 mm).
2. **Effect of Temporary Overload:** Cracks in beams caused by brief overloading tended to "heal" after ten months of exposure. No increase in corrosion was observed at these crack locations.
3. **Effect of Load Level:** No correlation between load level and corrosion was observed, with the exception of the specimens loaded to cracking.
4. **Effect of Cover:** Concrete cover of 1.5 in. (38.1 mm) and larger prevented corrosion in the uncracked specimens over the ten months of exposure. Corrosion was found in all specimens with 0.75 in. (19 mm) cover or less.

A.2.3.3 Perenchio, W.F., Fraczek, J., and Pfiefer, D.W.

Perenchio et al[A.47] performed exposure tests to evaluate the effectiveness of epoxy coated strand and the effect of cracks on the durability of pre-tensioned members. The specimens were 12 ft (3.66 m) long with a 6 x 10 in. (152 x 254 mm) cross section. The beams were pre-tensioned with two 0.5 in. (12.7 mm) dia. Gr 270 seven-wire strands. The strands were located symmetrically, one at the top of the member and one at the bottom, such that the eccentricity was zero.

A total of 8 beams were tested. In 4 of the specimens, the strand closest to the tension face was epoxy coated. The second strand in these specimens was bare. Half of the specimens, 2 with epoxy coated and 2 with all bare strands, were intentionally cracked under flexural loading to an average surface crack width of 0.01 in. (0.254 mm). The cracks were maintained during exposure testing by loading the specimens in pairs, back to back. Exposure consisted of a one week long wet-dry cycle (3.5 days wet, 3.5 days dry) using 15% NaCl solution. During the dry portion of the cycle, the specimens were subjected to a constant temperature of 100 deg. F (37.8 deg. C) to further accelerate corrosion. Exposure testing was continued for 10 months. The specimens were wired externally to allow direct measurement of macrocell corrosion current.

The experimental results for the beams with bare strands only indicated that corrosion was more severe in cracked beams. Macrocell corrosion currents were

significantly higher in the cracked specimens. No quantitative corrosion current data was reported by the authors. In addition, half-cell potential readings indicated a high probability of corrosion in the cracked beams after only 30 days of exposure. Similar readings were obtained in the uncracked beams only after an exposure period of 60 days. Visual examination of the strands after autopsy at the conclusion of testing showed heavy corrosion on all strands near the tension face of the beam. The amount of corrosion in the cracked beams was not significantly more than in the uncracked beams. Some amount of corrosion was also observed on all strands nearest the compression face. Chloride content measurements indicated that chlorides had reached the strands at the compression face through cracks in the cracked specimens. In the uncracked specimens, high chloride levels at these strands were attributed to spillage of the salt water solution.

The macrocell corrosion current measurements were essentially zero for the specimens with epoxy coated strands. Occasional non-zero measurements indicated a reversed corrosion macrocell had developed (i.e. the bare strand near the compression face was corroding). This occurrence was confirmed during destructive examination of the beams after conclusion of exposure testing. As in the specimens with bare strands only, this corrosion was attributed to penetration of chlorides at crack locations or due to spillage. Half-cell potential readings for the beams with epoxy coated strands were erratic and could not be used to draw any conclusions.

From the reported experimental results, the following observations can be made:

1. **Effect of Cracking:** Cracking (crack width = 0.01 in. (0.254 mm)) reduced the time to initiation of corrosion and increased corrosion severity. However, significant corrosion also occurred in companion uncracked specimens.
2. **Critical Crack Width:** No conclusions regarding critical crack width can be made from the results of this study.
3. **Concrete Cover:** 1 in. (25 mm) of clear cover was not sufficient to prevent corrosion in either cracked or uncracked specimens.
4. **Epoxy Coated Strand:** Epoxy coated strand showed no signs of corrosion during exposure testing. However, experimental results illustrate the importance of using epoxy coated strand throughout the member rather than just at the level of steel closest to the tension face.

Appendix A – References:

A.1) **Koester, Bradley D.,** "Evaluation of Cement Grouts for Strand Protection Using Accelerated Corrosion Tests," Master of Science Thesis, The University of Texas at Austin, December 1995.

A.2) **ACI Committee 318,** Building Code Requirements for Reinforced Concrete, ACI 318-95, American Concrete Institute, Detroit, MI, 1995, 369 pp.

A.3) **Gergely, P. and Lutz, L.A.,** "Maximum Crack Width in Reinforced Concrete Members," SP-20, American Concrete Institute, Detroit, MI, 1968, pp. 87-117.

A.4) **AASHTO**, LRFD Bridge Design Specifications, 2nd Edition, American Association of State Highway and Transportation Officials, Washington, D.C., 1998.

A.5) Design of Concrete Structures for Buildings, CAN3-A23.3-M84, Canadian Standards Association, Rexdale, Ontario, 1984.

A.6) Ontario Highway Bridge Design Code, 3rd Edition, Ontario Ministry of Transportation, Quality and Standards Division, Toronto, Ontario, 1991.

A.7) Commentary - Ontario Highway Bridge Design Code, Ontario Ministry of Transportation, Quality and Standards Division, Toronto, Ontario, 1991.

A.8) CEB-FIP Model Code 1990, CEB Information Report No. 213/214, Comite Euro-International Du Beton, Lausanne, May 1993.

A.9) Code of Practice for the Structural Use of Concrete - Part 1. Design, Materials and Workmanship, British Standards Institution Publication CP 110, London, England, November 1972 (Amended May 1977).

A.10) Concrete Structures, SIA Standard 162, Swiss Society of Engineers and Architects, Zurich, Switzerland, July, 1989.

A.11) Standard Specification for Design and Construction of Concrete Structures - 1986, Part 1 (Design), Japan Society of Civil Engineers, SP-1, Tokyo, Japan, 1986.

A.12) **ACI Committee 201,** "Guide to Durable Concrete," ACI 201.2R-92, American Concrete Institute, Detroit, Michigan.

A.13) **ACI Committee 222,** "Corrosion of Metals in Concrete," ACI 222R-89, American Concrete Institute, Detroit, Michigan.

A.14) **Atimtay, E., and Ferguson, P.M.,** "Early Chloride Corrosion of Reinforced Concrete - A Test Report," *Materials Performance*, V. 13, No. 12, 1974, pp. 18-21.

A.15) **Martin, H., and Schiessl, P.,** "The Influence of Cracks on the Corrosion of Steel in Concrete," *Preliminary Report*, RILEM International Symposium on the Durability of Concrete, Prague, 1969, V. 2.

A.16) **Raphael, M. and Shalon, R.,** "A Study of the Influence of Climate on the Corrosion of Reinforcement," *Proceedings*, RILEM Symposium on Concrete and Reinforced Concrete In Hot Countries, Building Research Station, Haifa, 1971, pp. 77-96.

A.17) **ACI Committee 224,** "Control of Cracking in Concrete Structures," ACI 224R-90, American Concrete Institute, Detroit, Michigan.

A.18) **Nawy, Edward, G.,** "Crack Control in Reinforced Concrete Structures," ACI JOURNAL, *Proceedings* V. 65, No. 10, Oct. 1968, pp. 825-836.

A.19) **U.S. Bureau of Public Roads - Bridge Division,** Strength and Serviceability Criteria - Reinforced Concrete Bridge Members, U.S. Department of Transportation, Washington, D.C., 1967.

A.20) **ACI Committee 350,** "Environmental Engineering Concrete Structures," ACI 350R-89, American Concrete Institute, Detroit, Michigan.

A.21) **CEB,** Durable Concrete Structures – CEB Design Guide, Bulletin D'Information No. 182, Comité Euro-International du Béton, Lausanne, June 1989, 310 pp.

A.22) **CEB,** Bulletin D'Information No. 148, "Durability of Concrete Structures" State of the Art Report, Comité Euro-International du Béton, Paris, January 1982.

A.23) **CEB,** Design Manual on Cracking and Deformations, Comité Euro-International du Béton, École Polytechnique Fédérale De Lausanne, Suisse, 1985, 231 pp.

A.24) **Kahhaleh, K.Z.,** "Corrosion Performance of Epoxy Coated Reinforcement," Doctor of Philosophy Dissertation, Department of Civil Engineering, The University of Texas at Austin, May 1994.

A.25) **Houston, J.T., Atimtay, E., and Ferguson, P.M.,** "Corrosion of Reinforcing Steel Embedded in Structural Concrete," Research Report 112-1F, Center for Highway Research, The University of Texas at Austin, March 1972.

A.26) **Vennesland, O. and Gjorv, O.E.,** "Effect of Cracks in Submerged Concrete Sea Structures on Steel Corrosion," *Materials Performance*, Vol. 20, August 1981, pp. 49-51.

A.27) **Lin, C.Y.,** "Bond Deterioration Due to Corrosion of Reinforcing Steel," *Performance of Concrete in Marine Environment*, ACI SP-65, American Concrete Institute, Detroit, Michigan, 1980, pp. 255-269.

A.28) **Makita, M., Mori, Y., and Katawaki, K.,** "Marine Corrosion Behavior of Reinforced Concrete Exposed at Tokyo Bay," *Performance of Concrete in Marine Environment*, ACI SP-65, American Concrete Institute, Detroit, Michigan, 1980, pp. 271-289.

A.29) **Misra, S. and Uomoto, T.,** "Reinforcement Corrosion under Simultaneous Diverse Exposure Conditions", *Durability of Concrete, Second International Conference*, ACI SP 126, American Concrete Institute, Detroit, MI, pp.423-441.

A.30) **Okada, K. and Miyagawa, T.,** "Chloride Corrosion of Reinforcing Steel in Cracked Concrete," *Performance of Concrete in Marine Environment*, ACI SP-65, American Concrete Institute, Detroit, Michigan, 1980, pp. 237-289.

A.31) **Swamy, R.N.,** "Durability of Rebars in Concrete", *Durability of Concrete, G.M. Idorn International Symposium*, ACI SP-131, American Concrete Institute, Detroit, MI, pp.67-98.

A.32) **Berke, N.S., Dalliare, M.P., Hicks, M.C., and Hoopes, R.J.,** "Corrosion of Steel in Cracked Concrete," *Corrosion*, V. 49, No. 11, Nov. 1993, pp. 934-943.

A.33) **Schiessl, P., and Raupach, M.,** "Laboratory Studies and Calculations on the Influence of Crack Width on Chloride-Induced Corrosion of Steel in Concrete," *ACI Materials Journal,* Vol. 94, No. 1, January-February 1997, pp. 56-62.

A.34) **Tremper, Bailey,** "The Corrosion of Reinforcing Steel In Cracked Concrete," *ACI JOURNAL, Proceedings* V. 43, No. 10, June 1947, pp. 1137-1144.

A.35) **Ohta, T.,** "Corrosion of Reinforcing Steel in Concrete Exposed to Sea Air", *Durability of Concrete, Second International Conference*, ACI SP-126, American Concrete Institute, Detroit, MI, pp.459-477.

A.36) **Francois, R. and Arliguie, G.,** "Reinforced Concrete: Correlation Between Cracking and Corrosion", *Durability of Concrete, Second International Conference*, ACI SP-126, American Concrete Institute, Detroit, MI, pp.1221-1238.

A.37) **O'Neil, E.F.,** "Study of Reinforced Concrete Beams Exposed to Marine Environment," *Performance of Concrete in Marine Environment*, ACI SP-65, American Concrete Institute, Detroit, Michigan, 1980, pp. 113-132.

A.38) **Schiessl, P.,** "Admissible Crack Width in Reinforced Concrete Structures", Contribution II 3-17, Inter-Association Colloquium on the Behavior in Service of Structures, Preliminary Reports, Vol. II, Liege 1975, pp.739-753.

A.39) **Schiessl, P.,** "Zur Frage der zulassigen Rissbreite und der erforderlichen Betondeckung im Stahlbetonbau unter besonderer Berucksichtigung der Karbonatisierung des Betons", Deutscher Ausschuss fur Stahlbeton, Heft 255, Berlin 1976.

A.40) **Tuutti, Kyosti,** "Cracks and Corrosion", CBI Research No. 6:78, Swedish Cement and Concrete Research Institute, Stockholm, 1978, 55 pp.

A.41) **Beeby, A. W.,** "Cracking, Cover, and Corrosion of Reinforcement", *Concrete International*, Vol. 5, No. 2, February 1983, pp.35-40.

A.42) **Beeby, A.W.,** "Corrosion of Reinforcing Steel in Concrete and its Relation to Cracking", *The Structural Engineer*, V. 56A, No. 3, London, March 1978, pp.77-81.

A.43) **Beeby, A.W.,** "Cracking and Corrosion", Concrete in the Oceans, Technical Report No. 1, Construction Industry Research and Information Association/Cement and Concrete Association, London 1978, 77 pp.

A.44) **Husain, S. I., and Ferguson, P. M.,** "Flexural Crack Width at the Bars in Reinforced Concrete Beams," Research Report No. 102-1F, Center for Highway Research, University of Texas at Austin, June 1968.

A.45) **Poston, R.W.,** "Improving Durability of Bridge Decks by Transverse Prestressing," Doctor of Philosophy Dissertation, The University of Texas at Austin, December 1984.

A.46) **Moore, D.G., Klodt, D.T., and Hansen, J.,** "Protection of Steel in Prestressed Concrete Bridges," NCHRP Report 90, 1970, 86 p.

A.47) **Perenchio, W.F., Fraczek, J., and Pfiefer, D.W.,** "Corrosion Protection of Prestressing Systems in Concrete Bridges," NCHRP Report 313, February 1989, 25 pp.

Appendix B:

Field Performance of Prestressed Concrete Bridges: Literature Review

This appendix provides a brief review of available literature on the field performance of prestressed concrete structures, with an emphasis on bridges. The review addresses the following areas:

B.1 Corrosion of Prestressing Strand Before Construction

B.2 Pretensioned Bridges

B.3 Unbonded Single Strand (Monostrand) Tendons

B.4 Unbonded Internal Tendons (Multistrand and Bar) in Bridges

B.5 External Multistrand Tendons in Bridges

B.6 Bonded Internal Post-Tensioned Tendons in Bridges

General occurrences of corrosion problems are described according to type of prestressing, time of occurrence and various aspects of the prestressing system. Where possible, specific case studies are provided for illustration. The findings and conclusions from the literature review are discussed in Chapter 2, Section 2.6.

B.1 Corrosion of Prestressing Strand Before Construction

Corrosion of prestressing strand occurring prior to construction can lead to failures before, during and after stressing. Corrosion prior to construction may result from improper storage and handling during shipping. Failures before stressing normally occur in cases where the prestressing strand is stored in tightly wound coils. This type of failure is generally attributed to stress corrosion cracking and is most common in quenched and tempered steel, which is more susceptible to stress corrosion. Quenched and tempered steel is not permitted by AASHTO or ACI (see Section 2.4.4.1), and is generally not available for use in North America. Reports of this type of failure have primarily been from Germany. Chemical contamination of the strand during storage, transport and handling can lead to embrittlement or pitting corrosion of the strand. Common sources of contamination are splashing with fertilizers, water containing lime and gypsum, animal wastes and raw oils.[B.1] Pitting corrosion may also occur as a result of exposure to moisture, saltwater or sea-mist during storage or transportation. Embrittlement and pitting corrosion may lead to failure prior to stressing. Corrosion occurring before stressing may also cause failure during stressing and after stressing in both pretensioned and post-tensioned structures.[B.1] Guidelines for assessing the degree of corrosion on prestressing strand before it is placed in the structure are provided by Sason[B.2] and PCI.[B.3]

B.2 Pretensioned Bridges

The types of corrosion problems in pretensioned structures are not significantly different from those in reinforced concrete structures. The absence of the post-tensioning duct and anchorages in pretensioned concrete makes it more similar to reinforced concrete in terms of the protection provided for the prestressing steel. The main influencing factors for corrosion in pretensioned structures are the prestressing steel, concrete and severity of environment. The effect of the concrete and environment is the same for pretensioned and reinforced concrete structures. Although prestressing steel is more susceptible to corrosion and the consequences of corrosion may be more severe than for mild steel reinforcement, corrosion of prestressing tendons in pretensioned structures is rare for two main factors. Pretensioned elements are always precast, generally resulting in improved overall quality control and good quality concrete. Also, pretensioned elements normally fit the classic definition of full-prestressing, that is, concrete tensile stresses are limited to prevent flexural cracking of the concrete. Where corrosion has been discovered in pretensioned structures, the cause is normally related to the structural form and details. Because pretensioned elements are precast, the structure may contain a large number of joints or discontinuities. Poor design and/or maintenance of these joints may direct moisture and chlorides onto the pretensioned elements of the structure in very localized areas.

Novokschenov[B.4] performed an extensive condition survey of several pretensioned and post-tensioned bridges, in both marine and de-icing salt environments. One bridge located in the Gulf of Mexico consisted of pretensioned girder approach spans and post-tensioned segmental box girder main spans. The bridge was 16 years old at the time of inspection. Corrosion damage consisting of concrete cracking caused by corrosion of the prestressing steel was found on the ends of the pretensioned girders adjacent to the

expansion/contraction joint at the transition between the approach and main spans. Corrosion was attributed to chloride laden moisture from the deck leaking through the expansion/contraction joint onto the ends of the girders, producing highly localized, severe exposure conditions. Novokschenov[B.4] also examined a precast pretensioned box girder viaduct that had been exposed to de-icing salts throughout its service life. The bridge was 29 years old at the time of inspection. Examination revealed that almost all longitudinal joints between box girders were leaking, ranging from very minor to extensive. The leakage appeared to have resulted from moisture and chlorides penetrating through cracks in the cast-in-place concrete deck overlay and progressing through the longitudinal joints between the girders, as shown in Figure B.1. In the areas of heaviest leakage, extensive staining and white deposits were visible, accompanied by corrosion of the prestressing strands and deterioration of the concrete cover. In some areas, spalling exposed the prestressing strands, leading to severe deterioration and failure of up to six of the seven wires in several strands. The specified concrete cover for this bridge was 45 mm (1.75 in.), and measured cover was up to 6 mm (0.25 in.) less than this value. Novokschenov mentioned that this type of damage was common in other, similar bridges, and concluded that is an inherent problem to this particular bridge design. A third bridge examined in this report[B.4] consisted of precast pretensioned I-girders. Corrosion related damage consisting of concrete cracking and spalling was found in girders adjacent to longitudinal expansion joints and at the ends of most girders at transverse joints, both expansion and fixed. The path of chloride laden water at a longitudinal expansion joint and the resulting deterioration are shown in Figure B.2. In areas where the strand was exposed due to spalling, wire fractures were common. Corrosion damage at the ends of the girders was less severe at fixed joints in comparison to expansion joints, attributed to less leakage of chloride laden moisture from the bridge deck. The specified cover was 50 mm (2 in.), and measured covers were up to 6 mm (0.25 in.) less than this value.

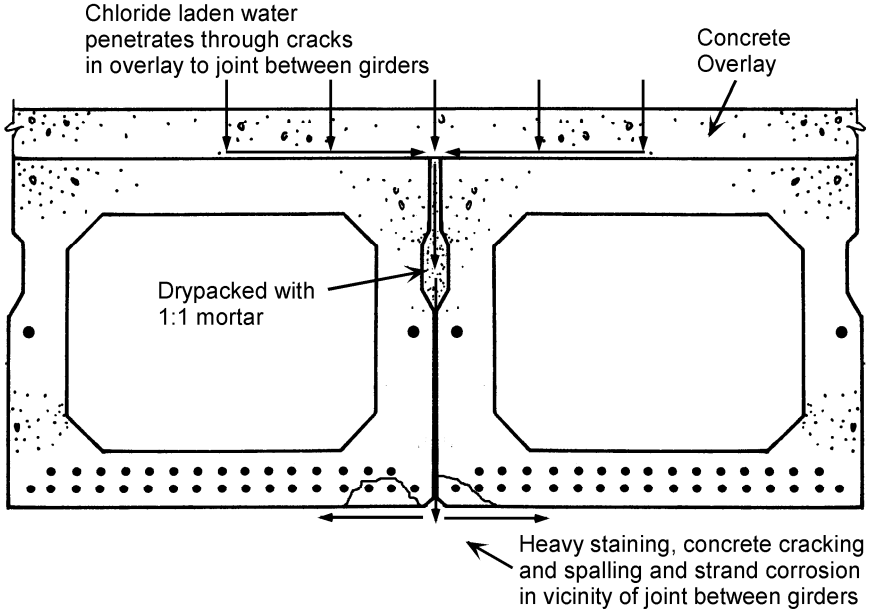

Figure B.1 - Mechanism for Moisture and Chloride Penetration Through Concrete Overlay in Precast Pretensioned Box Girders (adapted from Ref. B.4)

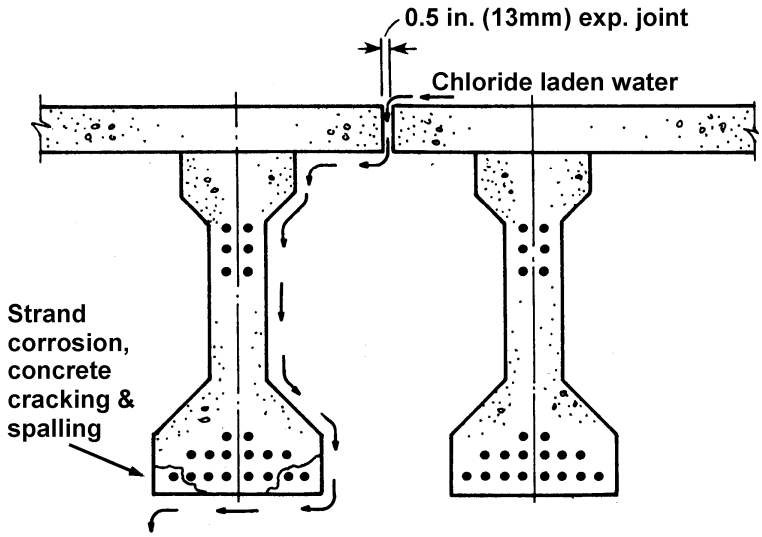

Figure B.2 - Mechanism for Moisture and Chloride Penetration at Longitudinal Expansion Joints in Precast I-Girder Bridges (adapted from Ref. B.4)

Others have performed similar condition studies of bridges with pretensioned elements.[B.5] In general, these surveys found corrosion related deterioration in pretensioned members to be localized in specific areas of the structure, primarily at transverse joints along the bridge. The findings of condition surveys of pretensioned bridges indicate that corrosion problems in this type of structure are primarily a function of the design of the structure, rather than the pretensioned elements. Improved joint design and maintenance or minimization of joints would appear to eliminate most corrosion problems.

B.3 Unbonded Single Strand Tendons

Unbonded single strand or monostrand tendons refer to greased and sheathed type single strand tendons commonly used in slabs. Monostrand unbonded tendons represented approximately 80% of post-tensioning used in the U.S. from 1965 to 1991.[B.6] The majority of this steel was used in buildings (including parking structures) and in slabs-on-grade. Although monostrand applications would be very limited in bridge substructures, they have been used for transverse post-tensioning in bridge decks and segmental box girders. Also, examination of corrosion problems in structures with monostrand tendons can provide insight into the overall picture of corrosion in post-tensioned structures, including bridges.

The evolution of the monostrand system for post-tensioning is shown in Figure B.3. Common locations of corrosion are indicated by the letter "C" in the figure. A very comprehensive discussion of corrosion of monostrand tendons is provided by ACI/ASCE

Committee 423.[B.7] Corrosion problems in monostrand tendons can be grouped into four areas:

1. Damage to the sheathing,
2. Poor anchorage protection,
3. System deficiencies,
4. Structural aspects.

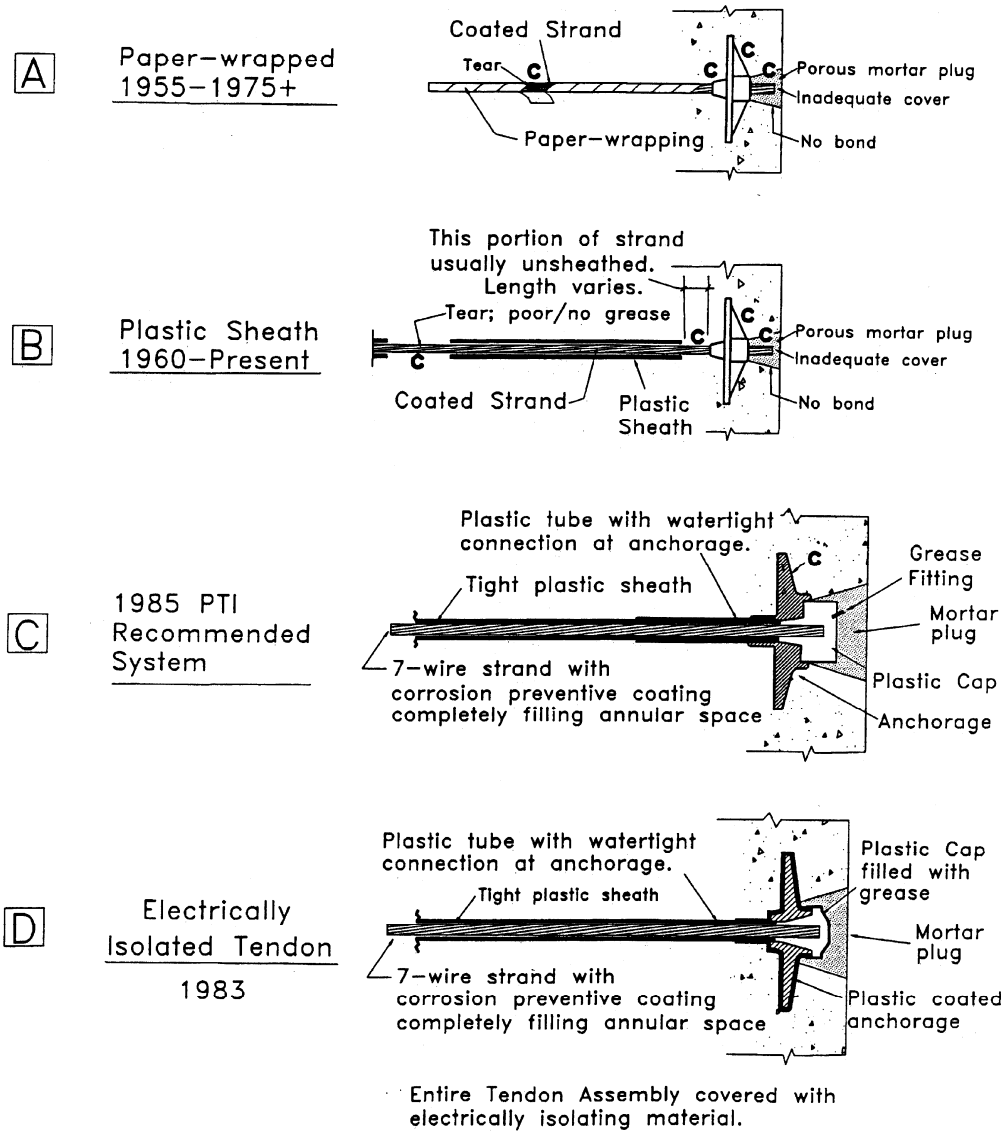

**Figure B.3 - Evolution of Monostrand Systems for Post-Tensioning (Ref. B.6)
(common locations for corrosion indicated by "c")**

B.3.1.1 Sheathing Damage

Damage to the sheathing during transportation, handling and placement can lead to corrosion by allowing moisture and chlorides to reach the tendon. This situation is worsened when cracks in the concrete or concrete with high permeability provides easy access for moisture and chlorides to reach the tendon. In some cases, water has been found inside the sheath of tendons located buildings where they were not exposed to moisture.[B.6] In this situation, it is likely that water entered the tendon sheath during fabrication, handling or prior to concrete placement.

B.3.1.2 Anchorage Protection

Inadequate anchorage protection can lead to multiple forms of corrosion problems in monostrand systems. Corrosion of the anchorage itself is a common problem. Failure of the anchorage in an unbonded system obviously leads to loss of the tendon. Corrosion of the anchorage typically occurs due to lack of a protective barrier or insufficient concrete cover. Concrete or mortar used to cover anchorage recesses after stressing is often low quality, allowing moisture penetration to the anchorage. Placement of the anchorage in locations where exposure to moisture and chlorides may occur, such as at or below construction or expansion joints, has also lead to corrosion related anchorage failures of monostrand tendons. Typical moisture and chloride access to the monostrand system is shown in Figure B.4.[B.8] Schupack[B.6] reported corrosion of live-end anchorages at expansion joints and at dead-end anchorages where the concrete was cracked. Kesner and Poston[B.9] reported corrosion of live-end anchorages at the edge of balconies in a residential building. In this situation, the anchorages were not sufficiently protected for their exterior exposure.

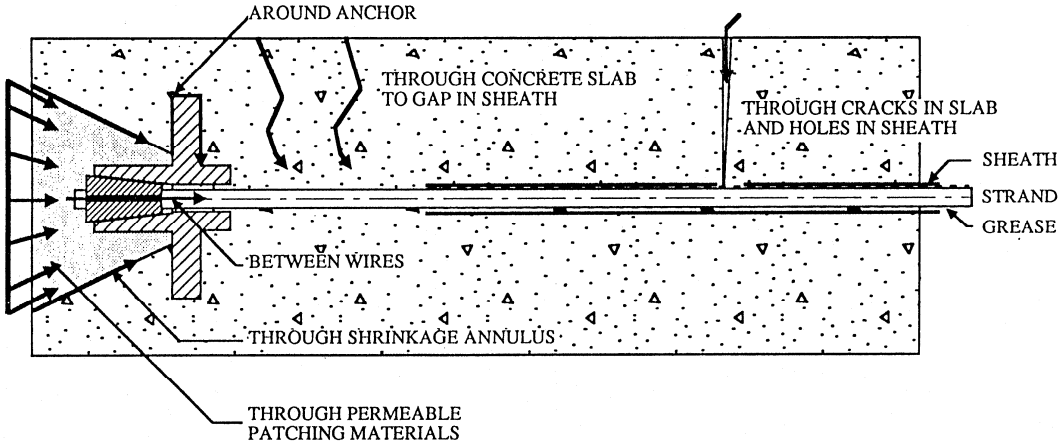

Figure B.4 - Possible Moisture and Chloride Access to Monostrand Systems (Ref. B.8)

Poor quality anchorage protection can also lead to corrosion of the strand stub that projects from the anchor. If the strand stub corrodes, it often provides a pathway for

moisture to reach the anchorage, or it may allow moisture to move along the interstices between the wires, and into the greased and sheathed length of the strand. Schupack[B.10] reports a situation where water was leaking through a light fixture in a flat slab post-tensioned building. The source of moisture was rain water penetrating a poorly protected end anchorage on the exterior of the building. Rain water entered the tendon thought the anchorage and moved along the tendon inside the sheath, exiting the tendon where the sheath was damaged.

B.3.1.3 System Deficiencies

Many corrosion problems in monostrand systems have been related to the system itself. Most of these problems occurred in older monostrand systems, such as A and B shown in Figure B.3. Modern developments in monostrand systems (C and D, Figure B.3) have eliminated many of the problems found in older systems.

The evolution of sheath types used in monostrand systems is shown in Figure B.5. Earlier sheath systems have shown poor long term corrosion protection. Paper wrapping is not waterproof and is easily damaged. Peterson[B.11] reports that paper wrapped monostrand tendons are a common corrosion problem in parking structures. Heat sealed sheaths have been found to split open over time, compromising the moisture barrier for the strand. A large number of monostrand corrosion problems have been encountered with the push-through sheath.[B.6] Even when the sheath is intact, the annular space around the strand allows movement of moisture and chlorides. Schupack[B.6] reported severe tendon corrosion and failures in a seven year old platform structure with push-through monostrand tendons. Water entered the sheathing at poorly protected end anchorages. Intermittent corrosion and wire failures were found throughout the structure. Tight fitting extruded sheaths should minimize this problem.

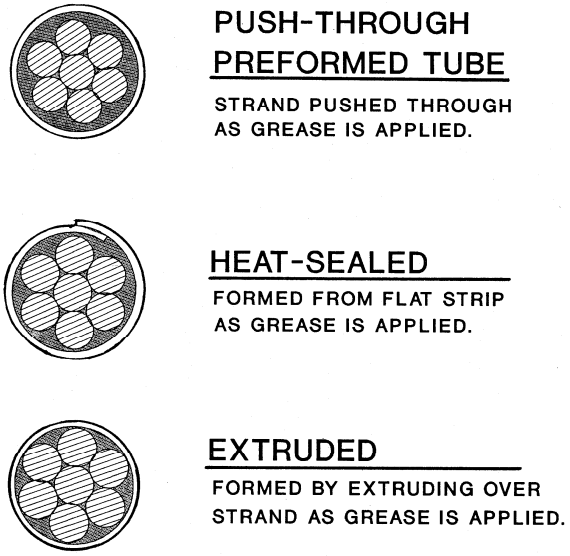

Figure B.5 - Evolution of Sheaths for Monostrand Systems (Ref. B.10)

Another common source of monostrand corrosion problems has been the discontinuity of sheathing and grease on the strand immediately behind the anchorage (see Figure B.3). Schupack[B.6] reported on a thirteen year old parking structure with extruded sheaths. The stressing anchorages in this structure were located at an expansion joint that permitted moisture and chlorides to come in contact with the anchorage. Removal of concrete behind the anchorages revealed severe corrosion of the prestressing strand where the sheath was not present. Examination of strand where the sheath was intact revealed bright strand with no evidence of corrosion. Schupack[B.6] also reported severe pitting corrosion on unsheathed strand at dead-end anchorages in a fourteen year old parking structure. The anchorages were located away form expansion and construction joints. Moisture appeared to reach the tendon through cracks in the vicinity of the anchorage, leading to corrosion.

The grease used in the monostrand systems also plays a critical role in corrosion protection in addition to providing lubrication. Grease related problems have included inadequate coverage, water soluble grease, contaminated grease and the lack of corrosion inhibitors in the grease.

B.3.1.4 Structural Design Aspects

Some aspects of the design process may lead to further corrosion problems. Electrical contact between the monostrand tendon and other reinforcement may provide the opportunity for macrocell corrosion with a large cathode (reinforcement) and small anode (monostrand tendon) in a non-isolated system. Large cathode to anode areas can lead to high corrosion rates and severe corrosion damage. The electrically isolated system shown in Figure B.3 should prevent this occurrence.

Reinforcement congestion or reinforcement ties may lead to sheathing damage during post-tensioning of the monostrand.

Inadequate concrete cover can play two roles in corrosion of monostrand systems. First, concrete is a barrier to penetration of moisture and chlorides. The second role is as protection for the monostrand system. Wiss, Janney, Elstener Associates, Inc.[B.12] reported a parking garage where corrosion of the mild steel reinforcement led to concrete spalling and delamination. A combination of low cover and severe spalling exposed the monostrand tendons at the high points of the tendon profile. Traffic wear and tear eventually damaged the tendons, allowing moisture penetration and corrosion of the tendons.

B.4 Unbonded Internal Tendons in Bridges

This section deals with unbonded internal tendons other than monostrand tendons. Included in this category are unbonded multistrand tendons and unbonded post-tensioning bars. Internal unbonded tendons are not commonly used for several reasons. The lack of grouting that provides bond between the tendon and concrete limits the ultimate load carrying capacity of the structure. Unbonded internal tendons also suffer a lack of corrosion protection options, primarily that provided by grout. Failure of an unbonded tendon, due either to tendon corrosion or anchorage corrosion, leads to a complete loss of prestress.

Novokschenov[B.4] reported a condition survey of a bridge with pretensioned and post-tensioned girders located in Salt Lake City. Post-tensioned girders were prestressed with unbonded post-tensioning bars. Two 25 mm (1 in.) diameter and two 38 mm (1.5 in.) diameter prestressing rods were used in each girder. Each post-tensioning bar was placed inside a galvanized steel duct, and no additional corrosion protection was provided. Bar anchorage was provided using end nuts and a steel bearing plate. Anchorages were located in pockets that were filled with mortar after stressing. The bridge was located in an environment where deicing salts were used. After thirteen years of service, failures of the post-tensioned bars began occurring. Failures were first indicated by loud noises heard by persons in the area, and by bars projecting from the ends of the girders. Additional failures were discovered by removing the mortar anchorage protection and checking for loose bar ends and nuts. No cracks or rust stains were found on the exterior of the girders. Twenty one bar failures were found in total. Pitting corrosion was found on the fractured bars, and the absence of necking or cross-section reduction suggested the failure was brittle in nature. The source of corrosion was attributed to moisture and chlorides entering the ducts at the anchorage zones and moving along the tendon. Corrosion of the steel anchorage plates was rated from moderate to very severe. Corrosion of the plates caused cracking and spalling of the mortar cover. Chloride measurements in the mortar were very high. A malfunctioning drainage system and leaking expansion joints allowed chloride laden moisture to drip onto the ends of the girders and the anchorage areas. Examination of the duct exterior at locations away from girder ends found no sign of corrosion activity. It was concluded that penetration of moisture and chlorides through the concrete cover and galvanized steel duct was unlikely, and that the sole cause of corrosion was penetration at end anchorages.

B.5 External Multistrand Tendons in Bridges

The most common forms of external multistrand tendons occur in bridges. Cable stays may also be considered in this category. Corrosion protection for multistrand external tendons typically consists of a plastic or metal sheath normally filled with grout or corrosion inhibiting grease. Observed corrosion related failures or problems have resulted from a breakdown in the sheathing system or insufficient protection of the anchorages. These situations are worsened by poor or incomplete filling of the void space around the tendon with grout or grease that allows movement of moisture along the tendon length after penetration.

Robson and Brooman reported[B.13] corrosion related distress in a precast segmental box girder bridge with external tendons. The external prestress was provided by 240 tendons, each consisting of nineteen wires (19 mm (3/4 in.) dia.) inside a plastic, grease filled sheath. Severe signs of distress were observed after approximately twenty years of service life. Two of the 240 tendons had failed completely, and evidence of individual wire fracture was observed in 121 of the remaining tendons. The fractures were attributed to corrosion of the wires in the anchorage zones. It was assumed that corrosion began during a ten month construction delay during which the tendon ends were left unprotected. Because the tendons were external, individual wire failures were detectable by visual inspection. Existing tendons were removed and the bridge was prestressed with new tendons after modifications to the anchorage areas.

B.6 Bonded Internal Post-Tensioned Tendons in Bridges

B.6.1 After Stressing, Before Grouting

The time period after stressing but before grouting provides an open opportunity for corrosion of post-tensioning tendons. During this period, the tendon is not fully protected, and tendon corrosion has occurred as a result of water penetrating the ducts through either the end anchorages or grouting ports and vents. Hydrogen embrittlement failures have been attributed to corrosion occurring during the period between stressing and grouting.[B.14] Many construction specifications limit the length of time between stressing and grouting of post-tensioned tendons to forty-eight hours to minimize the potential for corrosion during this period. Corrosion occurring after stressing but before grouting could also lead to failures after the structure has been in service for some period.

B.6.2 In Service

Incidents of corrosion in post-tensioned structures during service have been attributed to a variety of sources. The corrosion protection of a post-tensioning tendon in service is provided by a multi-layered system of variables, and a breakdown in any of the components may lead to tendon corrosion. In most cases, corrosion related deterioration is related to an inadequacy or breakdown in more than one component of the protection system.

B.6.2.1 Grouting

Many corrosion problems have resulted from various aspects of grouting. The effectiveness of the grout as corrosion protection is related both to its material properties and construction practices.

The most common grout related corrosion problems are attributed to incomplete grouting, that is, where the duct is not completely filled with grout. The extent of incomplete grouting may range from small voids to a complete lack of grouting. Common causes of incomplete grouting are construction difficulties, improper construction practices, blocked or damaged ducts and improper placement or usage of vents. The fresh properties of the grout may also affect the grouting process through insufficient or excessive fluidity and excessive bleed water, leading to entrapped air or the formation of bleed lenses. The severity of tendon corrosion is related to the extent of incomplete grouting and the availability of moisture, oxygen and chlorides. In general, the most severe attack occurs when the tendon is intermittently exposed and embedded in the grout. In this situation, a concentration cell may occur due to the variations in the chemical and physical environment along the length of the tendon. Concentration cells may result from differences in oxygen, moisture and chloride concentration, and often lead to severe macrocell corrosion.

Tendon corrosion may also occur in situations where the entire length of the tendon is well grouted. The most common cause of corrosion in these situations has been sources of chlorides in the grout itself. Examples include seawater used as the mixing water or chloride containing admixtures. A combination of severe exposure conditions

and low cover may lead to corrosion of the duct and subsequent penetration of moisture and chlorides from an external source.

Isecke[B.15] described a detailed examination of a bonded post-tensioned bridge in Germany. The bridge was demolished after less than twenty years of service due to corrosion related deterioration. Isecke reported varying levels of grouting: full grouting, partial grouting, partial or total coating of the steel surface with a thin film of grout and complete absence of grout. No corrosion was found where grouting was complete and the steel fully embedded in grout. Varying amounts of corrosion damage were found under all other grouting conditions. The most severe corrosion was reported in partially grouted ducts at the boundaries between exposed and embedded steel. In ducts that were completely ungrouted, the prestressing steel was covered with a thin film of rust, but the reduction of area due to corrosion was deemed very small.

Schupack[B.16,B.17] performed an extensive forensic examination on a thirty-five year old post-tensioned bridge. The extent of corrosion damage in this bridge was not significant enough to affect structural behavior.[B.16] Corrosion deterioration was attributed to two sources: poor and incomplete grouting throughout the bridge, and the use of grout containing high levels of chloride in some girders. Schupack found a range of grouting, from fully grouted, to partial grouting to a complete lack of grout. The extent of corrosion was dependent on the completeness of grouting, the type of grout, and the availability of moisture. No corrosion was found in tendons where the ducts were completely filled with grout that did not contain chlorides. In partially grouted tendons (with no chlorides in the grout) and in ungrouted tendons, most exposed wires had surface corrosion. Severe corrosion was found at tendon low points where water had collected in the duct. Several tendons that were completely ungrouted, but free of moisture, showed no signs of corrosion. Several girders in the bridge were grouted using an expansive grout that contained high levels of chloride. This grout was not recommended for post-tensioning applications by its manufacturer, as expansive properties were achieved by adding iron filings and chlorides to provide expansion though corrosion of the iron. Chloride analysis performed on grout samples from the bridge found chloride levels as high as 8000 ppm by weight of grout. Very severe tendon and duct corrosion was found where this grout was used. Deep pitting corrosion and random wire breaks were found. Schupack also reported significant longitudinal cracks in the webs of the girders following the tendon profile. In most cases, the cracks were attributed to freezing of water in partially grouted or ungrouted tendons, rather than from tendon corrosion, illustrating additional deterioration that may result from poor grouting.

B.6.2.2 Inadequate Concrete Cover

Concrete cover provides an additional level of protection for the tendon. In situations where the protection provided by the duct is less than adequate, low concrete cover has contributed to tendon corrosion.

Novokschenov[B.4] reported a condition survey of the Gandy Bridge in Florida. This bridge consisted of precast post-tensioned girders with reinforced concrete deck slab. Post-tensioning was provided using 28.6 mm (1.125 in.) diameter prestressing bars. Each bar was located inside a 38.1 mm (1.5 in.) grouted metal duct. The bridge was less than thirty-five years old at the time of inspection, and had experienced significant cracking

and spalling resulting from corrosion of the post-tensioning ducts and tendons. Measured values of concrete cover for the bottom tendons were less than the specified value of 70 mm (2.75 in.), ranging from 32 mm (1.25 in.) to 64 mm (2.5 in.), with an average of 53 mm (2.1 in.). Concrete in the girders was air-entrained with low water-cement ratio. Rapid chloride permeability measurements on concrete samples from the bridge indicated moderate to low permeability. Because the concrete was of good quality, Novokschenov concluded that insufficient concrete cover was the major cause of corrosion of the post-tensioning tendons.

B.6.2.3 Duct Problems

The post-tensioning duct is an important component of corrosion protection in post-tensioned structures. Many forms of ducts exist, ranging from non-permanent duct formers, to galvanized steel ducts, to plastic ducts, each providing an increasing level of protection. Incidents of corrosion have resulted from damaged ducts, improper splices between ducts, corroded ducts and situations where non-permanent duct formers have been used. Holes in the duct may allow concrete to enter the duct during casting. This may hamper placement and tensioning of the tendons, and may cause difficulties during grouting. Damage or misalignment during construction or concrete placing may also lead to post-tensioning and grouting difficulties.

As mentioned in the preceding section, Novokschenov[B.4] reported duct and tendon corrosion in a post-tensioned bridge in Florida. Novokschenov concluded that insufficient concrete cover led to severe corrosion of the metal ducts and post-tensioning tendons. If non-corroding plastic ducts had been used, it is possible that corrosion related deterioration of the post-tensioning system could have been eliminated in spite of low cover. Isecke[B.15] also reported total deterioration of metallic ducts due to corrosion in many areas of a post-tensioned bridge. Corrosion of the duct lead to moisture and chloride penetration into the grout. In most cases, deterioration of the duct corresponded to severe corrosion and occasionally fracture of the prestressing steel.

B.6.2.4 Anchorage Protection

Anchorage corrosion in bonded tendons is generally not deemed failure critical, unlike unbonded tendons. Bond between the tendons and concrete will prevent a complete loss of prestressing. However, anchorage corrosion and inadequate anchorage protection can lead to the ingress of moisture and chlorides into the tendon. This condition is particularly severe with poorly grouted ducts that may allow moisture to readily move along the length of the tendon. Corrosion of anchorage components can also cause cracking and spalling of concrete in the vicinity of the anchorage.

Most anchorage corrosion problems result from two factors: inadequate protection and location. Inadequate protection may include insufficient cover, permeable materials used to fill the anchorage recess and lack of bond between fill material and anchorage recess. The location of the anchorage plays a significant role. Normally anchorages are located at the end of the member. In many structure types, expansion joints are located over the member ends. Poor detailing and maintenance of the joints has permitted chloride laden moisture to come in direct contact with the anchorage zones of the member, creating particularly severe exposure conditions.

Dickson et al[B.18] reported a detailed evaluation of a thirty-four year old precast post-tensioned girder. The girder was removed from a bridge that had been subjected to deicing salts throughout its service life. The overall condition of the girder was excellent, and the observed corrosion deterioration was not deemed to affect structural behavior. The most severe corrosion was found on the anchorages of the girder. Anchorage protection was provided by a cast-in-place concrete end diaphragm. Surface corrosion was found on all anchorage and bearing plate surfaces. The post-tensioning wires within the anchorage were corroded more severely than the wires within the length of the duct. In general, the ducts were very well grouted with only one void found during dissection of the girder. Corrosion of the wires within the length of the tendon was very minor. Chloride analysis performed on grout samples indicated that chlorides had infiltrated the duct through one of the anchorages in spite of the cast-in-place concrete anchorage protection.

Isecke[B.15] also reported infiltration of moisture and chlorides through end anchorages during the examination of a post-tensioned bridge. The anchorages in this bridge were unprotected. Anchorages located in the vicinity of expansion joints were exposed to chloride laden moisture runoff from the bridge deck. Anchorages in these areas were heavily damaged by corrosion. Moisture and chlorides penetrated through the anchorages, leading to heavy corrosion on the post-tensioned bars used in the structure. In areas of the structure were the unprotected anchorages where not exposed to deck runoff, no corrosion was found on the anchorages.

Appendix B – References:

B.1) **Szilard, R.,** "Corrosion and Corrosion Protection of Tendons in Prestressed Concrete Bridges," *ACI Journal*, January 1969, pp. 42-59.

B.2) **Sason, A.S.,** "Evaluation of Degree of Rusting on Prestressed Concrete Strand," *PCI Journal*, Vol. 37, No. 3, May-June 1992, pp. 25-30.

B.3) **PCI,** Manual for Quality Control for Plants and Production of Precast and Prestressed Concrete Products, Precast/Prestressed Concrete Institute, Chicago, IL, 1985.

B.4) **Novokschenov, V.,** "Salt Penetration and Corrosion In Prestressed Concrete Members," Publication No. FHWA-RD-88-269, Federal Highway Administration, McLean, Va., 1989. (See also Novokschenov, V. "Condition Survey of Prestressed Concrete Bridges," *Concrete International*, Vol. 11, No. 9, September 1989, pp. 60-68, and Novokschenov, V., "Prestressed Bridges and Marine Environment," *Journal of Structural Engineering*, American Society for Civil Engineering, Vol. 116, No. 11, November 1990, pp. 3191-3205.)

B.5) **Whiting, D., Stejskal, B, and Nagi, M.** "Condition of Prestressed Concrete Bridge Components – Technology Review and Field Surveys," Publication No. FHWA-RD-93-037, Federal Highway Administration, McLean, VA, September 1993.

B.6) **Schupack, Morris,** "Unbonded Tendons – Evolution and Performance," *Concrete International*, Vol. 16, No. 12, December 1994, pp. 32-35.

B.7) **ACI Committee 423,** "Corrosion and Repair of Unbonded Single Strand Tendons," (ACI 423.4R-98), American Concrete Institute, Detroit, MI, 1998, 20pp.

B.8) **Demitt, A.,** "Evaluation and Repair of Unbonded Post-tensioned Slabs," Presentation at 1994 ACI Fall Convention, Tarpon Springs, FL, ADEM Engineering Ltd., Calgary, AB.

B.9) **Kesner, K. and Poston, R.W.,** "Unbonded Post-Tensioned Concrete Corrosion: Myths, Misconceptions and Truths," *Concrete International*, Vol. 18, No. 7, July 1996, pp. 27-32.

B.10) **Schupack, M.,** "Corrosion Protection for Unbonded Tendons," *Concrete International*, Vol. 13, No. 2, February 1991, pp. 51-57.

B.11) **Peterson, C.A.,** Survey of Parking Structure Deterioration and Distress," *Concrete International*, Vol. 2, No. 3, March 1980, pp. 53-61.

B.12) "Project Profile – Park Place Parking Garage," Wiss, Janney, Elstener Associates, Inc., Northbrook, IL.

B.13) **Robson, A., and Brooman, H.,** "A3/A31 Flyover - Case History of an Externally Post-tensioned Bridge," *Proceeding of the Seventh International Conference on Structural Faults and Repair - 1997*, Vol. 1, July 1997, pp. 307-315.

B.14) **Clark, L.A.,** "Performance In Service of Post-Tensioned Concrete Bridges," British Cement Association, October 1992.

B.15) **Isecke, B.,** "Long Term Behaviour of Materials in a Prestressed Concrete Bridge," Proceedings, International Symposium of Corrosion in Reinforced Concrete Construction, Warwickshire, England, Elsevier Applied Science, Essex, England, 1990, pp. 142-159.

B.16) **Schupack, M.,** "Durability Study of a 35-Year-Old Post-Tensioned Bridge," *Concrete International*, Vol. 16, No. 2, February 1994, pp. 54-58.

B.17) **Schupack, M.,** "Post-Tensioning Tendons After 35 Years," *Concrete International*, Vol. 16, No. 3, March 1994, pp. 50-54.

B.18) **Dickson, T.J., Tabatabai, H. and Whiting, D.A.,** "Corrosion Assessment of a 34-Year-Old Precast Post-Tensioned Concrete Girder," *PCI Journal*, Vol. 38, No. 6, November-December 1993, pp. 44-51.

Appendix C

Detail Drawings - Supplement to Appendix B

**** Page Numbers Printed Separately ****

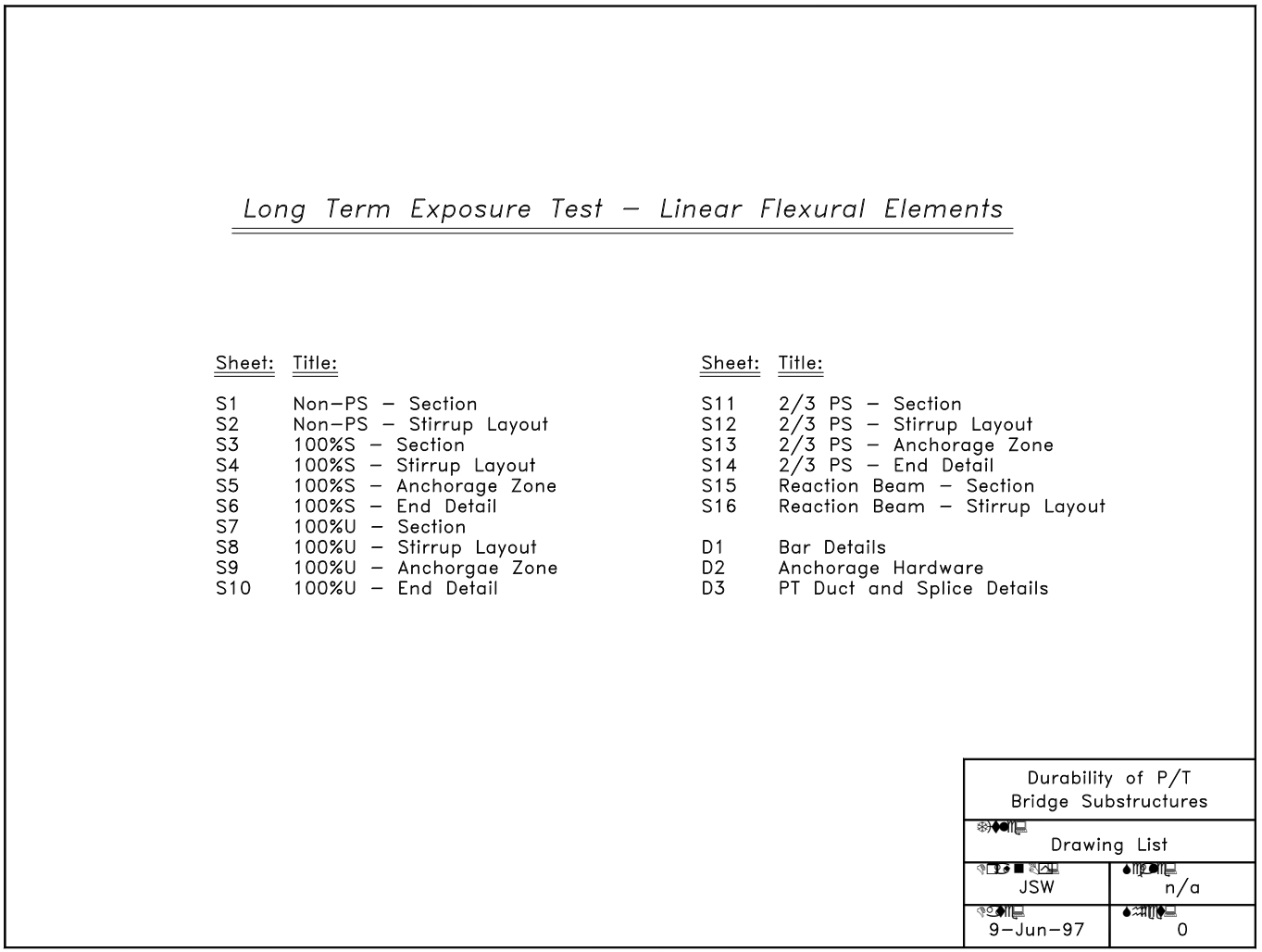

Figure C.1 – Sheet 0: Drawing List

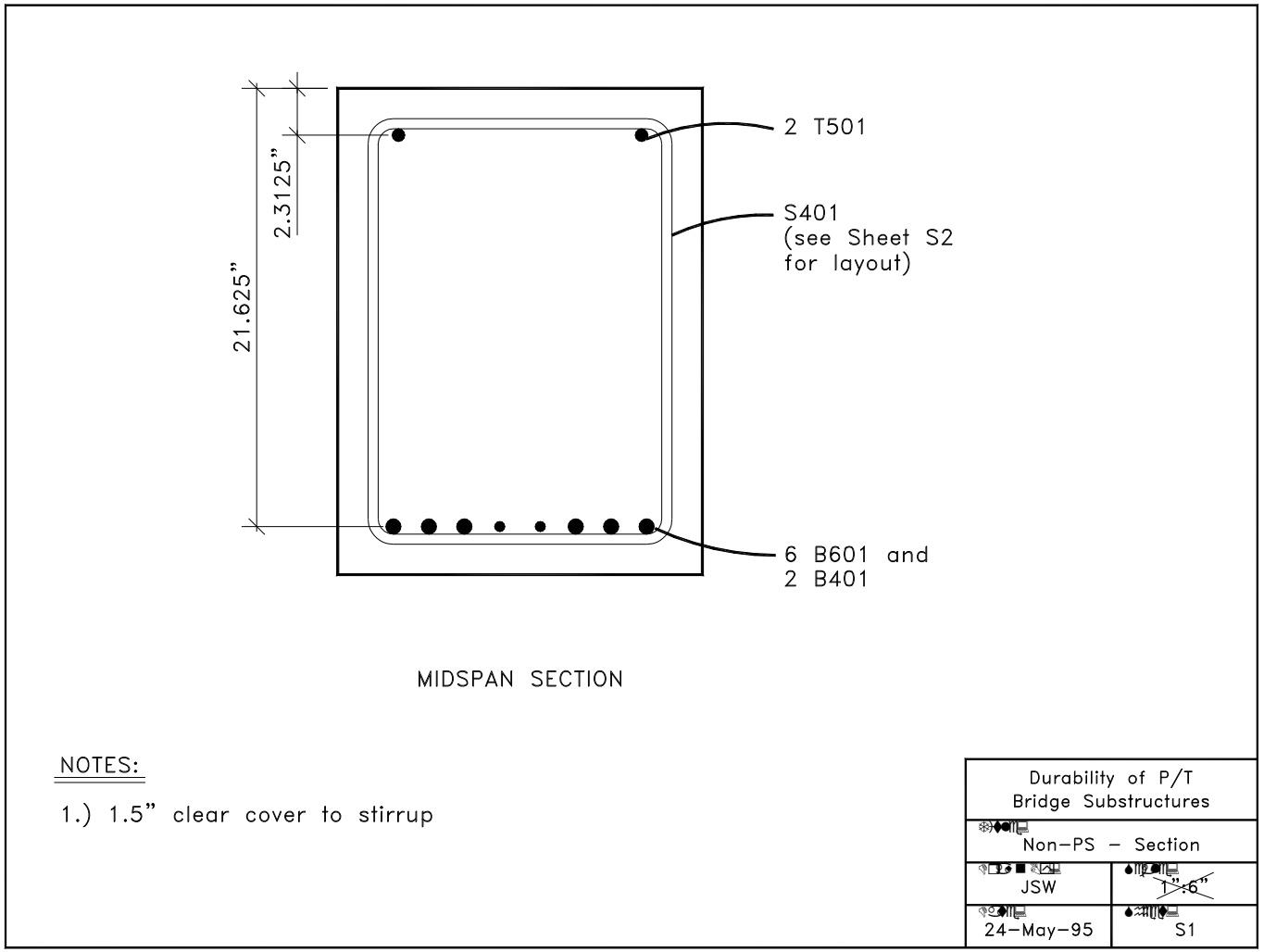

Figure C.2 - Sheet S1: Non-PS Section

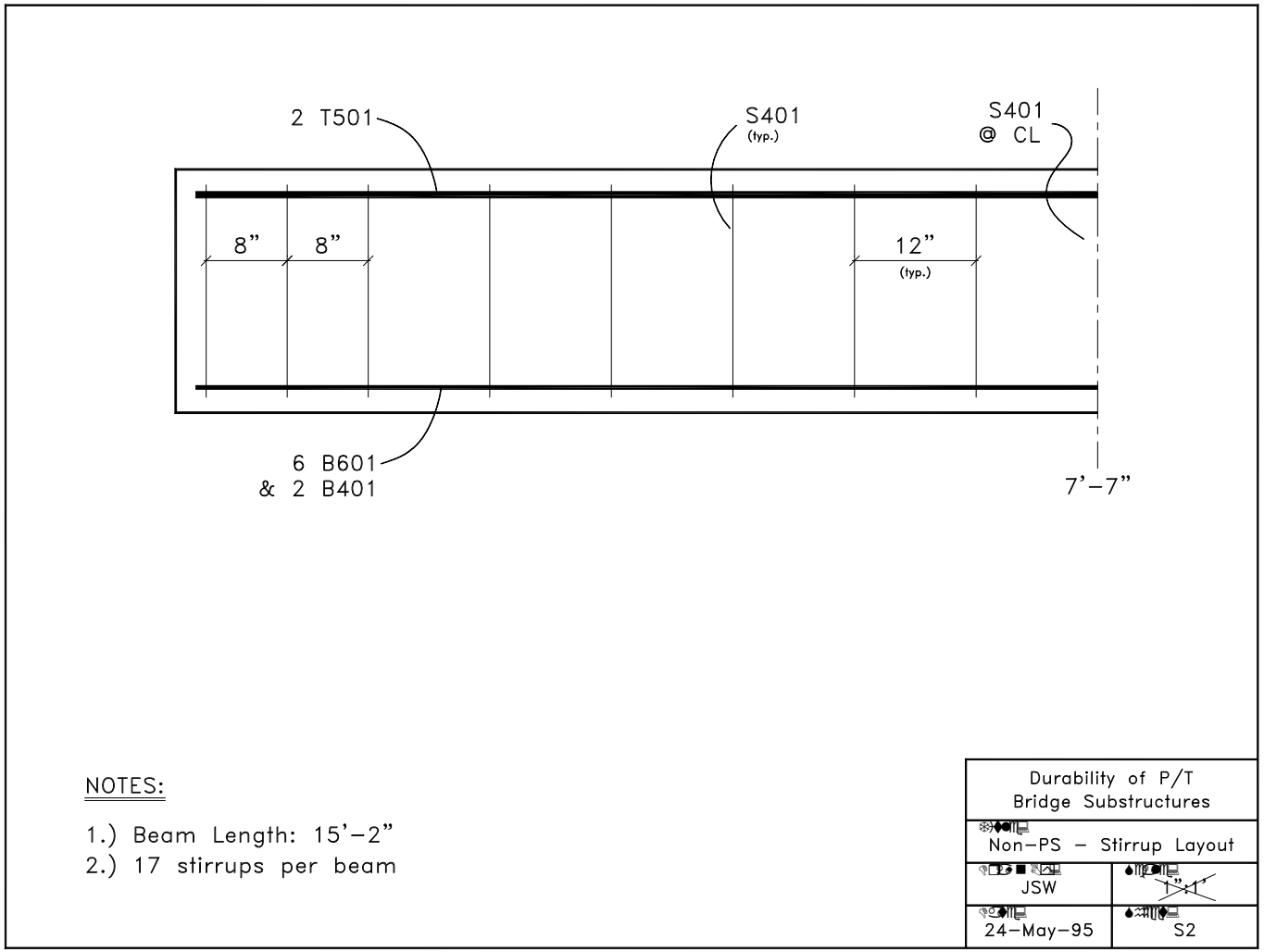

Figure C.3 - Sheet S2: Non-PS Stirrup Layout

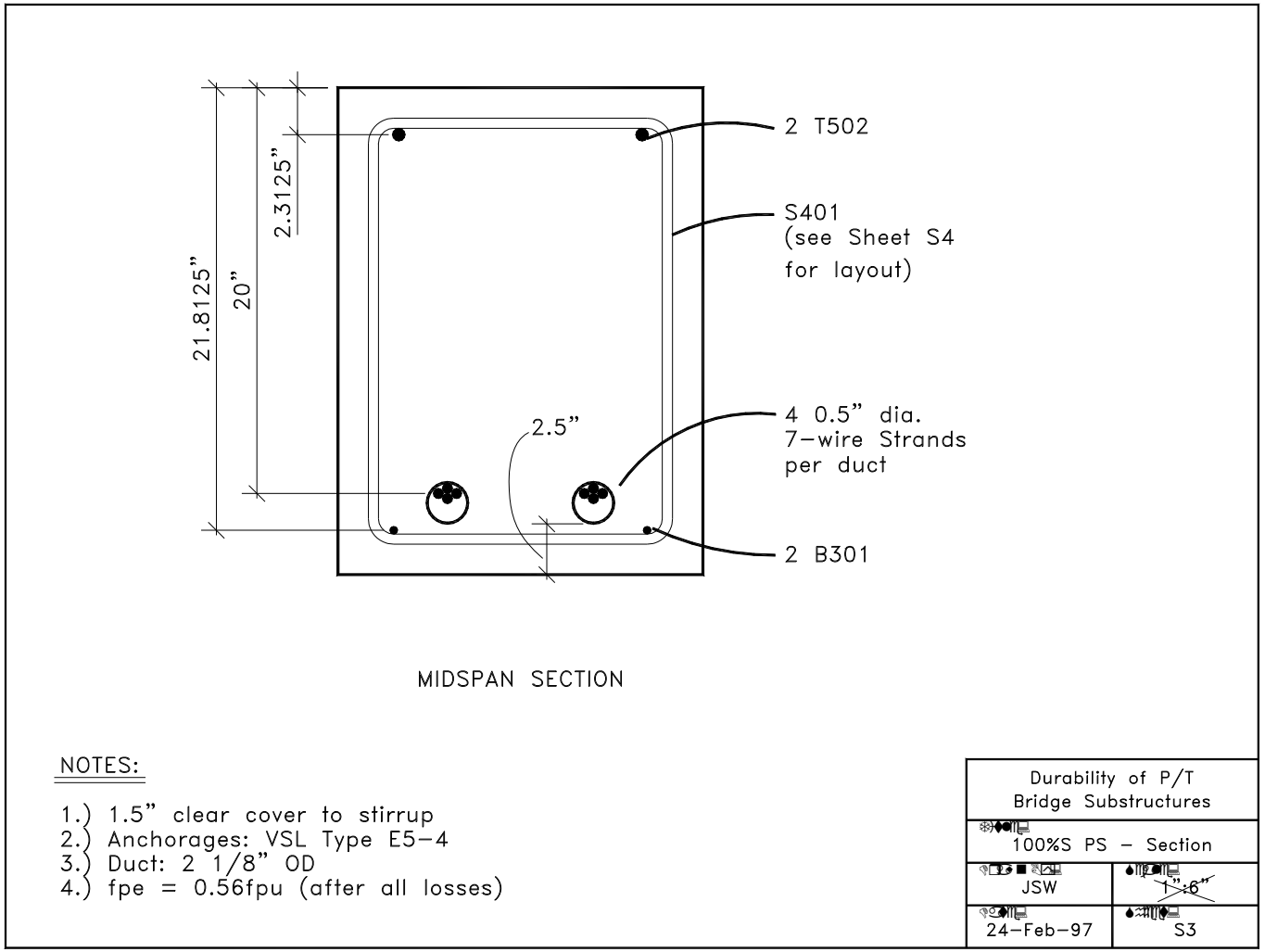

Figure C.4 - Sheet S3: 100%S PS Section

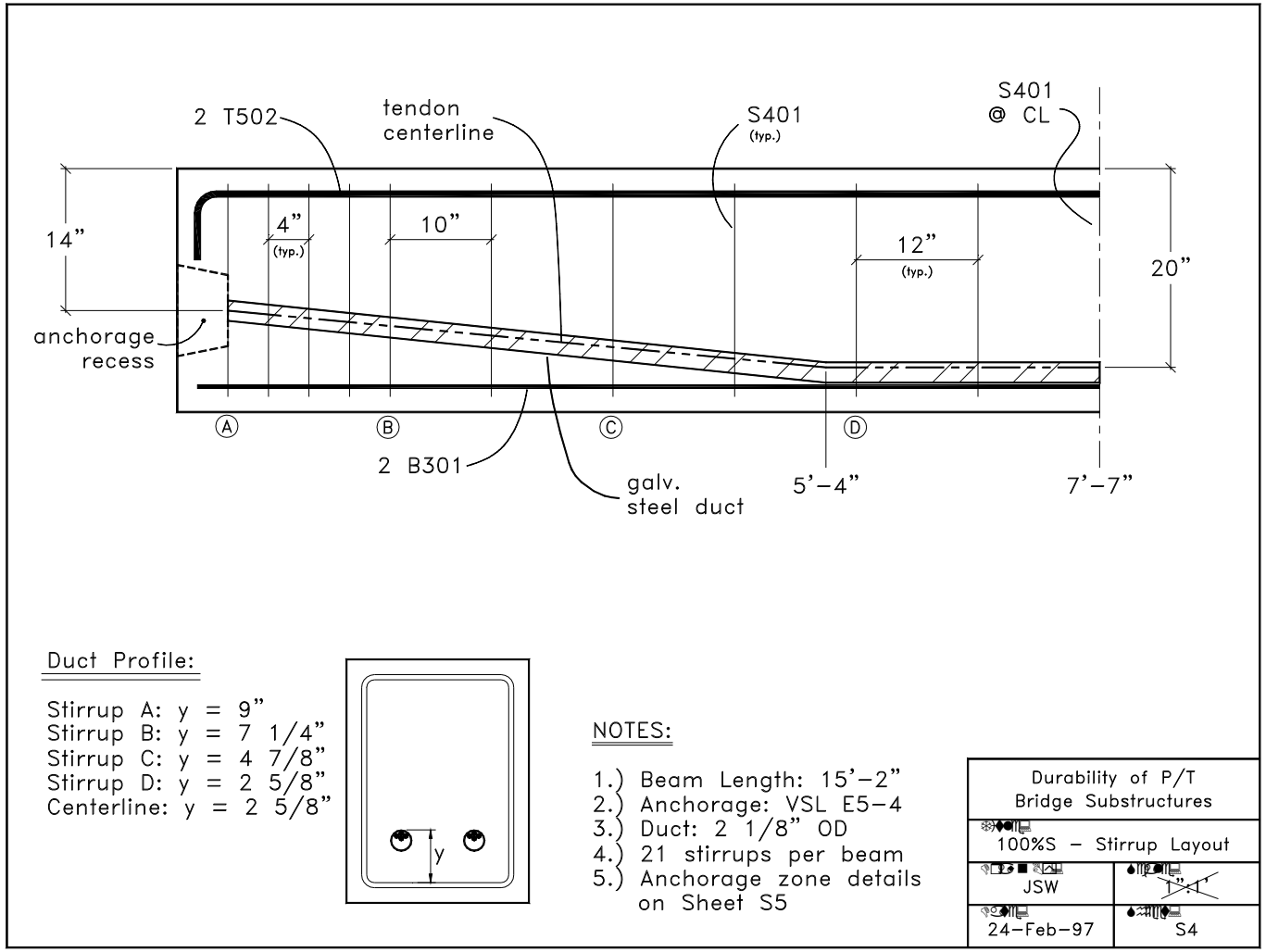

Figure C.5 - Sheet S4: 100%S Stirrup Layout

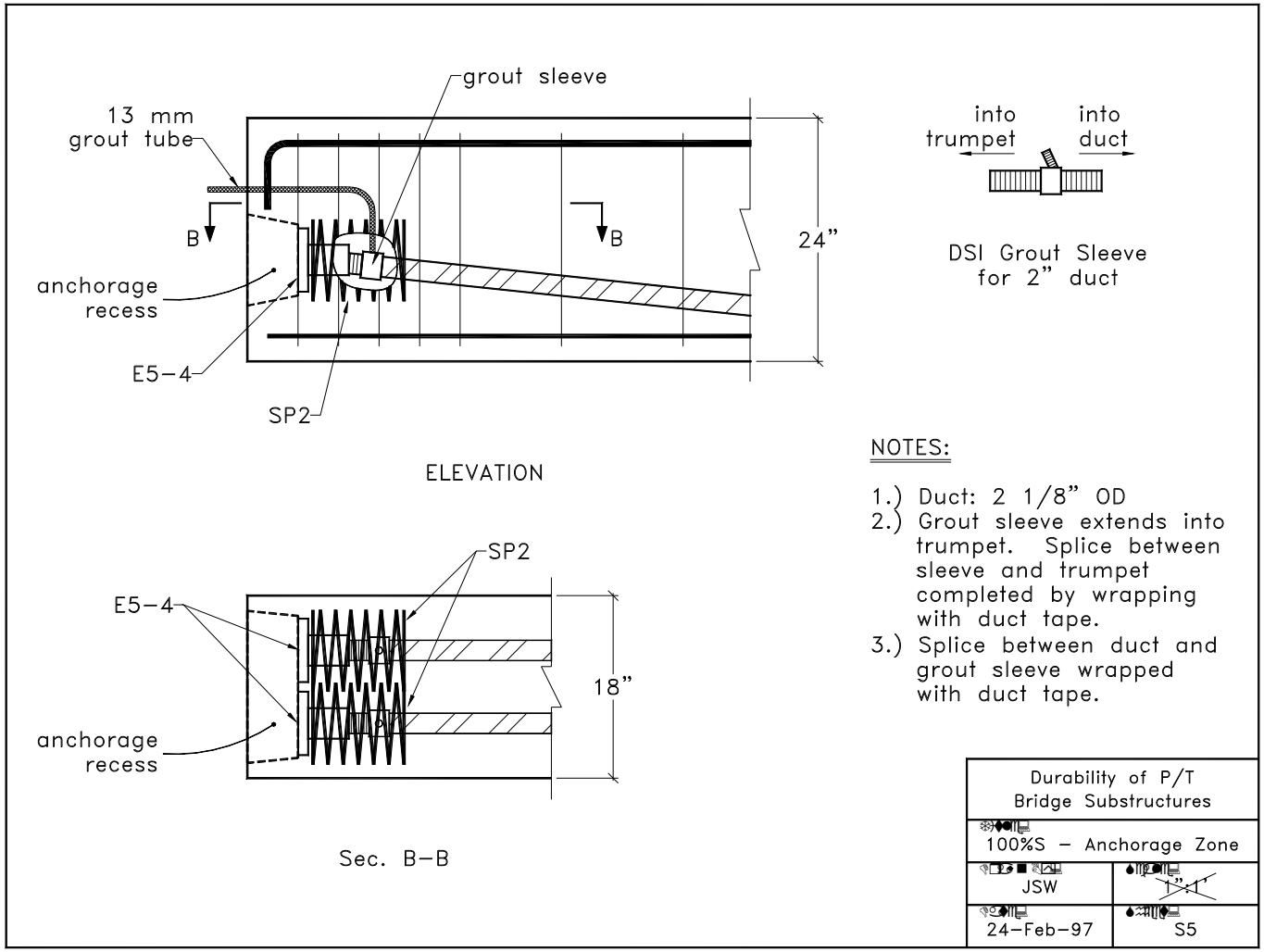

Figure C.6 - Sheet S5: 100%S Anchorage Zone

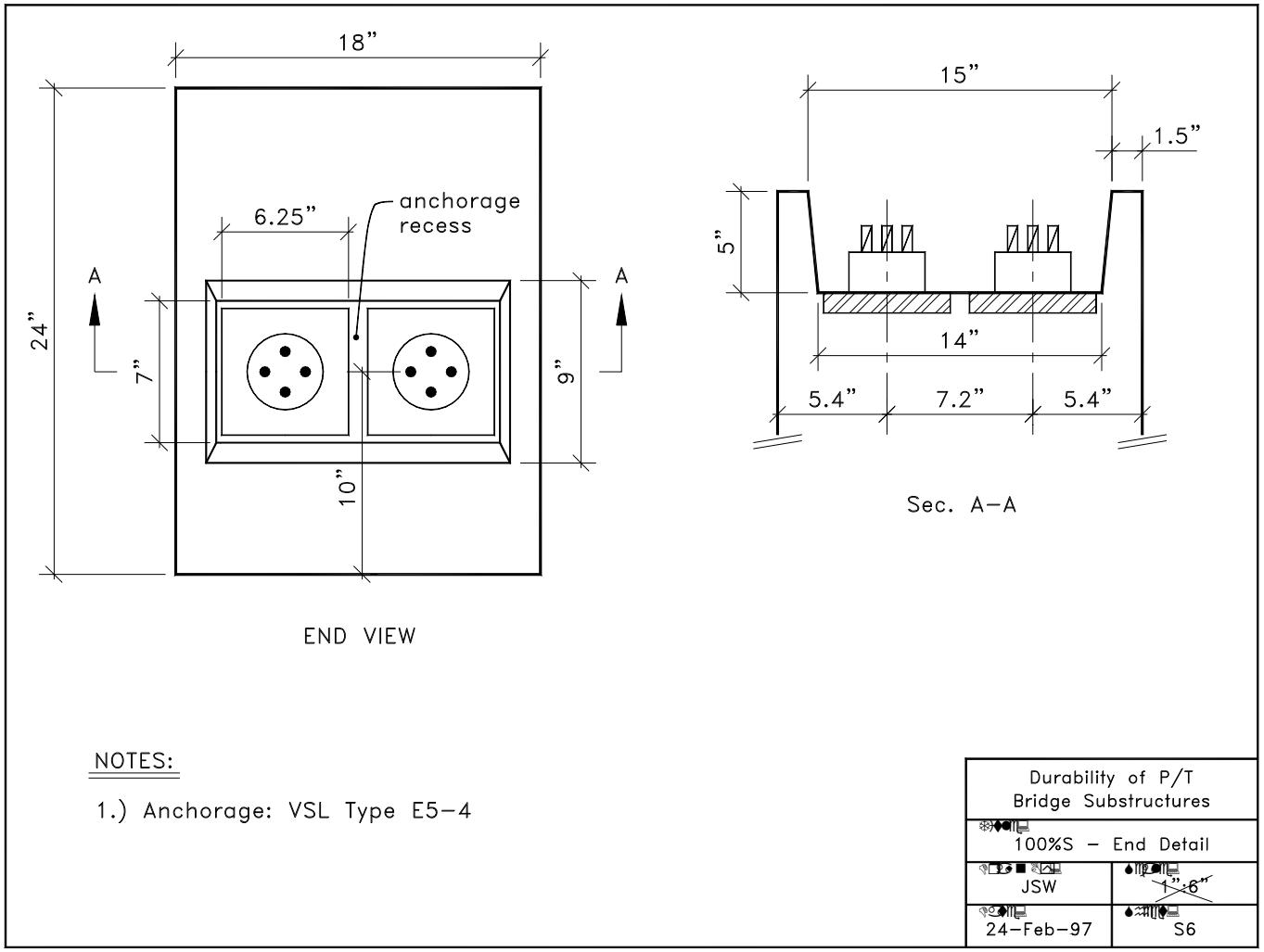

Figure C.7 - Sheet S6: 100%S End Detail

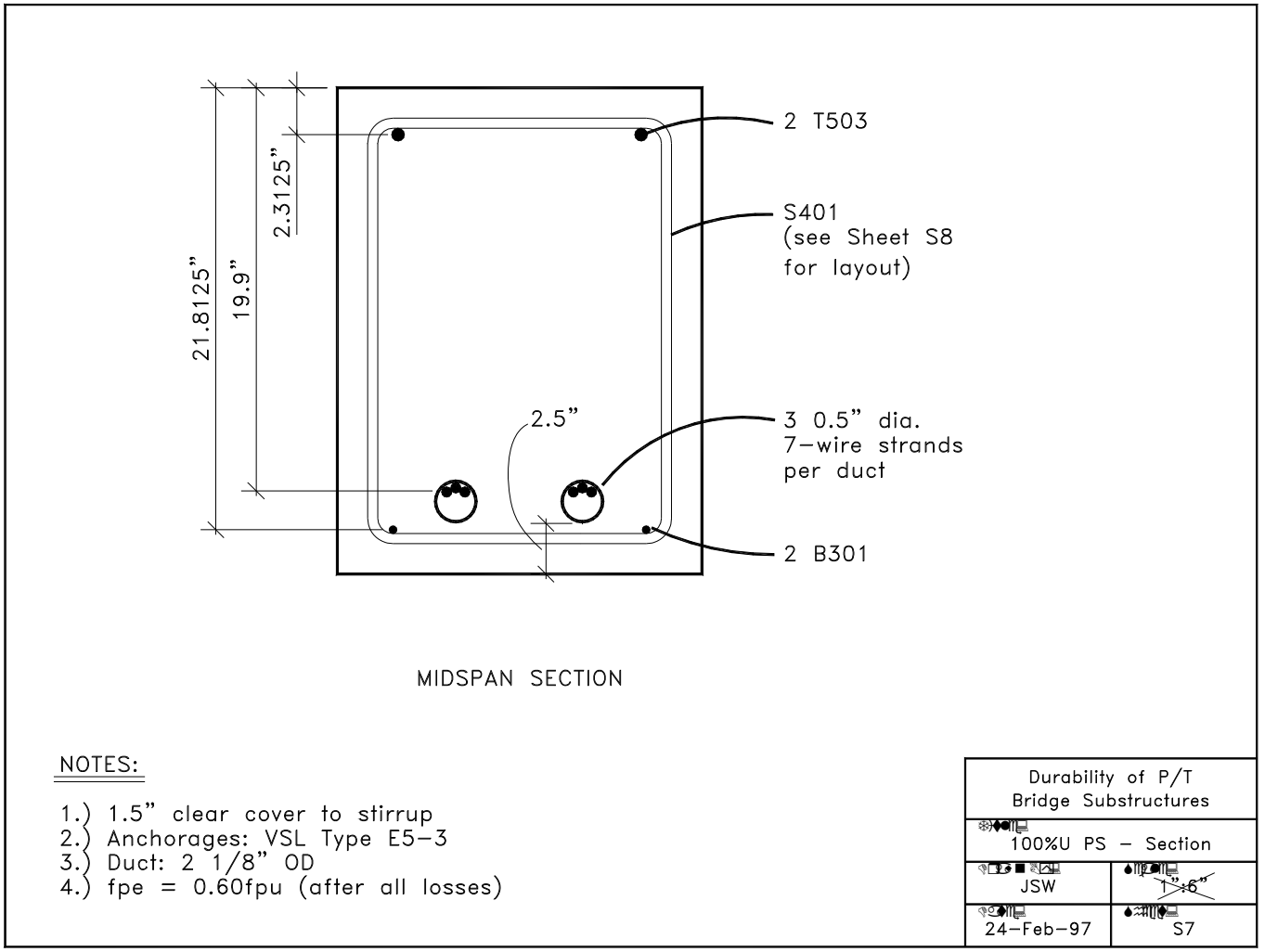

Figure C.8 - Sheet S7: 100%U PS Section

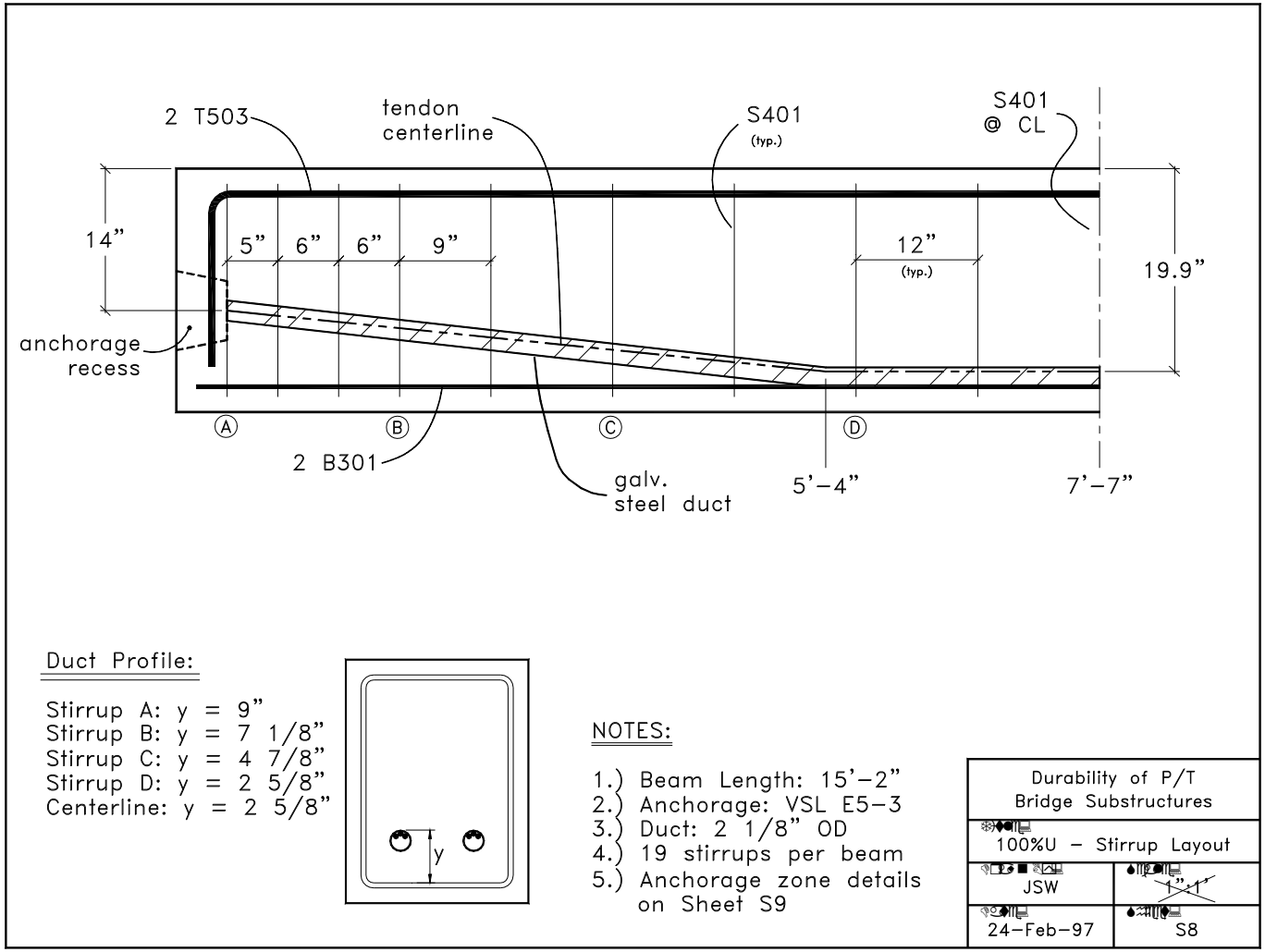

Figure C.9 - Sheet S8: 100%U Stirrup Layout

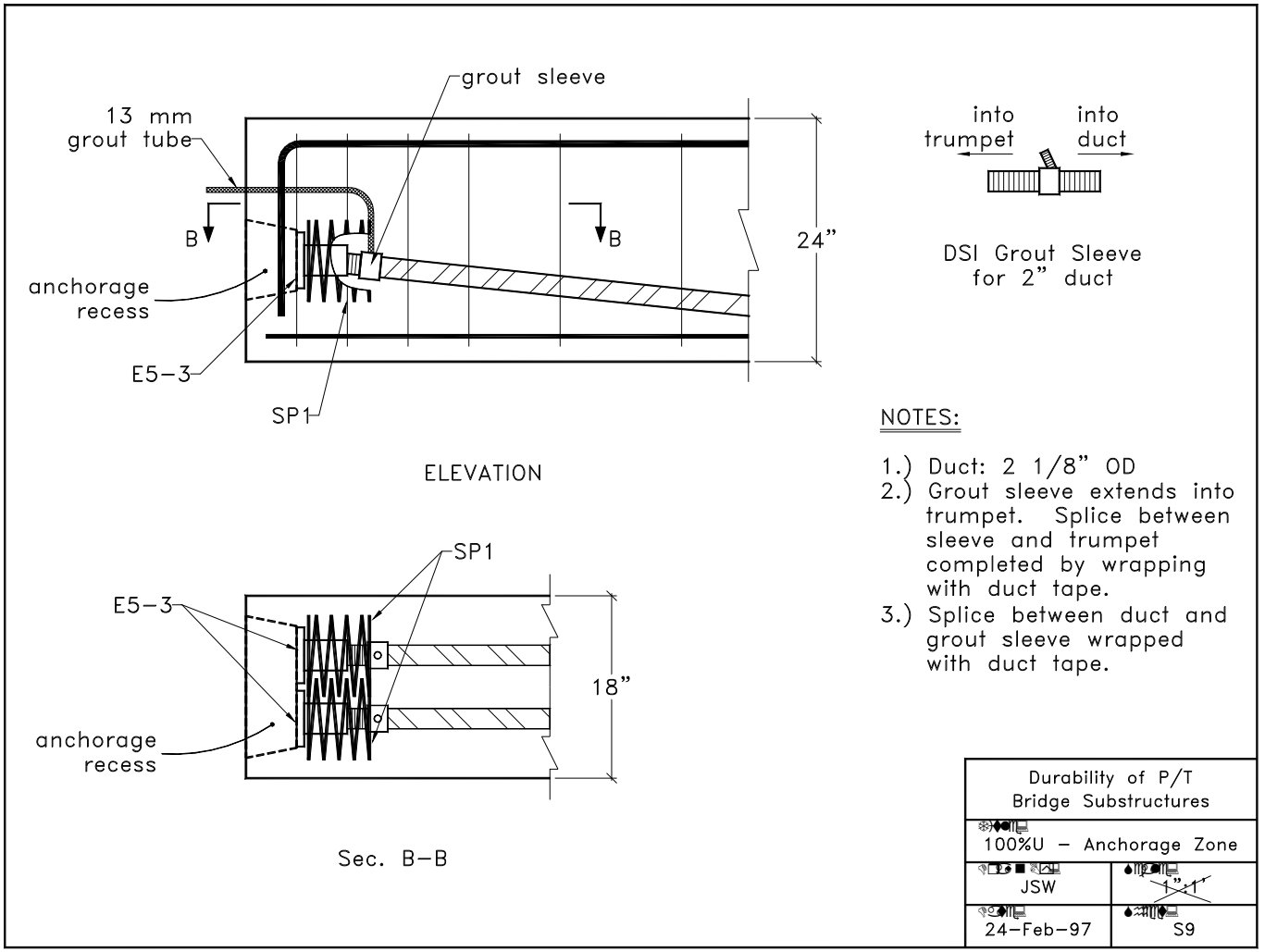

Figure C.10 - Sheet S9: 100%U Anchorage Zone

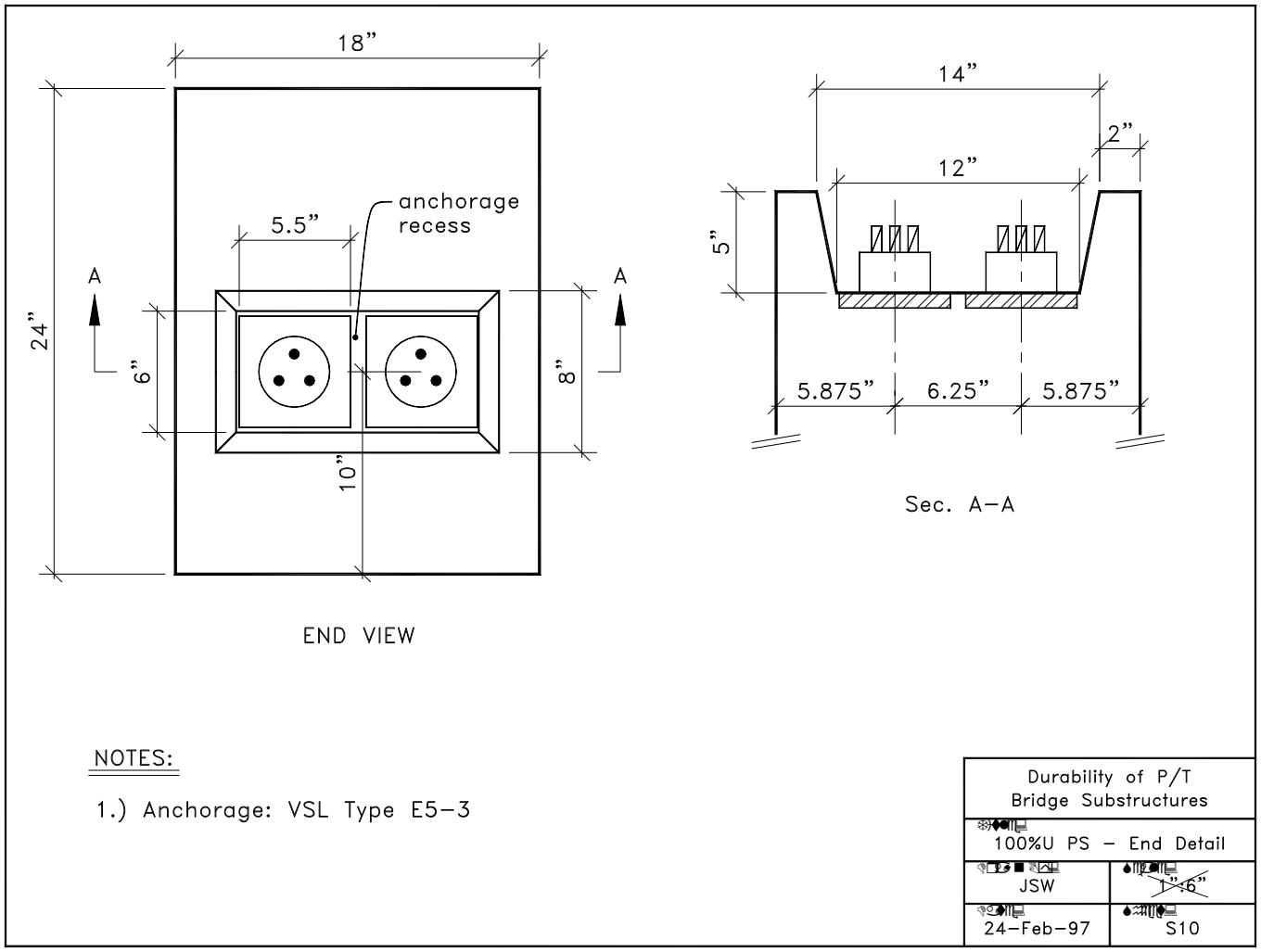

Figure C.11 - Sheet S10: 100%U End Detail

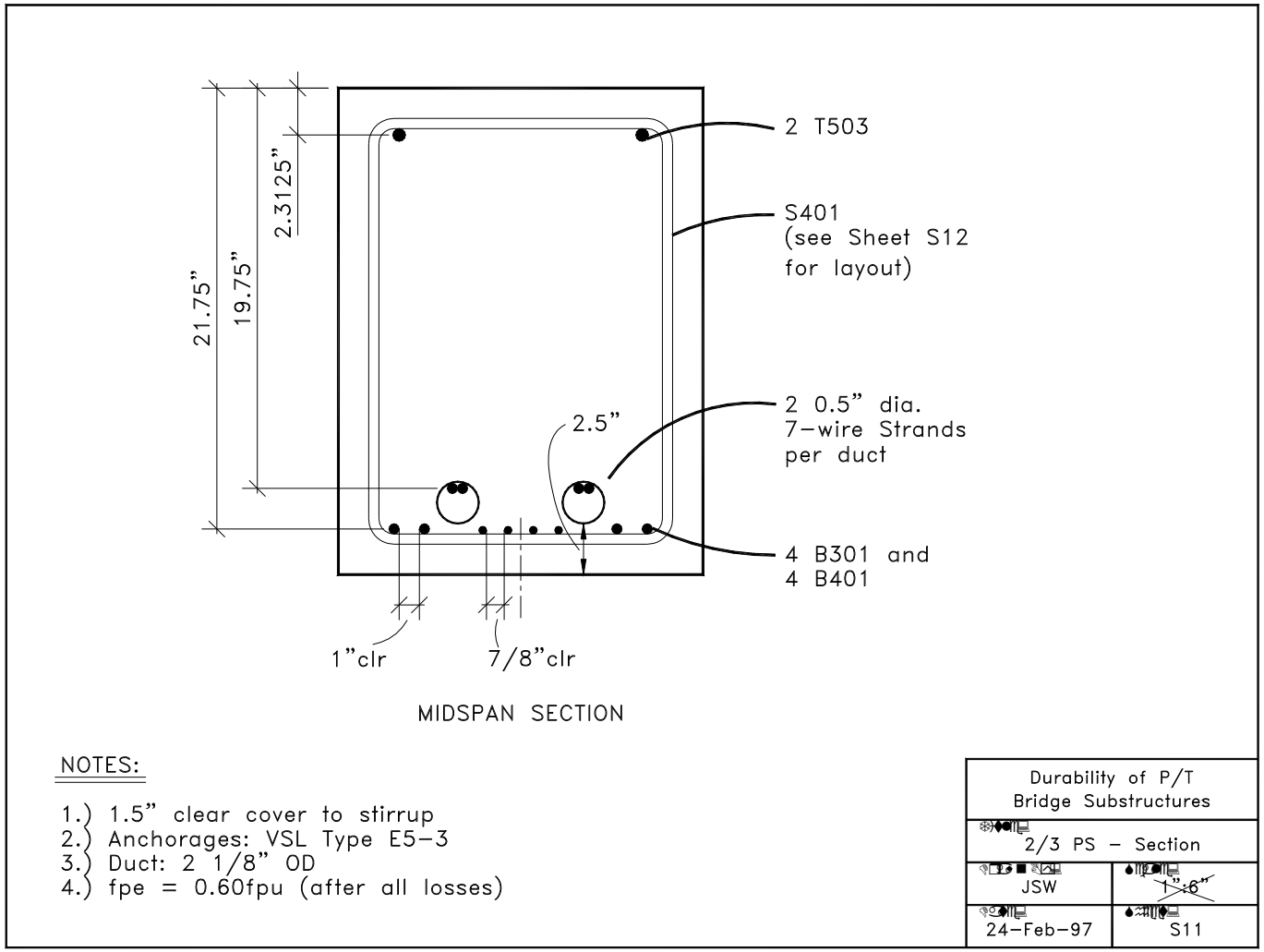

Figure C.12 - Sheet S11: 2/3 PS Section

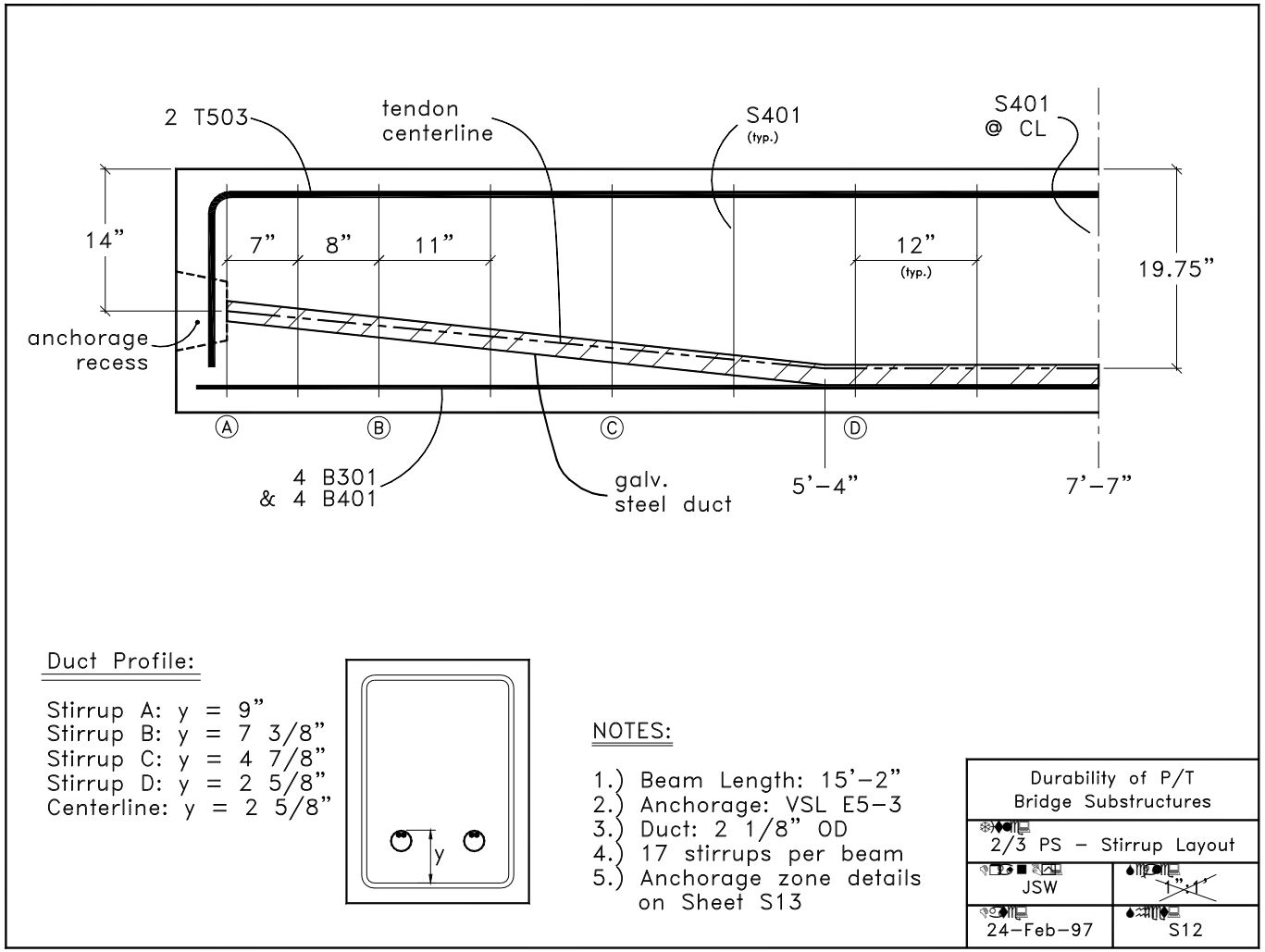

Figure C.13 - Sheet S12: 2/3 PS Stirrup Layout

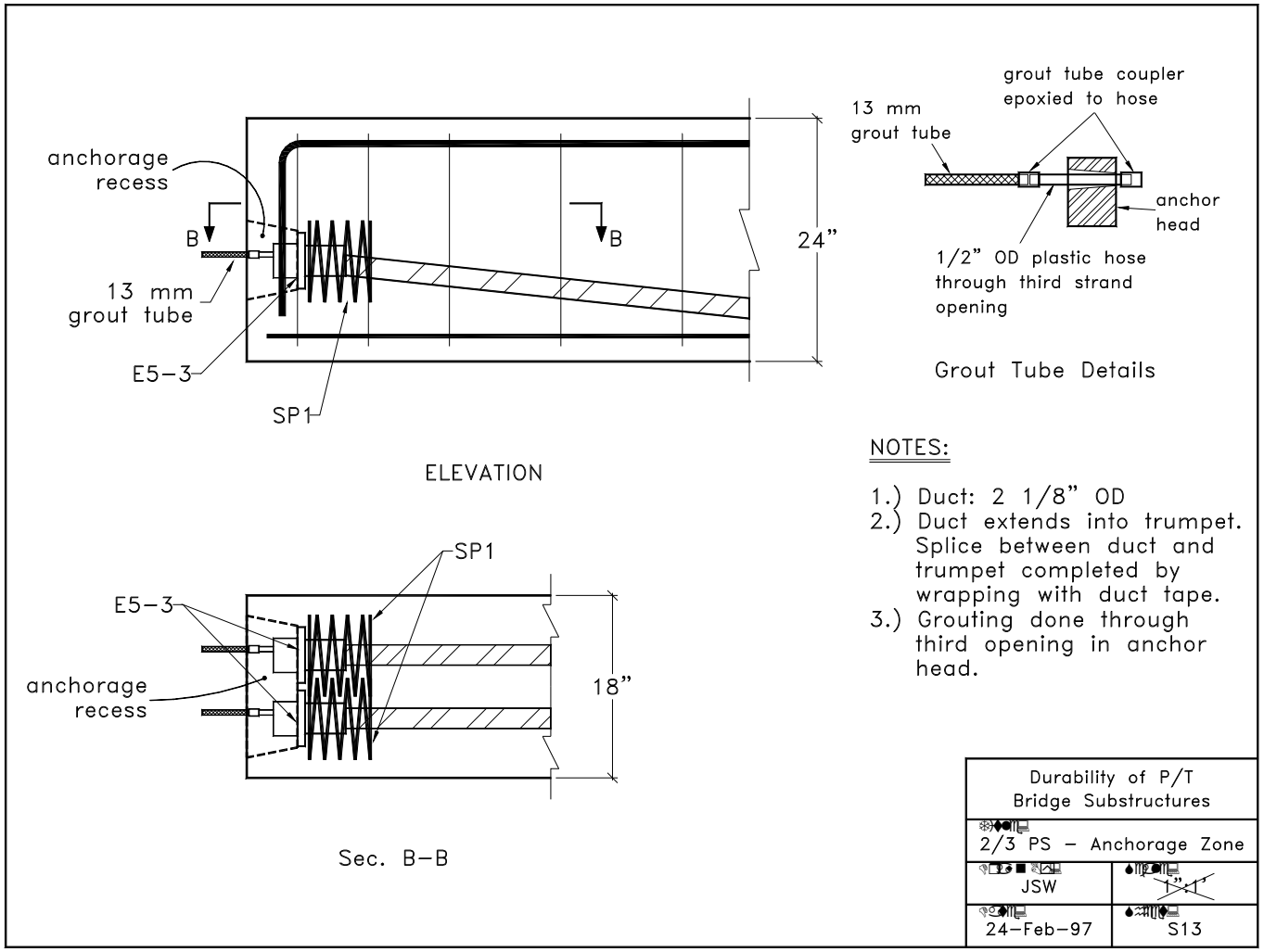

Figure C.14 - Sheet S13: 2/3 PS Anchorage Zone

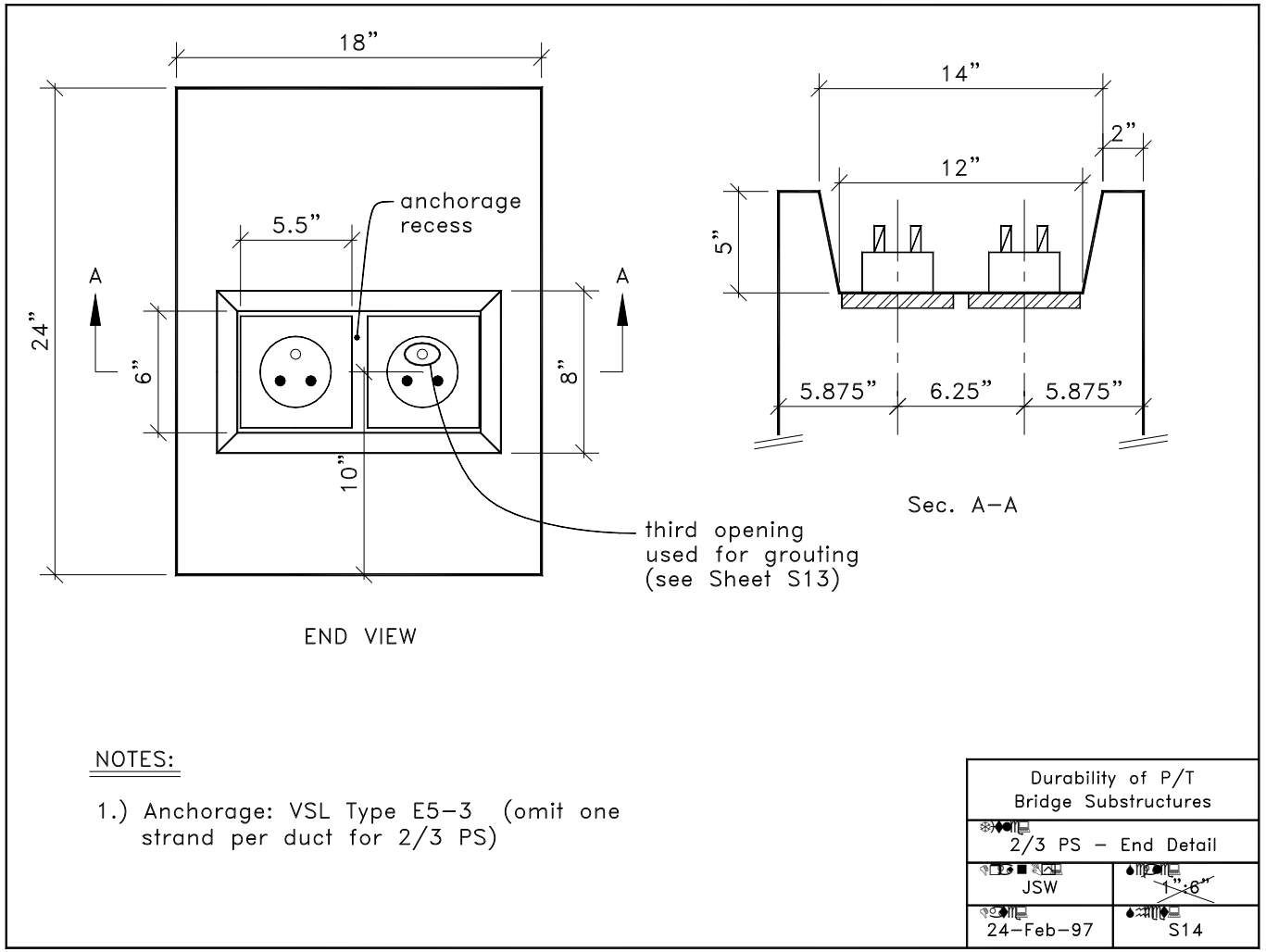

Figure C.15 - Sheet S14: 2/3 PS End Detail

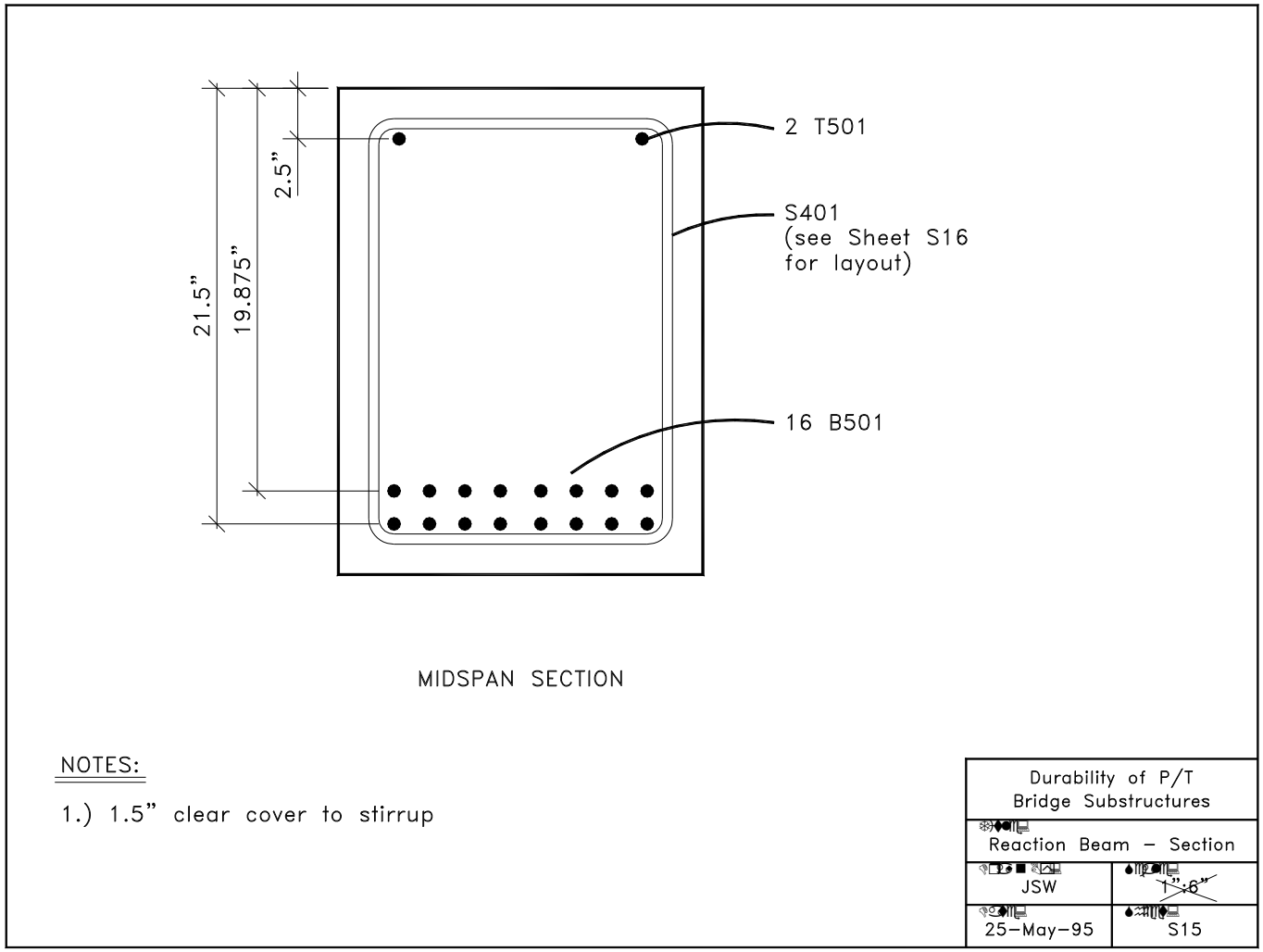

Figure C.16 - Sheet S15: Reaction Beam Section

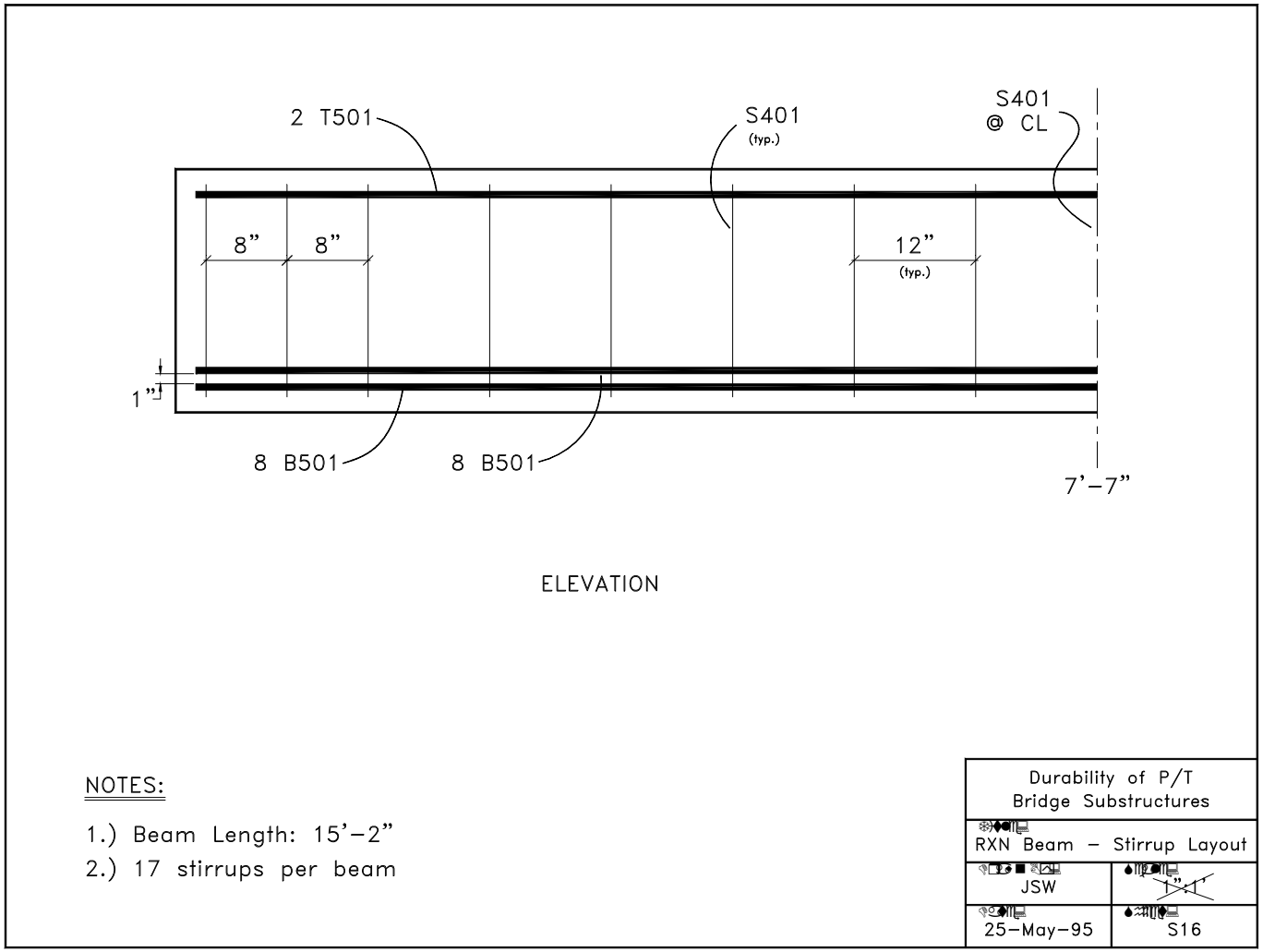

Figure C.17 - Sheet S16: Reaction Beam Stirrup Layout

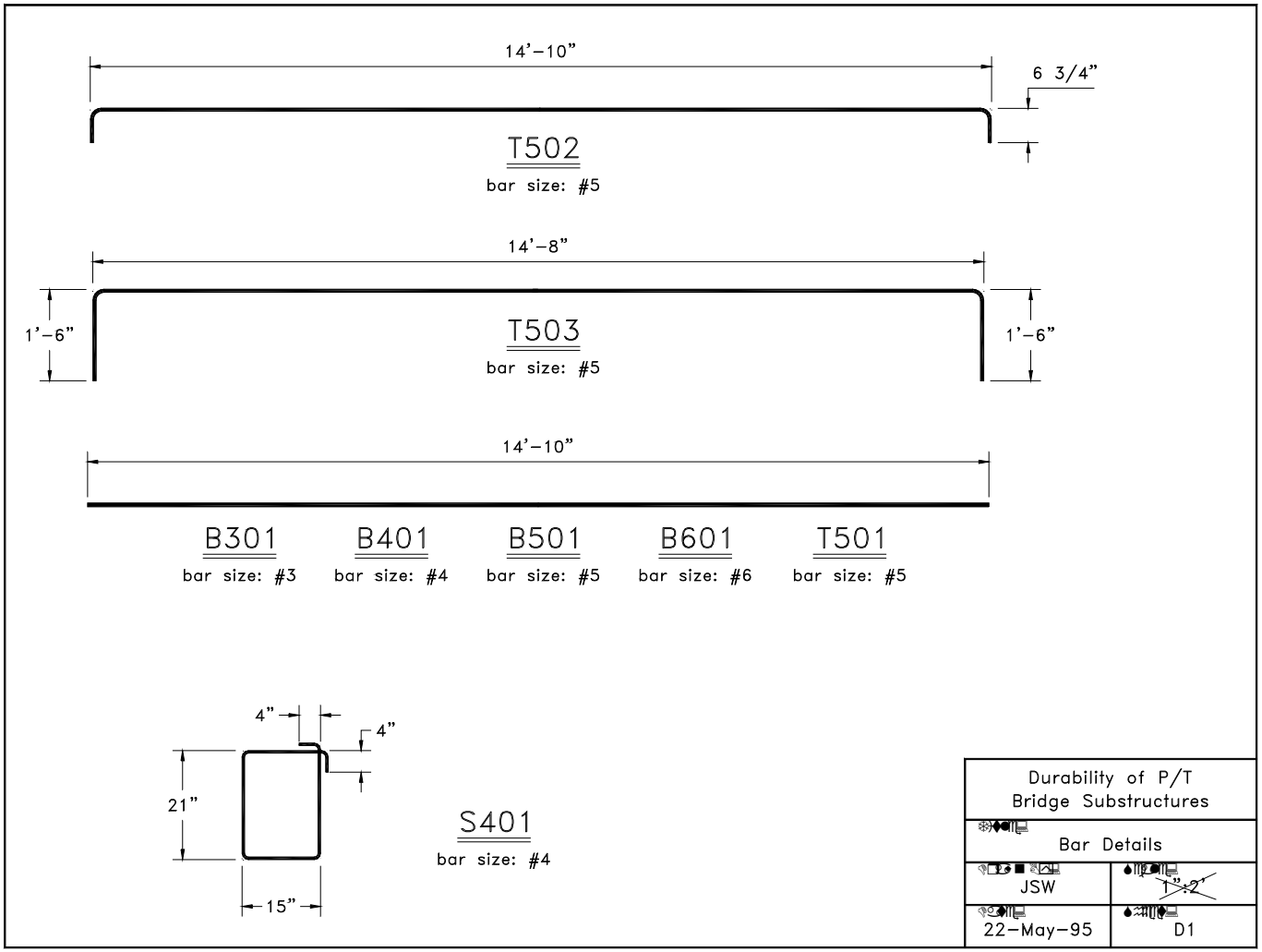

Figure C.18 - Sheet D1: Bar Details

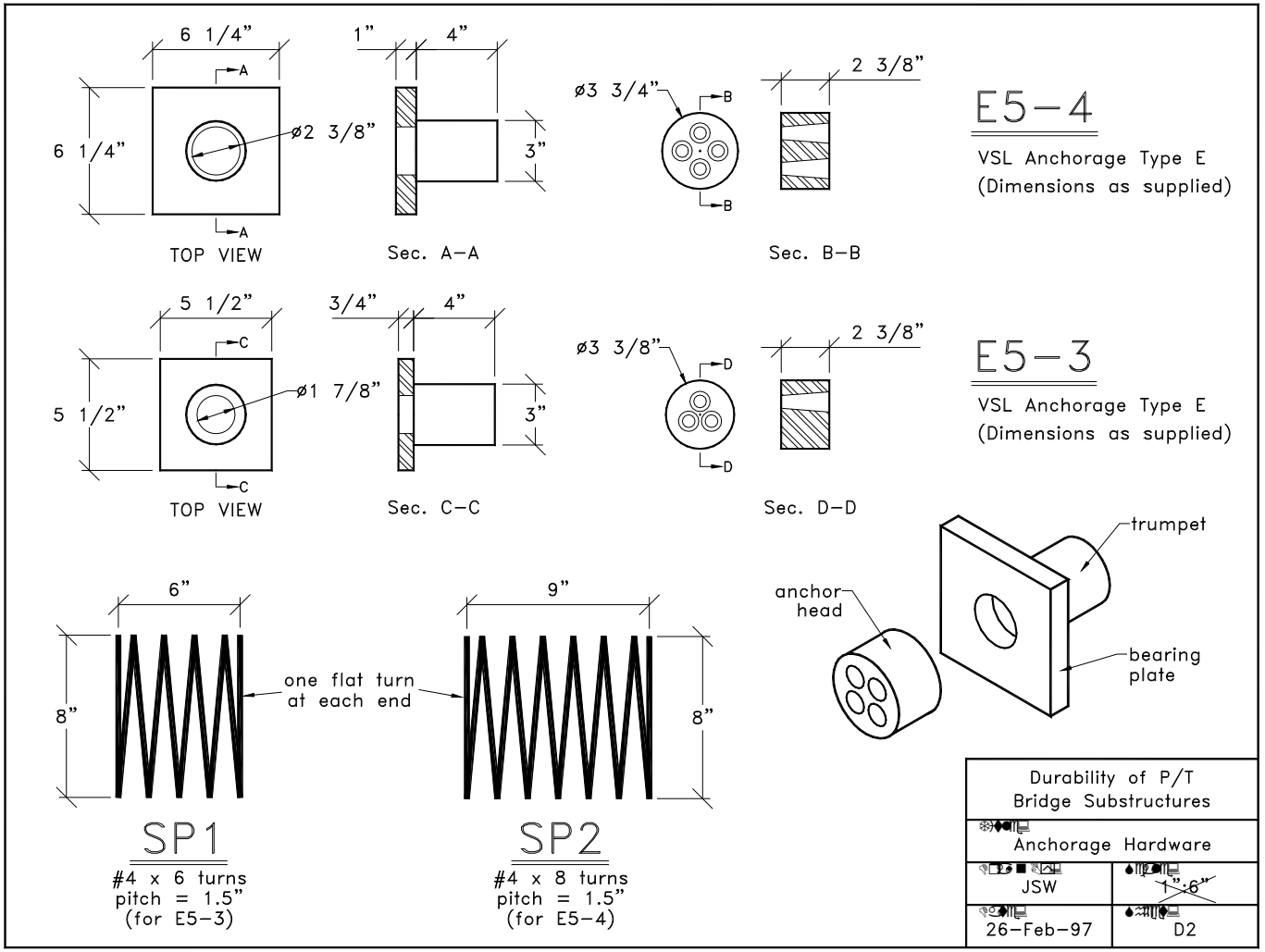

Figure C.19 - Sheet D2: Anchorage Hardware

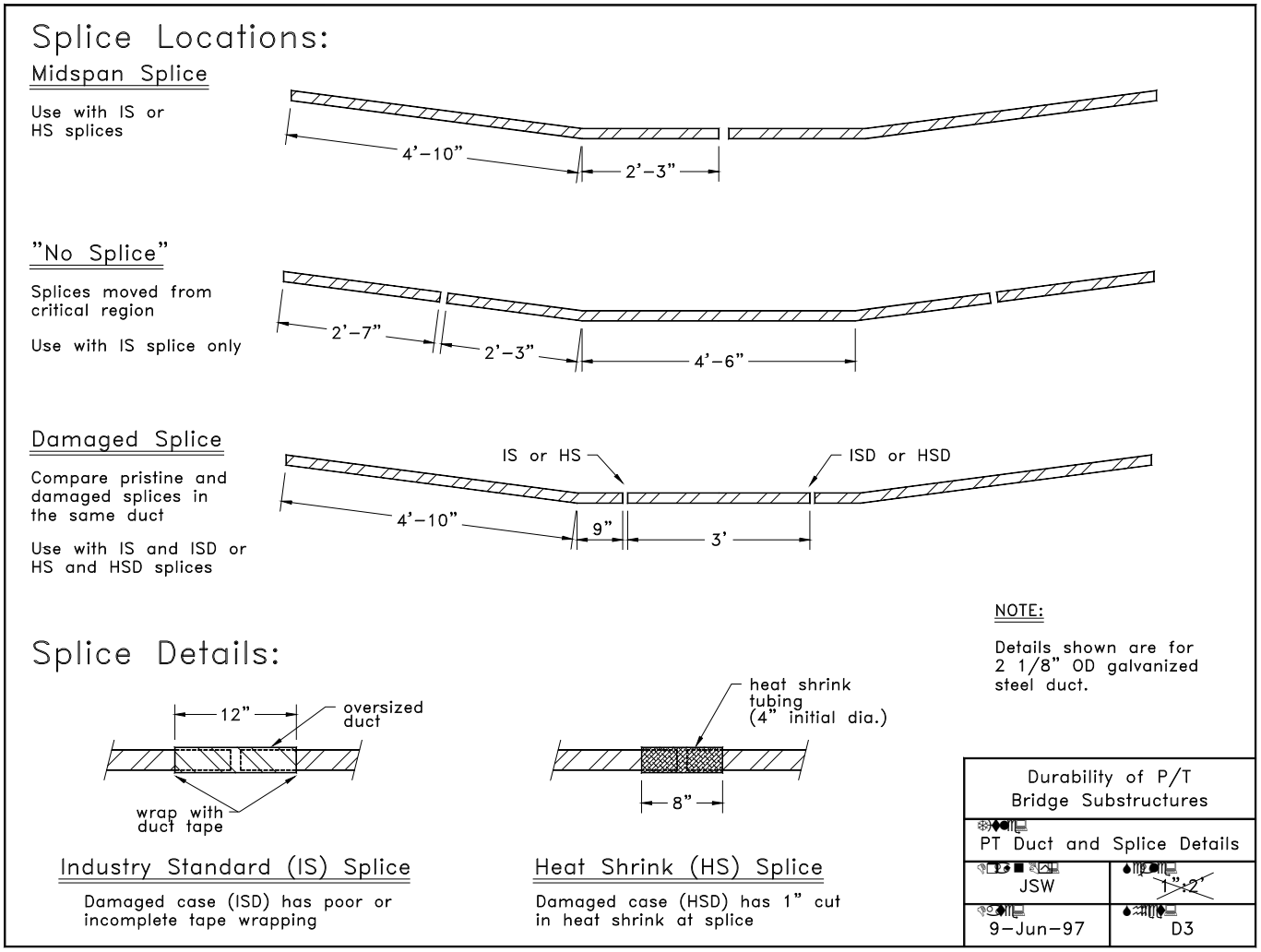

Figure C.20 - Sheet D3: Post-Tensioning Duct and Splice Details

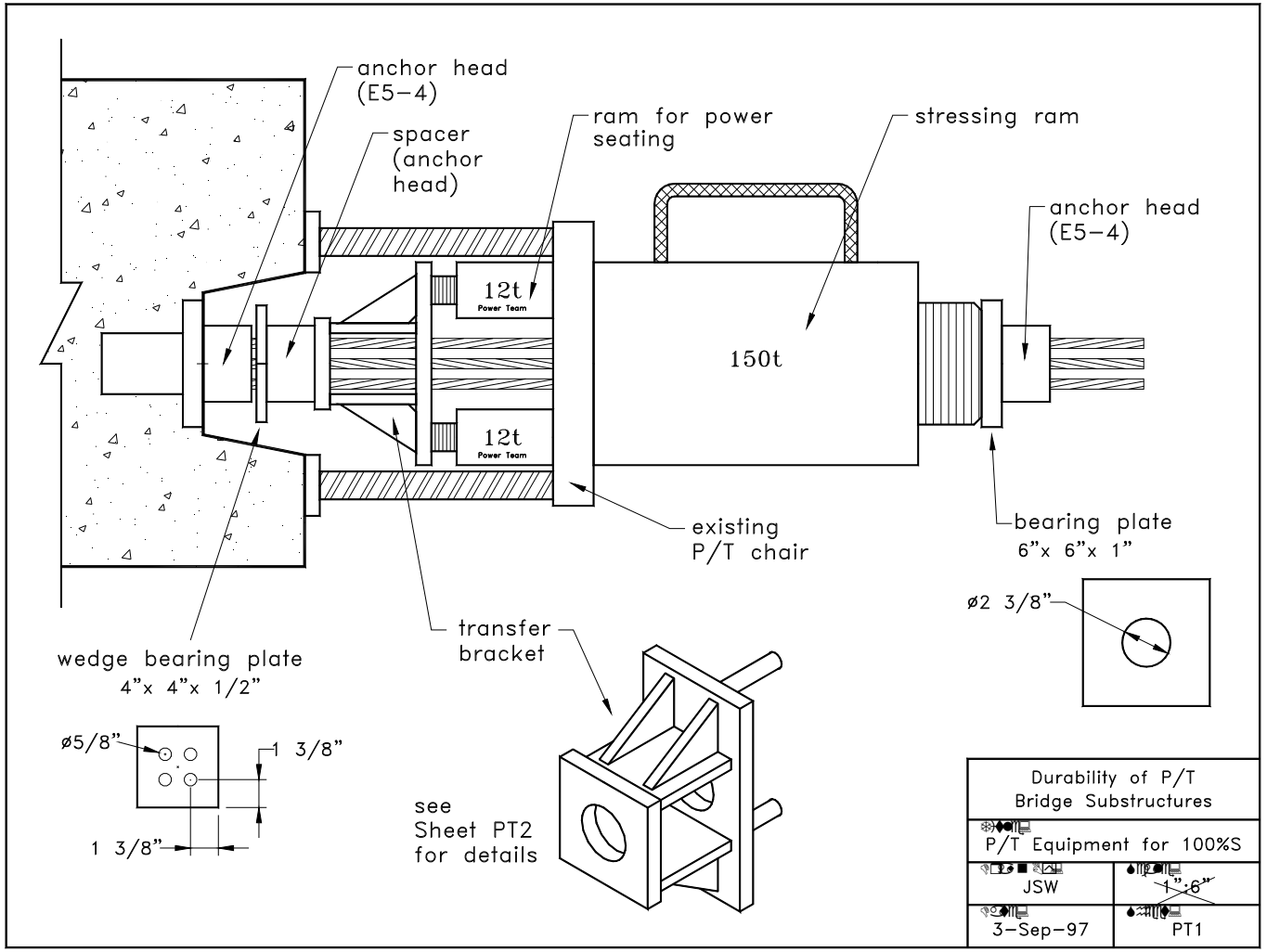

Figure C.21 - Sheet PT1: Post-Tensioning Equipment for 100%S Beams

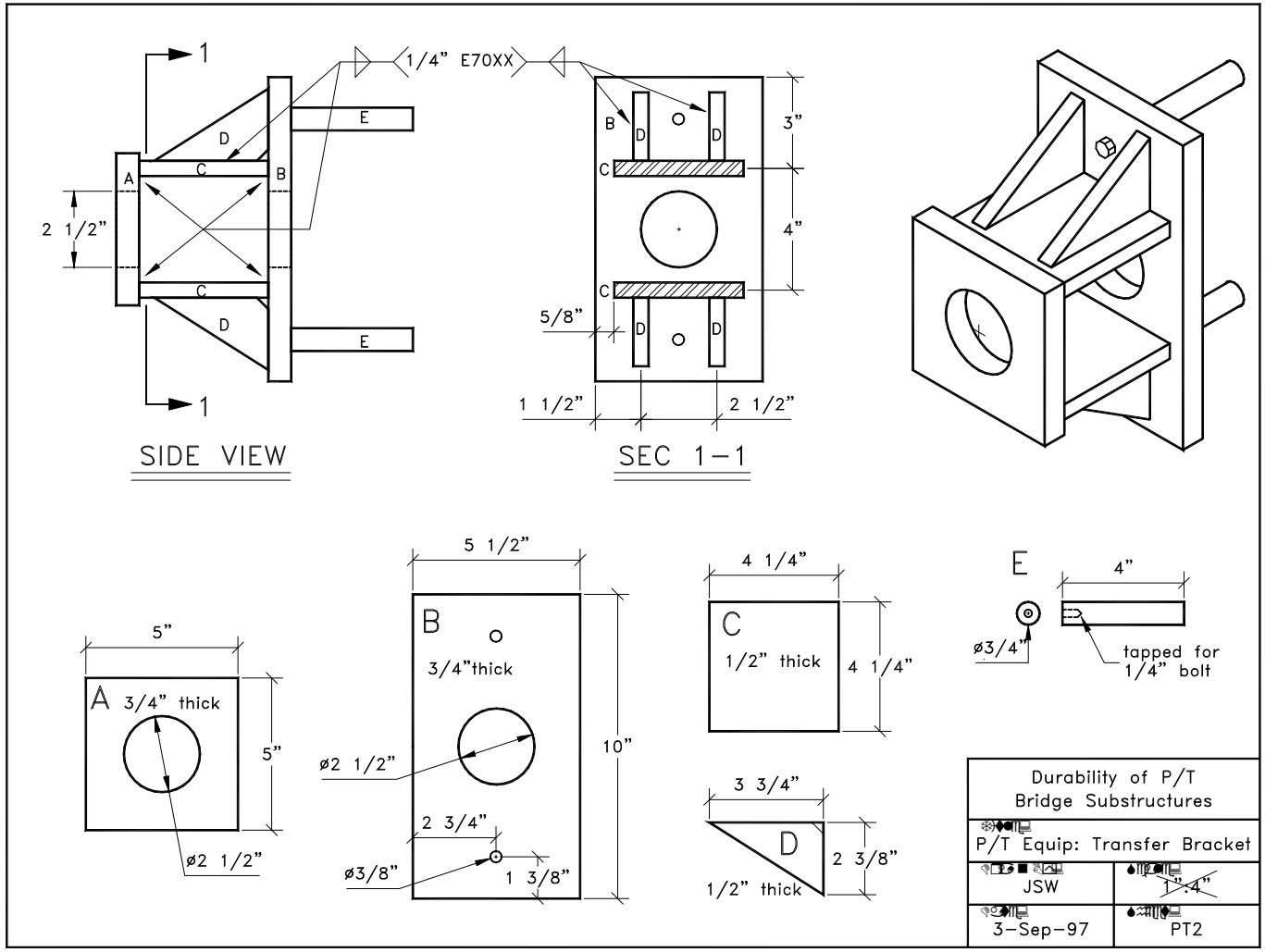

Figure C.22 - Sheet PT2: Post-Tensioning Equipment Transfer Bracket for Power Seating of Wedges

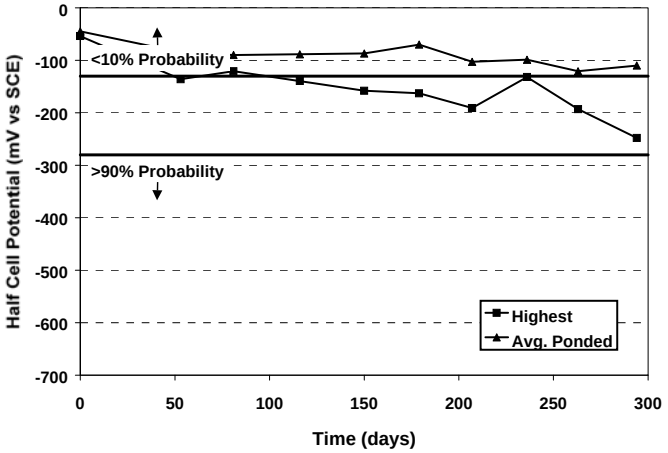

Figure C.34 - Half-Cell Readings: Beam 1.1

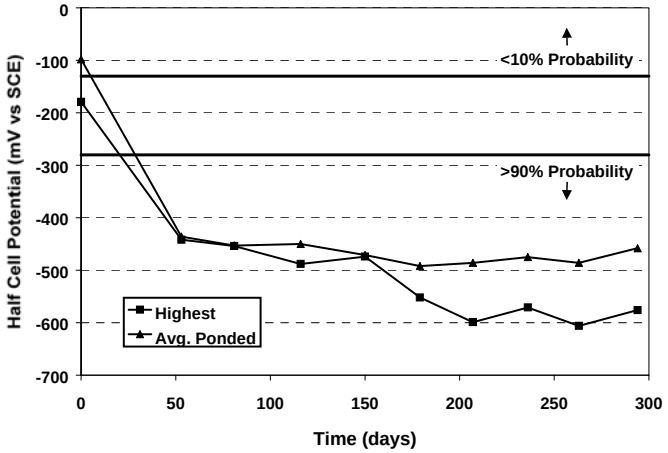

Figure C.35 - Half-Cell Readings: Beam 1.2

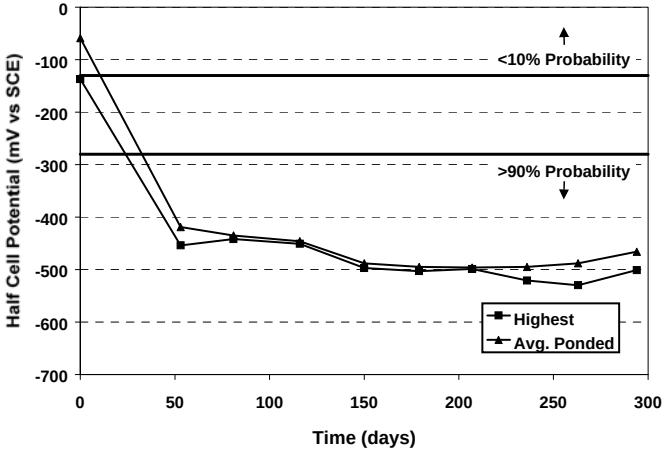

Figure C.36 - Half-Cell Readings: Beam 1.3

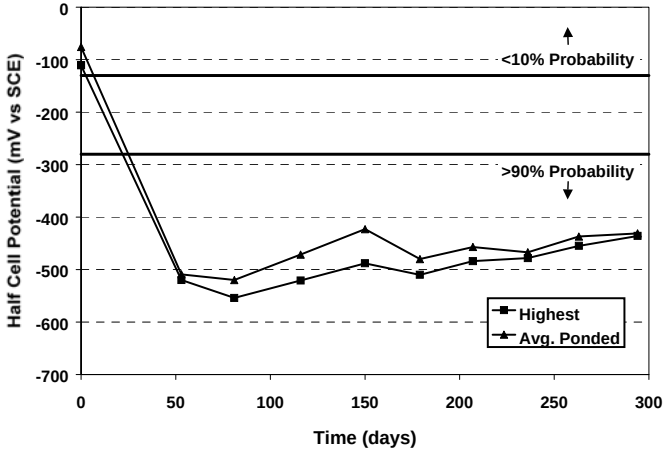

Figure C.37 - Half-Cell Readings: Beam 1.4

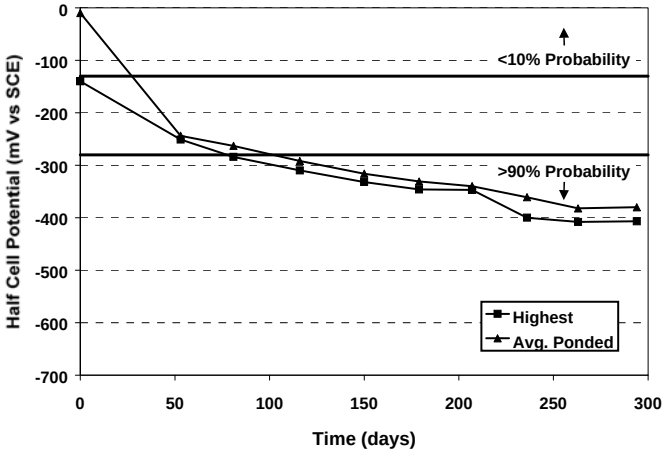

Figure C.38 - Half-Cell Readings: Beam 2.1

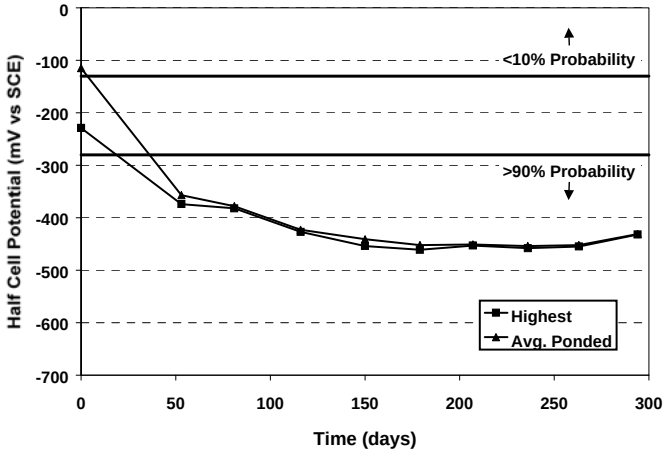

Figure C.39 - Half-Cell Readings: Beam 2.2

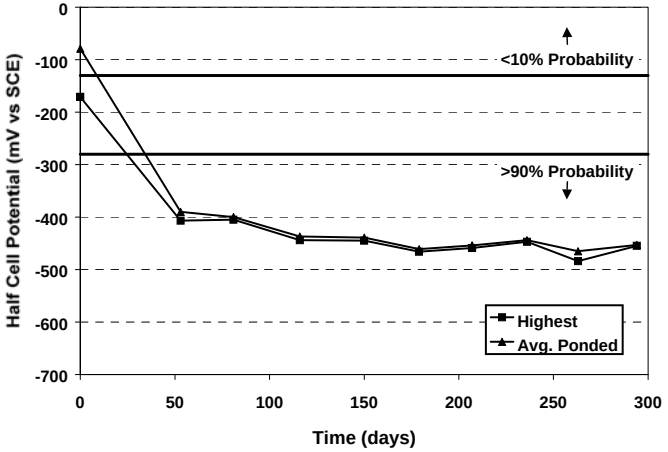

Figure C.40 - Half-Cell Readings: Beam 2.3

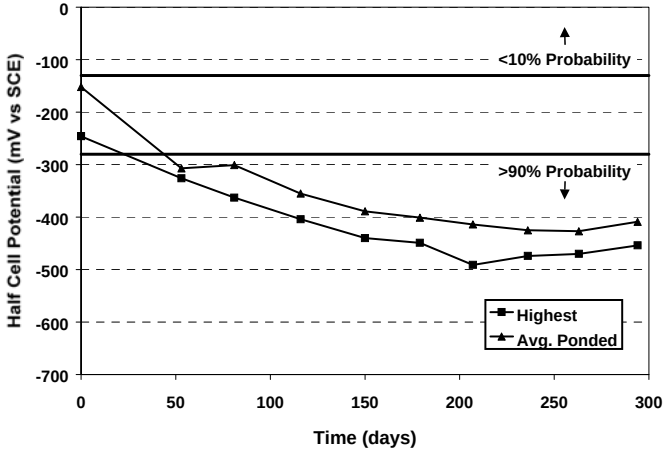

Figure C.41 - Half-Cell Readings: Beam 2.4

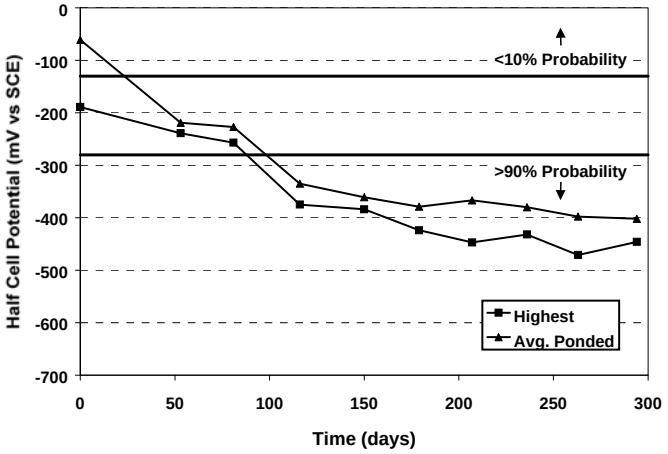

Figure C.42 - Half-Cell Readings: Beam 2.11

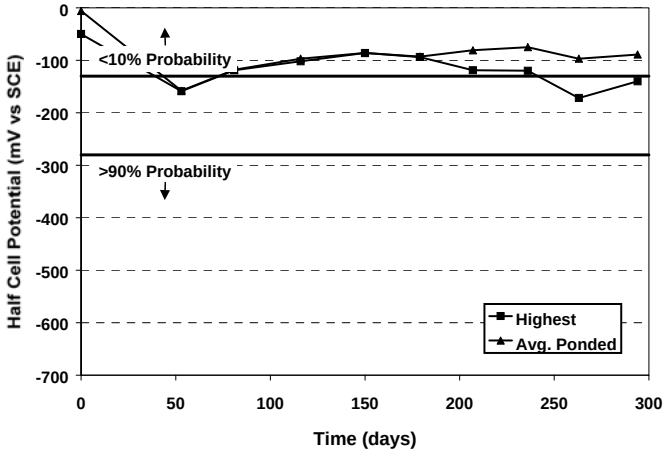

Figure C.43 - Half-Cell Readings: Beam 3.1

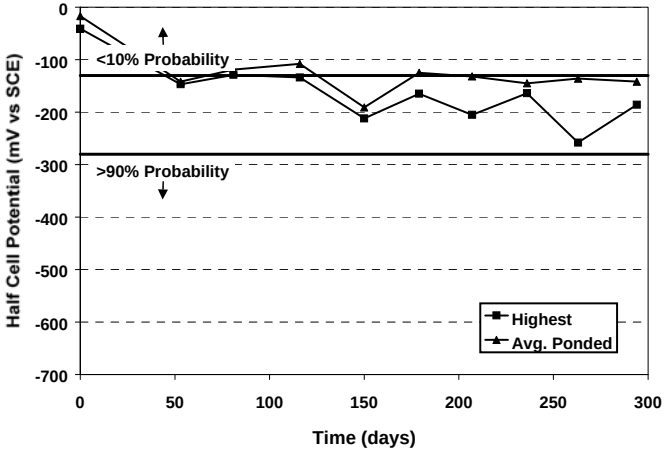

Figure C.44 - Half-Cell Readings: Beam 3.2

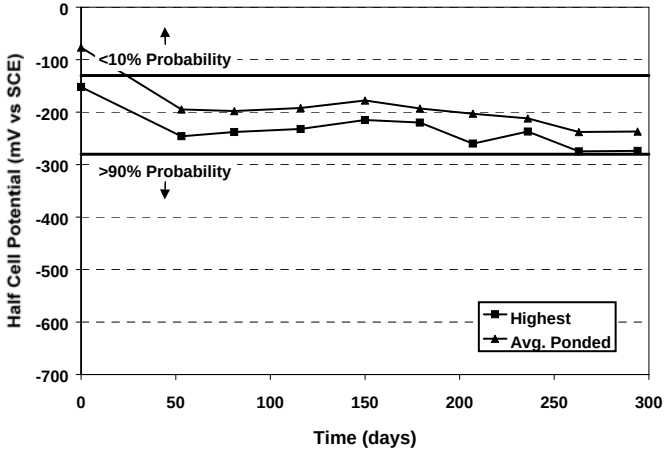

Figure C.45 - Half-Cell Readings: Beam 3.3

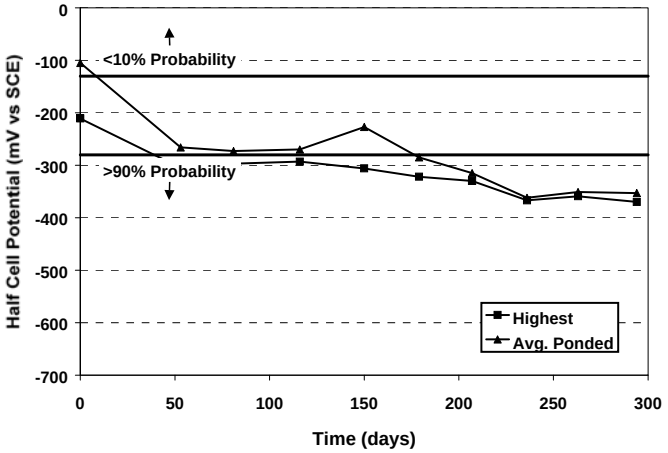

Figure C.46 - Half-Cell Readings: Beam 3.4

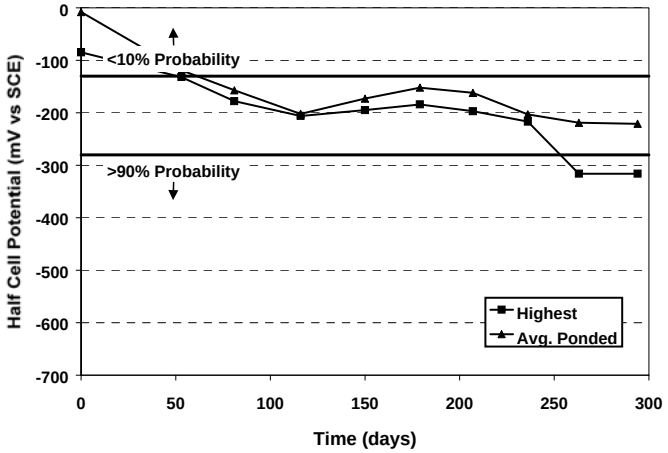

Figure C.47 - Half-Cell Readings: Beam 3.5

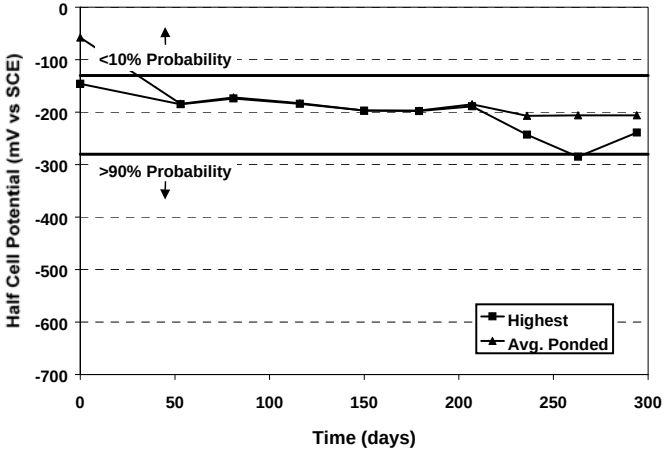

Figure C.48 - Half-Cell Readings: Beam 4.1

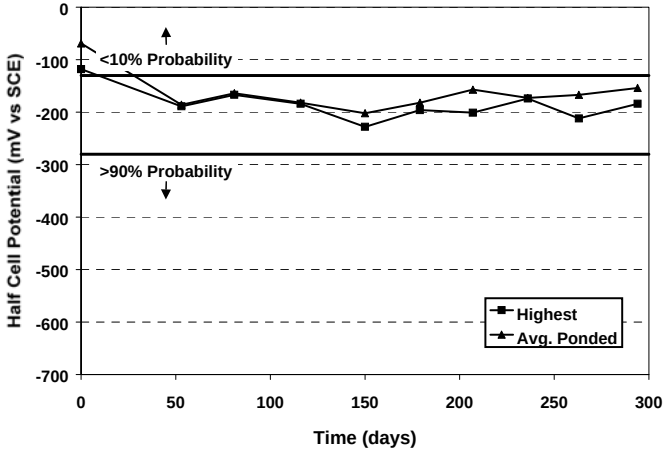

Figure C.49 - Half-Cell Readings: Beam 4.2

Appendix C:

Long Term Beam Corrosion Tests:

Supplementary Material

Analysis of Section 100%S for Maximum Allowable Loading

Gross Section Properties:

$$A_g = 457.2 \times 609.6 = 278{,}709 \text{ mm}^2$$

$$S_b = S_t = \frac{(457.2)(609.6)^2}{6} = 28{,}316{,}847 \text{ mm}^3$$

At Transfer:

extreme fiber stress compression, $f_c \le 0.60\, f'_{ci} = 21$ MPa (3 ksi)

extreme fiber stress tension, $f_t \le 0.25\sqrt{f'_{ci}} = 1.48$ MPa (0.214 ksi)

prestress force at transfer, $T_i = 8 \times 0.65(1860 \text{ MPa}) \times 99 \text{ mm}^2$

$= 958$ kN (215 kips)

tendon eccentricity at midspan, $e = 200$ mm (8 in.)

$$f_c = \frac{958{,}000}{278{,}709} + \frac{(958{,}000)(200)}{28{,}316{,}847} = 10.2 \text{ MPa (1.48 ksi)}$$

$$f_t = \frac{958{,}000}{278{,}709} - \frac{(958{,}000)(200)}{28{,}316{,}847} = -3.33 \text{ MPa } (-.483 \text{ ksi})$$

- At transfer, the extreme fiber stress in tension exceeds the allowable value, and a portion of the superimposed loading will have to be applied to satisfy stress limits.
- The tendon profile will be draped to reduce the tendon eccentricity near the member ends to satisfy stress limits.

Compute Maximum Permissible Service Loading:

extreme fiber stress compression, $f_c \le 0.45\, f'_c = 15.75$ MPa (2.28 ksi)

extreme fiber stress tension, $f_t \le 0.5\sqrt{f'_c} = 2.96$ MPa (0.429 ksi)

effective prestress force, $T_e = 8 \times 0.55(1860 \text{ MPa}) \times 99 \text{ mm}^2$

$= 814$ kN (183 kips)

tendon eccentricity at midspan, $e = 200$ mm (8 in.)

Case 1: $f_c = 0.75f_{cmax}$

$$f_c = 0.75 \times 15.75 = \frac{814{,}000}{278{,}709} - \frac{(814{,}000)(200)}{28{,}316{,}847} + \frac{M_{serv}}{28{,}316{,}847}$$

$$M_{serv} = 414.6 \text{ kN} - \text{m} \quad (3670 \text{ k} - \text{in.})$$

$$f_t = \frac{814{,}000}{278{,}709} + \frac{(814{,}000)(200)}{28{,}316{,}847} - \frac{414.6 \times 10^6}{28{,}316{,}847} = -5.97 \text{ MPa } (-.866 \text{ ksi}) \text{ too high!}$$

Case 2: $f_t = 0.75f_{tmax}$

$$f_t = 0.75 \times (-2.96) = \frac{814{,}000}{278{,}709} + \frac{(814{,}000)(200)}{28{,}316{,}847} - \frac{M_{serv}}{28{,}316{,}847}$$

$$M_{serv} = 308.4 \text{ kN} - \text{m} \quad (2730 \text{ k} - \text{in.})$$

$$f_c = \frac{814{,}000}{278{,}709} - \frac{(814{,}000)(200)}{28{,}316{,}847} + \frac{308.4 \times 10^6}{28{,}316{,}847} = 8.06 \text{ MPa } (1.17 \text{ ksi}) \quad \text{O.K.}$$

- Base total permissible service load on Case 2.
- Use M_{serv} = 310.7 kN-m (2750 k-in.)

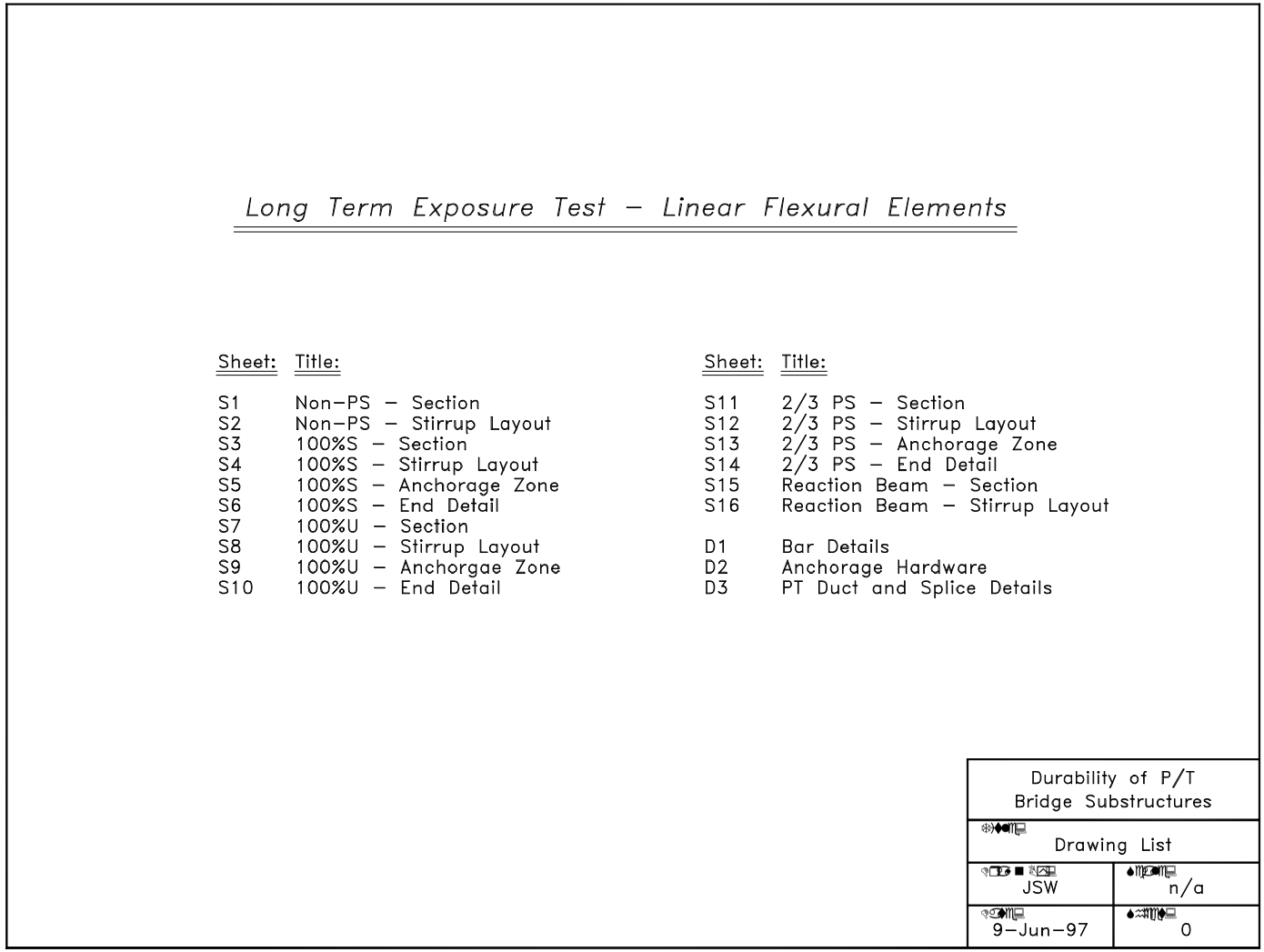

Figure C.1 - Sheet 0: Drawing List

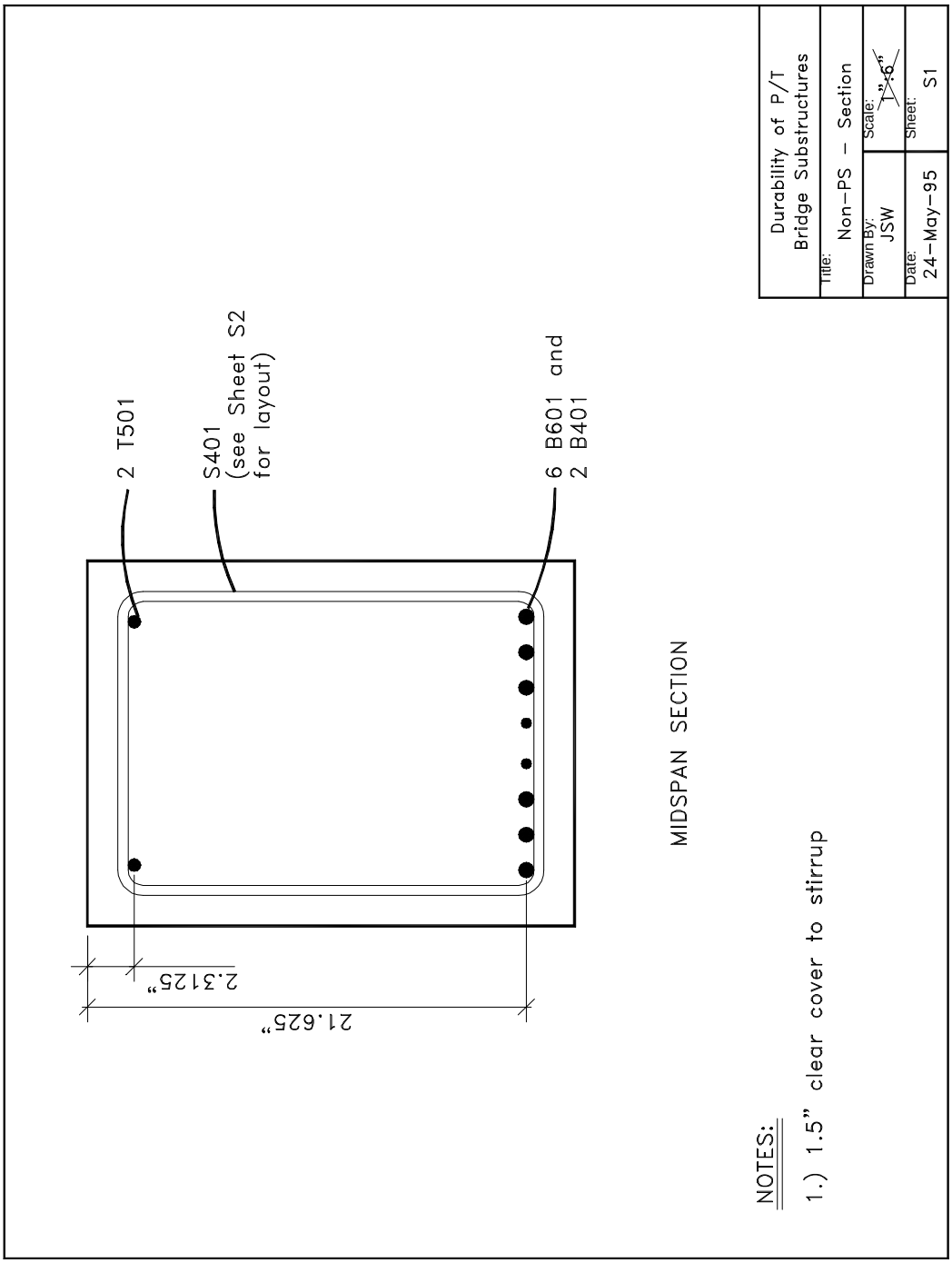

Figure C.2 - Sheet S1: Non-PS Section

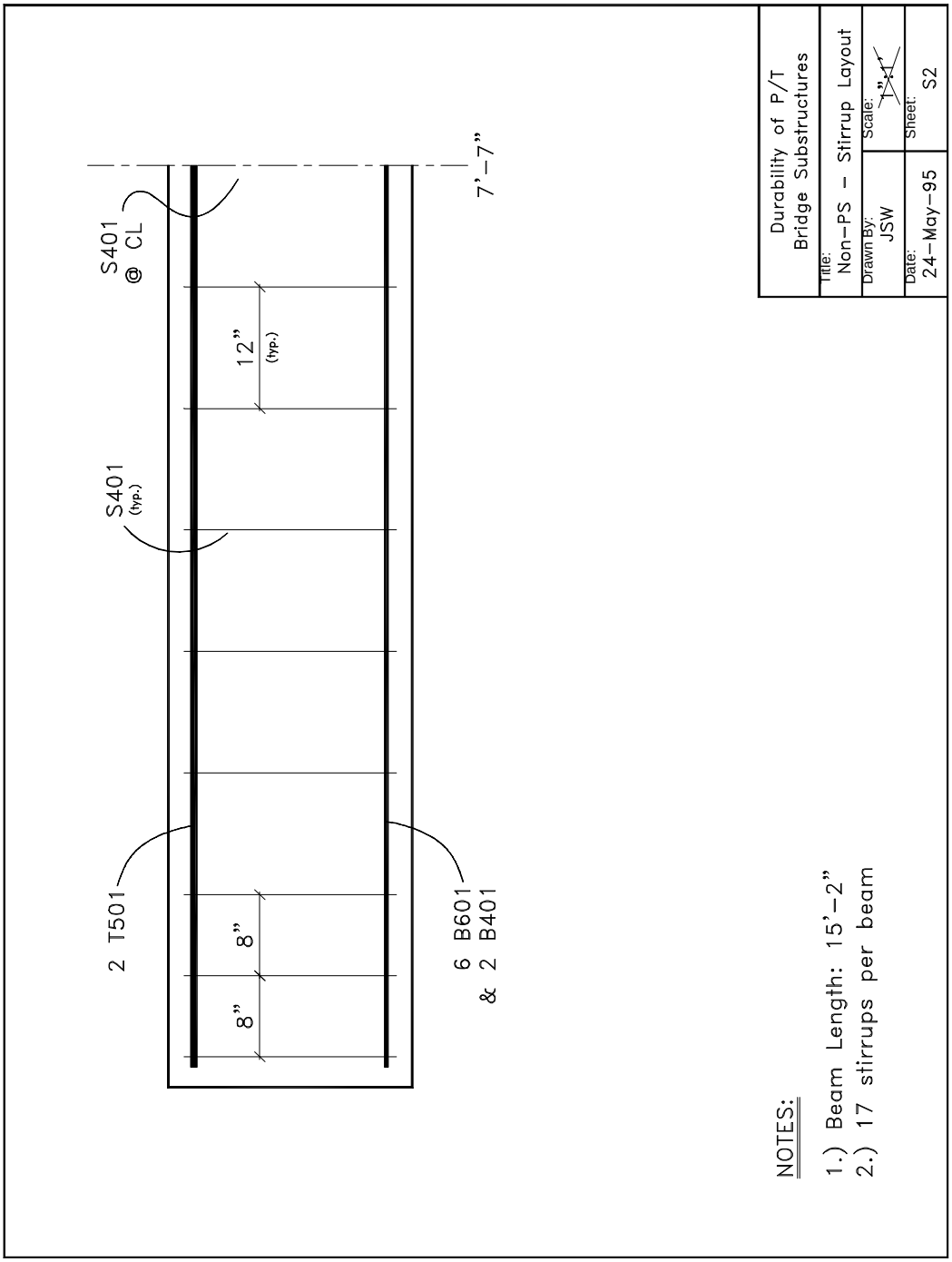

Figure C.3 - Sheet S2: Non-PS Stirrup Layout

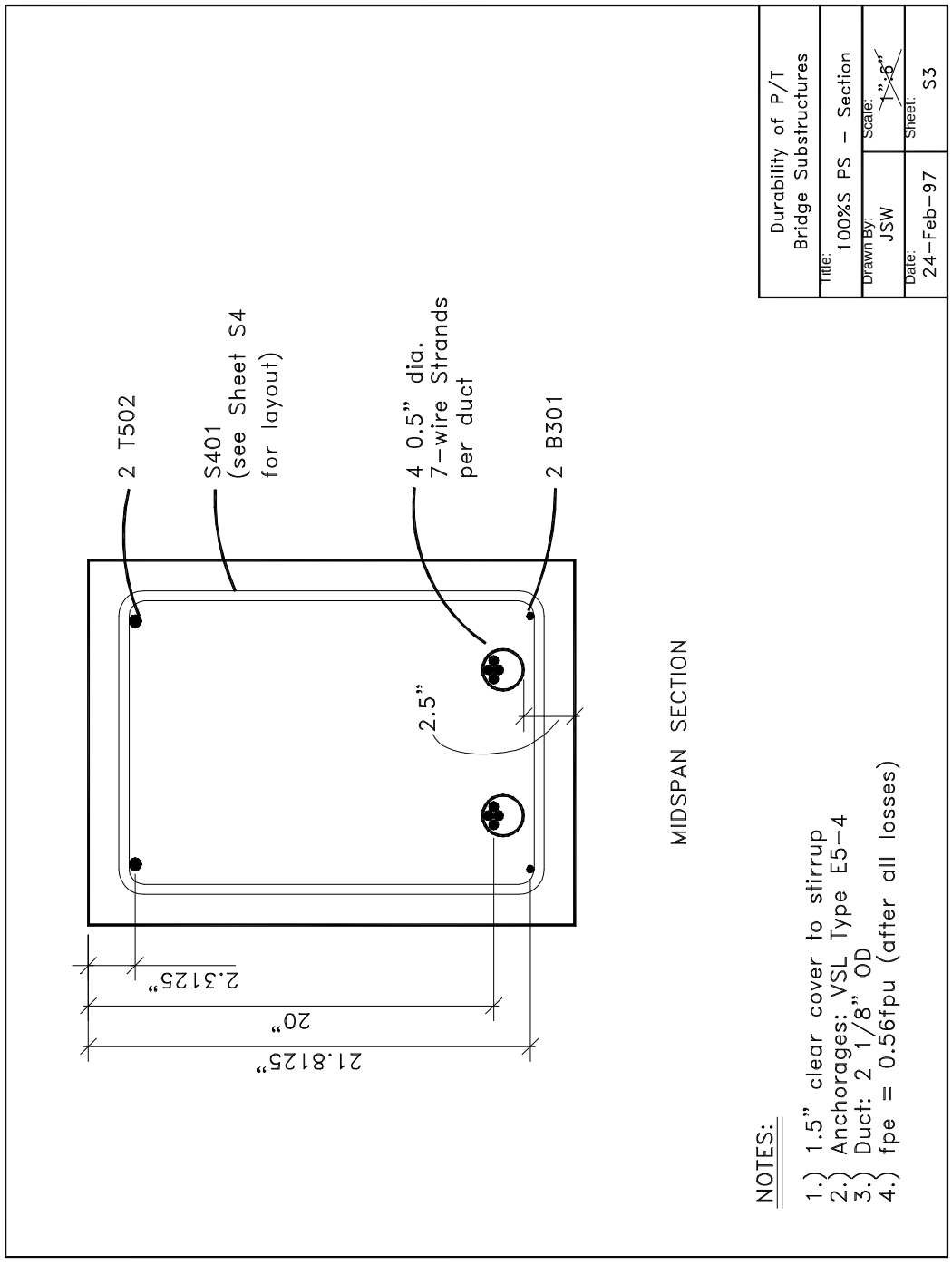

Figure C.4 - Sheet S3: 100%S PS Section

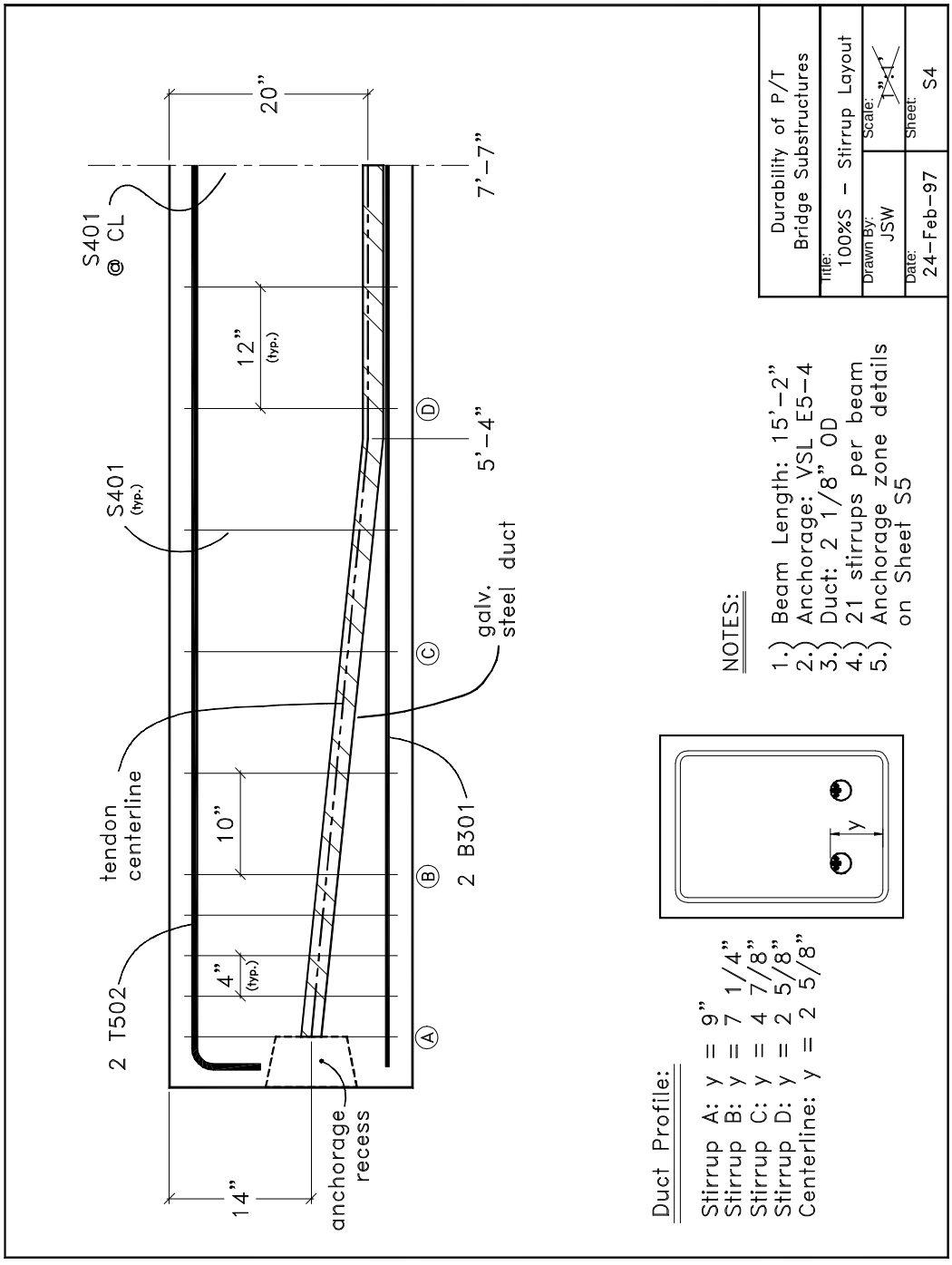

Figure C.5 - Sheet S4: 100%S Stirrup Layout

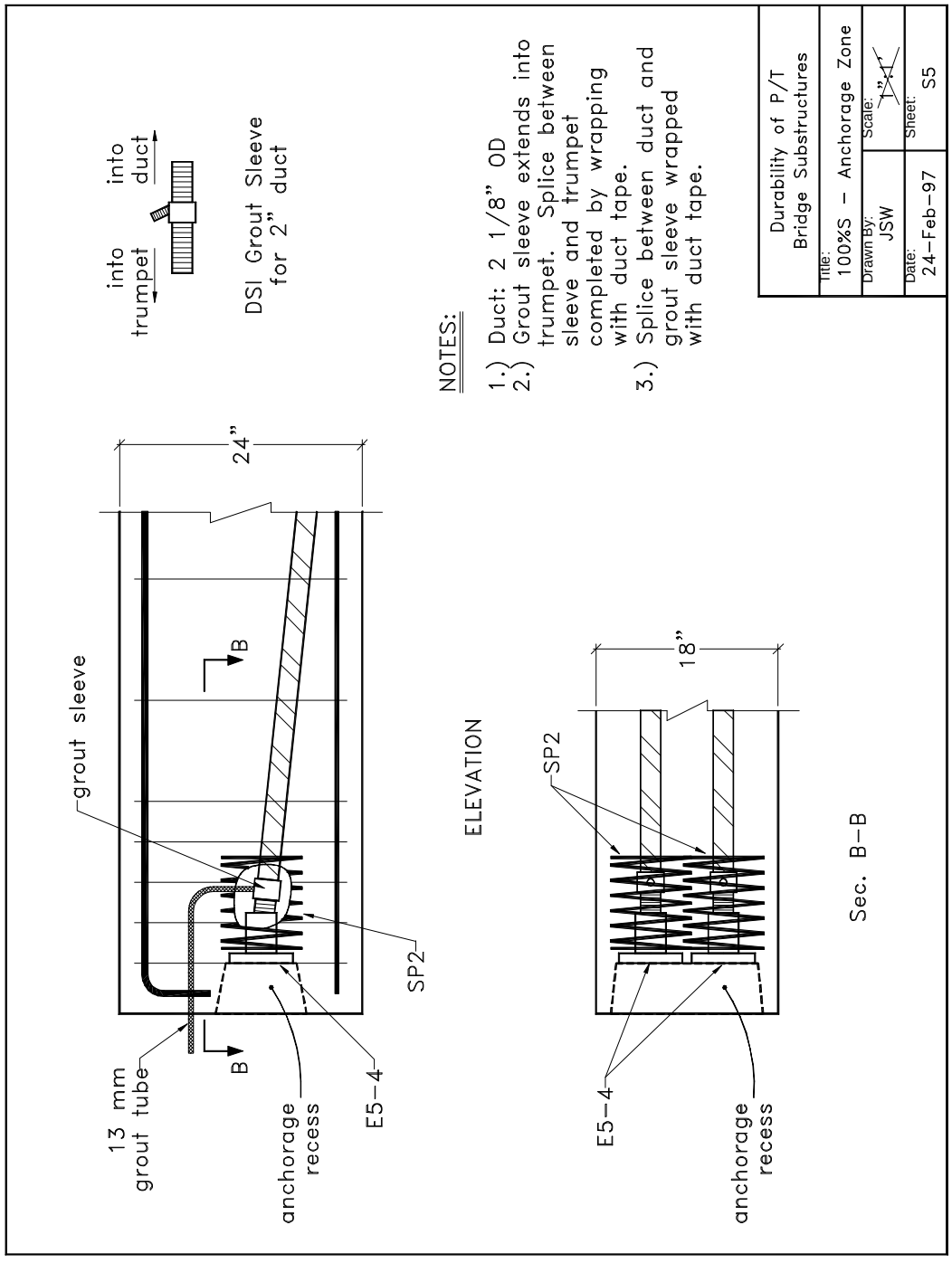

Figure C.6 - Sheet S5: 100%S Anchorage Zone

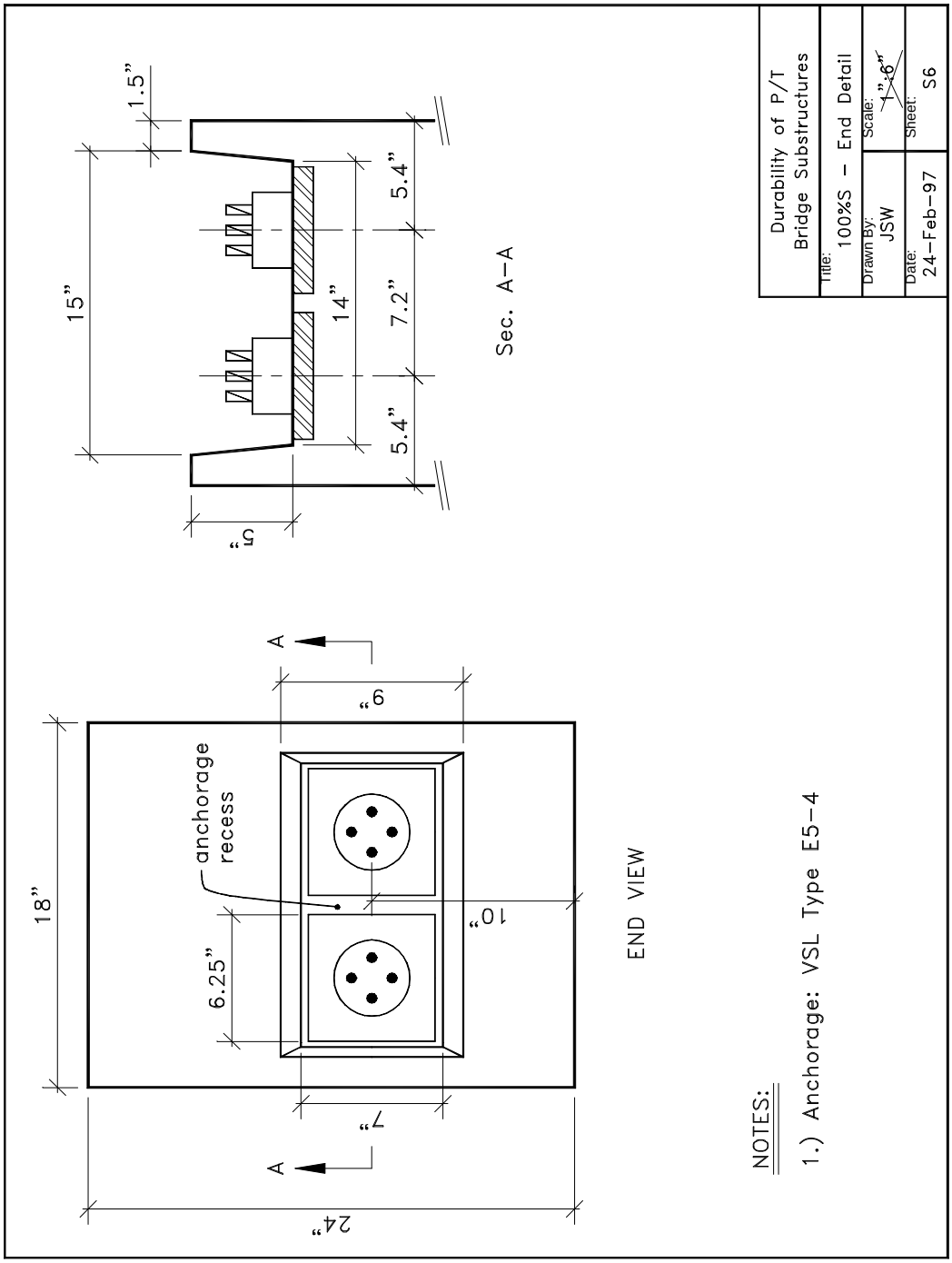

Figure C.7 - Sheet S6: 100%S End Detail

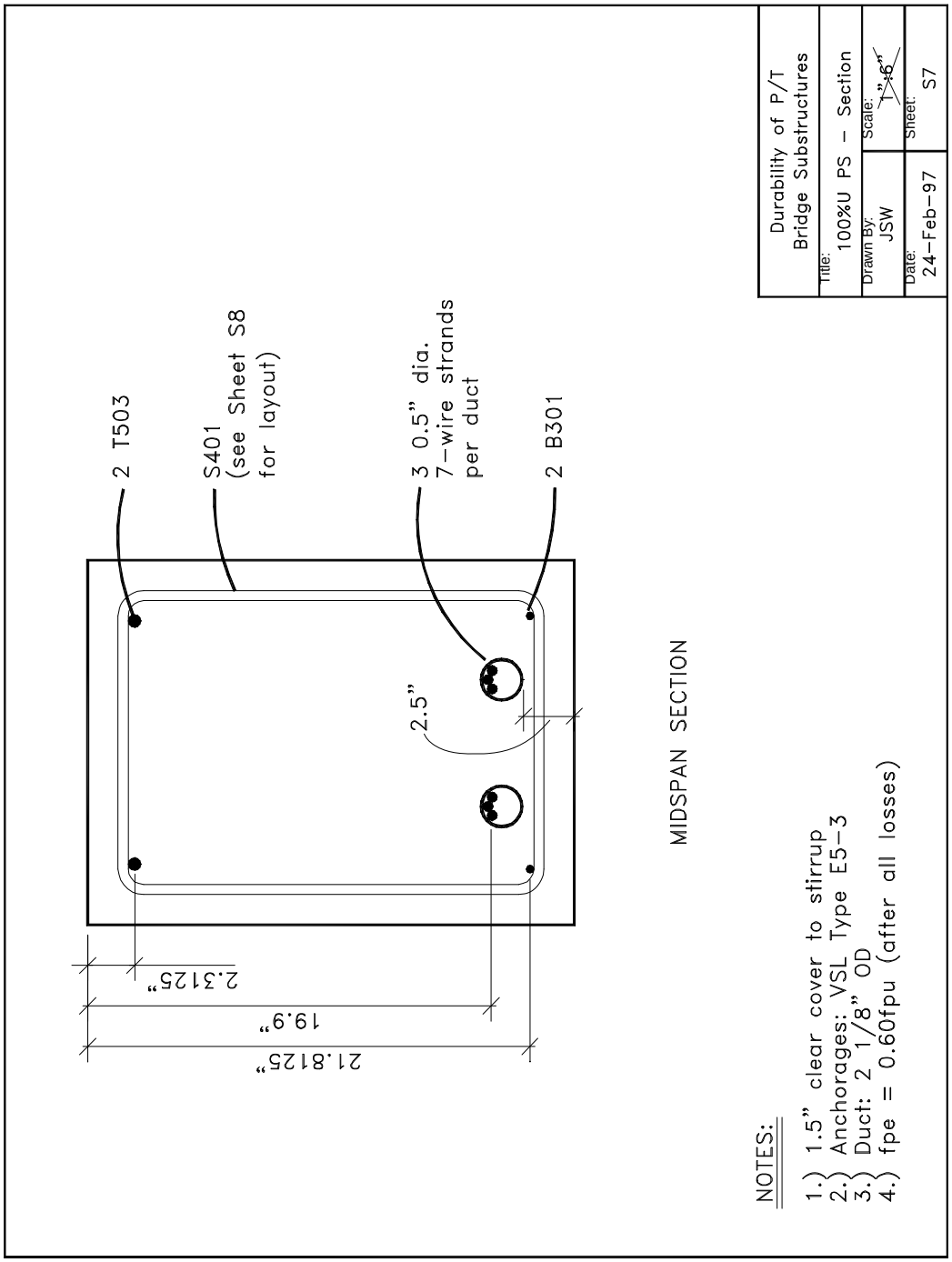

Figure C.8 - Sheet S7: 100%U PS Section

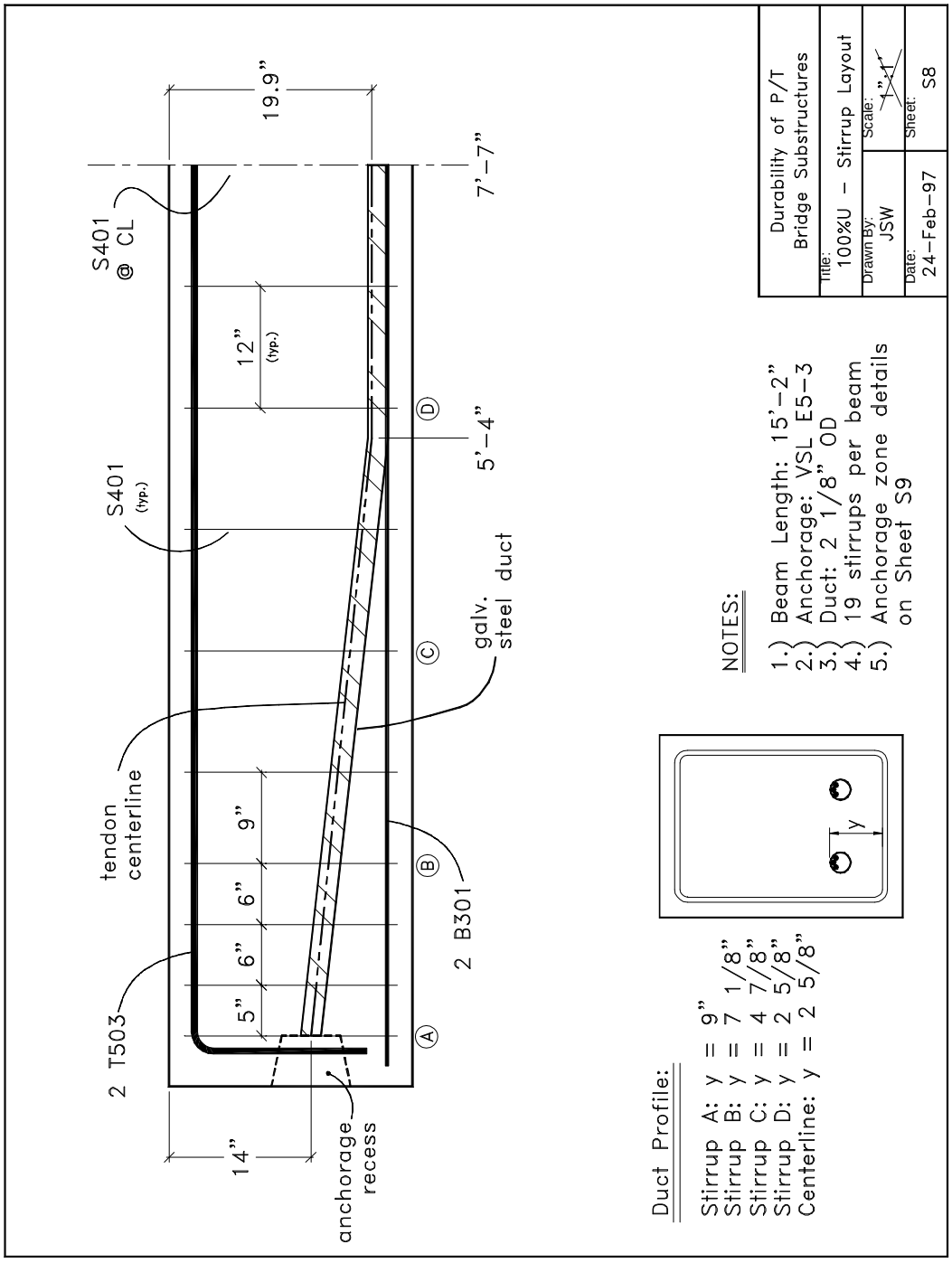

Figure C.9 - Sheet S8: 100%U Stirrup Layout

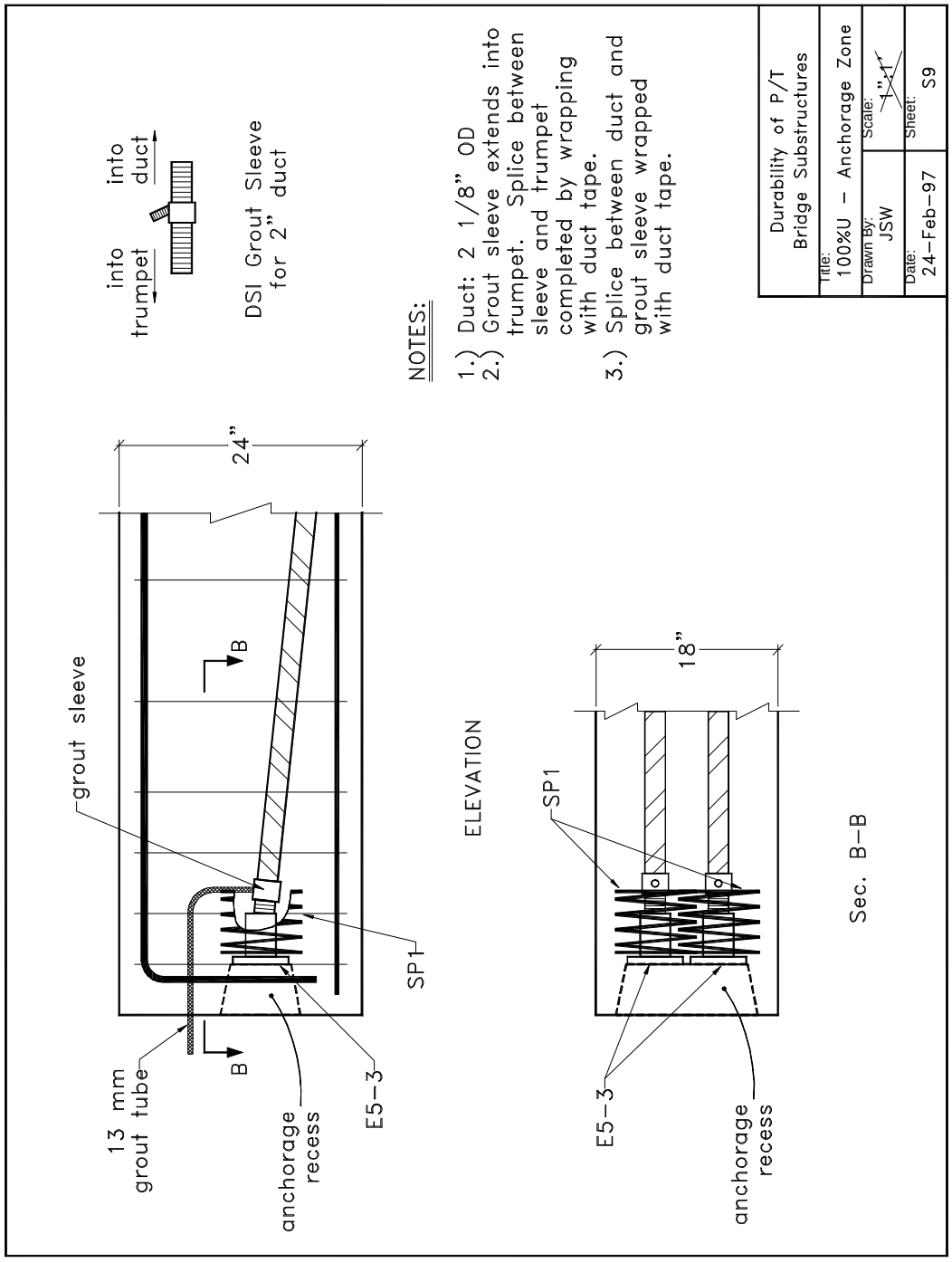

Figure C.10 - Sheet S9: 100%U Anchorage Zone

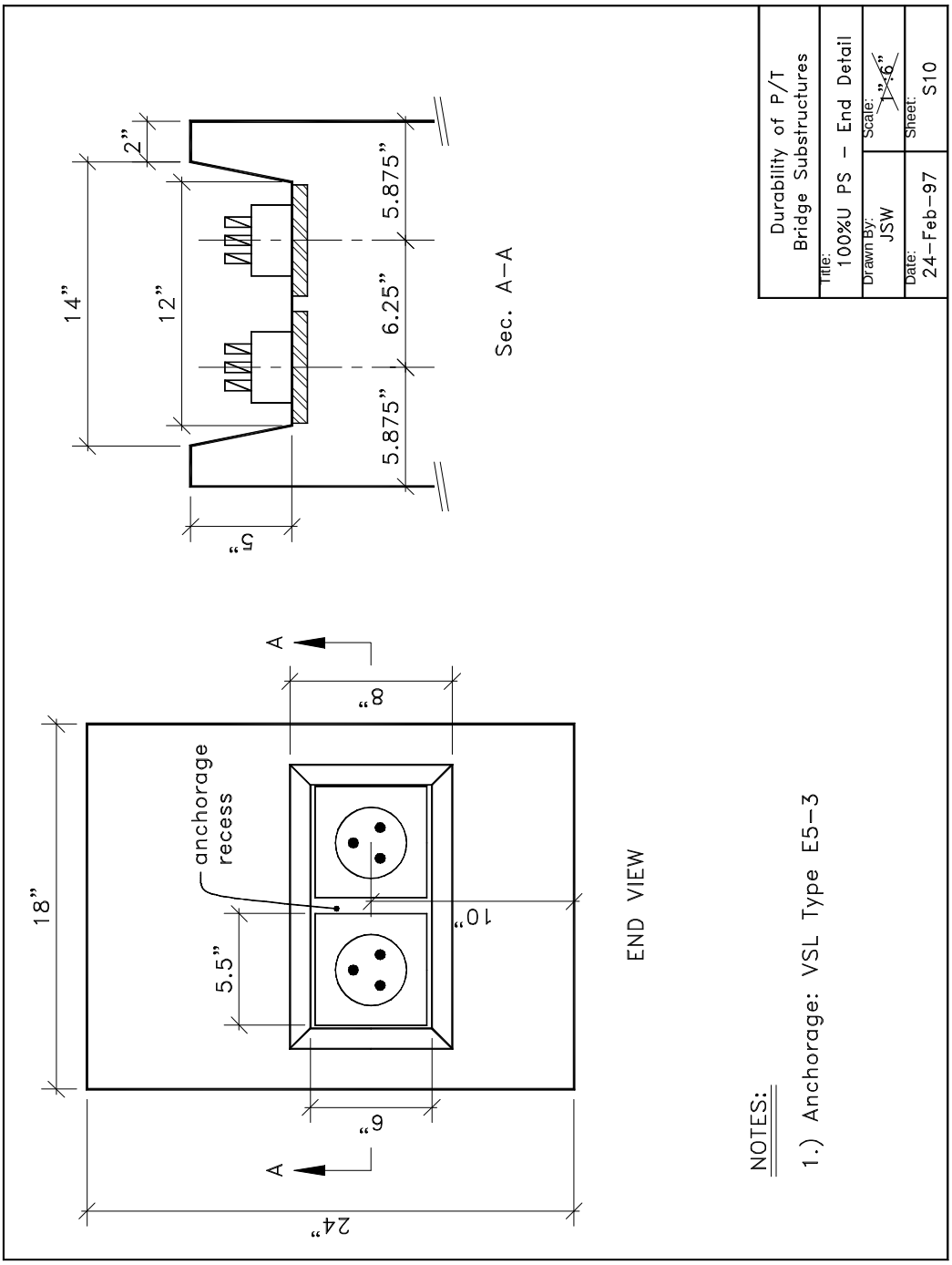

Figure C.11 - Sheet S10: 100%U End Detail

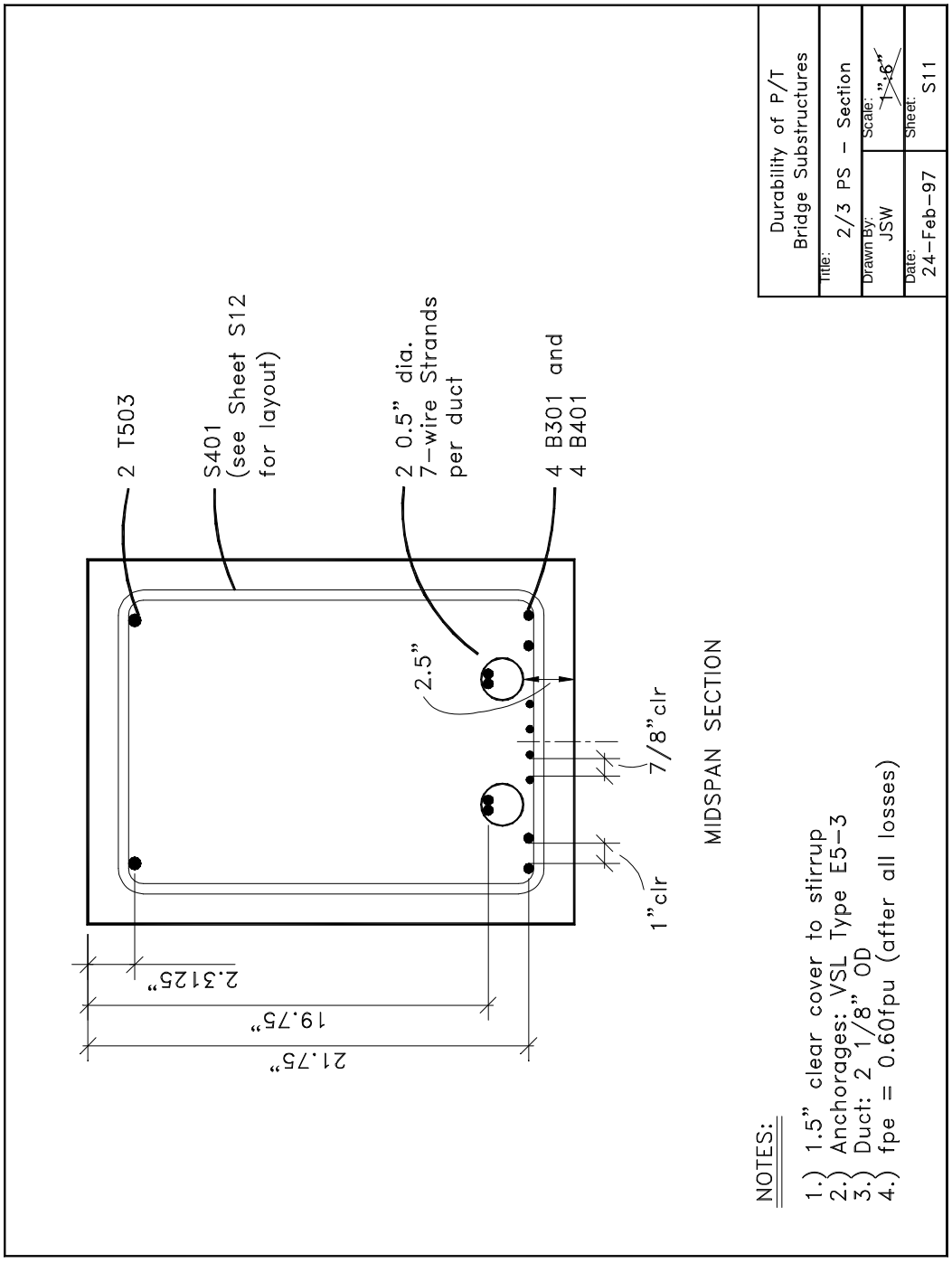

Figure C.12 - Sheet S11: 2/3 PS Section

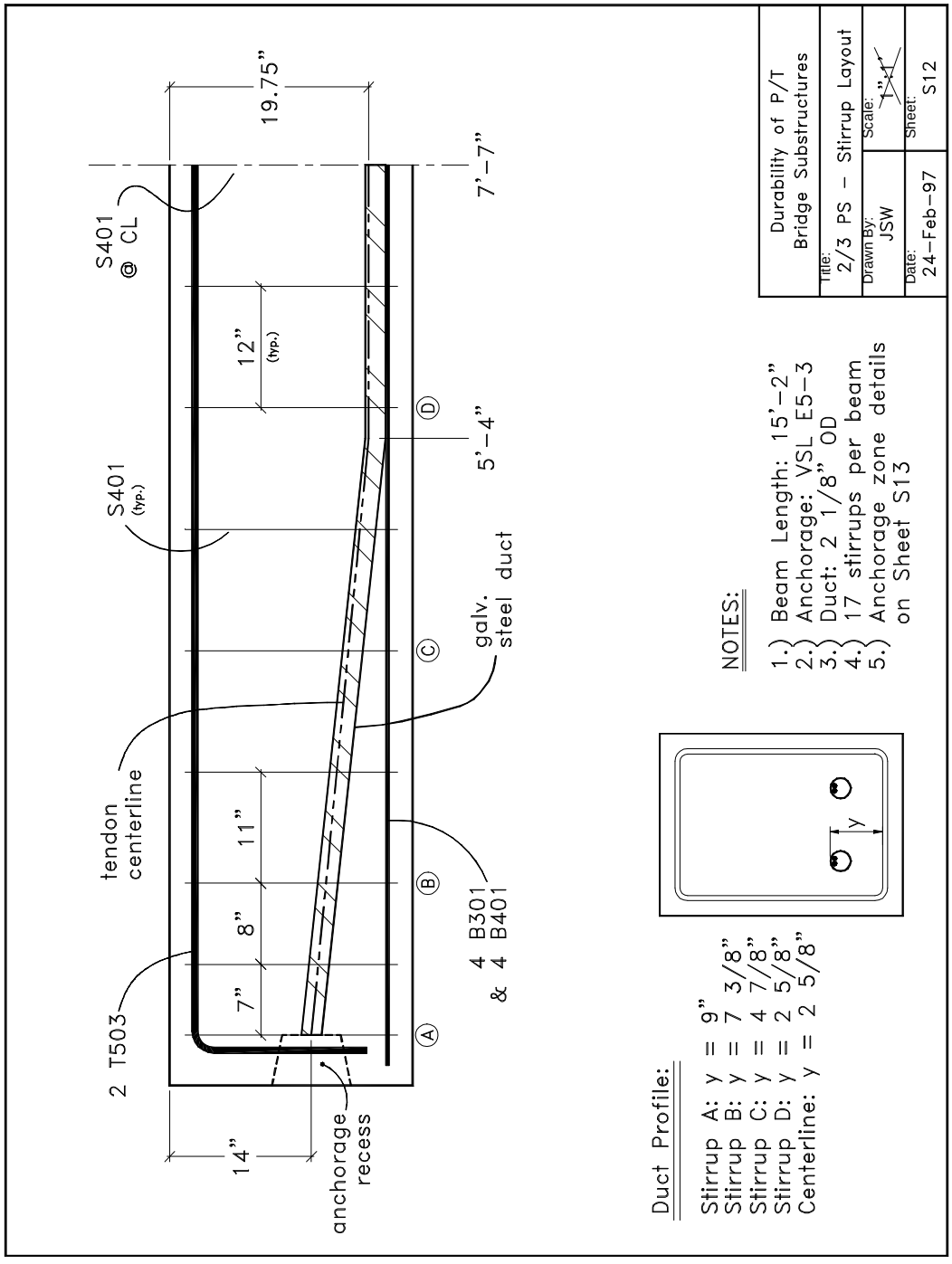

Figure C.13 - Sheet S12: 2/3 PS Stirrup Layout

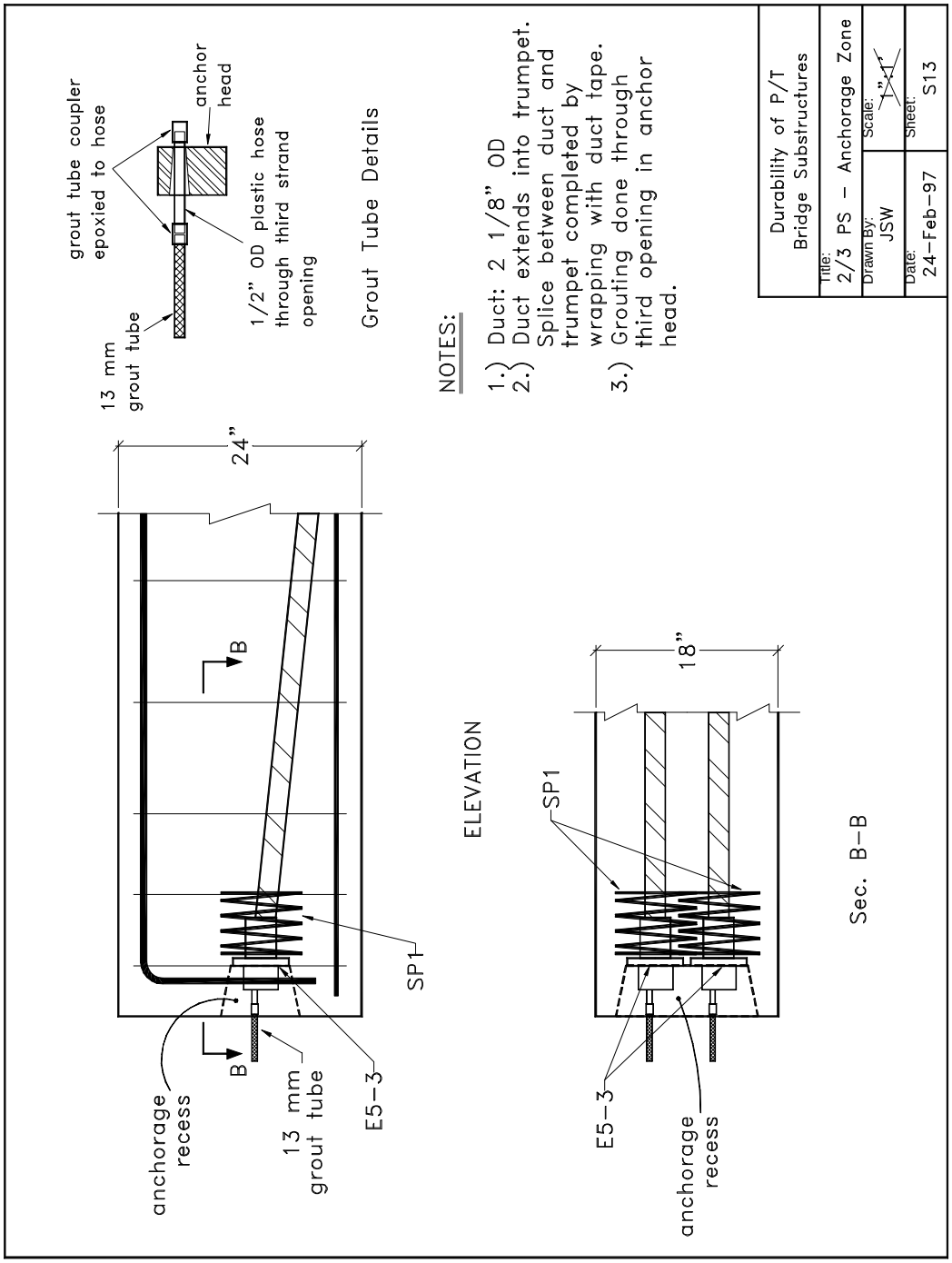

Figure C.14 - Sheet S13: 2/3 PS Anchorage Zone

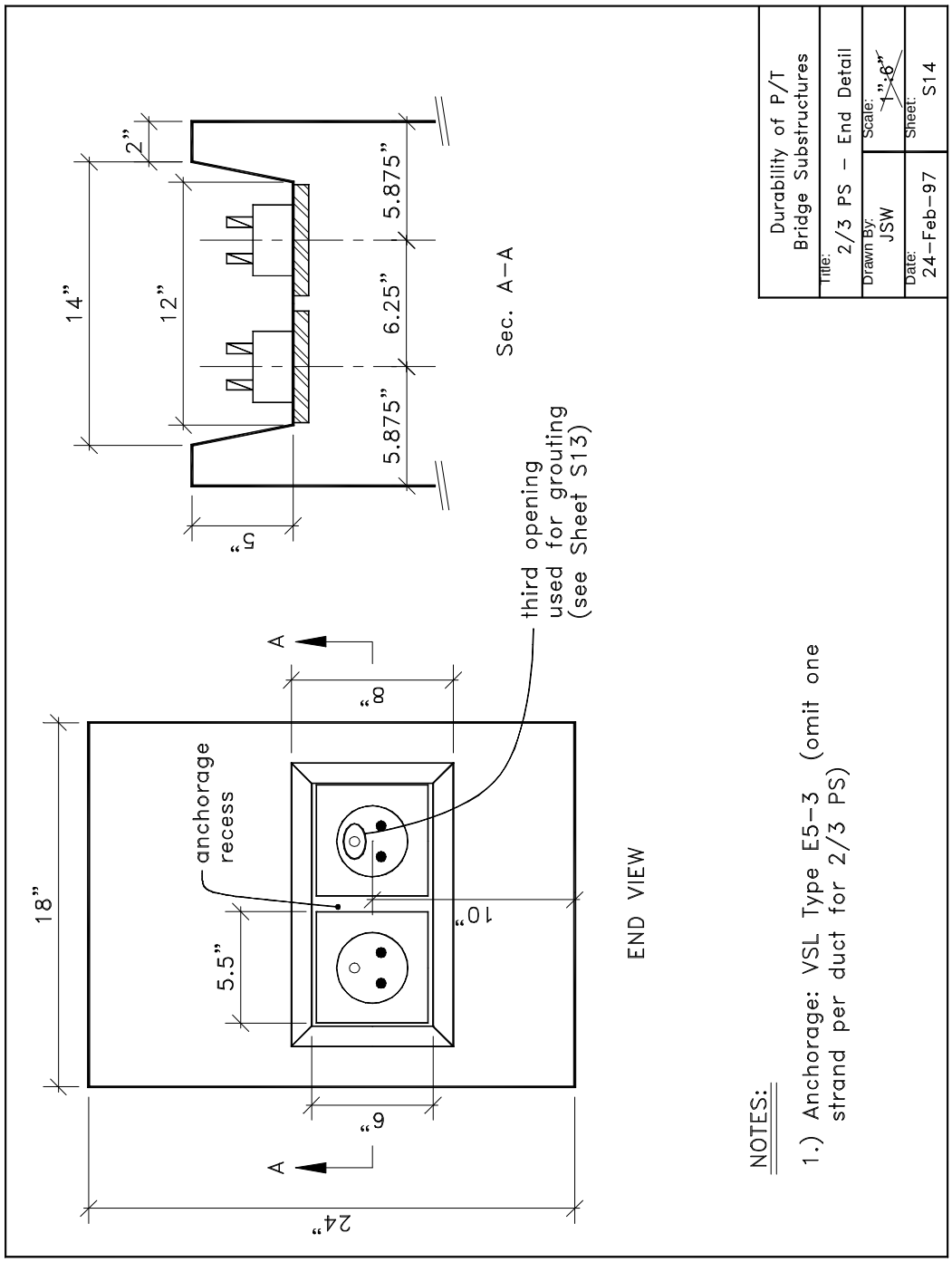

Figure C.15 - Sheet S14: 2/3 PS End Detail

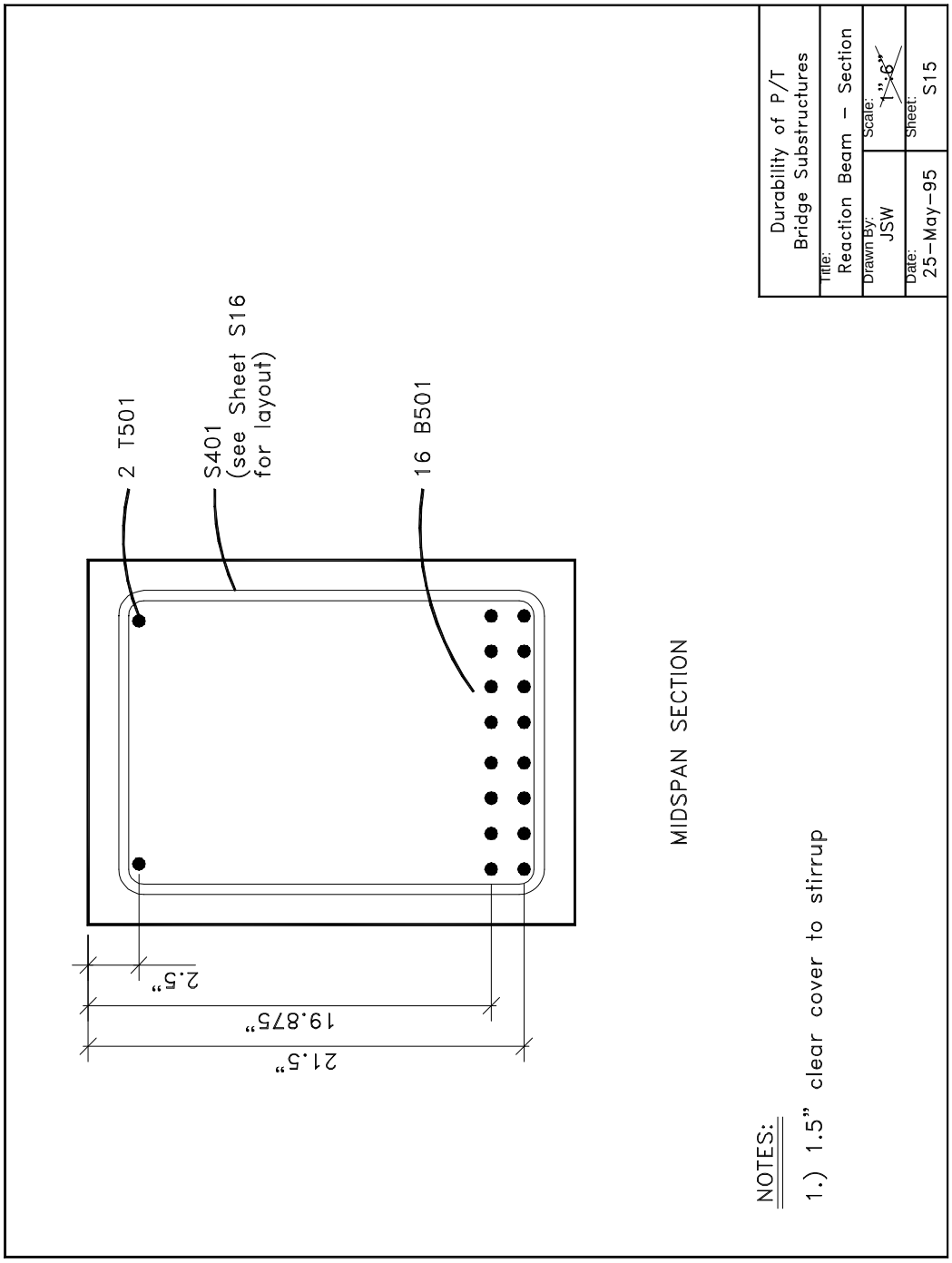

Figure C.16 - Sheet S15: Reaction Beam Section

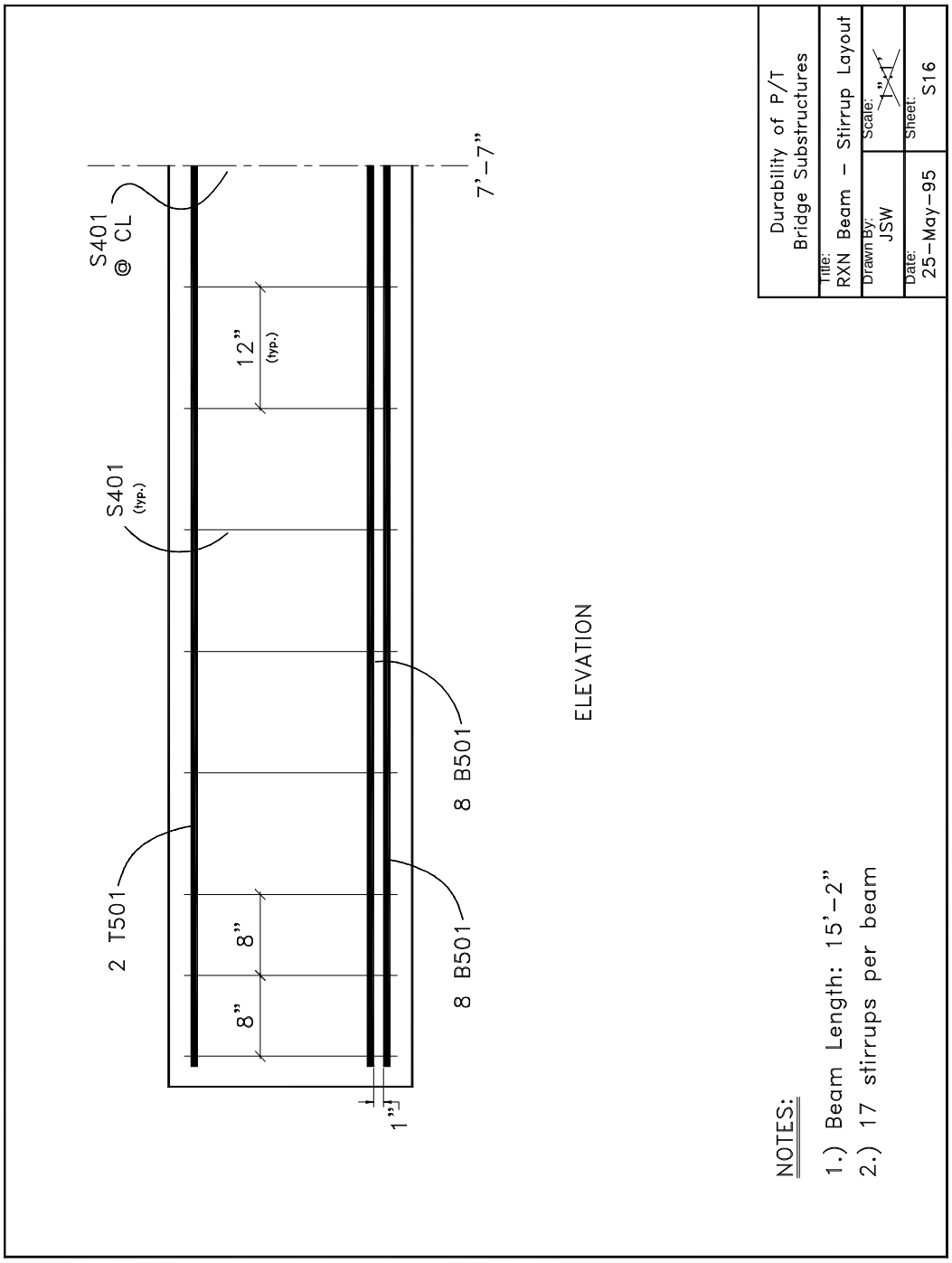

Figure C.17 - Sheet S16: Reaction Beam Stirrup Layout

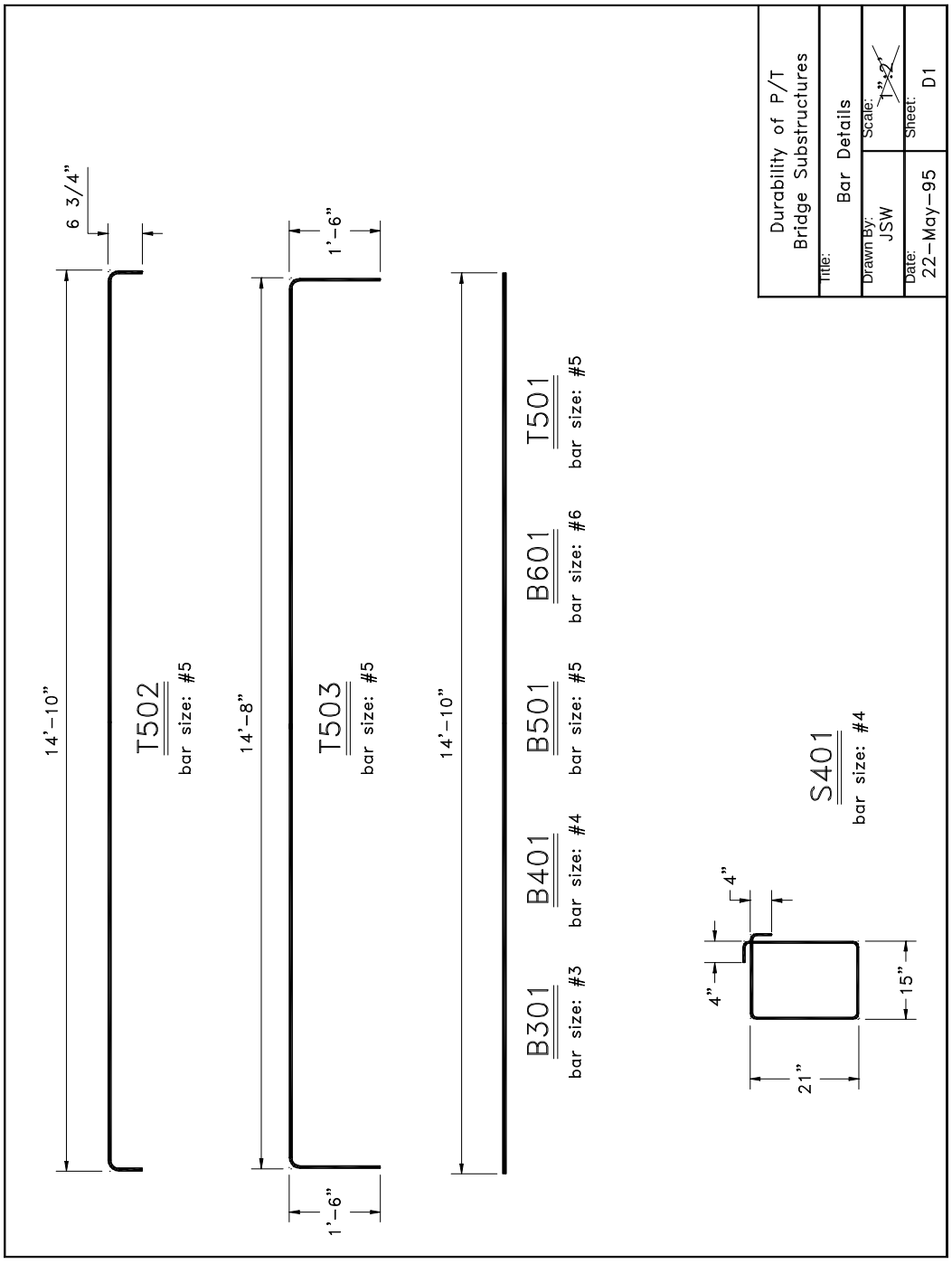

Figure C.18 - Sheet D1: Bar Details

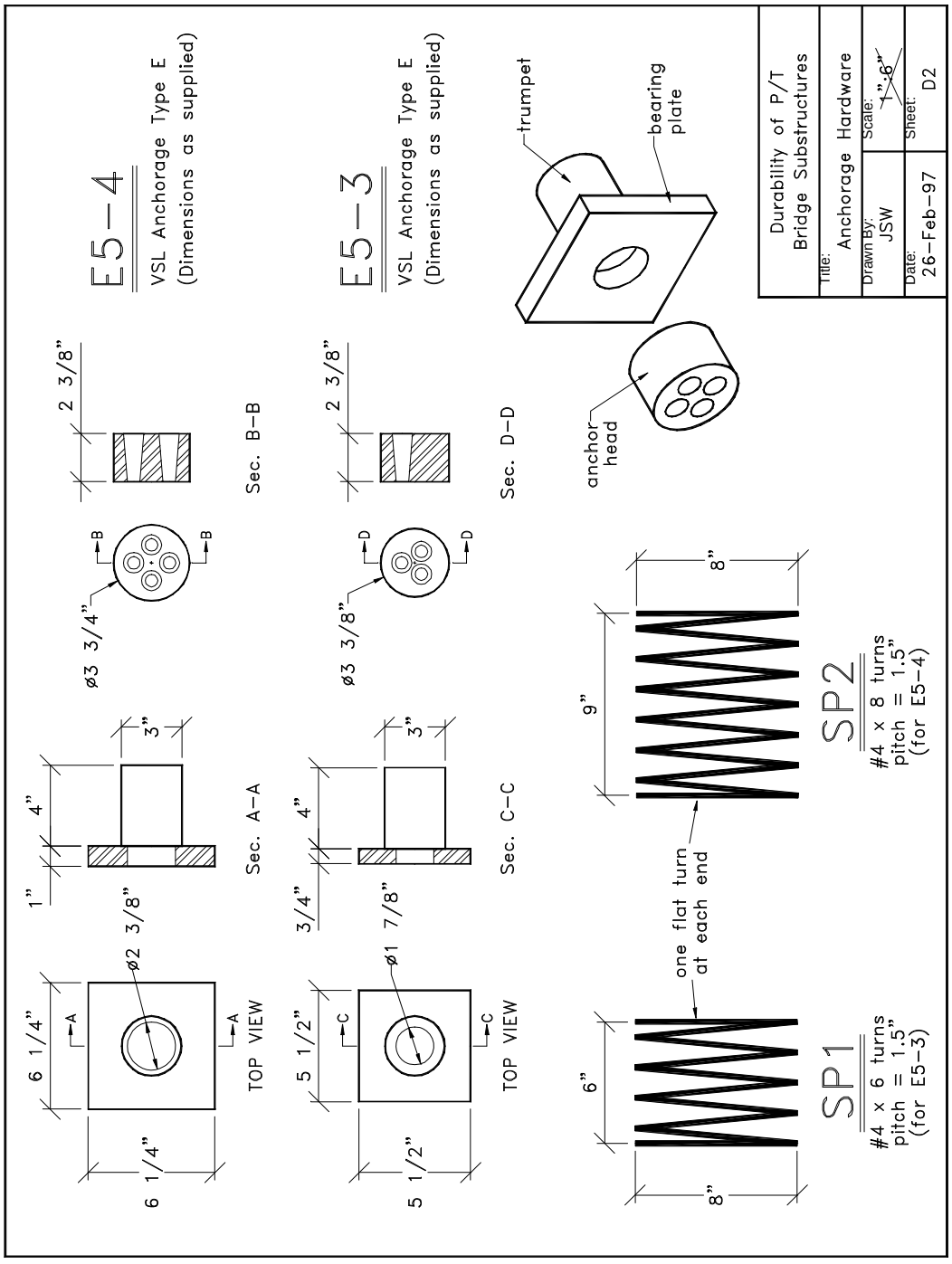

Figure C.19 - Sheet D2: Anchorage Hardware

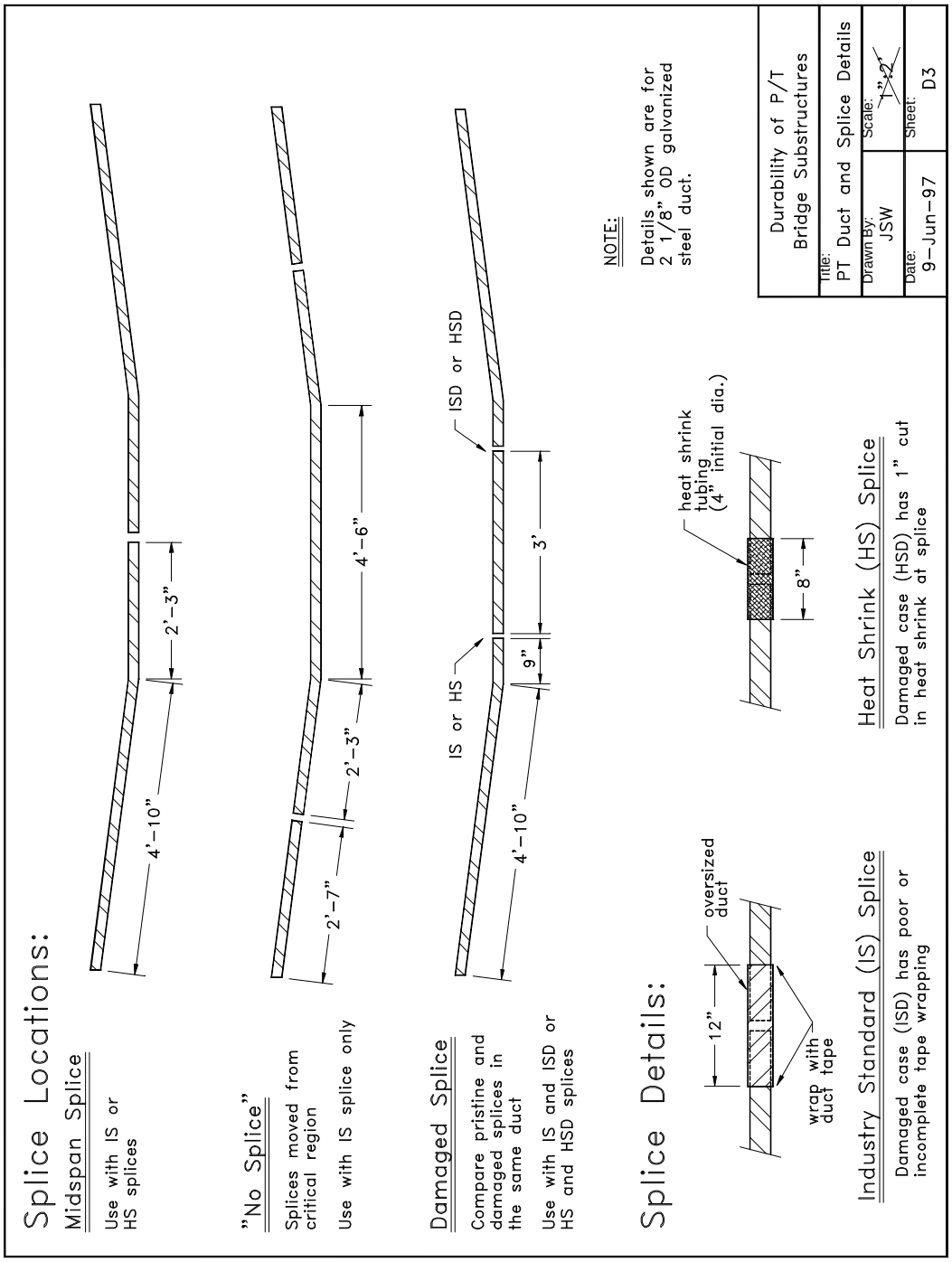

Figure C.20 - Sheet D3: Post-Tensioning Duct and Splice Details

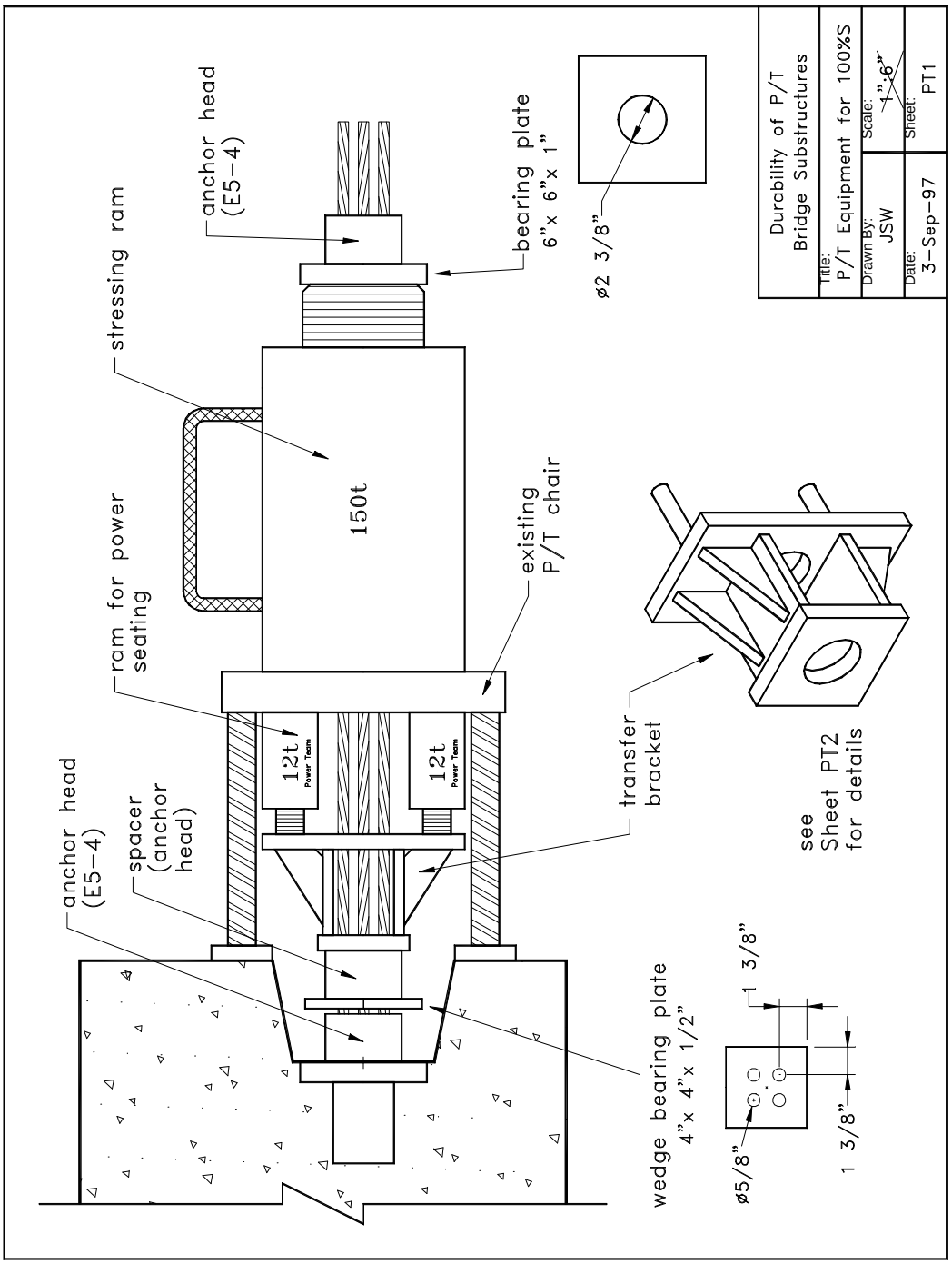

Figure C.21 - Sheet PT1: Post-Tensioning Equipment for 100%S Beams

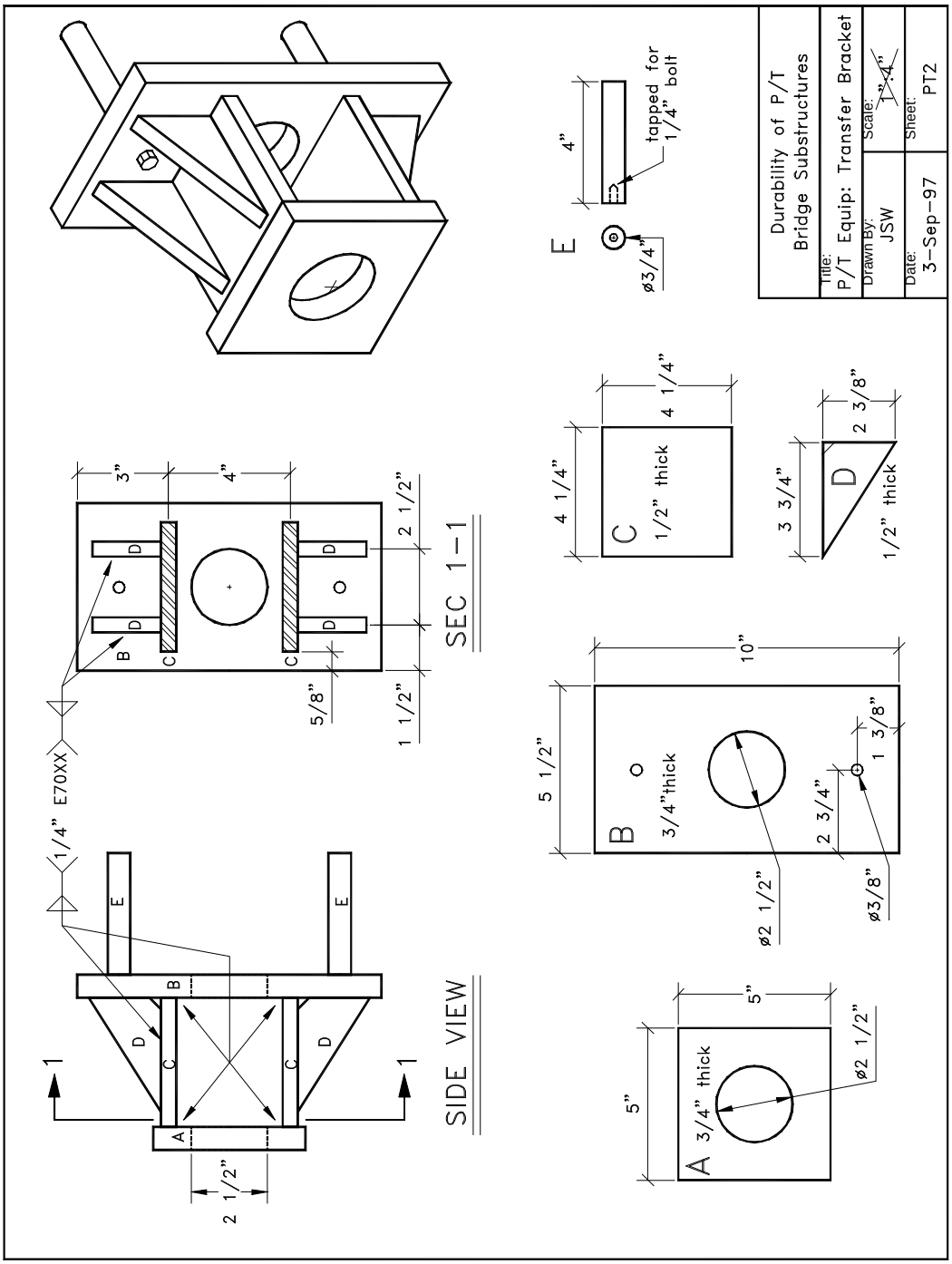

Figure C.22 - Sheet PT2: Post-Tensioning Equipment Transfer Bracket for Power Seating of Wedges

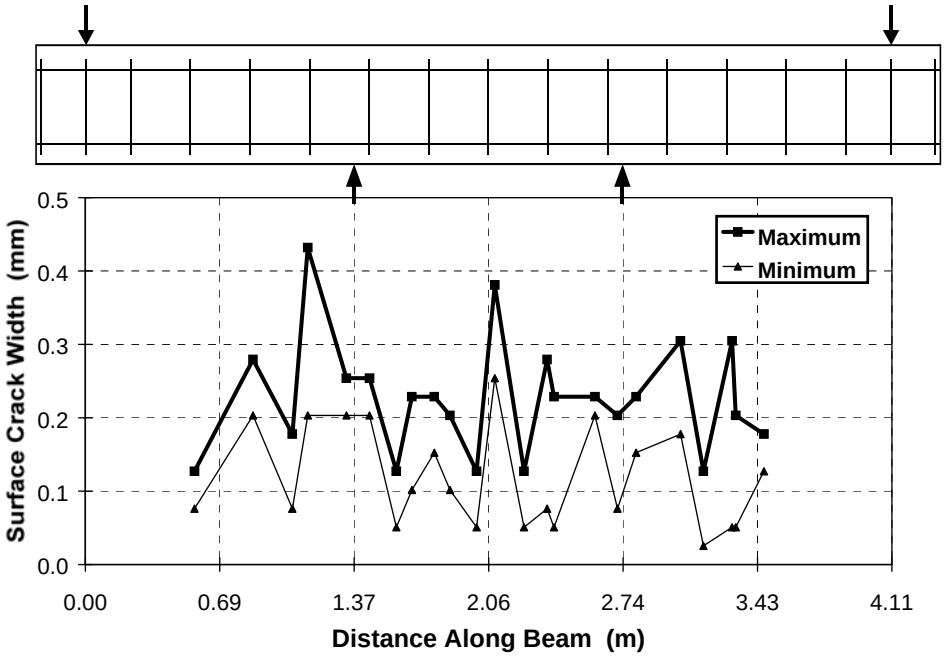

Figure C.23 – Measured Crack Widths: Beam 1.2 at Service

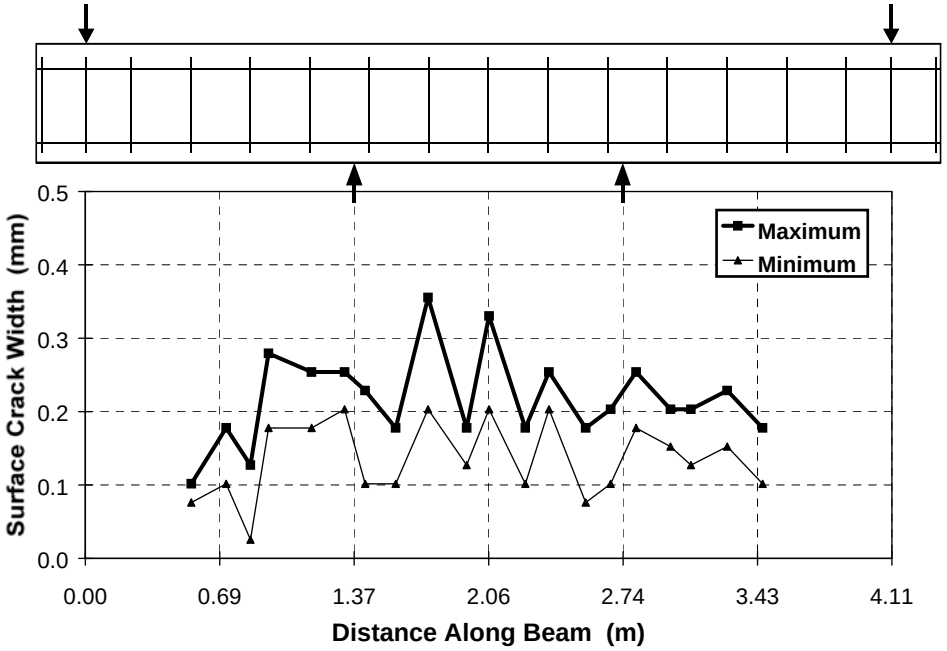

Figure C.24 - Measured Crack Widths: Beam 1.3 at Service

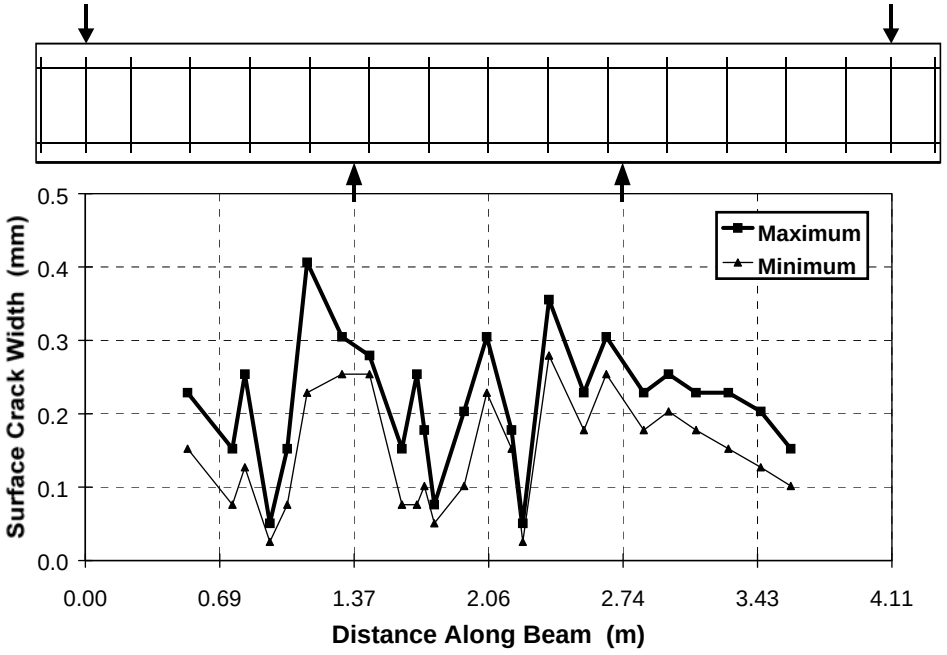

Figure C.25 - Measured Crack Widths: Beam 1.4 at Service After 25% Overload

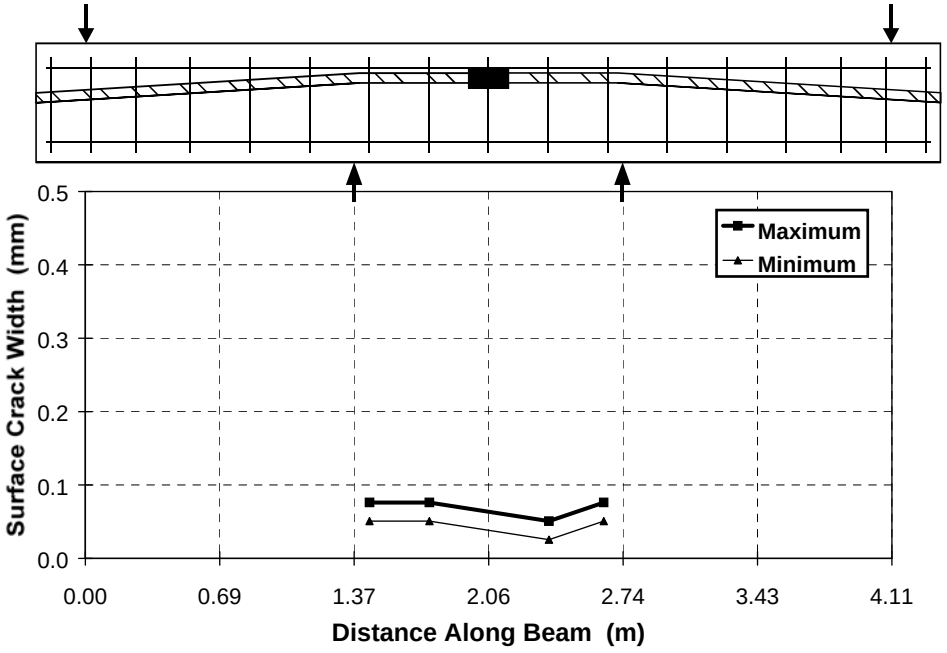

Figure C.26 - Measured Crack Widths: Beam 2.1 at 84% of Service

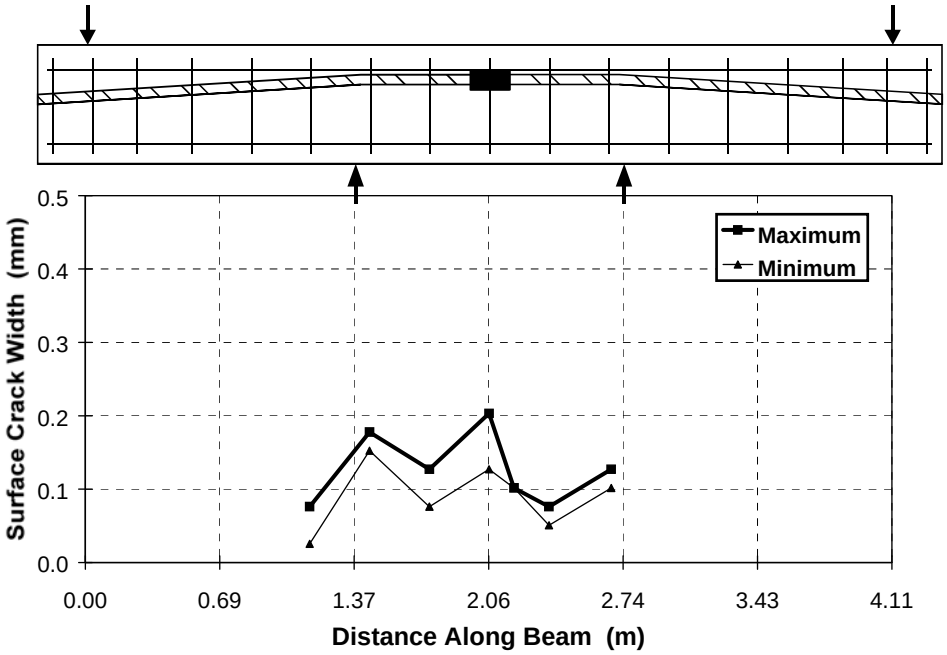

Figure C.27 - Measured Crack Widths: Beam 2.2 at Service

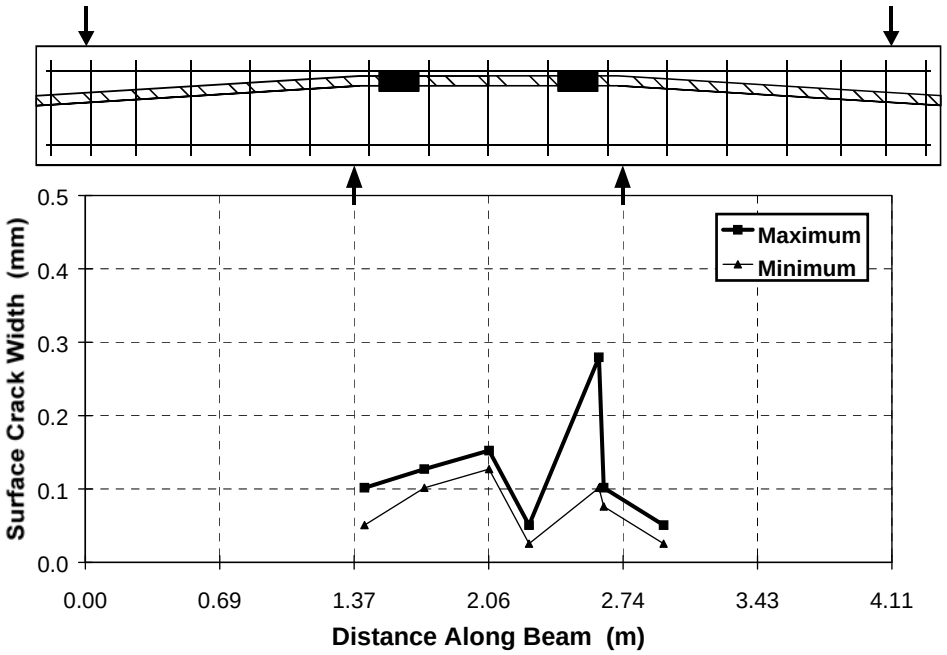

Figure C.28 - Measured Crack Widths: Beam 2.3 at Service

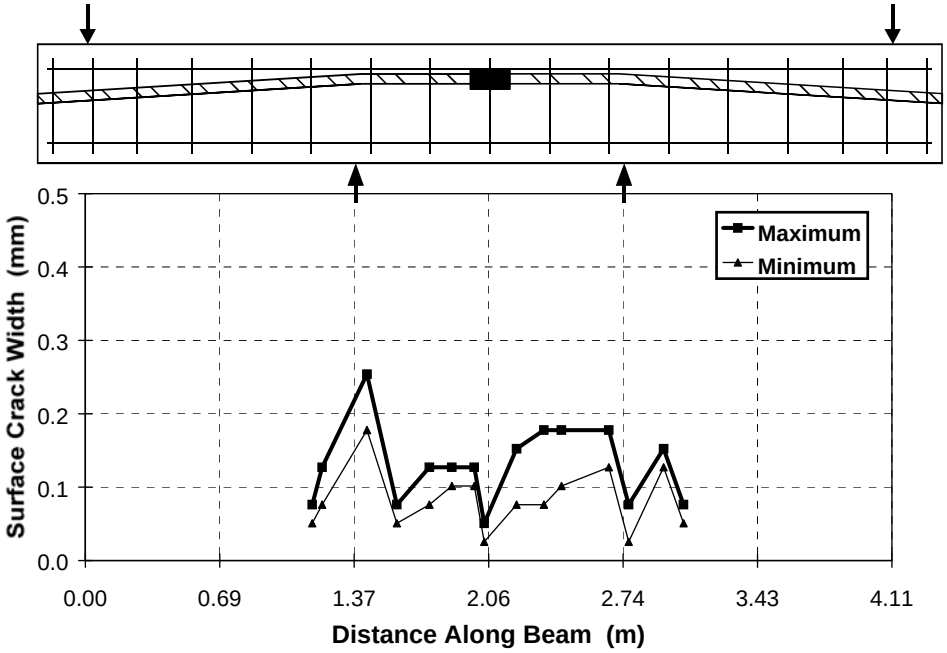

Figure C.29 - Measured Crack Widths: Beam 2.4 at Service After 25% Overload

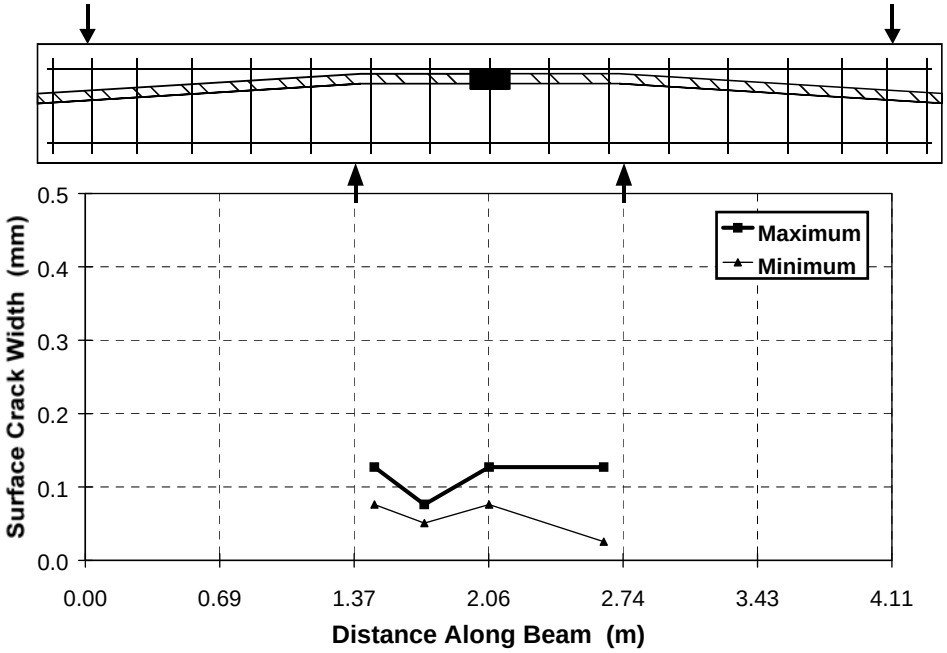

Figure C.30 - Measured Crack Widths: Beam 2.11 at Service

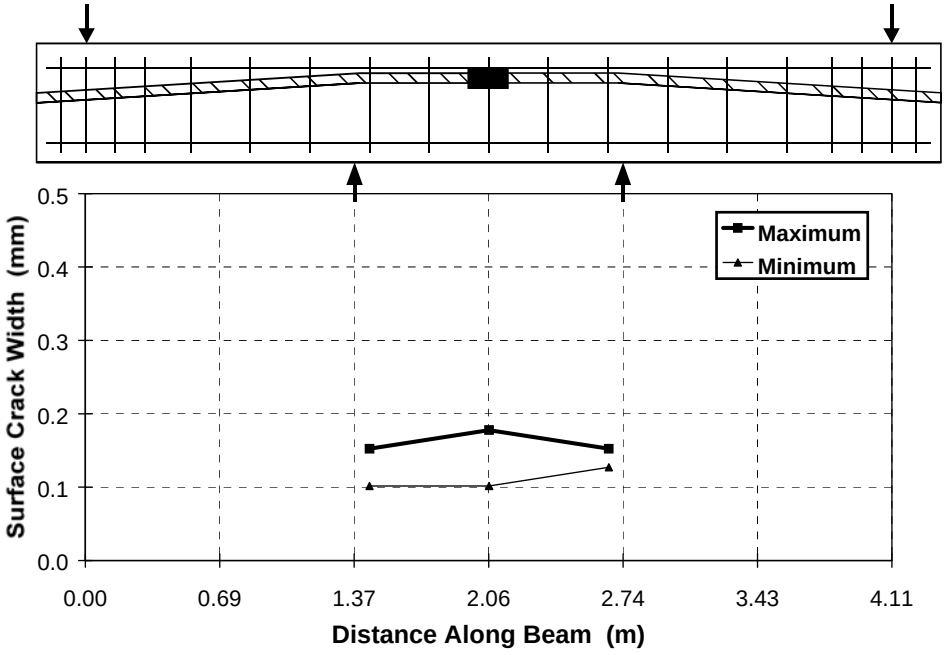

Figure C.31 - Measured Crack Widths: Beam 3.3 at Service After 25% Overload

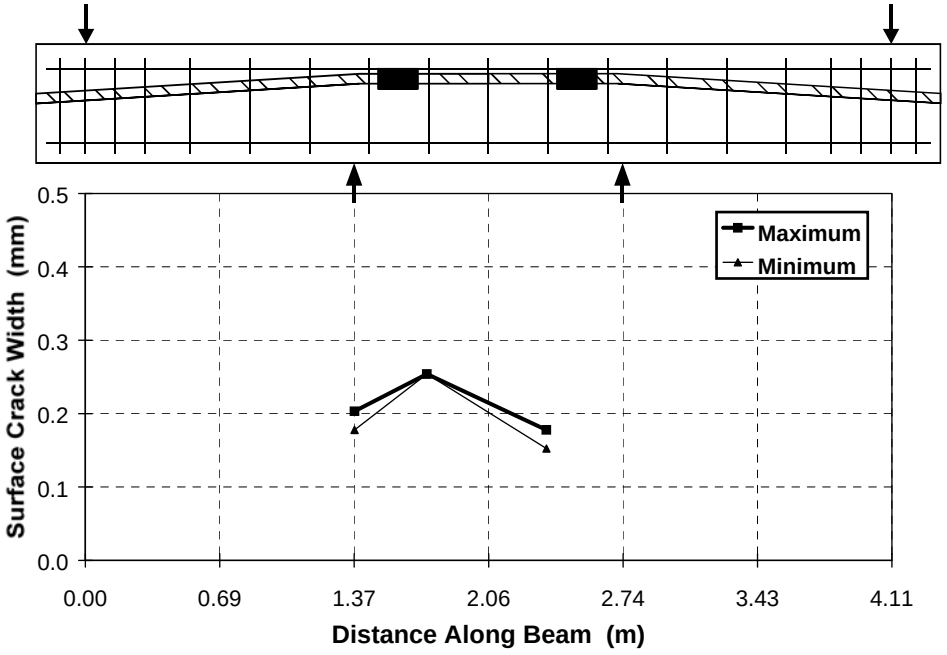

Figure C.32 - Measured Crack Widths: Beam 3.4 at Service After 33% Overload

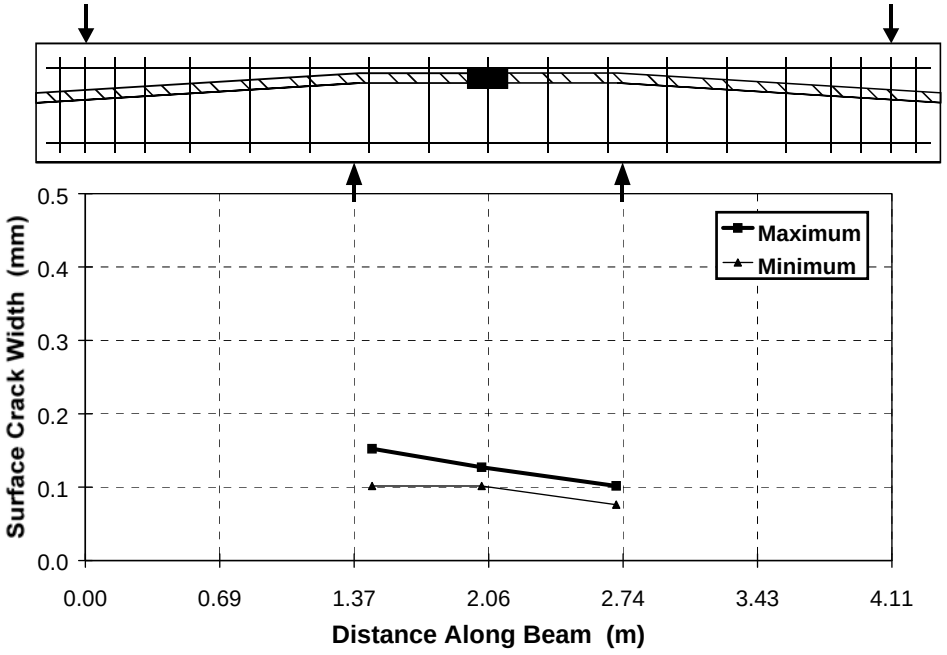

Figure C.33 - Measured Crack Widths: Beam 3.5 at Service After 25% Overload

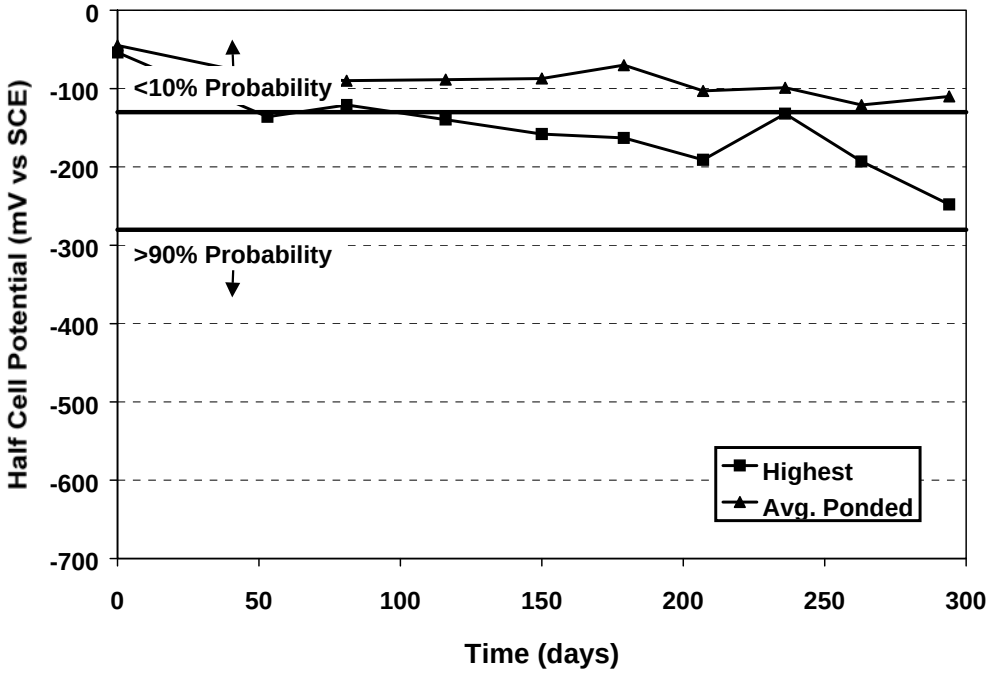

Figure C.34 - Half-Cell Readings: Beam 1.1

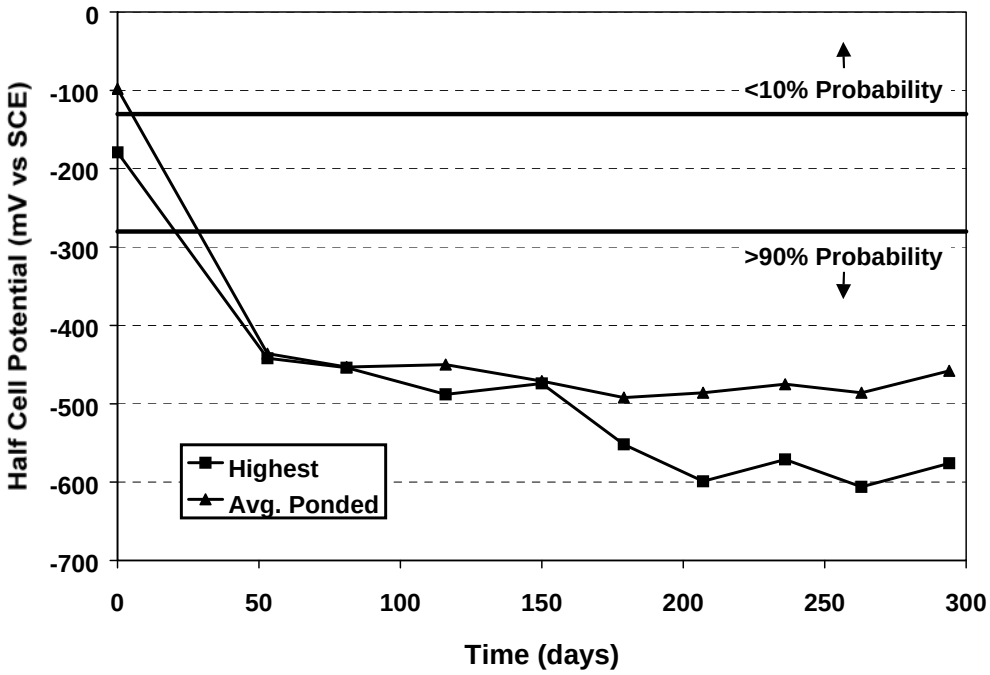

Figure C.35 - Half-Cell Readings: Beam 1.2

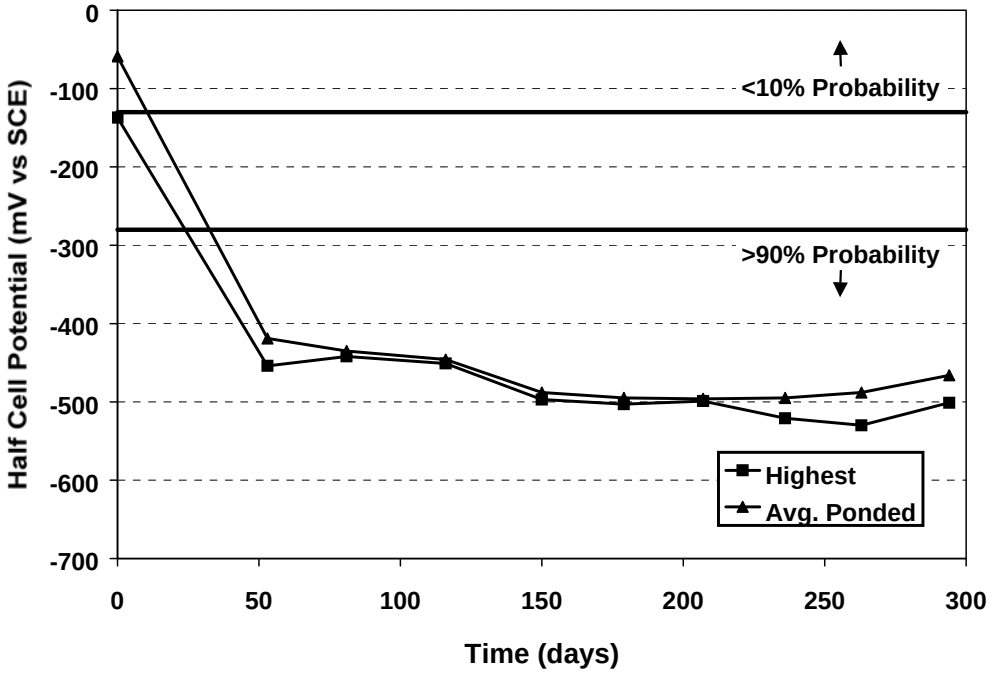

Figure C.36 - Half-Cell Readings: Beam 1.3

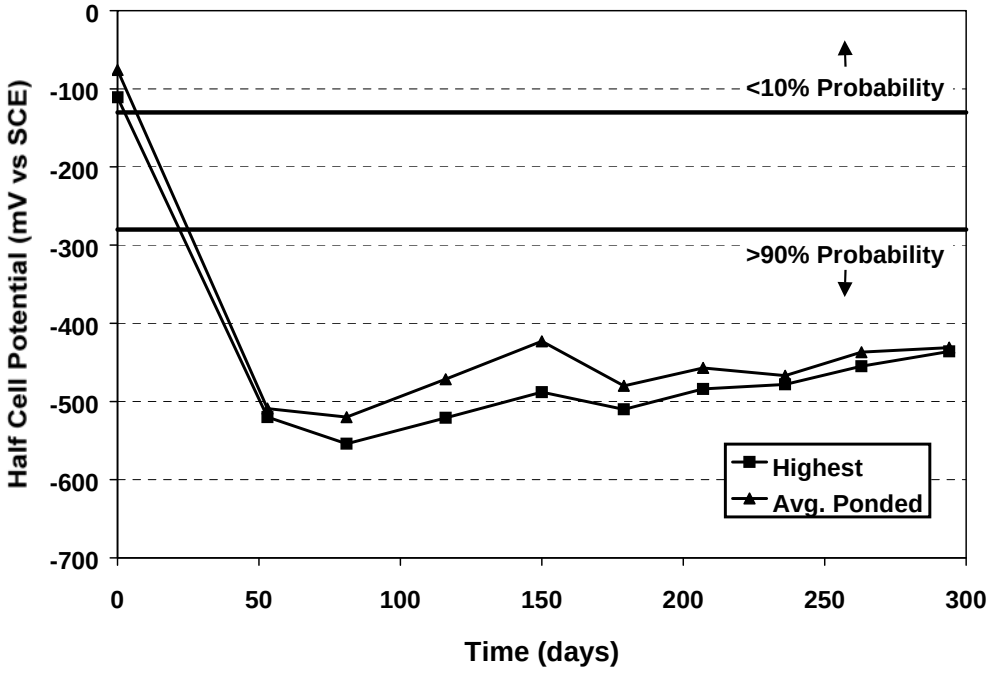

Figure C.37 - Half-Cell Readings: Beam 1.4

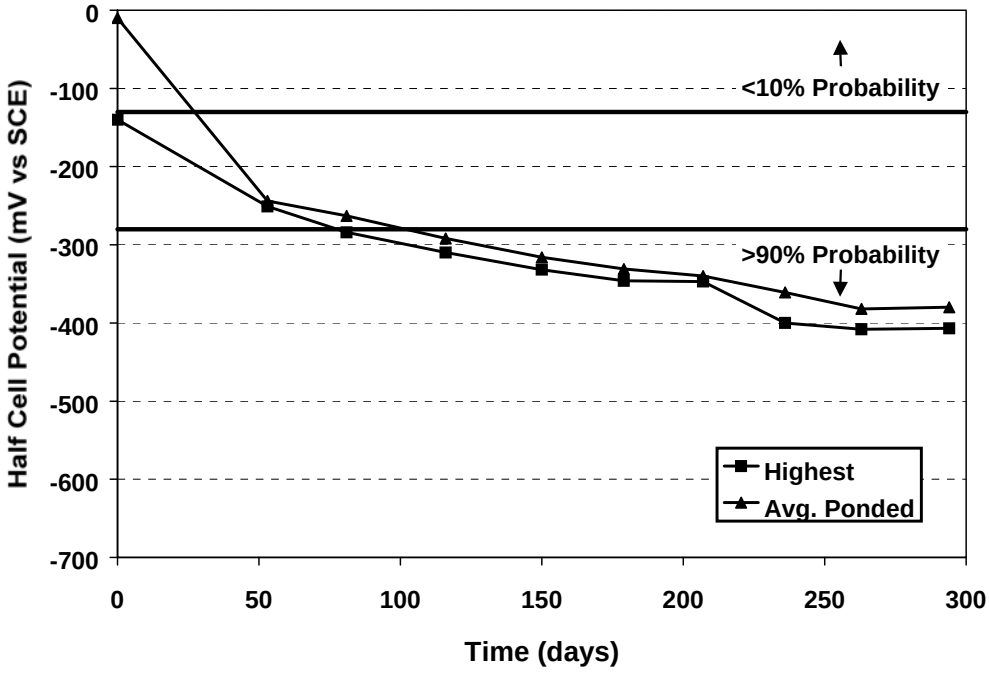

Figure C.38 - Half-Cell Readings: Beam 2.1

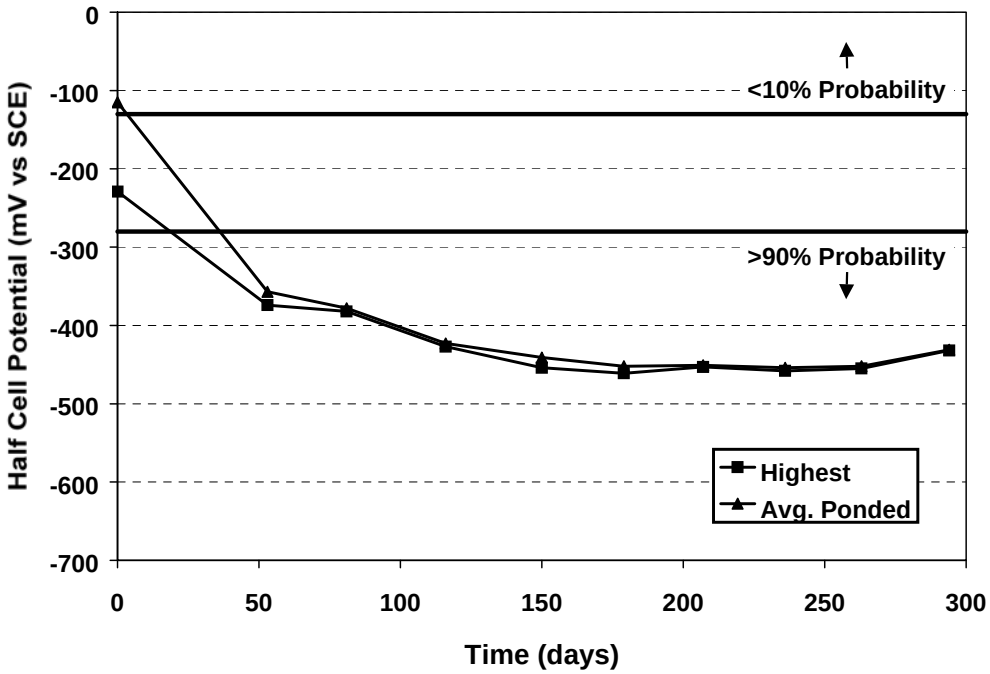

Figure C.39 - Half-Cell Readings: Beam 2.2

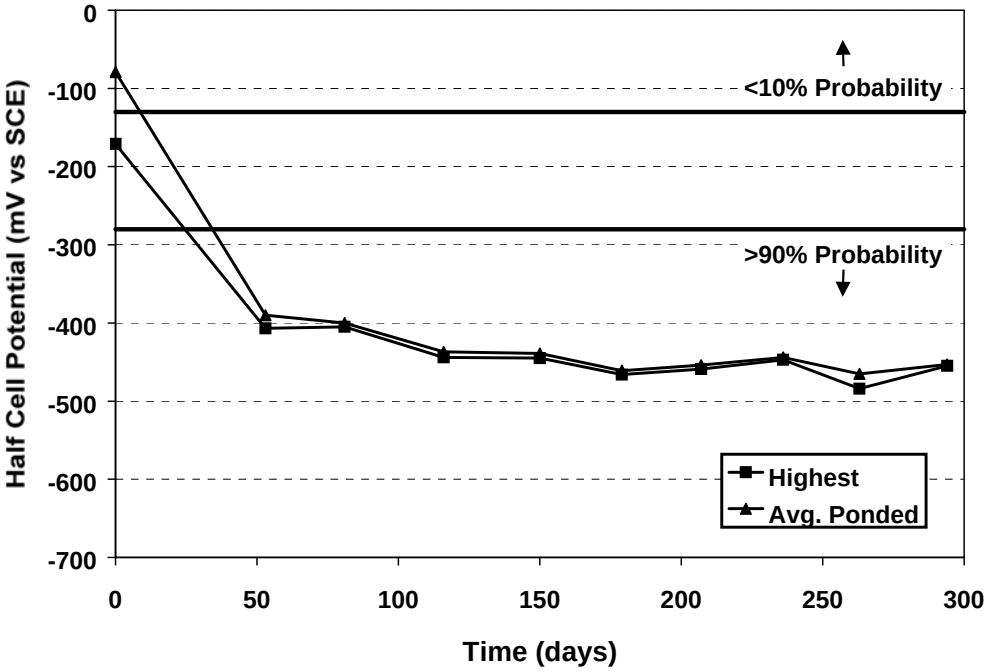

Figure C.40 - Half-Cell Readings: Beam 2.3

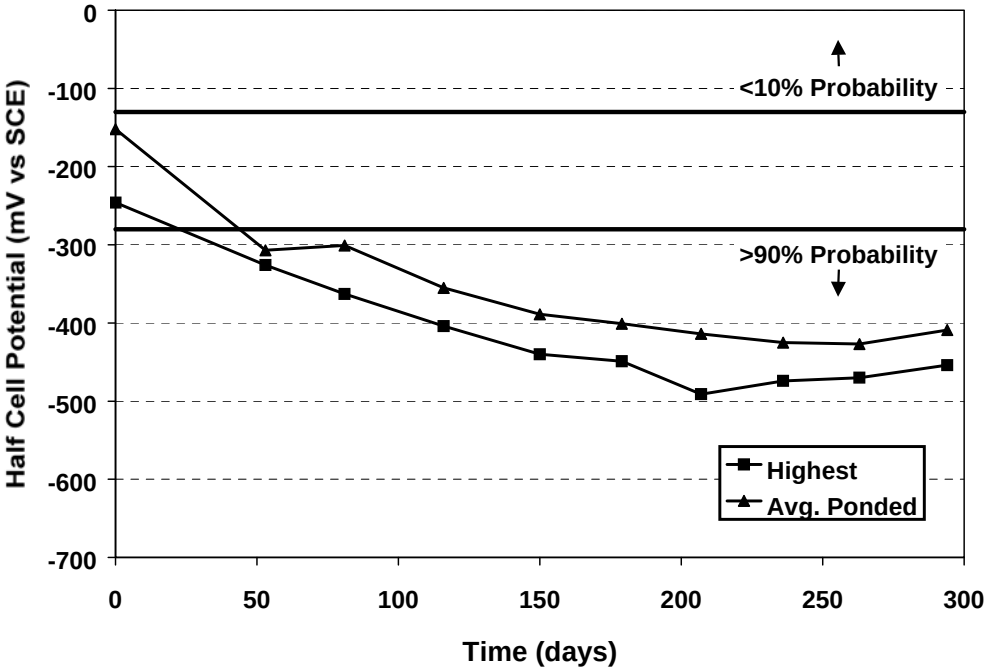

Figure C.41 - Half-Cell Readings: Beam 2.4

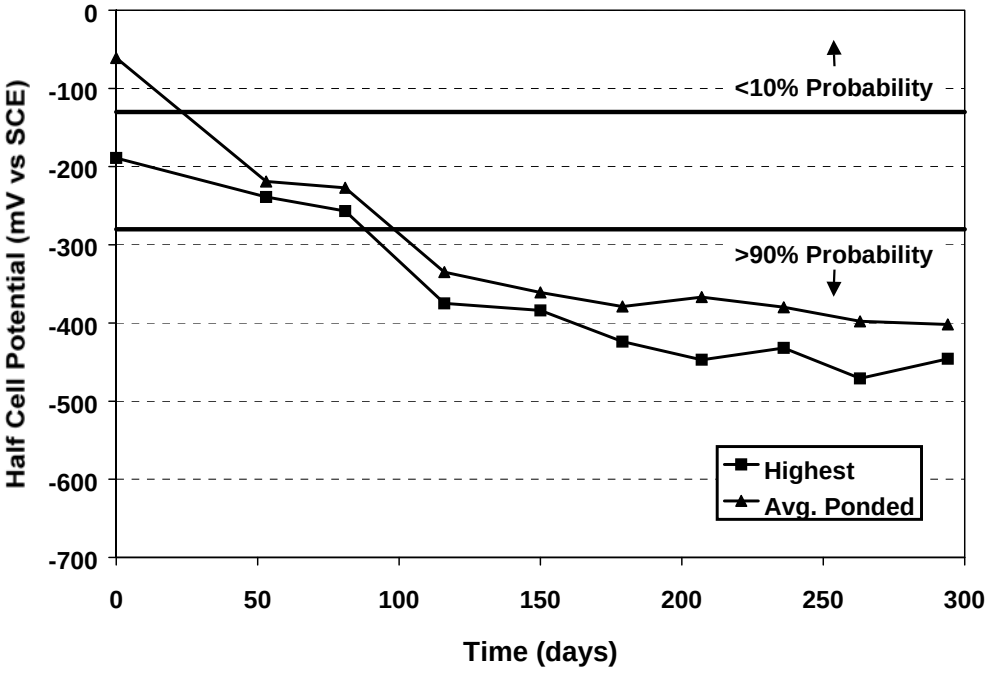

Figure C.42 - Half-Cell Readings: Beam 2.11

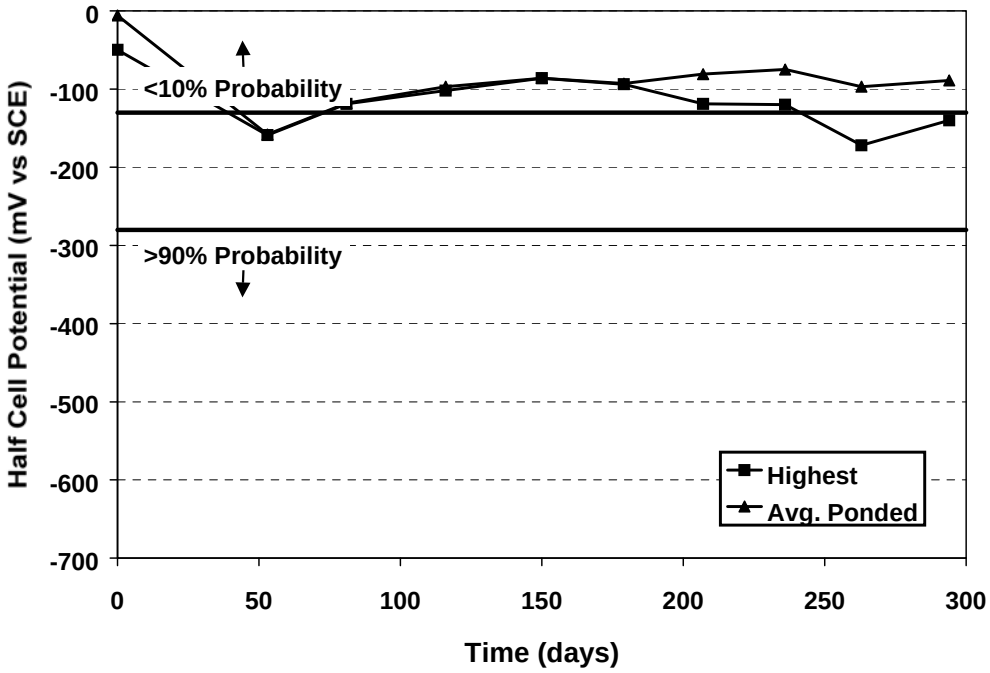

Figure C.43 - Half-Cell Readings: Beam 3.1

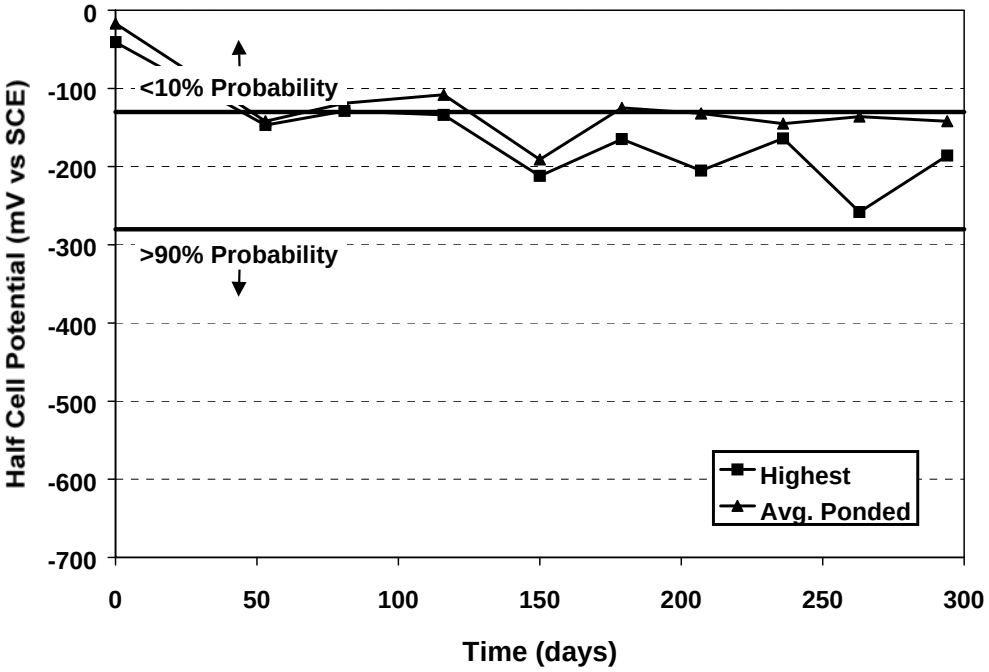

Figure C.44 - Half-Cell Readings: Beam 3.2

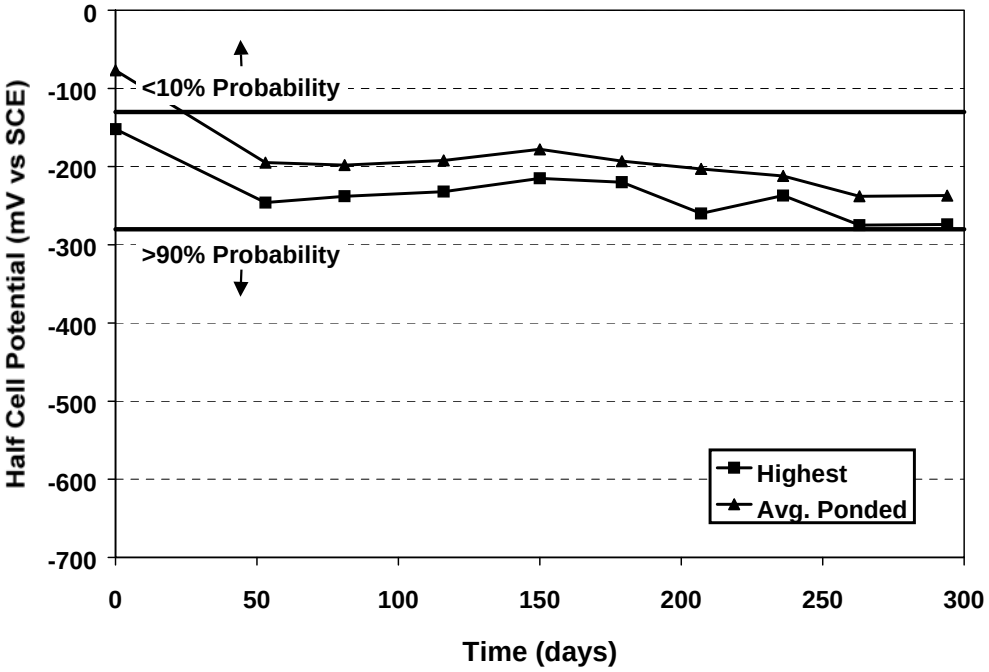

Figure C.45 - Half-Cell Readings: Beam 3.3

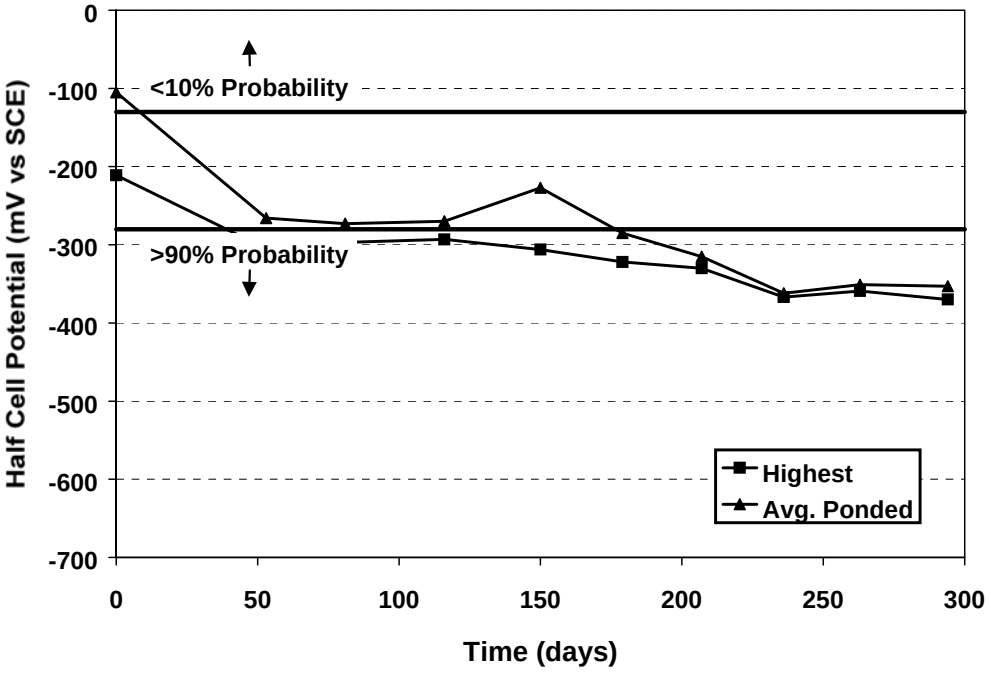

Figure C.46 - Half-Cell Readings: Beam 3.4

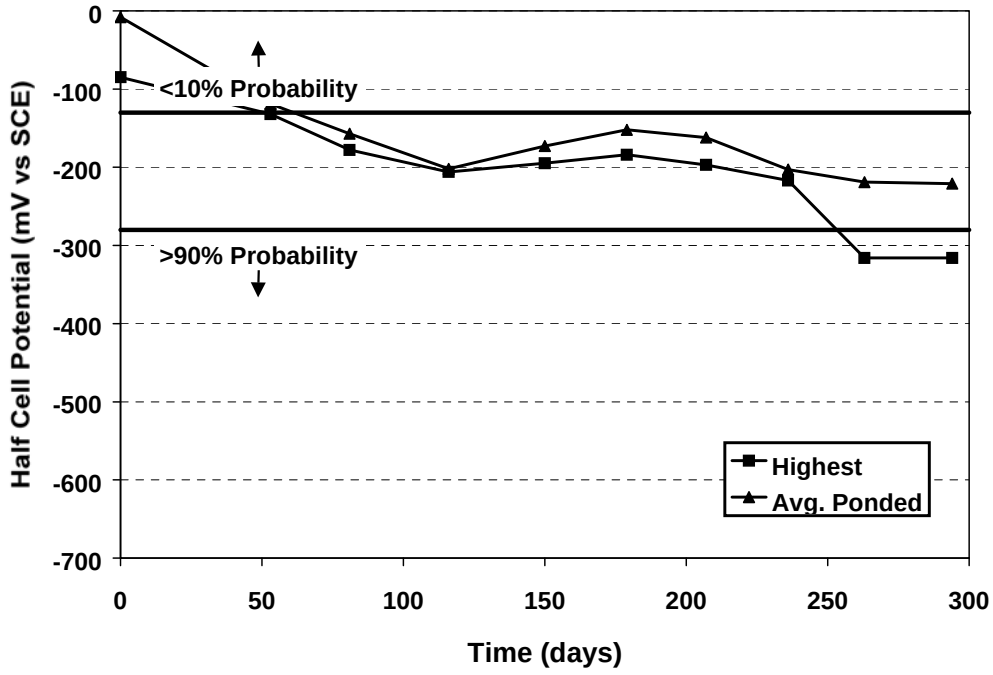

Figure C.47 - Half-Cell Readings: Beam 3.5

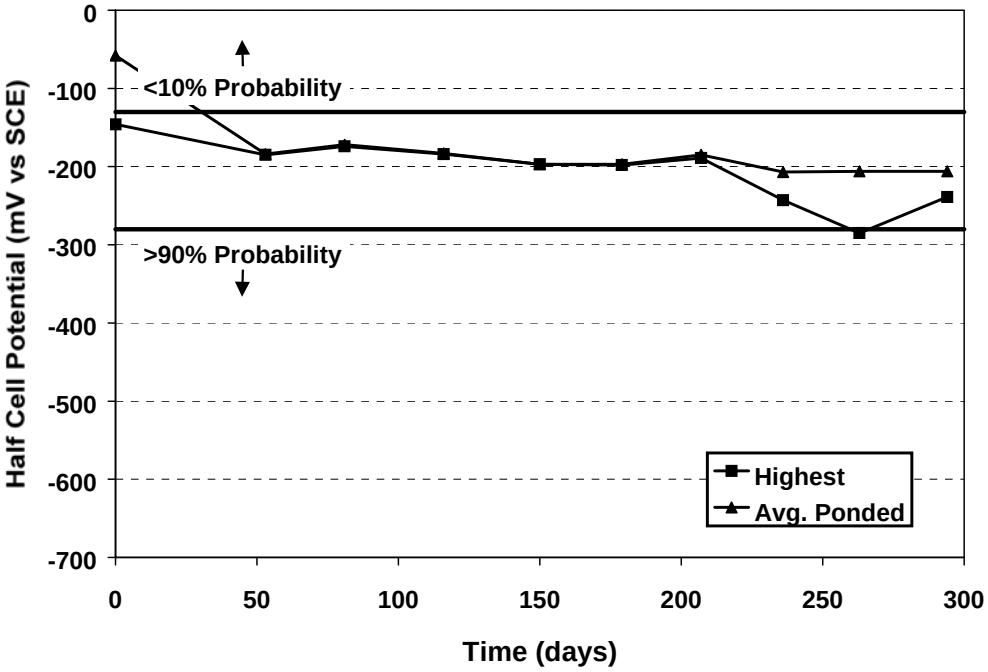

Figure C.48 - Half-Cell Readings: Beam 4.1

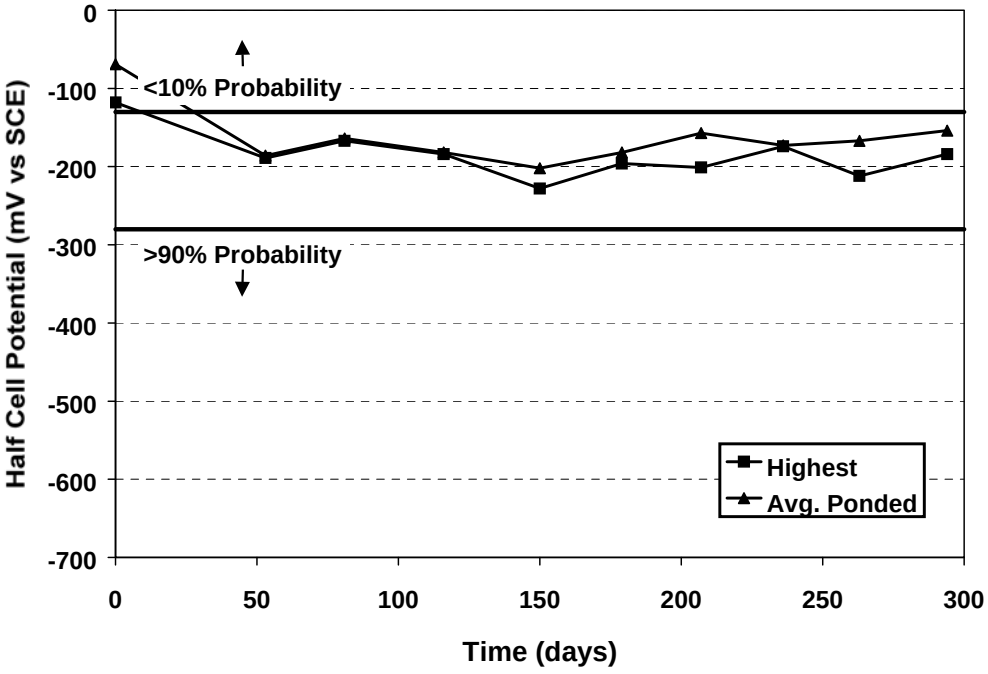

Figure C.49 - Half-Cell Readings: Beam 4.2

Appendix D:

Long Term Column Corrosion Tests:

Supplementary Material

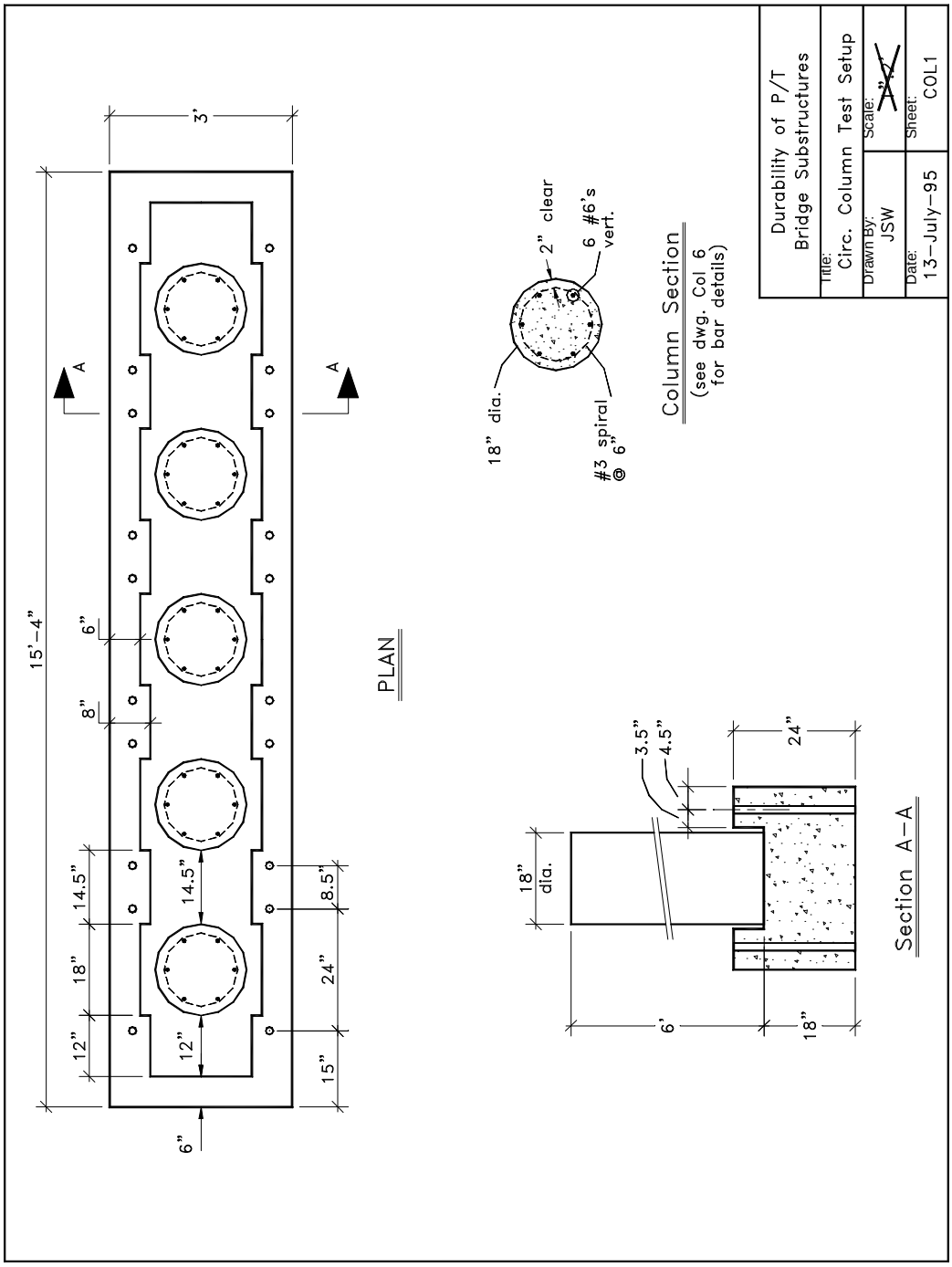

Figure D.1 – Sheet COL1: Column Foundation

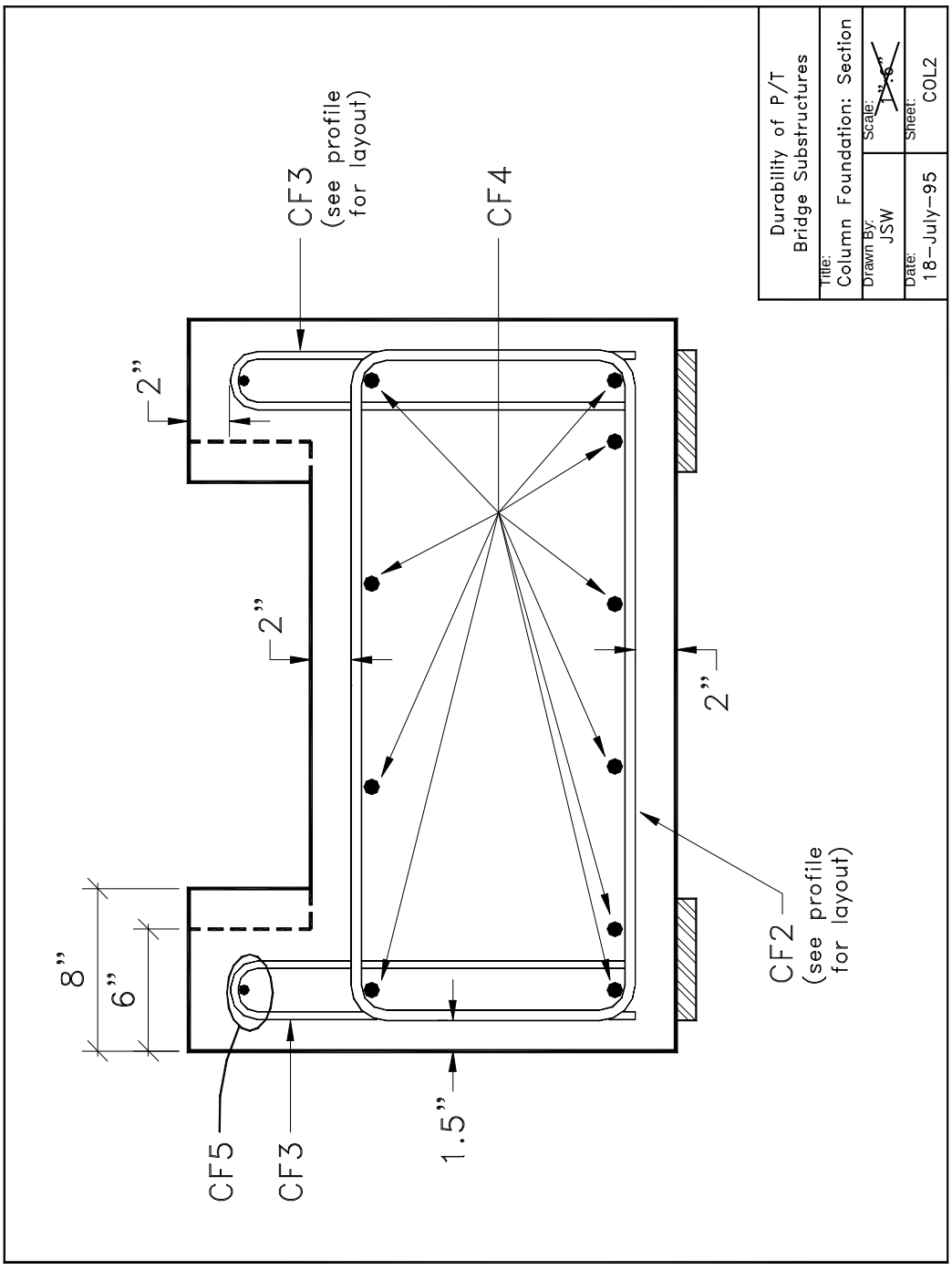

Figure D.2 - Sheet COL2: Column Foundation Section

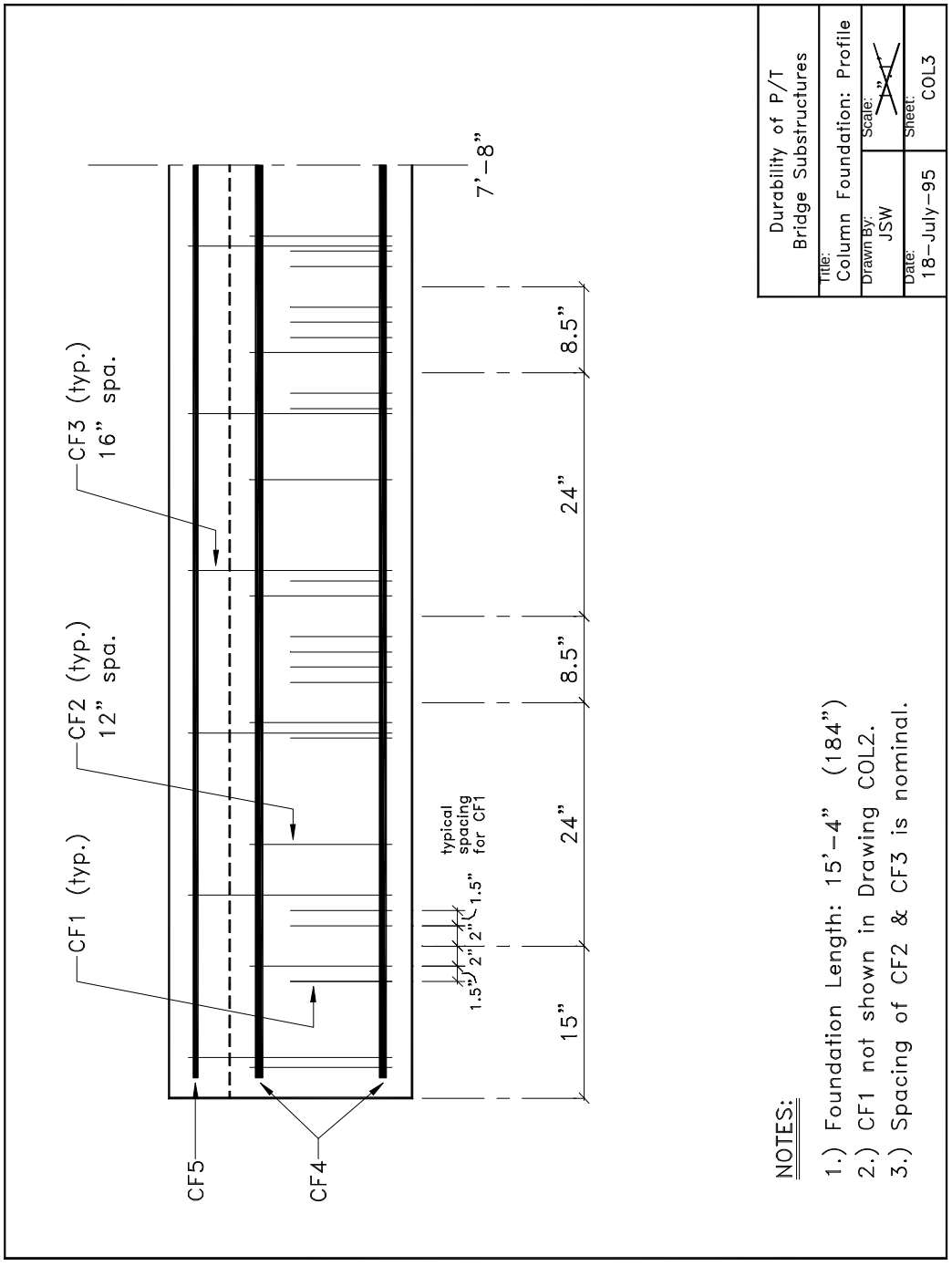

Figure D.3 - Sheet COL3: Column Foundation Profile

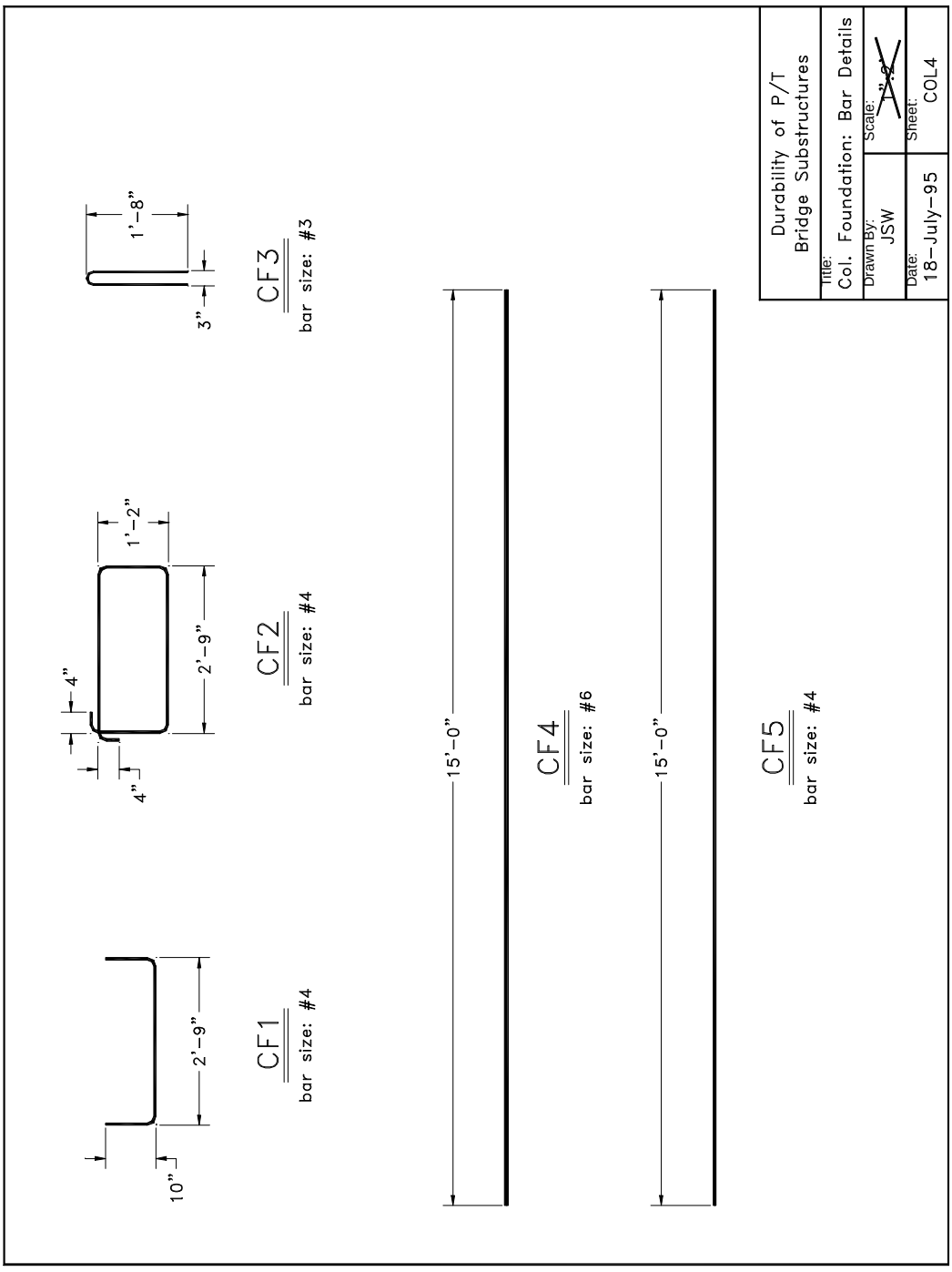

Figure D.4 - Sheet COL4: Column Foundation Bar Details

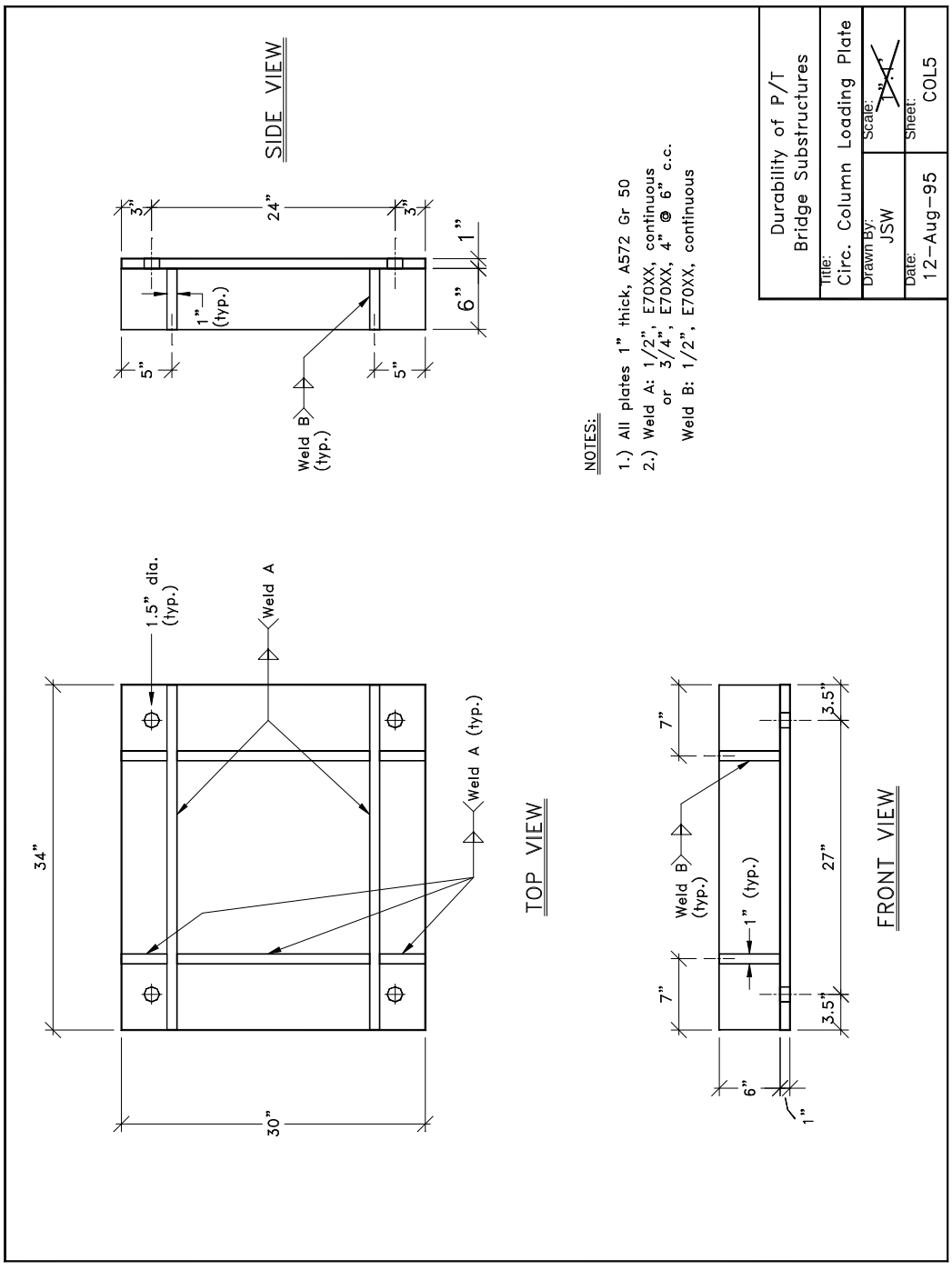

Figure D.5 - Sheet COL5: Column Loading Plate

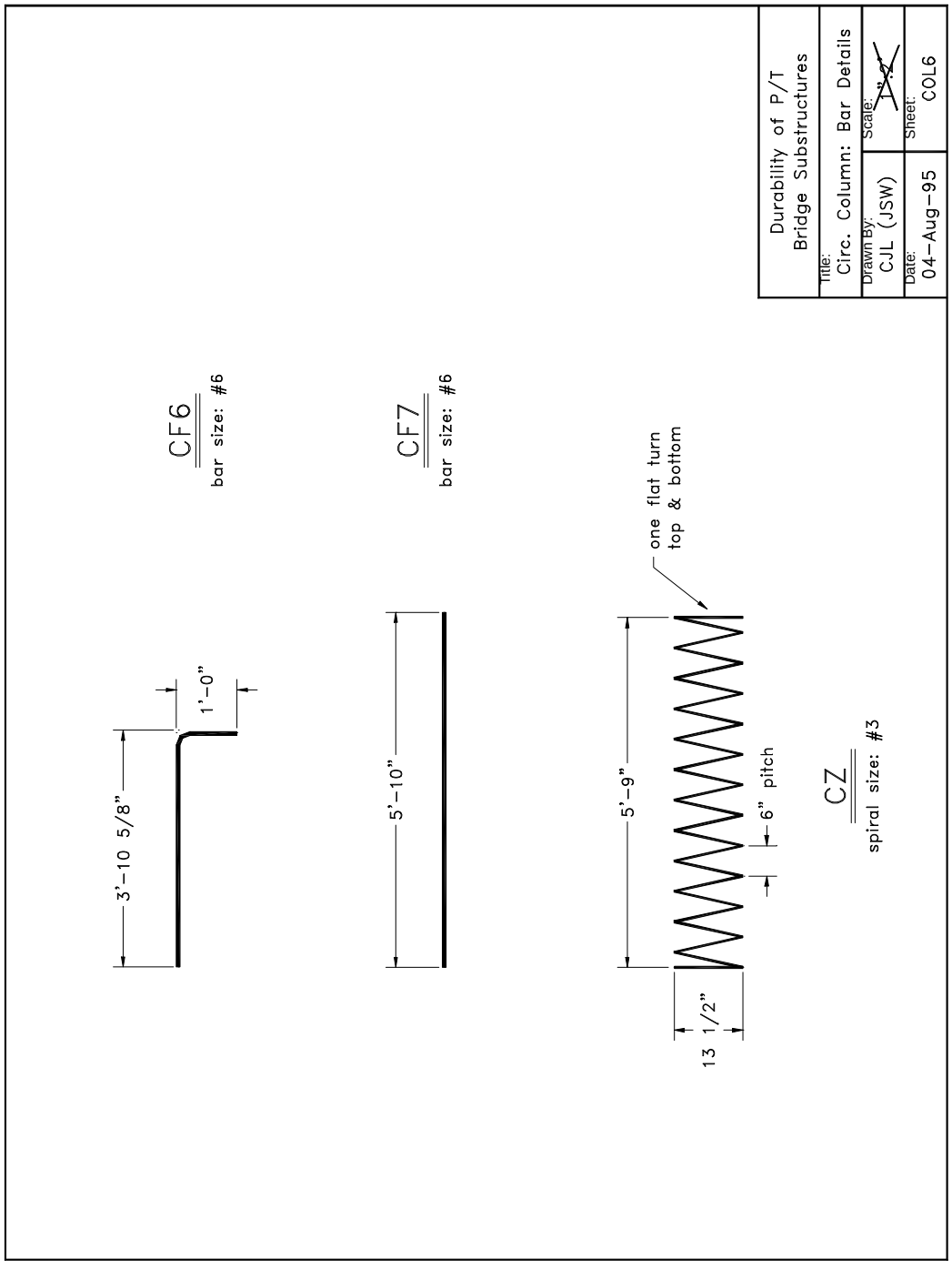

Figure D.6 - Sheet COL6: Column Reinforcing Bar Details

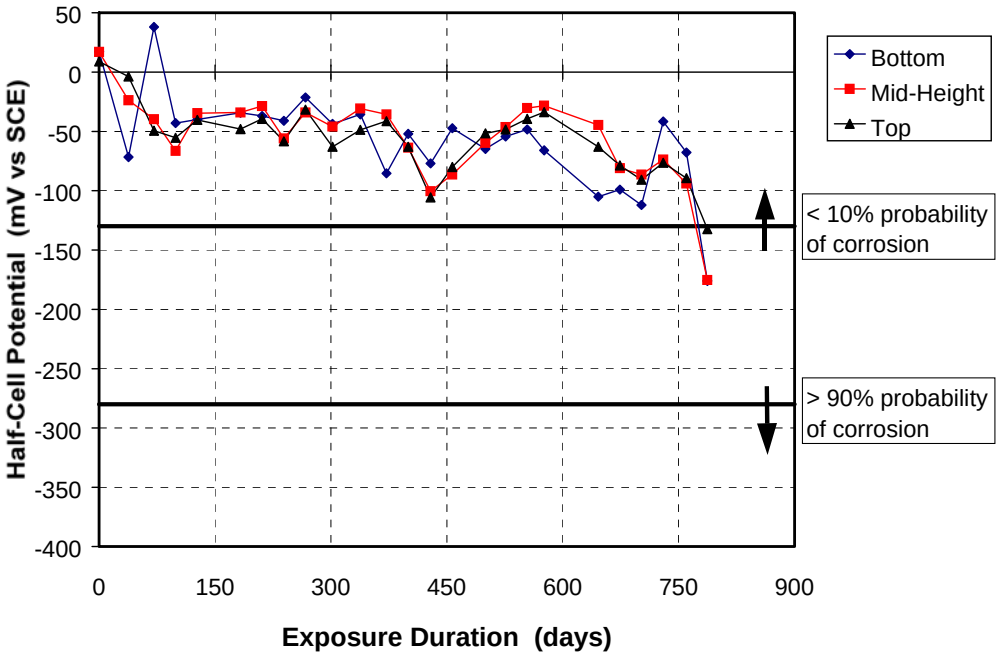

Figure D.7 – Average Half-Cell Potentials: Column NJ-TC-N

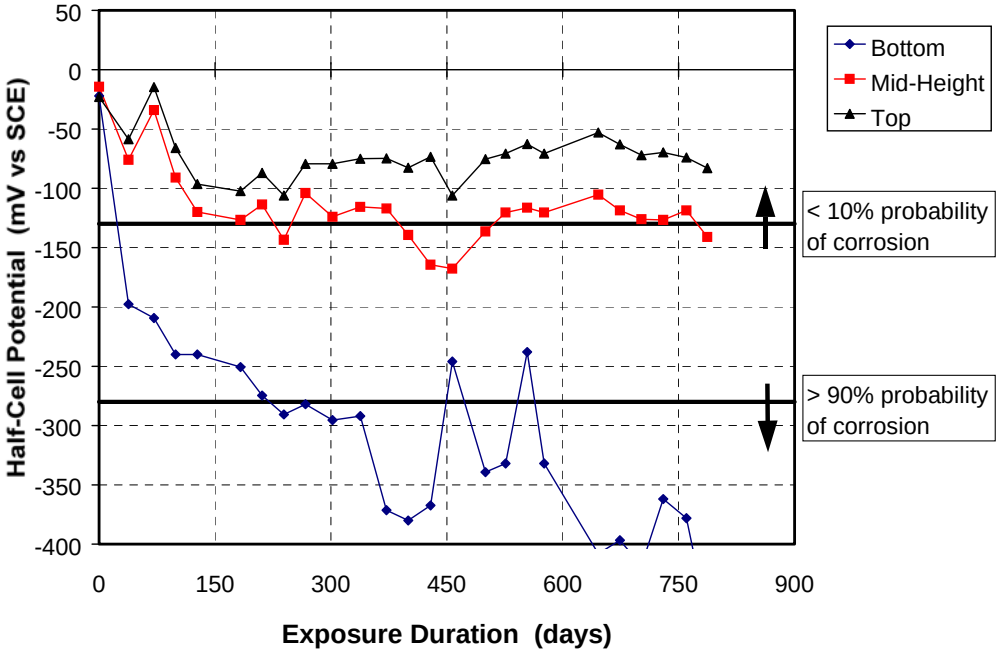

Figure D.8 - Average Half-Cell Potentials: Column NJ-TC-S

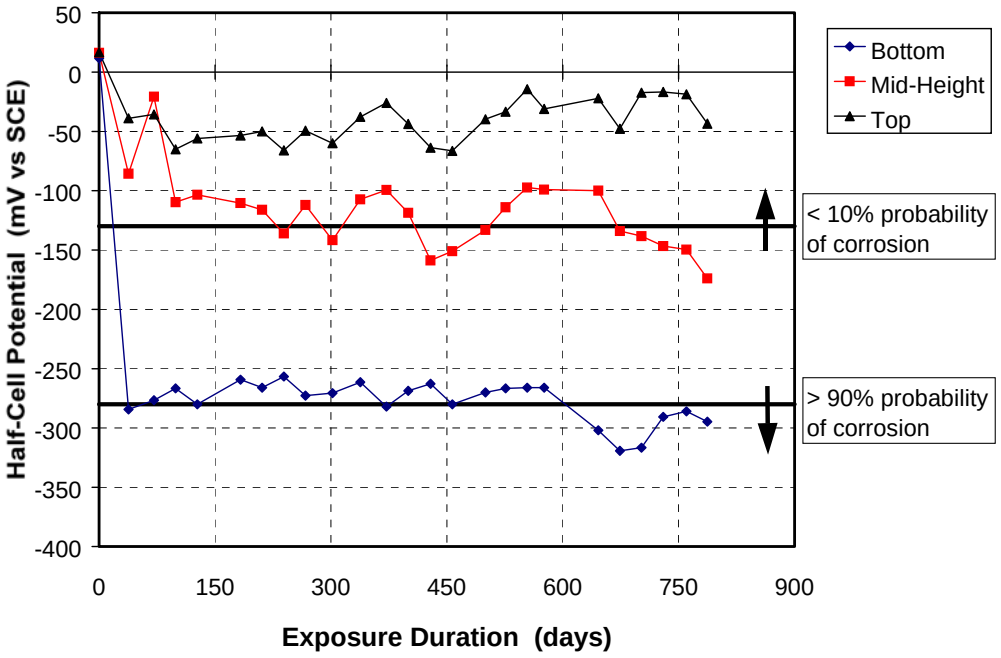

Figure D.9 - Average Half-Cell Potentials: Column DJ-TC-N

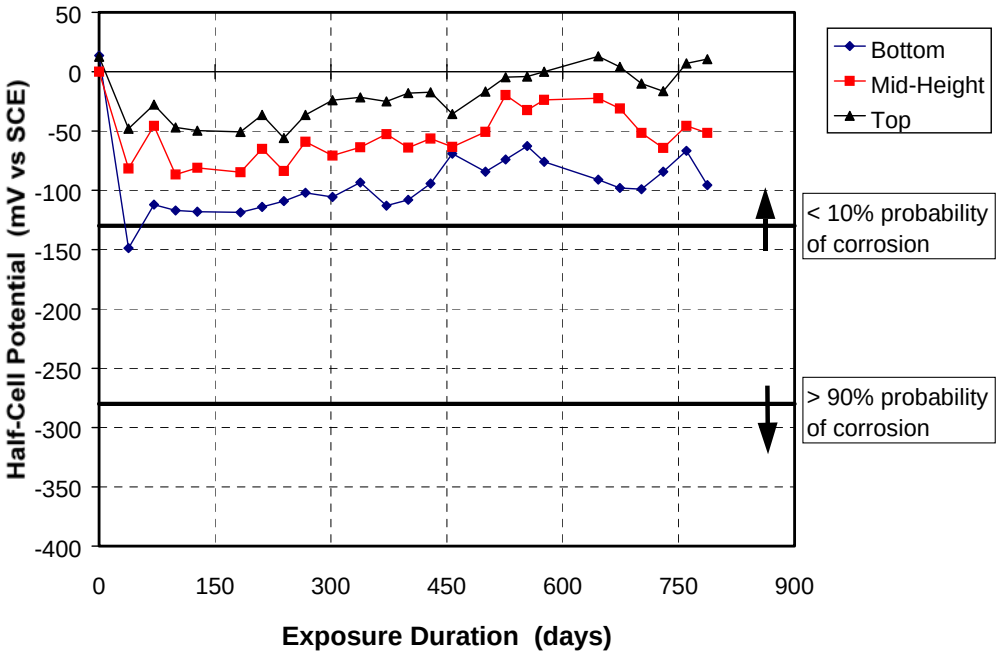

Figure D.10 - Average Half-Cell Potentials: Column DJ-TC-S

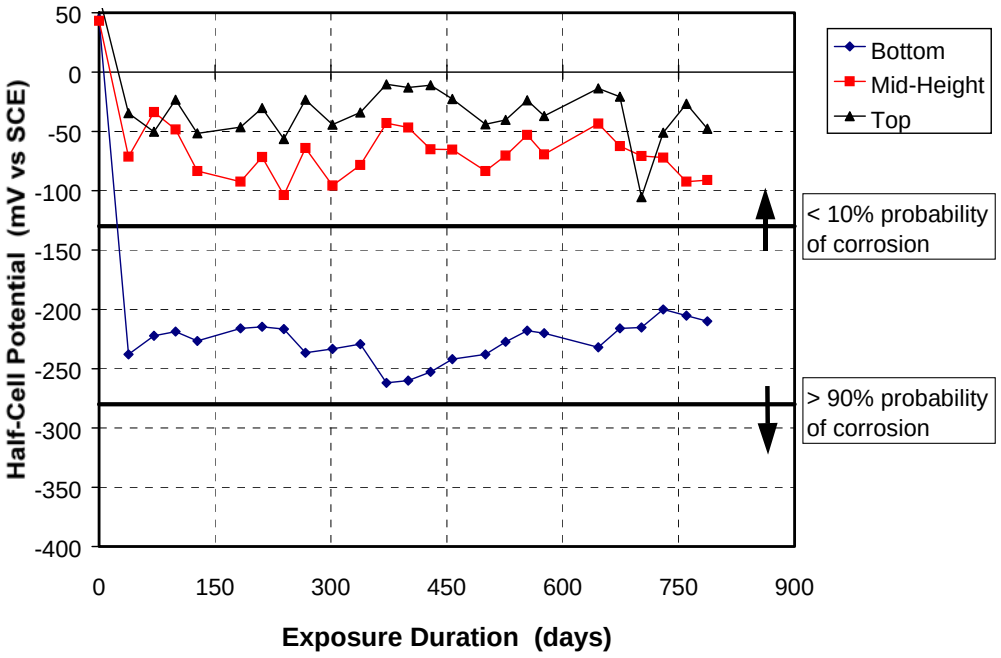

Figure D.11 - Average Half-Cell Potentials: Column DJ-FA-S

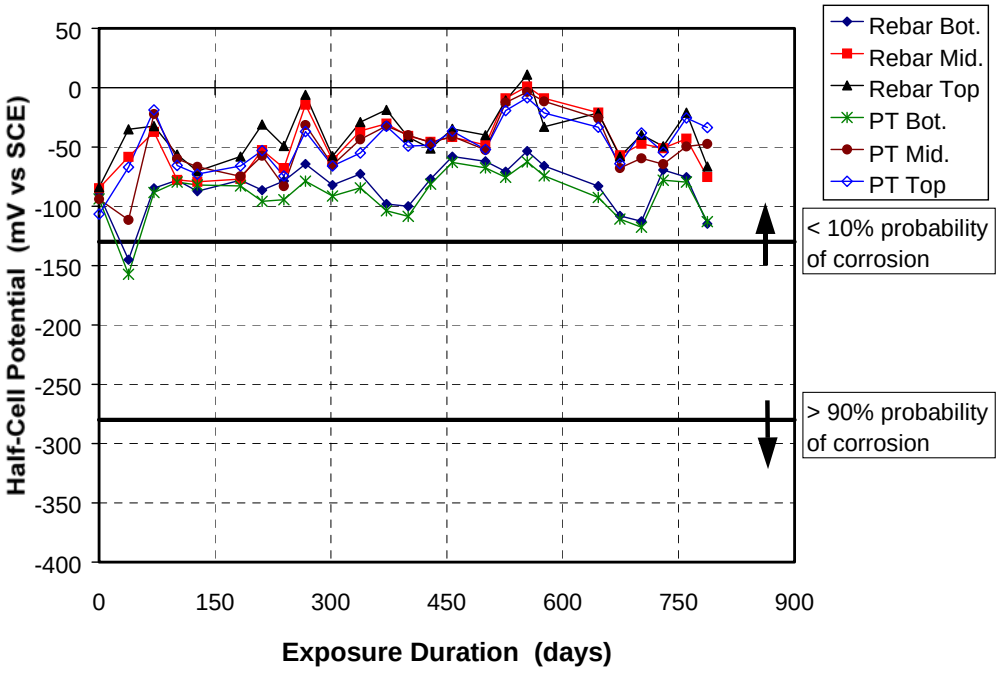

Figure D.12 - Average Half-Cell Potentials: Column PT-TC-N-PD

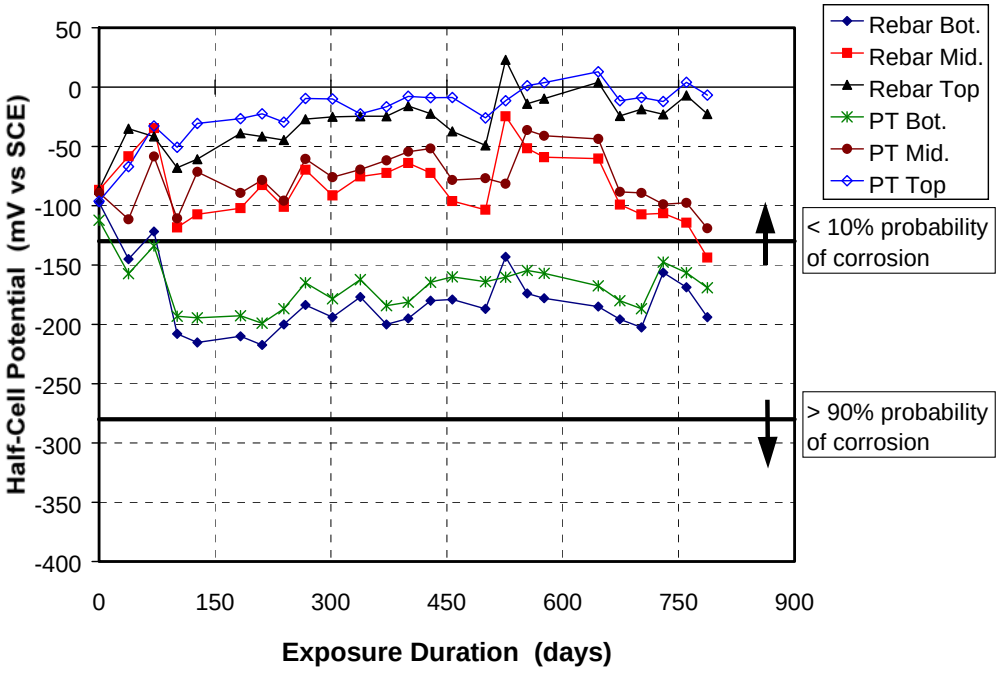

Figure D.13 - Average Half-Cell Potentials: Column PT-TC-S-PD

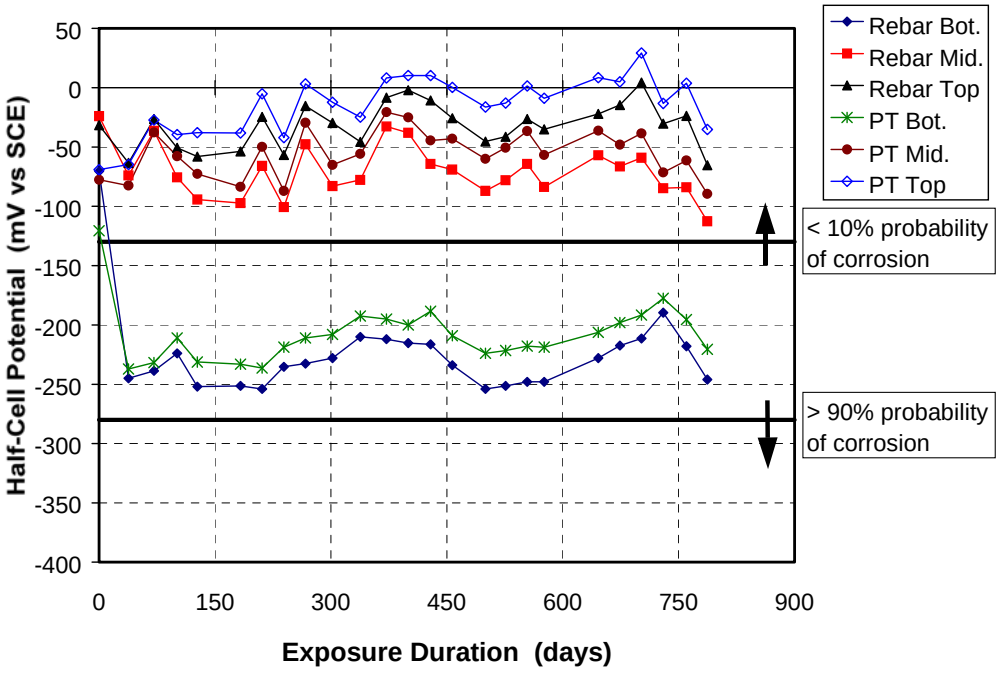

Figure D.14 - Average Half-Cell Potentials: Column PT-FA-S-PD

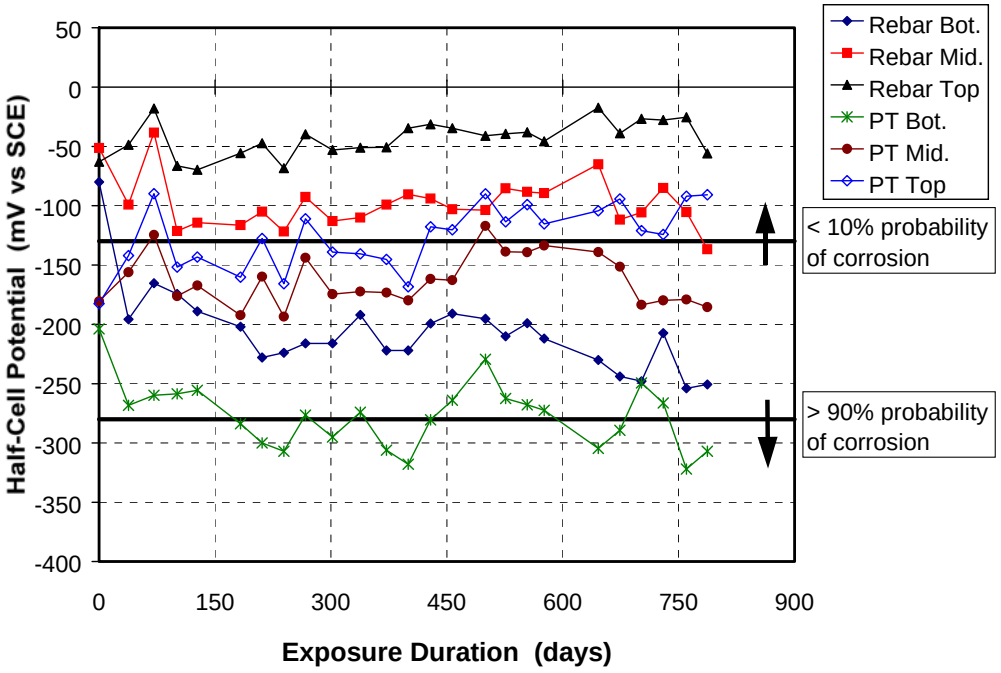

Figure D.15 - Average Half-Cell Potentials: Column PT-TC-S-EB

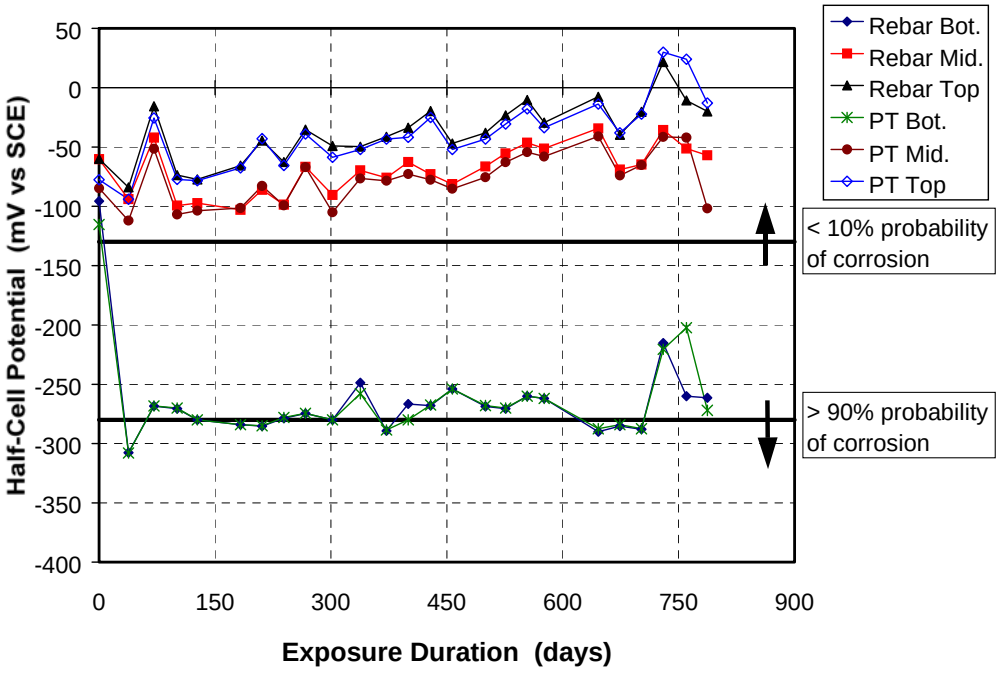

Figure D.16 - Average Half-Cell Potentials: Column PT-TC-S-GB

Appendix D

Detail Drawings - Supplement to Appendix C

**** Page Numbers Printed Separately ****

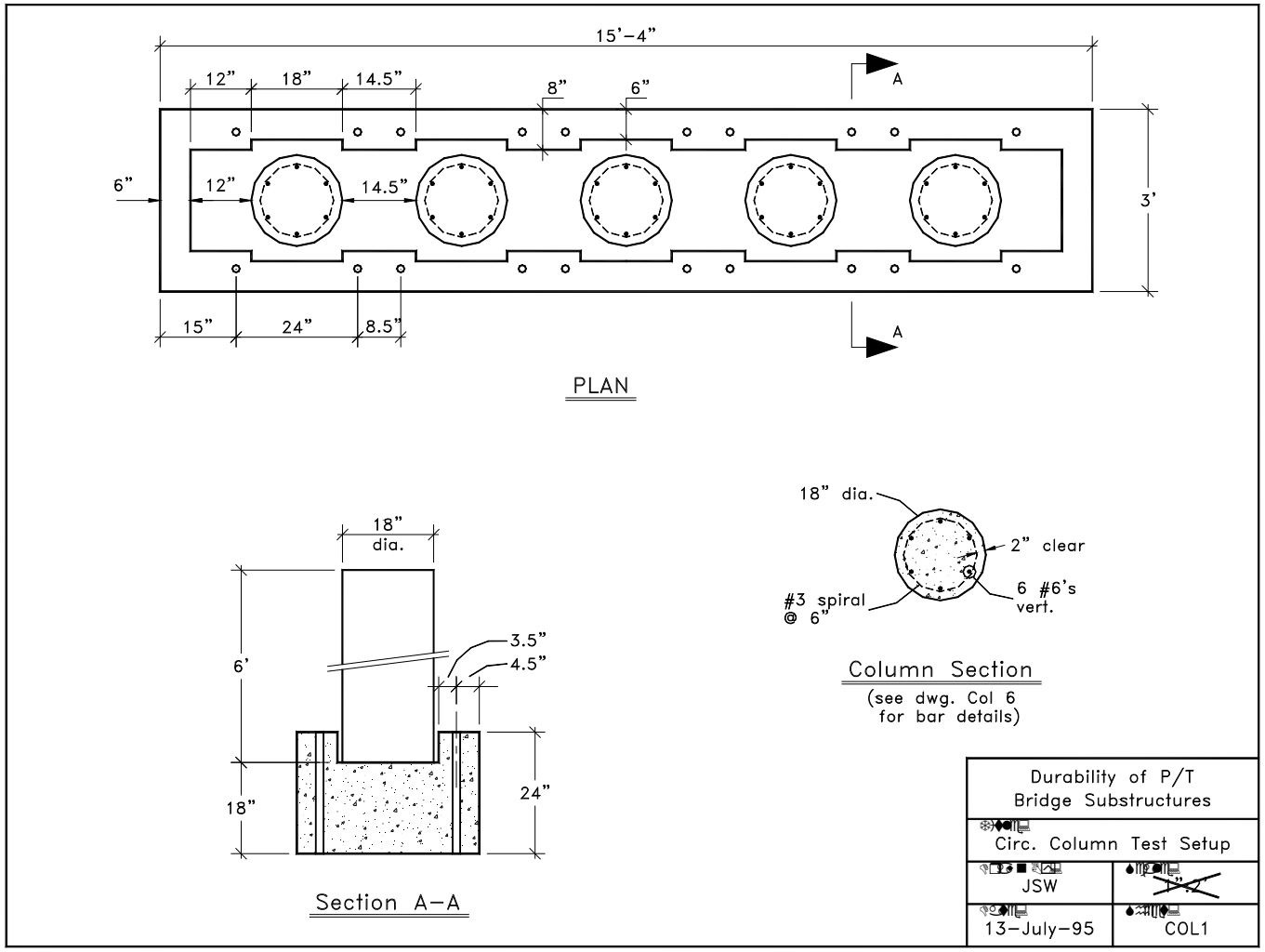

Figure D.1 – Sheet COL1: Column Foundation

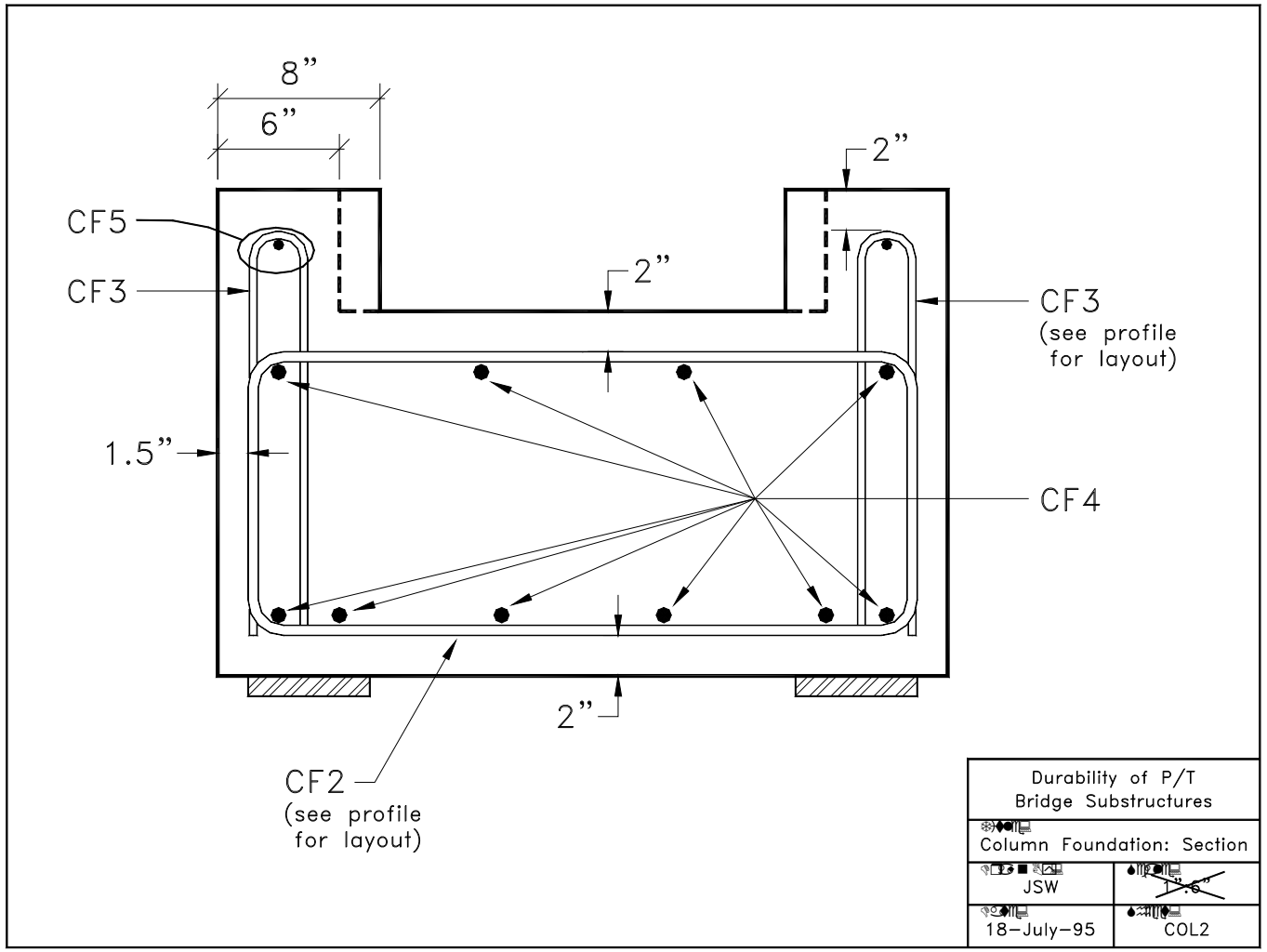

Figure D.2 - Sheet COL2: Column Foundation Section

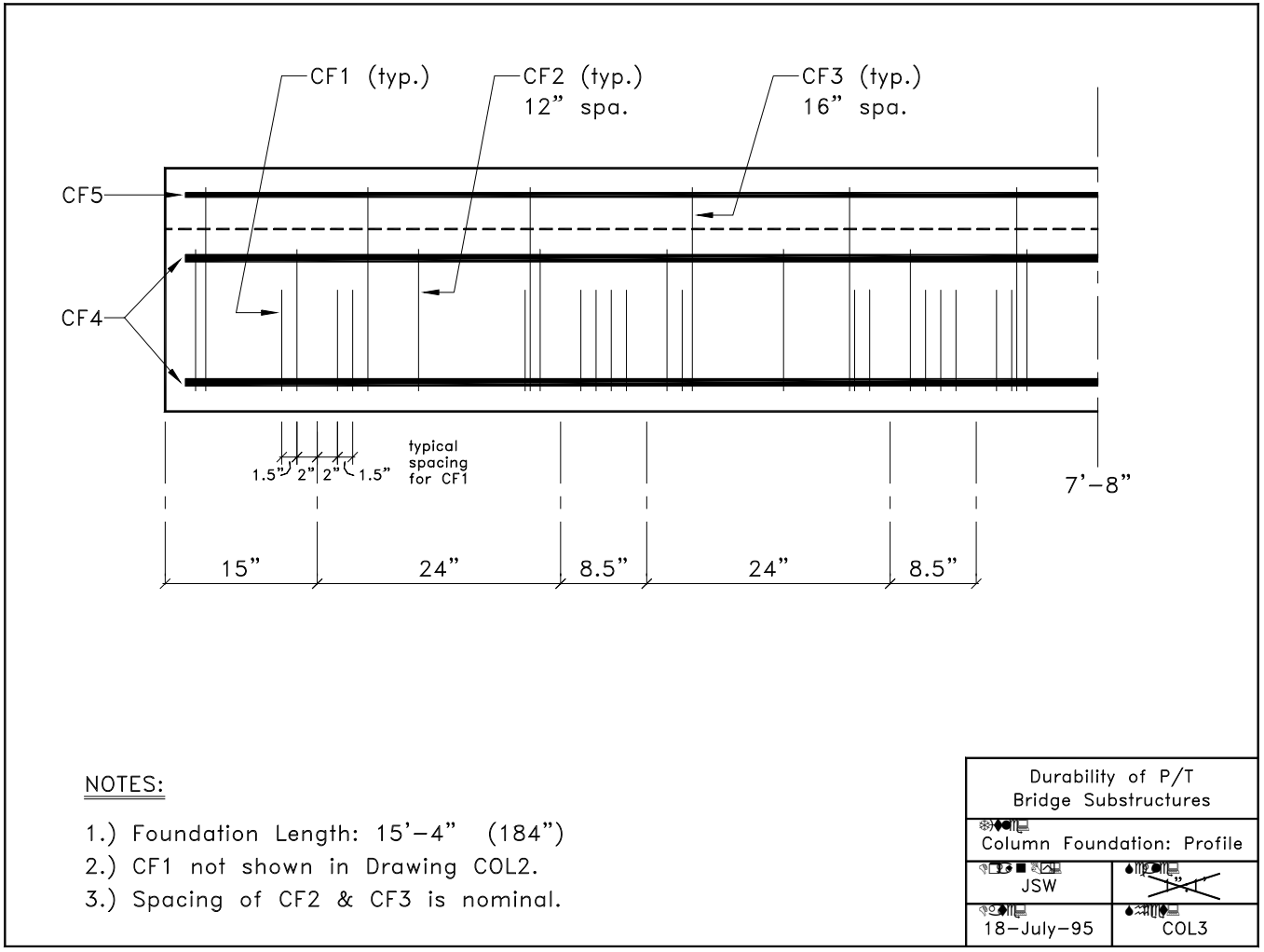

Figure D.3 - Sheet COL3: Column Foundation Profile

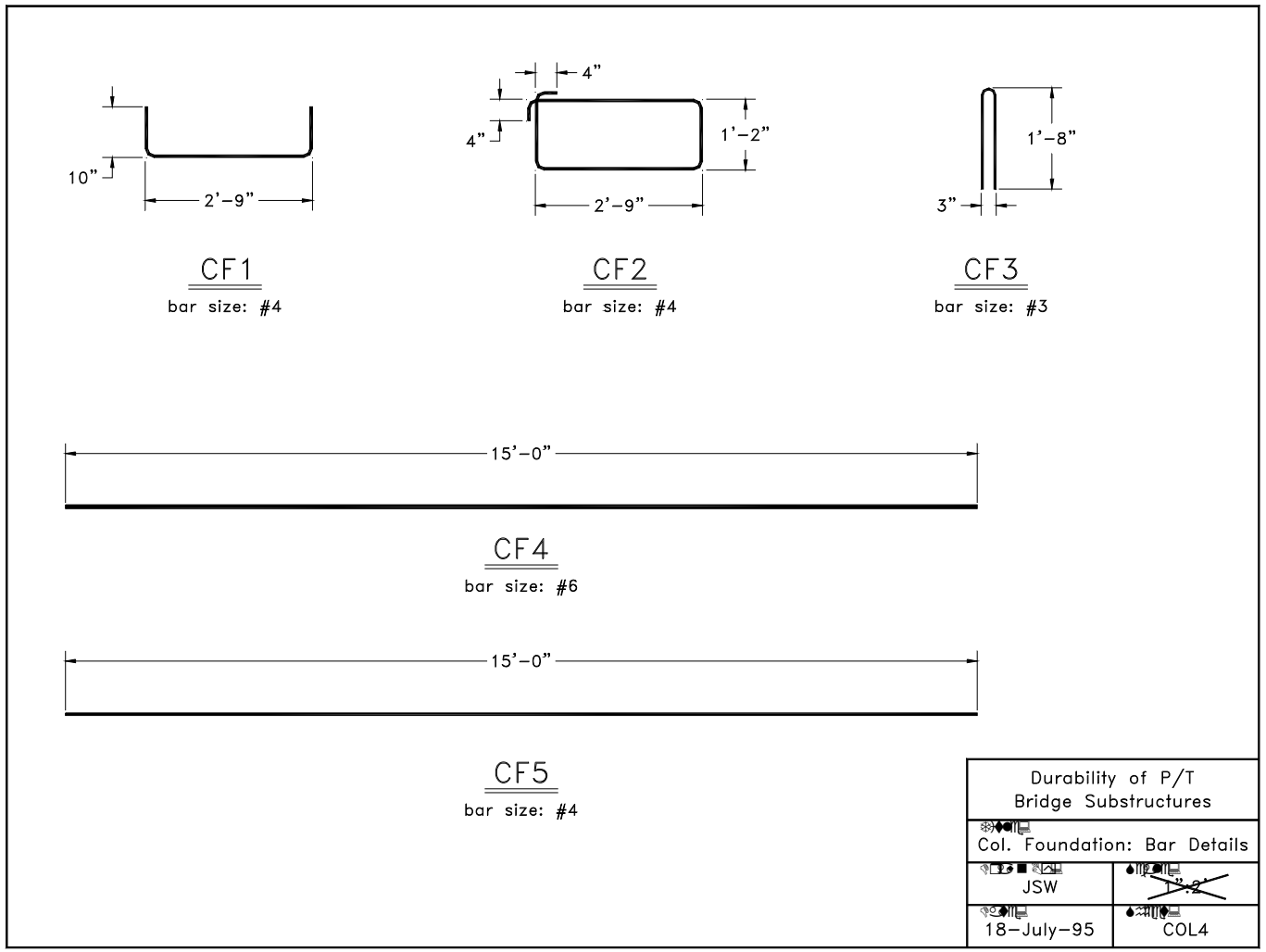

Figure D.4 - Sheet COL4: Column Foundation Bar Details

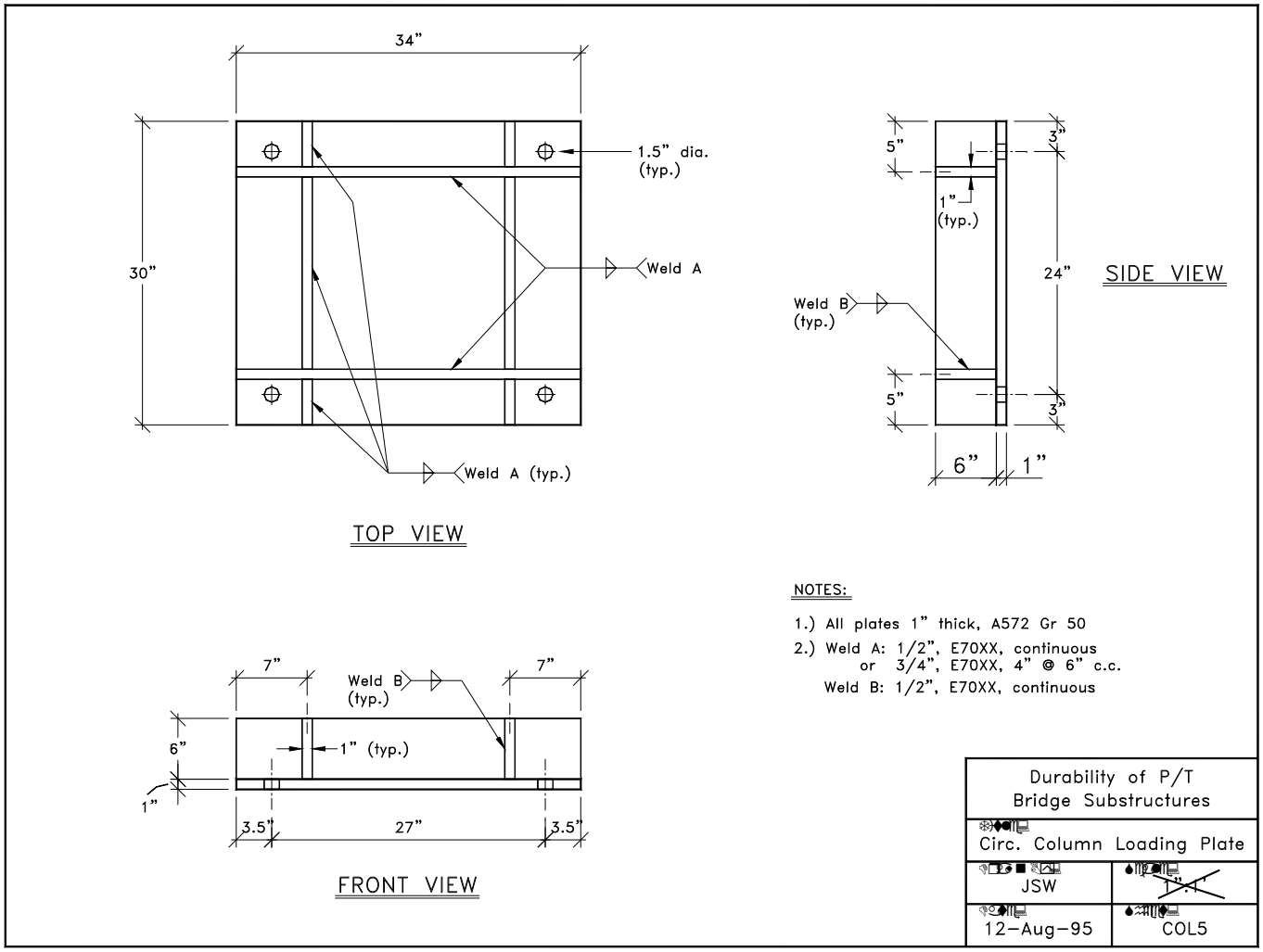

Figure D.5 - Sheet COL5: Column Loading Plate

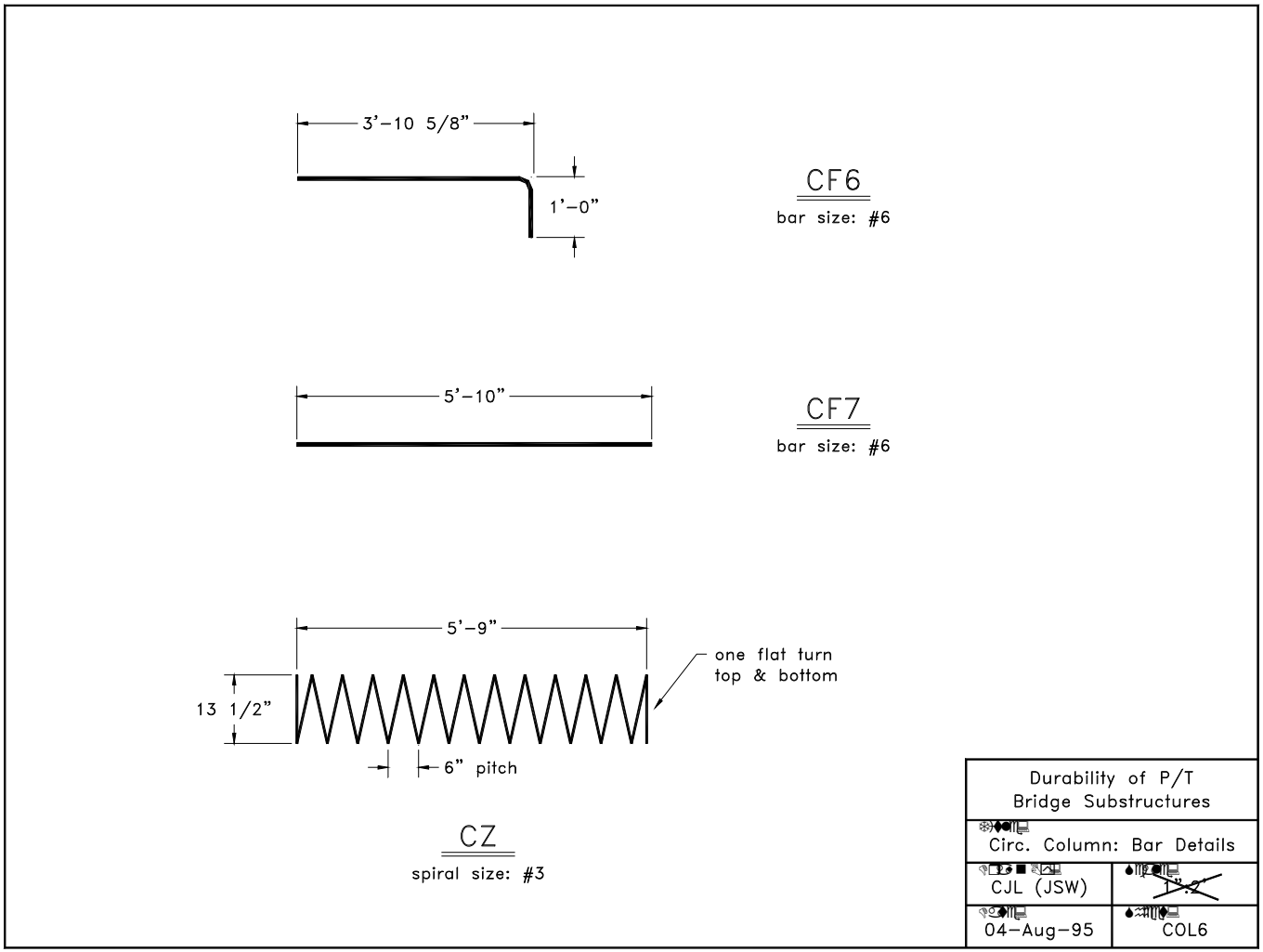

Figure D.6 - Sheet COL6: Column Reinforcing Bar Details

Appendix E:

Macrocell Corrosion Tests:

Supplementary Material

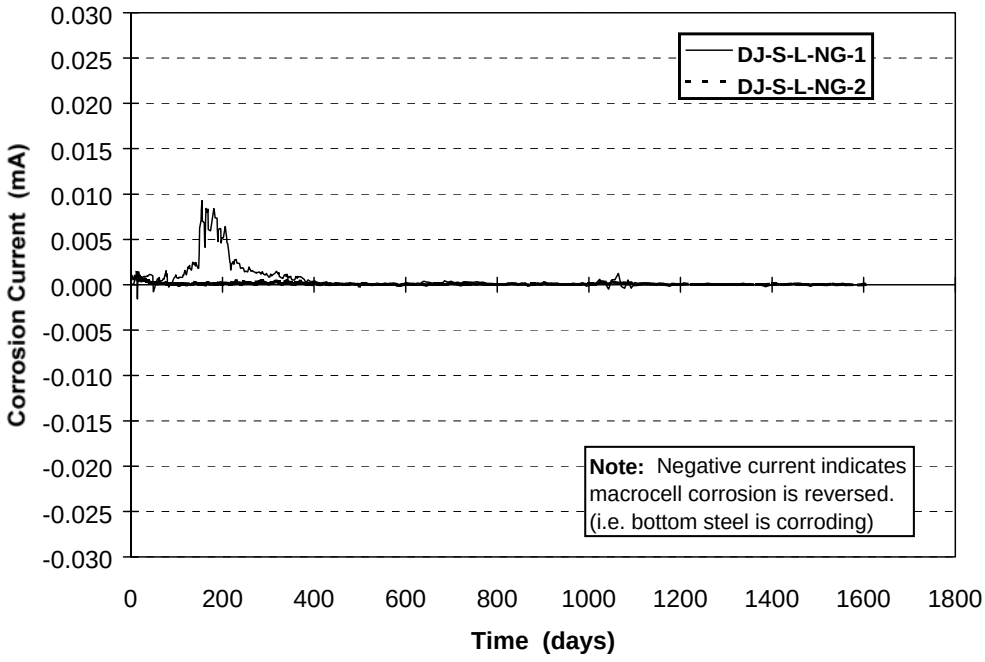

Figure E.1 - Macrocell Corrosion Current: DJ-S-L-NG

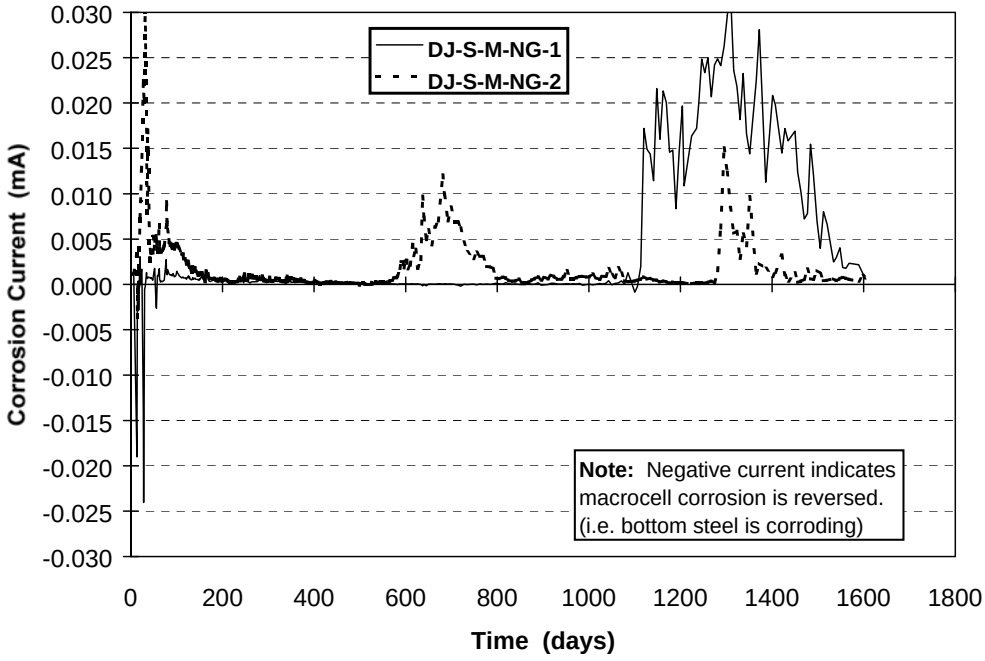

Figure E.2 - Macrocell Corrosion Current: DJ-S-M-NG

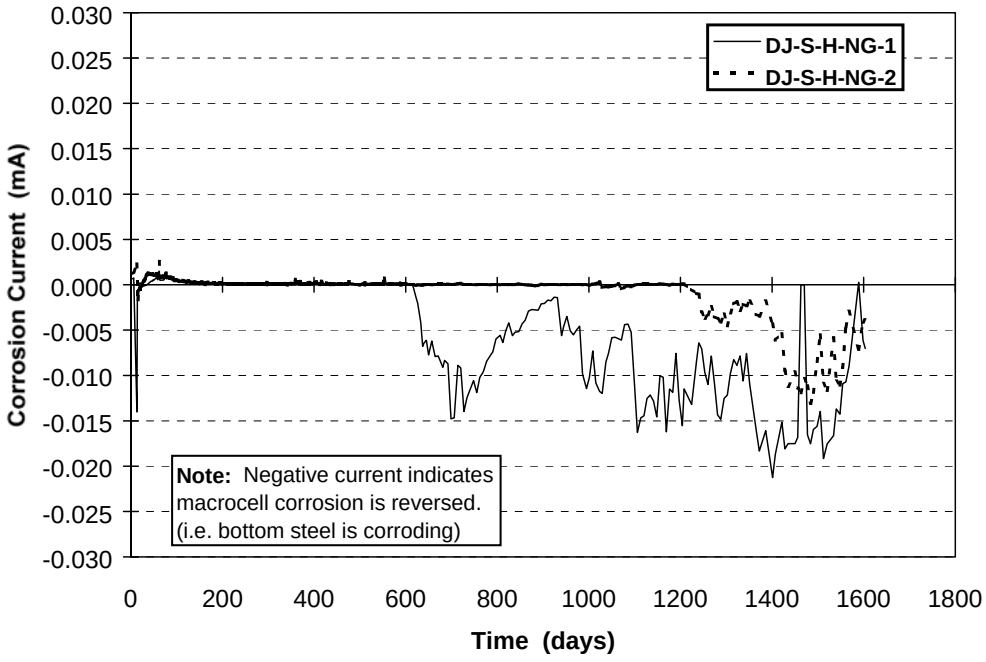

Figure E.3 - Macrocell Corrosion Current: DJ-S-H-NG

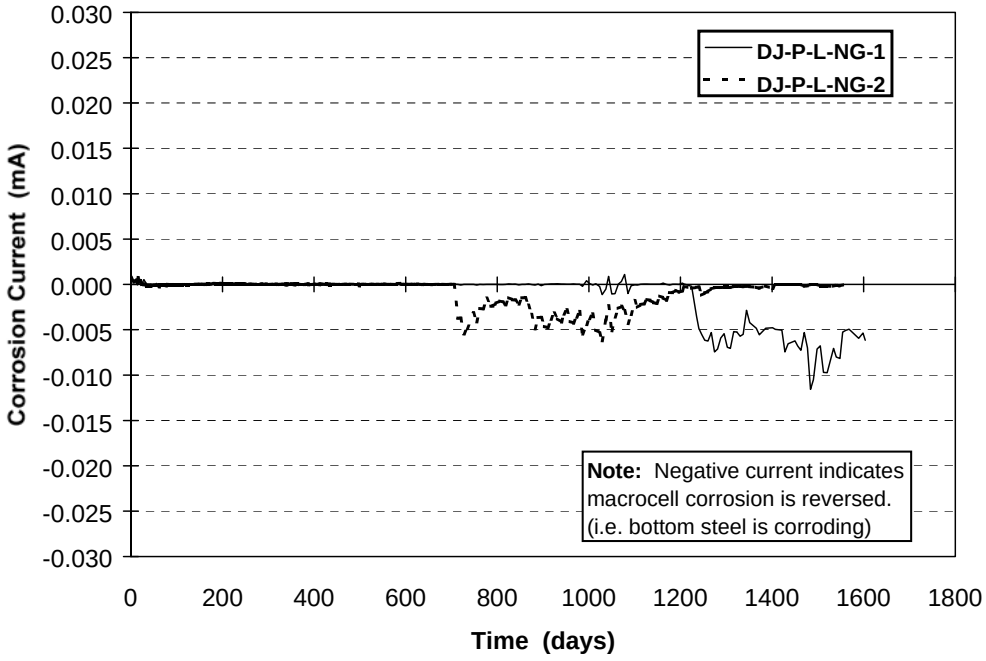

Figure E.4 - Macrocell Corrosion Current: DJ-P-L-NG

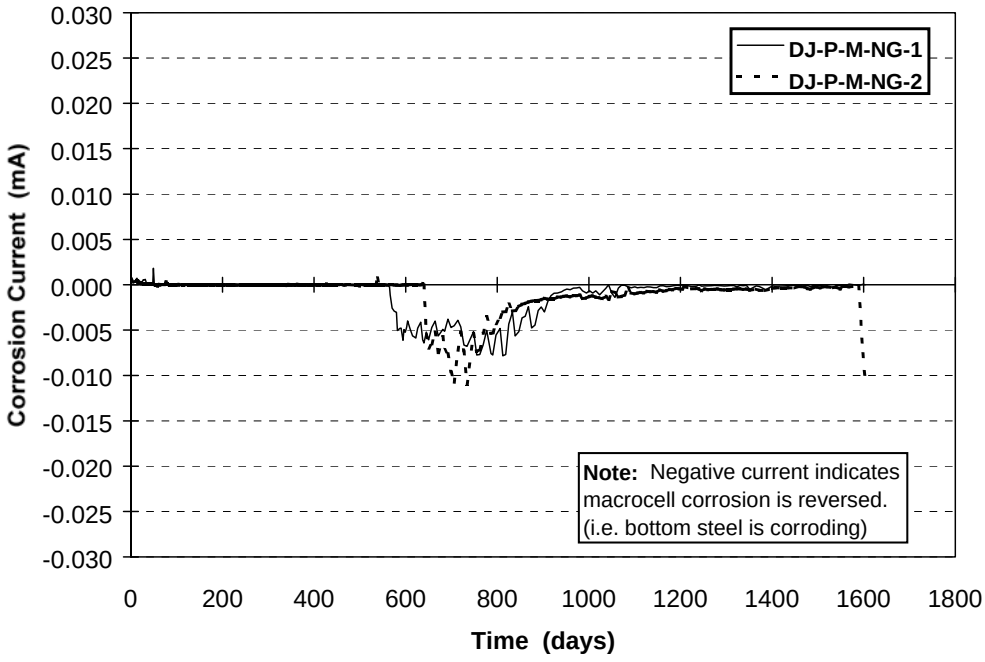

Figure E.5 - Macrocell Corrosion Current: DJ-P-M-NG

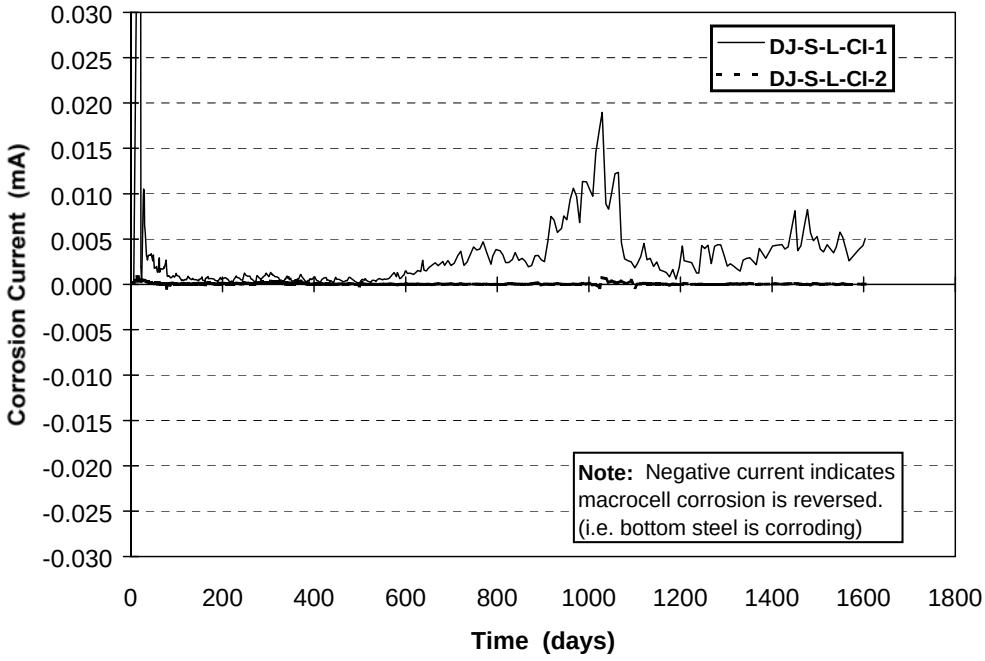

Figure E.6 - Macrocell Corrosion Current: DJ-S-L-CI

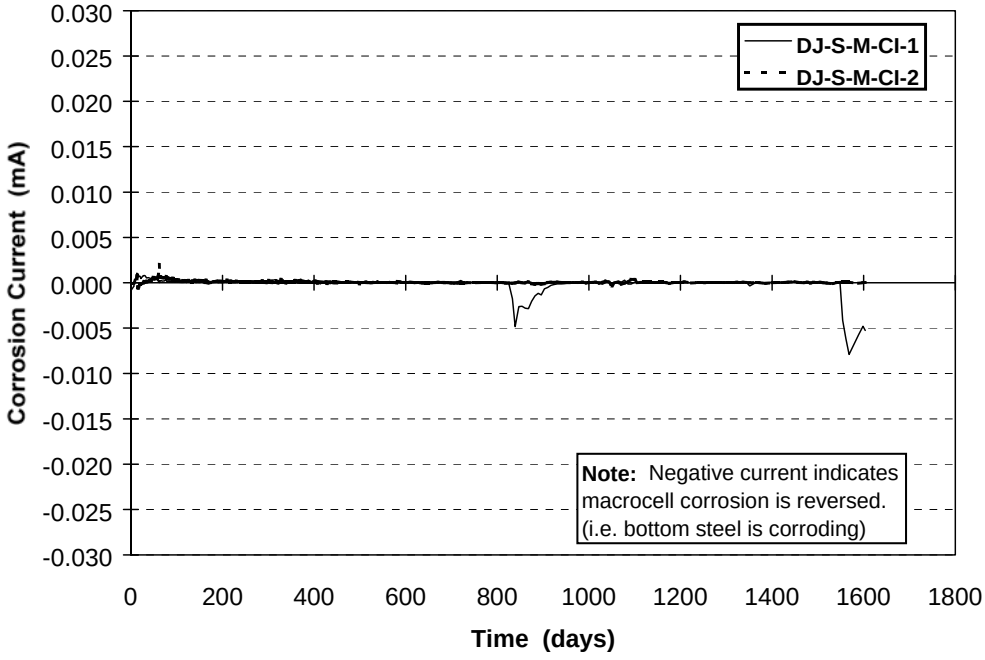

Figure E.7 - Macrocell Corrosion Current: DJ-S-M-CI

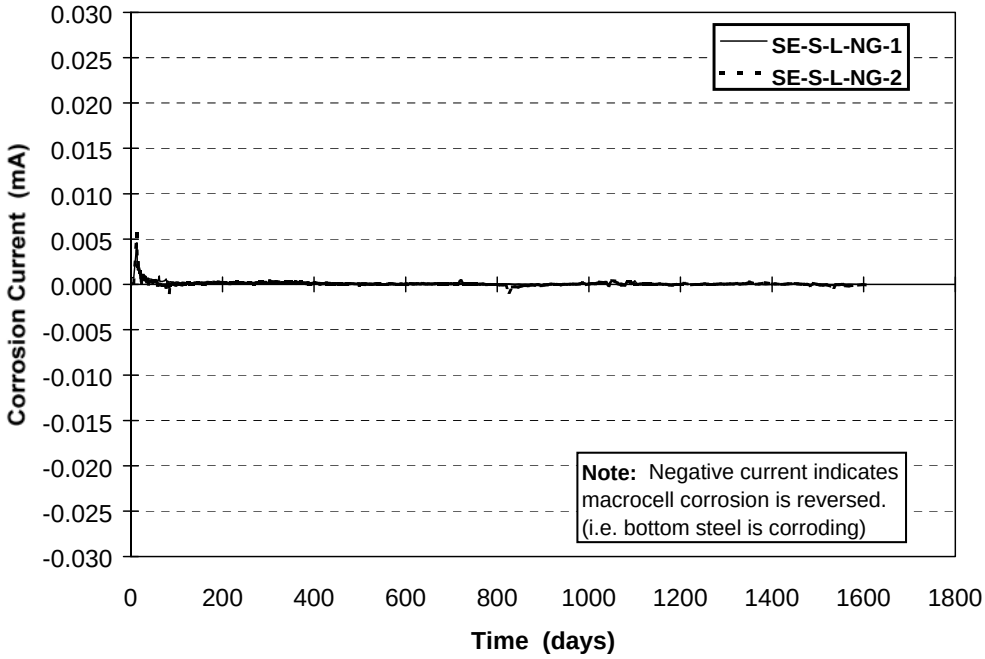

Figure E.8 - Macrocell Corrosion Current: SE-S-L-NG

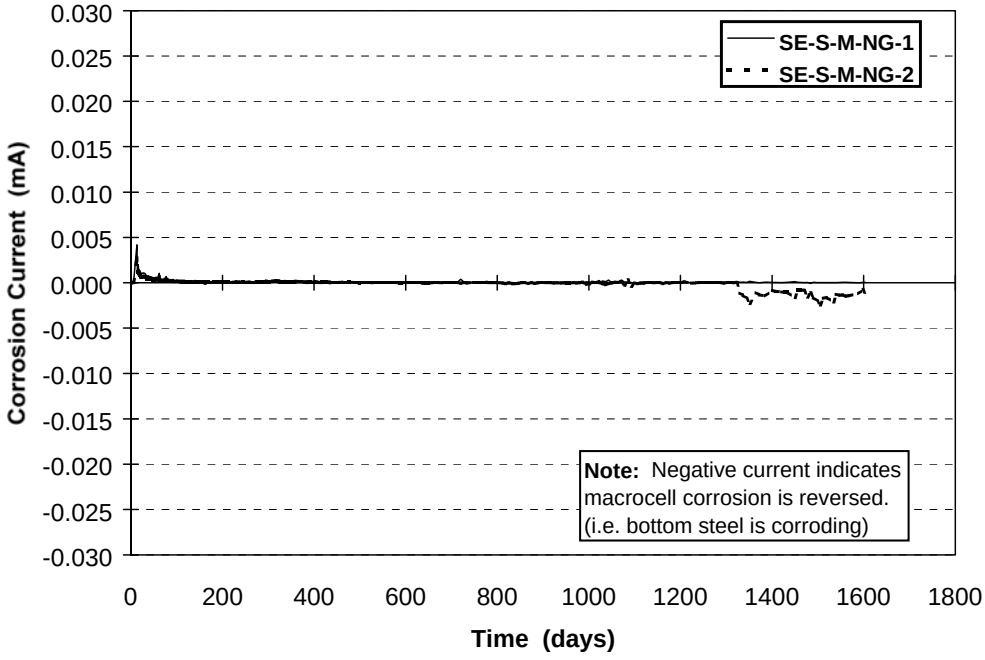

Figure E.9 - Macrocell Corrosion Current: SE-S-M-NG

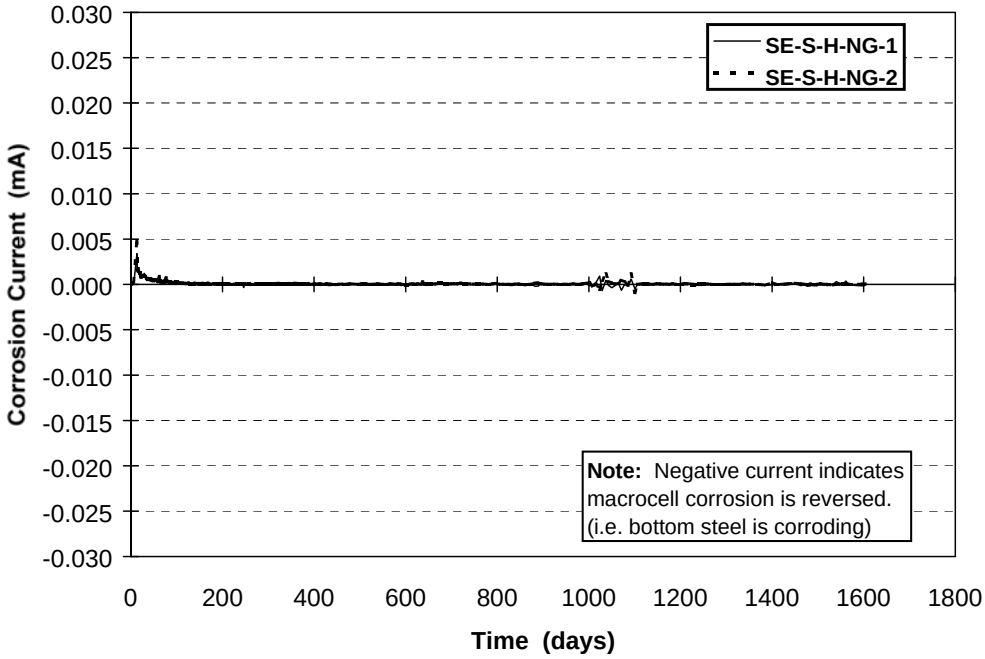

Figure E.10 - Macrocell Corrosion Current: SE-S-H-NG

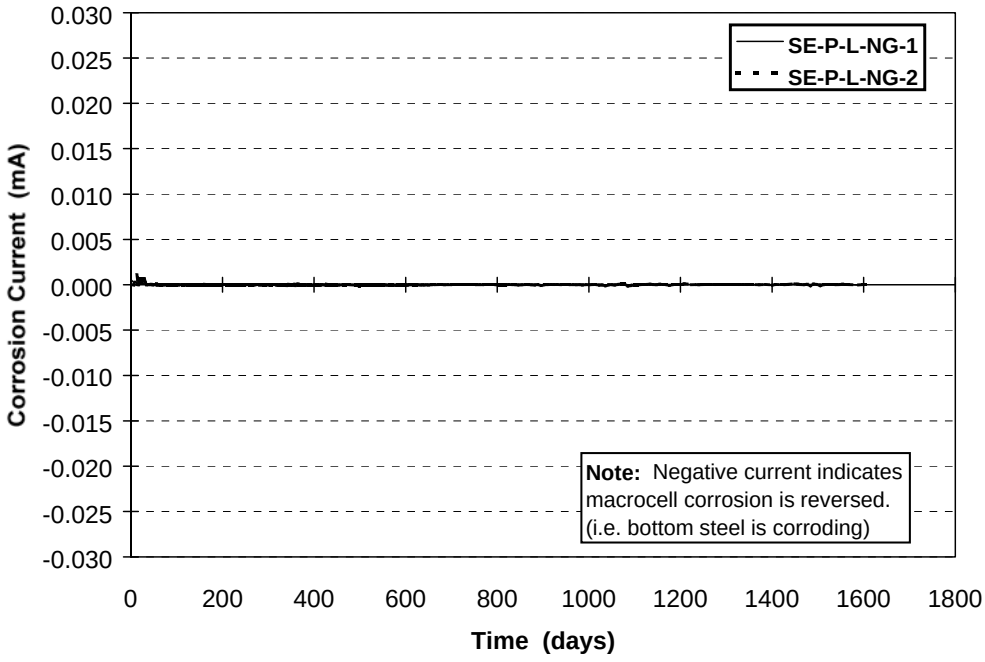

Figure E.11 - Macrocell Corrosion Current: SE-P-L-NG

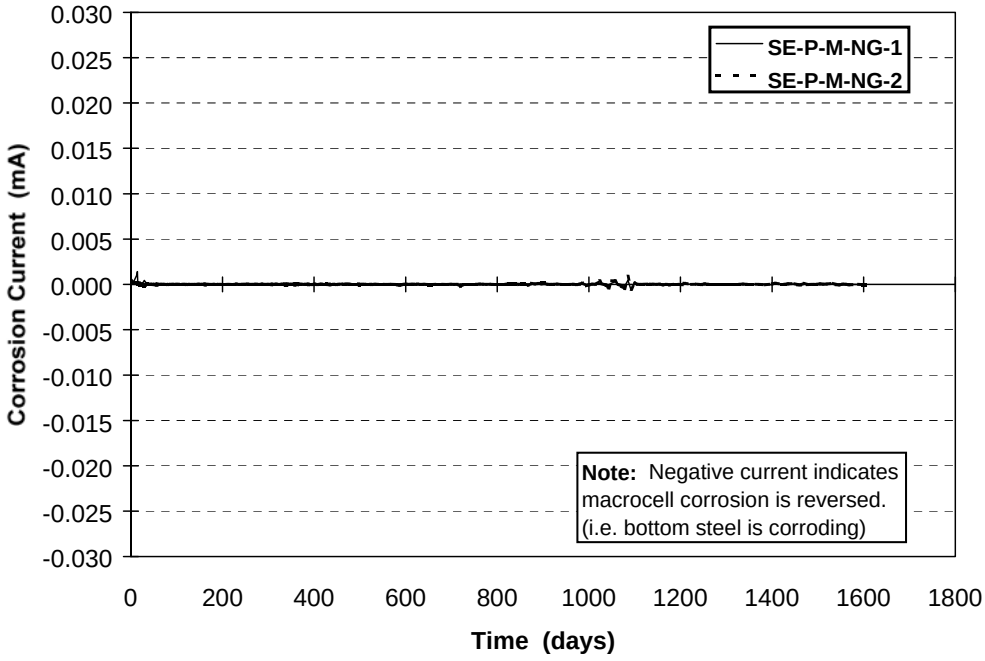

Figure E.12 - Macrocell Corrosion Current: SE-P-M-NG

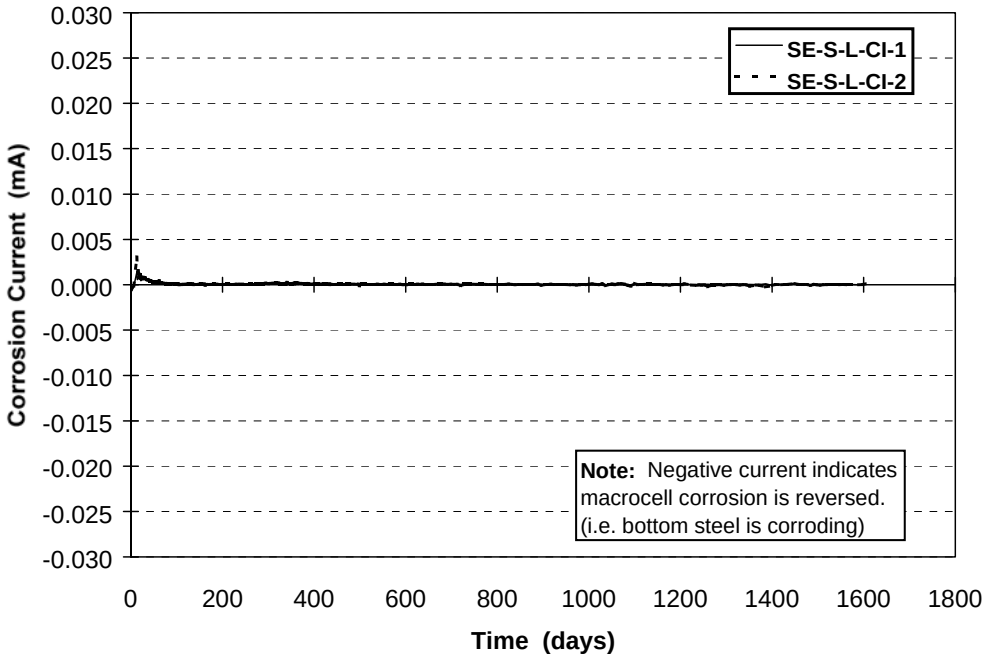

Figure E.13 - Macrocell Corrosion Current: SE-S-L-CI

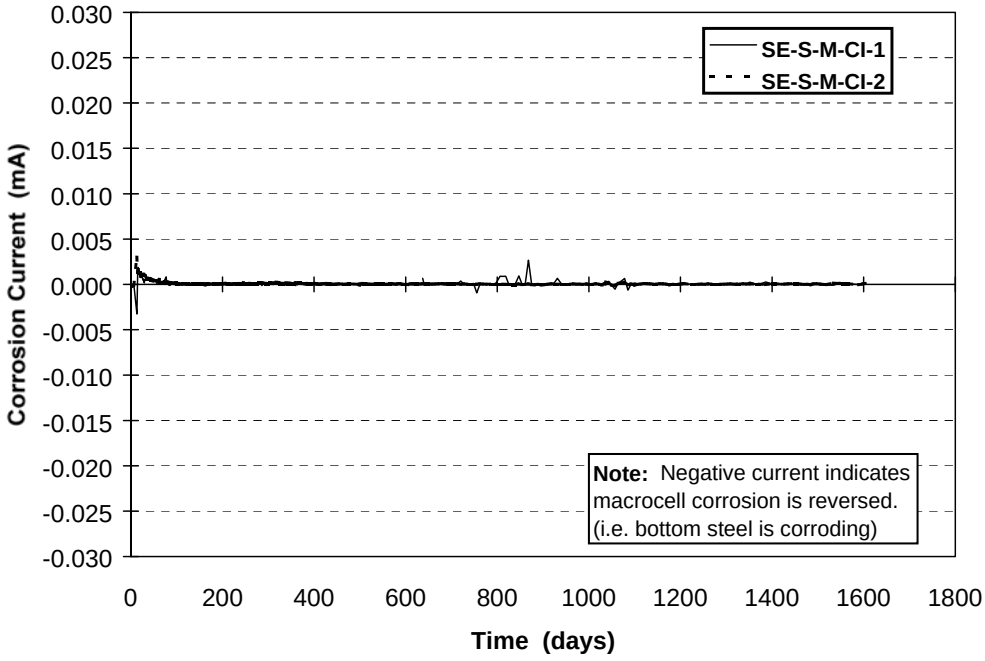

Figure E.14 - Macrocell Corrosion Current: SE-S-M-CI

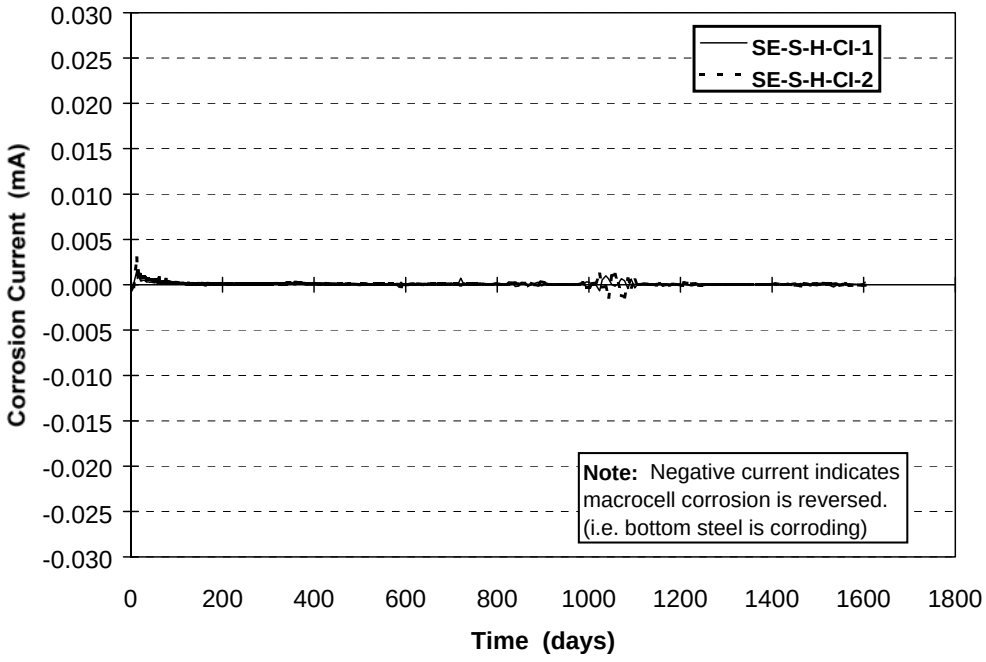

Figure E.15 - Macrocell Corrosion Current: SE-S-H-CI

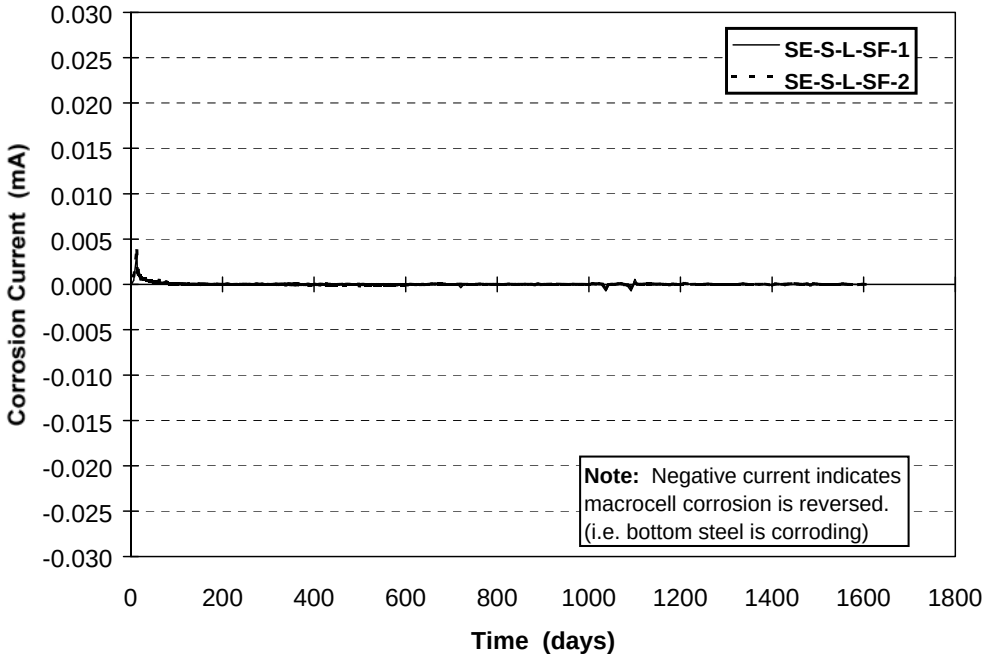

Figure E.16 - Macrocell Corrosion Current: SE-S-L-SF

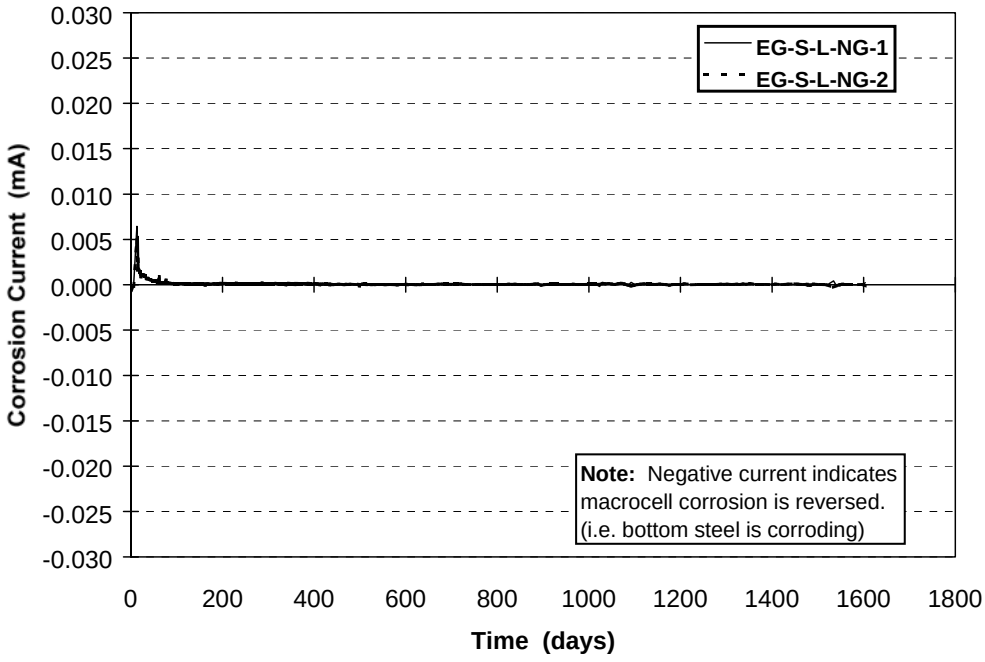

Figure E.17 - Macrocell Corrosion Current: EG-S-L-NG

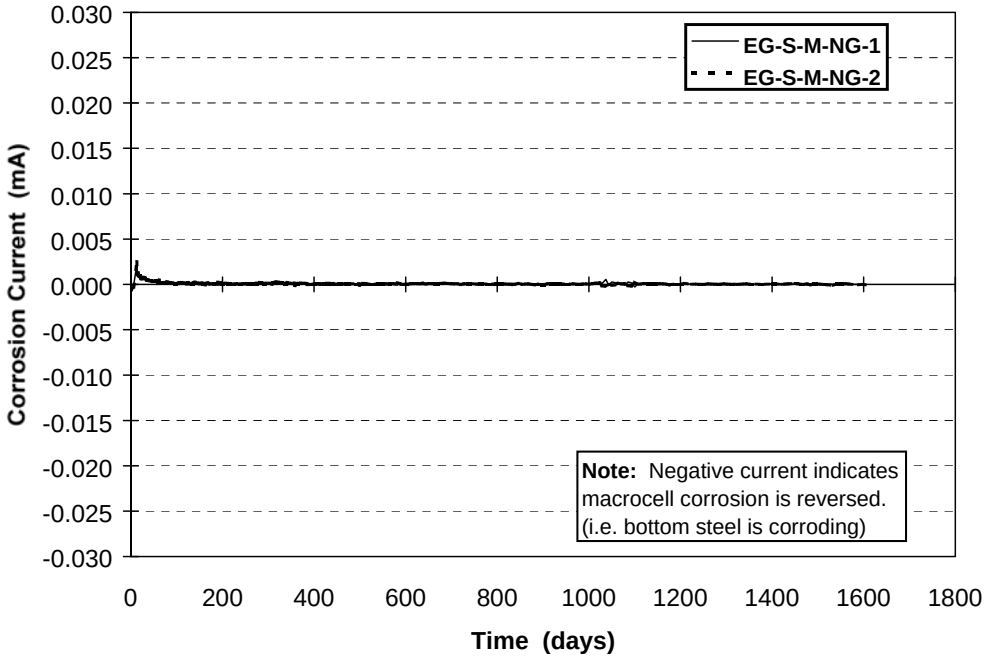

Figure E.18 - Macrocell Corrosion Current: EG-S-M-NG

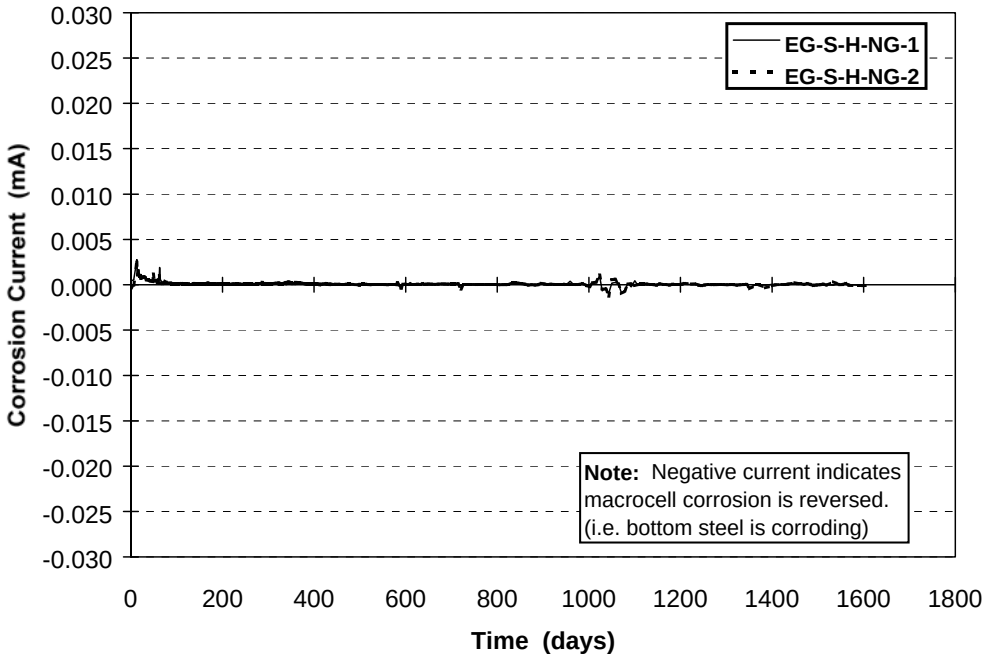

Figure E.19 - Macrocell Corrosion Current: EG-S-H-NG

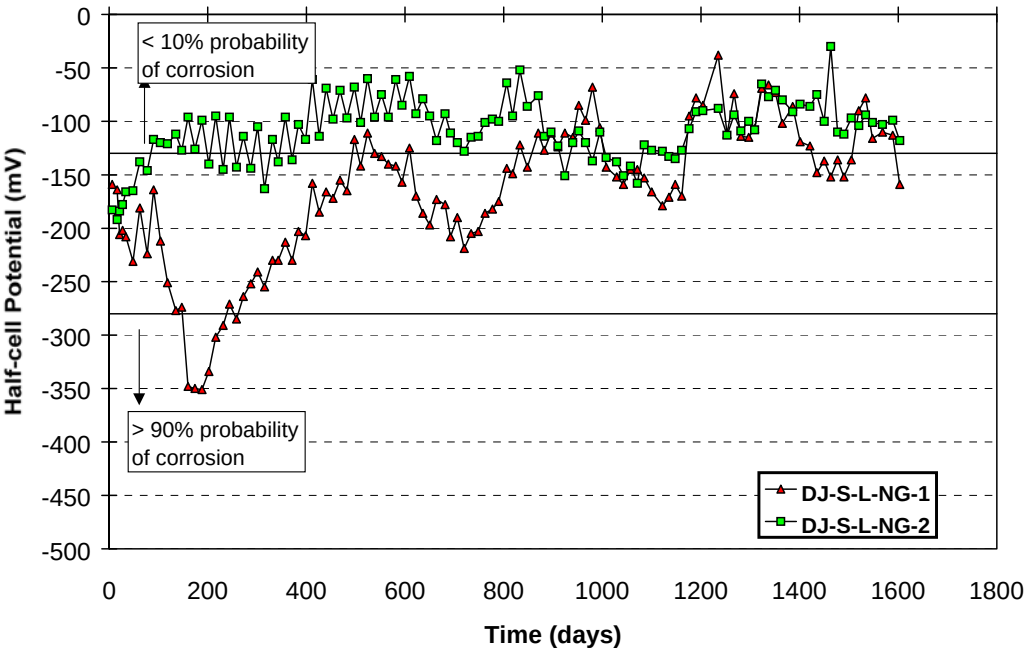

Figure E.20 - Half-Cell Potential Readings: DJ-S-L-NG

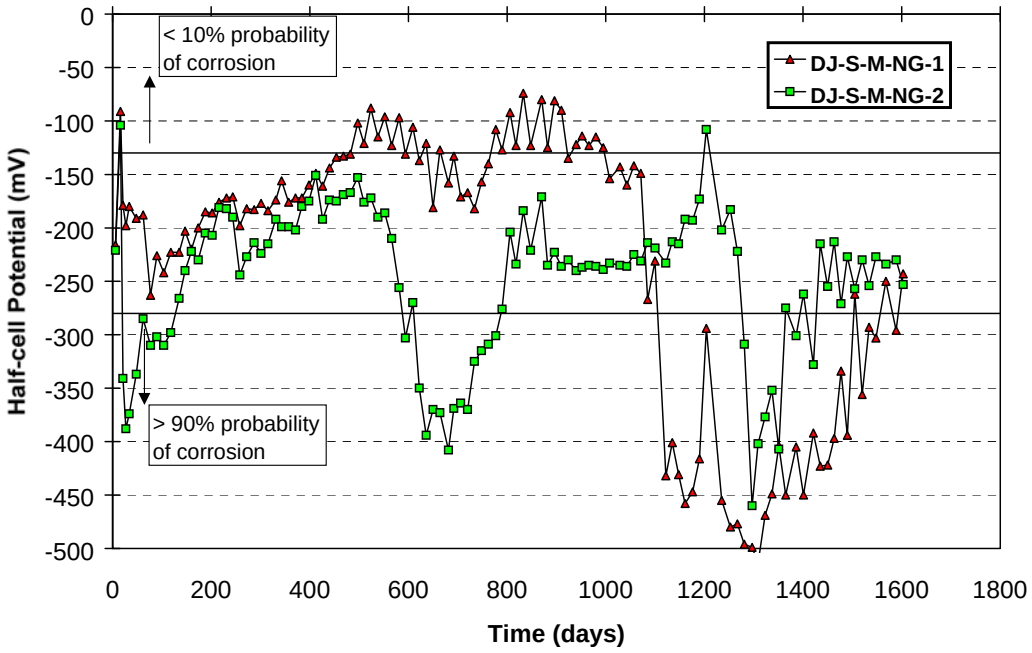

Figure E.21 - Half-Cell Potential Readings: DJ-S-M-NG

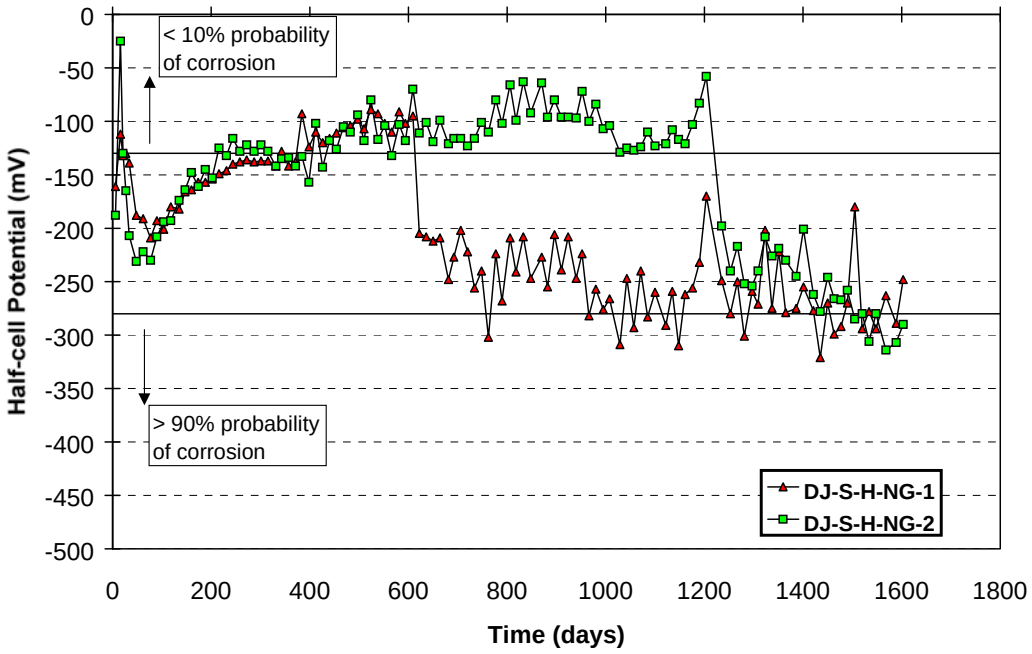

Figure E.22 - Half-Cell Potential Readings: DJ-S-H-NG

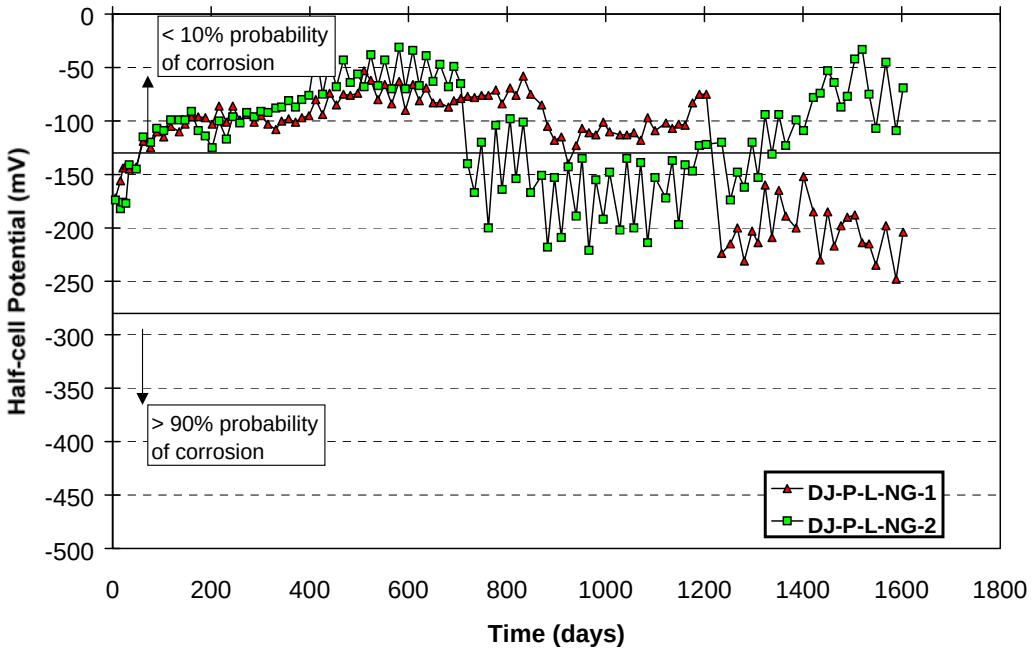

Figure E.23 - Half-Cell Potential Readings: DJ-P-L-NG

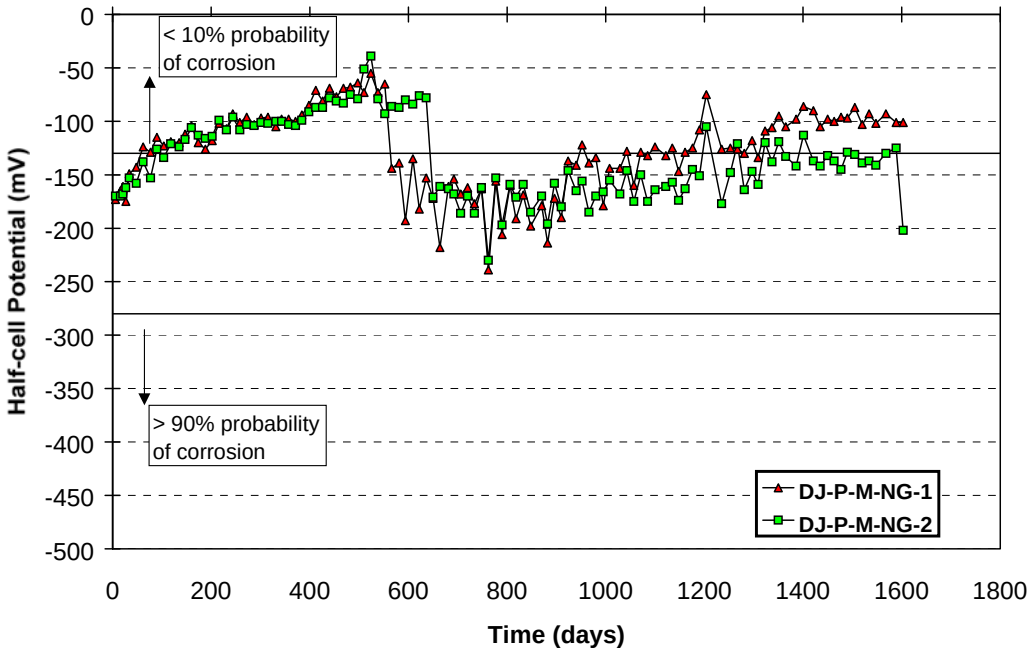

Figure E.24 - Half-Cell Potential Readings: DJ-P-M-NG

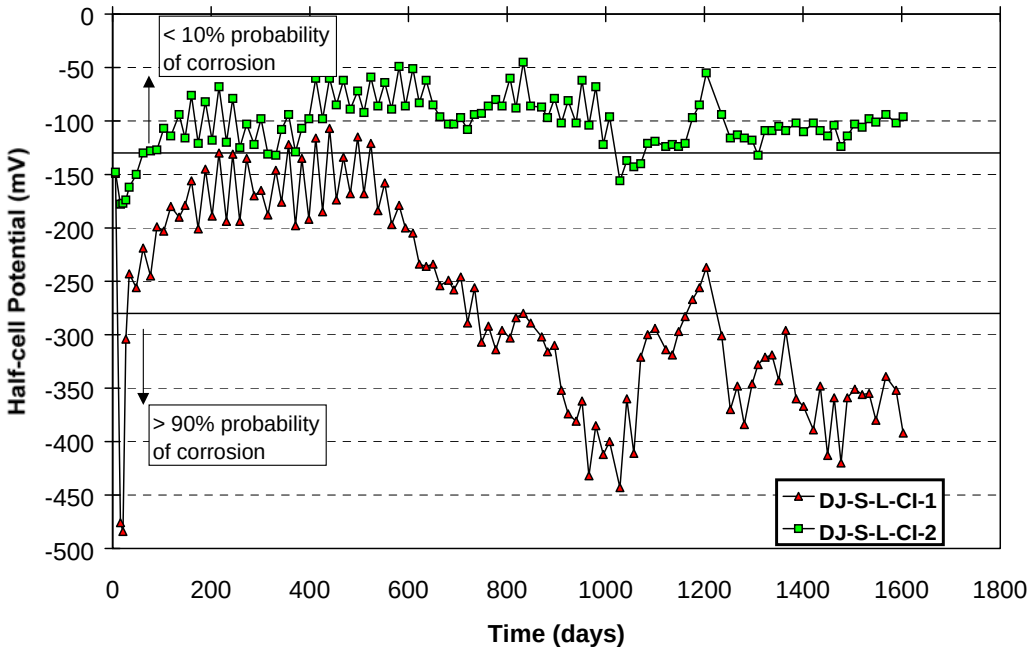

Figure E.25 - Half-Cell Potential Readings: DJ-S-L-CI

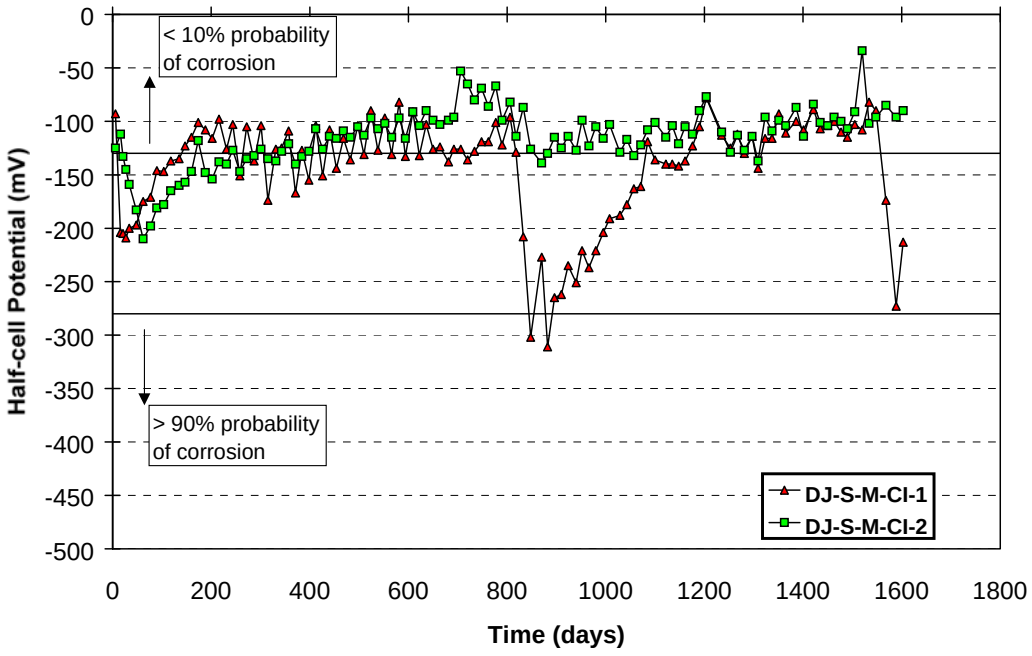

Figure E.26 - Half-Cell Potential Readings: DJ-S-M-CI

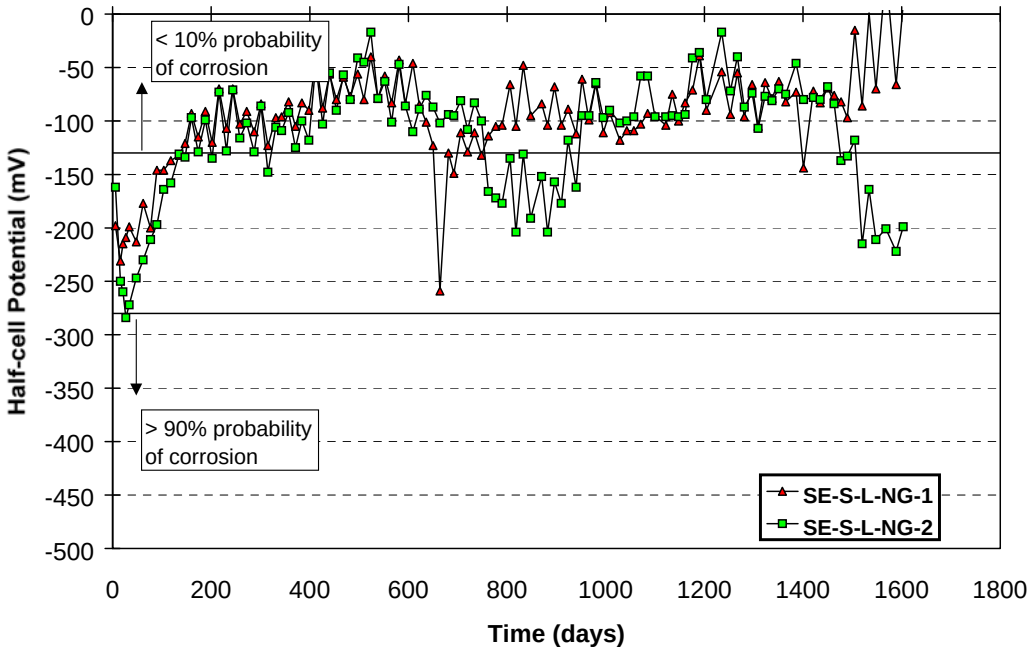

Figure E.27 - Half-Cell Potential Readings: SE-S-L-NG

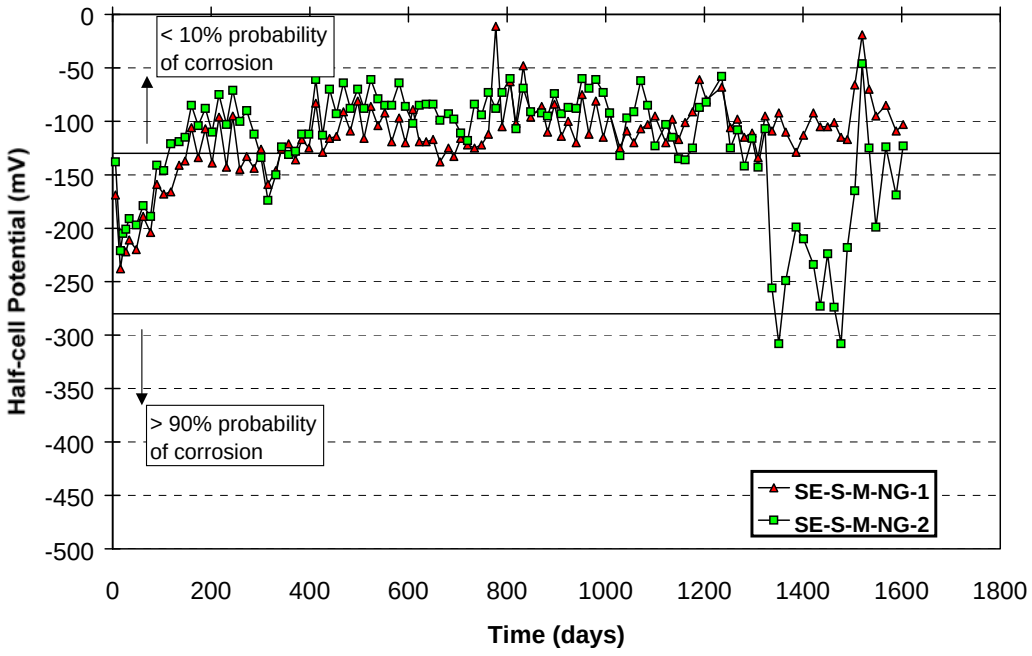

Figure E.28 - Half-Cell Potential Readings: SE-S-M-NG

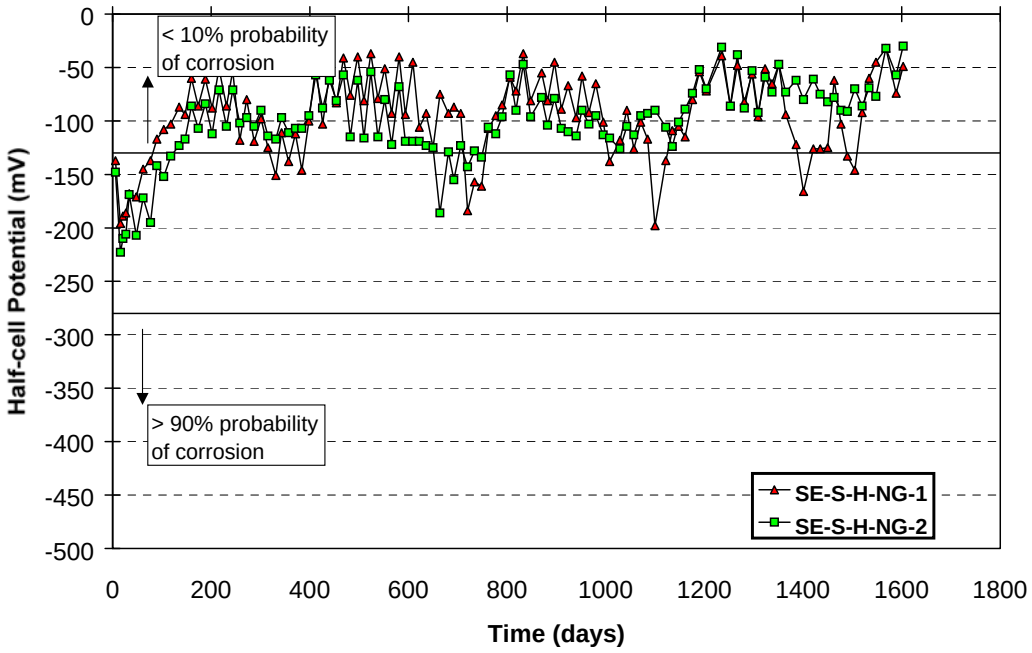

Figure E.29 - Half-Cell Potential Readings: SE-S-H-NG

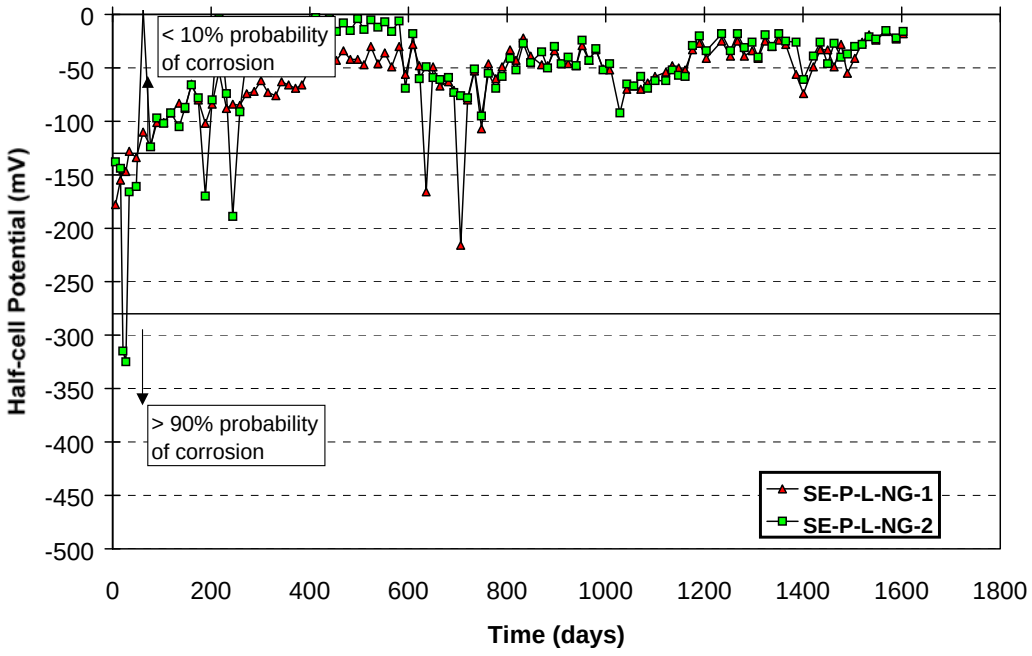

Figure E.30 - Half-Cell Potential Readings: SE-P-L-NG

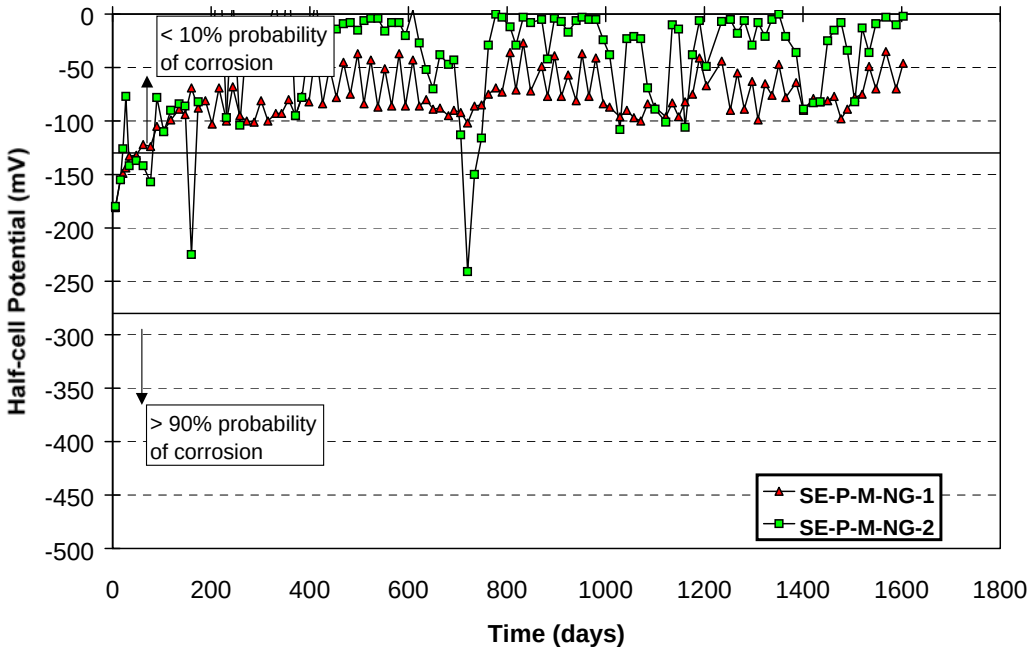

Figure E.31 - Half-Cell Potential Readings: SE-P-M-NG

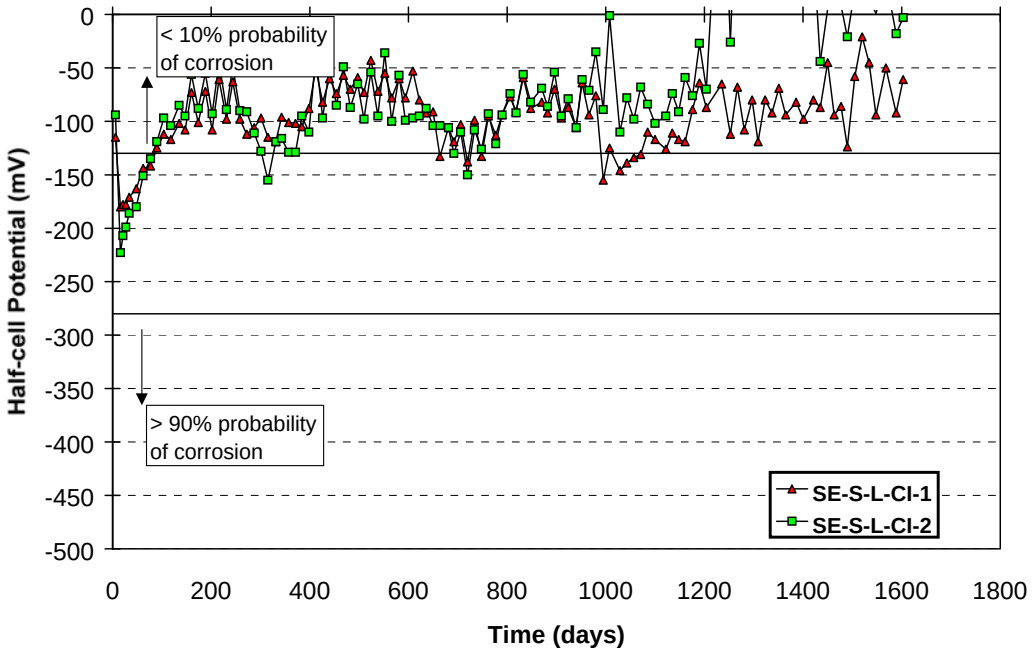

Figure E.32 - Half-Cell Potential Readings: SE-S-L-CI

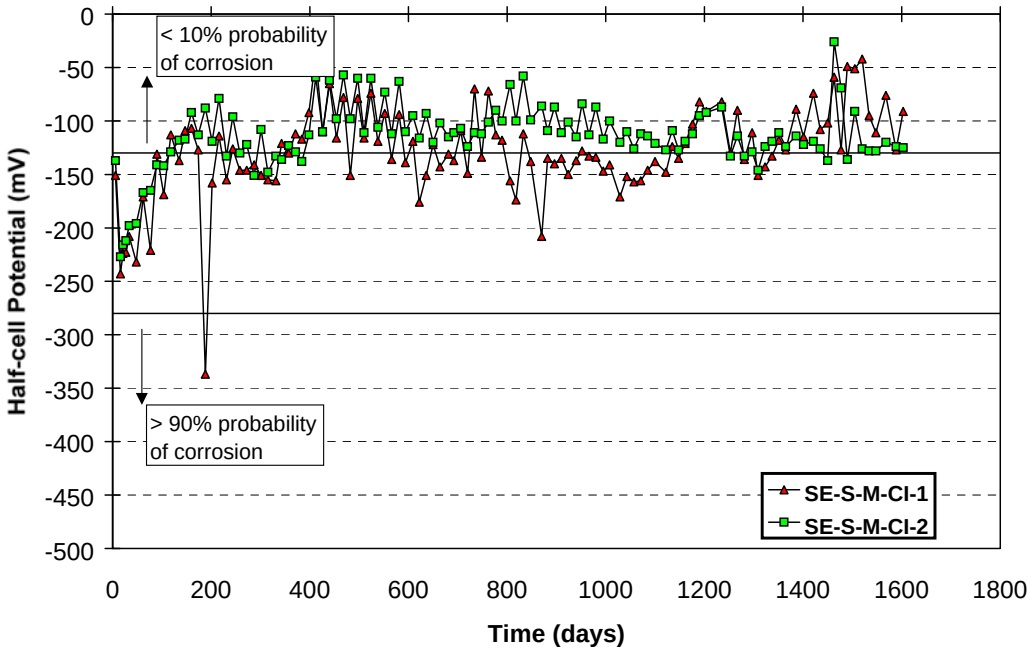

Figure E.33 - Half-Cell Potential Readings: SE-S-M-CI

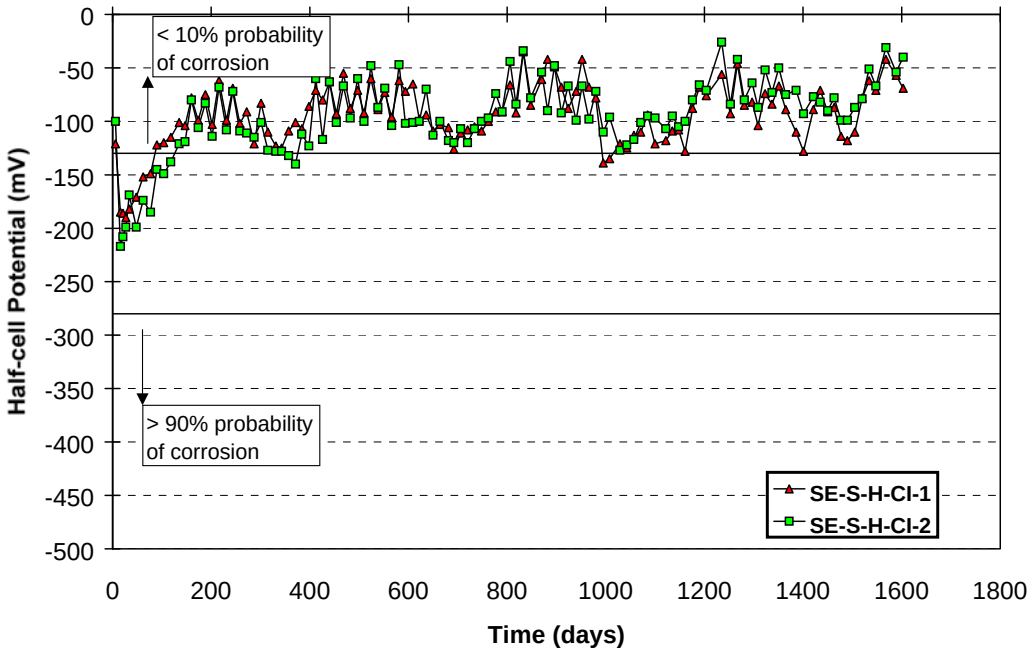

Figure E.34 - Half-Cell Potential Readings: SE-S-H-CI

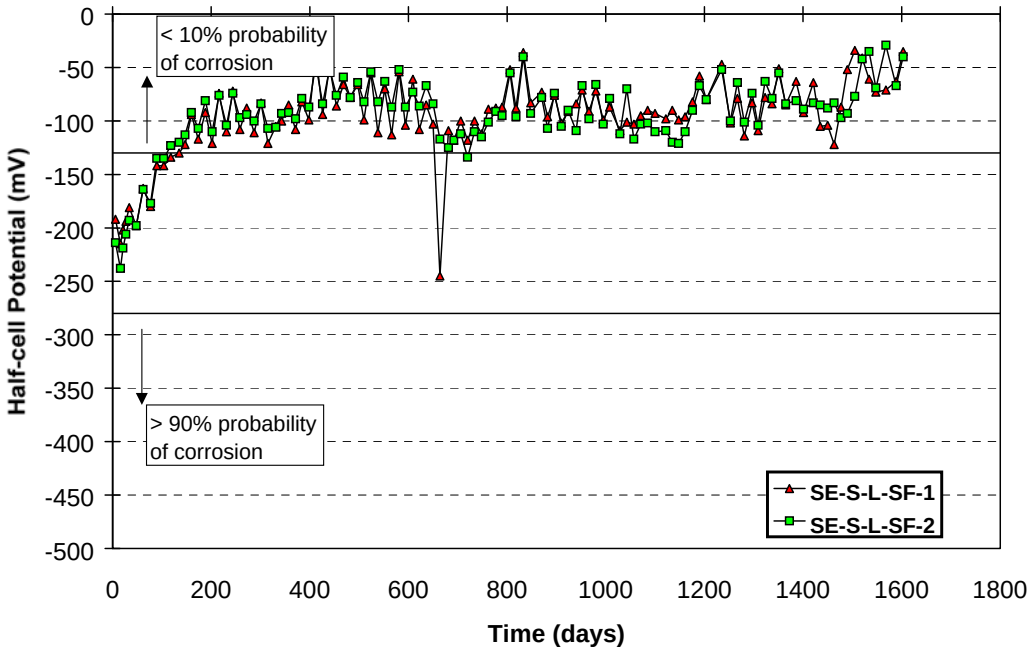

Figure E.35 - Half-Cell Potential Readings: SE-S-L-SF

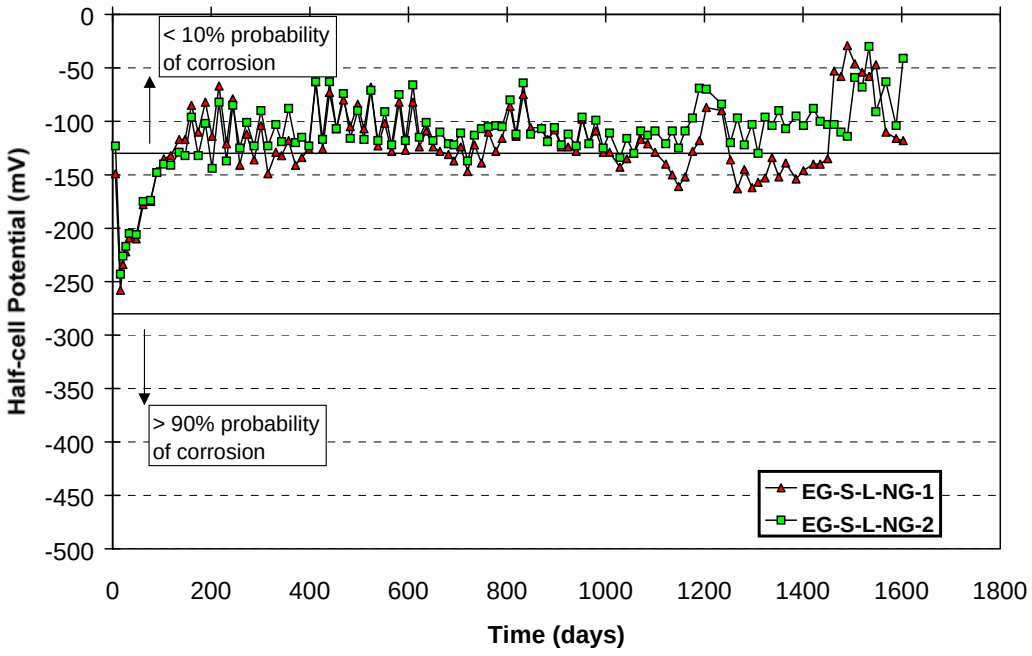

Figure E.36 - Half-Cell Potential Readings: EG-S-L-NG

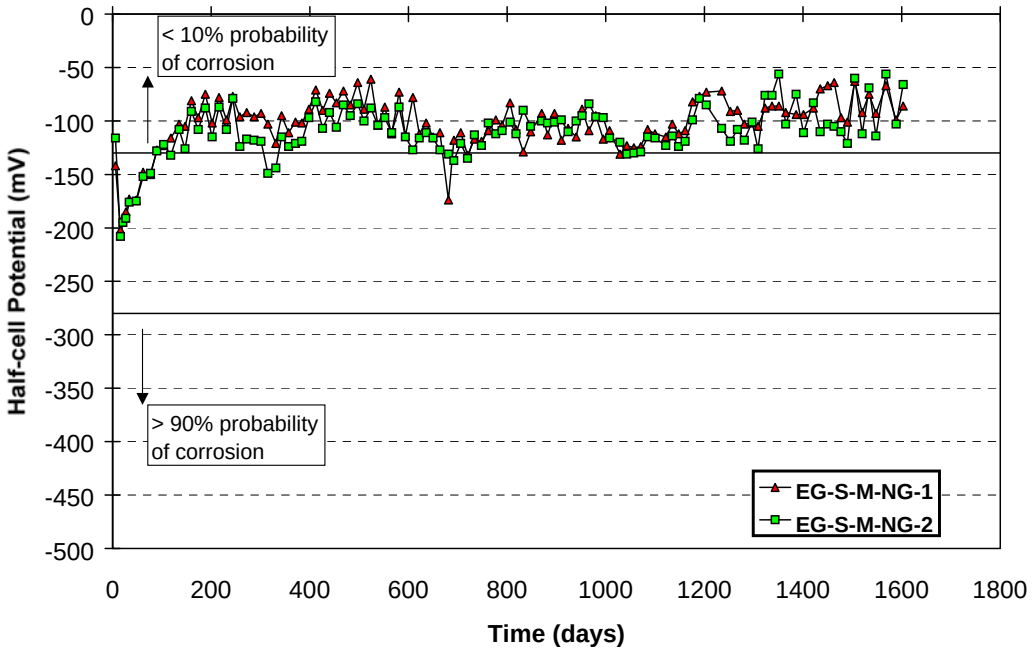

Figure E.37 - Half-Cell Potential Readings: EG-S-M-NG

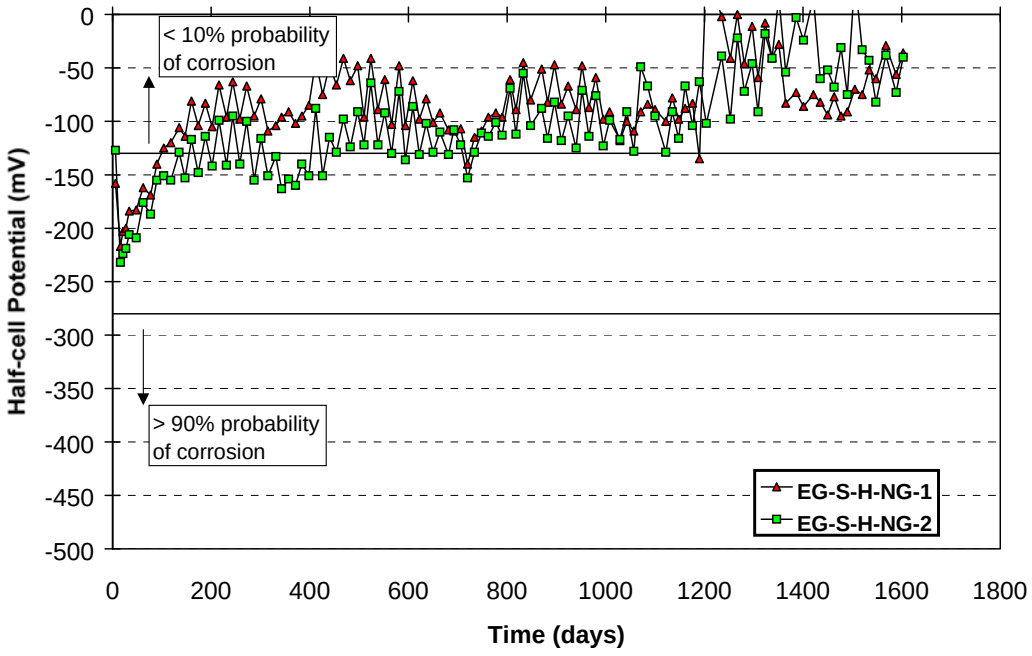

Figure E.38 - Half-Cell Potential Readings: EG-S-H-NG

Calculation of Metal Loss Corresponding to I_{wa} = 10 μA

Equations:

$$\text{Charge Flux} = \int I_{corr} dt \times \frac{86400\text{sec}}{\text{day}} \quad \text{(Coulombs)}$$

$$I_{wa} = \frac{\int I_{corr} dt}{t_i - t_o} \quad \text{(amps)}$$

$$\text{Metal Loss} = \text{Charge Flux} \times \frac{1\text{hr}}{3600\text{sec}} \times \frac{1.04\text{g}}{\text{amp} - \text{hr}} \times \frac{1000\text{mg}}{\text{g}} \quad \text{(mg)}$$

where,

Charge Flux	=	total current passed, Coulombs (amp-sec)
I_{corr}	=	corrosion current, amps
I_{wa}	=	weighted average corrosion current, amps
	=	0.000010 amps (based on "failure" criteria of ASTM G109)
t_i - t_o	=	exposure duration, days
	=	1603 days

Thus,

$$\int I_{corr} dt = 0.000010 \text{ amps} \times 1603 \text{ days}$$

$$= 0.01603 \text{ amp} - \text{days}$$

$$\text{Charge Flux} = (0.01603 \text{ amp} - \text{days}) \times \frac{86400\text{sec}}{\text{day}}$$

$$= 1385.0 \text{ Coulombs}$$

$$\text{Metal Loss} = 1385.0 \times \frac{1\text{hr}}{3600\text{sec}} \times \frac{1.04\text{g}}{\text{amp} - \text{hr}} \times \frac{1000\text{mg}}{\text{g}}$$

$$= 400.1 \text{ mg}$$

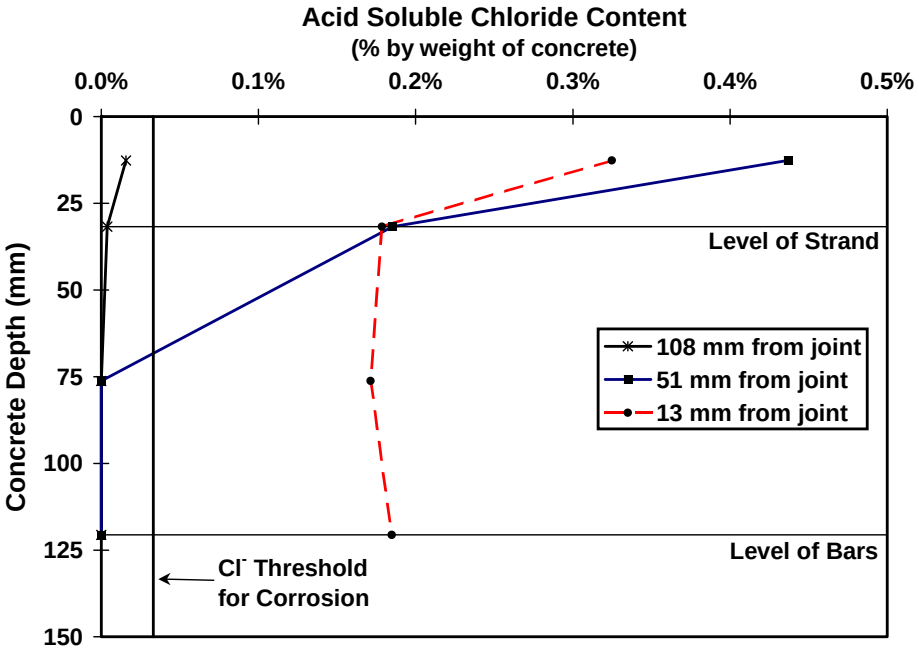

Figure E.39 - Concrete Chloride Profiles for DJ-S-L-NG-1

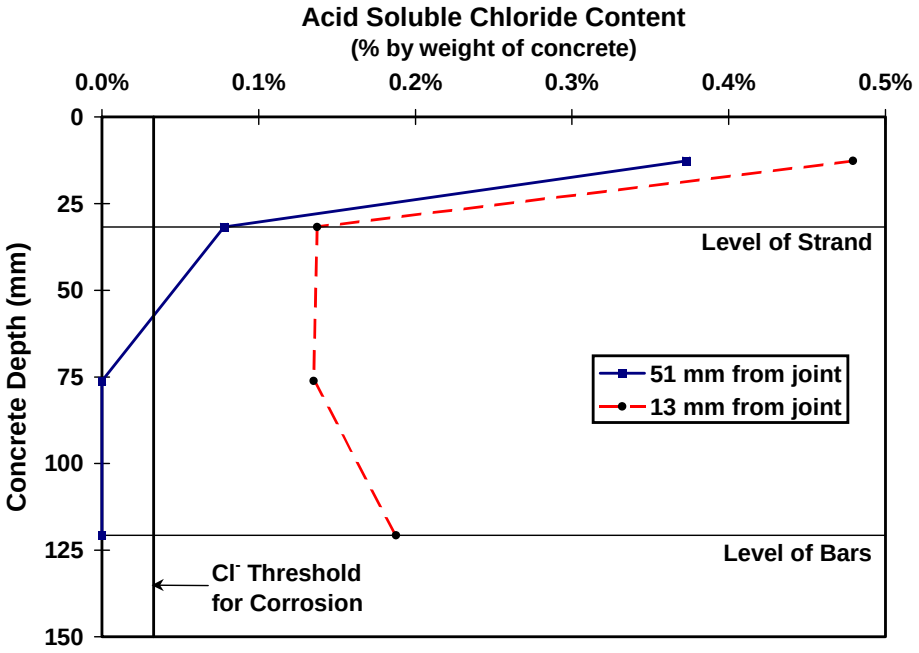

Figure E.40 - Concrete Chloride Profiles for DJ-S-M-NG-1

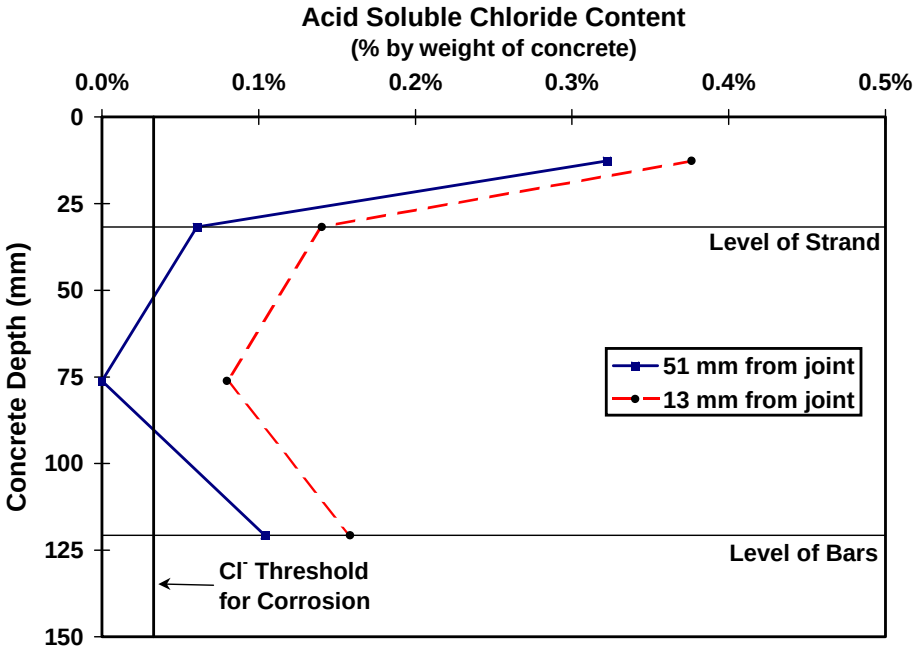

Figure E.41 - Concrete Chloride Profiles for DJ-S-H-NG-1

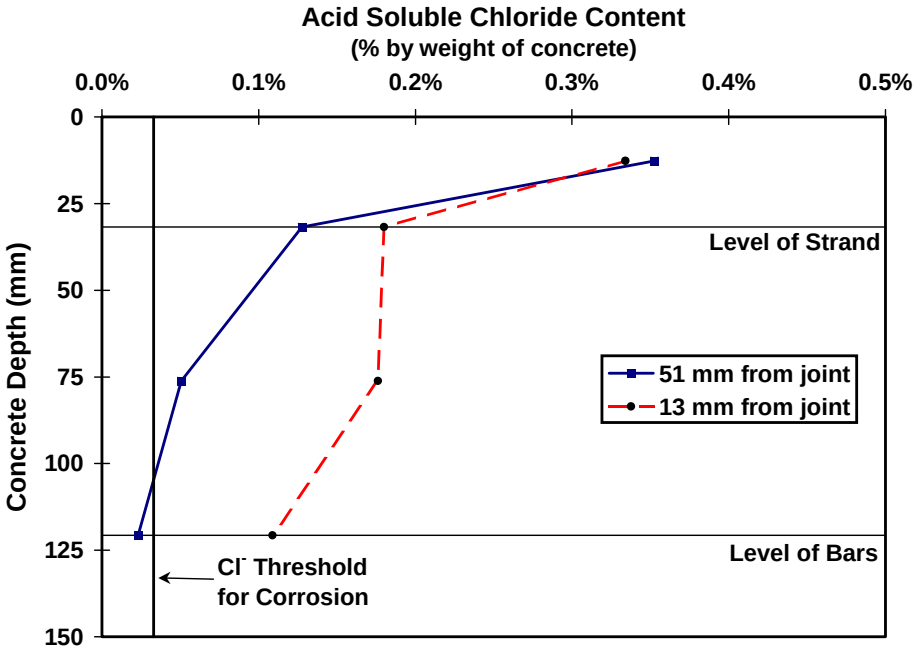

Figure E.42 - Concrete Chloride Profiles for DJ-P-L-NG-1

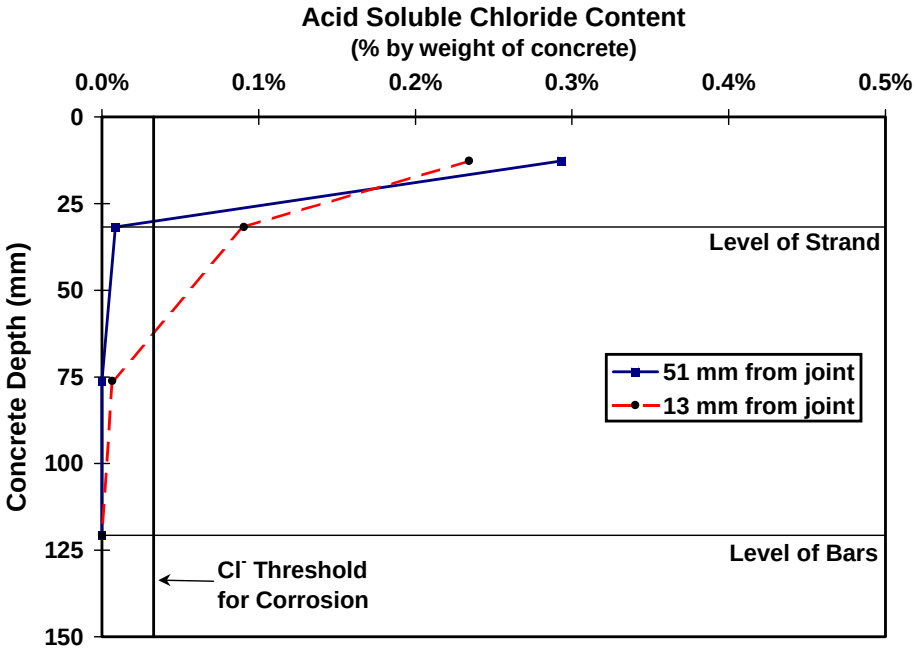

Figure E.43 - Concrete Chloride Profiles for DJ-S-L-CI-1

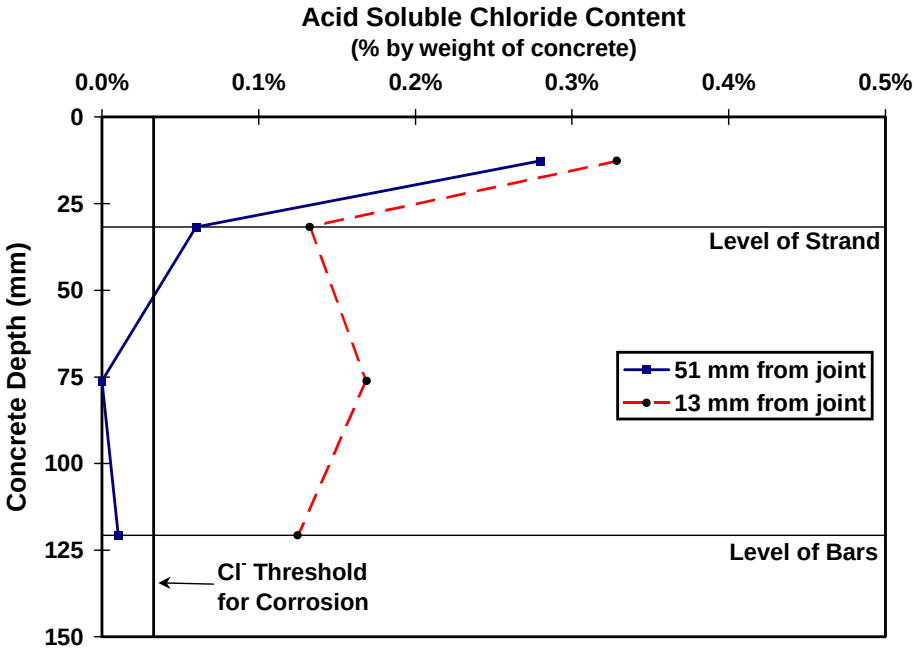

Figure E.44 - Concrete Chloride Profiles for DJ-S-M-CI-1

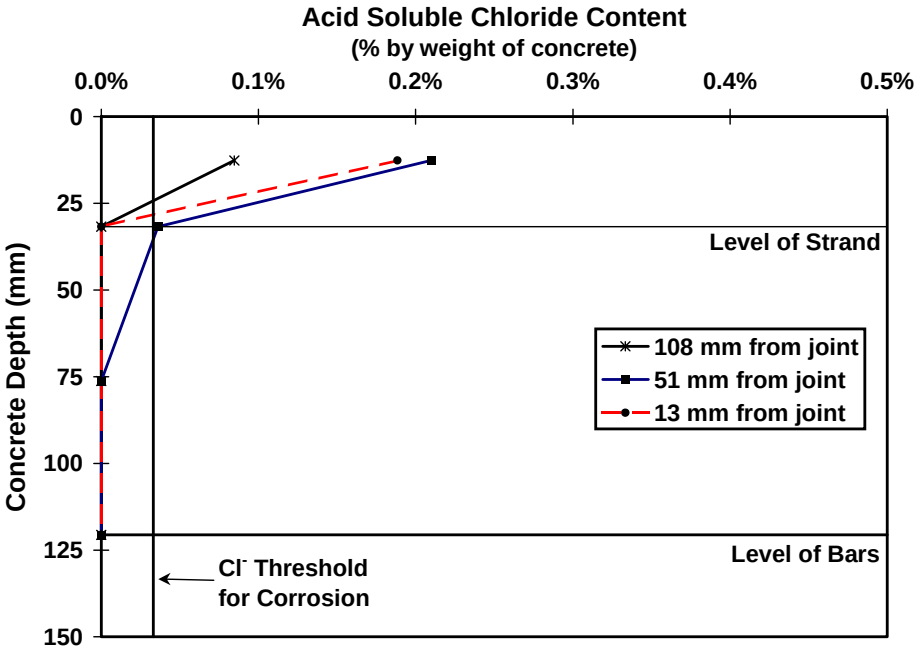

Figure E.45 - Concrete Chloride Profiles for SE-S-L-NG-2

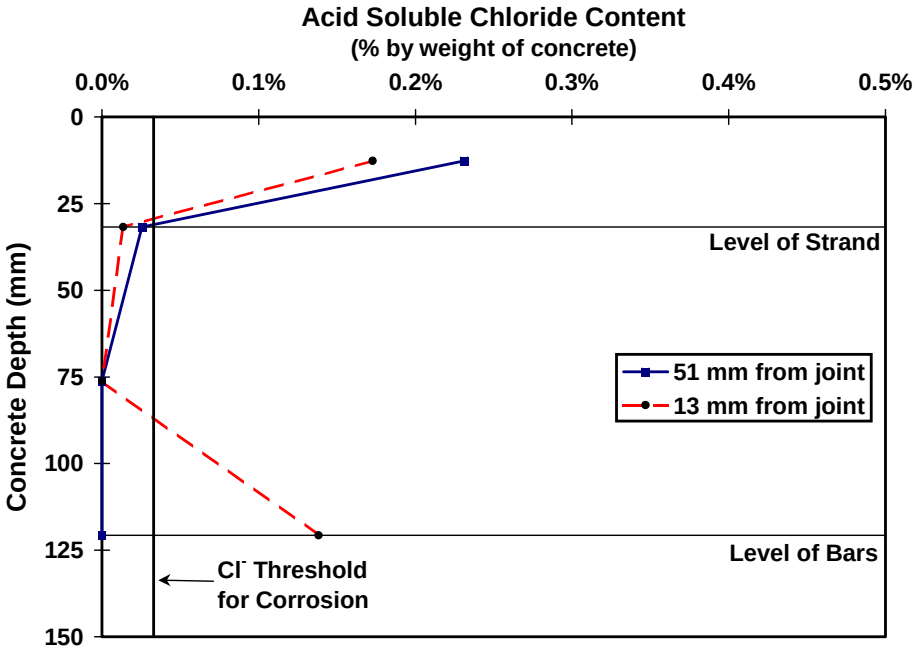

Figure E.46 - Concrete Chloride Profiles for SE-S-M-NG-2

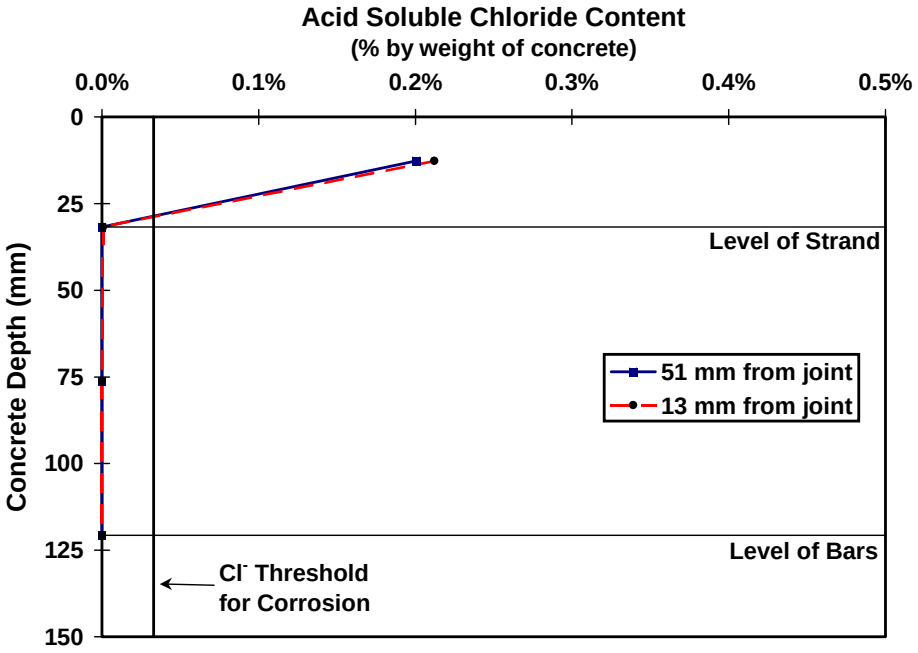

Figure E.47 - Concrete Chloride Profiles for SE-S-H-NG-2

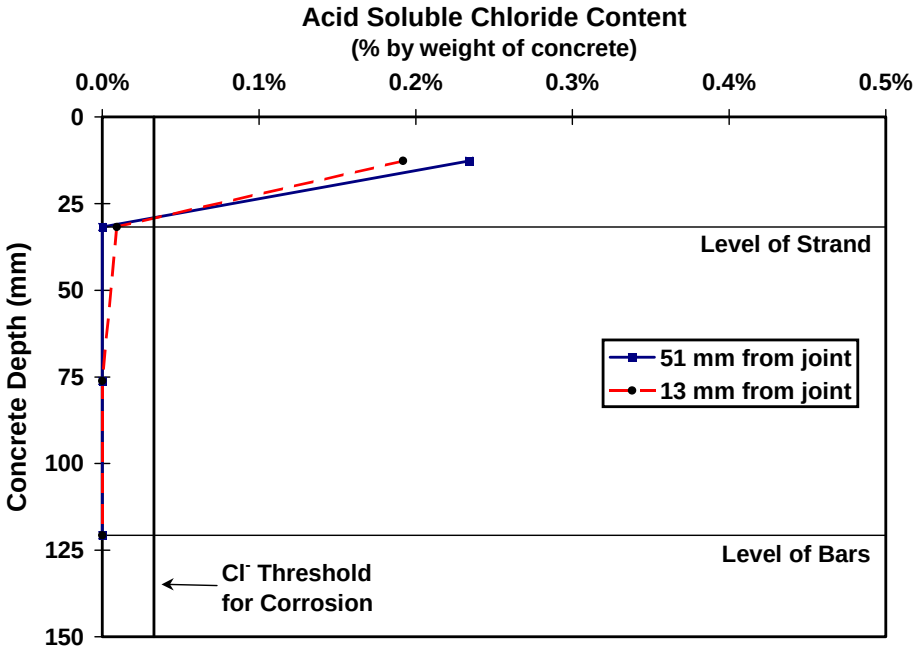

Figure E.48 - Concrete Chloride Profiles for EG-S-L-NG-2

Reference List

Chapter 1 References

1.1) **Larosche, C.J.,** "Test Method for Evaluating Corrosion Mechanisms in Standard Bridge Columns," Master of Science Thesis, The University of Texas at Austin, August 1999.

1.2) **Aeberhard, H.U., Ganz, H.R., Marti, P., and Schuler, W.,** Post-Tensioned Foundations, VSL International Ltd., Berne, Switzerland, 1988, 24 pp.

1.3) **AASHTO**, LRFD Bridge Design Specifications, 2nd Edition, American Association of State Highway and Transportation Officials, Washington, D.C., 1998.

1.4) **Billington, S.L.,** "Behavior of Two-Span Continuous Pier Caps With Varying Levels of Prestress," Master of Science Thesis, The University of Texas at Austin, December 1994.

1.5) **Thürlimann, Bruno,** "Considerations to the Design of Prestressed Concrete Bridges," *IABSE Proceedings,* No. 70, 1983, pp. 237-?.

1.6) **Armstrong, S.D., Salas, R.M., Wood, B.A., Breen, J.E. and Kreger, M.E.,** "Behavior and Design of Large Structural Bridge Pier Overhangs," Research Report 1364-1, Center for Transportation Research, The University of Texas at Austin, 1997, 272 pp.

1.7) **Billington, S.L.,** "Improving Standard Bridges Through Aesthetic Guidelines and Attractive, Efficient Concrete Substructures," Doctor of Philosophy Dissertation, The University of Texas at Austin, December 1997.

1.8) **Barnes, R.W.,** "Development of a High Performance Substructure System for Prestressed Concrete Girder Highway Bridges," Master of Science Thesis, The University of Texas at Austin, 1996.

1.9) **Koester, B.D.,** "Evaluation of Cement Grouts for Strand Protection Using Accelerated Corrosion Tests," Master of Science Thesis, The University of Texas at Austin, December 1995.

1.10) **Schokker, A.J.,** "Improving Corrosion Resistance of Post-Tensioned Substructures Emphasizing High Performance Grouts," Doctor of Philosophy Dissertation, The University of Texas at Austin, May 1999.

1.11) **Vignos, R.P.**, "Test Method for Evaluating the Corrosion Protection of Internal Tendons Across Segmental Bridge Joints." Master of Science Thesis, The University of Texas at Austin, May 1994.

Chapter 2 References

2.1) **CEB,** Durable Concrete Structures – CEB Design Guide, Bulletin D'Information No. 182, Comité Euro-International du Béton, Lausanne, June 1989, 310 pp.

2.2) **Texas State Department of Highways and Public Transportation,** Bridge Design Guide, First Edition, Austin, Texas, 1990.

2.3) **Watkins, D.A.,** "Specification of Air Entrainment for Freezing and Thawing Environments," Master of Science Thesis, The University of Texas at Austin, August 1997.

2.4) **Schiessl, P., and Raupach, M.,** "Laboratory Studies and Calculations on the Influence of Crack Width on Chloride-Induced Corrosion of Steel in Concrete," *ACI Materials Journal,* Vol. 94, No. 1, January-February 1997, pp. 56-62.

2.5) **Hime, W., and Erlin, B.,** "Some Chemical and Physical Aspects of Phenomena Associated with Chloride-Induced Corrosion," ACI SP-102, *Corrosion, Concrete and Chlorides – Steel Corrosion in Concrete: Causes and Restraints,* F.W. Gibson, Editor, American Concrete Institute, Detroit, MI, 1987, pp. 1-12.

2.6) **Fraczek, J.,** "A Review of Electrochemical Principles as Applied to Corrosion of Steel in a Concrete or Grout Environment," ACI SP-102, *Corrosion, Concrete and Chlorides – Steel Corrosion in Concrete: Causes and Restraints,* F.W. Gibson, Editor, American Concrete Institute, Detroit, MI, 1987, pp. 13-24.

2.7) **Martin, F.J.,** "Corrosion Damage of Reinforced Concrete," Presentation Notes, Purdue University, 1995.

2.8) **Beeby, A.W.,** "Cracking and Corrosion", Concrete in the Oceans, Technical Report No. 1, Construction Industry Research and Information Association/Cement and Concrete Association, London 1978, 77 pp.

2.9) **Popovics, S., Simeonov, Y., Bozhinov, G., and Barovsky, N.,** "Durability of Reinforced Concrete in Sea Water," *Chapter 2, Corrosion of Reinforcement in Concrete Construction,* A.P. Crane, Editor, Ellis Horwood, New York, NY, 1983, pp. 19-34.

2.10) **Vaysburg, A.M.,** "Some Durability Considerations for Evaluating and Repairing Concrete Structures," *Concrete International,* Vol. 15, No. 3, March 1993, pp. 29-35.

2.11) **ACI Committee 222,** "Corrosion of Metals in Concrete" (ACI 222R-96), American Concrete Institute, Detroit, MI, 1996, 30pp.

2.12) **Tuutti, K.,** Corrosion of Steel in Concrete, Report 4-82, Swedish Cement and Concrete Research Institute, Stockholm, Sweden, 1982, 469 pp.

2.13) **Arya, C., and Wood, L.A.,** "The Relevance of Cracking in Concrete to Corrosion of Reinforcement," Concrete Society Technical Report No. 44, The Concrete Society, Slough, Berkshire, UK, 1995, 32 pp.

2.14) **Rostam, S.,** "Service Life Design – The European Approach," *Concrete International,* Vol. 15, No. 7, July 1993, pp. 24-32.

2.15) **Fontana, M.G.,** Corrosion Engineering, 3rd Edition, McGraw-Hill, Inc., New York, New York, 1986.

2.16) **Jones, D.A.,** Principles and Prevention of Corrosion, 2nd Edition, Prentice Hall, Inc., Upper Saddle River, NJ, 1996.

2.17) **Hamilton, H.R.,** "Investigation of Corrosion Protection Systems for Bridge Stay Cables," Doctor of Philosophy Dissertation, The University of Texas at Austin, September 1995.

2.18) **Freytag, G.,** "Development of a Field Corrosion Detection and Monitoring Program for Reinforced Concrete Bridges," Master of Science Thesis, The University of Texas at Austin, 1994.

2.19) **Neville, A.M.,** Properties of Concrete, 4th Edition, John Wiley & Sons, New York, NY, 1997, 844 pp.

2.20) **Rasheeduzzafar, Hussain, S.E. and Al-Saadoun, S.S.**, "Effect of Tricalcium Aluminate Content of Cement on Chloride Binding and Corrosion of Reinforcing Steel in Concrete", *ACI Materials Journal*, V. 89, No. 1, Jan.-Feb. 1992, pp. 3-12.

2.21) **Rasheeduzzafar,** "Influence of Cement Composition on Concrete Durability," *ACI Materials Journal*, V. 89, No. 6, Nov.-Dec. 1992, pp. 574-586.

2.22) **Nagataki, S., Otsuki, N., Wee, T. and Nakashita, K.**, "Condensation of Chloride Ion in Hardened Cement Matrix Materials and on Embedded Steel Bars", *ACI Materials Journal*, V. 90, No. 4, July-Aug. 1993, pp. 323-332.

2.23) **Hime, W.G.**, "The Corrosion of Steel - Random Thoughts and Wishful Thinking", *Concrete International*, October 1993, pp. 54-57.

2.24) **Mehta, P.K.**, "Durability of Concrete in Marine Environment - A Review", *Performance of Concrete in Marine Environment*, ACI SP-65, American Concrete Institute, Detroit, Michigan, 1980, pp. 1-20.

2.25) **Lerch, W., Ashton, F.W. and Bogue, R.H.**, "The Sulfoaluminates of Calcium", *Portland Cement Association*, Skokie, Fellowship Paper No. 19, 1929.

2.26) **Kalousek, G.L. and Benton, E.J.** "The Mechanism of Seawater Attack on Cement Pastes", *ACI Journal*, V. 67, No. 2, Feb. 1970, pp. 187-192.

2.27) **Hussain, S.E., Al-Gahtani, A.S., and Rashedduzzafar,** "Chloride Threshold for Corrosion of Reinforcement in Concrete," *ACI Materials Journal,* Vol. 93, No. 6, November-December 1996, pp. 534-538.

2.28) **Hausmann, D.A.,** "Steel Corrosion in Concrete: How Does it Occur?" *Materials Protection,* Vol. 6, No. 11, November 1967, pp. 19-23.

2.29) **Kahhaleh, K.Z.,** "Corrosion Performance of Epoxy Coated Reinforcement," Doctor of Philosophy Dissertation, Department of Civil Engineering, The University of Texas at Austin, May 1994.

2.30) "ACI Forum: Influence of Chlorides in Reinforced Concrete," *Concrete International,* Vol. 7, No. 9, September 1985, pp. 13-19.

2.31) **ACI Committee 318,** "Building Code Requirements for Structural Concrete" (ACI 318-95), American Concrete Institute, Detroit, MI, 1995, 369 pp.

2.32) **Moore, D.G., Klodt, D.T. and Hensen, R.J.,** "Protection of Steel in Prestressed Concrete Bridges," National Co-operative Highway Research Program Report 90, 1970., 86 pp.

2.33) **Nagi, M, and Whiting, D.,** "Corrosion of Prestressed Reinforcing Steel in Concrete Bridges: State-of-the-Art," *Concrete Bridges in Aggressive Environments,* ACI SP-151, American Concrete Institute, Detroit, MI, 1994, pp. 17-41.

2.34) **Woodward, R.J. and Williams, F.W.,** "Collapse of the Ynys-y-Gwas Bridge, West Glamorgan," *Proceeding of The Institution of Civil Engineers*, Part 1, Vol. 84, August 1988, pp. 635-669.

2.35) **ACI Committee 201,** "Guide to Durable Concrete" (ACI 201.2R-92), American Concrete Institute, Detroit, MI, 1992, 41 pp.

2.36) **Saleh, M.A., Einea, A., and Tadros, M.K.,** "Creating Continuity in Precast Girder Bridges," *Concrete International,* Vol. 17, No. 8, August 1995, pp. 27-32.

2.37) **ACI Committee 224**, "Control of Cracking in Concrete Structures," ACI 224R-90, American Concrete Institute, Detroit, MI, 1990, 43 pp.

2.38) **ACI Committee 224,** "Causes, Evaluation, and Repair of Cracks in Concrete Structures," (ACI 224.1R-93), American Concrete Institute, Detroit, MI, 1993, 20 pp.

2.39) **Mindess, S., and Young, J.F.,** Concrete, Prentice-Hall Inc., Englewood Cliffs, New Jersey, 1981.

2.40) **Whiting, D.,** "Permeability of Selected Concretes," *Permeability of Concrete,* ACI SP-108, American Concrete Institute, Detroit, MI, 1988, pp. 195-221.

2.41) **Clear, K.C.,** "Time-to-Corrosion of Reinforcing Steel in Concrete Slabs, Vol. 3: Performance After 830 Daily Salt Applications," Report No. FHWA-RD-76-70, Federal Highway Administration, Washington, D.C., 1976, 64 pp.

2.42) **Al-Amoudi, O.S.B., Rasheeduzzafar, Maslehuddin, M. and Al-Mana, A.I.**, "Prediction of Long-Term Corrosion Resistance of Plain and Blended Cement Concretes," *ACI Materials Journal*, V. 90, No. 6, Nov.-Dec. 1993, pp. 564-570.

2.43) **Mehta, P.K.,** "Pozzolanic and Cementitious By-Products as Mineral Admixtures for Concrete – A Critical Review," *Fly Ash, Silica Fume, Slag and Other Mineral By-Products in Concrete,* ACI SP-79, Vol. 1, American Concrete Institute, Detroit, MI, 1983, pp. 1-46

2.44) **ACI Committee 226**, "Use of Fly Ash in Concrete," ACI 226.3R-87, American Concrete Institute, Detroit, Michigan.

2.45) **Berke, N.S., Scali, M.J., Regan, J.C. and Shen, D.F.**, "Long Term Corrosion Resistance of Steel in Silica Fume and/or Fly Ash Containing Concretes," *Durability of Concrete, Second International Conference*, ACI SP-126, American Concrete Institute, Detroit, Michigan, 1991, pp. 393-415.

2.46) **Sivasundaram, V., Carette, G.G. and Malhotra, V.M.**, "Properties of Concrete Incorporating Low Quantity of Cement and High Volumes of Low-Calcium Fly Ash, *Fly Ash, Silica Fume, Slag and Natural Pozzolans in Concrete - Proceedings, Third International Conference*, ACI SP-114, American Concrete Institute, Detroit, Michigan, 1989, pp. 45-71.

2.47) **Haque, M.N., Kayyali, O.A. and Gopalan, M.K.**, "Fly Ash Reduces Harmful Chloride Ions in Concrete," *ACI Materials Journal*, V. 89, No. 3, May-June 1992, pp. 238-241.

2.48) **Ellis, W.E., Jr., Riggs, E.H. and Butler, W.B.**, "Comparative Results of Fly Ash, Silica Fume and GGBFS in Reducing the Chloride Permeability of Concrete," *Durability of Concrete, Second International Conference*, ACI SP-126, American Concrete Institute, Detroit, Michigan, 1991, pp. 443-447.

2.49) **Saricimen, H., Maslehuddin, M., Al-Tayyib, A.J., and Al-Mana, A.I.,** "Permeability and Durability of Plain and Blended Cement Concretes Cured in Field and Laboratory Conditions," *ACI Materials Journal,* Vol. 92, No. 2, March-April 1995, pp. 111-116.

2.50) **Alhozaimy, A., Soroushian, P., and Mirza, F.,** "Effects of Curing Conditions and Age on Chloride Permeability of Fly Ash Mortar," *ACI Materials Journal,* Vol. 93, No. 1, January-February 1996, pp. 87-95.

2.51) **ACI Committee 308,** "Standard Practice for Curing Concrete" (ACI 308-92), American Concrete Institute, Detroit, MI, 1992, 110 pp.

2.52) **Perenchio, W.F., Fraczek, J., and Pfeifer, D.W.,** "Corrosion Protection of Prestressing Systems in Concrete Bridges," NCHRP 313, Transportation Research Board, Washington, D.C., 1989, 25 pp.

2.53) **Griffin, D.F.,** "Corrosion Inhibitors for Reinforced Concrete," ACI SP-49, *Corrosion of Metals in Concrete,* American Concrete Institute, Detroit, MI, 1975, pp. 95-102.

2.54) **Montani, R.,** "Corrosion Inhibitors – New Options and Possibilities," *Concrete Repair Bulletin,* July-August 1996, pp. 10-14.

2.55) **Berke, N.S.,** "Corrosion Inhibitors in Concrete," *Concrete International,* Vol. 13, No. 7, July 1991, pp. 24-27.

2.56) **AASHTO**, LRFD Bridge Design Specifications, 2nd Edition, American Association of State Highway and Transportation Officials, Washington, D.C., 1998.

2.57) **AASHTO**, LRFD Bridge Construction Specifications, 1st Edition, American Association of State Highway and Transportation Officials, Washington, D.C., 1998.

2.58) **ACI Committee 301,** "Standard Specifications for Structural Concrete" (ACI 301-96), American Concrete Institute, Detroit, MI, 1996, 43 pp.

2.59) **American Society for Testing and Materials,** "Standard Specification for Steel Strand, Uncoated Seven-Wire for Prestressed Concrete," ASTM A416-97, Philadelphia, PA, 1997.

2.60) **American Society for Testing and Materials,** "Standard Specification for Uncoated Stress-Relieved Steel Wire for Prestressed Concrete ," ASTM A421-98, Philadelphia, PA, 1998.

2.61) **American Society for Testing and Materials,** "Standard Specification for Uncoated High-Strength Steel Bar for Prestressing Concrete ," ASTM A722-98, Philadelphia, PA, 1998.

2.62) **McDonald, D.B., Pfeifer, and Blake, G.T.,** "The Corrosion Performance of Inorganic, Ceramic and Metallic-Clad Reinforcing Bars and Solid Metallic Reinforcing Bars in Accelerated Screening Tests," FHWA-RD-96-085, Federal Highway Administration, Mclean, Va, October 1996, 112 pp.

2.63) **Prestressed Concrete Institute Ad Hoc Committee on Epoxy-Coated Strand,** "Guidelines for the Use of Epoxy-Coated Strand," *PCI Journal,* Vol. 38, No. 4, July-August 1993, pp. 26-32.

2.64) **American Society for Testing and Materials,** "Standard Specification for Epoxy-Coated Seven-Wire Prestressing Steel Strand," ASTM A882-92, Philadelphia, PA, 1992.

2.65) **Moore, M.,** "Use of Epoxy-coated Prestressing Strand in Concrete Bridge Structures," FIP - 12th International Congress, Washington, D.C., June 2, 1994.

2.66) **American Society for Testing and Materials,** "Standard Specification for Epoxy-Coated Reinforcing Steel Bars," ASTM A775-97, Philadelphia, PA, 1997.

2.67) **Florida Wire and Cable, Inc.,** Product Information Pamphlet, (not dated).

2.68) "Specifications for Galvanizing DYWIDAG High Strength Threadbar," Dywidag-Systems International, (not dated).

2.69) **American Society for Testing and Materials,** "Standard Specification for Zinc (Hot-Dip Galvanized) Coatings on Iron and Steel Products," ASTM A123-97, Philadelphia, PA, 1997.

2.70) **ACI Committee 440,** "State-of-the-Art Report on Fiber Reinforced Plastic (FRP) Reinforcement for Concrete Structures" (ACI 440R-96), American Concrete Institute, Detroit, MI, 1996, 68 pp.

2.71) **Ganz, H.R.,** "PT-PLUS Plastic Duct System," Report No. 241e, VSL International Ltd., Berne, Switzerland, October 1992, 13 pp. (see also Ganz, H.R., and Gnaegi, A., "Plastic Ducts for Enhanced Performance of Post-tensioning Tendons," http://www.vsl-intl.com/ptplus2.htm).

2.72) **Wollman, G.P., Yates, D.L., and Breen, J.E.,** "Fretting Fatigue in Post-Tensioned Concrete," Research Report 465-2F, Center for Transportation Research, The University of Texas at Austin, November 1988.

2.73) "VSL Post-Tensioning Systems," Product Information Pamphlet, VSL Corporation, (undated).

2.74) **PTI Committee on Grouting Specifications,** "Guide Specification for Grouting of Post-Tensioned Structures," 5th Draft, Post-Tensioning Institute, Phoenix, AZ, November 1997, 37 pp.

2.75) **Kittleman, W.M., Davis, R.T., Hamilton, H.R., Frank, K.H., and Breen, J.E.,** "Evaluation of Agents for Lubrication and Temporary Corrosion Protection of Post-Tension Tendons," Research Report CTR 0-1264-1, Center for Transportation Research, The University of Texas at Austin, August 1993, 104 pp.

2.76) **Thompson, N.G., Lankard, D., and Sprinkel, M.,** "Improved Grouts for Bonded Tendons in Post-Tensioned Bridge Structures," Report No. FHWA-RD-91-092, Federal Highway Administration, McLean VA, January 1992, 146 pp.

2.77) **Schokker, Andrea J.,** "Improving Corrosion Resistance of Post-Tensioned Substructures Emphasizing High Performance Grouts," Doctor of Philosophy Dissertation, The University of Texas at Austin, May 1999.

2.78) "Durable Bonded Post-Tensioned Concrete Bridges," Technical Report No. 47, The Concrete Society, Slough, Berkshire, U.K., August 1996, 64 pp.

2.79) "VSL Composite System," Product Information Pamphlet, VSL Corporation, (undated).

2.80) Post-Tensioning Manual, 5th Edition, Post-Tensioning Institute, Phoenix, AZ, 1990, 406 pp.

2.81) "Specifications for Unbonded Single Strand Tendons," revised 1993, Post-Tensioning Institute, Phoenix, AZ, 1993, 20 pp.

2.82) **ACI Committee 423,** "Recommendations for Concrete Members Prestressed with Unbonded Tendons" (ACI 423.3R-96), American Concrete Institute, Detroit, MI, 1996, 19 pp.

2.83) **Freeman, R.B.,** "Optimization of the Physical and Compositional Characteristics of Fly Ash Cement for the Production of Sulfate Resistant Concrete," Doctor of Philosophy Dissertation, The University of Texas at Austin, August 1992.

2.84) **Wolf, Lloyd,** Personal Communication, Texas Department of Communication, February 1994.

2.85) **Tikalsky, P.J.,** "The Effect of Fly Ash on the Sulfate Resistance of Concrete," Doctor of Philosophy Dissertation, The University of Texas at Austin, August 1989.

2.86) **American Society for Testing and Materials,** "Standard Specification for Portland Cement," ASTM C150-97a, Philadelphia, PA, 1997.

2.87) **Ellis, W.E., Jr.,** "For Durable Concrete, Fly Ash Does Not Replace Cement," *Durable Concrete,* ACI Compilation 24, American Concrete Institute, Detroit, Michigan, 1993.

2.88) **American Society for Testing and Materials,** "Standard Specification for Coal Fly Ash and Raw or Calcined Natural Pozzolan for Use as a Mineral Admixture in Concrete," ASTM C618-98, Philadelphia, PA, 1998.

2.89) **Hooton, R.D.,** "Influence of Silica Fume Replacement of Cement on Physical Properties and Resistance to Sulfate Attack, Freezing and Thawing, and Alkali-Silica Reactivity," *ACI Materials Journal,* Vol. 90, No. 2, March-April 1993, pp. 143-151.

2.90) **Mangat, P.S., and Khatib, J.M.,** "Influence of Fly Ash, Silica Fume, and Slag on Sulfate Resistance of Concrete," *ACI Materials Journal,* Vol. 92, No. 5., September-October 1995, pp. 542-552.

2.91) **Pierce, James,** "Use of Fly Ash in Combating Sulfate Attack in Concrete," U.S. Bureau of Reclamation, 1982.

2.92) **ACI Committee 212,** "Chemical Admixtures for Concrete," ACI 212.3R-91, American Concrete Institute, Detroit, MI, 1991, 32 pp.

2.93) **Nasser, K.W., and Lai, P.S.H.,** "Resistance of Fly Ash Concrete to Freezing and Thawing," *Fly Ash, Silica Fume, Slag and Natural Pozzolans in Concrete,* Vol. 1, ACI SP-132, V.M. Malhotra, Editor, American Concrete Institute, Detroit, MI, 1992, pp. 205-226.

2.94) **Yamoto, T, Emoto, Y., and Soeda, M.,** "Strength and Freezing-and-Thawing Resistance of Concrete Incorporating Condensed Silica Fume", *Fly Ash, Silica Fume, Slag and Natural Pozzolans in Concrete,* Vol. 2, ACI SP-91, V.M. Malhotra, Editor, American Concrete Institute, Detroit, MI, 1986, pp. 1095-1117.

2.95) **Naik, T.R., Ramme, B.W., and Tews, J.H.,** "Pavement Construction with High-Volume Class C and Class F Fly Ash Concrete," *ACI Materials Journal,* Vol. 92, No. 2, March-April 1995, pp. 200-210.

2.96) **Johnston, C.D.,** "Durability of High Early Strength Silica Fume Concretes Subjected to Accelerated and Normal Curing," *Fly Ash, Silica Fume, Slag and Natural Pozzolans in Concrete,* Vol. 2, ACI SP-132, V.M. Malhotra, Editor, American Concrete Institute, Detroit, MI, 1992, pp. 1167-1187.

2.97) **Hooton, R.D.,** "Influence of Silica Fume Replacement of Cement on Physical Properties and Resistance to Sulfate Attack, Freezing and Thawing, and Alkali-Silica Reactivity," *ACI Materials Journal,* Vol. 90, No. 2, March-April 1993, pp. 143-151.

2.98) **American Society for Testing and Materials,** "Standard Test Method for Resistance of Concrete to Rapid Freezing and Thawing," ASTM C666-97, Philadelphia, PA, 1997.

2.99) **American Society for Testing and Materials,** "Standard Test Method for Critical Dilation of Concrete Specimens Subjected to Freezing," ASTM C671-94, Philadelphia, PA, 1994.

2.100) **American Society for Testing and Materials,** "Standard Practice for Evaluation of Frost Resistance of Coarse Aggregates in Air-Entrained Concrete by Critical Dilation Procedures," ASTM C682-98, Philadelphia, PA, 1998.

2.101) **Spencer, T.E., and Blaylock, A.J.,** "Alkali-Silica Reaction in Marine Piles," *Concrete International,* Vol. 19, No. 1, January 1997, pp. 59-62.

2.102) **Carrasquillo, R.L., and Snow, P.G.,** "Effect of Fly Ash on Alkali-Aggregate Reaction in Concrete," *ACI Materials Journal,* Vol. 84., No. 4, July-August 1987, pp. 299-305.

2.103) **Tobin, R.E.,** "Reactive Aggregates and Popouts – Causes and Prevention," *Concrete International,* Vol. 17, No. 1, January 1995, pp. 52-54.

2.104) **Kakodkar, S., Ramakrishnan, V., and Zimmerman, L.,** "Addition of Class C Fly ash to Control Expansions Due to Alkali-Silica Reaction," *Transportation Research Record 1458,* Materials and Construction, Concrete Research, National Academy Press, Washington, D.C., 1994, pp. 109-117.

2.105) **American Society for Testing and Materials,** "Standard Test Method for Effectiveness of Mineral Admixtures or Ground Blast-Furnace Slag in Preventing Excessive Expansion of Concrete Due to the Alkali-Silica Reaction," ASTM C441-97, Philadelphia, PA, 1997.

2.106) **FIP Commission on Durability.** Report. Proceedings of the Sixth FIP Congress, Prague, 1970, pp. 59-66.

2.107) **Freyermuth, C.L.,** "Durability of Post-Tensioned Prestressed Concrete Structures," *Concrete International,* Vol. 13, No. 10, October 1991, pp. 58-65.

2.108) **Szilard, R.,** "Survey on Durability of Prestressed Concrete Structures in the United States, Canada, and Pacific and Far Eastern Countries," *Prestressed Concrete Institute Journal*, Vol. 14, October 1969, pp. 62-73.

2.109) **Moore, D.G., Klodt, D.T. and Hensen, R.J.,** "Protection of Steel in Prestressed Concrete Bridges," National Co-operative Highway Research Program Report 90, 1970.

2.110) **Schupack, M.A.,** "A Survey of Durability Performance of Post-Tensioning Tendons," *Proceedings of the American Concrete Institute*, Vol. 75, No. 10, October 1978, pp. 501-510.

2.111) **Dunker, K.F. and Rabbat, B.G.,** "Performance of Highway Bridges," *Concrete International*, Vol. 12, No. 8, August 1990, pp. 40-42.

2.112) **Miller, M.D.,** "Durability Survey of Segmental Concrete Bridges," *PCI Journal*, Vol. 40, No. 3, May-June 1995, pp. 110-123.

2.113) **Tanaka, Y., Kurauchi, M., and Masuda, Y.,** Ten Year Marine Atmosphere Exposure Test of Unbonded Prestressed Concrete Prisms, Post-Tensioning Institute, Phoenix, AZ, 1988, 35 pp.

2.114) **Etienne, C.F., Binnekamp, D.C., Copier, W.J., Hendrickx, R., and Smit, C.L.,** "Corrosion Protection of Unbonded Tendons," *Heron,* Vol. 26, No. 3, 1981, 74 pp.

2.115) **O'Neil, E.F.,** "Durability and Behavior of Prestressed Concrete Beams – Report 4: Post-tensioned Concrete Beam Investigation with Laboratory Tests From June 1961 to September 1975," Technical Report No. 6-570, Dept. of the Army, Washington, DC, February 1977, 172 pp.

2.116) **Schupack, M.,** "Behavior of 20 Post-Tensioned Beams Subjected to up to 2200 Cycles of Freezing and Thawing in the Tidal Zone at Treat Island, Maine," *Performance of Concrete in a Marine Environment,* ACI SP-65, American Concrete Institute, Detroit, MI, 1980, pp. 133-152.

2.117) **O'Neil, E.F., and Odom, G.L.,** "Durability and Behavior of Prestressed Concrete Beams – Report 6: Post-tensioned Concrete Beam Investigation, Supplemental Laboratory Tests of Beams Exposed From 1961 to 1982," Technical Report No. 6-570, Dept. of the Army, Washington, DC, October 1984, 40 pp.

2.118) **Poston, R.W.,** "Improving Durability of Bridge Decks by Transverse Prestressing," Doctor of Philosophy Dissertation, The University of Texas at Austin, December

1984. (see also Poston, R.W., Carrasquillo, R.L., and Breen, J.E., "Durability of Post-Tensioned Bridge Decks," *ACI Materials Journal,* Vol. 84, No. 4, July-August 1987, pp. 315-326.)

2.119) **Batchelor, B.,DEV., and El Shahawi, M.,** "A Review of Cracking of Partially Prestressed Concrete Members," *Canadian Journal of Civil Engineering*, Vol. 12, 1985, pp. 645-652.

2.120) **Gergely, P., and Lutz. L.A.,** "Maximum Crack Width in Reinforced Concrete Flexural Members," ACI SP-20, American Concrete Institute, Detroit, MI, 1968, pp. 87-117.

2.121) **Armstrong, S.D., Salas, R.M., Wood, B.A., Breen, J.E. and Kreger, M.E.,** "Behavior and Design of Large Structural Bridge Pier Overhangs," Research Report 1364-1, Center for Transportation Research, The University of Texas at Austin, 1997, 272 pp.

2.122) **CEB-FIP,** Model Code for Concrete Structures: CEB-FIP International Recommendations, 3rd Edition, Comité Euro-International du Béton, Paris, 1978, 348 pp.

2.123) **CEB,** Design Manual on Cracking and Deformations, Comité Euro-International du Béton, École Polytechnique Fédérale De Lausanne, Suisse, 1985, 231 pp.

2.124) **CEB-FIP,** CEB-FIP Model Code for Concrete Structures 1990, Bulletin D'Information No. 213/214, Comité Euro-International du Béton, Lausanne, May 1993, 437 pp.

2.125) **Suri, K.M., and Dilger, W.H.,** "Crack Width of Partially Prestressed Concrete Members," *ACI Journal,* Vol. 83, No. 5, September-October 1986, pp. 784-797.

Chapter 3 References

3.1) **Schokker, Andrea J.,** "Improving Corrosion Resistance of Post-Tensioned Substructures Emphasizing High Performance Grouts," Doctor of Philosophy Dissertation, The University of Texas at Austin, May 1999.

3.2) "VSL Post-Tensioning Systems," Product Information Pamphlet, VSL Corporation, (undated).

3.3) **AASHTO**, LRFD Bridge Design Specifications, 2nd Edition, American Association of State Highway and Transportation Officials, Washington, D.C., 1998.

3.4) **ACI Committee 318,** "Building Code Requirements for Structural Concrete" (ACI 318-95), American Concrete Institute, Detroit, MI, 1995, 369 pp.

3.5) **Breen, J.E., Burdet, O., Roberts, C., Sanders, D. and Wollman, G.,** "Anchorage Zone Reinforcement for Post-Tensioned Concrete Girders," NCHRP Report 356, Transportation Research Board, Washington, D.C., 1994, 204pp.

3.6) **Armstrong, S.D., Salas, R.M., Wood, B.A., Breen, J.E. and Kreger, M.E.,** "Behavior and Design of Large Structural Bridge Pier Overhangs," Research Report 1364-1, Center for Transportation Research, The University of Texas at Austin, 1997, 272 pp.

3.7) **Gergely, P., and Lutz. L.A.,** "Maximum Crack Width in Reinforced Concrete Flexural Members," ACI SP-20, American Concrete Institute, Detroit, MI, 1968, pp. 87-117.

3.8) **Collins M.P., and Mitchell, D.,** Prestressed Concrete Structures, Prentice Hall, NJ, 1991.

3.9) **Park R., and Paulay, T.,** Reinforced Concrete Structures, John Wiley and Sons, Inc., New York, 1975.

3.10) **Klingner, R.,** "Advanced Reinforced Concrete Structures," Course Notes CE383N, The University of Texas at Austin, 1994.

3.11) **Ghali, A., and Favre, R.**, Concrete Structures: Stresses and Deformations, 2nd. Edition, E & FN Spon, London, 1994. (see also Ghali, A., "Stress and Strain Analysis in Prestressed Concrete: A Critical Review," *PCI Journal*, Vol. 34, No. 6, November-December 1989, pp. 80-97.)

3.12) **ACI Committee 209,** "Prediction of Creep, Shrinkage and Temperature Effects in Concrete Structures" (ACI 209R-92), American Concrete Institute, Detroit, Michigan, 1992.

3.13) Standard Specifications for Construction of Highways, Streets and Bridges, Texas Department of Transportation, March 1995.

3.14) Standard Specifications for Construction of Highways, Streets and Bridges, Special Provision to Item 426 (Prestressing), Sub-Section: Construction Methods, Texas Department of Transportation, 1995. (also, personal communication with Dean Van Landuyt, Texas Department of Transportation, April 1997.)

3.15) **ASTM,** "Standard Specification for Coal Fly Ash and Raw or Calcined Natural Pozzolan for Use as a Mineral Admixture in Concrete," ASTM C618-98, American Society for Testing and Materials, Philadelphia, PA, 1998.

3.16) **PTI Committee on Grouting Specifications,** "Guide Specification for Grouting of Post-Tensioned Structures," 5th Draft, Post-Tensioning Institute, Phoenix, AZ, November 1997, 37 pp.

3.17) **ASTM**, "Standard Test Method for Determining the Effects of Chemical Admixtures on the Corrosion of Embedded Steel Reinforcement in Concrete Exposed to Chloride Environments," ASTM G109-92, American Society for Testing and Materials, Philadelphia, PA, 1992.

3.18) **Silvestri, Giovanni**, Personal Communication, VSL Corporation, Grand Prairie, TX, March 1997.

3.19) **AASHTO**, LRFD Bridge Construction Specifications, 1st Edition, American Association of State Highway and Transportation Officials, Washington, D.C., 1998.

3.20) **ASTM**, "Standard Test Method for Half-Cell Potentials of Uncoated Reinforcing Steel in Concrete," ASTM C876-91, American Society for Testing and Materials, Philadelphia, Pa., 1991.

3.21) **AASHTO**, Standard Method of Test for Resistance of Concrete to Chloride Ion Penetration," AASHTO Designation T 259-80, American Association of State Highway and Transportation Officials, Washington, D.C., 1980.

3.22) **AASHTO**, Standard Method of Test for Sampling and Testing for Chloride Ion in Concrete and Concrete Raw Materials," AASHTO Designation T 260-94, American Association of State Highway and Transportation Officials, Washington, D.C., 1994.

3.23) **Fontana, M.G.,** Corrosion Engineering, 3rd Edition, McGraw-Hill, Inc., New York, New York, 1986.

3.24) **Jones, D.A.,** Principles and Prevention of Corrosion, 2nd Edition, Prentice Hall, Inc., Upper Saddle River, NJ, 1996.

3.25) **Flis, J., Sehgal, A., Li, D., Kho, Y, Sabol, S., Pickering, H., Osseo-Asare, K, and Cady, P.D.,** "Condition Evaluation of Concrete Bridges Relative to Reinforcement Corrosion, Volume 2: Method for Measuring the Corrosion Rate of Reinforcing Steel," SHRP-S/FR-92-104, Strategic Highway Research Program, Washington, D.C., 1992, 105 pp.

3.26) **Clear, K.,** "Measuring the Rate of Corrosion of Steel in Field Concrete Structures," Transportation Research Record 1211, pp. 28-37, 1989.

3.27) **Andrade, C., Castelo, V., Alonso, C. and Gonzalez, J.A.,** "The Determination of Corrosion Rate of Steel Embedded in Concrete by the Polarization Resistance and AC Impedance Methods," Corrosion Effect of Stray Currents and the Techniques for Evaluating Corrosion of Rebars in Concrete, ASTM STP 906, V. Chaker, Editor, American Society for Testing and Materials, Philadelphia, PA, 1986, pp. 43-63.

3.28) **CONCORR, Inc.,** "FHWA – SHRP Showcase: Assessment of Physical Condition of Concrete Bridge Components," Federal Highway Administration, Washington, D.C., July 1996.

3.29) **Cady, P., and Gannon, E.,** "Condition Evaluation of Concrete Bridges Relative to Reinforcement Corrosion, Volume 8: Procedure Manual," SHRP-S/FR-92-330, Strategic Highway Research Program, Washington, D.C., 1992, 124 pp.

3.30) **Kahhaleh, K.Z.,** "Corrosion Performance of Epoxy-Coated Reinforcement," Doctor of Philosophy Dissertation, The University of Texas at Austin, May 1994.

3.31) **Wheat, H.G., and Eliezer, Z.,** "Some Electrochemical Aspects of Corrosion of Steel in Concrete," *Corrosion*, Vol. 41, No. 11, November 1985, pp. 640-645.

3.32) **ACI Committee 222,** "Corrosion of Metals in Concrete," ACI 222R-96, American Concrete Institute, Detroit, Michigan, 1996.

3.33) **CEB-FIP,** Model Code for Concrete Structures: CEB-FIP International Recommendations, 3rd Edition, Comité Euro-International du Béton, Paris, 1978, 348 pp.

3.34) **CEB-FIP,** CEB-FIP Model Code for Concrete Structures 1990, Bulletin D'Information No. 213/214, Comité Euro-International du Béton, Lausanne, May 1993, 437 pp.

3.35) **Batchelor, B.DEV., and El Shahawi, M.,** "A Review of Cracking of Partially Prestressed Concrete Members," *Canadian Journal of Civil Engineering*, Vol. 12, 1985, pp. 645-652.

3.36) **Suri, K.M., and Dilger, W.H.,** "Crack Width of Partially Prestressed Concrete Members," *ACI Journal,* Vol. 83, No. 5, September-October 1986, pp. 784-797.

3.37) **Verhulst, S.M.,** "Evaluation and Performance Monitoring of Corrosion Protection Provided by Fiber-Reinforced Composite Wrapping," Master of Science Thesis, The University of Texas at Austin, May 1999.

Chapter 4 References

4.1) **AASHTO**, LRFD Bridge Design Specifications, 2nd Edition, American Association of State Highway and Transportation Officials, Washington, D.C., 1998.

4.2) **Texas State Department of Highways and Public Transportation,** Bridge Design Guide, First Edition, Austin, Texas, 1990.

4.3) **Collins M.P., and Mitchell, D.,** Prestressed Concrete Structures, Prentice Hall, NJ, 1991.

4.4) Standard Specifications for Construction of Highways, Streets and Bridges, Texas Department of Transportation, March 1995.

4.5) **ASTM,** "Standard Specification for Coal Fly Ash and Raw or Calcined Natural Pozzolan for Use as a Mineral Admixture in Concrete," ASTM C618-98, American Society for Testing and Materials, Philadelphia, PA, 1998.

4.6) **ASTM**, "Standard Specification for Epoxy-Coated Reinforcing Steel Bars," ASTM A775-97, Philadelphia, PA, 1997.

4.7) **ASTM**, "Standard Test Method for Determining the Effects of Chemical Admixtures on the Corrosion of Embedded Steel Reinforcement in Concrete Exposed to Chloride Environments," ASTM G109-92, American Society for Testing and Materials, Philadelphia, PA, 1992.

4.8) **ASTM**, "Standard Test Method for Half-Cell Potentials of Uncoated Reinforcing Steel in Concrete," ASTM C876-91, American Society for Testing and Materials, Philadelphia, Pa., 1991.

4.9) **AASHTO**, Standard Method of Test for Sampling and Testing for Chloride Ion in Concrete and Concrete Raw Materials," AASHTO Designation T 260-94, American Association of State Highway and Transportation Officials, Washington, D.C., 1994.

4.10) **ACI Committee 222,** "Corrosion of Metals in Concrete," ACI 222R-96, American Concrete Institute, Detroit, Michigan, 1996.

4.11) **Kahhaleh, K.Z.,** "Corrosion Performance of Epoxy-Coated Reinforcement," Doctor of Philosophy Dissertation, The University of Texas at Austin, May 1994.

4.12) **Wheat, H.G., and Eliezer, Z.,** "Some Electrochemical Aspects of Corrosion of Steel in Concrete," *Corrosion*, Vol. 41, No. 11, November 1985, pp. 640-645.

4.13) **Fontana, M.G.,** Corrosion Engineering, 3rd Edition, McGraw-Hill, Inc., New York, New York, 1986.

4.14) **Elsener, B., and Böhni, H.,** "Potential Mapping and Corrosion of Steel in Concrete," Corrosion Rates of Steel in Concrete, ASTM STP 1065, Berke, N.S., Chaker, V., and Whiting, D., Editors, American Society for Testing and Materials, Philadelphia, PA, 1990, pp. 143-156.

4.15) **Vaca-Cortes, Enrique**, "Corrosion Performance of Epoxy-Coated Reinforcement in Aggressive Environments," Doctor of Philosophy Dissertation, The University of Texas at Austin, May 1998.

4.16) **Schokker, Andrea J.,** "Improving Corrosion Resistance of Post-Tensioned Substructures Emphasizing High Performance Grouts," Doctor of Philosophy Dissertation, The University of Texas at Austin, May 1999.

Chapter 5 References

5.1) **AASHTO**, Guide Specifications for Design and Construction of Segmental Concrete Bridges, American Association of State Highway and Transportation Officials, Washington, D.C., 1989.

5.2) **Woodward, R.J. and Williams, F.W.,** "Collapse of the Ynys-y-Gwas Bridge, West Glamorgan," *Proceeding of The Institution of Civil Engineers*, Part 1, Vol. 84, August 1988, pp. 635-669.

5.3) **Miller, Maurice D.**, "Durability Survey of Segmental Concrete Bridges," *PCI Journal*, Vol. 40, No. 3, May-June 1995, pp. 110-123.

5.4) **Vignos, R.P.**, "Test Method for Evaluating the Corrosion Protection of Internal Tendons Across Segmental Bridge Joints." Master of Science Thesis, The University of Texas at Austin, May 1994.

5.5) **ASTM**, "Standard Test Method for Determining the Effects of Chemical Admixtures on the Corrosion of Embedded Steel Reinforcement in Concrete Exposed to Chloride Environments," ASTM G109-92, American Society for Testing and Materials, Philadelphia, PA, 1992.

5.6) **ASTM**, "Standard Test Method for Half-Cell Potentials of Uncoated Reinforcing Steel in Concrete," ASTM C876-91, American Society for Testing and Materials, Philadelphia, Pa., 1991.

5.7) **Broomfield, J.P., Rodriguez, J., Ortega, L.M., and Garcia, A.M.**, "Corrosion Rate Measurement and Life Prediction for Reinforced Concrete Structures," Proceedings of the 5th International Conference on Structural Faults and Repair held on June 29, 1993, Vol. 2, Venue, University of Edinburgh, pp 155-163.

5.8) **Al-Qadi, I.L., Peterson, J.E., and Weyers, R.E.**, "A Time to Cracking Model for Critically Contaminated Reinforced Concrete Structures," Proceedings of the 5th International Conference on Structural Faults and Repair held on June 29, 1993, Vol. 3, Venue, University of Edinburgh, pp 91-99.

5.9) **Concrete Reinforcing Steel Institute**, "CRSI Performance Research: Epoxy-Coated Reinforcing Steel," Interim Report, CRSI, Schaumburg, Ill, January 1992.

5.10) **Virmani, Y.P., Clear, K.C., and Pasko, T.J.**, "Time-to-Corrosion of Reinforcing Steel in Concrete Slabs, Vol. 5,: Calcium Nitrite Admixture or Epoxy-Coated Reinforcing Bars as Corrosion Protection Systems," Report No. FHWA/RD-83/012, Federal Highway Administration, Washington, D.C., September 1983, 71p.

5.11) **AASHTO.** "Sampling and Testing for Chloride Ion in Concrete and Concrete Raw Materials," AASHTO T 260-94, American Association of State Highway and Transportation Officials, Washington, D.C., 1994.

5.12) **Poston, R.W.,** "Improving Durability of Bridge Decks by Transverse Prestressing," Doctor of Philosophy Dissertation, The University of Texas at Austin, 1984.

5.13) **Hamilton, H.R.,** "Investigation of Corrosion Protection Systems for Bridge Stay Cables," Doctor of Philosophy Dissertation, The University of Texas at Austin, 1995.

5.14) **Sason, A.S.,** "Evaluation of Degree of Rusting on Prestressed Concrete Strand," *PCI Journal*, Vol. 37, No. 3, May-June 1992, pp. 25-30.

5.15) **Wouters, J.P.,** Personal Communication, Whitlock Dalrymple Poston and Associates, Inc., Manassas, Virginia, July 1998.

5.16) **ACI Committee 222,** "Corrosion of Metals in Concrete," ACI 222R-96, American Concrete Institute, Detroit, Michigan, 1996.

5.17) **Vaca-Cortes, Enrique**, "Corrosion Performance of Epoxy-Coated Reinforcement in Aggressive Environments," Doctor of Philosophy Dissertation, The University of Texas at Austin, May 1998.

5.18) **Koester, B.D.,** "Evaluation of Cement Grouts for Strand Protection Using Accelerated Corrosion Tests," Master of Science Thesis, The University of Texas at Austin, December 1995.

5.19) **Berke, N.S., Dallaire, M.P., Hicks, M.C. and Hoopes, R.J.,** "Corrosion of Steel in Cracked Concrete," *Corrosion*, Vol. 49, No. 11, November 1993, pp. 934-943.

5.20) **Pfeifer, D.W., Landgren, J.R. and Zoob, A.,** "Protective Systems for New Prestressed and Substructure Concrete," FHWA/RD-86/193, Federal Highway Administration, Washington, D.C., April 1987.

Chapter 6 References

6.1) **Watkins, D.A.,** "Specification of Air Entrainment for Freezing and Thawing Environments," Master of Science Thesis, The University of Texas at Austin, August 1997.

6.2) **ACI Committee 201,** "Guide to Durable Concrete" (ACI 201.2R-92), American Concrete Institute, Detroit, MI, 1992, 41 pp.

6.3) **American Society for Testing and Materials,** "Standard Test Method for Resistance of Concrete to Rapid Freezing and Thawing," ASTM C666-97, Philadelphia, PA, 1997.

6.4) **American Society for Testing and Materials,** "Standard Test Method for Critical Dilation of Concrete Specimens Subjected to Freezing," ASTM C671-94, Philadelphia, PA, 1994.

6.5) **American Society for Testing and Materials,** "Standard Practice for Evaluation of Frost Resistance of Coarse Aggregates in Air-Entrained Concrete by Critical Dilation Procedures," ASTM C682-98, Philadelphia, PA, 1998.

6.6) **American Society for Testing and Materials,** "Standard Specification for Portland Cement," ASTM C150-97a, Philadelphia, PA, 1997.

6.7) **American Society for Testing and Materials,** "Standard Specification for Coal Fly Ash and Raw or Calcined Natural Pozzolan for Use as a Mineral Admixture in Concrete," ASTM C618-98, Philadelphia, PA, 1998.

6.8) **AASHTO**, LRFD Bridge Construction Specifications, 1st Edition, American Association of State Highway and Transportation Officials, Washington, D.C., 1998.

6.9) **Freeman, R.B.,** "Optimization of the Physical and Compositional Characteristics of Fly Ash Cement for the Production of Sulfate Resistant Concrete," Doctor of Philosophy Dissertation, The University of Texas at Austin, August 1992.

6.10) **AASHTO**, LRFD Bridge Design Specifications, 2nd Edition, American Association of State Highway and Transportation Officials, Washington, D.C., 1998.

6.11) Standard Specifications for Construction of Highways, Streets and Bridges, Texas Department of Transportation, March 1995.

6.12) **American Association of State Highway and Transportation Officials,** "Rapid Determination of the Chloride Permeability of Concrete," AASHTO T277, Washington, D.C., 1983.

6.13) **American Society for Testing and Materials,** "Standard Test Method for Electrical Indication of Concrete's Ability to Resist Chloride Ion Penetration," ASTM C1202-97, Philadelphia, PA, 1997.

6.14) **Goodspeed, C.H., Vanikar, S., and Cook, R.A.,** "High Performance Concrete Defined for Highway Structures," *Concrete International*, Vol. 18, No. 2, February, 1996, pp. 62-67.

6.15) **Vaca-Cortes, Enrique**, "Corrosion Performance of Epoxy-Coated Reinforcement in Aggressive Environments," Doctor of Philosophy Dissertation, The University of Texas at Austin, May 1998.

6.16) **Kahhaleh, K.Z.,** "Corrosion Performance of Epoxy Coated Reinforcement," Doctor of Philosophy Dissertation, Department of Civil Engineering, The University of Texas at Austin, May 1994.

6.17) **Koester, B.D.,** "Evaluation of Cement Grouts for Strand Protection Using Accelerated Corrosion Tests," Master of Science Thesis, The University of Texas at Austin, December 1995.

6.18) **Hamilton, H.R.,** "Investigation of Corrosion Protection Systems for Bridge Stay Cables," Doctor of Philosophy Dissertation, The University of Texas at Austin, September 1995.

6.19) Standard Specifications for Construction of Highways, Streets and Bridges, Special Provision to Item 426 (Prestressing), Sub-Section: Construction Methods, Texas Department of Transportation, 1995. (also, personal communication with Dean Van Landuyt, Texas Department of Transportation, April 1997.)

6.20) **Vincentsen, L.J. and Henriksen, K.R.**, "The Great Belt Link - Built to Last," *Concrete International*, Vol. 14, No. 7, July, 1992, pp. 30-33.

6.21) **Rasheeduzzafar, Dakhil, F.H., Bader, M.A., and Kahn, M.M.**, "Performance of Corrosion Resisting Steels in Chloride-Bearing Concrete," *ACI Materials Journal*, Vol. 89, No. 5, September-October 1992, pp. 439-448.

6.22) **McDonald, D.B., Sherman, M.R., Pfeifer, D.W., and Virmani, Y.P.**, "Stainless Steel Reinforcing as Corrosion Protection," *Concrete International*, Vol. 17, No. 5, May 1995.

6.23) **McDonald, D.B., Pfeifer, and Blake, G.T.,** "The Corrosion Performance of Inorganic, Ceramic and Metallic-Clad Reinforcing Bars and Solid Metallic Reinforcing Bars in Accelerated Screening Tests," FHWA-RD-96-085, Federal Highway Administration, Mclean, Va, October 1996, 112 pp.

6.24) **Perenchio, W.F., Fraczek, J., and Pfeifer, D.W.,** "Corrosion Protection of Prestressing Systems in Concrete Bridges," NCHRP 313, Transportation Research Board, Washington, D.C., 1989, 25 pp.

6.25) **Schokker, Andrea J.,** "Improving Corrosion Resistance of Post-Tensioned Substructures Emphasizing High Performance Grouts," Doctor of Philosophy Dissertation, The University of Texas at Austin, May 1999.

6.26) **American Society for Testing and Materials,** "Standard Test Method for Flow of Grout for Preplaced-Aggregate Concrete (Flow Cone Method)," ASTM C939-97, Philadelphia, PA, 1997.

6.27) "Durable Bonded Post-Tensioned Concrete Bridges," Technical Report No. 47, The Concrete Society, Slough, Berkshire, U.K., August 1996, 64 pp.

6.28) **Silvestri, Giovanni**, VSL Corporation, Grand Prairie, Texas, Personal Communication, June 1996.

Appendix A References

A.1) **Koester, Bradley D.,** "Evaluation of Cement Grouts for Strand Protection Using Accelerated Corrosion Tests," Master of Science Thesis, The University of Texas at Austin, December 1995.

A.2) **ACI Committee 318,** Building Code Requirements for Reinforced Concrete, ACI 318-95, American Concrete Institute, Detroit, MI, 1995, 369 pp.

A.3) **Gergely, P. and Lutz, L.A.,** "Maximum Crack Width in Reinforced Concrete Members," SP-20, American Concrete Institute, Detroit, MI, 1968, pp. 87-117.

A.4) **AASHTO**, LRFD Bridge Design Specifications, 2nd Edition, American Association of State Highway and Transportation Officials, Washington, D.C., 1998.

A.5) Design of Concrete Structures for Buildings, CAN3-A23.3-M84, Canadian Standards Association, Rexdale, Ontario, 1984.

A.6) Ontario Highway Bridge Design Code, 3rd Edition, Ontario Ministry of Transportation, Quality and Standards Division, Toronto, Ontario, 1991.

A.7) Commentary - Ontario Highway Bridge Design Code, Ontario Ministry of Transportation, Quality and Standards Division, Toronto, Ontario, 1991.

A.8) CEB-FIP Model Code 1990, CEB Information Report No. 213/214, Comite Euro-International Du Beton, Lausanne, May 1993.

A.9) Code of Practice for the Structural Use of Concrete - Part 1. Design, Materials and Workmanship, British Standards Institution Publication CP 110, London, England, November 1972 (Amended May 1977).

A.10) Concrete Structures, SIA Standard 162, Swiss Society of Engineers and Architects, Zurich, Switzerland, July, 1989.

A.11) Standard Specification for Design and Construction of Concrete Structures - 1986, Part 1 (Design), Japan Society of Civil Engineers, SP-1, Tokyo, Japan, 1986.

A.12) **ACI Committee 201,** "Guide to Durable Concrete," ACI 201.2R-92, American Concrete Institute, Detroit, Michigan.

A.13) **ACI Committee 222,** "Corrosion of Metals in Concrete," ACI 222R-89, American Concrete Institute, Detroit, Michigan.

A.14) **Atimtay, E., and Ferguson, P.M.,** "Early Chloride Corrosion of Reinforced Concrete - A Test Report," *Materials Performance*, V. 13, No. 12, 1974, pp. 18-21.

A.15) **Martin, H., and Schiessl, P.,** "The Influence of Cracks on the Corrosion of Steel in Concrete," *Preliminary Report*, RILEM International Symposium on the Durability of Concrete, Prague, 1969, V. 2.

A.16) **Raphael, M. and Shalon, R.,** "A Study of the Influence of Climate on the Corrosion of Reinforcement," *Proceedings*, RILEM Symposium on Concrete and Reinforced Concrete In Hot Countries, Building Research Station, Haifa, 1971, pp. 77-96.

A.17) **ACI Committee 224,** "Control of Cracking in Concrete Structures," ACI 224R-90, American Concrete Institute, Detroit, Michigan.

A.18) **Nawy, Edward, G.,** "Crack Control in Reinforced Concrete Structures," ACI JOURNAL, *Proceedings* V. 65, No. 10, Oct. 1968, pp. 825-836.

A.19) **U.S. Bureau of Public Roads - Bridge Division,** Strength and Serviceability Criteria - Reinforced Concrete Bridge Members, U.S. Department of Transportation, Washington, D.C., 1967.

A.20) **ACI Committee 350,** "Environmental Engineering Concrete Structures," ACI 350R-89, American Concrete Institute, Detroit, Michigan.

A.21) **CEB,** Durable Concrete Structures – CEB Design Guide, Bulletin D'Information No. 182, Comité Euro-International du Béton, Lausanne, June 1989, 310 pp.

A.22) **CEB,** Bulletin D'Information No. 148, "Durability of Concrete Structures" State of the Art Report, Comité Euro-International du Béton, Paris, January 1982.

A.23) **CEB,** Design Manual on Cracking and Deformations, Comité Euro-International du Béton, École Polytechnique Fédérale De Lausanne, Suisse, 1985, 231 pp.

A.24) **Kahhaleh, K.Z.,** "Corrosion Performance of Epoxy Coated Reinforcement," Doctor of Philosophy Dissertation, Department of Civil Engineering, The University of Texas at Austin, May 1994.

A.25) **Houston, J.T., Atimtay, E., and Ferguson, P.M.,** "Corrosion of Reinforcing Steel Embedded in Structural Concrete," Research Report 112-1F, Center for Highway Research, The University of Texas at Austin, March 1972.

A.26) **Vennesland, O. and Gjorv, O.E.,** "Effect of Cracks in Submerged Concrete Sea Structures on Steel Corrosion," *Materials Performance*, Vol. 20, August 1981, pp. 49-51.

A.27) **Lin, C.Y.,** "Bond Deterioration Due to Corrosion of Reinforcing Steel," *Performance of Concrete in Marine Environment*, ACI SP-65, American Concrete Institute, Detroit, Michigan, 1980, pp. 255-269.

A.28) **Makita, M., Mori, Y., and Katawaki, K.,** "Marine Corrosion Behavior of Reinforced Concrete Exposed at Tokyo Bay," *Performance of Concrete in Marine Environment*, ACI SP-65, American Concrete Institute, Detroit, Michigan, 1980, pp. 271-289.

A.29) **Misra, S. and Uomoto, T.,** "Reinforcement Corrosion under Simultaneous Diverse Exposure Conditions", *Durability of Concrete, Second International Conference*, ACI SP 126, American Concrete Institute, Detroit, MI, pp.423-441.

A.30) **Okada, K. and Miyagawa, T.,** "Chloride Corrosion of Reinforcing Steel in Cracked Concrete," *Performance of Concrete in Marine Environment*, ACI SP-65, American Concrete Institute, Detroit, Michigan, 1980, pp. 237-289.

A.31) **Swamy, R.N.,** "Durability of Rebars in Concrete", *Durability of Concrete, G.M. Idorn International Symposium*, ACI SP-131, American Concrete Institute, Detroit, MI, pp.67-98.

A.32) **Berke, N.S., Dalliare, M.P., Hicks, M.C., and Hoopes, R.J.,** "Corrosion of Steel in Cracked Concrete," *Corrosion*, V. 49, No. 11, Nov. 1993, pp. 934-943.

A.33) **Schiessl, P., and Raupach, M.,** "Laboratory Studies and Calculations on the Influence of Crack Width on Chloride-Induced Corrosion of Steel in Concrete," *ACI Materials Journal,* Vol. 94, No. 1, January-February 1997, pp. 56-62.

A.34) **Tremper, Bailey,** "The Corrosion of Reinforcing Steel In Cracked Concrete," *ACI JOURNAL, Proceedings* V. 43, No. 10, June 1947, pp. 1137-1144.

A.35) **Ohta, T.,** "Corrosion of Reinforcing Steel in Concrete Exposed to Sea Air", *Durability of Concrete, Second International Conference*, ACI SP-126, American Concrete Institute, Detroit, MI, pp.459-477.

A.36) **Francois, R. and Arliguie, G.,** "Reinforced Concrete: Correlation Between Cracking and Corrosion", *Durability of Concrete, Second International Conference*, ACI SP-126, American Concrete Institute, Detroit, MI, pp.1221-1238.

A.37) **O'Neil, E.F.,** "Study of Reinforced Concrete Beams Exposed to Marine Environment," *Performance of Concrete in Marine Environment*, ACI SP-65, American Concrete Institute, Detroit, Michigan, 1980, pp. 113-132.

A.38) **Schiessl, P.,** "Admissible Crack Width in Reinforced Concrete Structures", Contribution II 3-17, Inter-Association Colloquium on the Behavior in Service of Structures, Preliminary Reports, Vol. II, Liege 1975, pp.739-753.

A.39) **Schiessl, P.,** "Zur Frage der zulassigen Rissbreite und der erforderlichen Betondeckung im Stahlbetonbau unter besonderer Berucksichtigung der Karbonatisierung des Betons", Deutscher Ausschuss fur Stahlbeton, Heft 255, Berlin 1976.

A.40) **Tuutti, Kyosti,** "Cracks and Corrosion", CBI Research No. 6:78, Swedish Cement and Concrete Research Institute, Stockholm, 1978, 55 pp.

A.41) **Beeby, A. W.,** "Cracking, Cover, and Corrosion of Reinforcement", *Concrete International*, Vol. 5, No. 2, February 1983, pp.35-40.

A.42) **Beeby, A.W.,** "Corrosion of Reinforcing Steel in Concrete and its Relation to Cracking", *The Structural Engineer*, V. 56A, No. 3, London, March 1978, pp.77-81.

A.43) **Beeby, A.W.,** "Cracking and Corrosion", Concrete in the Oceans, Technical Report No. 1, Construction Industry Research and Information Association/Cement and Concrete Association, London 1978, 77 pp.

A.44) **Husain, S. I., and Ferguson, P. M.,** "Flexural Crack Width at the Bars in Reinforced Concrete Beams," Research Report No. 102-1F, Center for Highway Research, University of Texas at Austin, June 1968.

A.45) **Poston, R.W.,** "Improving Durability of Bridge Decks by Transverse Prestressing," Doctor of Philosophy Dissertation, The University of Texas at Austin, December 1984.

A.46) **Moore, D.G., Klodt, D.T., and Hansen, J.,** "Protection of Steel in Prestressed Concrete Bridges," NCHRP Report 90, 1970, 86 p.

A.47) **Perenchio, W.F., Fraczek, J., and Pfiefer, D.W.,** "Corrosion Protection of Prestressing Systems in Concrete Bridges," NCHRP Report 313, February 1989, 25 pp.

Appendix B References

B.1) **Szilard, R.,** "Corrosion and Corrosion Protection of Tendons in Prestressed Concrete Bridges," *ACI Journal*, January 1969, pp. 42-59.

B.2) **Sason, A.S.,** "Evaluation of Degree of Rusting on Prestressed Concrete Strand," *PCI Journal*, Vol. 37, No. 3, May-June 1992, pp. 25-30.

B.3) **PCI,** Manual for Quality Control for Plants and Production of Precast and Prestressed Concrete Products, Precast/Prestressed Concrete Institute, Chicago, IL, 1985.

B.4) **Novokschenov, V.,** "Salt Penetration and Corrosion In Prestressed Concrete Members," Publication No. FHWA-RD-88-269, Federal Highway Administration, McLean, Va., 1989. (See also Novokschenov, V. "Condition Survey of Prestressed Concrete Bridges," *Concrete International*, Vol. 11, No. 9, September 1989, pp. 60-68, and Novokschenov, V., "Prestressed Bridges and Marine Environment," *Journal of Structural Engineering*, American Society for Civil Engineering, Vol. 116, No. 11, November 1990, pp. 3191-3205.)

B.5) **Whiting, D., Stejskal, B, and Nagi, M.** "Condition of Prestressed Concrete Bridge Components – Technology Review and Field Surveys," Publication No. FHWA-RD-93-037, Federal Highway Administration, McLean, VA, September 1993.

B.6) **Schupack, Morris,** "Unbonded Tendons – Evolution and Performance," *Concrete International*, Vol. 16, No. 12, December 1994, pp. 32-35.

B.7) **ACI Committee 423,** "Corrosion and Repair of Unbonded Single Strand Tendons," (ACI 423.4R-98), American Concrete Institute, Detroit, MI, 1998, 20pp.

B.8) **Demitt, A.,** "Evaluation and Repair of Unbonded Post-tensioned Slabs," Presentation at 1994 ACI Fall Convention, Tarpon Springs, FL, ADEM Engineering Ltd., Calgary, AB.

B.9) **Kesner, K. and Poston, R.W.,** "Unbonded Post-Tensioned Concrete Corrosion: Myths, Misconceptions and Truths," *Concrete International*, Vol. 18, No. 7, July 1996, pp. 27-32.

B.10) **Schupack, M.,** "Corrosion Protection for Unbonded Tendons," *Concrete International*, Vol. 13, No. 2, February 1991, pp. 51-57.

B.11) **Peterson, C.A.,** Survey of Parking Structure Deterioration and Distress," *Concrete International*, Vol. 2, No. 3, March 1980, pp. 53-61.

B.12) "Project Profile – Park Place Parking Garage," Wiss, Janney, Elstener Associates, Inc., Northbrook, IL.

B.13) **Robson, A., and Brooman, H.,** "A3/A31 Flyover - Case History of an Externally Post-tensioned Bridge," *Proceeding of the Seventh International Conference on Structural Faults and Repair - 1997,* Vol. 1, July 1997, pp. 307-315.

B.14) **Clark, L.A.,** "Performance In Service of Post-Tensioned Concrete Bridges," British Cement Association, October 1992.

B.15) **Isecke, B.,** "Long Term Behaviour of Materials in a Prestressed Concrete Bridge," Proceedings, International Symposium of Corrosion in Reinforced Concrete Construction, Warwickshire, England, Elsevier Applied Science, Essex, England, 1990, pp. 142-159.

B.16) **Schupack, M.,** "Durability Study of a 35-Year-Old Post-Tensioned Bridge," *Concrete International*, Vol. 16, No. 2, February 1994, pp. 54-58.

B.17) **Schupack, M.,** "Post-Tensioning Tendons After 35 Years," *Concrete International*, Vol. 16, No. 3, March 1994, pp. 50-54.

B.18) **Dickson, T.J., Tabatabai, H. and Whiting, D.A.,** "Corrosion Assessment of a 34-Year-Old Precast Post-Tensioned Concrete Girder," *PCI Journal*, Vol. 38, No. 6, November-December 1993, pp. 44-51.

Vita

Jeffrey Steven West was born in Calgary, Alberta on September 10, 1968 to David and Sharon West. After graduating as class Valedictorian from Sturgeon Creek Regional Secondary School in Winnipeg, Manitoba in 1986, he entered the engineering program at the University of Manitoba in Winnipeg. Choosing civil engineering as a major, he followed the Co-operative Education track and spent work terms in the Small Craft Harbours branch of Fisheries and Oceans Canada, the Air Transportation Sector of Architectural and Engineering Services in Public Works Canada, and in the Structures Laboratory at the University of Manitoba. He received his Bachelor of Science Degree in Civil Engineering with Distinction in the Fall of 1990, and was awarded the University Gold Medal. He enrolled in the Master of Science program at the University of Manitoba in the Spring semester of 1991 to study structural engineering under the supervision of Dr. Sami Rizkalla. After completing his Master's Degree, he entered to Graduate School at The University of Texas at Austin in September 1993 to pursue a Ph.D. in structural engineering.

Permanent Address: 9 Magnolia Lane
Guelph, Ontario
Canada N1G 4X7

This dissertation was typed by the author.